MATERIALS SCIENCE AND TECHNOLOGY FOR ADVANCED APPLICATIONS

DONALD R. MASH, EDITOR

MATERIALS SCIENCE AND TECHNOLOGY FOR ADVANCED APPLICATIONS

DONALD R. MASH, EDITOR

IN *MATERIALS SCIENCE AND TECHNOLOGY FOR ADVANCED APPLICATIONS*, edited by Donald R. Mash, electronic applications and space auxiliary nuclear power are covered with regard to important materials aspects. Special attention is given to aerospace applications. This book is a collection of technical papers published in book form for the 1962 Golden Gate Metals Conference program.

CONTRIBUTORS:

Irving Silver, *Bureau of Naval Weapons*

Charles J. Thelen, *U.S. Naval Ordnance*

C. M. Frey, *United Technology Corporation*

Abraham Hurlich, *General Dynamics/ Astronautics*

Dr. John E. Hove, *Aerospace Corporation*

H. Todd, F. Barcatta, D. Clark, R. Worlock; *Electro-Optical Systems, Inc.*

D. W. Gates, *Research Projects Division George C. Marshall, Space Flight Center*

Dr. Harry L. Reynolds, *Lawrence Radiation Laboratory*

Donald P. MacMillan, *Los Alamos Scientific Laboratory*

Dr. F. J. Clauss, C. F. O'Hara, S. P. Drake, S. B. Cooke; *Lockheed Missiles and Space Company*

Dr. R. E. Gaumer, *Lockheed Missiles and Space Company*

Jackson R. Stalder, *Vidya, Incorporated*

Dr. Daniel Schiff, *High Temperature Materials, Inc.*

Nicholas J. Hoff, *Stanford University*

W. D. Buntin, *General Dynamics, Fort Worth*

L. P. Spalding, *North American Aviation, Inc.*

Paul H. Denke, *Douglas Aircraft Company, Inc.*

(Continued from front flap)

Dr. Paul H. Egli, *U.S. Naval Research Laboratory*

Dr. F. L. Rosi, *RCA Laboratories*

Dr. Bernd Ross, *Hoffman Electronics Corporation, Semiconductor Division*

Coleman Kaplan, *The Marquardt Corporation*

Dr. Walter L. Knecht, *Astronautical Systems Division*

John E. Allegretti, Peter I. Pollak; *Merck, Sharp & Dohme Research Labs.*

Dr. Bruce Barnaby, *Eitel-McCullough, Inc.*

Dr. Roger Chang, G. G. Bentle, F. E. Ekstrom; *Atomics International*

Dr. David W. Levinson, *Armour Research Foundation*

Warren L. Pollock, *E. I. duPont deNemours & Company*

H. C. Emerson, *Rohr Corporation*

Warren G. Mang, *General Dynamics Corporation*

Dr. Donald R. Mash, *Advanced Materials and Processes, Inc.*

Cecil C. Lacy, Leopold Albertin; *The Boeing Company*

Dr. John R. Weeks, *Brookhaven National Laboratory*

G. M. Slaughter, C. W. Fox, E. A. Franco-Ferreira, R. G. Gilliland; *Oak Ridge National Laboratory*

Charles C. Woolsey, *Atomics International*

The Editor

DR. DONALD R. MASH is President and Technical Director of Advanced Materials and Processes, Inc., Los Altos, California.

PRENTICE-HALL, Inc.

Other books of interest . . .

PROPERTIES OF SOLIDS

by GEORGE G. KOERBER, *Iowa State University*

The basic purpose of PROPERTIES OF SOLIDS is to provide a modern, unified approach to materials science. The properties of materials are characterized in such a way that they can be represented as tensors of various ranks. Thus it is possible to bring the phenomenological treatment of all material properties into the operational framework of tensor algebra. Among the many advantages of this approach are: (1) the influence of structural symmetry upon anisotropy can be explored thoroughly but concisely, and (2) complex cross-effects such as galvanomagnetic, thermoelectric, and electromechanical interactions can be treated with simplicity.

Certain mathematical techniques, not usually included in the background of many engineers, have been employed. Therefore, Dr. Koerber devotes the first three chapters to the development of some elementary vector analysis, matrix algebra and tensor operations. Anyone already familiar with this material could still profit from a quick reading of these chapters in order to familiarize himself with the notation used later in the text.

PRENTICE-HALL SERIES IN ENGINEERING OF THE PHYSICAL SCIENCES

Published 1962 — *286 pages*

MECHANICAL BEHAVIOR OF ENGINEERING MATERIALS

by JOSEPH MARIN, *The Pennsylvania State University*

This book was written especially to meet the need for an up-to-date treatment of the mechanical properties of materials (sometimes referred to as solid state mechanics), which covers the macroscopic stress-strain behavior of materials under various environments encountered in modern engineering constructions.

Such new environmental conditions which arise in conjunction with space vehicles, nuclear engineering applications, as well as more conventional construction, make it mandatory for the engineer to possess a thorough understanding of the behavior of materials. The author gives primary consideration to the mechanical properties of materials for static, fatigue, shock, impact and high-temperature stresses. Utilization of these properties in analysis and design is included in order to integrate the study of mechanics of materials and design.

Published 1962 — *502 pages*

PRENTICE-HALL, INC.

MATERIALS SCIENCE AND TECHNOLOGY FOR ADVANCED APPLICATIONS

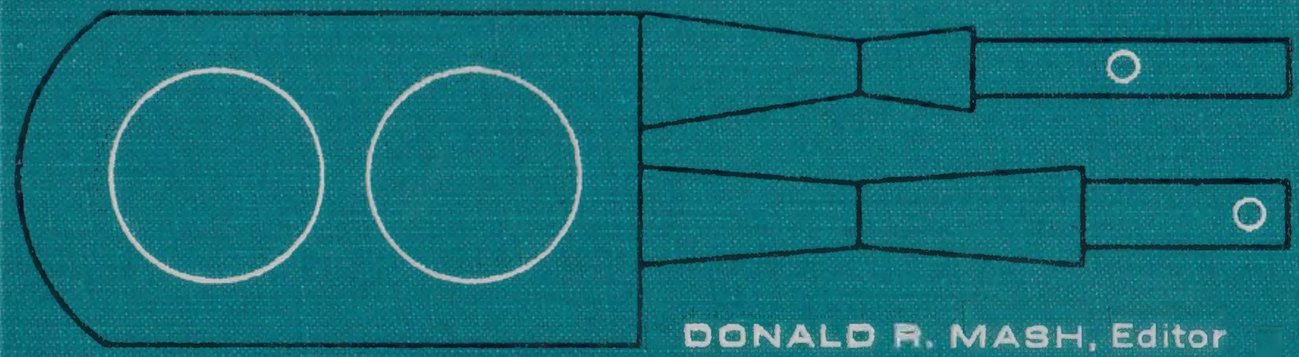
DONALD R. MASH, EDITOR

MATERIALS SCIENCE AND TECHNOLOGY FOR ADVANCED APPLICATIONS

MASH

Prentice-Hall

MATERIALS SCIENCE AND TECHNOLOGY FOR ADVANCED APPLICATIONS



DONALD R. MASH, Editor

Materials Science and Technology for Advanced Applications

Materials Science and Technology for Advanced Applications

Edited by DONALD R. MASH

President and Technical Director
Advanced Materials and Processes
Los Altos, California

For the Golden Gate Chapter of the American Society for Metals

PRENTICE-HALL, INC.
Englewood Cliffs, N. J. 1962

PRENTICE-HALL INTERNATIONAL, INC.
London Tokyo Sydney Paris

PRENTICE-HALL OF CANADA, LTD.

PRENTICE-HALL DE MEXICO, S.A.

© 1962 by Prentice-Hall, Inc., Englewood Cliffs, N. J. All rights reserved. No part of this book may be reproduced in any form, by mimeograph or any other means, without permission in writing from the publishers.

Library of Congress Card Catalog No. 62-18202

Printed in the United States of America

56090 —C

FOREWORD

It is not often that technical papers delivered at a regional conference are published in book form. However, the enthusiasm with which the 1962 Golden Gate Metals Conference program was received by those in attendance appears to warrant the current exception. As a result of excellent cooperation between the American Society for Metals and the Prentice-Hall Publishing Company, papers presented at the bienniel San Francisco meeting are collected in this volume for distribution in the entire technical community, both here and abroad. Especial thanks are extended to the individual contributors whose efforts have resulted in this important publication.

Although the Golden Gate Metals Conference traditionally emphasizes materials applications of interest to the West, the unprecedented technological growth of this region has effectively removed most restrictions on program scope and content. As a result, papers presented are of widespread interest and have a contribution to make on a country-wide basis. For example, considerable attention is given aerospace applications in keeping with the recent ascendancy of this field in the San Francisco Bay Area and with the emphasis currently given space exploration as part of our national program.

Problem areas and recent progress in connection with materials for propulsion, space vehicles, missiles, and supersonic aircraft are given rather thorough treatment. In addition, electronic applications and space auxiliary nuclear power have been covered with regard to important materials aspects. Finally, recent developments in materials and in fabrication techniques are discussed without connection to specific engineering applications.

Effective performance by the metallurgist and materials engineer in meeting their responsibilities in the Space Age can

be sustained only if progress in materials technology is accompanied by an appreciation of current and planned engineering applications. Recognition of this important relationship is the basic, unifying theme of this book. It is sincerely hoped that these collected papers will provide both information and incentive for all concerned with materials for advanced applications.

Donald R. Mash

TABLE OF CONTENTS

Problems in Chemical Propulsion Systems and Limiting Factors
Irving Silver, Bureau of Naval Weapons 1

Materials Requirements for Storable Liquid Propellant Rocket Motors
Charles J. Thelen, U.S. Naval Ordnance Test Station, China Lake 19

Materials Requirements for Solid Propellant Rocket Motors
C. M. Frey, United Technology Corporation..... 38

Materials Requirements for Cryogenic Temperature Applications
Abraham Hurlich, General Dynamics/ Astronautics 45

Introduction to Space Propulsion Problems
John E. Hove, Aerospace Corporation 85

Materials Requirements for Ion Propulsion
H. Todd, F. Barcatta, D. Clark, R. Worlock; Electro-Optical Systems, Inc. 94

Materials Requirements for Plasma Propulsion
D. W. Gates, Research Projects Division, George C. Marshall Space Flight Center 123

Materials Requirements for Nuclear Ramjets
Harry L. Reynolds, Lawrence Radiation Laboratory 136

Material Requirements for Nuclear Rockets
Donald P. MacMillan, Los Alamos Scientific Laboratory 151

Sliding Contacts and Friction Phenomena in Space
F. J. Clauss, C. F. O'Hara, S. P. Drake, S. B. Cooke; Lockheed Missiles and Space Company 164

Problems of Thermal Control Surfaces in the Space Environment
R. E. Gaumer, Lockheed Missiles and Space Company 199

Re-entry Environment
Jackson R. Stalder, Vidya, Incorporated 215

Pyrolytic Materials for Re-entry Applications
Daniel Schiff, High Temperature Materials, Inc. .. 236

Materials Problem Areas Peculiar to Supersonic Aircraft
Nicholas J. Hoff, Stanford University 267

Some Materials and Structures Problems Associated with Designing B-58 Type Structure for Supersonic Cruise Capability
W. D. Buntin, General Dynamics/ Fort Worth 281

The Use of Precipitation Hardening Stainless Steels in Supersonic Aircraft
L. P. Spalding, North American Aviation, Inc. ... 309

Materials for the Supersonic Transport
Paul H. Denke, Douglas Aircraft Company, Inc. 334

History and Recent Developments in Direct Energy Conversion Systems
Paul H. Egli, U.S. Naval Research Laboratory... 371

Semiconducting Materials for Thermoelectric Power Generation
F. L. Rosi, RCA Laboratories 408

Solar Energy Converters
Dr. Bernd Ross, Hoffman Electronics Corporation, Semiconductor Division 431

Materials for Thermionic Converters
Coleman Kaplan, The Marquardt Corporation 453

Advanced Electron Tubes for High Frequency, High Power, and Long Life
Dr. Walter L. Knecht, Aeronautical Systems Division 467

Epitaxial Deposition
John E. Allegretti, Peter I. Pollak, Merck, Sharp & Dohme Research Labs. 498

Electron Emission from Single Crystals
Bruce Barnaby, Eitel-McCullough, Inc. 512

Some Recent Studies of the High-Temperature Mechanical Properties of Refractory Oxides and Carbides
Roger Chang, G. G. Bentle, F. E. Ekstrom; Atomics International 533

Fiber-Reinforced Structural Materials
David W. Levinson, Armour Research Foundation 559

Recent Developments in Columbium Physical Metallurgy
Warren I. Pollock, E. I. duPont deNemours & Company 576

Welding and Brazing of Space Age Materials
H. C. Emerson, Rohr Corporation 606

High Energy Rate Forming of Space Age Materials
Warren G. Mang, General Dynamics Corporation 632

Plasma-arc Spraying of Space Age Materials
Donald R. Mash, Advanced Materials and Processes, Inc. 656

Heat Treatment of Space Age Materials
Cecil C. Lacy, Leopold Albertin; The Boeing Company 682

Corrosion and Mass Transfer in Alkali Liquid Metal Systems
John R. Weeks, Brookhaven National Laboratory.. 709

Joining of Refractory Metals for Space Power Applications
G. M. Slaughter, C. W. Fox, E. A. Franco-Ferreira, R. G. Gilliland; Oak Ridge National Laboratory..... 728

A Nuclear Fuel Element for Space Application 747
Charles C. Woolsey, Atomics International

PROBLEMS IN CHEMICAL PROPULSION SYSTEMS AND LIMITING FACTORS

Irving Silver
Branch Engineer, Missile Propulsion Branch
Bureau of Naval Weapons
Washington 25, D.C.

ABSTRACT

The energy limitations of chemical propulsion systems are discussed in terms of molecular weight, bond energy and molecular dissociations. Based on the above consideration, a specific impulse in the order of 425 seconds appears to be the maximum value attainable. Other factors affecting the performance of chemical propulsion systems are mass ratio and combustion efficiency.

Problems associated with advancing the state of technology in chemical propulsion in solids, liquids and hybrid engines are discussed. These include the sensitivity of energetic ingredients used in solid propellants, the design and engineering of liquid engines employing cryogenic oxidizers and fuels, the use of more energetic and dense propellants in storable liquid engines, and problems in combustion and development of hybrid engines.

INTRODUCTION

For many years, rocket propulsion has been synonymous with chemical reaction systems. Today, as a result of the latest advances in nuclear, thermoelectric and other

related technologies, rocket motors based on physical rather than chemical properties are now being developed. It is not anticipated that these new developments will materially affect the position of chemical propulsion systems; instead, these new systems will find their own unique place fulfilling special functions based on new requirements now being established for outer space and other missions.

It is important that we define the area in which chemical systems operate and to indicate the limitation on performances set by the maximum available energy in chemical propellants. These performance limitations are real but this in no way implies that no further advancements are possible. Although ultimate performance limitations can be indicated with a fair degree of accuracy, these limits have not yet been attained and further advances in the state of the art will permit significant improvements over our present capabilities. This paper will discuss the energy limitations of chemical propulsion systems and outline the problem areas which need resolution if we are to develop higher energy and more efficient chemical propulsion systems.

The most serious limitations to chemical propulsion systems are those that are imposed by the laws of nature. The maximum available energy that can be obtained from known chemical structures can be determined from a consideration of bond energies, heats of formation and reaction. It is possible then to establish a maximum value for specific impulse which is a fundamental parameter depicting the performance of a propellant. In its simplest form, specific impulse can be described by the following equation:

$$I_s = \frac{F}{W} \ ;$$

F = Thrust in pounds force
W = Rate of propellant consumption in pounds/second or the thrust generated by a flow of one pound of propellant per second.

From Table I, the relative position of various rocket propulsion systems is shown. In terms of specific impulse chemical systems are the least energetic. Non-chemical systems are capable of performance of at least one order of magnitude over any performance possible by chemical propulsion systems, although chemical air-breathers employing oxygen from the atmosphere as an oxidizer offer the possibility of extending the impulse performance by a factor of 2-3.

TABLE I

COMPARISON OF PROPULSION SYSTEMS

System	Specific Impulse (lb(F)sec/lbm)
Chemical	130 - 450
Chemical Air Breathers	300 - 1,200
Solar Heating	300 - 600
Nuclear	500 - 7,000
Arc Jet	1,000 - 5,000
Ion Jet	5,000 - 15,000
Plasma	3,000 - 6,000

The use of specific impulse as a basis of comparison can lead to misleading conclusions. Although some of the non-chemical systems are capable of generating high specific impulse, the mass flow rate of the thrust is extremely low limiting these systems to only certain applications where high thrust requirements do not have to be met. Thrust can be shown to be equivalent to the product of the velocity of the exhaust particle and the mass flow rate. The advantage of the chemical propulsion system is that by varying the burning rate of the propellant and the internal design of the grain tremendous mass expulsion rates can be attained to give thrusts equivalent to hundreds of thousands of pounds. By reducing the burning rate, the

same propellants may be useable in sustainer operations where lower thrusts but increased burning times are required.

A specific impulse of about 425 appears to be the maximum value attainable in chemical propulsion systems. The reasons for this are essentially related to the reactions of chemical constituents in rocket combustion chambers. The barriers preventing the attainment of performance higher than this are: bond energy, molecular weight and molecular dissociation. To appreciate these factors, we need to redefine specific impulse in terms of thermochemical and dynamic relationships such as:

$$I_s = \sqrt{\frac{2J}{g}\ (H_c - H_e)}$$

where

J = Mechanical Equivalent of Heat
g = Gravitational Constant
H_c = Combustion Enthalpy
H_e = Exit Enthalpy.

Another representation of the specific impulse equation is:

$$I_s = 9.797 \sqrt{\frac{k}{k-1} \times \frac{Tc}{M} \left[1 - \left(\frac{Pe}{Pc}\right)^{\frac{k-1}{k}}\right]}$$

where

k = Average Specific Heats C_p / C_v
Pe = Exit Pressure
Pc = Chamber Pressure
M = Average Molecular Weight
Tc = Combustion Chamber Temperature.

The significant points in this equation are that specific impulse is defined by the temperature of the combustion process Tc and the molecular weight of the reactant gases, M. The specific heat, k, and pressure effects are contributing factors but not of major consideration in this discussion. The above equation can be reduced to the following:

$$I_s \sim \sqrt{\frac{Tc}{M}}$$

Table II lists theoretical values for specific impulse for some typical liquid propellants. From these values, it is possible to establish relationships between specific impulse and composition, temperature and molecular weight. From consideration of molecular weight according to the foregoing equation, the approach to higher specific impulse is the selection of propellants which result in low molecular weight combustion products. The absolute minimum which can be achieved of course is hydrogen--with a molecular weight of 1.5 to 2 involving both molecular and atomic species. However, since reactions between different atomic and molecular species other than hydrogen will be involved in chemical propulsion molecular weights greater than 2 will generally result, the latter being possible only in a nuclear rocket employing hydrogen as a fuel. Some typical rocket exhaust compositions are shown in Table III. Typical rocket exhaust molecular weights generally range from 18 to 32. From Table III, it can also be seen that second period light metals such as lithium, beryllium and boron with molecular weights of 7, 9 and 11 permit them to be considered as possible constituents in rocket engine combustion. A value for the hydrogen-fluorine system is 8.9 which is the minimum molecular weight attainable. The limiting value, of course, is one but this value is unattainable for chemical propulsion systems. The species hydrogen, carbon, nitrogen, oxygen and fluorine have long been and will probably be for some years to come the basic atomic species participating in the rocket combustion and expansion cycle. It is here then, with the molecular weight that the first barrier to extremely high specific impulse values is to be found.

The temperature is a measure of the thermal energy imparted to the combustion products as a result of the fuel-oxidizer reaction in the combustion chamber resulting from the breaking of valence bonds and forces in the oxidizer and fuel and forming of new and usually stronger valence bonds in the reaction products. Table IV shows comparative values of chemical bond energies of reactants and products.

TABLE II

SPECIFIC IMPULSE VALUES

Oxidizer	Fuel	Tc (°F)	M	k	Isp (500 psi)	
Hydrogen Peroxide	Gasoline	4830	21	1.20	248	(286)
Hydrogen Peroxide	Hydrazine	4690	19	1.22	262	
Nitric Acid	Gasoline	5150	--	1.23	240	
Nitric Acid	Aniline	5100	21	--	235	
Nitric Acid	Ammonia	4220	22	1.24	237	
Oxygen	Alcohol	5560	22	1.22	259	
Oxygen	Gasoline	5770	22	1.24	264	
Oxygen	Hydrazine	5370	18	1.25	280	(313)
Oxygen	Hydrogen	4500	9	1.26	360	(391)
Fluroine	Ammonia	7224	19	1.33	306	(357)
Fluorine	Hydrazine	7940	19	1.33	316	(363)
Fluorine	Hydrogen	5100	8.9	1.33	373	(410)

Bracketed figures -- 1000 → 14.7 psia

TABLE III

MOLECULAR WEIGHTS

Reactants		Combustion Products	
Hydrogen	1.00	H	1.00
Helium	4.00	H_2	2.02
Lithium	6.94	C	12.01
Beryllium	9.01	N	14.01
Boron	10.82	O	16.00
Carbon	12.01	OH	17.01
Nitrogen	14.01	H_2O	18.02
Oxygen	16.00	F	19.00
Fluorine	20.18	HF	20.01
Sodium	23.00	CO	28.01
Magnesium	24.32	NO	30.01
Aluminum	26.97	CF	31.01
Silicon	28.06	O_2	32.00
Phosphorus	30.98	F_2	38.00
Sulfur	32.07	CO_2	44.01
Chlorine	35.45	CF_2	50.01
		C_2F_2	62.02
		COF_2	66.01
		CF_3	69.01
		CF_4	88.01

TABLE IV

VALENCE BOND ENERGIES
(Kcal/mol)

Reactants		Combustion Products	
C-O	81	C=O	256
C-C	78	N≡N	225
C-N	70.5	N=O	150
O-O	117	N-F	134
H-H	33	C-F	106
N-H	85	H-O	103
C-H	80		
F-F	36		

In selecting propellant combinations that will yield high combustion temperatures, the choice of fuel and oxidizer will be centered on compounds which in themselves have positive heats of formation and will in reaction lead to products which have high bond energies and very negative heats of formation. One of the objectives of the ingredient synthesis program for higher energy propellant is to prepare chemical structures which have low negative or even positive heats of formation so as to produce the maximum heat balance. The bond energies or heats of formation of basic chemical structures then represent another limitation in the attainment of higher specific impulse since the combustion temperature on which specific impulse depends is directly related to the energy balance resulting from the combustion reaction.

Another limitation is that there is a temperature level beyond which it is extremely difficult to go. At higher temperatures, the exhaust products begin to absorb substantial quantities of energy by first dissociating to free radicals. Unless these radicals recombine in the nozzle this energy absorbed in dissociation is not available to do useful work. In Table V, the lower order flame temperatur

TABLE V

DISSOCIATION OF EXHAUST SPECIES

Species	% Dissociation (4,000°F)	(6,000°F)	(8,000°F)	(10,000°F)
CO_2	5	40	--	--
H_2O	2	12	22	--
H_2	1	6	18	--
O_2	1	5	14	--
HF	--	1	2	--
CO	--	--	--	2
N_2	--	--	--	2

are low primarily because of lower order bond energy, although in some cases the low temperatures are a result of advanced dissociation of some of the reactant ingredients, particularly water and carbon dioxide. Water begins to dissociate low in the temperature scale, 5% being dissociated at 5000°F. Rocket engine flame temperature, Tc, is therefore limited by the dissociation of the reaction products which begin about 5000°F and reach advanced levels at 8000°F to 10,000°F. However, the practical limit in combustion temperature is approximately 7000°F. Table V shows the percent dissociation of various exhaust species against temperature at 500 psi. From this, one can gather that higher temperature systems are more probable in those reactions which have a minimum of CO_2 and H_2O and an optimum amount of N_2 and CO. Theoretical considerations and experimental firings prove that this is the case.

To the propulsion engineers, performance is generally expressed in terms of vehicle range, size, payload or velocity at burnout. The latter parameter which can be shown to be related to the other performance criteria is described by the following equation:

$$V_b = I_s \, g \log \frac{W_i}{W_b}$$

$$\frac{W_i}{W_b} = \text{mass ratio} = \frac{\text{vehicle initial weight}}{\text{vehicle burn-out weight}}$$

The mass ratio can also be written as:

$$\frac{W_i}{W_b} = \frac{W_b + W_p}{W_b} = 1 + \frac{W_p}{W_b} = 1 + \frac{vd}{W_b}$$

where

v = volume of propellant
d = density of propellant
W_p = propellant weight.

There is little doubt that these performance parameters are all enhanced to a greater or lesser degree by the increase in specific impulse. However, there are certain aspects of the foregoing equation apart from specific impulse which are limiting factors in achieving maximum performance in a chemical propulsion system. These aspects are discussed below:

Combustion Efficiency

The specific impulse is generally calculated to give a theoretical value assuming 100% efficiency and assuming complete equilibrium flow along the nozzle. In actual practice, the performance is limited by the combustion efficiency of the propellant and of the motor, and the efficiency or available energy is generally around 90 to 97% of the theoretical value. The difference between theoretical and actual delivered specific impulse may be attributable to several factors. Heat losses from the motor, failure to maintain equilibrium flow throughout the nozzle, and thermal-velocity lags of condensed phases in the exhaust all lead to reduced efficiency. This factor is of considerable importance in that the selection of a propellant for a given motor is not necessarily based on its theoretical

value but on the delivered impulse. It is possible that some propellant may actually deliver higher impulse even though their theoretical values may be somewhat less than other propellants.

The addition to metals to propellants either as a fuel or as a means of increasing density may seriously affect the combustion efficiency. The use of Al as a fuel, for example, will give significant increases in specific impulse but large amounts of Al are increasingly more difficult to burn efficiently so that the improvement in performance is less than proportional. The presence of Al_2O_3 in the exhaust creates two phase flow in which there exists thermal and velocity lags which dissipate the energy in the system. There is also the problem of obtaining complete combustion of the aluminum to aluminum oxide. If the aluminum particles are only oxidized on the surface during the combustion process then the full potential of the aluminum as a fuel is not realized. This type of combustion inefficiency may occur where metal fuels are present in the propellant formulation. As other metals are employed, one of the major problems anticipated is that of obtaining acceptable combustion efficiencies in the development of higher energy propellants. In general, values below 90% are undesirable and may result in deliverable impulses not significantly above available systems. Considerable effort is being placed on the combustion efficiency problem with the idea of understanding the basic mechanisms affecting the dissipation of energy and in developing propellants and propulsion systems in which combustion efficiencies of 95% or over for solid fuels are possible.

Mass Ratio

The mass ratio factor in the equation for burnout velocity shows that improved performance can be obtained through an increase in the proportion of propellant by weight to the inert constituents of the motor. Motor designs are generally optimized to give the highest mass ratio consistent within the state of the art. Table VI shows the variation in range and velocity of a one stage rocket for different

TABLE VI

MASS RATIO EFFECTS

Mass Ratio $\frac{W_f}{W_i}$	Isp (lb sec)	Range (mile)	Burnout Velocity (ft sec)
1.43	200	50	2,305
	300	75	3,460
	400	140	4,610
	500	200	5,760
	600	275	6,900
2.00	200	130	4,460
	300	250	6,700
	400	440	8,920
	500	700	11,160
	600	1,050	13,400
3.33	200	330	7,750
	300	750	11,600
	400	1,450	15,550
	500	2,700	19,400
	600	4,850	23,200
10.1	200	1,300	14,800
	300	4,150	22,200
	400	Satellite	29,000
	500	Escape	37,000
	600	Escape	44,400

specific impulses. It is apparent that the rewards for achieving high mass ratio propulsion systems are significant in terms of increased performance. Even for relatively low impulse such as 200 seconds, a mass ratio increase from 200 (50% propellant and 50% inerts) to 10 (90% propellant to 10% inerts) can increase the range from 130 to 1300 miles.

The limiting factors on which the mass ratio depends are as follows:

Pressure: A higher specific impulse can be obtained by designing the motor for higher combustion pressures. Increased combustion pressure results in decreased dissociation of some species, thereby increasing the flame temperatures and making possible a more complete combustion. There is a practical limit to the increase in pressure as determined by the trade-off between the improvement in specific impulse and the increase in the thickness and therefore weight of combustion chamber to accommodate the increase in pressure. In some instances, it may be desirable to operate the motor at lower pressures; for example, in the upper stage of some of the space motors at some sacrifice in impulse so that higher mass ratios can be attained. The development and use of higher strength light weight materials may make it possible to operate motors at higher pressure realizing higher impulse values and reducing at thickness and weight of the chamber so that simultaneously an increase in mass ratio is obtained. On the other hand, the increase in impulse and temperature may offset this improvement since the use of additional insulation in the chamber and nozzle to resist thermal erosive effects may be required thereby effectively reducing the mass ratio.

Propellant Density: For volume limited applications, it is sometimes desirable to incorporate the maximum amount of propellant by weight. This is essentially accomplished by using a propellant with a relatively high density. This maneuver not only is effective in increasing the mass ratio but also can result in a higher total impulse for the motor. The addition of metals to the propellant is

one of the best methods for obtaining really significant increases in density. The selection of the metal is of considerable importance in that some metals, such as Al, are effective fuels and can effect significant increases in specific impulse in addition to adding to the density of the propellant. Other metals such as titanium, tungsten and zirconium can add significantly to the density of the propellant but generally result in a decrease in specific impulse. In some applications, particularly boosters, the improvement in mass ratio is more than enough to offset the drop in impulse so that in effect improvements in performance are possible. The increase in propellant density has certain limitations in that the total weight of the motor may be in excess of the maximum launch weight which can be tolerated. In many applications a better indication of performance than specific impulse is impulse-density, which gives consideration to the density of the propellant. The importance of the impulse-density ban be described by the following equation:

$$p = k I_s d^{\mu}$$

where

p is a performance parameter
I_s = specific impulse
d = density
μ = variable with stage = 1st stage about 0.70 = 2nd stage 0.28 = 3rd stage 0.23.

Thus the effect of high density impulse is greatest in the first stage. In upper stages, the density effect is less important and specific impulse is the more critical criterion. This is one of the reasons liquid engines employing high impulse propellants are considered more appropriate for upper stages for high altitude and space shots.

Solid Propellants

Although solid propellants cannot match the specific impulse of the cryogenic liquids, it is possible theoretically to achieve values of over 300 seconds. To date, the addition of aluminum and ammonium perchlorate coupled with

an increase in solid loadings form the basis of many of the solid propellants in use today. To attain even higher performance, the Services in conjunction with the Advanced Research Projects Agency are supporting major research efforts in the synthesis of new fuels and oxidizers. The syntheses of these ingredients are based on computer performance calculations using thermal constants for various postulated molecular structures. Since these performance calculations serve as guides in determining the selection of promising avenues of research, considerable effort is devoted to obtaining accurate thermodynamic characterization of these ingredients, many of which have not been previously prepared or inaccurately characterized. Currently, the major interest is in those chemical structures based on combinations of N, O, B or F which theoretically are capable of forming compounds of higher energy content.

The research effort is now resulting in many new ingredients of higher energy content. The main problem is in translating these new ingredients into usable propellant systems which are safe to process and handle and economically acceptable. The proper utilization of some of these ingredients presents serious problems for which solutions are required. The greater reactivity of these ingredients and their attendant tendency toward greater sensitivity to impact or friction, degradation by moisture and heat, and incompatibility with other ingredients require new techniques for their processing and building. One serious approach towards the solution of problems associated with these new ingredients is encapsulation. The chemistry and physics of encapsulation, the development of new encapsulation coatings, techniques of encapsulation and the incorporation of encapsulated coatings into propellant compositions are all aspects of the problem. The objective is an encapsulated ingredient impervious to moisture and other atmospheric influences and unreactive with other propellant ingredients when stored for long periods of time.

Since encapsulation is by no means a panacea to the use of these more energetic ingredients, other means of utilizing these materials are being investigated. One approach is that of segregating the fuel and oxidizer into compartments

so that only their combustion products are brought into intimate contact. The combustion of solid propellants in which the oxidizer and fuel are separated is not thoroughly understood and it is anticipated that problems concerning the ignition and control of burning rate will need to be solved. If successful, this approach could mean major changes in solid propellant technology with respect to assembly and loading.

Liquid Propellants

In liquid rocket propulsion, the ultimate propellants are on hand and current work is being carried out to develop practicable engines employing these materials. In the field of cryogenics, liquid hydrogen and fluorine are the most promising advanced materials. The high heat of reaction of hydrogen with all oxidizers and the low molecular weight of the reaction products produces high specific impulse. However, its low density (0.58 lb/gal) means that the payload capability of vehicles using this fuel must be examined carefully. Mission analyses would indicate that the hydrogen fueled engines are most applicable in top stages where significant gains in payloads are possible. The late entry of hydrogen into present day rocketry can be ascribed to concern over handling as a liquid.

Fluorine is the most promising cryogenic oxidizer for near future applications. Its reactivity is well known and in a sense is the chief drawback to its development and use as a liquid engine oxidizer. Fluorine attacks most metals and organics and is extremely toxic. It presents special handling problems in disposition either in the laboratory or out in the field at a launching site. Combustion temperatures of liquid F_2 are much higher than with O_2 so that the problems of engine cooling is further aggravated. Other cryogenic materials such as liquid ozone, oxygen bifluoride and nitrogen fluorides are of general interest and their applicability as cryogenics is under study.

A major drawback to the use of cryogenic liquids is the need for venting the tanks to permit the propellant to boil

off until the instant of firing. Because of this, the engines cannot be stored in the loaded condition and substantial preparation time is required to load the tanks and top them off prior to launching. For this reason, they are not suited to certain military applications where instant readiness is a basic requirement. Another limitation is the low density of cryogenics.

In order to meet the requirement of instant readiness and to avoid some of the problems of cryogenic bipropellant systems, the packaged storable engines have been developed by the Navy. These engines operate on the principle that the liquid propellants with suitable energetic and physical properties can be permanently housed in sealed compartments without deterioration in storage and on the sudden application of pressure can be injected into a combustion chamber where they react chemically. The advantages of these storable liquid engines derive from their inherent capability to operate at temperature extremes which solid motors only now do with great difficulty.

Current research work in liquids is concerned with upgrading the performance of storable liquid engines. For this purpose, work is being directed towards the synthesis and evaluation of denser and more energetic liquid propellants. Increased performance is being achieved through the addition of light metal additives. The synthesis of more energetic liquid propellants is being concentrated in B, N, O and F compounds. In fact, the synthesis program for solid propellants is yielding liquid ingredients which are being characterized for evaluation in liquid engine firings.

Hybrid Engines

A more recent approach towards improving the performance of chemical propulsion system is the hybrid engine. A hybrid engine combines both solid and liquid propellants in a single engine for the purpose of deriving the major advantages of each technology and possibly avoiding some of their major drawbacks. The advantages which make hybrids so attractive are (a) new liquid or

solid propellants, as well as the standard ones, can be utilized to full advantage in a large variety of combustions, (b) increased safety because of the separation of oxidizers and fuel, (c) optimization of specific impulse and density impulse according to the specific needs of a mission, (d) retention of on-off restart capability, full thrust throttling and other advantages of the liquid engines.

Although the hybrid represents a marriage of liquid and solid rocket technology, new problems are created which require investigation. Among these areas under study are the following: (a) a better understanding of liquid-solid combustion processes and chemical kinetics; (b) research and development of propellants specifically tailored for the hybrid engine; (c) establishment of the feasibility and design criteria for hybrid engines and the enhancement of the hardware state of the art.

CONCLUSION

The energetic limits of chemical propulsion have been indicated in this report. In the last decade, considerable progress in both solid and liquid rocket technology have formed the basis for the current advanced missile and space vehicles currently under development. Further gains in technology are possible through the development of more energetic propellants, improved materials and advanced design concepts to make possible a closer proximity to maximum performance possible with chemical propulsion.

MATERIALS REQUIREMENTS FOR STORABLE LIQUID PROPELLANT ROCKET MOTORS

Charles J. Thelen
Head, Propellants Division
U.S. Naval Ordnance Test Station
China Lake, California

ABSTRACT

As a frame of reference a generalized design of a storable liquid propellant propulsion system and the general military requirements for this type of system are briefly described. Current material requirements for the critical parts of the propulsion system are then discussed with emphasis given to compatability of propellants with metals and plastics used in the fabrication of propellant tanks, liners and valves. Since the storable liquid propulsion system has great potential for positioning and attitude control of space vehicles because of its variable thrust and on-off capabilities, the anticipated effect of space environment on the aforementioned material requirements are also discussed.

INTRODUCTION

One of the most significant recent developments in the field of liquid propellants has been the re-awakened interest in storable* bipropellant** propulsion systems for military

---

* In this paper no attempt will be made to rigidly define a storable propellant since the definition varies dependent upon the lifetime environment encountered by the missile. In general terms, storable propellants are oxidizers and

applications. This renewed interest, as evidenced by the development of storable liquid propulsion systems for the Bullpup and Titan II missiles, has been largely the result of the propellant research and engineering studies which have been conducted in the last several years. These studies have shown the advantages of these systems to be excellent performance, simplicity of motor design, instant readiness, high reliability, safety, missile mobility, long term storage, suitability for volume limited applications, wide temperature cycling capability, minimum requirements of ground support equipment and maintenance, and low cost.

The design of a storable liquid propellant rocket motor is quite similar to that of a cryogenic liquid propellant motor. The only difference is a slight change of materials in the critical components due largely to the corrosive activity of the storable oxidizers, the effect of materials of construction on the chemical stability of the storable oxidizers and fuels, and the relaxation of some of the stringent operational requirements imposed by the low temperatures of the cryogenic oxidizer, normally liquid oxygen.

Before discussing the materials requirements, it might be well to briefly review the major components of a liquid propellant propulsion system. This system consists of three main parts: the thrust chamber, the propellant feed system and the propellant tankage. The thrust chamber consists of an injector with its manifold, a combustion chamber which may be regenerative cooled, *** a nozzle, and

---

fuels which can be stored in tankage in the missile for a minimum period of two years under the environmental conditions specified in the missile specification.

** This paper will be concerned only with liquid bipropellant systems. However, the general principles outlined for the selection of materials for bipropellants also pertain to those for storable monopropellants.

*** Regenerative cooling is the term applied to the technique used to cool a combustion chamber and nozzle by transferring the heat contained in their inner walls to a moving stream of propellant prior to its injection.

sometimes an ignition system. The propellant feed system consists of the propellant feed lines, the valves required for the control of the flow of the propellants and a device for expelling the propellants from their tankage to the thrust chamber. Two designs, gas pressurization and turbopump, for moving the propellants to the thrust chamber, are shown schematically in Figures 1 and 2.

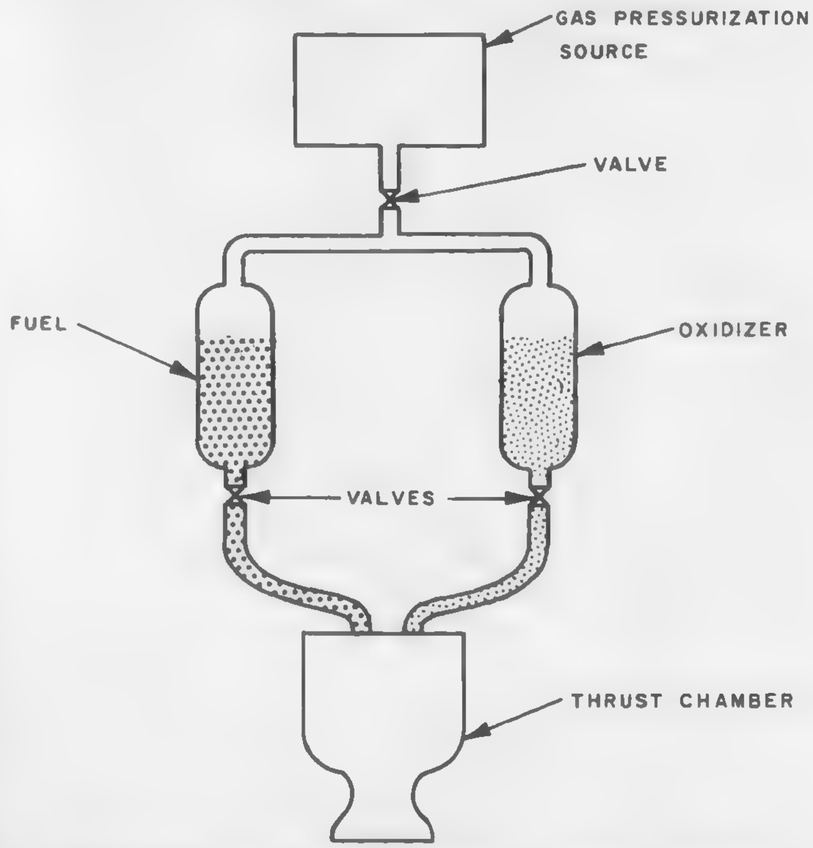


FIGURE 1 SIMPLIFIED SCHEMATIC DIAGRAM OF LIQUID PROPELLANT PROPULSION SYSTEM UTILIZING A PRESSURIZED FEED SYSTEM

The propellant tankage consists of containers which are usually cylindrical and arranged either in tandem or concentrically. Although their design is influenced usually by the method used for expelling the propellants, consideration must also be given to movement of the propellants by acceleration forces caused by maneuvers of the missile. To ensure that the tank outlets are continually fed with liquids, several different pressurization designs have been developed

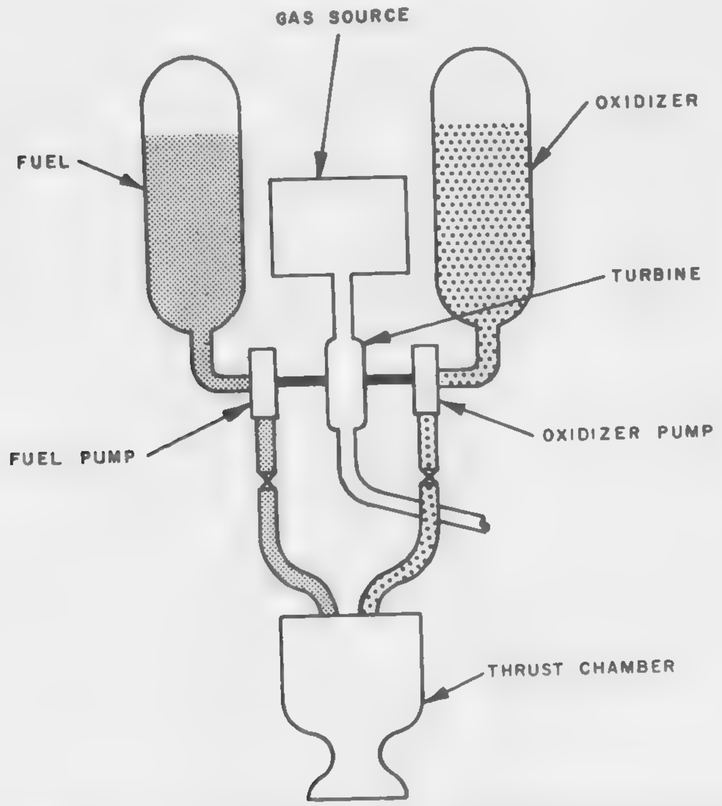


FIGURE 2 SIMPLIFIED SCHEMATIC DIAGRAM OF LIQUID PROPELLANT PROPULSION SYSTEM UTILIZING A TURBOPUMP FEED SYSTEM

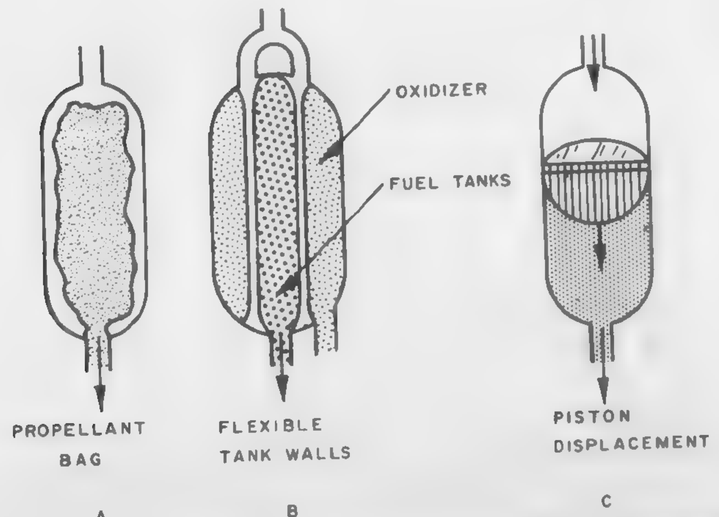


FIGURE 3 METHODS FOR ASSURING POSITIVE PROPELLANT FLOW IN PRESSURIZED FEED DESIGNS

which are shown in Figure 3. The first design incorporates a plastic bag which either encloses the liquid volume at all times as shown in Figure 3A or encloses the pressurizing gas when it is injected into the tank. Figure 3B illustrates an extension of the bag principal which utilizes flexible metal tank walls (ballonets) thereby avoiding some of the convoluted shapes which prevent complete expulsion of the propellant. The third design, Figure 3C, incorporates a piston for assuring continuous flow of the propellant but suffers from the drawback of not being adaptable at the present time to storage in the loaded condition.

FACTORS INFLUENCING MATERIALS SELECTION

In any design of a propulsion system considerations are given to selection of materials upon strength and stiffness both at storage and operational temperatures, availability, cost, storability, resistance to corrosion, minimum weight and ease of manufacture. This latter factor also includes considerations as to availability of tooling required for the manufacture of the various propulsion components. Other important factors which play a role in the selection of materials for certain components are high thermal conductivity, high specific heat, low thermal expansion, erosion and fatigue resistance, and effect on propellant stability.

In military applications the anticipated environment which the system will see during its lifetime also must be considered in the selection of materials. For this reason, the military specifications for the design and development of the specific system includes, besides the operational requirements (total thrust, burning time, etc.), qualification tests which tend to duplicate the worst type of environments which might be encountered during the shipping, handling and storage phases. Examples of some of these tests* for a Navy air fired system are as follows:

---

* These tests are run with the propulsion system encased in its shroud or skin and normally detached from the guidance and control and warhead sections of the missile.

1. Temperature cycling over the range of -65 to 160°F.
2. Drops of 6 feet and 40 feet onto a steel plate embedded in concrete. The propulsion system is required to operate satisfactorily after the 6 foot drop test but not after the 40 foot drop test. However, in the latter case the system should be in a condition which would allow safe disposal.
3. Temperature and humidity tests--14 cycles between -65°F and ambient humidity and 160°F and 95% relative humidity.
4. Salt spray test--168 hours of spraying with a 20% sodium chloride solution.

A very important factor which has a great influence on the selection of materials which will come into contact with storable propellants is compatibility. Compatibility in this case not only refers to the resistance of the materials to chemical attack by the propellants but also to the effect of the materials on the chemical stability of the propellants. Based upon propulsion and industrial experience and laboratory studies, a number of materials have been recommended for application with current and potential storable oxidizers and fuels, and these are listed in Tables I and II. It should be pointed out that the metals and non-metals listed in these tables are not only the ones which can be used. However, if other materials are selected adequate compatibility tests should be conducted under environments which will simulate their use in the propulsion system, in order to determine their useability in the proposed application.

Besides the aforementioned corrosion, other types which may be encountered in a propulsion system are galvanic, intergranular and stress corrosion cracking. The latter two are common mainly with the tankage system and will be briefly mentioned later. The first type, galvanic or electrolytic corrosion, is normally considered by the propulsion designer when he specifies the use of dissimilar metals in a component. However, once in a while this type of corrosion is overlooked and, as a result, a severe corrosion problem is encountered which does not make its appearance until well into the development phase.

TABLE I

MATERIALS WHICH CAN BE USED WITH VARIOUS STORABLE LIQUID FUELS

Fuel	Metals	Non-Metals
Ammonia (99.5% minimum purity)	300 and 400 series stainless steel, carbon steels, Hastelloys, Inconel, gold, platinum, tantalum, nickel and lead	Teflon Kel F Pure asbestos
Hydrazine* (97% minimum purity, approx. 1% water)	Stainless steel types 302, 304, 304 ELC, 316, 347, 416, 17-7 PH Nickel Aluminum types 356, 716, 1100, 2017, 2020, 3003, 4043, 5052, 6061 Titanium alloy 6A1-4V	Teflon High density polyethylene Garlock 735 Mylar film Unplasticized Kel F Silastic elastomer Asbestos
Unsymmetrical dimethylhydrazine (98% min. purity, approx. 0.1% water)	Mild steel Aluminum and its alloys Nickel Stainless steel types 303, 304, 321, 347, 416, 17-7 PH 4130 steel Titanium 6A1-4V	Teflon Unplasticized Kel F Polyethylene Garlock gasket 900 Nylon

* Hydrazine should not be brought into contact with carbon and low alloy steels, copper and its alloys, molybdenum and stainless steels containing greater than 0.5% molybdenum, 40E aluminum, magnesium, zinc, and lead for these metals and alloys cause its decomposition.

TABLE II

MATERIALS WHICH CAN BE USED WITH VARIOUS STORABLE LIQUID OXIDIZERS

Oxidizer	Metals	Non-Metals
Chlorine trifluoride[a]	Copper, brass, steel, aluminum, Monel, nickel	Kel F Teflon
Hydrogen peroxide[b]	Aluminum types 1060, 1100, 1160, 1260, 7072, B-356, tantalum, zirconium	Kel F
Inhibited red fuming nitric acid (IRFNA)	Aluminum types EC, 356, 1060, 1100, 2014, 2017, 2026, 3003, 3004, 5052, 5154, 6061, 7075 Stainless steel types 302, 303, 304, 304 ELC, 316, 321, 347, 430, 17-7 PH, 19-9 DL, 19-9 DX, Chromium	Kel F Teflon Polyethylene
Nitrogen tetroxide (normally with less than 0.1% water)	Carbon steels, mild and 1020 steels, aluminum, stainless steels,[c] titanium[d] alloys, gold, platinum, lead	Teflon Kel F (unplasticized) Albestos, Ceramic Polyvinyl fluoride (Teslar 30)
Perchloryl fluoride[e] fluoride[e]	Carbon steel, aluminum, stainless steel, copper, brass, bronze	Teflon, Kel F Unmodified phenolics Epoxy resins GRS rubber Silicone rubber

[a] Most common metals can be used with chlorine trifluoride because of the formation of a passivating fluoride coating. Normally nickel, Monel and 18-8 stainless steel are preferred.

[b] Metals must be passivated before use. For limited applications, the 300 series of stainless steels may be used.

[c] For nitrogen tetroxide containing over 0.1% water, the 300 series of stainless steel are recommended.

[d] Recent tests indicate that titanium alloys are satisfactory for use with nitrogen tetroxide. However, it is recommended that tests be made of any proposed application of titanium alloys in the configuration that they will be used and under conditions which they will be subjected to during the lifetime of the missile.

[e] At ordinary temperatures, perchloryl fluoride is not corrosive to most metals. The following metals are recommended for use with moist perchloryl fluoride: Types 304, 310, 314 and 316 stainless steels; Hastelloy; titanium, tantalum, Durimet "T" and Durimet 20.

MATERIALS REQUIREMENTS FOR THE PROPULSION SYSTEM COMPONENTS

Uncooled Combustion Chambers

Uncooled chambers* are used for applications which require short operational times during which thermal equilibrium is not attained. Operating temperatures and, therefore, operating times of this type of chamber are limited largely by the high temperature materials used in their construction. Longer operating times can be obtained by reducing heat transfer to the wall by the use of an inner refractory liner or coating as shown in Figure 4.

The properties which are sought in an uncooled-combustion-chamber, wall material are high strength at elevated temperatures, high strength to weight ratio, resistance to chemical attack by the hot propellant vapors, high specific heat, resistance to corrosion and erosion by the propellant combustion products, resistance to mechanical and thermal shock, high melting point, low thermal expansion and good fatigue resistance. If an inner refractory liner or coating is to be used the following parameters should be considered in its selection: resistance to thermal shock, refractory properties, low density, oxidation and corrosion resistance, erosion resistance, and thermal conductivity.

Past designs have usually used high strength steels such as 4130 as the outer wall material. Refractory liner graphite, silicon carbide, silicon carbide bonded with silicon nitride, and zirconium boride. Of these graphite has perhaps found the widest usage largely because of its low density, machineability, good refractory properties and resistance to thermal shock.

In reviewing the future requirements for uncooled combustion chambers, it appears the greatest need will be in small thrust units for applications where on-off operation

*Since nozzle material requirements are essentially the same as those for combustion chambers and nozzle and chambers are made integrally, nozzle materials will not be discussed separately.

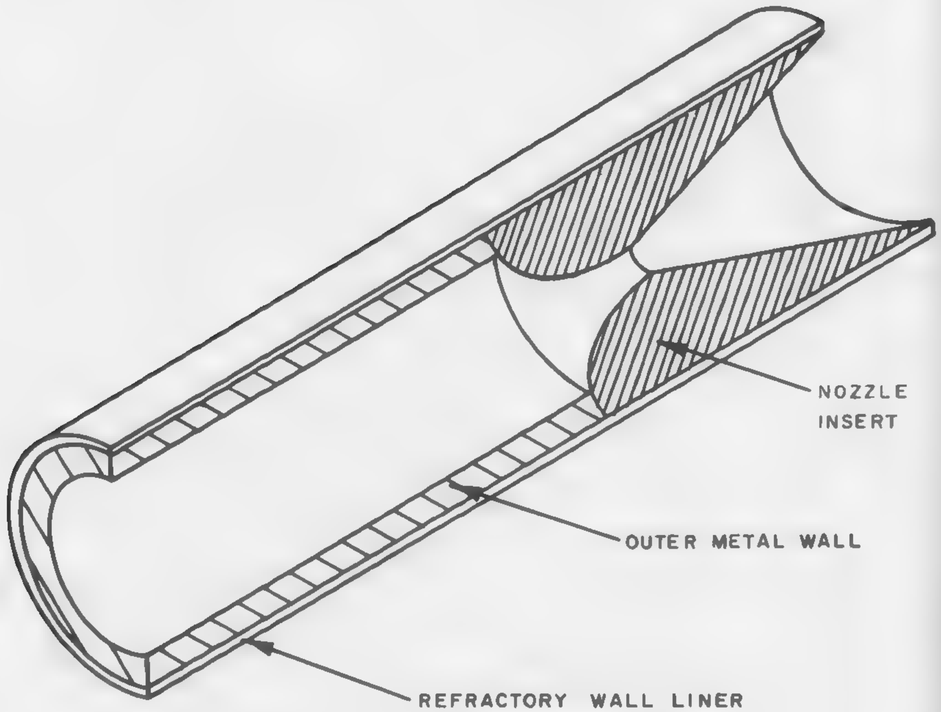


FIGURE 4 UNCOOLED COMBUSTION CHAMBER

and variable thrust are required and regenerative cooling is not feasible. In these applications refractory metals and alloys appear to be desirable as the structural metal. Therefore, problems relative to joining (welding and brazing) these metals and alloys need to be developed which will insure reliability for these applications. Also, refractory liners will be needed which are easy to fabricate and having improved resistance to erosion, corrosion and thermal shock.

Cooled Combustion Chambers

At the present time no materials are available which are sufficiently heat resistant to permit the design of uncooled combustion chambers for high impulse, long duration rocket motors. However, by the use of regenerative cooling, chambers can be designed which will operate under steady state thermal conditions. This type of chamber may be constructed by using either a double wall or a formed-assembled tubular design. Material requirements for both types are essentially similar.

In selecting materials for the cooled combustion chamber a very important consideration is the strength-to-weight ratio. Also a high thermal conductivity is desirable to eliminate hot spot difficulties. Other parameters which must be considered are resistance to corrosion and erosion action by high velocity combustion products, resistance to corrosion by the propellants used as coolants, resistance to mechanical and thermal shock, low thermal expansion and good fatigue resistance. All these requirements must be considered and compromises made when materials are selected for specific designs.

Metals which have been utilized in the design of cooled combustion chambers include 304 stainless steel, 17-7 PH and AM-350 stainless steels, Haynes 25 cobalt-based alloy, and 5052 and 6061 aluminum alloys. Problems which have been encountered with the application of these materials have been (1) hot spots (areas of localized over heating), (2) reduction of innerchamber wall thickness by corrosion-erosion action of the high velocity combustion products, and

(3) process problems associated with maintaining proper design tolerances and obtaining reliable joints.

Presently available alloys permit inner wall temperatures of 1200 to 1600°F for cooled thrust chambers. Future applications may require higher operating temperatures. Therefore, improved high temperature alloys which are reasonably compatible with the propellants at or near their boiling points need to be developed along with adequate fabrication techniques. Also, attention should be given to improved refractory coatings which are corrosion-erosion resistant and which can be adequately bonded to the inner wall of the cooled chamber.

Injectors

The material requirements associated with injectors are common both to cooled and uncooled chamber designs. These requirements may be briefly listed as follows: (1) easily machineable (passages and many small orifices are usually required), (2) high purity (minimum non-metallic inclusions), and (3) resistance to corrosion by the propellants and erosion by their combustion products. Stainless steel and aluminum alloys have been the main materials used for this application. Recently, injector assemblies have been prepared from aluminum alloys brazed to high strength steels in order to reduce time of fabrication and cost.

A common problem encountered with injectors is erosion of the face. This has been eliminated largely through design changes which involve considerable trial and error and sometimes loss in performance. Therefore, the development of an easily applied erosion resistant coating which would strongly adhere to the structural metal appears to be needed at the present time.

Turbines

Turbine drive systems employ the energy of hot combustion gases to produce useful mechanical energy to drive

the pumps used for expelling the propellants. The hot gases are derived either by gas generator systems* or by gas bled directly from the main combustion chamber.**

Materials for the turbine wheel must possess a high strength to density ratio both in tension and compression, low creep rate and high rupture strength over a wide temperature range (1300 to 2400°F) for reasonable periods of time. High thermal shock resistance (high thermal conductivity and low thermal expansion) is desired, and corrosion and erosion resistance to the hot gases is necessary. Materials which have been used in turbine wheels are cast cobalt base alloys and precipitation-hardened, iron-base austenitic alloys. However, requirements for higher operating temperatures and increased strength have directed attention to the new nickel base and molybdenum alloys as well as titanium carbide-base cermets.

Pumps

Experience with large thrust, liquid propellant propulsion systems have shown that the centrifugal design is the best for delivering propellants at the desired pressures and flow rates. The criteria used in the selection of structural materials for this type of pump are high resistance to corrosion by the propellants, high yield strength, high ductility and low density without porosity. Also, materials used in this application should have physical properties which do not change when brought into contact with the propellants.

---

* These systems are essentially uncooled liquid or solid propellant combustion chambers which deliver gases at temperatures significantly lower than those obtained in thrust chambers. Since their material requirements are similar to uncooled combustion chambers, gas generator systems will not be discussed.

** In this case some means must be available to cool the gas to a temperature which will not cause a severe materials problems. This is accomplished normally by injecting controlled amounts of one of the propellants into the gas stream.

In the past, 355 and 356 aluminum casting alloys have been used as a structural material for pump housings and impellers. The porosity problem associated with these alloys has been overcome to some extent by impregnants. While this solution has been adequate generally for handling fuels, it has not been satisfactory for storable oxidizers because of their reactivity with the commercially available impregnants.

Teflon, Kel F and Kel F elastomers have been the main materials used in seals and O-rings. While satisfactory for short contact times, they have been only marginal over extended contact times with propellants because of cold flow and, in the case of the Kel F materials, slow attack by some of the propellants.

Valves and Pipes

The main criterion to be used in selecting materials for the valves and pipes is compatibility with the propellants. For this reason stainless steel and aluminum alloys have been used. Materials for seals have generally been of the Kel F and Teflon types.

Propellant Tanks

Propellant tanks are generally of two types, pressurized tanks (300 to 700 psia) which are used for propellants expelled by pressure-fed systems and low pressure tanks (0 to 50 psia) used with turbo pump systems. In either type, the criteria used for the selection of materials for the tanks are compatibility with the fuel and oxidizer, high strength to weight ratio, and fabricability.

In determining compatibility of metallic materials for tank structures, considerable attention should be given to the effect of fabrication operations on the corrosion resistance of the materials to the propellants. Past experience has shown that metals which have been found to be

made susceptible to intergranular corrosion and stress corrosion cracking by fabrication techniques. For example, cold worked 304 stainless steel, normally resistant to attack by red fuming nitric acid, when welded undergoes intergranular corrosion in the weld and heat affected areas when exposed to fuming nitric acid. A good example of the other type of corrosion is 410 stainless steel which, when subjected to certain heat treatment conditions and then placed under a stress condition, undergoes rapid faliure because of stress corrosion cracking when exposed to fuming nitric acid.

In those pressurized tank designs which incorporate plastic bags, material selection parameters which must be considered for the bag material are ability to withstand repeated flexing due to thermal expansion and contraction of the liquids, abrasion resistance, ability to be sealed with a leak-proof joint to metals, good flexibility and minimum change of flexibility over the anticipated environment temperatures, highly resistant to diffusion by propellant vapors and, in certain cases, heat resistant. In the case of the flexible metal wall design, the additional criteria needed to be considered are flexibility and fatigue resistance.

Stainless steel and aluminum alloys have been the main materials used in tank fabrication. However, new alloys which are compatible with the propellants, which have a higher strength-to-weight ratio, and which are easy to fabricate into tank designs without change in physical and corrosion resistant properties are foreseen as a requirement for future pressurized propellant tank designs.

The non-metallic materials used in tank construction have been largely Teflon and Kel F materials with Teflon being used almost exclusively in the propellant bag designs. In this application it has not been too satisfactory because of diffusion of propellants and difficulty to obtain reliable seals to metals. The Kel F materials in general have not been satisfactory because of a slow attack by some of the propellants.

EFFECT OF SPACE ENVIRONMENT ON MATERIAL REQUIREMENTS

Based upon the information available at the present time on the nature of the space environment, the conditions which will have the most effect on material selection appear to be the extreme low pressure environment, meteoroid impact and radiation. Of these, the latter one is probably the least important.

Studies of space indicate that it is a dilute plasma having a pressure of approximately 10^{-11} millimeters of mercury. Under this condition of near vacuum, one can expect loss of volatiles and cold welding. Since the propellants are volatile materials, improved joining techniques will be required in order to obtain 100% leak-proof joints between metals used in the fabrication of propellant tanks; this may require a more judicious choice of metals. This leak-proof requirement also pertains to the valves thus requiring improved materials for the valve seats. In regard to plastic and elastomeric materials used in seals and other applications, they will have to be carefully scrutinized to make sure their physical properties do not degrade over a period of time because of the loss of volatile ingredients (e.g., plasticizers, unpolymerized monomers, low molecular weight polymers, etc.).

Cold welding is a problem which will probably only be encountered in valves. In this case the possibility of welding of the pintle to the valve seat should be considered. In order to overcome this, it may be necessary to use nonmetallic valve seats such as ruby or ceramic.

Meteoroid impact will largely affect the design of the propellant tanks and the thrust chamber. The concern with this problem is penetration by the larger meteoroids, particles which are comparable to or larger than the thickness of the wall upon which it impinges. Although improved metals as wall materials may be desirable, based upon available data the best solution appears to be the use of a "meteor bumper." The desired properties of materials for the bumper are unknown at the present time. However, it

appears that materials which have high strength and high density would be desirable.

Studies by A. D. Little, Incorporated, indicate that the only type of radiation which may have an influence on material selection is electromagnetic radiation. Here the main concern is with the ratio of solar absorptivity (α) to low-temperature emissivity (ϵ) of the outside surface. If this ratio increases with time as it may for some materials because of "sputtering"* or micrometeoroid impacts, the temperature of the liquid propellants will increase because of absorption of energy which is transmitted as a heat input to the propellant. This condition will be serious if the temperature raises to a value such that the vapor pressure of the propellant becomes sufficiently large to rupture the tank or such that degradative chemical reactions of the oxidizer and/or fuel begin to occur.

---

* Sputtering is the term applied to the removal of atoms from the surface layer through bombardment by the atomic particles (electrons and positive nuclei) which exist in space.

BIBLIOGRAPHY

1. Allen, J. M., "Environmental Factors Influencing Metals Applications in Space Vehicles," Defense Metals Information Center, Battelle Memorial Institute, Report 142 (December 28, 1960).

2. Barrere, M. A., A. Jaumotte, B. Fraeija De Veubeke and J. Vandenkerckhove, Rocket Propulsion, Elsevier Publishing Company (1960).

3. Beighley, C. M., "Storables Stir Renewed Interest," Missiles and Rockets (February 15, 1960), pp. 30-33.

4. Bell Aerosystems Company, "Titan II Storable Propellant Handbook," Prepared for the Air Force Flight Test Center, Report 8111-933003 (June 1961).

5. Bonney, E. A., M. J. Zucrow, and C. W. Besserer, Principles of Guided Missile Design - Aerodynamics, Propulsion, Structures and Design Practice, Edited by Grayson Merrill, Captain, U. S. N., D. Van Norstrand Company, Inc. (1956).

6. Bortczak, G., "Missile Materials," Advanced Materials (February 1961), p. 57.

7. Defense Metals Information Center, Battelle Memorial Institute, "Compatibility of Rocket Propellants with Materials of Construction," Memorandum 65 (September 15, 1960).

8. Frank, R. G., and W. F. Zimmerman, Materials for Rockets and Missiles, The Macmillian Company (1959).

9. Gerard, G., "Structures and Materials - State of the Art 1960," Astronautics, Vol. V, No. 11 (November (1960), pp. 47, 158-164.

10. Goldsmith, M., "Liquid Propellants - State of the Art 1960," Astronautics, Vol. V, No. 11 (November 1960), pp. 38, 169-170.

11. Judge, J. F., "Temperature Barrier Slows Progress," Missile and Rockets (November 23, 1959), pp. 15-16.

12. Kilner, S. B., and L. B. Rapp, "Application of Storable Propellants to Space Flight," Presented at the American Rocket Society Space Flight Report to the Nation Meeting, New York (October 9-15, 1961), ARS Preprint No. 2267-61.

13. Kopituk, R. C., "Compatibility of Materials for Rocket Service," Presented at the First Meeting of the Joint Army-Navy-Air Force Liquid Propellant Group, New Orleans (November 3-5, 1959).

14. Lee, Y. C., "Liquid Rockets - State of the Art 1959," Astronautics, Vol. IV, No. 11 (November 1959), pp. 38, 148.

15. Office of the Director of Defense Research and Engineering, The Handling and Storage of Liquid Propellants, Department of Defense (March 1961).

16. Simmons, J. C., Jr., "Behavior of Materials in Space," Astronautics, Vol. IV, No. 6 (June 1959), pp. 32-33, 84-88.

17. Sutton, G. P., Rocket Propulsion Elements, 2nd Edition, John Wiley and Sons, Inc. (1956).

18. Wiederhorn, N. M., "The Space Environment and Its Interactions with Liquid Propellants and Their Storage Systems," Presented at the Third Meeting of the Joint Army-Navy-Air Force - NASA-ARPA Liquid Propellant Group, Miami (November 7-9, 1961).

19. Zeilberger, E. J., "Plastics for Liquid Rocket Engines," Astronautics, Vol. 3, No. 8 (August 1958), pp. 26-27, 76-79.

MATERIALS REQUIREMENTS FOR SOLID-PROPELLANT ROCKET MOTORS

C. M. Frey
Manager, Materials Branch
United Technology Corporation
Sunnyvale, California

ABSTRACT

The entrance of solid-propellant rockets into the field of truly large boosters for space exploration has brought with it new requirements for materials and a relaxation of some of the problems associated with much smaller motors. The development of current solid-propellant ballistic rockets, for instance, has compelled the designer to adopt the extreme philosophy of reduced weight at any cost--in contrast to the criteria for projected space boosters wherein cost and reliability are the paramount factors.

Casing materials applicable to motors in excess of 160 inches in diameter are discussed in this article. The materials requirements for nozzles having throat diameters in excess of 60 inches and exit diameters greater than 150 inches are presented together with comments on internal ballistic considerations and how these affect the demands made on nozzle materials. The author predicts that, before 1970, fiber- or tape-reinforced composite materials will almost completely supplant homogeneous metals and solid ceramics.

INTRODUCTION

The decision has been made to develop truly large solid-propellant rocket motors for application as boosters for space missions. This entrance of "solids" into the domain previously held exclusively by "liquids" was prompted by the demonstrated reliability and low cost of solid-propellant motors. Applications for which these boosters are to be used require that boosters be reliable and inexpensive rather than lightweight or compact. Nozzle throats can be permitted to erode at a faster rate than could be tolerated in smaller motors.

SIZE

The smallest of these space boosters will be approximately ten feet in diameter and contain over one million pounds of propellant. A single casing will weigh roughly 60 tons and the nozzle throat diameter will be about five feet. Motor lengths will approach 100 feet. Larger space boosters with casing diameters exceeding 25 feet are being considered.

In contrast to the smaller motors, such as those of Minuteman and Polaris where economics permit sixty or more test firings before committing the system to the task of boosting a warhead, the cost of these truly large space boosters suggests that manned flights occur after about five test firings of the full-size motors. For these reasons, the materials and fabrication processes selected must produce highly reliable casings and nozzles.

DESIGN AND FABRICATION CONSIDERATIONS

Casings

When considering the manufacture, shipment, and inspection of motors ten feet in diameter and 100 feet long, it is found desirable to fabricate them in segments. A typical motor 100 feet in length might be made of ten cylindrical segments, each one ten feet long. These segments or

"building blocks" will be fabricated, loaded with propellant, inspected, and shipped to a launching site. The ends of each of the segment casings will have mechanical joints permitting easy attachment of segments at the site. Bolted flange, radial pin, and Ortman key-type joints have been used for this purpose. All of these joints require that the ends of the cylindrical walls be thicker than the central portion and suggest the use of thick end rings welded to the cylinders.

If the material selected for the casing requires that plates be rolled and welded, it would be desirable to eliminate the requirement for heat-treating the welded assembly because of facility requirements and processing costs. One of these motors constructed of steel would have at least one-sixth mile of girth welds in plates approximately 3/4-inch thick.

Nozzles

The amount of throat erosion permissible in rocket nozzle is generally expressed as the increase in the throat area. This parameter is selected because the pressure maintained within the motor and the thrust delivered depend upon the throat area. Unlike small nozzle throats, where a small amount of material ablated would have a marked effect on the throat area, the very large nozzles can tolerate rather large erosion rates. For instance, if a four-inch diameter throat were to be ablated 1/2-inch on each side, the resulting five-inch diameter would have a throat area 56 percent greater than the initial one; on the other hand, if an 80-inch diameter throat were to be increased to 81 inches, the area increase would be less than 1.5 percent. A two-inch increase in the throat diameter of an 80-inch nozzle would increase the area only four percent. It is obvious that the acceptable erosion rates for large nozzles are far greater than those for the smaller nozzles. This fact permits the consideration of materials that lack the excellent erosion resistance of graphite and the refractory metals.

MATERIALS CONSIDERATIONS

Casings

Materials which are of low cost and lend themselves to low-cost fabrication techniques are desirable. The strength-to-weight ratio need not be greater than that available from steel heat-treated to a yield strength of 160,000 psi. Sheet materials should be readily weldable without the requirement for rigid controls on preheat, post-heat, or other welding procedures. Because the only machining necessary is on the joints at the casing ends, it would be desirable to weld the rings containing the joints to the casing after final machining, thereby eliminating the need for machine tools large enough to handle the assembled casing. This suggests that the material be weldable in the heat-treated condition without greatly reducing the strength of the casing at the weld.

When considering a casing made of tons of metal with weld lengths measured in fractions of a mile, it is inconceivable that it would be completely free of cracks, notches, or inclusions. This signifies that the material and heat treatment selected must result in production of casings which are not sensitive to these defects, at a stress level below the design stress.

The strength of filaments or thin tapes is almost unaffected by the presence of cracks and can be used to fabricate casings which have no welds and do not require large heat-treatment facilities. Fiberglass filaments are currently the only type in use, but the filament winding process is sufficiently flexible to permit the utilization of almost any conceivable type of material in the form of thin wires or filaments. The new saying that "old metallurgists never die - they just turn to glass," is becoming popular. The question arises: why aren't they turning to filaments of nylon, celluloid, cellulose acetate, titanium, or other promising materials? Surely fiberglass does not possess all of the best properties of all materials.

Nozzles

When one considers the fabrication and thermal-stress problems associated with nozzles having throat diameters of 80 inches and exit diameters on the order of 200 inches, the need for new forms of materials becomes apparent. Solid graphite, the workhorse nozzle-throat material for small motors, is not available in these large sizes and the brittle nature of solid pieces of graphite and other ceramics presents design problems when applied to large structures. It is the author's opinion that the use of refractory filaments, in the form of rovings, cloth, or tapes, bonded with resins such as phenolic or pitch, will replace the homogeneous structures for nozzle throat applications. This conclusion is based on the following:

Coat considerations
Notch sensitivity
Reliability
Availability
Facility requirements.

The ability to tape-wrap or wind continuous fibrous materials to the shape needed, with very little subsequent machining required, has been demonstrated in the fabrication of large nozzle exit cones. By also eliminating the need for large high-pressure tooling, costs are further reduced. Because the sensitivity to crack propagation of a material is inversely proportional to its thickness, the use of a multitude of fibers is preferred to one homogeneous part. For instance, nearly 100,000 filaments of fiberglass would be found in a three-inch thickness of a composite material. If 10,000 of these filaments had serious flaws, the strength of the structure might be reduced 10 percent but, if a solid piece were used, one flaw could lead to a failure of the whole piece through crack propagation. Also, test samples of the fibers could be taken during the fabrication of the part so that the quality of each laminate could be determined, thus providing a method of continuous quality control of the composite wall during its fabrication. The small thickness of the laminates would insure that large

voids, cracks, or inclusions would not be present in the composite part.

Because composite walls of filaments can be fabricated to any thickness without regard to the thickness of the filaments themselves, the lead time needed to produce a given part is reduced to a minimum. Rather than await the production of forgings, castings, sheets, or billets to the specific size required, the wrapping technique allows the part to be fabricated to the specified dimensions by merely winding the required amount.

The lay-up technique also eliminates the need for furnaces, ovens, and mills large enough to accommodate the final part because the fibers are formed and fully treated prior to their fabrication into the final part. This is analogous to the drawing and heat treatment of fine wire, when compared to the rolling and heat treatment of large sheets.

CONCLUSION

The advent of the truly large space boosters presents new facets of rocket-materials technology and circumvents some of the problems associated with smaller motors. Low cost and high reliability are the paramount considerations, and the conditions under which these motors will be launched obviate the necessity for extreme compactness and extreme efficiency.

It is the author's opinion that the most fruitful areas for materials development at this time is in the development of adhesive-bonded fibrous materials which lend themselves well to the filament winding process. This approach permits the fabrication of low-cost motors free of welds and circumvents the need for large rolling mills, large machine tools, and large heat-treatment facilities. The probability of the occurrence of rapidly propagating cracks leading to catastrophic failures is also markedly diminished.

It is significant to note that in all competitive motor-development programs where filament-wound casings were

selected by one contractor and metal casings by another, the contractor proposing filament-wound motors won the competition.

MATERIALS REQUIREMENTS FOR CRYOGENIC TEMPERATURE APPLICATIONS

Abraham Hurlich
Supervisor, Materials Research Group
General Dynamics/Astronautics
San Diego, California

ABSTRACT

The general effects of low temperatures upon the mechanical properties of metals and alloys are discussed, including effects upon strength, ductility, and touchness (resistance to brittle fracture). Metallurgical variables such as crystal structure, microstructure, chemical composition, and impurities influence the low temperature mechanical properties of metals, as do factors such as notches, stress concentrators, multiaxial stress distributions and rate of loading. The criteria for the selection of metals for application in cryogenic fueled missiles and space craft are discussed, including consideration of strength/density ratios, resistance to brittle fracture and crack propagation, corrosion resistance, weldability and formability.

Mechanical properties of high strength heat-treatable steels, austenitic steels, aluminum, magnesium, nickel, cobalt, and titanium base alloys are discussed and data are presented on various alloys of these classed which are recommended for use at extreme sub-zero temperatures.

Recent data on effects of combined environments of cryogenic temperatures and nuclear radiation are presented in reference to the use of liquid hydrogen as the propellant in nuclear engined space craft.

FACTORS AFFECTING THE LOW TEMPERATURE MECHANICAL PROPERTIES OF METALS

Before considering the effects of low temperatures upon the engineering properties of specific metals and alloys, it is well to review the general effects of low temperature upon the properties of metals. As the temperature is lowered, the hardness, yield strength and modulus of elasticity increase as does, with few exceptions, the tensile strength and fatigue resistance of all metals and alloys. The effects of low temperatures upon the ductility and toughness of metals are, however, complex and merit considerable discussion. To begin with, it is essential to clearly differentiate between ductility and toughness since these characteristics are all too often considered the same and the two terms used interchangeably.

Ductility is commonly expressed in terms of percentage elongation in gage length and reduction in area of a tensile test specimen that is tested to fracture. Ductility is thus a measure of the deformation undergone by a smooth test specimen of uniform cross-section which is slowly stressed until fracture occurs. Toughness, on the other hand, is a characteristic which permits a metal to absorb energy by undergoing plastic deformation rather than fracturing in the presence of high stress concentrations (cracks or notches) and multiaxial stress distributions, under high rates of loading, or at low temperatures.

It is possible for a metal to exhibit high ductility in a tension test, yet behave in a catastrophically brittle fashion in service at moderate temperatures; witness the plague of fractures in Liberty ships during World War II, when many ship plates broke apart with virtually no deformation anywhere near the fracture and yet tensile test coupons removed from adjacent areas exhibited 40% elongation and 60% reduction in area.

Whereas ductility is measured as deformation occurring in a tension test of a uniaxially loaded smooth specimen, toughness is commonly measured in terms of the energy absorbed in breaking, under impact loading, a test specimen

which is notched with a circular or sharp groove on the side at which fracture initiates. At a given test temperature a metal may manifest high ductility in the tensile test and practically no toughness in a notched-bar impact test. Consequently, any statement regarding the effects of low temperature upon the tendency of metal to behave in a ductile or brittle fashion must be qualified by the conditions under which the fracture is produced.

In general, metals fall into two distinct classes with respect to the influence of low temperatures upon their ductility and toughness; a relatively small class of metals which retain a high order of ductility and resistance to brittle fracture down to very low temperatures, and a much larger class of metals which undergo, at some temperature or in some range of temperature, a transition from ductile to brittle behavior. And, as pointed out above, the temperature level at which this transition in fracture behavior occurs is influenced by the test conditions.

The metals which remain ductile at extreme sub-zero temperatures include nickel, copper, aluminum, lead, and silver among others. These metals all have a face-centered cubic crystal structure, and ductility at low temperatures appears to be a characteristic common to metals of this crystal family. The explanation of this phenomenon is as yet obscure. Metals which have a body-centered cubic structure (iron, chromium, molybdenum, tantalum, tungsten, etc.) undergo a marked decrease in ductility over a range of temperatures, see Figure 1, and the range of transition temperatures may occur from well above boiling water temperature to several hundred degrees below $0^{o}F$. Several common metals, such as magnesium, zinc, titanium, and beryllium, have a hexagonal crystal structure, and these metals, with the exception of titanium, are generally brittle or have limited ductility at room and at moderately elevated temperatures. Titanium and several of its alloys may exhibit high ductility and toughness down to very low temperatures.

The different effects of low temperatures upon the ductility of metals is explained in terms of the effects of

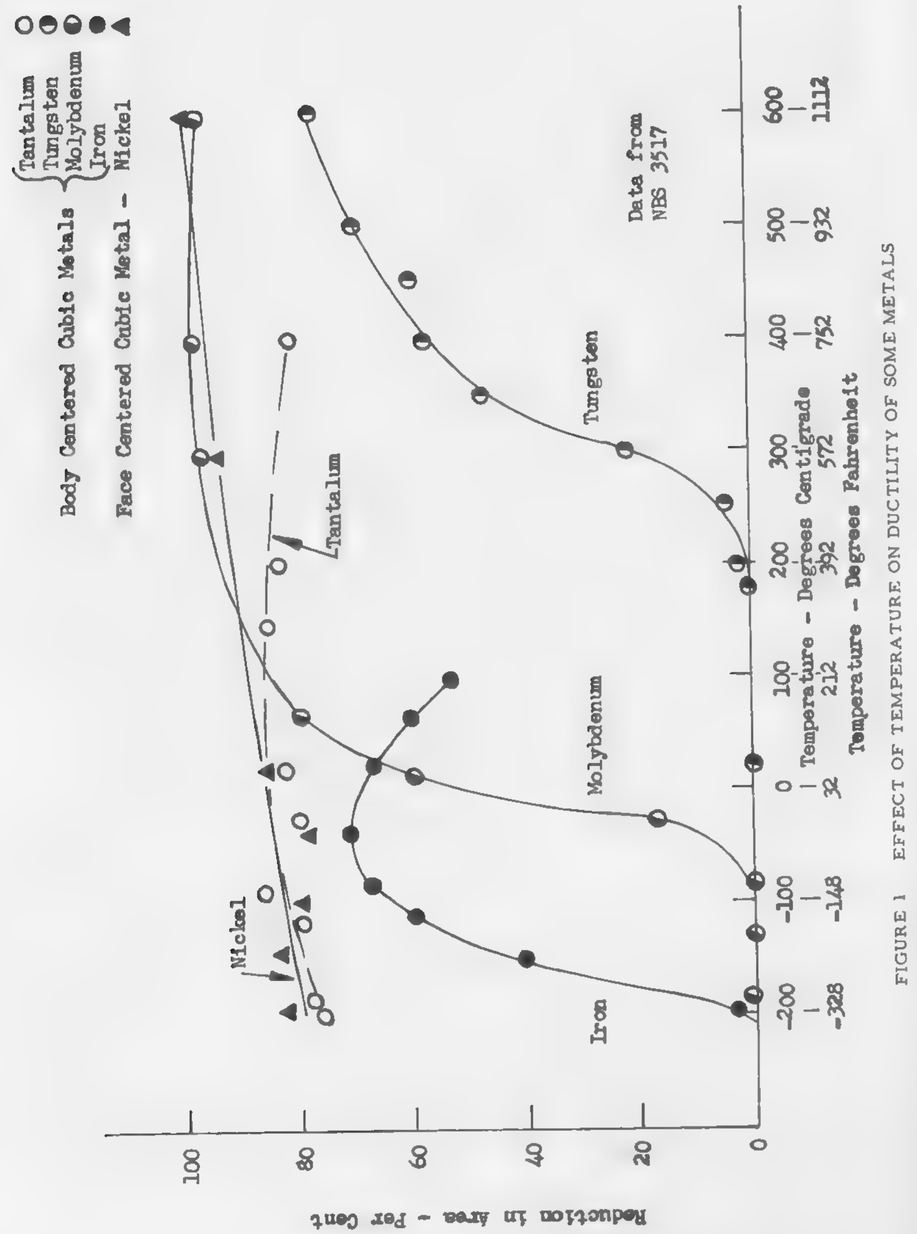


FIGURE 1 EFFECT OF TEMPERATURE ON DUCTILITY OF SOME METALS

the effects of low temperatures upon the flow strength (stress level at which plastic yielding starts) and upon the fracture strength of metals (stress level at which undeformed metal fractuers). Low temperatures cause an increase in both flow and fracture strengths of metal, but they may increase at characteristically different rates. In the case of aluminum and copper, as well as other face-centered cubic metals, the fracture strength increases at the same or greater rate than does the yield strength. Greater spreads between the yield and fracture strengths permit more deformation to occur prior to fracture; hence these metals retain or increase their ductility at low temperatures. Iron, on the other hand, exhibits a more rapid increase in flow strength than in fracture strength as the temperature is lowered. As the spread between flow and fracture strengths decreases less plastic deformation occurs, and finally, at some reduced temperature, fracture takes place with no plastic deformation and the flow and fracture strengths coincide. Figures 1 and 2 indicate the effects of low temperatures upon the ductility and flow strength of several metals.

In the metals which undergo a transition from ductile to brittle performance with decreasing temperature, it is found that a large number of factors may influence to a marked extent, the temperatures at which this transition occurs. As discussed earlier, at a given test temperature, a metal may be ductile in the tension test and brittle in an impact test.

The top graph of Figure 3 shows, in the case of mild steel, the wide variations in transition temperature revealed in torsion, tensile, and impact tests. Heindlhofer[1] explained the difference in transition behavior in the three tests in terms of the ratios between maximum principal and shearing stresses, which were 1:1 in torsion, 2:1 in tension, and greater than 2:1 in impact. Since, in iron, the yield strength increases more rapidly than does the fracture strength, the resistance to shear increases more rapidly than does resistance to rupture. In view of the ratios of maximum principal to shear stress, the conditions for brittle fracture are met first in the impact test (highest

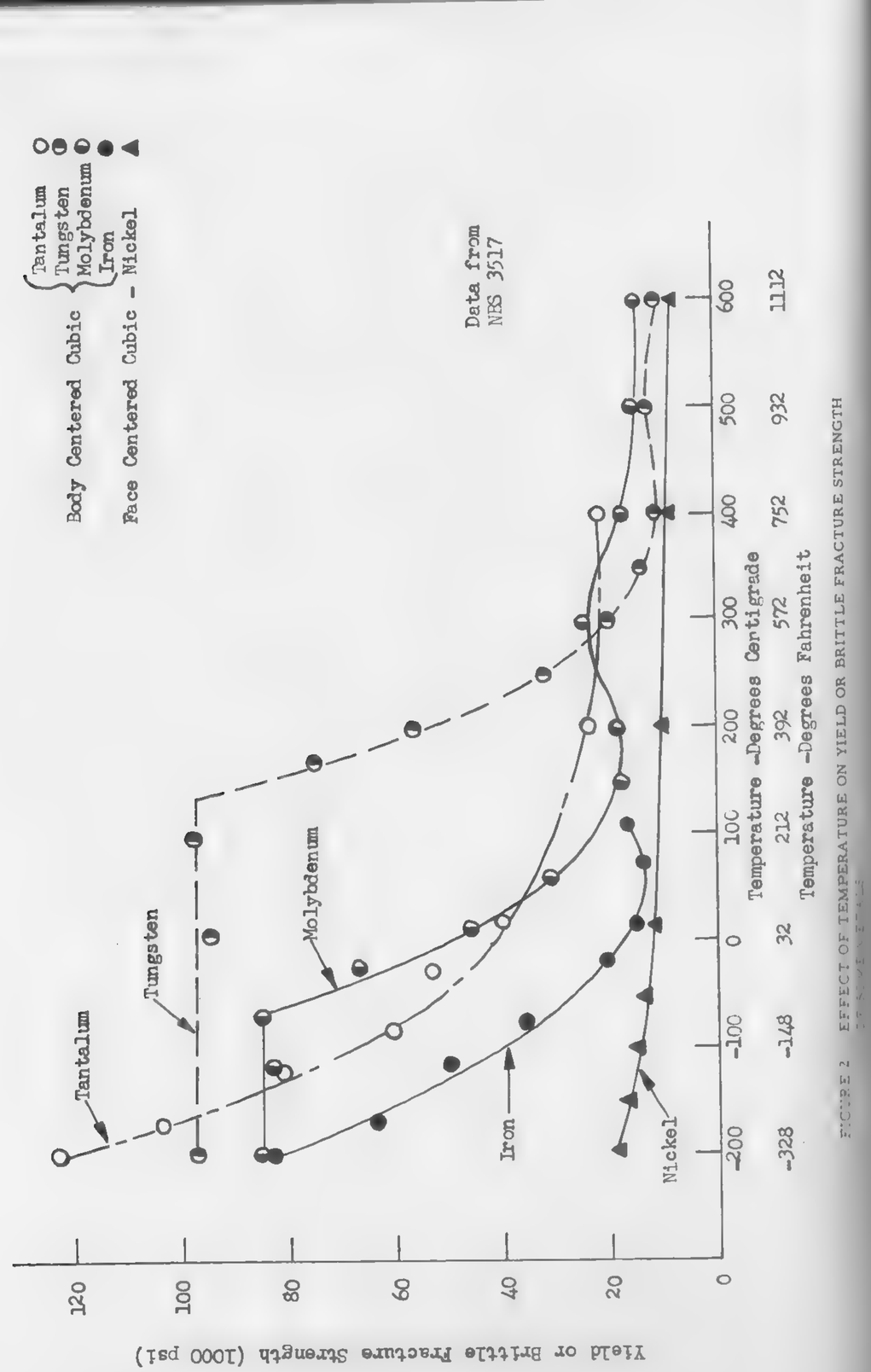
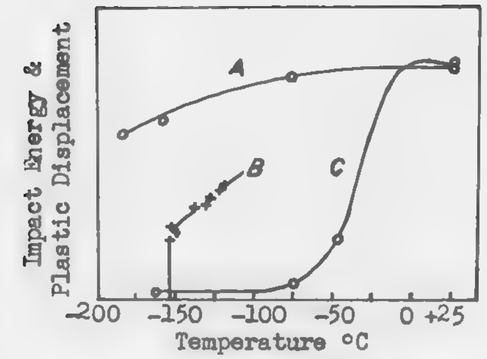
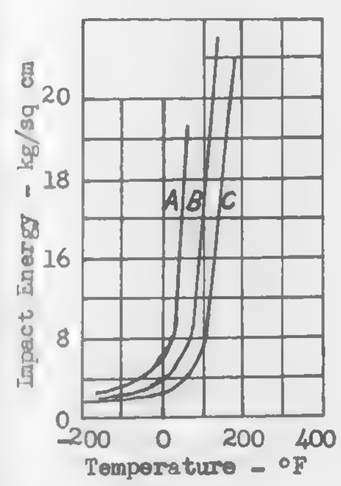


FIGURE 2 EFFECT OF TEMPERATURE ON YIELD OR BRITTLE FRACTURE STRENGTH



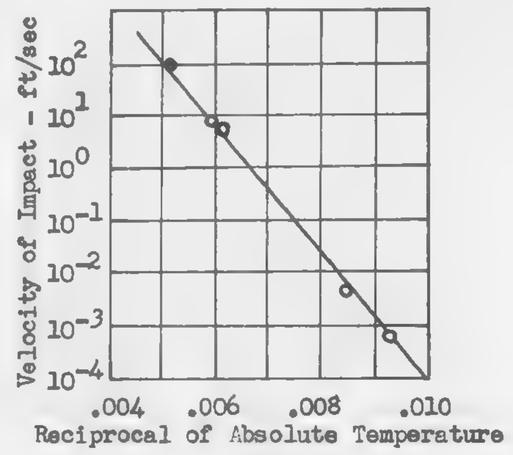
EFFECT OF MECHANICAL FACTORS ON EMBRITTLEMENT OF FERRITIC STEELS AT VARIOUS TEMPERATURES

Transition from ductile to brittle fracture in low carbon steel tested in: A - Torsion, showing angular displacement as function of test temperature, B - Tension test, showing % Elongation, C - Impact, showing energy absorbtion. (Heindlhofer)



EFFECT OF WIDTH OF SPECIMEN ON TEMPERATURE OF TRANSITION FROM DUCTILE TO BRITTLE FRACTURE. (After Maurer & Mailander)

A - Specimen width - 7.5 mm
B - Specimen width -15.0 mm
C - Specimen width -30.0 mm



EFFECT OF IMPACT VELOCITY ON TEMPERATURE OF ONSET OF BRITTLE FRACTURE (After Witman & Stepanoff)

FIGURE 3

transition temperature), next in the tension test and last in the torsion test (lowest transition temperature).

Other mechanical factors which influence the temperature level at which brittle fracture transitions occur are geometry of test specimen, rate of load application, and the presence and sharpness of notches. Large or wide specimens, as illustrated in the lower left hand graph of Figure 3, tend to raise the temperature at which brittle fracture occurs because of the greater degree of restraint imposed upon the deformation capabilities of the material. Increasing the rate of load application also raises the temperature of transition from ductile to brittle behavior, as shown in the lower right hand graph of Figure 3.

The effect of increasing the sharpness of notches upon the transition from ductile to brittle fracture in a notched bar impact test is shown in Figure 4, which is taken from work done by Armstrong and Gagnebin.[2] The notched-bar impact test, by combining complex stress distributions, high rates of loading, and a sharp notch, all of which favor brittle fracture and raise the temperature of transition from ductile to brittle performance, provides a sensitive index of the tendency of materials to perform in a brittle fashion at extreme sub-zero temperatures.

In addition to crystal structure, a considerable number of metallurgical factors influence the low temperature properties of metals. Chemical composition affects the low temperature toughness of alloys; for example, increasing amounts of nickel up to 13% significantly raise the notched bar impact properties of low carbon steels, see the lower left graph of Figure 5. For this reason, low carbon alloy constructional steels containing up to 9% nickel are commercially employed for cryogenic fluid storage tanks and transfer equipment. Similarly, increasing the carbon content of alloy steels lowers the toughness and raises the ductile to brittle transition temperature of alloy steels as shown in the upper right of Figure 5.

Microstructure also greatly affects the low temperature mechanical properties, especially toughness, of alloys. In

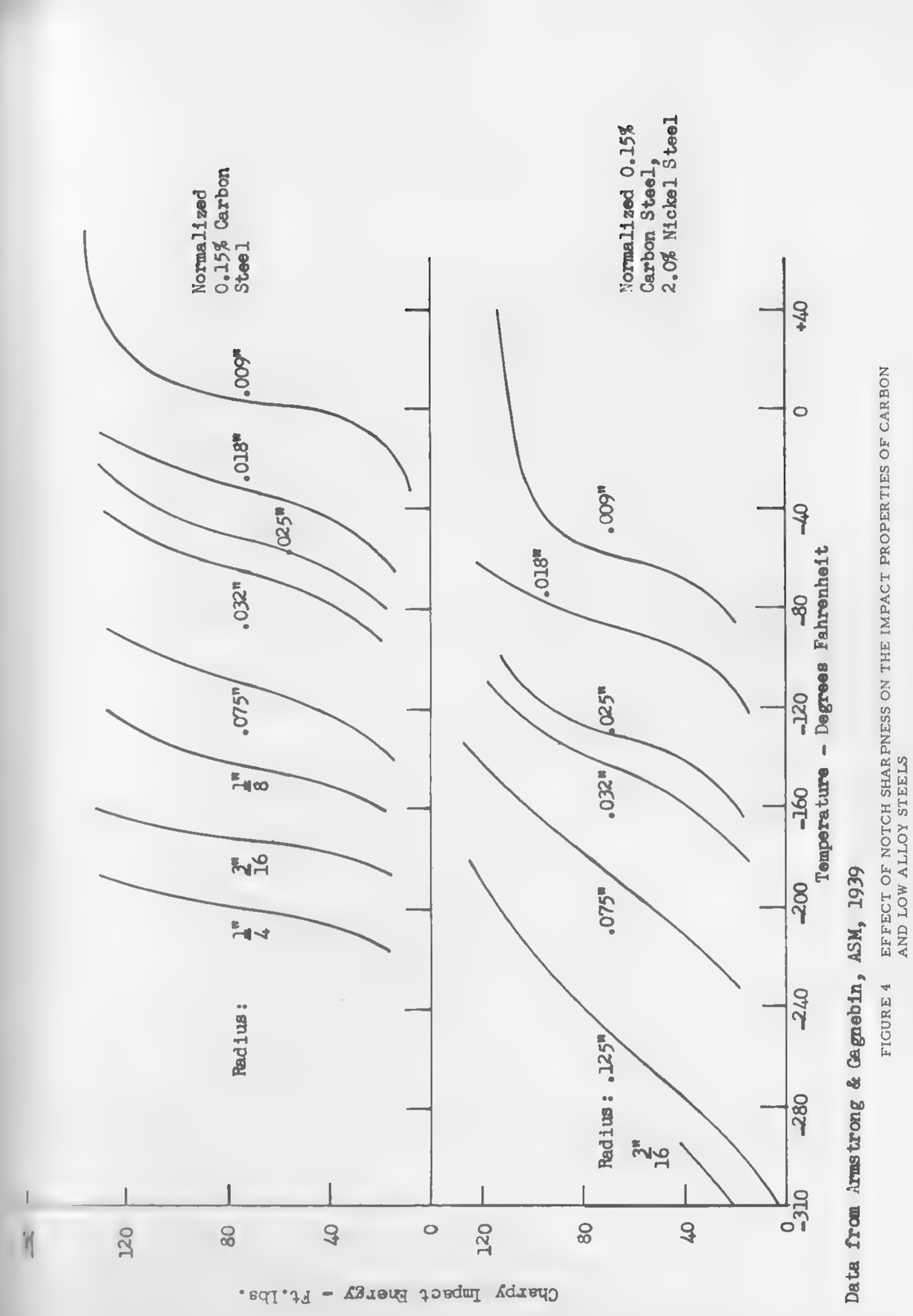
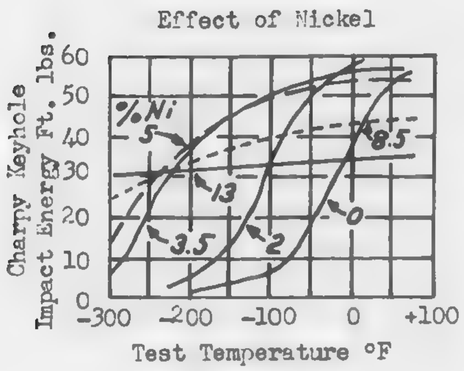
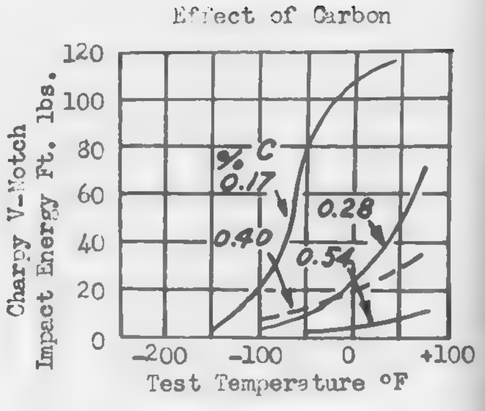


FIGURE 4 EFFECT OF NOTCH SHARPNESS ON THE IMPACT PROPERTIES OF CARBON AND LOW ALLOY STEELS



Normalized 0.10% carbon steels, except 2% Ni steel which contained 0.15% C. ASM Metals Handbook, 1961.



0.70% Cr, 0.32% Mo steel transformed to pearlite at 1200°F.

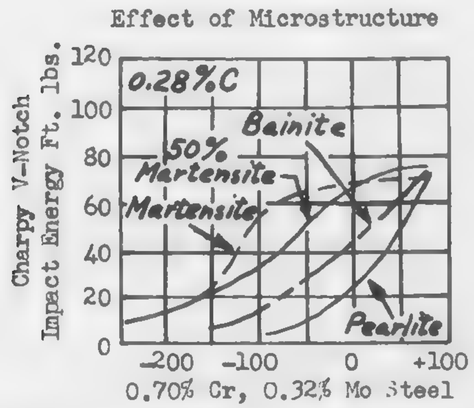


FIGURE 5 EFFECT OF CHEMICAL COMPOSITION AND MICROSTRUCTURE ON THE TOUGHNESS OF WROUGHT STEELS AT LOW TEMPERATURES

the case of heat-treatable low and medium alloy steels, heat treatment to a tempered martensitic microstructure develops the best combination of strength and toughness at sub-zero temperatures, with tempered bainite being less tough and tempered pearlite still less tough at temperatures below approximately 50°F, see the lower graph of Figure 5.

Non-metallic inclusions, intermetallic compounds, and other impurity constituents which may form or precipitate at grain boundaries will reduce the toughness of metals, especially at low testing temperatures.[3], It has recently been determined at General Dynamics/Astronautics that impurity levels which cause no apparent embrittlement in titanium alloys when tested at room temperature may cause excessive embrittlement at extreme sub-zero temperatures. Table I presents data on the effects of oxygen and iron contents upon the tensile and notched tensile properties of the 5Al-2.5Sn-titanium alloy at temperatures down to -423°F (liquid hydrogen). Resistance to brittle fracture was evaluated by side-notched tensile tests, using a specimen having a stress concentration factor, K_t, of 6.3, and the notched/unnotched tensile ratio is employed as a criterion of brittle fracture tendency. Note the decreasing notched/unnotched ratio with increasing oxygen content in tests at -423°F, whereas tests at room temperature show no effect and tests at -320°F (liquid nitrogen) only very slight effects with change in oxygen contents in the range of 0.09% to 0.24%.

CRITERIA FOR SELECTION OF AEROSPACE MATERIALS FOR CRYOGENIC APPLICATIONS

Until the advent of cryogenic fueled aerospace vehicles, liquefied gases were produced for commercial applications such as steel processing, welding, chemical synthesis, refrigeration, and medical uses. Low strength aluminum alloys, annealed stainless steels, and low carbon nickel alloy steels having tensile yield strengths in the range of 20,000 to 50,000 psi, or ratios of yield strength to density of 150,000 to 200,000 in. lbs. per lb. were adequate for the construction of storage tanks, transfer vehicles, and

TABLE I

EFFECT OF OXYGEN AND IRON IMPURITY CONTENTS ON MECHANICAL PROPERTIES OF 5Al-2.5Sn-TITANIUM ALLOY SHEET*

A. Effect of Oxygen Content (All other elements controlled within narrow range)
Fe-0.02 to 0.10%, C-0.03 to 0.04%, N-0.01 to 0.02%, H_2-0.009 to 0.014%

Oxygen Content	Test Temperature (°F)	F_{t_y} (psi)	F_{t_u} (psi)	Elongation (%)	Notched Tensile Strength, psi (K_t = 6.3)	Notched/Unnotched Tensile Strength Ratio
0.09%	+ 78	106,000	115,000	16.2	154,000	1.34
	-320	169,000	181,000	16.8	227,000	1.25
	-423	198,000	223,000	13.3	254,000	1.14
0.15%	+ 78	105,000	116,000	17.3	157,000	1.35
	-320	173,000	186,000	14.8	231,000	1.24
	-423	214,000	230,000	11.3	234,000	1.02
0.24%	+ 78	117,000	123,000	16.7	172,000	1.40
	-320	188,000	201,000	15.0	236,000	1.17
	-423	238,000	252,000	4.8	196,000	0.78

* All tests in longitudinal direction and represent average of duplicate specimens. Gages of sheet were in range of 0.035" - 0.045" and sheet was rolled from laboratory size melts.

TABLE I (continued)

B. Effect of Oxygen and Iron Contents (All other elements controlled with narrow range)

Oxygen	Iron	Test Temp. (°F)	F_{t_y} (psi)	F_{t_u} (psi)	Elongation (%)	Notched Tensile Strength, psi (K_t = 6.3)	Notched/Unnotched Tensile Strength Ratio
0.07	0.15	-423	211,000	232,000	14.3	233,000	1.00
0.08	0.50	-423	226,000	252,000	6.3	180,000	0.71
0.20	0.27	-423	256,000	265,000	7.0	166,000	0.65

refrigeration equipment required for the manufacture and handling of liquefied gases.

Such materials are, however, prohibitively heavy for use in aerospace vehicles and would not have permitted the development of several successful and standardized aerospace vehicles which are currently available for both military and scientific uses. High strength aluminum alloys and steels presently used in aircraft and missiles for the containment of liquid oxygen and liquid hydrogen have room-temperature yield strength to density ratios of 500,000 to 600,000 in. lbs. per lb., and a titanium alloy pressure vessel used for the storage of chilled high pressure helium gas in the Atlas missile has a yield strength to density ratio of over 800,000. Thus, aerospace vehicle materials are from 3 to 4 times as strong as comparable alloys used for non-aerospace cryogenic applications; and a high strength-to-weight ratio remains a necessary requirement for all structural materials employed in aircraft and missiles.

Tanks for cryogenic fuels, propellant lines and ducts, and engine components must be leak tight to both liquid and gas phases of the fuels. Fabrication by welding is then essential since bolted joints are not only difficult to make gas tight, but are also very heavy due to the requirement for stiff flanges and a large number of sturdy bolts. To minimize weight, the weld joint should, ideally, be as strong as the parent metal, but this is not a firm requirement since design procedures have been developed which overcome the loss in strength of weld joints with only very slight weight penalties. It is important, however, that both the weld joint and the parent metal be tough at the lowest service temperatures.

High strength is of little practical significance if stress concentrators and discontinuities, minute flaws, and other metallurgical, mechanical, or service factors result in brittle fracture of aerospace structures. A material or structure which fails by brittle fracture can do so at very low gross stress levels, often as low as 10% of yield stress. Consequently, it is important that materials selected for critically stressed applications be tough under the environmental conditions to which they may be exposed. This is

particularly important in cryogenic temperature applications since low temperature in itself can exert a severely embrittling effect.

As previously described, notched bar impact tests have been used for a moderately long time for evaluating the toughness of metals. While it is true that such tests involve impact loading, the rate of loading is moderately low and is not especially significant. It is the notch, which acts as a stress concentrator as well as a source of multiaxial stress distributions, which is the important feature of these tests. The most commonly used notched-bar impact test specimen is the V-notch Charpy specimen which is illustrated in Figure 6. This specimen is 0.394" square

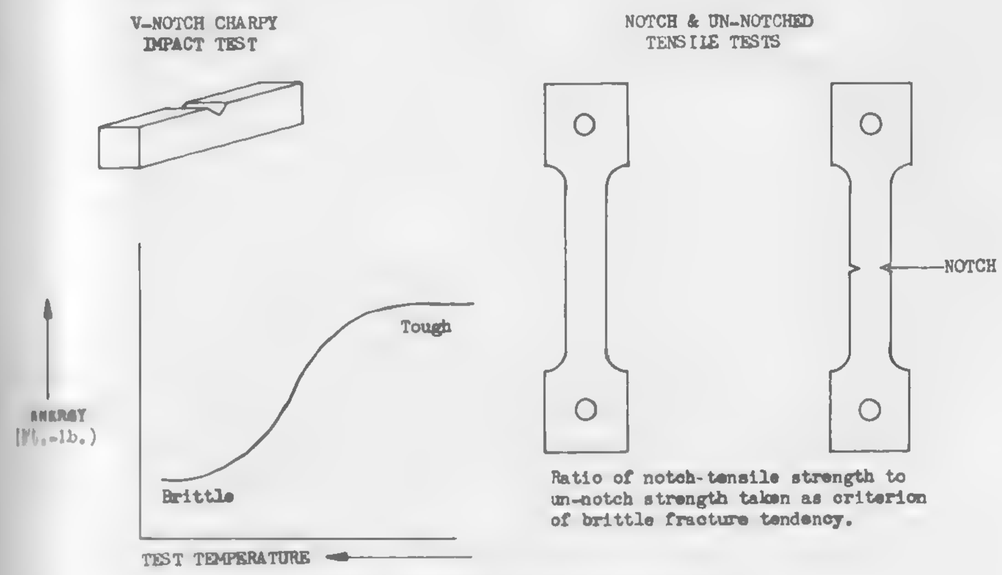


FIGURE 6 TOUGHNESS EVALUATION TESTS

and approximately 2" in length. A 0.079" deep 60° V-notch with a root radius of 0.010" is machined across one face of the specimen. The bar is broken by being supported at both ends and struck by a pendulum supported weight impacting the face opposite the notch. The energy absorbed in rupturing the bar is determined by measuring the loss in kinetic energy of the pendulum. These tests may be performed over a range in temperatures to determine the tough-to-brittle transition behavior of the material, reference Figures 4 and 5.

While the notched-bar impact test is very useful for evaluating the toughness of forgings, plate, and bar stock, it is not applicable to very thin sheet materials such as are often employed in aerospace vehicles and airborne pressure vessels. Another type of test specimen which has been employed to evaluate the brittle fracture tendency of heavy sections of steel, and more recently of sheet alloys, is the notched tensile test specimen, such as depicted on the right side of Figure 6. In round specimens the notch is circumferential and in sheet materials the notches are machined in both edges as shown in Figure 6.

A variety of notches have been employed by various investigators, with stress concentrations ranging from 3 for mild notches to as high as 18 for severely notched specimens (ASTM and NASA standard specimens). General Dynamics/ Astronautics has standardized on a notched tensile test specimen having a stress concentration factor of 6.3 since this specimen was found to yield results which correlated with the fracture behavior of full scale thin skinned cryogenic pressure vessels and with the behavior of large specimens containing complex welded joints.[4, 5] With materials that are notch tough, the effect of the biaxial stress distribution at the notched section is to increase the effective strength of the material, and the notched tensile strength may range from 1.0 to approximately 1.5 times the smooth tensile strength. In notch brittle or notch sensitive steels, the effect of the notch is to induce premature brittle fracture, and the notched tensile strength will be less than the smooth tensile strength. In notch sensitive steels, the higher the stress concentration factor the lower

will be the notched tensile strength and the notched/unnotched tensile strength ratio. This ratio thus serves as an index of the brittle fracture characteristics of materials.

Precaution must be taken to compare the stress concentration factors employed by different investigators when comparing notched tensile data and notch sensitivity data reported from different laboratories.

Notched and unnotched tensile tests can be readily performed over a range of temperatures down to the boiling point of liquid helium (-451°F) to evaluate the effect of low temperatures upon the brittle fracture characteristics of metals. For the sake of convenience and economy low temperature mechanical property tests are generally conducted at some of the following temperatures:

-100°F (dry ice and alcohol)
-320°F (liquid nitrogen)
-423°F (liquid hydrogen)

Smooth and notched tensile tests can also be conducted on fusion weld joints (weld being transverse to the direction of loading) to evaluate the mechanical properties and brittle fracture characteristics of weld joints. Center notched specimens have also been devised to determine the critical crack extension force, critical crack length beyond which catastrophically rapid crack propagation ensues, or the stress level at which a crack-like flaw or defect will propagate to result in failure.[6, 7]

Additional requirements for aerospace vehicles are corrosion resistance and formability. Corrosion resistance is important for a number of reasons; one being the fact that cryogenic propellant tanks, lines, and ducts are of extremely thin gauge, and only a slight amount of corrosion attack may be sufficient to result in pinhole leaks. Furthermore, aerospace vehicles may be maintained for prolonged periods in a state of readiness on launch platforms located at seacoast launch areas permeated by corrosive environments of high temperatures, high humidity, and seacoast atmosphere. Formability is required for the fabrication of aerospace

vehicle components such as elbows, bellows, ducts, bulkheads, and other items which must be stamped, deep-drawn, or stretch formed from sheet materials.

Aerospace vehicle applications therefore present an exacting set of materials requirements; only a limited number of metals and alloys are available which simultaneously possess a satisfactory combination of high strength-to-density ratio, weldability, toughness in both base metal and weld joints at extreme sub-zero temperatures, corrosion resistance, and formability.

MECHANICAL PROPERTIES OF HIGH STRENGTH ALLOYS FOR CRYOGENIC APPLICATIONS

During the past three years, low temperature mechanical property evaluation tests have been conducted on more than 50 high strength sheet alloys at General Dynamics/Astronautics. These alloys included steels, aluminum, titanium, nickel, and cobalt base alloys having yield strength/density ratios in the range of approximately 500,000 to 1,000,000 in. lbs. per lb. and were tested in the form of relatively thin sheet in the range of 0.010" to approximately 0.100" in thickness. While the mechanical property data presented in Figures 7 through 16 of this paper represent tests conducted at General Dynamics/Astronautics on 16 alloys, many of the generalizations and viewpoints expressed in the following paragraphs are based upon work performed at other laboratories as well as our own.

In general, evaluation tests conducted at Astronautics included determination of the smooth and notched tensile properties, in both longitudinal and transverse directions, at room temperature (approximately 75°F), -100°, -320°, and -423°F. In addition, the tensile strength and ductility of simple fusion butt welds was determined. Because of the thinness of many of the sheet alloys, the butt welds were often made by the inert-gas tungsten-arc process with no filler metal added. Notched tensile tests were also often made on weld joint specimens.

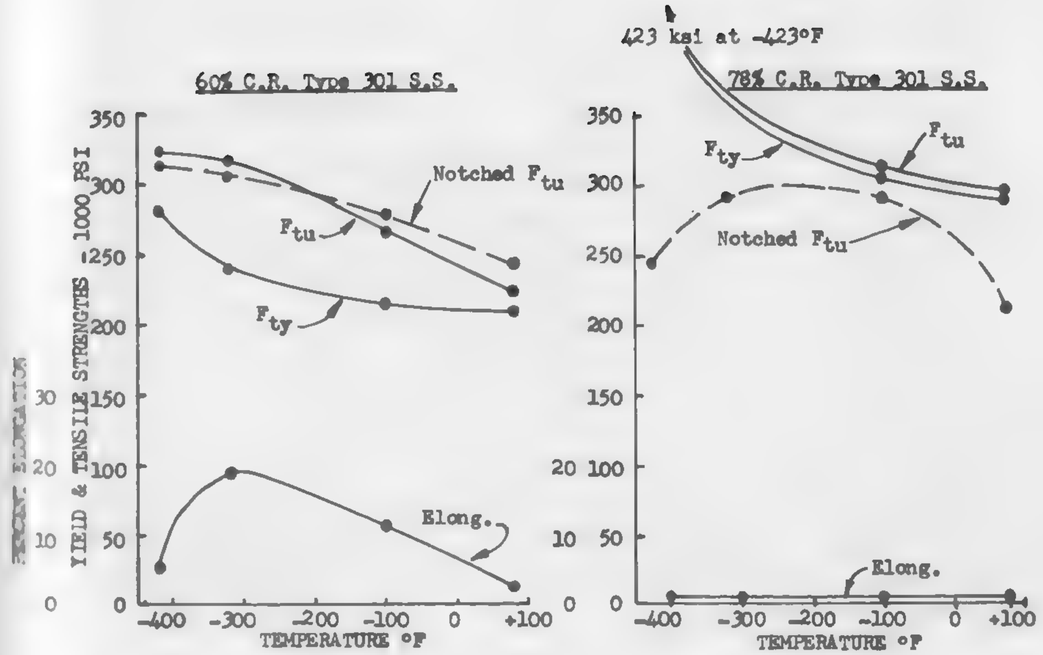
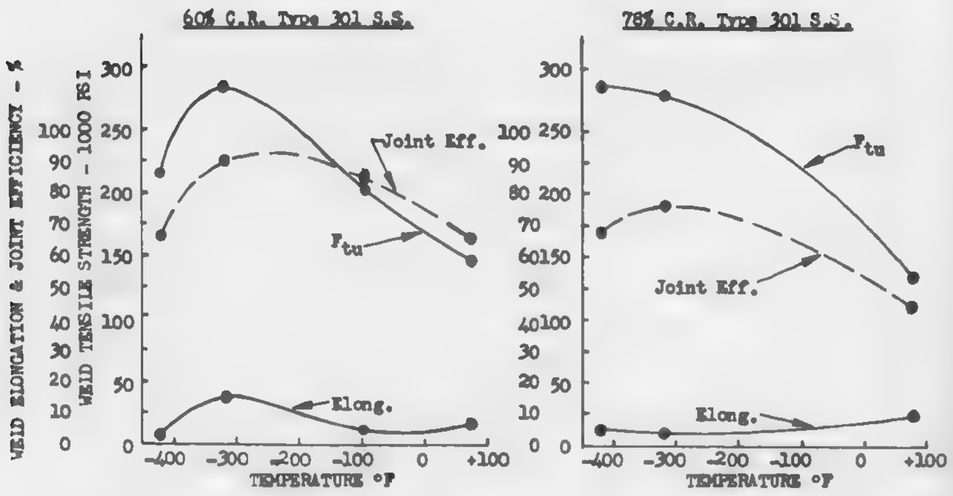


FIGURE 7 STAINLESS STEELS



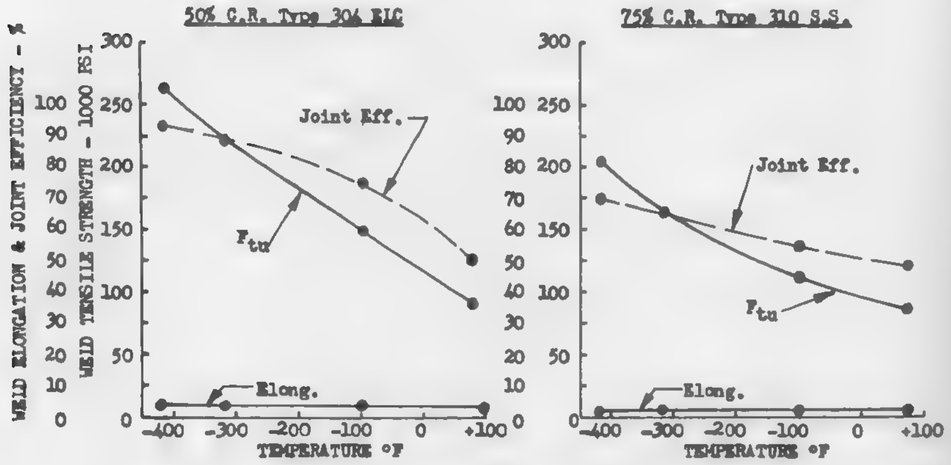
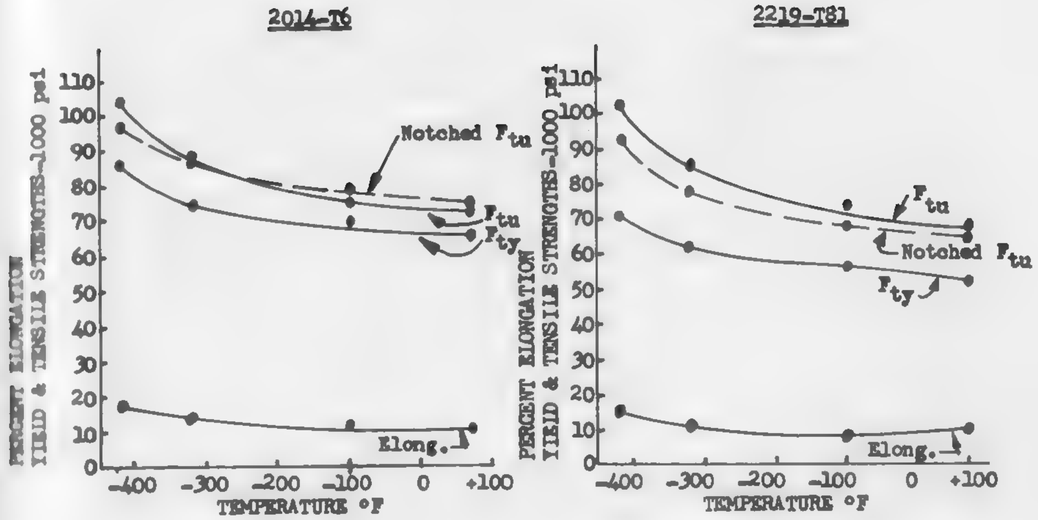


FIGURE 8 PROPERTIES OF HELIARC BUTTWELDS IN STAINLESS STEELS



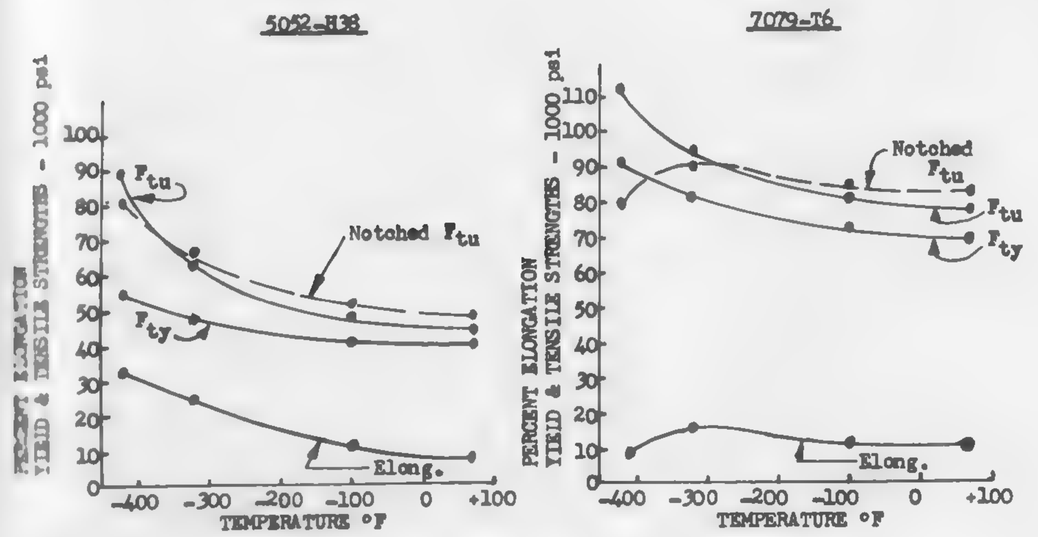
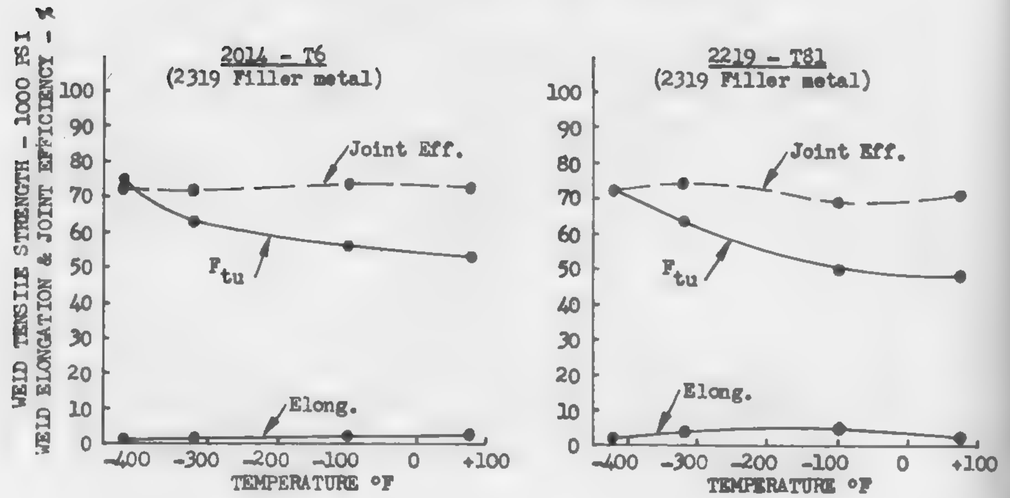


FIGURE 9 ALUMINUM ALLOYS

PROPERTIES OF FUSION BUTT WELDS IN ALUMINUM ALLOYS



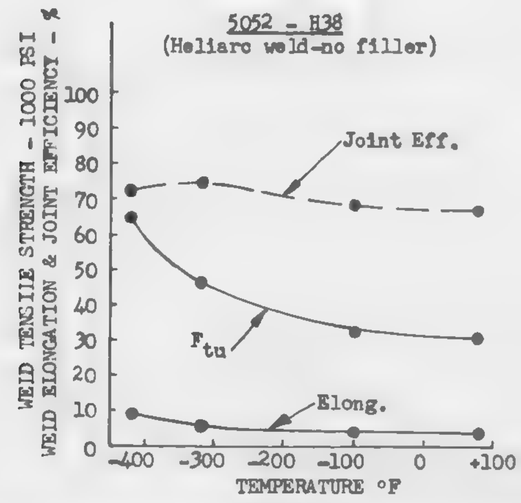
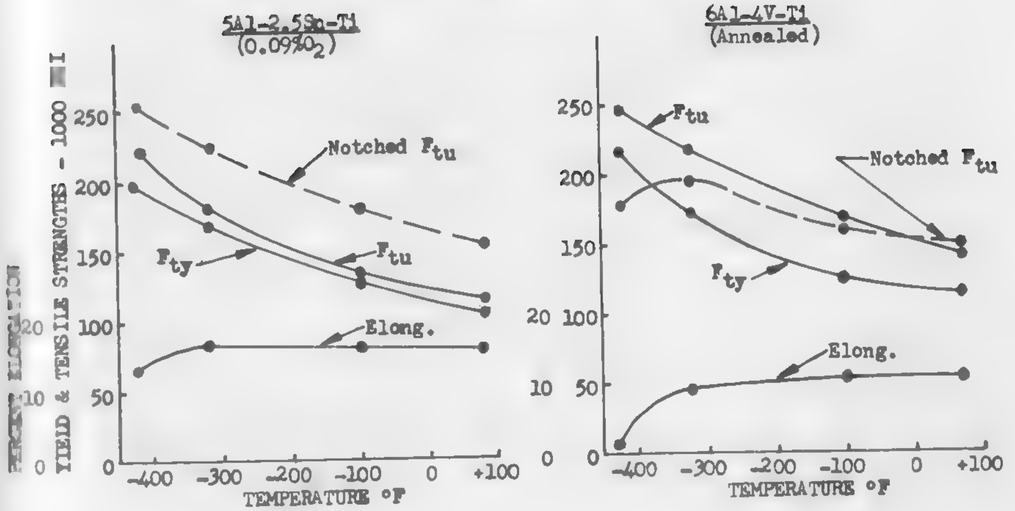


FIGURE 10 PROPERTIES OF FUSION BUTT WELDS IN ALUMINUM ALLOYS

TITANIUM ALLOYS



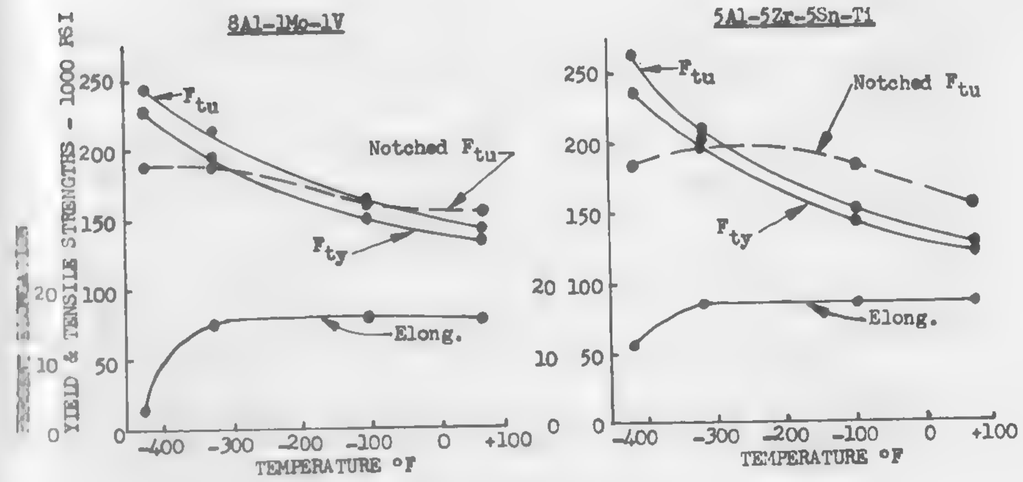
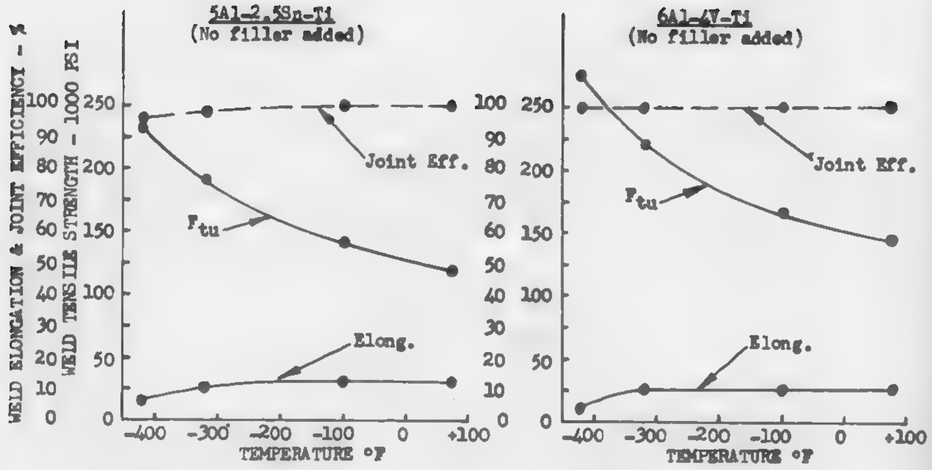


FIGURE 11 TITANIUM ALLOYS



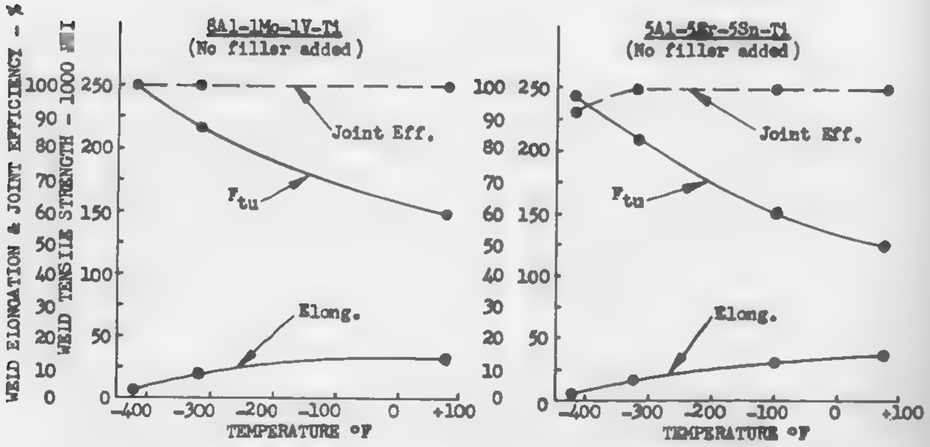
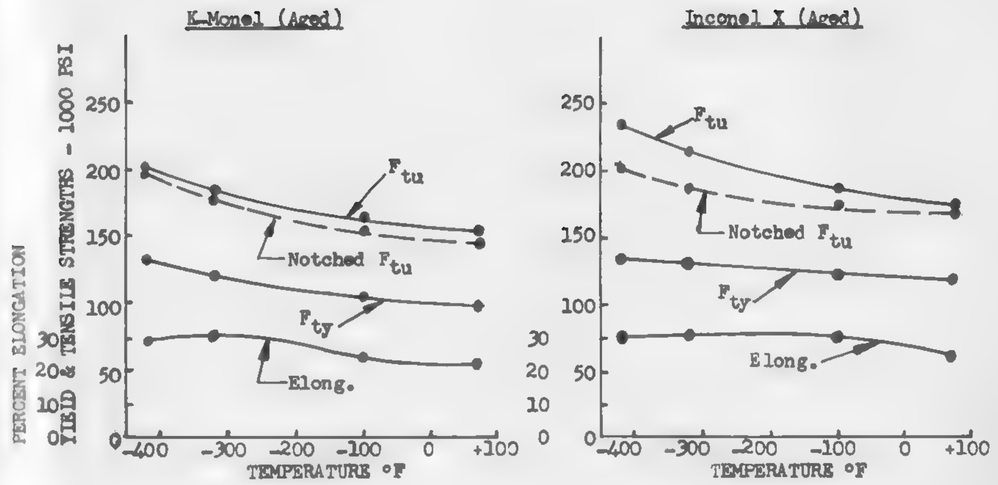


FIGURE 12 PROPERTIES OF HELIARC BUTT WELDS IN TITANIUM ALLOYS

NICKEL BASE ALLOYS



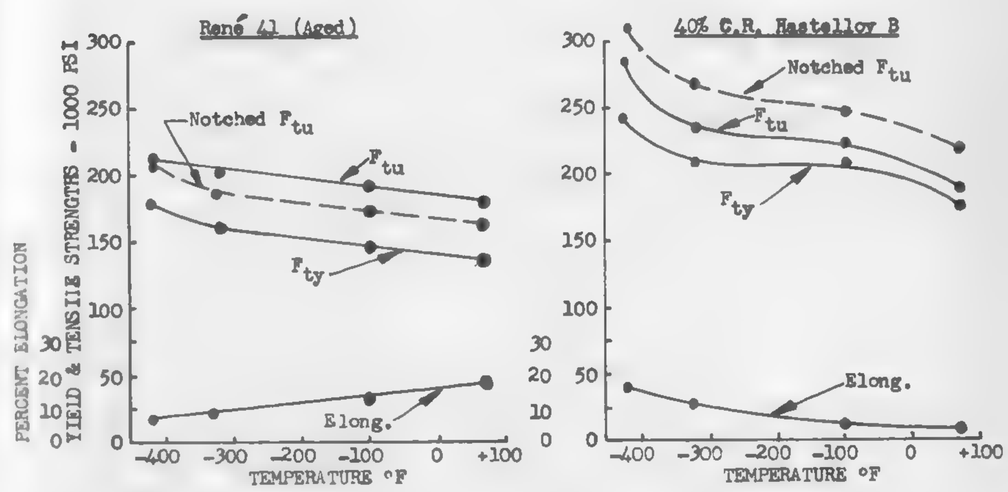


FIGURE 13 NICKEL BASE ALLOYS

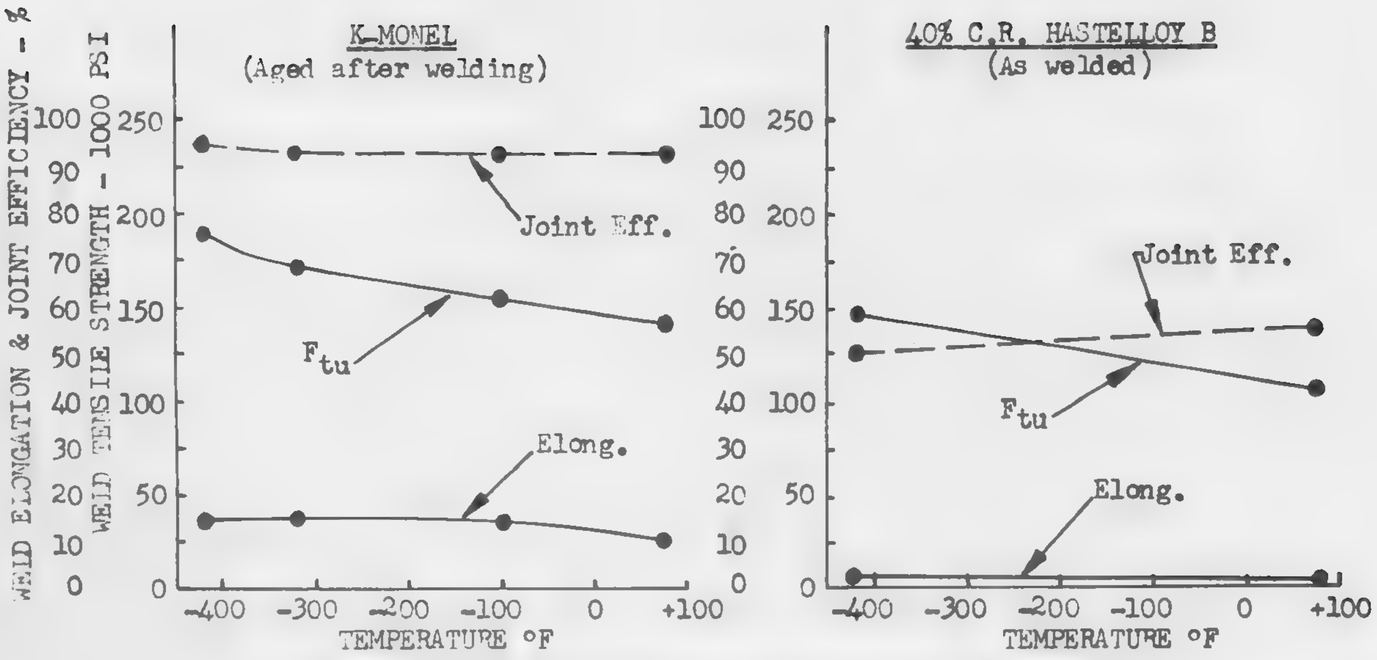


FIGURE 14 PROPERTIES OF HELIARC BUTT WELDS IN NICKEL BASE ALLOYS

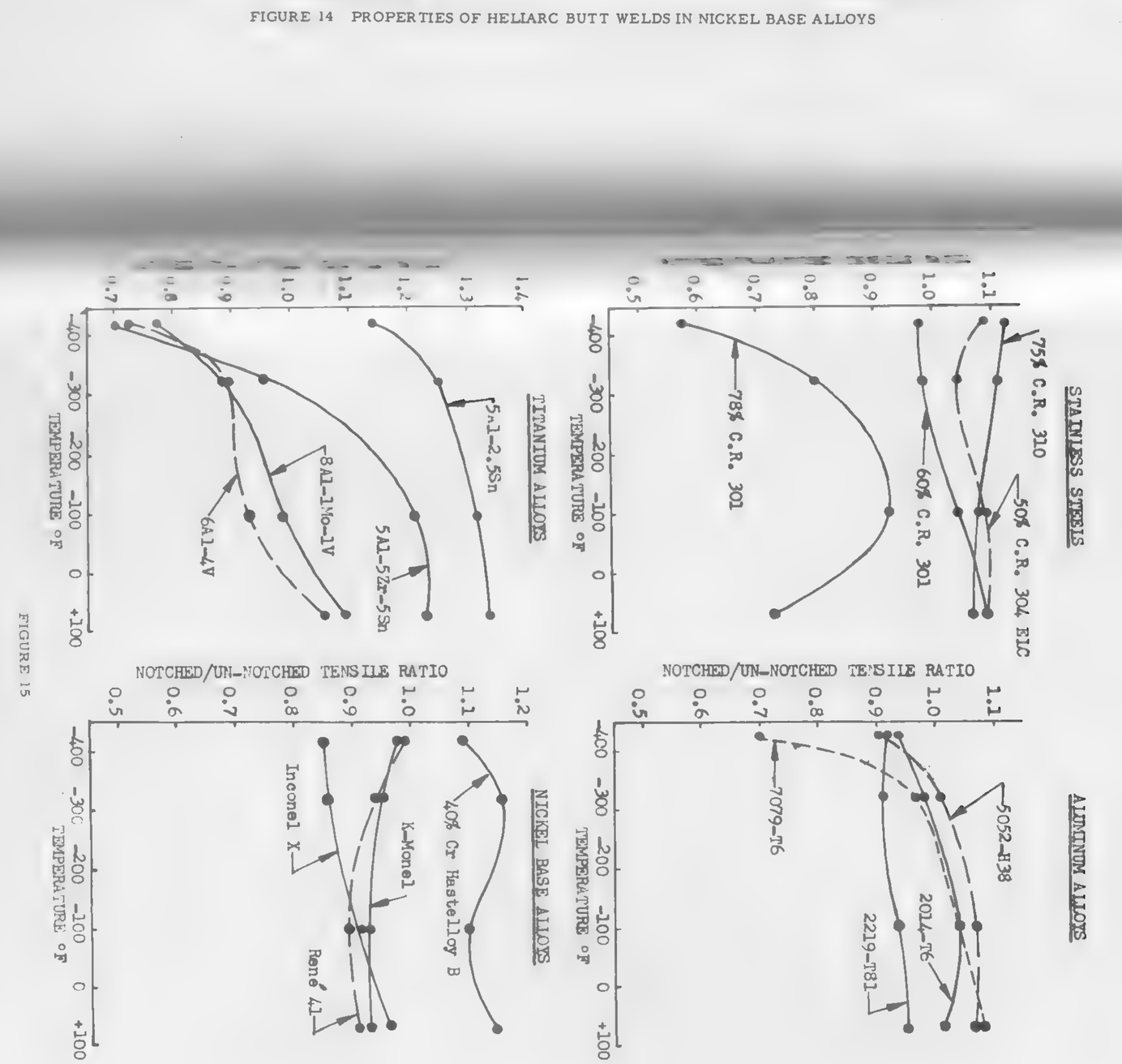
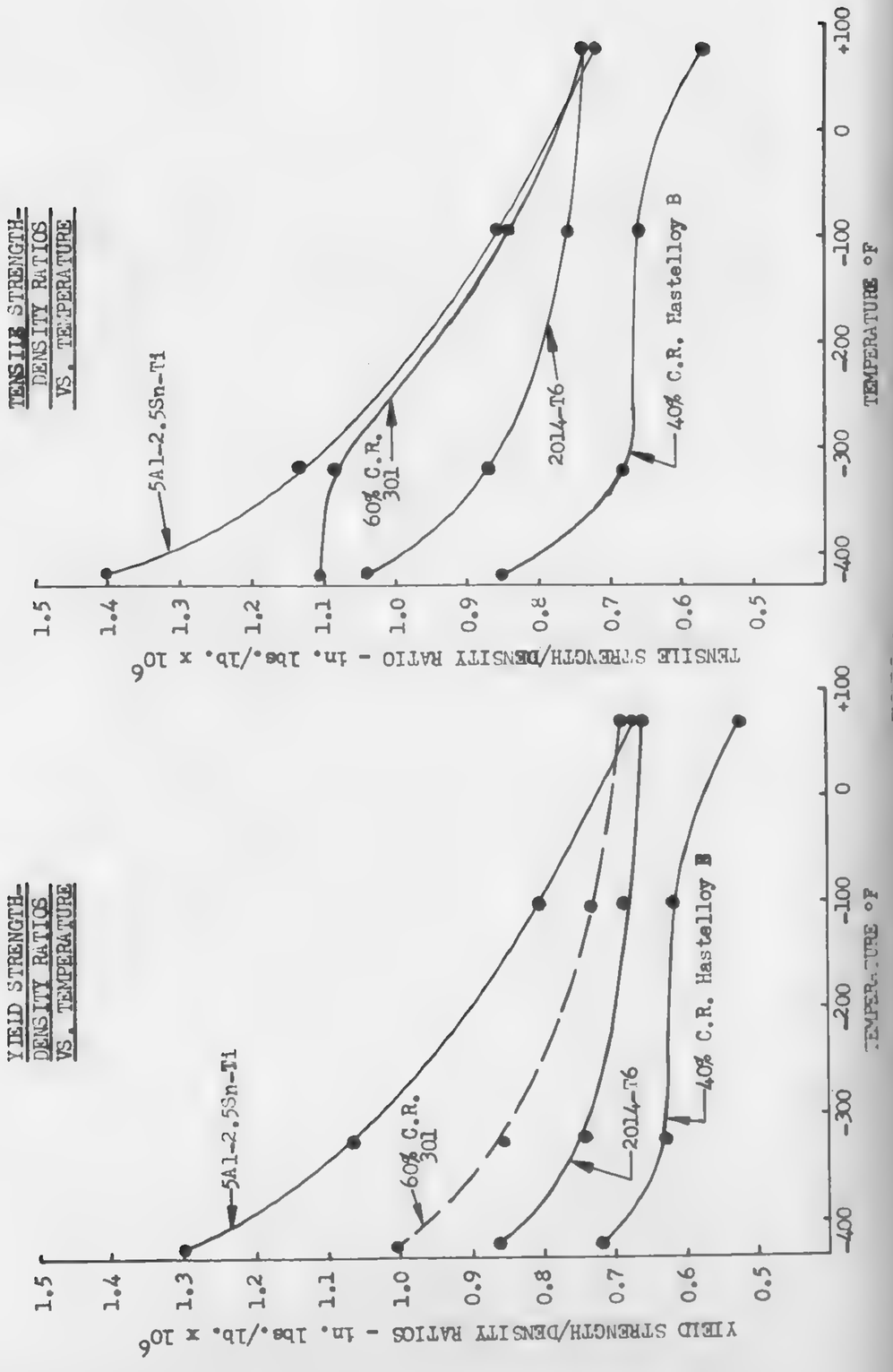


FIGURE 15



The more promising materials which merited more thorough evaluation were subjected to additional tests, including shear and cross-tension tests of individual spot welds over the forementioned range of temperatures, static tension and axial fatigue tests of complex welded joints, and the determination of physical properties such as thermal conductivity, expansion coefficients, etc. at extreme sub-zero temperatures when such information was required for design purposes. All tensile tests discussed in the following sections were conducted in the following types of specimens:

a. Smooth tensile test specimens - Standard 0.500" wide, 2" gage length, 9" long specimens with holes for pin grips.

b. Notched tensile test specimens --0.400" wide with 0.10" deep notches, 60° included angle, and 0.0025" root radii. Stress concentration

$$\left(K_t = \sqrt{\frac{1/2 \text{ width between notches}}{\text{radius at root of notch}}}\right)$$

of 6.3. Specimens 9" in length with holes for pin grips.

Steels

For the purpose of considering their low temperature mechanical properties, high strength steels may be divided into three categories; low and medium alloy steels, heat-treatable semi-austenitic steels, and austenitic steels.

Low and medium alloy steels properly heat treated to a fine grained tempered martensitic microstructure free from temper embrittlement and at tensile strengths up to approximately 280,000 psi may possess reasonably adequate toughnesses at temperatures down to approximately -100°F. Below this temperature a ductile-to-brittle transition occurs and such steels become prone to brittle fracture. Consequently, the low and medium alloy steels such as 4130, 4340, AMS 6434, etc. are not recommended for use at extremely sub-zero temperatures.

Similarly, heat-treatable semi-austenitic stainless steels which develop high strength by partial transformation to martensite (17-7 PH, PH 15-7Mo, AM-350, AM-355, etc.) are also embrittled at temperatures below approximately -100°F and are not recommended for applications at liquid nitrogen to liquid hydrogen temperatures. These alloys evidence considerable notch sensitivity and reduced ductility at extreme sub-zero temperatures,[8] even when tested with mildly notched specimens having a stress concentration factor, K_t, of 3.

On the other hand, the heat-treatable stainless steel A-286 (hardening results primarily from a precipitation rather than a martensite transformation mechanism) is very tough and ductile even when moderately severely notched and tested at temperatures down to -423°F.

The austenitic steels possess the maximum toughness and insensitivity to notches and high rates of loading at extreme sub-zero temperatures. In the fully annealed condition, these steels of the Type 300 series have very low yield strengths in the range of 30,000 to 50,000 psi and are consequently not efficient for use in aerospace vehicles particularly in structural applications. The austenitic stainless steels may be strengthened by cold rolling, and this procedure is particularly adaptable to sheet material. Cold rolling of Type 301 to a 60% reduction in thickness achieves yield and tensile strengths in excess of approximately 160,000 and 200,000 psi respectively. This degree of cold reduction results in a considerable degree (60-70%) of transformation of autenite to martensite, but the martensite thus formed has a low carbon content (up to 0.10% carbon in the Type 301 used in the Atlas missile) and is very tough at extreme suz-zero temperatures in contrast to the 0.30-0.45% carbon martensites in medium alloy steels which are severely embrittled at low temperatures.

The longitudinal base metal tensile properties of 60 and 78% cold rolled Type 301, 50% cold rolled Type 304 ELC and 75% cold rolled type 310 stainless steels (0.020" to 0.030" thick) are shown in Figure 7, and the strength and elongation of heliarc butt weld joints in Figure 8. These

data were obtained in tests conducted at Astronautics.[9] The notched tensile strength and notched/unnotched strength ratios of these steels are shown in the upper left of Figure 15. With the exception of the 78% cold rolled Type 301, all the stainless steels were reasonably tough at temperatures down to -423°F, with the 75% cold rolled Type 310 being best, followed by the 50% cold rolled Type 304 ELC, with the 60% cold rolled Type 301 in third place, see Figure 15.

The higher numbered Type 300 series steels contain increasing chromium and nickel contents and are consequently more stable austenitic steels (face-centered cubic crystal structure). Type 310, for example, which contains 25% Cr and 20% Ni, remains 100% austenitic even when cold rolled 75% and then strained to fracture at -423°F. Type 301 is approximately 60% martensitic when cold rolled 60% at room temperature, and transforms to essentially 100% martensite in the vicinity of the fracture when broken at extreme sub-zero temperatures.

The maximum spread between the yield and tensile strengths of 60% sold rolled Type 301 and 50% cold rolled Type 304 ELC when tested at -320°F are reflected in maxima in the elongation values at this test temperature.

Note that percent elongation bears no relation to toughness as evaluated by notched/unnotched tensile ratios. Type 304 ELC has its maximum percent elongation and minimum notched/unnotched tensile ratio at -320°F, while the notched/unnotched tensile ratio of 78% cold rolled Type 301 varies widely with test temperature whereas the elongation remains constant at 1% from room temperature to -423°F.

Alumunim Alloys

While the mechanical properties of only four aluminum alloys are presented in this paper, extensive tests conducted at Astronautics on many alloys permit their characterizations into the following classes with respect to their over-all toughness and utility at extreme sub-zero temperatures:

Very Tough	Moderately Tough
2014-T6	5086-H34
2024-T4	5086-H38
2219-T8	5154-H38
5052-H38	6061-T4
6061-T6	7079-T6
5083-H38	

Moderately Brittle	Very Brittle
7075-T6	7178-T6
7275-T6	

The above tabulation of the toughness characteristics of aluminum alloys was based upon the results of notched tensile tests conducted on sheet from 0.020" to 0.080" in thickness over the temperature range of 78°F to -423°F. Mechanical property tests on 2014-T6, 2219-T81, 5052-H38 and 7079-T6 aluminum alloys in base metal and weld joint conditions are shown in Figures 9, 10, and the upper right hand of Figure 15.

The 2000 series aluminum alloys contain copper and lesser amounts of other alloying elements and are hardenable by precipitation of intermetallic compounds by low temperature aging after a solution quenching heat-treatment. While the base metal of these alloys may be extremely tough down to very low temperatures, weld joints may be very brittle at sub-zero temperatures and alloys such as 2014 and 2024 may be regarded as marginally weldable. Increasing the thickness of the material at weld joints to reduce stress levels and careful control of weld quality to insure freedom from cracks, lack of fusion, incomplete penetration, undercutting, and other stress concentrating flaws must be resorted to in weldments intended for sub-zero temperature applications.

The 5000 series aluminum alloys are essentially solid solution alloys with magnesium, are not heat-treatable, and are hardenable only by cold working as in the case of the austenitic stainless steels. These alloys are extremely weldable with most of them retaining excellent ductility and toughness in the weld joint at reduced temperatures. There are, however, some exceptions; for example, the 5086-H34

alloy is quite touch down to -320°F, but becomes embrittled at -423°F. In the -H38 temper, this alloy is much tougher at -423°F than in the -H34 temper.[10] While many of the 5000 series alloys possess the desirable qualities of weldability and low temperature toughness, their generally low strengths often make them disadvantageous for aerospace applications, with the result that the much less weldable but stronger 2014-T6 alloy may be chosen instead.

The 6000 series alloys contain low quantities of copper, magnesium, and silicon and are hardenable by heat-treatment. 6061-T6 is weldable and very touch at extreme sub-zero temperatures, but like the 5000 series alloys, suffers from low strength in comparison to the 2000 series alloys.

The 7000 series alloys are the most highly alloyed ones, containing zinc, copper, and magnesium, and are heat-treatable to very high strengths in the range of 70,000 to 90,000 psi tensile strength. While the 7079-T6 alloy is reasonably tough down to -320°F, it is brittle at -423°F and the remaining 7000 series alloys range from moderately to severely brittle at sub-zero temperatures. Furthermore, the 7000 series alloys are generally unweldable by presently available welding techniques. As a result of these circumstances, the 7000 series alloys are not recommended for cryogenic uses, except that the 7079-T6 alloy may safely be used down to liquid oxygen and liquid nitrogen temperatures if mechanical attachment rather than welding is employed for joining this alloy.

Magnesium Alloys

Magnesium alloys are generally quite brittle in notched-bar impact tests at room and slightly reduced temperatures[5] and are hence not recommended for structural applications involving sub-zero temperatures. Magnesium alloys can, however, be used in such applications as housings, pump parts, and minor accessories in cryogenic fluid systems where severe stresses and impact loads do not occur, and where low toughness and ductility can be tolerated.

Titanium Alloys

Titanium alloys are being increasingly employed in aerospace vehicles, particularly for pressure vessel applications involving the storage of gases at high pressures. The pneumatic systems of many aircraft and missiles depend upon titanium alloy storage vessels. High strength-to-weight ratios, good formability and weldability and excellent corrosion resistance are factors in the selection of titanium for such applications. An outstanding example of the use of titanium in pressure vessels is the 6Al-4V-titanium alloy helium storage bottle, a half-dozen of which are employed in each Atlas Missile to contain the gas used for pressurization of the propellant tanks.[11] These bottles are chilled to liquid nitrogen temperature (-320°F) to increase their gas storage capacity and the 6Al-4V-Ti alloy, heat treated to tensile strengths in the range of 160,000-170,000 psi, is tough and fracture resistant at the service temperature.

More recently, titanium alloys have been evaluated at temperatures down to -423°F for possible application as liquid hydrogen propellant tanks and pneumatic pressure vessels operating at this temperature. The all-beta titanium alloy, 13V-11Cr-3Al-Ti, is extremely brittle at very low temperatures, as are many of the heat-treatable alpha-beta alloys, such at the 16V-2.5Al-Ti, 4Al-3Mo-1V-Ti and 8Mn-Ti alloys.[12] As mentioned above, the 6Al-4V-Ti alloy is extremely tough at temperatures down to -320°F, but tests at Astronautics have disclosed that this alloy displays notch sensitivity and lowered toughness at -423°F in both the annealed and heat-treated conditions, and this alloy is not recommended for use at liquid hydrogen temperature, note the mechanical properties of the annealed condition of this alloy shown in Figures 11 and 15.

The most promising titanium alloys for extreme low temperature applications are the all-alpha type, the best of which is the 5Al-2.5Sn-Ti alloy, see the upper left of Figure 11, and the notched/unnotched tensile ratios shown in the lower left of Figure 15. As discussed in a previous section, impurities such as oxygen, carbon, nitrogen, hydrogen, and iron embrittle titanium alloys, especially at

low temperatures, and their contents must be carefully limited and controlled to optimize the cryogenic temperature properties of titanium alloys. General Dynamics/Astronautics has developed a specification for the 5Al-2.5Sn-Ti alloy for low temperature applications that limits the oxygen content to a maximum of 0.12% and iron to 0.25%, whereas the commercial alloy may contain oxygen up to 0.20% and iron up to 0.50%. The latter quantities, as shown in Table I, greatly reduce the low temperature notch toughness and ductility of the alloy.

The low temperature mechanical properties of more recently developed essentially alpha titanium alloys are shown in the lower portion of Figures 11 and 15. Both the 8Al-1Mo-1V-Ti and 5Al-5Zr-5Sn-Ti alloys have reduced toughness at temperatures below approximately -100°F, but this may be due to the high oxygen contents of these alloys. Oxygen is deliberately added to some titanium alloys to enhance their elevated temperature creep resistance. Development work is currently underway to evaluate the cryogenic properties of a number of titanium alloys carefully made from high purity constituents having low interstitial contents.

An important characteristic of the all-alpha or annealed alpha-beta and beta titanium alloys is that they develop essentially 100% weld tensile efficiency which is retained down to extremely low temperatures, see Figure 12. Finally, titanium alloys increase in strength more rapidly with decreasing temperatures than do steel, aluminum, copper, and nickel base alloys. Many titanium alloys display a 100% increase in tensile strength between +70°F and -423°F, whereas steels may increase from 50 to 75°F in strength, and aluminum alloys from 25 to 40% in strength over this same temperature range. Thus, in those cases where the intended service conditions permit, the use of low temperature design allowable yield and tensile strengths results in very significant weight reductions when titanium can be used. This is illustrated by the curves shown in Figure 16; where, as an example, titanium has approximately the same room temperature yield strength/density ratio as cold rolled austenitic steel (Type 301) and the 2014-T6 aluminum alloy,

but is 30% higher than the steel alloy and more than 50% higher than the aluminum alloy in yield strength/density ratio at -423°F.

Nickel and Cobalt Base Alloys

The face-centered cubic crystal structure of nickel and cobalt base alloys indicate that they would be expected to retain ductility and toughness at extreme sub-zero temperatures and this generalization is true of these alloy classes. Many of these alloys have been developed primarily for high temperature applications, but their low temperature properties have been found to be also promising.[13] Haynes 25, a cobalt base alloy, possesses excellent ductility and toughness down to -423°F in the 20% cold rolled condition, but is excessively brittle at extremely low temperatures in the 40% cold rolled condition.

The mechanical properties from +75°F to -423°F of nickel base alloys such as K-Monel, Inconel X, Rene' 41, and Hastelloy B (40% cold rolled) are shown in Figures 13, 14, and the lower right of Figure 15. Nickel base alloys display the least increase in strength with decreasing temperature over the above temperature range of the four classes of alloys discussed in this paper, and some of them, such as K-Monel and Inconel X, have very high ductilities in the range of 25-30% elongation over the entire temperature range.

K-Monel has been successfully employed as ducting for the fuel and liquid oxygen propellants of the Atlas missile. The excellent formability, weldability, corrosion resistance, and development of moderately high strength upon a simple, relatively distortion-free, low temperature aging cycle made this alloy attractive of such applications.

The excellent low temperature mechanical properties as well as the outstanding elevated temperature properties of Inconel X, Rene' 41, and cold worked Hastelloy B make these alloys of interest in applications where extremely wide ranges of temperatures may be encountered in cryogen-

fueled aircraft or missiles having atmosphere re-entry flight profiles.

COMBINED EFFECTS OF NUCLEAR RADIATION AND CRYOGENIC TEMPERATURES

Recently developed interest in nuclear propelled aerospace vehicles has prompted concern about the effects of certain combined environments on the mechanical properties of structural engineering alloys. The best practicable working fluid for nuclear propulsion systems is hydrogen which would be stored as liquid in tanks, piped to the reactor, heated to a high temperature, and expelled through nozzles to provide thrust. The tankage and accessory components and structure would be subjected to high radiation levels, so that some of the structural materials would be simultaneously exposed to very low temperatures and a high neutron flux density.

Radiation damage to metals often anneals out at room or moderately elevated temperatures because of diffusion processes which occur. However, diffusion is extremely restricted at a temperature of -423°F, so radiation damage may be expected to be more permanent. Inasmuch as low temperatures themselves exert an embrittling effect on many high strength aerospace alloys, radiation effects superimposed upon these might be expected to produce serious results.

In an attempt to explore this problem area, the General Dynamics/Astronautics and Fort Worth Divisions cooperated in a test program during which base metal and welded, notched and smooth tensile test specimens of a number of steel, aluminum, and titanium alloys were kept immersed in liquid hydrogen for 100 hours during which they were subjected to an integrated radiation flux of 2×10^{17} fast neutrons per square cm. The specimens were strained to fracture without any intervening raise in temperature, and the results compared to the normal low temperature properties of the same alloys.

It was determined that the threshold of radiation damage was reduced from the room temperature range of 10^{18} to 10^{20} ntv. by at least one magnitude when the temperature of exposure was reduced to -423°F. The effect of radiation damage was to lower the tensile strength (from 3% in the case of the 5Al-2.5Sn-titanium alloy to 27% in the case of 60% cold rolled Type 301 stainless steel) and to reduce the ductility of the alloys. The reduction in deformation capability is believed associated with the introduction of lattice vacancies and interstitial elements by the neutron bombardment. The 2014-T6 aluminum alloy, while slightly lower in strength after irradiation, displayed no reduction in ductility. The notched strength and notched/unnotched tensile ratios were not deleteriously affected in any of the alloys investigated, but it must be borne in mind that only the toughest alloys of each type were selected for this investigation.

It may be concluded that suitable structural materials are presently available for the fabrication of liquid hydrogen tanks for nuclear propelled aerospace vehicles which will have a high order of reliability under the operating and environmental conditions encountered during service.

ACKNOWLEDGMENTS

Much of the data discussed in the paper were developed by Dr. J. F. Watson and Mr. J. L. Christian of the Materials Research Group, General Dynamics/Astronautics. The permission of the General Dynamics/Astronautics Division to publish this paper is appreciated.

BIBLIOGRAPHY

1. Heindlhofer, K., "The Plasticity of Iron at Low Temperatures," Transactions AIMME, Vol. 116, 1935, p. 232.

2. Armstrong, T. N., and A. P. Gagnebin, "Impact Properties of Some Low Alloy Nickel Steels at Temperatures Down to -200°F," Transactions ASM, Vol. 28, 1940, p. 1.

3. Hemes, S. A., and C. H. Lorig, "Influence of Metallurgical Factors on the Mechanical Properties of Steel," Transactions ASM, Vol. 40, p. 775.

4. Watson, J. F., J. L. Christian, T. T. Tanalski, and A. Hurlich, "The Correlation of Notch/Unnotch Tensile Ratios with Tensile Fatigue Properties of Complex Welded Joints in High Strength 300 Series Stainless Steels at Cryogenic Temperatures," presented at annual meeting, ASTM, Atlantic City, New Jersey, June 1961.

5. Hurlich, A., "Summation: Symposium on Low Temperature Properties of High-Strength Aircraft and Missile Materials," ASTM Special Technical Publication No. 287, June 1960.

6. Irwin, G. R., "Onset of Crack Propagation in High-Strength Steel and Aluminum Alloys," Naval Research Laboratory Report 4763, May 24, 1956.

7. Irwin, G. R., J. A. Kies, and H. L. Smith, "Fracture Strengths Relative to Onset and Arrest of Crack Propagation," Proceedings ASTM, Vol. 58, 1958.

8. Campbell, J. E., and L. P. Rice, "Properties of Some Precipitation - Hardening Stainless Steels and Low-Alloy High-Strength Steels at Very Low Temperatures," ASTM Special Technical Publication No. 287, June 1960.

9. Watson, J. F., and J. L. Christian, "Low-Temperature Properties of Cold-Rolled AISI Types 301, 302, 304 ELC, and 310 Stainless Steel Sheet," ASTM Special Technical Publication No. 287, June 1960.

10. Watson, J. F., J. L. Christian, and J. Hertz, "Cryogenics - Selection Data for Structural Materials," Electro-Technology, November 1961, Vol. 68, No. 5.

11. Hurlich, A., "Metals and Fabrication Methods Used for the Atlas," Metal Progress, Vol. 76, No. 5, November 1959.

12. Espey, G. B., M. H. Jones, and W. F. Brown, Jr., "Sharp-Edge-Notch Tensile Characteristics of Several High Strength Titanium Sheet Alloys at Room and Cryogenic Temperatures," ASTM Special Technical Publication No. 287, June 1960.

13. Watson, J. F., and J. L. Christian, "Low Temperature Properties of K-Monel, Inconel X, Rene' 41, Haynes 25 and Hastelloy B Sheet," ASME Winter Annual Meeting, Nov. 26 - Dec. 1, 1961.

INTRODUCTION TO SPACE PROPULSION PROBLEMS

J. E. Hove
Director, Materials Sciences Laboratory
Aerospace Corporation
Los Angeles, California

ABSTRACT

Considerations of space propulsion mainly involve the possible trade-offs between propellant mass, structure and auxiliary equipment mass and payload in order to accomplish a prescribed mission. For long-time deep space missions, chemical propulsion is not normally feasible with any reasonable payload requirements. This is principally because the low specific impulse of such engines gives rise to the requirement of prohibitively large propellant mass transfer and hence initial propellant mass. Thus, electrical and nuclear systems are under study, principally ion and plasma propulsion using nuclear auxiliary power units, and reactor heating of a propellant by surface heat transfer. Other systems are under consideration, such as photon propulsion, but will not be discussed in this talk. Some of the advantages and disadvantages of the various propulsion schemes will be presented and the general problems discussed, particularly those relating to materials. Since atmospheric nuclear propulsion schemes (such as the ram-jet) give rise to technology useful to the solution of some of the space problems, a brief discussion of such systems will be included.

INTRODUCTION

The problem of propelling a vehicle in space involves different considerations than the problem of placing a vehicle into orbit. In the latter case, a high thrust is of paramount importance. At our present state of technology, this requirement can generally be satisfied only by chemical means. However, a deep space mission does not need high total thrust since retarding forces, such as gravity, are low. Furthermore a high total thrust necessarily means a high rate of loss of mass, a situation to be avoided since the high initial propellant mass so required eats into the available payload mass. Thus the various schemes for space propulsion rarely involve chemical energy as a primary source, but usually emphasize nuclear power. There have also been some investigations of photon propulsion,[1] i. e. a utilization of the light pressure from the sun on a large sail in much the same way that an ordinary sailboat uses wind pressure. This idea appears to have some merit for certain applications, but as a sole propulsion source, there are problems. For example, its acceleration capacity is so low that a photon-powered vehicle could not leave an earth orbit unaided. Also, the sail area has to be rather large, about 10,000 square feet per pound of vehicle weight for a typical 300 day Mars journey. This introduces over-all weight difficulties. In any case, photon propulsion will not be discussed herein.

Assuming, then, that a nuclear reactor provides the energy for propulsion, the next question is how to utilize this energy for useful thrust. There are two general approaches, one using a reactor to provide electrical power which in turn operates an ion or plasma propulsion engine and the other using the reactor as a direct source of heat to give high thermal energy to a propellant. In the latter case, at the present state of knowledge, we can speak only of a fission reactor which transfers heat to a gas across a solid surface. There are no practicable methods as yet for either a controlled themonuclear engine or a fission engine where the reaction takes place in the gas phase. This solid surface heat transfer aspect of nuclear propulsion forms a great handicap since it means that the gas can never be hotter than the walls of the reactor and thus

the specific impulse is limited. It is for this reason that the materials problems are generally more severe for nuclear propulsion than for any other method, since the operating temperatures must be as high as possible and, of course, no system of cooling the walls is possible.

PROPULSION PARAMETERS OF VARIOUS PROPULSION METHODS

It seems worthwhile to present a brief comparison of propulsion parameters for the three major schemes, chemical, direct nuclear and electrical, before discussing the systems themselves. The rocket engine operates by ejecting mass. If this mass moves with an (assumed constant) exhaust velocity V with respect to the rocket, then the thrust force due to the rocket engine is

$$F = MV$$

where M is the mass time rate of change. In the simplified case where no other forces act and the propellant velocity and direction are constant with time, this can be equated to the mass times acceleration of the rocket and the equation integrated to give

$$\Delta v = v_1 - v_0 = V \ln \frac{M_0}{M_1}$$

where v is the rocket's velocity and the subscripts 0 and 1 refer to initial and final values. Δv is sometimes called the characteristic velocity. The specific impulse, I_{sp}, is defined as the ratio of the total thrust to the rate of mass loss and hence is equal to, or proportional to, the exhaust velocity, depending on the system of units used. Actually, I_{sp} is usually defined in terms of force and rate of weight (not mass) loss, so that

$$I_{sp} = \frac{V}{g}$$

and has units of seconds instead of velocity. The importance

of a high specific impulse in attaining a given characteristic velocity van be immediately seen since the effect of mass flow rate is only logarithmic. This means that for ambitious space missions where extremely high Δv's are required, a high specific impulse system is the only way to avoid impossibly high mass ratios. It should be noted that no explicit time appears in the above equation. Thus, while the total thrust does not (at least in this simple case) strongly affect the magnitude of the characteristic velocity, it does affect the time needed to achieve this velocity. Clearly both a high thrust and a high specific impulse would be desirable, but also are difficult to obtain.

In chemical systems, there is no real limitation on the thrust, but the maximum specific impulse is about 500 seconds, corresponding to an exhaust velocity of about 15,000 feet per second. In nuclear heat transfer systems, the thrust can also be very high but also specific impulses of over 1000 seconds are possible. In electrical systems, the specific impulse can be made very high, up to 10,000 or 20,000 seconds, but thrusts are limited to fractions of a pound or, at best, a few pounds. They can, therefore, only be used in deep space flights where gravitational forces are unimportant. For such missions, however, the high specific thrust allows a sizeable increase in payload to be achieved. It has been estimated[2] that for a round trip from an Earth to a Mars orbit, the payload using electrical propulsion (with a SNAP-8 type of system) is some ten times larger than that for chemical propulsion and about 50% greater than for direct nuclear propulsion.

It is, naturally, true that the attractive payloads for electrical systems can be substantially eaten into by the additional weight of the power source, conversion system and acceleration system. Considerable effort is going into attempts to make the auxiliary power units lighter for a given amount of power delivered in the jet, but this subject will be considered at a later session of this meeting.

ELECTRICAL SYSTEMS

Since later papers will deal in some detail with the types of electrical systems, it is only the intent here to introduce these types in a very general manner. In electropulsion systems the propellant is made up of charged particles and the difference between the two methods presently under study is reflected in the nature of the ionized gas and the manner of accelerating the gas. Basically in all ion-propulsion schemes, positive ions are produced and then electrostatically accelerated by an arrangement of suitably biased electrodes. Provision must be made to emit electrons into the stream of exhaust ions to neutralize the beam and prevent a net charge from building up on the rocket. In plasma-propulsion devices, a neutral plasma discharge is produced and accelerated by intense and rapidly varying magnetic fields which are often provided by the discharge of large currents through the plasma and associated circuit elements.[3]

For ion-propulsion devices, the exit ion velocity (i.e. specific impulse) depends on the voltage between electrodes and the ion mass, whereas the thrust can be shown to depend only on the electric field intensity.[3] Thus for a given desired I_{sp}, it is necessary to minimize the interelectrode spacing to maximize the thrust. However, ion optics sets a lower limit on the spacing and, in effect, prevents the attainment of large thrusts. To get an idea of typical numerical values, an accelerating voltage of 10 kilovolts (giving, for singly ionized cesium, an I_{sp} of 12,000 seconds) over a spacing of one centimeter (with a like beam diameter) yields a specific thrust of about 0.2 pounds per square foot. One of the major materials problems in such schemes is the sputtering of ions of atoms on the electrode causing an erosion effect.

For plasma-drive devices, there is a greater variety of methods available. Since specific impulse and thrust can be determined in a more independent fashion than for ion devices, plasma devices appear on paper to have great advantages. Thus,[3] it is possible to talk about thrusts of 20,000 pounds per square foot (or 10^5 greater than ion-drive with similar orders of specific impulse) if a continuous

operation is assumed. However, this gets into problems similar to MHD generator devices, i. e. the gas must be highly conductive which implies high temperatures and the containment gets into a severe materials problem. At the present, the furthest advanced technology, therefore, is in the area of pulsed field operation, where the duty cycle is of the order of 10^{-5}. Hence, for such devices, the advantage over ion-drive disappears. Nevertheless, the potential of plasma propulsion seems very great.

DIRECT NUCLEAR SYSTEMS

Direct nuclear propulsion implies a system where the fission energy is used in as direct a manner as possible to put energy into the propellant. Here we will discuss propulsion in general, not just space propulsion, so that atmospheric engines will also be considered. At the present time, there are only two schemes under major development, the nuclear rocket and the nuclear ram-jet. Both use what might be called a brute force technique, i. e., a reactor of as high a power and power density as possible simply heats the propellant to the highest temperature feasible considering the materials capabilities. For reasons of fuel economy as well as ease of power control, these reactors are usually thermal (i. e. the fission event takes place when a neutron of thermal energy is captured) or nearly so which causes an additional materials problem, namely the bulk of the materials used must not be nuclear poisons. This severely restricts the choice of possible materials useful either as moderator or structure. Thus, in large amounts (greater than 25% of the bulk, say), only He, Be, C, O, F and D are tolerable although H is an exception because it is such an excellent moderator. Of these, only D(H), Be, and C can be considered as practical moderator elements. In somewhat smaller amounts (between 5 and 25%, say) only Mg, Al, Si, P, Zr, Pb and Bi are tolerable.

One of the advantages of using a nuclear reactor heat source in the rocket is that the propellant can be picked to give the highest possible specific impulse, i. e. hydrogen can be used. If used as a booster, the wall temperature of

the propellant channels must be very high, however, to permit the high heat flow into the gas which is needed to attain the required thrusts. These temperatures are in the range of 2000-2500°C and indicate why so much attention has been paid to the use of graphite, since, if the reactor is thermal, only carbon and ZrC are feasible as bulk materials. This gives rise to one of the major problems which had to be overcome, that of corrosion of the graphite by hydrogen at these temperatures. This difficulty is somewhat alleviated, of course, by the relatively short duration of full power, which is of the order of minutes. For space use, the high thrust is no longer as important and the temperature can be somewhat lower, although not a great deal since the specific impulse is then decreased. Naturally the system reliability must be then assured over a much longer time span.

For the case of the nuclear ram-jet, the propellant of necessity is air which means that the reactor materials, in addition to withstanding high temperatures (say 1200-1500°C wall temperature) and being neutronically tolerable, must also be very oxidation resistant. This makes the oxides of Be, Mg, Al, Si and Zr of particular interest with a sharp focus on BeO since it is the least poisonous from a nuclear standpoint and is a good moderator. There is, however, a water vapor corrosion difficulty to be considered. SiC is a possible material (either for structural use or as a coating on graphite) since it forms a self-sealing protective silica coating upon oxidation at high temperatures. Some care must be taken since there is a (lower) temperature region where the silica is formed at a reasonable rate but where it does not flow to form a continuous coating. The remaining possible material is the highest beryllide of zirconium (probably not $ZrBe_{13}$ at high temperatures, but more likely Zr_2Be_{17}) which is oxidation resistant at these temperatures, presumably due to the formation of a BeO film. There is a similar difficulty here to that of SiC in that zirconium beryllide is rapidly attacked by air in the region of 900°C, although the reasons for this attack do not seem altogether clear as yet. It may be worth mentioning that the zirconium compound appears to be the worst of the transition metal compounds in this regard. The best seems

to be tantalum beryllide which has never shown any sign of air corrosion, but unfortunately the element tantalum is essentially intolerable in a thermal reactor. The big advantage of a nuclear ram-jet over a chemical engine is that of range, particularly at low altitudes. This means that for the system to be interesting from an operational standpoint, the reactor must operate well for periods of many hours, at least. Thus, even though the temperatures are lower than for the nuclear rocket, the much longer times involved make the materials problems of perhaps equivalent difficulty.

CONCLUDING COMMENTS

In summary, the materials problems inherent in the propulsion schemes discussed center about the need for reliable, predictable performance at very high temperatures and a variety of atmospheres. There is still very little basic understanding about the chemistry and physics of materials and their interactions under these conditions, but there is a great deal more known now than there was just a few years ago and this is largely due to the technological impetus of the various propulsion programs. In some ways, this increase in the technology of refractory materials may, in the long run, be as important a result of these programs as the actual achievement of the systems themselves.

Character

The sun set, but set not his hope;
Stars rose; his faith was earlier up;
Fixed on the enormous galaxy,
Deeper and older seemed his eye;
And matched his suffrance sublime
The taciturnity of time.
He spoke, and words more soft than rain
Brought the Age of Gold again;
His action won such reverence sweet
As hid all measure of the feat.

BIBLIOGRAPHY

1. Hock, McMillan and Tanguay, Proceeding IRE 48, 492 (April 1960).

2. Finger, H. B., "Nuclear Energy for Advanced Space Missions," Proceeding of the NASA Industry Program Plans Conference, July 1960, p. 54.

3. For a review of these methods, see S. W. Kash, Proceedings IRE 48, 458 (April 1960).

Fable

The mountain and the squirrel
Had a quarrel,
And the former called the latter "Little Prig";
Bun replied,
"You are doubtless very big;
But all sorts of things and weather
Must be taken in together,
To make up a year
And a sphere.
And I think it no disgrace
To occupy my place.
If I'm not so large as you,
You are not so small as I,
And not half so spry.
I'll not deny you make
A very pretty squirrel track;
Talents differ; all is well and wisely put;
If I cannot carry forests on my back,
Neither can you crack a nut."

MATERIAL REQUIREMENTS FOR ION PROPULSION*

H. Todd, F. Barcatta, D. Clark, R. Worlock
Electro-Optical Systems, Inc.
Pasadena, California

ABSTRACT

Ion propulsion devices impose new and unique material requirements. High operating temperatures, low pressures, the presence of cesium vapor, and the necessity for high ionization efficiencies, and low electrode sputtering rates create formidable problems.

In the ion engine, ionization of cesium is accomplished by effecting its evaporation from a clean porous tungsten surface. During this process the cesium atom loses an electron to the tungsten and becomes positively charged. The resulting ion is accelerated away from the ionizing surface through a negatively charged annular electrode. Neutralization of the cesium ion beam is accomplished downstream by electrons emitted from a high temperature, low work function material developed for this application.

---

* Work described in this paper was performed under the following contracts:
DA-04-495-ORD-1191, for the United States Army Ordnance District, Los Angeles
AF 33(616)-6958, for the Aeronautical Systems Division, Air Force Systems, Command, United States Air Force
NAS 8-1545, for the National Aeronautics and Space Adm.
NAS 8-1537, for the National Aeronautics and Space Adm.

Material requirements for the porous tungsten ionizing surface are particularly critical. Permeability, pore size, and spacing must be carefully regulated if a high degree of ionization efficiency is to be obtained. Present porous materials produced by powder metallurgy methods are far from uniform in pore size and spacing and permeability. Wire bundle techniques appear particularly promising as a method of producing improved porous materials.

Metal joining problems have proven rather difficult of solution in ion propulsion devices, particularly that of effecting a seal between the porous ionizing material and the cesium box. Brazing has been adopted as the most practical joining method since it can be easily carried out in vacuum or protective atmosphere environments and results in an assembly substantially free of stress at operating temperatures. Brazing alloys for these applications must satisfy a number of requirements, among which are: lack of infiltration of the porous ionizing surface, high temperature strength, cesium compatibility, and low vapor pressure. Special alloys have been developed at Electro-Optical Systems which satisfy these conditions and have proven satisfactory for several hundred hours of ion engine operation.

Ion engine lifetime is seriously affected by the sputtering rate of the accelerating electrodes. A number of studies of this phenomenon have been completed which indicate that sputtering rate increases as the number of d shell electrons of the target material increases.

INTRODUCTION

Electrostatic ion propulsion methods offer formidable advantages for deep space missions. Such methods of propulsion are designed to operate after chemical propulsion systems have achieved orbital velocities, and to operate for long periods of time on small quantities of fuel. In

addition, high specific thrust, and low weight-to-thrust ratios make this propulsive method exceedingly attractive.

Study of the unique material requirements imposed by the environmental phenomena of deep space is of prime importance in the development of an ion propulsion system, and Electro-Optical Systems, Inc. (EOS) has made significant progress in this direction.

To better understand the nature of the various material requirements for an ion engine, the following sections attempt to explain in detail the requirements of individual engine components, and to give the conclusions arrived at through extensive preliminary research and experimentation.

FUNCTIONING OF THE ION ENGINE

Familiarity with the component parts of the ion engine and their functions is prerequisite to comprehension of the material requirements. Figure 1 shows a sectional view of the engine components. The cesium vapor passes from the boiler through a delivery tube into the cesium box and thence through the porous ionizer where it emerges as a positive ion. Just ahead of the ionizer is the annular acceleration electrode charged to a high negative potential. The positive ion is accelerated in the negative field and passes through the annular accelerating electrode. Downstream from the accelerating electrode you will note a positively charged decelerating electrode whose function is to bring the ion beam to the desired final exhaust velocity. As the positive ion leaves the apparatus it is necessary that it be neutralized, otherwise the space craft would soon become negatively charges to such a potential that ions would no longer leave the ship. Neutralization of the ion beam is accomplished through the injection of electrons from the surface of the neutralizing electrode.

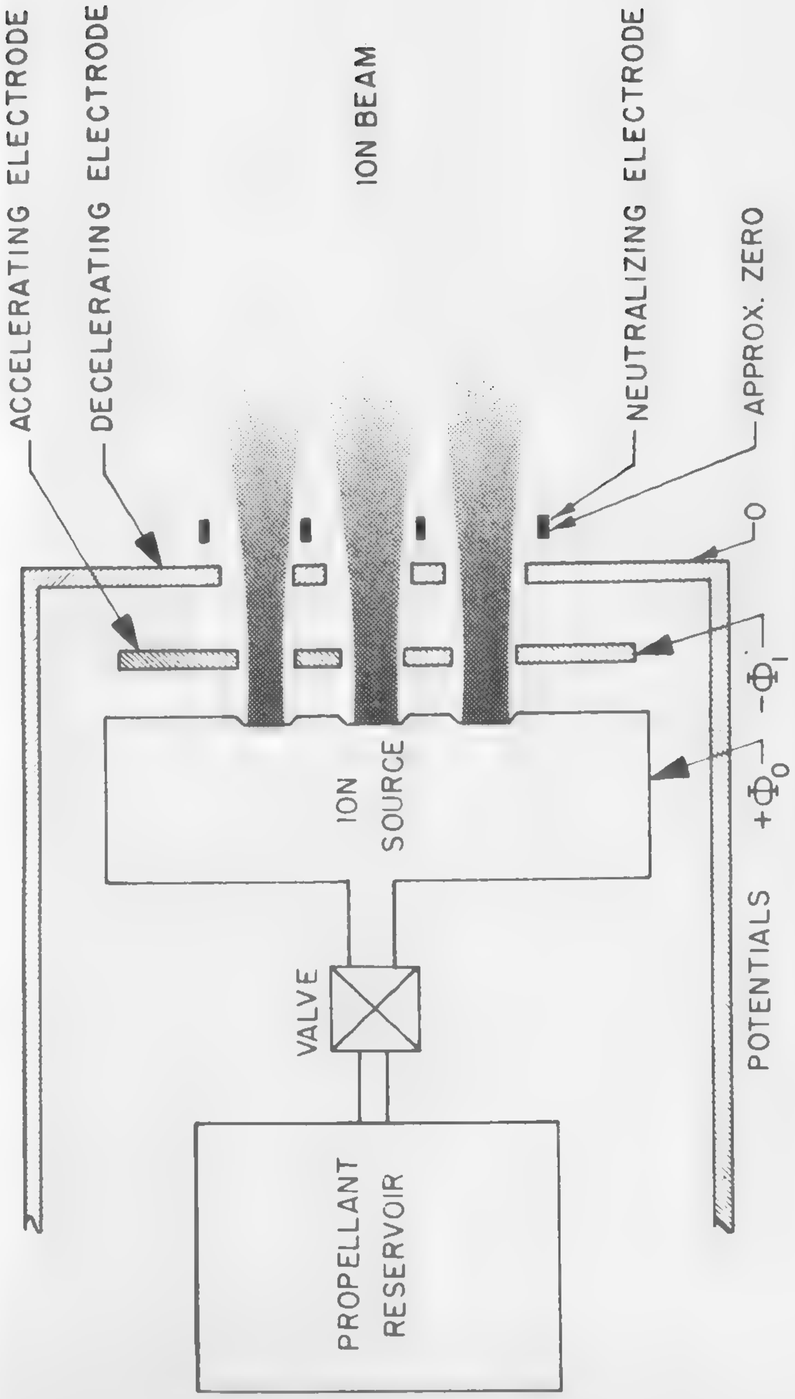


FIGURE 1 SCHEMATIC REPRESENTATION OF ION ENGINE

MATERIAL REQUIREMENTS FOR THE IONIZER

One of the most critical components of the engine is the ionizer. It is the heart of the engine without whose efficient functioning this form of propulsion would be impractical. This component must operate for long periods of time with a high efficiency of ionization and low energy requirements.

Various techniques may be utilized to effect ionization of a number of gaseous materials, such as, high frequency fields, electron bombardment, high temperatures, etc. Various gases, such as mercury vapor, alkali metal vapors, rare gases, etc., can be ionized by such techniques; however one of the most efficient methods of ionization yet discovered is that known as surface ionization which occurs whenever an alkali metal of low work function is evaporated from a metal surface of high work function. During this process, an electron is stripped from the alkali metal atom and the metal evaporates from the surface as an ion. The efficiency of ionization by such a process is unusually high, often exceeding 95%, and this factor makes the process appear extremely attractive for ion propulsive devices.

Supplying alkali metal vapor to a surface from whence the ions evaporate is, however, not a simple matter. For example, if the vapor is merely directed against the ionizing surface, outgoing ions will interact with the incoming neutral atoms, and will result in charge exchange phenomena which are deleterious to engine operation. This problem can best be solved by making the ionizer in the form of a porous diaphragm. If this is done, the alkali metal vapor can be supplied to the rear of the diaphragm where it can diffuse through to the front surface, be ionized, and then accelerated away finder the influence of the electrostatic field without danger of collision with incoming neutral atoms.

Material requirements for the porous ionizer are particularly critical, as efficient functioning of the engine is directly dependent on this component. Among these requirements are the following:

1. High work function
2. Uniform pore size and spacing
3. Pores of the proper diameter and spacing
4. Uniform permeability
5. High temperature stability
6. High melting point
7. Cesium compatibility.

For efficient ionization of the alkali metal, evaporation must occur from a surface whose work function is 4.5 electron volts or greater. Elements such as chromium, iron, nickel, tungsten, tantalum, and metals of the platinum group satisfy this requirement.

PRESENT METHODS OF PRODUCING POROUS MATERIALS FOR IONIZER FABRICATION

Now let us discuss present methods of producing these porous materials having the previously mentioned characteristics. Powder metallurgy techniques lend themselves well to this application. Carefully sized tungsten powder in the size range of 4 to 8 microns is placed in small rectangular dies and cold pressed into a rectangular bar using 15 to 20 tons of pressure per square inch. After cold-pressing, the small bar is sintered. During the sintering operation, shrinkage of the pressed compact occurs rapidly at first, and then reduces in rate as time continues. For a given temperature and time, a point will be reached at which further densification of the compact becomes extremely slow. The selected temperature must be above that to which the ionizer will be subjected in use. In actual practice, this is about 1500°C. The final density achieved after the sinter will depend upon several factors such as:

1. Powder characteristics
2. Powder size
3. Pressing pressure
4. Sintering time
5. Sintering temperature.

Fine powders, high pressing pressures, high sintering temperatures, and long times at temperature give dense compacts. The surface energy of powders in the range of 1-2 microns is extremely high; therefore, while powder within this size range would be of the proper size for proper pore size and spacing, the rapid sintering rate precludes its use. Powder characteristics vary greatly from lot to lot of powder, even though all manufacturing techniques have apparently remained the same. Differences in sintering rates, pressing characteristics, density, etc., also occur as a result of variations in temperature of reduction, oxide powder size, purity of the reducing gas, and the presence of interstitial impurities in the finished product. Therefore, it is common practice for the concerns manufacturing these porous materials to purchase large lots of tungsten powder, work out the necessary processing techniques to get the desired results, and proceed until the particular lot is used, at which time a new procedure is worked out for the next lot of powder.

After pressing and sintering to the desired density, the porous compact is infiltrated with a metal in which tungsten exhibits no solubility, such as copper or gold. Infiltrating the porous tungsten skeleton with the metal matrix material serves two purposes; it strengthens the skeleton so as to permit machining the material into its final configuration, and it acts as a lubricant for the cutting tool, serving to prevent smearing of the material across the pore openings.

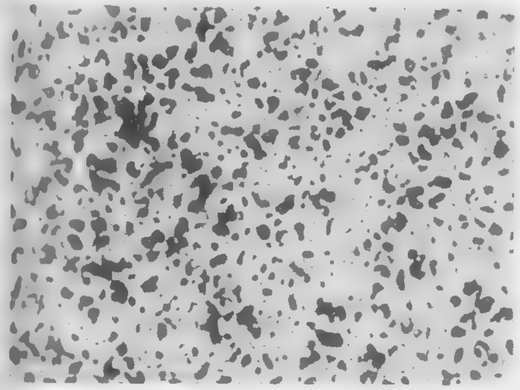
After machining, the copper is removed from the finished part by high temperature evaporation in a vacuum furnace. The rate of copper evaporation more or less limits the thickness of porous material which can be produced by this technique. A thickness of about 0.090 inch appears to be a practical upper limit from which the copper can be completely removed.

Other techniques of producing porous tungsten are those in which a volatile material is incorporated into the powder prior to pressing and wintering. This method, however, does not give the structural support during machining or the uniformity of structure possible with the copper infiltration technique.

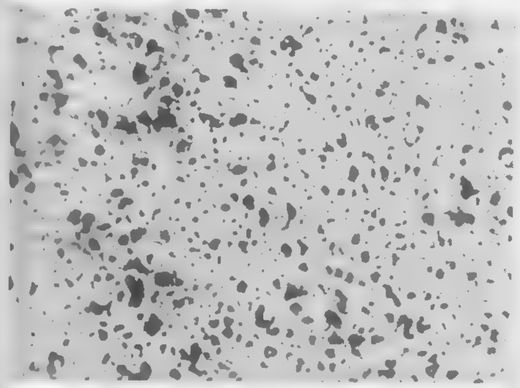
METHODS OF EVALUATING POROUS MATERIALS

Porous tungsten produced for emitter surfaces must meet stringent requirements with regard to pore size and spacing, porosity or permeability for vapor flow, thermal emissivity, and mechanical characteristics that may influence the mounting problem.

Photomicrographic examination of porous tungsten is invaluable for the measurement of pore size and spacings. The photomicrographs in Figure 2 show the difference in pore size and spacings from samples of two different suppliers. Successful examinations of this type require careful lapping, polishing and etching of the tungsten surface so as not to smear over the pores or cause their enlargement. The use of diamond lapping compound and hydrogen peroxide as an etchant has proven satisfactory as a means of surface preparation.



POROUS TUNGSTEN - VENDOR A



POROUS TUNGSTEN - VENDOR B

FIGURE 2 POROUS TUNGSTEN
Magnification 400X

Microscopic studies shown in Figures 3 and 4 indicate that the best available commercial porous materials have pore openings in the order of 2-4 microns with pore center to center spacing of 6-8 microns. For optimum efficiency, theoretical considerations indicate that pore openings should be in the order of 1 micron with spacings of approximately 2 microns. Such microscopic studies are very important for analyzing ionization efficiency, but they give no information on premeability to cesium flow through the material. This characteristic can best be determined by making measurements of gas flow permeability.

A device for making these measurements which is used routinely in the ion engine test program is shown in Figure 5. Here it can be seen that a chamber of known volume is charges to a predetermined gas pressure, then the rate of pressure drop occurring in this known gas volume resulting from the gas flow through the test object can be used as a measure of permeability. A standard of known porosity is checked before each ionizer measurement to be sure the instrument is calibrated properly. Results are easily reproducible and accurate, and clearly reveal variations in permeability between individual porous tungsten emitters.

Density is a critical variable in attaining uniform permeability between individual lots of porous material. For example, in the range of 79-83 percent theoretical density, nearly all of the pores of the emitters appear to be through pores, while at 90% density the permeability drops to zero (that is, no pores interconnect). This large variation in permeability with small change in density greatly aggravates the problems of producing ionizers of uniform characteristics from one button to another. Figure 6 is that of a 61 hole ionizer showing the array of porous tungsten buttons mounted on the cesium box.

Since all of the porous buttons connect to a common cesium supply, variations in permeability between buttons may result in some of the buttons being cesium starved during operation, while other button surfaces are receiving more cesium than can effectively be ionized. This proces-

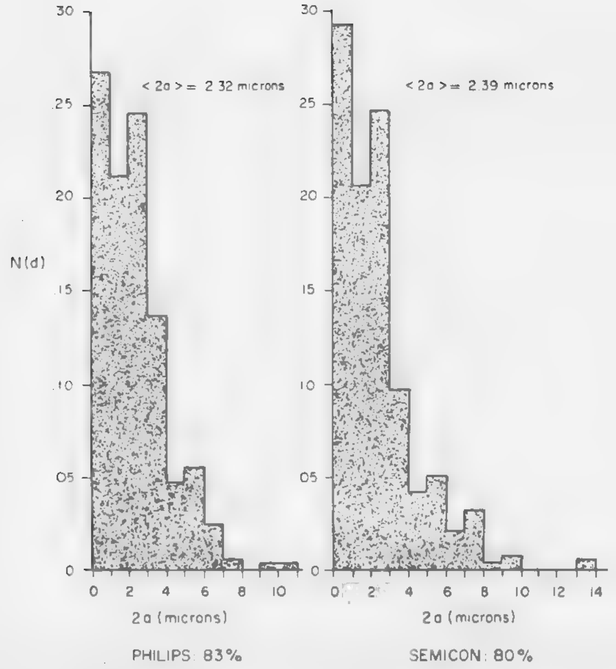


FIGURE 3 PORE SIZE DISTRIBUTIONS FOR TWO TYPES OF SINTERED POROUS TUNGSTEN FROM 1387-60

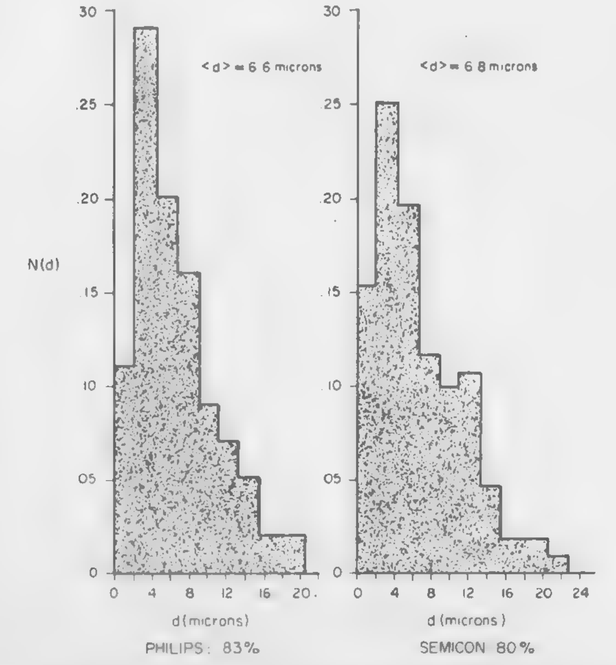


FIGURE 4 PORE SIZE DISTRIBUTIONS FOR TWO TYPES OF SINTERED POROUS TUNGSTEN FROM 1387-60

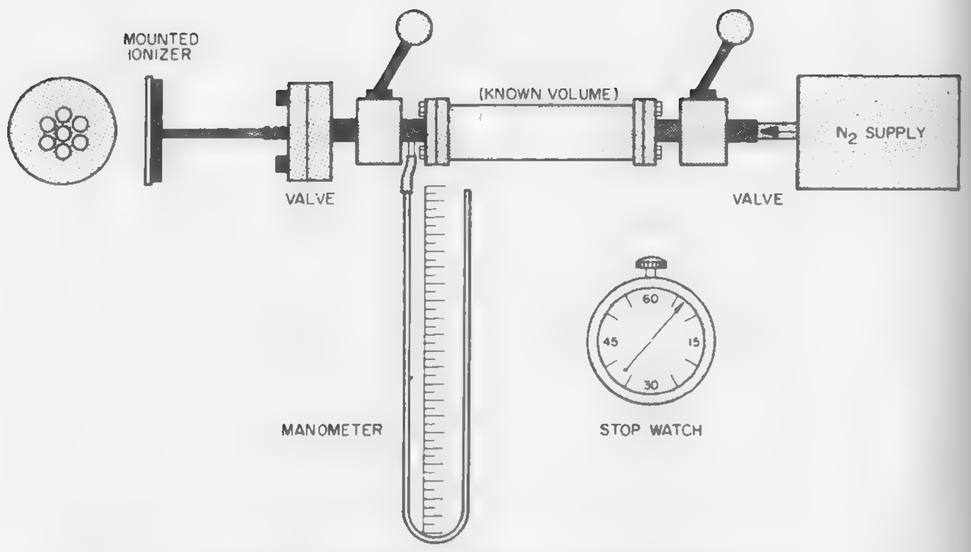


FIGURE 5 PERMEABILITY CHECKING DEVICE FROM 60-90A

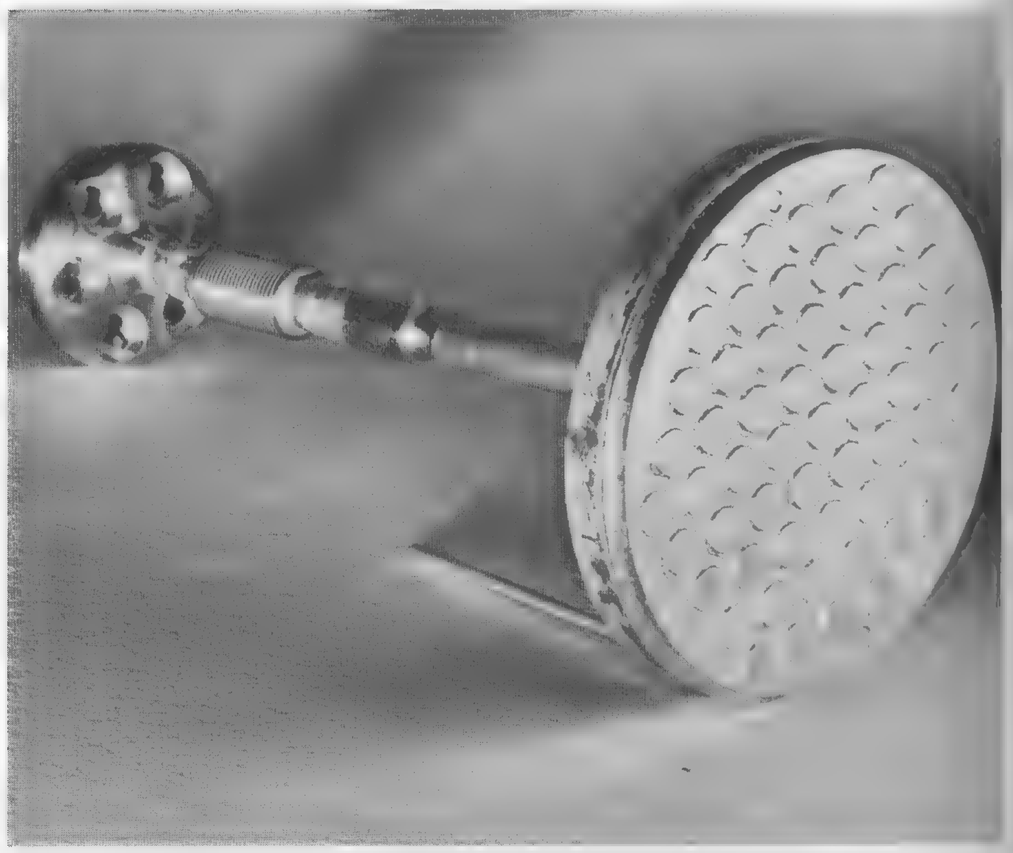


FIGURE 6 61 HOLE IONIZER SHOWING POROUS TUNGSTEN BUTTONS

not only lowers the efficiency of ionization, but results in accelerated electrode sputtering as a result of the large amount of neutrals introduced into the space between ionizer and accelerating electrode.

Electro-Optical Systems has made a careful study of permeability variations existing between porous tungsten buttons of a given thickness. Figure 7 will demonstrate the wide variations in permeability encountered. Figure 8 shows the relationship between density and permeability. In several instances all buttons were produced from a single pressed ingot, without noticeable improvement in the permeability spread. It was noted that buttons cut from the centers of ingots tended to be more permeable than those cut from near the ends. This was no doubt the result of density variations occurring as a result of internal friction within the powder during pressing.

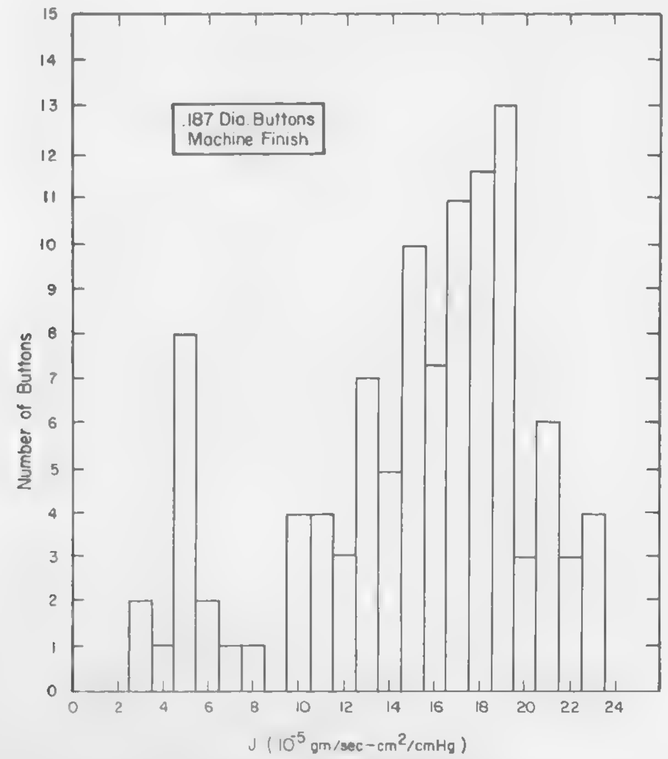


FIGURE 7 PERMEABILITY DISTRIBUTIONS FROM 61-506

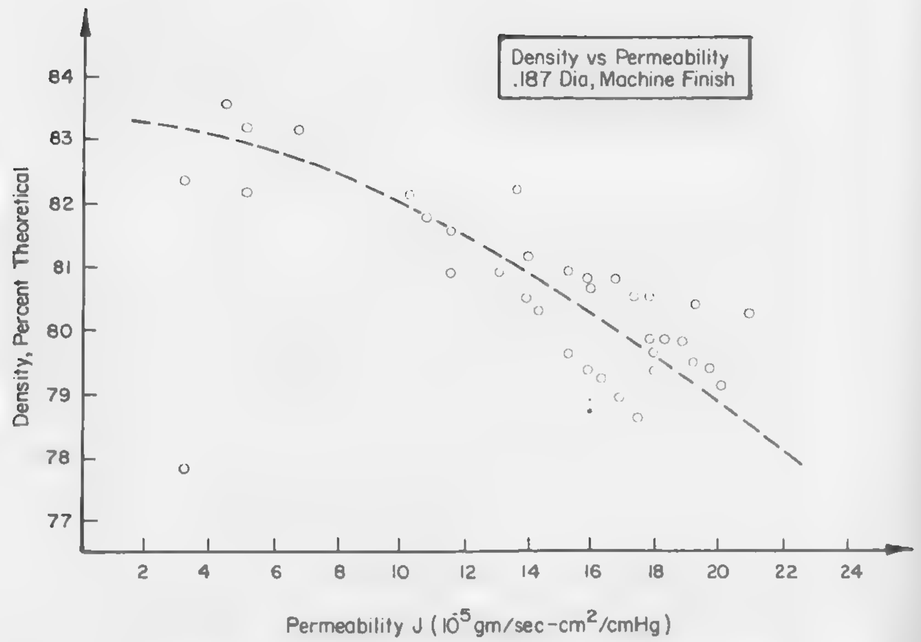


FIGURE 8 PERMEABILITY CHECKING DEVICE FROM 61-506

These variations in button permeability are being partially overcome at the present time by careful selection of buttons of similar characteristics.

ADVANCED TECHNIQUES OF PRODUCING POROUS MATERIALS

The following two advanced techniques are presently being pursued in an attempt to create porous materials whose characteristics can be duplicated:

1. Wire bundles
2. Spherical powders.

Both these techniques appear very promising as a means of producing porous ionizer materials of nearly perfect pore size and distribution. In the wire bundle method, tungsten wire of small diameter is wound on a mandrel. The bundle of wire is cut, opened up, and pulled into a tantalum tube. The tantalum tube is then swaged down about the wire bundle

so as to hold the wires into a close packed configuration. The encapsulated wires are sintered at a high temperature to bond them together, after which thin slices are cut from the bundle perpendicular to the wire axis so as to form the porous tungsten diaphragm. The pores in this instance are formed by the openings between wires (see Figure 9). The problem in this technique is to get all of the wires into perfect close packed configuration. A few small problems are also encountered in winding wire which is too fine for the eye to see.

The other technique of utilizing spherical powders allows the use of standard powder metallurgy methods. Spherical powders in a size range suitable for ionizer use have only recently become available. Present programs at producing ionizer materials from these powders appear most promising. Some of the problems encountered are: higher pressing pressures, higher sintering temperatures, and some difficulty in joining the porous material to the cesium box.

It is believed that either of the above techniques will offer the following advantages.

1. Uniform pore sizes and spacings
2. Uniform permeability
3. No blind pores

DEVELOPMENT OF JOINING METHODS FOR MATERIALS

Joining problems proved to be rather difficult to solve for this particular ion propulsion device as a result of the following stringent requirements for joining materials:

1. Low vapor pressure at high temperature
2. Cesium compatibility
3. High melting point
4. No infiltration of ionizer surface

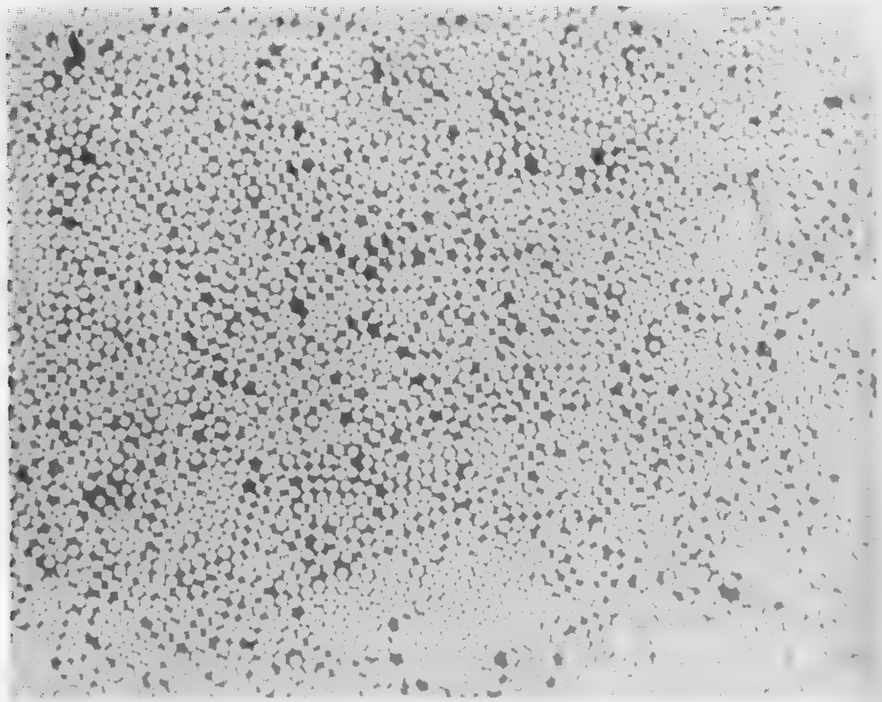


FIGURE 9 POROUS IONIZER PRODUCED BY USE OF 12 MICRON TUNGSTEN WIRE BUNDLE

Several joining methods were examined, including welding, brazing, and various mechanical seals. Brazing was selected as the method which appeared to satisfy the greatest number of requirements, and research was accordingly directed.

Brazing offered the following advantages as a joining method:

1. The joining operation could be performed in vacuum or inert atmospheres thus assuring a clean surface on the refractory metals.

2. At the moment of joining the components were at a high temperature and therefore free of stress.

3. The temperature of the porous ionizer surfcce could be accurately controlled during joining so as to prevent further sintering thereby resulting in permeability changes.

To carry out this research effort, a large vacuum furnace was designed and built under Air Force Contract No. AF 33(616)-6958. Figure 10 shows a few of the constructional details of the furnace. Note that the furnace is 3 ϕ, and uses tantalum or tungsten sheet as the resistor elements. The resistor elements are surrounded by 20 sheets of tantalum foil which serve as effective heat shielding. The present internal dimensions of the chamber are 6 in. diameter by 4 in. depth. This can be expanded to a 12 in. diameter by simply expanding the resistor elements and the shielding. Tungsten-Rhenium thermocouples are used in conjunction with a standard controller for temperature control.

The most critical and difficult of the joining problems was that of sealing the porous tungsten ionizer to the cesium box. The brazing operation is itself dependent upon the use of the surface tension of the joining alloy to create capillary flow of the braze material into the joint. However, in the case of the porous ionizer material, we were to attempt to braze the porous button to the cesium box, and during this process, to depend upon the joining material flowing around the porous ionizing surface forming a seal, while at the same moment preventing infiltration of the button. At first glance this might be compared to lifting one's self by the boot straps. However, one feasible approach which suggested itself, was that of finding an alloy or metal in which small changes in composition would result in a large variation in melting point.

The platinum group metals, platinum and ruthenium were tested as joining materials and it was found that gas-tight bonds could be effected between the cesium box and the porous material. After operating at high temperature in cesium vapor for a number of hours, however, it was found that these metals interacted with the ionizer material to create buckling at the joint which resulted in leakage and

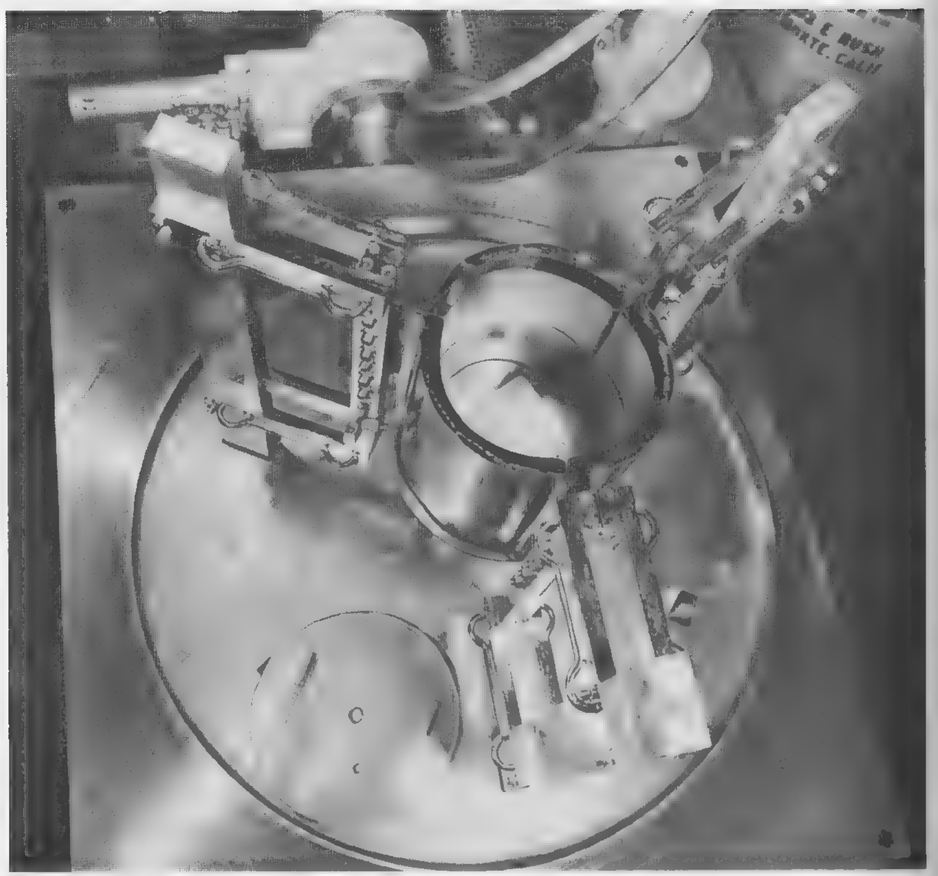


FIGURE 10 TOP VIEW OF 3 HIGH TEMPERATURE VACUUM FURNACE

distortion of the ion beam. After this initial brazing attempt a number of tests were run to determine the compatibility of several of the more common metals and alloys in liquid cesium. Carefully weighed samples were placed in the cesium reservoir prior to various ion engine test runs. After being exposed to the cesium environment for a number of hours, the samples were again weighed and the surfaces examined for signs of attack. These results were as follows:

TABLE I

CESIUM COMPATIBILITY TESTS
5 Hours in Cesium at 1375°C

Metal	Percent Weight Change
W	0
Pt	+0.08
Ta	0
Ni	0
Mo	+2.2
302 SS	0

The maximum pressure at which the ion engine may be operated is approximately 10^{-5} mm of Hg. Therefore, any structural material or joining alloy must exhibit a vapor pressure below this operating pressure at operating temperatures. The upper operating temperature for a number of materials is illustrated in Figure 11.

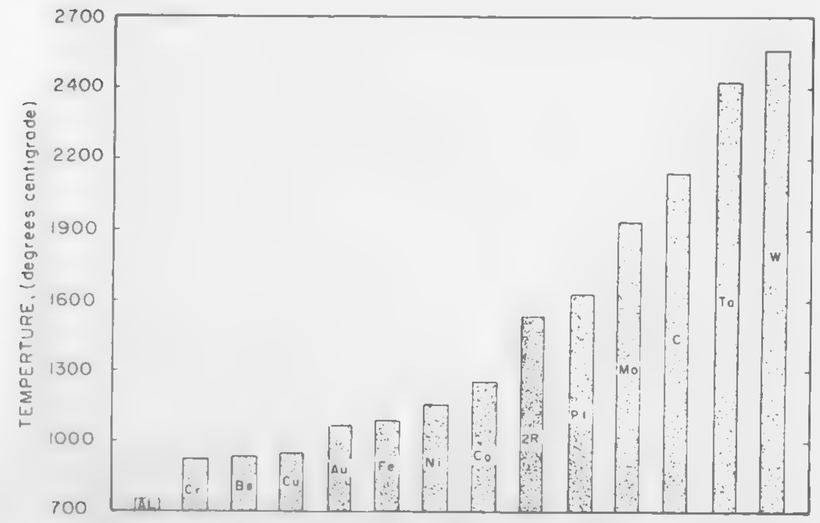


FIGURE 11 TEMPERATURE AT WHICH VAPOR PRESSURE IS LESS THAN 10^{-5} mm Hg

An examination of the phase diagrams of various alloy systems indicates that those of molybdenum-carbon and molybdenum-boron exhibited extremely steep liquidus curves corresponding to small compositional variations. Joining attempts were first tried utilizing the eutectic mixture of molybdenum-carbide and molybdenum powder as the braze material; however, the high melting point of 2200°C caused a considerable amount of sintering to occur in the ionizer material, with the result that permeability was reduced. Similar drawbacks were noted with the eutectic mixture of molybdenum boride and molybdenum powder. The illustrated phase diagrams in Figures 12 and 13 show the lowest melting point which might be expected with such mixtures.

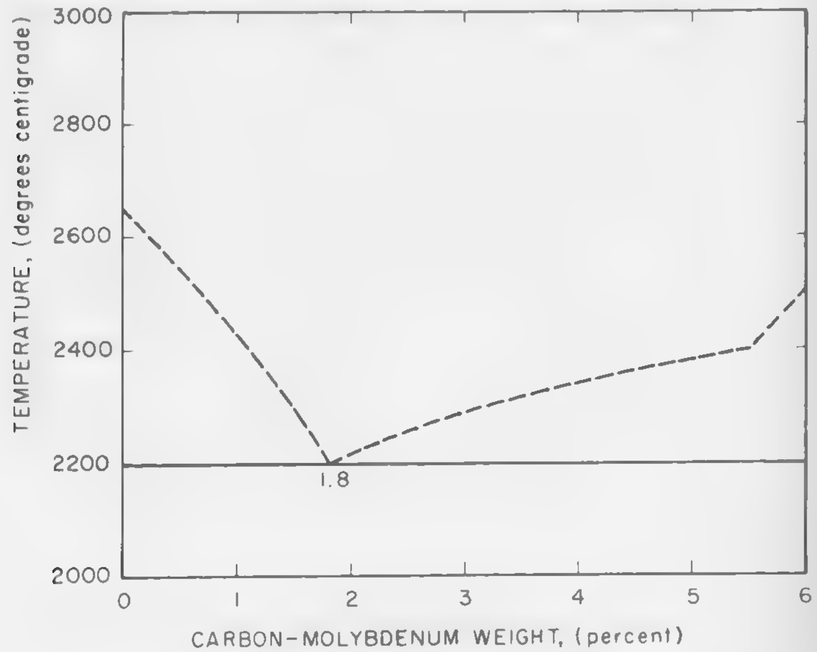


FIGURE 12 CARBON-MOLYBDENUM

Brazing studies made with the molybdenum-boron and molybdenum-carbon eutectics demonstrated one point, however; by careful temperature control, either of these two mixtures could be used to braze the porous tungsten ionizer to the cesium box without infiltration of the tungsten. The problem now remained of developing an alloy with these characteristics, but in addition having sufficiently low

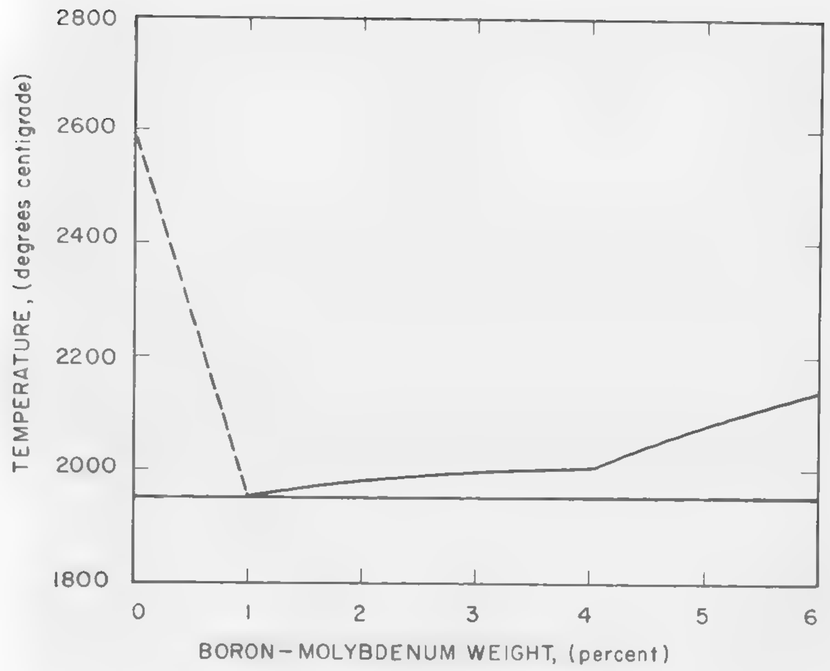


FIGURE 13 BORON-MOLYBDENUM

melting point so as to prevent sintering of the ionizers. An investigation of a ternary alloy system of molybdenum-carbon and boron was then initiated. A variety of these mixtures were evaluated with respect to melting point; smoothness of fillet, capillary flow, and lack of penetration of the porous tungsten. A ternary alloy of molybdenum-carbon and boron was developed under Air Force Contract AF 33(616)-6958 having a melting point of 1850°C. Photomicrographs of joints, made by this alloy appear to be primarily eutectic as shown by the photomicrograph in Figure 14. You will note that the penetration of brazing alloy into the porous tungsten is extremely shallow. Porous buttons joined by the use of this alloy have been run in vacuum at temperatures up to 1200°C for times up to 200 hours with no indication that the work function of the ionizer has changed or that further penetration of the braze material into the ionizer has occurred.

We have found during the course of our brazing alloy investigation that alloys containing nickel, cobalt, iron, or platinum when in contact with the ionizing, rapidly diffuse over the surface, changing the work function, and accelerating sintering of the porous material. However, alloys of

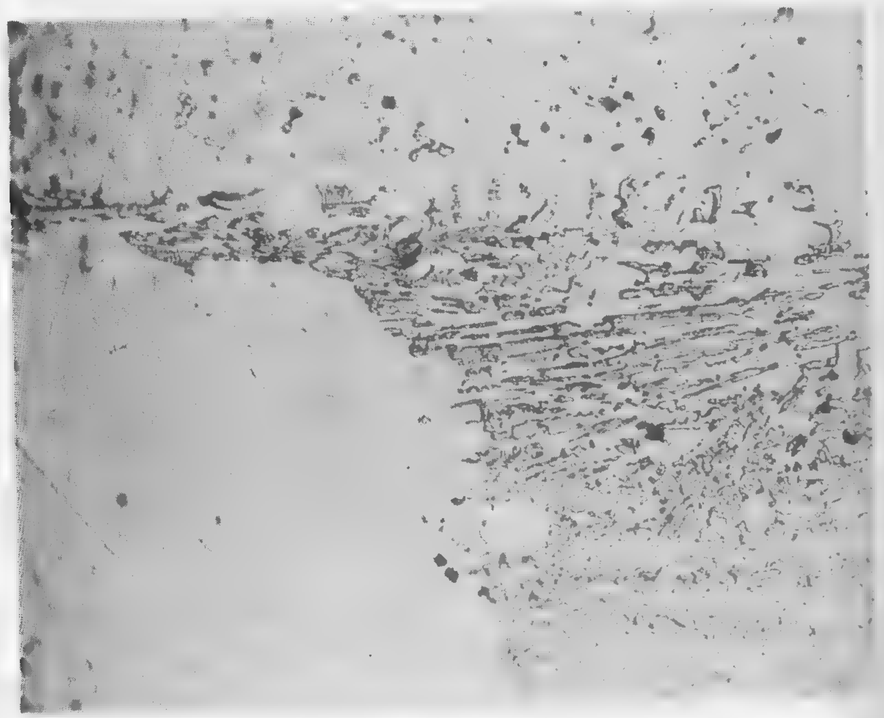


FIGURE 14 BRAZE BETWEEN POROUS TUNGSTEN AND MOLYBDENUM CESIUM BOX MADE WITH TERNARY OF Mo-C-B.
The porous tungsten is at bottom of the picture and the braze material at upper left.

these metals may be used for other joining purposes. For example, a number of useful alloys of differing melting points may be made of varying proportions of molybdenum and cobalt. Two of the alloys are used for fabrication of the cesium box. One alloy composed of 40% cobalt and 60% Mo and melting at 1540°C is used to braze the front surface of the cesium box to that of the rear. The other alloy melts at 1340°C and is composed of 60% Co and 40% Mo and is used for brazing the heater to the ionizer assembly.

The joint between the tantalum cesium feed tube and the ionizer is brazed with the 60% cobalt alloy. The low temperature end of the tantalum feed tube is joined to the bellows assembly by the use of an 88% gold - 12% nickel alloy. This alloy melts at 1750°F, has excellent cesium compatibility,

and low vapor pressure. Silver manganese was tried as a joining material for this joint but failed due to evaporation of the silver.

During the assembling of the ionizer, the sequence of brazing alloys is selected to enable each succeeding joint to be made at a reduced temperature. The ionizer is assembled in the following order - first, the porous tungsten buttons are brazed into the front plate of the cesium box using moly-carbon-boron alloy. After checking to make certain that all buttons are tight, this plate is joined to the cesium box by the use of the moly-cobalt alloy. The tantalum tube and heater are attached last to complete the assembly.

All brazing operations are performed in a vacuum of at least 4×10^{-4} mm of mercury to avoid embrittlement of the tantalum delivery tube by nitrogen or oxygen.

The cesium delivery tube in early engine designs was of 0.005 inch wall molybdenum tubing. However, it was found that after a short time at operating temperature, considerable grain growth had occurred, and the thin wall of the tube became extremely fragile--so much so in fact, that leakage appeared to occur spontaneously during the engine runs. Tantalum has proven quite satisfactory for this application providing that carbon, oxygen, or nitrogen are avoided while at high temperatures. For this reason the heat shielding selected for use about the ionizer must not outgas excessively when heated to high temperatures, or must not contain any carbonaceous material capable of reacting with the tantalum delivery tube. Tantalum foil in multiple layers has proven quite satisfactory as an insulating material. It is necessary that each layer of foil be separated from the other if possible. Points of contact between tantalum at high temperature in a vacuum environment rapidly sinter together to form a path of continuous heat conduction.

Various techniques have been used to prevent this sintering from occurring; these include painting the tantalum surfaces with various refractory oxides, placing

refractory spacers of various kinds between the plates, and chemical treatment of the tantalum surface. A satisfactory proprietary method has been developed for solving this problem.

The present insulators are made of sintered alumina. These have a metallic base brazed to them so that it can be brazed to the ion engine support plate, thereby furnishing a gas-tight seal through which the high-tension electrical leads are introduced to the engine. The condensation of cesium vapor on these insulators can render them conducting; two methods are used to prevent this. One method utilizes an encapsulating stainless steel sleeve which slips over the insulator to prevent the impingement of cesium vapor against the insulator. The second method employs the use of special glazes we have found which prevent the condensation of a continuous film of cesium over the insulator.

Because many insulators have been manufactured with cracks in them, we have resorted to X-ray inspection techniques as a means of eliminating defective insulator suppo

ELECTRODE MATERIAL REQUIREMENTS

The operating life of the ion engine at the present time appears to be limited to the life of the accelerating electrodes. Sputtering, which occurs on these electrodes as a result of ion bombardment, eventually enlarges and distorts the annular openings through which the ion beam passes to the point that engine operating efficiency falls off drastically. At present, accelerating electrode life is limited to a few hundred hours at the most. This may be expected to increase as improved ionizer materials, along with improved focusing techniques are developed. The ideal electrode material should have the following characteristics.

1. Lowest possible sputtering rate
2. Complete insolubility in the porous ionizer material

3. A thermal coefficient of the expansion fairly close to that of the ionizer assembly.

Sputtering data was accumulated for several materials exposed to cesium ion bombardment; ion energies in the range of 2 to 5 kilovolts were employed. This corresponds to the ion energy from present EOS motors so that sputtering in this range is of particular interest. As can be seen in Figure 17 a definite trend is evident. Laegreid and Wehner have pointed out that there appears to be a correlation between sputtering activity and the number of electrons present in the d shell of the target material, the increase in the number of d shell electrons being accompanied by an increased sputtering rate. The sputtering work at EOS has shown this to be the case. Table II shows some of the materials tested and their number of d shell electrons. Sputtering measurements were made by allowing the beam from one of our motors to impinge on a holder containing prepared samples of several materials. Figure 15 shows the arrangement, with samples gripped by metal fingers. The samples were carefully cleaned and weighed before and after each run. Sputtering ratios were then obtained from the measured weight loss and a measurement of ion beam current density. Photomicrographs of a typical sputtered material are shown in Figure 16. Figure 16a shows a nickel sample before sputtering. Figure 16b shows the same sample after bombardment by a total integrated current density of 0.36 coulombs per square centimeter, at a cesium ion energy of 2 kv. Figure 16c shows a different nickel sample after bombardment by a total integrated current density of about 20 coulombs per square centimeter. All photomicrographs were taken at a magnification of 60x.

Of the sample materials tested, beryllium showed the lowest sputtering rate and copper the highest. The materials tested, listed in order of increasing sputtering susceptibility were: beryllium, titanium, tantalum, molybdenum, tungsten, nickel, silver, gold, platinum, palladium, and copper.

TABLE II

SPUTTERING DATA

Target Material	Atomic Weight	Number of d Shell Electrons	Weight loss of Typical Sample (milligrams)
Titanium	47.90	2	1.3
Nickel	58.69	8	3.6
Copper	63.54	10	6.2
Molybdenum	95.95	5	3.7
Palladium	106.70	10	10.0
Silver	107.88	10	9.9
Tantalum	180.88	3	6.9
Tungsten	183.92	4	8.2
Platinum	195.23	9	23.5
Gold	197.20	10	9.9

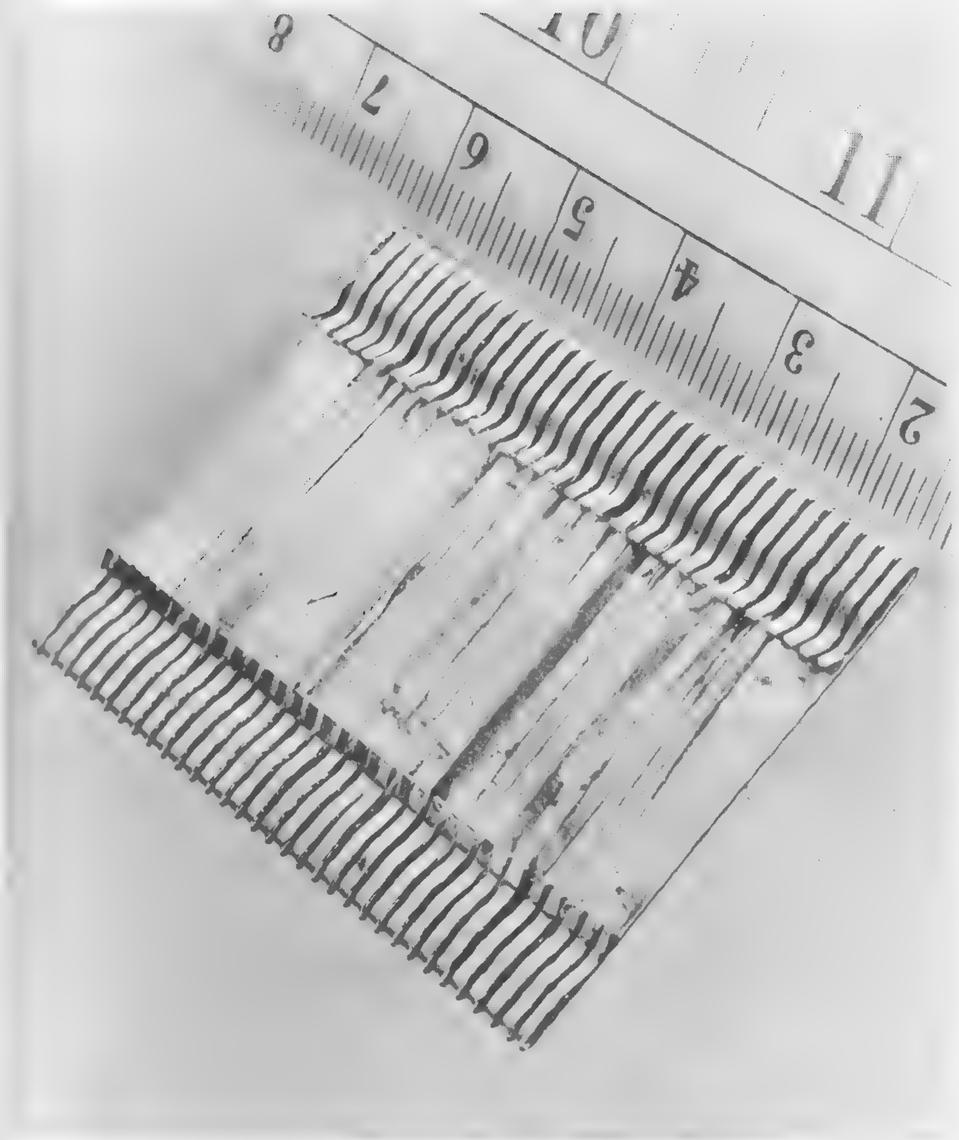


FIGURE 15 SPUTTERING SAMPLES



(a)

(b)

(c)

FIGURE 16 PHOTOMICROGRAPHS OF SPUTTERING SAMPLES

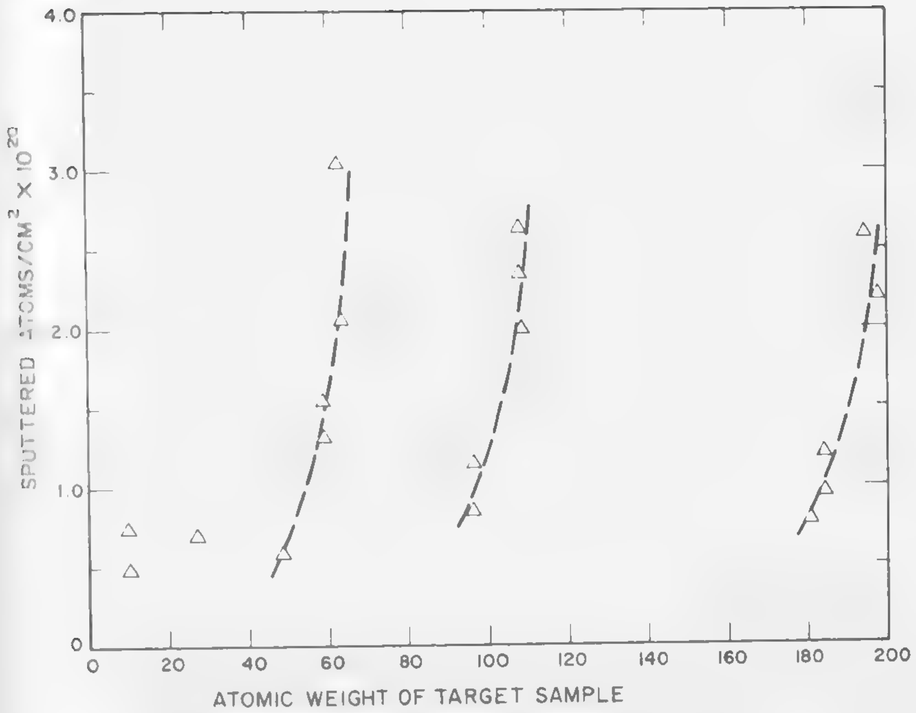


FIGURE 17 SPUTTERING VS ATOMIC WEIGHT OF SAMPLES

Several factors limited the accuracy of this experiment. First, gas pressure near the test sample was as high as 10^{-5} mm Hg and considerable oxygen was available to form layers on the surface of the sample. These layers may greatly influence the sputtering rate. Also, measurement of the incident ion current was difficult due to secondary electron emission and ion reflection at the surface of the sample. The relative values of the sputtering ratios given in Table II are not affected by this.

For use in an accurate evaluation of sputtering as a factor in engine lifetime, measurements must be made more accurate and extended to voltages up to 20 kv (ionizer - accelerator voltage difference), temperature of sputtered surface to 800°C, and various angles of incidence.

As an example of the activity of the sputtering process, consider a flat copper plate bombarded at normal incidence by cesium ions of 2000 electron volt energy. At a current

density of 10 ma/cm^2 the erosion rate would be of the order of 0.005 inches/hour. While this example is only an idealized case and not a true representation of the complicated geometry of ion motor electrodes, it indicates the magnitude of the sputtering problem. In some instances the erosion rate could be much higher, especially in cases where the angle of incidence is large.

CONCLUSIONS

1. Ion propulsion devices impose unique material problems not encountered in other propulsion or electrical devices.

2. Physical as well as electrical characteristics of the materials must be developed to a high degree if optimum efficiency and lifetime of these devices are to be achieved.

3. Additional research effort must be directed toward achieving more uniform ionizer materials of optimum pore size and spacing.

4. Basic research studies must be made of the mechanism of sputtering with the ultimate objective of increasing the lifetimes of engine electrodes.

5. Progress made in the past two years on the solution of ion engine materials problems has allowed the fabrication of several engines which have proven the value of these devices as a means of propulsion.

MATERIALS REQUIREMENTS FOR PLASMA PROPULSION

D. W. Gates
Ceramic Engineer
Research Projects Division
George C. Marshall Space Flight Center

ABSTRACT

A brief description is given of the engines under discussion, with some of the operation parameters pertinent to the selection of materials. Various propellants and their effects are noted. Some areas beyond present-known technology and/or desirable attributes are given to indicate the desired direction for future research and development. Materials problems external of the engine are mentioned, but concentration is on the electrode and nozzle considerations.

With an acceptable solution to the problems associated with low electrical power and high thrust-to-power ratio thrust devices, the "arc jet" is about ready for flight testing in the progress toward early use in attitude and position control systems.[1-4] The major problem areas beyond the basic design might be:

(1) nozzle, electrode, insulator, and associated thrustor materials
(2) starting or rather restarting for 10,000 cycles
(3) propellant feed and storage (especially cryogenic)
(4) power supply and in particular coupling of battery or alternator to the arc.

Each of these areas has materials problems necessary of solution to achieve a unit with the established reliability and reproducibility necessary for the use of the "arc jet"

as an integral part of a space vehicle. Some of the parameters of interest might be noted as:

(1) temperature - liquid hydrogen (14°K) to arc core (above 10,000°K for hydrogen ions and double to triple this for electron temperatures)
(2) time of operation - cyclic during a period up to two years for about 3% of the total time of the mission
(3) power requirements - 1 to 5 KW for attitude and position control - 20 to 40 KW and up for orbital transfer and supply missions as power supplies become available[5, 6]
(4) compatibility with propellant - for the present, hydrogen and ammonia are probable propellants, and lithium may soon be available.[7] Some of these "arc jet" designs which have been recently published include the following:

    (a) rail-type 3-phase AC (Fig. 1)
    (b) vortex stabilized DC with propellant injected at nozzle for cooling (Fig. 2)
    (c) vortex stabilized DC with propellant injected at rear (Fig. 3)
    (d) vortex stabilized DC with extended nozzle section (Fig. 4).

Presently because of power supplies and development times required it is believed that 1 to 3 KW is the immediate future (2 or 3 years) and that both batteries with recharge capabilities and AC must be ground and flight tested concurrently. Such a conclusion immediately forces the materials problems of the thrustor: very small nozzle diameters, many cyclic restarts, low Reynolds numbers, available size (hence space) for sophisticated cooling designs, reproducibility of parts, propellant limited to hydrogen because of temperatures associated with high specific impulse of ammonia and other propellants, maximum temperature of gas and actual wall temperature achieved through film cooling and conductivity of gas at operating conditions, and always light-weight and extreme reliability which indeed approaches perfection. Specifically what follows will be directed to the area of the low power unit.

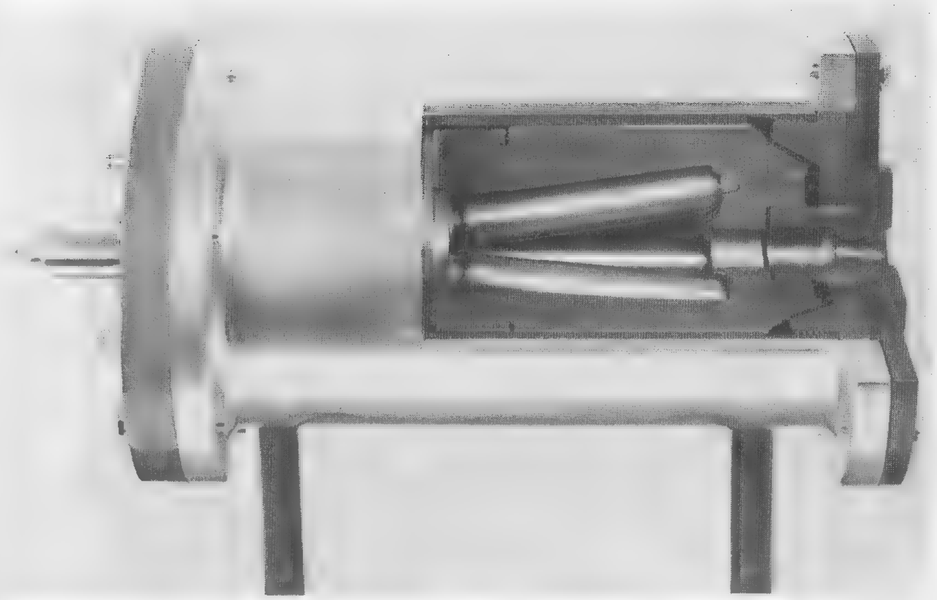


FIGURE 1 3-PHASE AC "RAIL-TYPE" ARC ENGINE



FIGURE 2 DC ARC ENGINE WITH PROPELLANT INJECTED AT FRONT

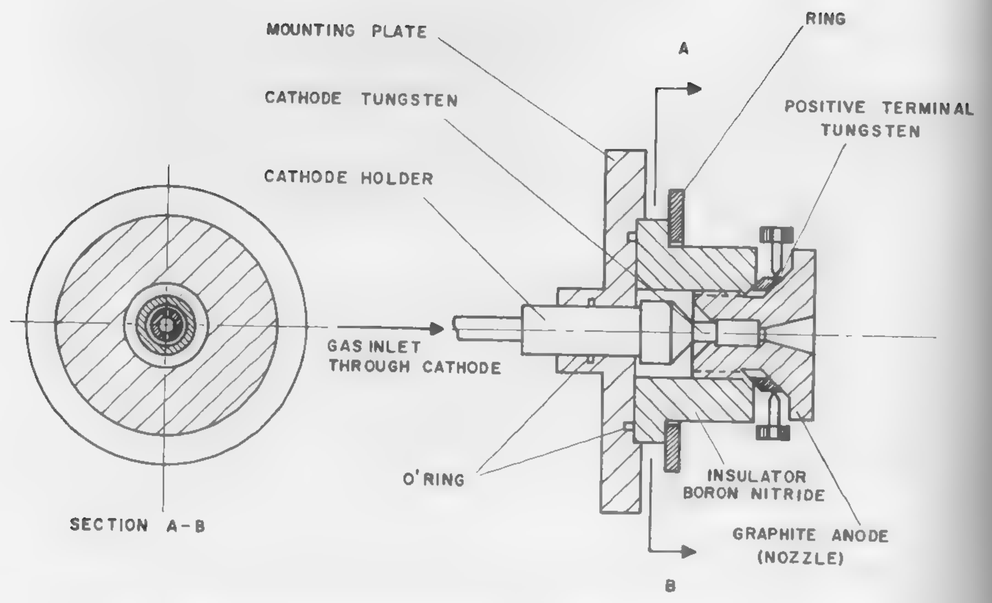


FIGURE 3 DC ARC ENGINE WITH PROPELLANT INLET THROUGH REAR ELECTRODE

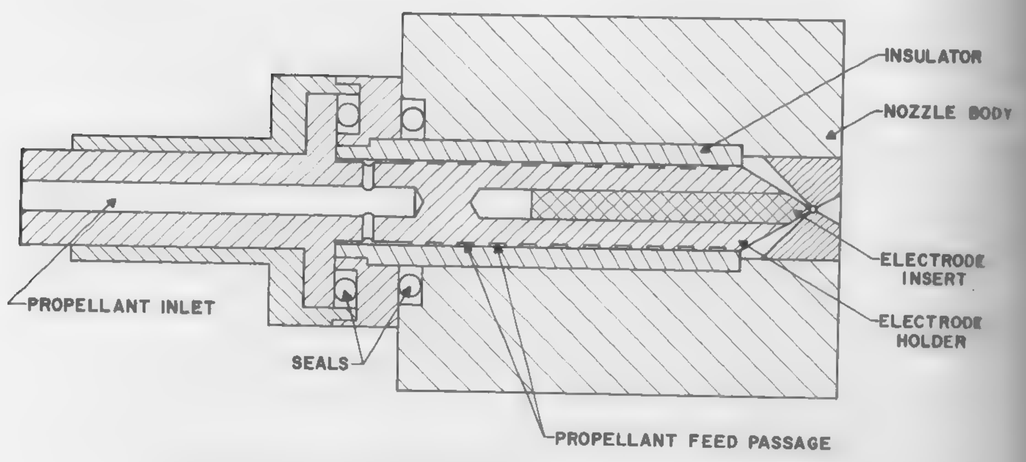


FIGURE 4 DC ARC ENGINE WITH EXTENDED NOSE SECTION

It is well known that conductivity increases with the temperature of hydrogen and that higher power in the gas (enthalpy increase) leads to higher conductivity to the wall. But at any enthalpy, at least in the arc filament complete ionization must take place with associated temperatures of the electrons of about 30, 000°K. Materials used in conjunction with exposure to this level of temperature require that times be very short, i. e. the arc striking point must be kept moving by some method, as vortex gas flow or magnetic field. It is also desirable to have the wall of a material of high conductivity so that local hot spots are quickly cooled. If in the areas of anode and cathode fall the heat transfer to the gas could be maximized, the gas temperature and hence adjacent material temperature would be minimum. Core or filament temperature necessary for ionization of lithium (when used as propellant or contaminant) is lower than hydrogen, hence the interest to obtain lower peak temperatures at equivalent enthalpies, if mixing can be obtained (Table I). Storage volume is low for lithium because of relatively high specific gravity of the light metal, but I_{sp} possibility would indicate use as contaminant and this only if associated reactions (erosion problems of compatible materials) are minimized.

The chart (Table I) of I_{sp} at the 2 KW level indicate what is likely some sort of maximum, and the present measured losses are shown on Fig. 5. [1] Certainly hot wall operation is mandatory to obtain some of the 40-60% cooling water loss for the low power thrustors, and regenerative cooling passages for the incoming propellant should reduce the indicated waste energy to a more nearly tractable value.

There are certain advantages in locating the nozzle away from the power and propellant connections (Fig. 4), such as:

(1) removal of the heat source from seals for the incoming propellant
(2) removal of the heat source from the electrical connections

TABLE I

PROPERTIES OF SELECTED PROPELLANTS

Propellants	Operating Volts at 1 atm. Pressure	Enthalpy to Ionization (Kcal/gm) x 10^{-3}	Enthalpy to Ionization (Kcal/gm-mole) x 10^{-3}	I_{sp} at Constant Enthalpy of 50,000 (Kcal/gm)
Hydrogen	100	217	217	1150
Water	64	18	324	--
0.1% Li in Hydrogen	20/25	*	--	1100**
NH_3	75	27	270	700**
Lithium	--	8	56	900
Helium	60	17	64	1380

* Enthalpy to first ionization will be approximately that of lithium, providing the contaminant will furnish sufficient number of charged particles to carry the current.

** Approximate

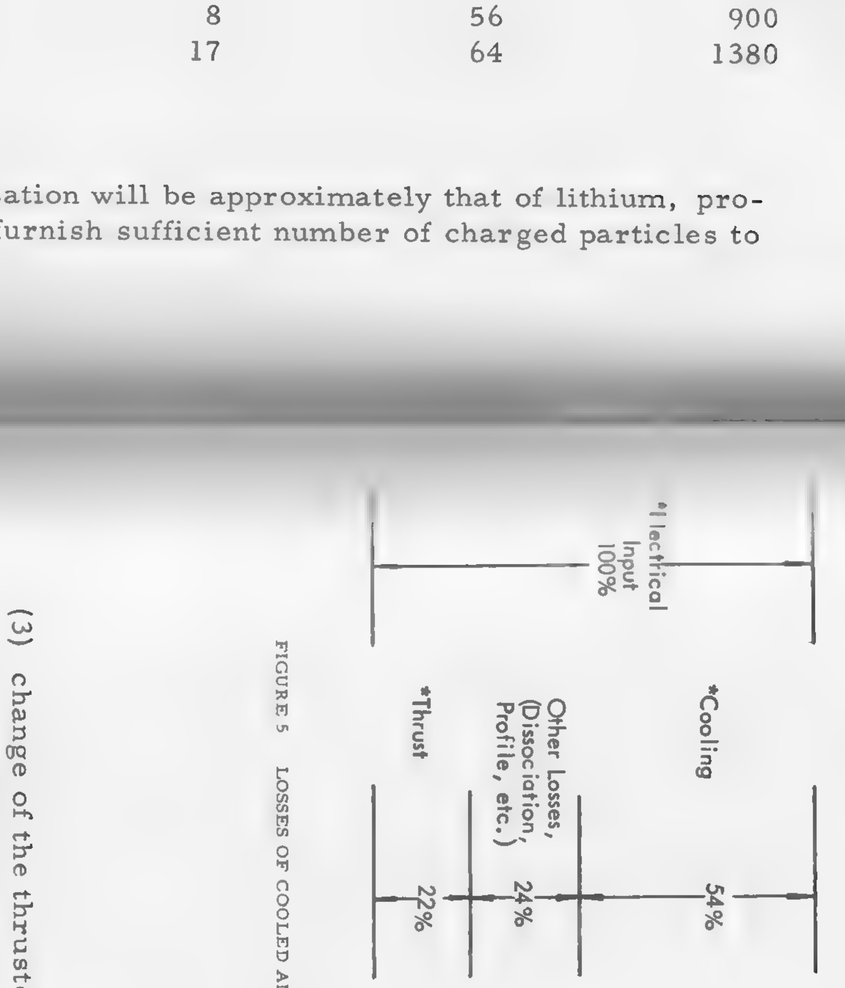


FIGURE 5 LOSSES OF COOLED AND HOT WALL DESIGN ARC ENGINES

(3) change of the thrustor anode body from carbon to molybdenum or tungsten and elimination of of the anode connection ring and its problems of good electrical contact

(4) larger area to dissipate heat through radiation and possibility of introduction of regenerative cooling passages in the extended section

(5) lower operating temperature of the electrical insulator adjacent to the rear center electrode

(6) in conjunction with (5) the possibility of introducing "pyro-deposited" materials with thermal conductivity maximum in the direction of propellant flow and minimizing electrical losses.

Though the over-all mass of the device is increased, the many advantages and more reliable operation outweigh the additional weight. Diameters may be further increased

through the use of lower density materials, to keep down the weight, while gaining the larger surface and greater emitting area. "Pyro-deposited" boron nitride or similar material would help in allowing heat flow back to the incoming gas and maintaining low electrical conductivity across the section. The laminar structure of these materials resulting from the process is a natural effect of the method of application, and the properties that might be expected are presently being investigated to determine the feasibility of the application to the insulator.

Another loss in early designs was in the mixing chamber just after the arc. This area provided large areas of wall loss, and has now been largely eliminated. Consideration has also been given to the 40-60% loss of power from the batteries in a resistance load for DC operated arcs.[8] By proper power supply this has been reduced to 11-15% as shown by Boehme and Cagle.[9] A comprehensive treatment of this subject will be presented in a forthcoming paper at an early ARS meeting, but briefly the open circuit voltage is reduced by a control circuit of high efficiency. As well as reducing the problem of the extra batteries needed to supply the higher voltage open circuit requirement, the heat dissipation from the load resistor is reduced to a small fraction. Operation with this device has been accomplished, and results are excellent. Due to extremely fast development time, the reporting of this "advance in the art" is only now being made ready for publication. One of the sources of energy that is lost to thrust is that in dissociation and ionization in the gas that leaves the nozzle. Much effort is not being placed on the recovery of this energy of recombination in the nozzle, though the method of converting to useful kinetic thrust is still obtuse, and indeed some results seem to indicate that the amount may be small.[10] Some recombination may be able to be achieved by the use of wall catalytic activity.[11-13]

Some of what is now needed in materials is shown in the following outline:

(1) A low-weight-loss high-operating-temperature material. It is stated thus to emphasize that for a given BTU input per foot square second, a weight loss below some level

will be minimum, but above this level ablation must occur.[14] Below this achieved surface temperature the weight loss due to erosion can not be entirely eliminated, but by maintaining the surface below the ablation temperature, long life and minimum weight loss may be achieved. Such a material may be used as the nozzle in its entirety or as an insert to hold down over-all weight. Materials that suggest themselves and some of the considerations are:[15]

(a) tungsten - melting point 3410°C, good thermal conductivity (0.245 at 1727°C, cal/cm^2/sm/sec/°C, low electrical resistivity at operating temperature (34 microhm-cm at 1000°C), good tensile strength, high specific gravity, low emissivity. Generally the material used for hot-wall design nozzles at least as an insert.

(b) molybdenum - melting point 2610°C, good thermal conductivity (0.35 cal/cm^2/sec/°C), low electrical resistivity at operating temperature (81.4 microhm-cm at 2622°C), good tensile strength, high specific gravity, low emissivity. Generally the second choice to tungsten for nozzles.

(c) graphite - sublimes at 3500°C, fair thermal conductivity (0.01 to 0.07 cal/cm^2/cm/sec/°C), fair electrical resistivity at operating temperature (78 to 140 microhm-cm at 1600°C), low tensile strength, high emissivity, low specific gravity. Usually used for laboratory models because of ease of machine work, but weight loss in operation needs improvement.

(d) hafnium boride and tantalum boride - melting points 3250°C and 3120°C respectively, thermal conductivity will probably be fairly low, electrical resistivity in the range of tungsten and molybdenum. Forming of parts is a difficulty, and little information on properties.

(e) tantalum carbide - melting point 3875°C, electrical resistivity low, thermal conductivity fairly low. Spalls in operational trials.

(2) A similar material with the specific properties necessary for the electrical insulator to surround the rear center electrode and allow for good thermal conductivity away from the electrode tip to the incoming gas, while maintaining high electrical resistance through the cross-section at operating temperatures. Some of the materials considered and some of the difficulties encountered to date are evident in the following partial list. It might be noted that the peak operating temperature is not as severe a requirement for the electrical insulator as for the nozzle or insert, and cooling can be provided. However, thermal shock stability in cyclic operation (after cooling by gas flow is stopped) and thermal expansion to match surround for good gas flow are necessary.

(a) hafnium carbide - melting point 3887°C, electrical resistivity high, obtaining samples may be a problem.

(b) beryllium oxide - melting point 2570°C, electrical resistivity is high (8×10^8 ohms per cm at 2100°C) and both resistivity and thermal conductivity (0.04 cal/cm^2/cm/sec/°C at 1400°C) are able to be made highly directional. Thermal shock properties should be excellent, but present supply is apparently difficult, and forming is a specialty.

(c) boron nitride - melting point 3000°C (but practical limit due to binders is much lower), electrical resistivity is high (10^7 ohm-cm at 1000°C), thermal conductivity fairly low (0.04 to 0.12 cal/cm^2/cm/sec/°C), thermal shock properties good, but strength rather low. Due to ease of machining and simple forming from bulk this is usually the immediate choice for the insulator, unfortunately specifications for the pieces to be used are still a difficulty, better quality control for this specific end use is desirable. Pyro-deposited boron nitride may facilitate the optimization of directional properties.

(3) For fabrication of the cryogenic tankage is needed a weldable, low conductivity, light-weight (especially in the case of the larger volume needed for hydrogen) material that is not shock sensitive at the storage temperature during launch vibration and shock loading. Titanium is

presently used at this early stage of design. If higher internal pressures are used, stainless may be a contender as thin wall structures become apparent. As the amount of propellant used decreases below the bleed off rate, better insulation is necessary and long time cryogenic storage becomes a prime consideration in the system. This may indeed force the use of other propellants with a higher bulk density storage or an alternate source of hydrogen such as water (necessary for the crew) and the use of the oxygen for addition to the air supply.

(4) All parts must be vacuum stable and with as low vapor pressure as possible at operating temperature.

From this brief outline it may be seen that many problems remain, certainly optimization for a specific mission is yet to be accomplished. We are now at the early stage of the automobile in that the machine runs, but your wife has not yet tried it out. Space may be a difficult marriage, but flight testing will establish the areas requiring immediate application of effort toward useful systems.

BIBLIOGRAPHY

1. Heller, G. B. and B. P. Jones, Survey of Arc Propulsion, paper presented at the Space-Nuclear Conference, 3-5 May 1961.

2. Heller, G. B., The Plasma Jet as an Electric Propulsion System for Space Application, 14th Annual ARS Meeting, Washington, D.C., 16-20 Nov. 1959.

3. Heller, G. B., Propulsion for Space Vehicles by the Thermodynamic Process, Ninth Tripartite AXP Conference, Quebec, Canada, 20 April-1 May 1953.

4. Page, R. J., R. D. Buhler, W. A. Stoner, and P. S. Masser, Arc Plasma Thrustor Studies, 15th Annual ARS Meeting, Washington, D.C., 5-8 Dec. 1960.

5. Stoner, W. A. and J. Rosener, Investigation of a Thermal Arc Jet for High Specific Impulse and High Power Level, PTL-12-459, 26 June 1961.

6. Masser, P. S. and J. Rosener, Advanced Research and Development of a 30 to 60 KW Plasma Jet Thrustor, PTL-12-440, 26 June 1961.

7. Noeske, H. O., The Lithium-Hydrogen Bi-Propellant Plasmajet, Rocketdyne, Canoga Park, California, 1960.

8. Graff, Charles B., Circuitry for Electric Arc Engines, M-RP-INT-61-24, December 13, 1961. (Private communication).

9. Boehme, R. and G. Cagle, DC Arc Power Supply, paper to be presented at March 1962 ARS Meeting.

10. Chen, Che-Jen, High Temperature Gas Recombination Effects on Supersonic Nozzle Flow - Theoretical and Experimental Study, Reports on Contract NAS 8-844, to December 1961.

11. Wood, B. J. and H. Wise, "Diffusion and Heterogeneous Reaction. II. Catalytic Activity of Solids for Hydrogen-Atom Recombination," Jnl. Chem. Phys., Vol. 29, pp. 1416-1417, 1958.

12. Goulard, R., On Catalytic Recombination Rates in Hypersonic Stagnation Heat Transfer, paper presented at the ARS 12th Annual Meeting, New York, N. Y., December 2-5, 1957, and revised July 1958.

13. Amdur, I., "Recombination of Hydrogen Atoms," Jnl. Am. Chem. Soc., Vol. 60, pp. 2347-2355, October 1938.

14. Steurer, W. H., Criteria in the Selection of Materials for High Temperature Structures, paper presented at the 3rd Symposium, High Speed Aerodynamics and Structures, San Diego, California, 25-27 March 1958.

15. McKenna, Q. H., The Use of Refractories for Very High Temperature Applications, PLR-69, 25 May 1960, Revised December 1960.

MATERIALS REQUIREMENTS FOR NUCLEAR RAMJETS

Harry L. Reynolds
Assistant Division Leader Pluto
Livermore, California

ABSTRACT

The nuclear ramjet, as presently conceived, is an unmanned missile traveling at sea level at a velocity in the vicinity of Mach 3, approximately forty miles per minute. Stagnation temperatures are about 1050°F at this velocity. Material requirements for the air frame are similar to those of any supersonic airframe with the exception that weight is a minor consideration and temperatures somewhat higher than stagnation are achieved in the vicinity of the reactor due to radiation heating. The reactor is made of a homogeneous mixture of beryllium oxide and uranium oxide. These ceramic pieces operating at temperatures in excess of 2000°F are held together by an assembly of high temperature nickel base alloys and cooled refractory metals such as molybdenum and niobium. The first reactor in this program has recently been tested at the Nevada proving grounds. A description of this reactor and the test facility will be given together with the materials requirements and performance.

INTRODUCTION

The Pluto program was established at the Lawrence Radiation Laboratory by the AEC with a goal of showing the feasibility of a nuclear reactor which would be able to propel a supersonic ramjet missile. Feasibility has been defined as the successful ground operation for short times of

a reactor with the desired characteristics, together with suitable laboratory experiments to allow extrapolation to the desired lifetime. With the exception of the lifetime and the expected missile accelerations, the reactor will perform on the ground in the same environment as expected in the missile flight.

Although the nuclear ramjet can be designed for flight at altitudes from sea level to over 100,000 ft, it possesses a unique ability for supersonic flight over long distances at sea level. Overcoming the supersonic missile drag at sea level requires a large amount of energy, which can be supplied only by a reactor if flight over significant distances is required. The present Pluto program is directed toward the design of a reactor for sea-level flight.

The nuclear ramjet consists of an inlet diffuser followed by a single-pass, straight-through heat exchanger (the reactor) and an exhaust nozzle. The purpose of the diffuser is to reduce the velocity of the intake air and recover as much of the ram, or stagnation, pressure as possible. In passing through the reactor, heat is added to the air. The random heat energy is changed into directed motion in the nozzle, resulting in an increase in air momentum and a net thrust for the missile. The sea-level nuclear ramjet develops a maximum thrust in the vicinity of Mach 3. This is illustrated in Figure 1, where thrust is plotted as a function of the flight Mach number for several reactor temperatures. The design has been optimized at each velocity and temperature. It is apparent that the ramjet performance increases rapidly with temperature increase and that a Pluto reactor will be a high-temperature reactor by today's standards.

The choice of material for the reactor is severely restricted. The material must have reasonable strength and resist oxidation at elevated temperatures. In addition, it must be a good moderator and a poor neutron absorber. Moderating ability is required because a fast, unmoderated reactor would be prohibitively expensive in terms of nuclear fuel. The only material that can meet the requirements for the moderator is the ceramic, beryllium oxide. Uranium

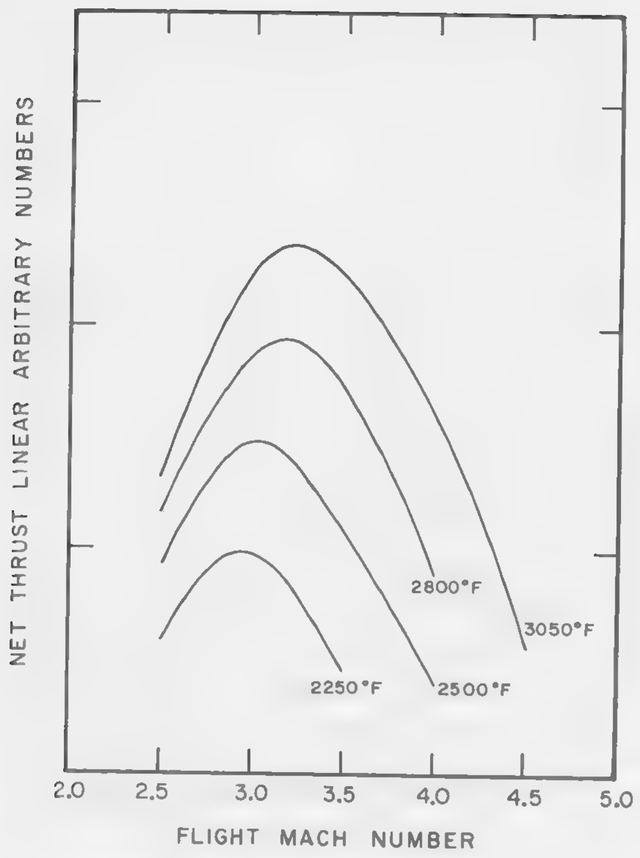


FIGURE 1 NUCLEAR RAMJET PERFORMANCE

forms a refractory oxide, UO_2, which unfortunately turns to a volatile oxide at high temperatures in air. Cladding is impractical at these temperatures, and thus the fuel is mixed homogeneously with the BeO moderator.

The reactor radiation creates a problem due to the large gamma and neutron heating in non-nuclear components both in and near the reactor. As an example, power densities in metallic structures in the reactor can be several times larger than the power density in the fuel elements themselves. Also, radiation damage of some materials can have serious consequences. These problems are under investigation by computation and experiment.

The mechanical designer is faced with formidable difficulties. The pressure drop in the direction of the air

stream results in a force of several hundred thousands of pounds tending to push the reactor out of the nozzle. In addition, accelerations of many g's due to air turbulence in flight must be reacted. The materials for supporting structures are limited in volume and nature because of neutronic requirements and high temperatures. Cooling air has a minimum temperature of 1000°F. The usual weight limitations are also present for structural elements. The fuel elements are ceramic and thus are brittle. Methods of design had to be utilized which did not rely upon ductility to take care of inevitable errors in fabrication and design.

After suitable laboratory experiments and tests, it was deemed desirable to attempt the solution of all of these problems (and others unmentioned such as thermodynamics, neutronics and fluid flow) in a reactor to be tested upon the ground.

For a Mach 3 sea-level ramjet, air is supplied to the reactor at a pressure of approximately 350 psi and a temperature of about 1000°F. Flow rates greater than 2000 lb/sec can be achieved. It is immediately apparent that the ground-test facility, and in particular the air supply, for such a reactor is large and complex. Also, a considerable amount of BeO is required for a full-scale reactor. At the beginning of the program, the fabrication of BeO was expensive and time-consuming.

Therefore, it was decided that the first ground test would be of a small reactor, so that the air supply and BeO requirements would be minimized. The small, high-temperature fueled core of this reactor would be tested to obtain data on the materials, physics, and engineering required for the design of the full-scale reactor. To enable the reactor to reach criticality, the core would be surrounded with a thick carbon reflector operating at room temperature. In addition, the reactor controls would be placed in this reflector so that the problem of operating control rods in a reactor at high temperature could be avoided in the first tests. The reflector with controls has no bearing whatsoever upon the missile reactor, since it is present only to satisfy neutronic requirements for the small test core.

This concept is called the Tory II-A reactor which has been operated a number of times. The Tory II-C reactor, to be tested after the II-A series, will be a full-scale, missile-like reactor and is intended to demonstrate the feasibility of the Pluto ramjet reactor.

The facility for testing the reactors is at the Nevada Test Site. A map of the facilities appears in Figure 2. The reactors are tested on unshielded railroad flat cars which can be remotely moved between a test bunker and a disassembly facility. Electrical, air, and water-cooling connections and disconnections to the test bunker can be made remotely. The control room is located approximately two miles from the test bunker. The shielded test bunker contains electronic and air-supply equipment, which must be located close to the reactor. Access to the bunker can be made through a 500 ft long shielded tunnel while a radioactive reactor is in place. Compressed air at 3600 psi (120,000 lb) is stored in long steel bottles.

During a reactor operation, the air passes into the bunker through a stack of previously heated steel, and then out of the bunker and into the reactor at 350 psi and 1060°F. For the Tory II-A reactor, approximately as much heat is added to the air before it reaches the reactor as is added in the reactor itself. This amount of stored air allows full-power operation of the Tory II-A reactor for approximately two minutes. The air bottles and heater can be recharged in less than two days.

Figure 3 shows the Tory II-A test vehicle in place at the bunker face with approximately 700 lb of air per second passing out of the nozzle. The air storage capacity will be increased to approximately one million pounds for operation of the Tory II-C reactor.

The main design parameters of the Tory II-A reactor are as follows:

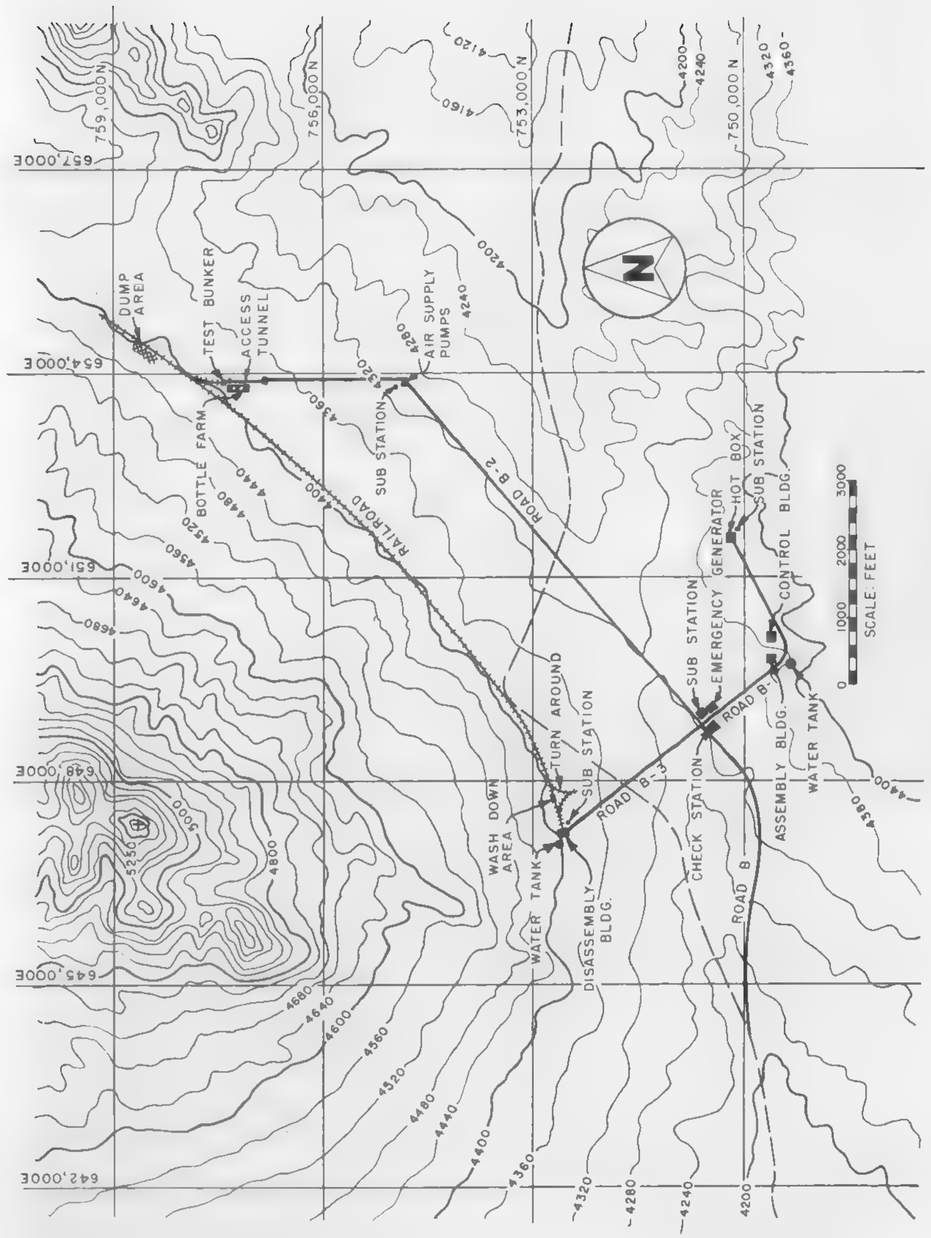


FIGURE 2 TEST SITE LAYOUT

Power, Mw	155
Flow rate, lb/sec	708
Maximum fuel-element wall temp, F	2250
Exit gas temp. (tube), F	1975
Core diameter, in.	32
Core length, in.	48
Side reflector thickness (graphite), in.	24

The core contains approximately 100,000 hexagonal fuel elements 4 in. long and 297 mils across flats with 200-mil-diam holes for the passage of air. These tubes are arranged in hexagonal bundles about 5 in. across. The bundles are contained in unfueled BeO structural elements, as shown in Figure 4. The fuel elements are not shown in this figure. An air-cooled Hastelloy R-235 tube is placed in each corner of the hexagonal bundles. The R-235 tubes are attached to a massive front support structure. At the exit end of the reactor the R-235 tubes are attached to coated molybdenum baseplates. The pressure drop through the fueled tubes appears at these baseplates. This load on the baseplates is reacted through the R-235 tubes and appears finally at the front support structure.



FIGURE 3 TORY IIA TEST VEHICLE AT BUNKER FACE

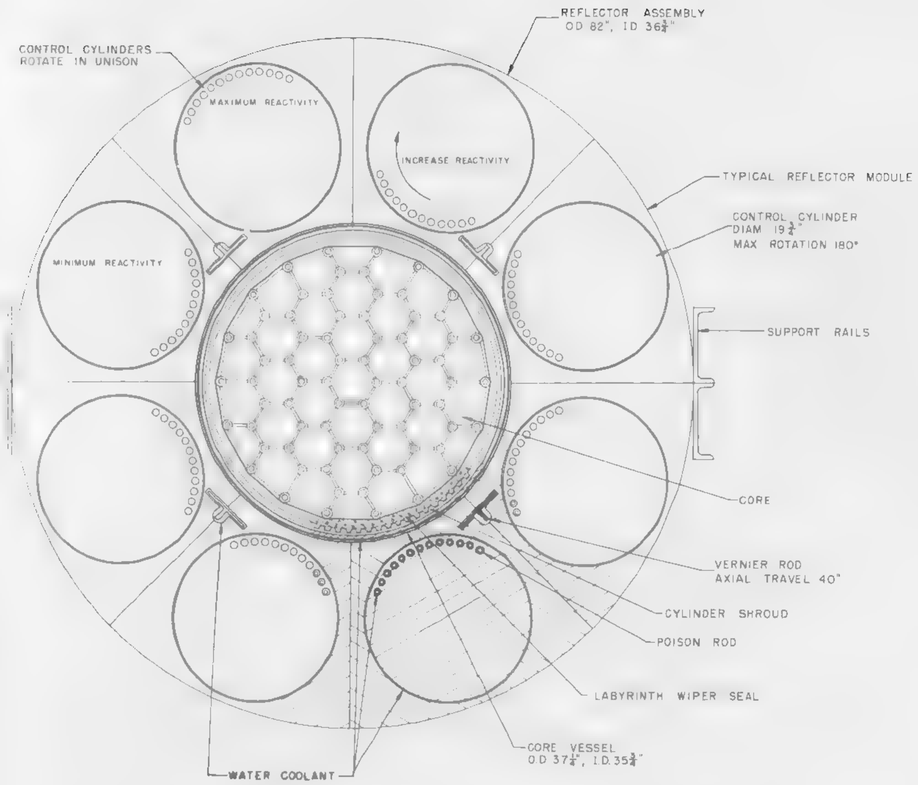


FIGURE 4 CROSS SECTION OF TORY IIA CORE AND REFLECTOR

The core is cantilevered from the front support structure by an air-cooled R-235 shroud. The core is separated from the reflector by a water-cooled aluminum pressure shell. The graphite reflector is in two sections which can be separated horizontally so that the aluminum pressure shell can be removed from the reflector. The reflector contains eight graphite cylinders with boron steel at the outer edge of one quadrant of each. These cylinders rotate and control the reactor by increasing or decreasing the effective size of the reflector. Additional fast control is obtained from four linear rods placed near the inner wall of the reflector. All control elements are moved by hydraulic actuators and can be operated singly or in unison. The reflector is water-cooled.

Figures 5 and 6 shows the core during assembly--the BeO structural elements and R-235 tubes can be seen. A few of the outside structural elements are in place. The dark tubes are fueled. The painted dots are a code system to indicate the percentage of uranium content. Strain gauges and thermocouples are in place. Figure 7 shows the front (upstream end) of the core, where the front-support structure and R-235 tubes can be clearly seen, and Figure 8 the fully assembled core in the pressure vessel.

The Tory II-C design is essentially complete, and fabrication of some parts has begun. A drawing, see Figure 9, shows the test vehicle and ducting. There will be no water-cooling on the test vehicle. The nozzle and reactor duct will be air-cooled. The reactor will be controlled by linear rods in the hot core. The rods are moved by pneumatic actuators located in front of the reactor in the 1060°F inlet air stream. These actuators together with servo valves and motors have been successfully operated at temperature of 1200°F for periods of several hours.

It should be apparent by now that the nuclear ramjet program is placing large demands upon present day materials technology. The test facility requires large diameter (~6 ft. diameter) piping to operate at pressures up to 600 psi and temperatures of 1200°F. A precipitation hardened alloy AM 355 caused considerable difficulty from cracks due to inadequate heat treatment. Future piping in the vicinity of

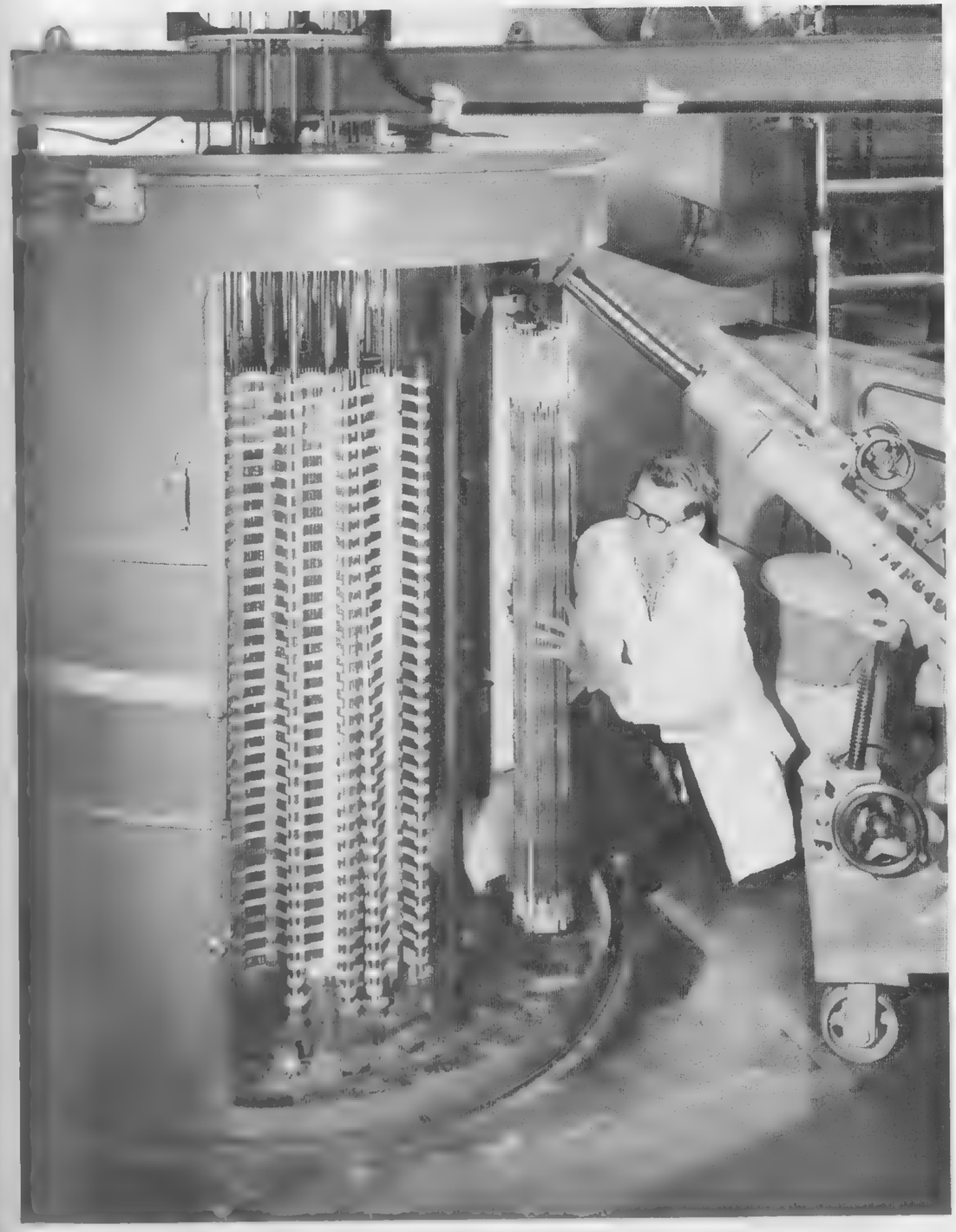


FIGURE 5 TORY IIA CORE DURING ASSEMBLY

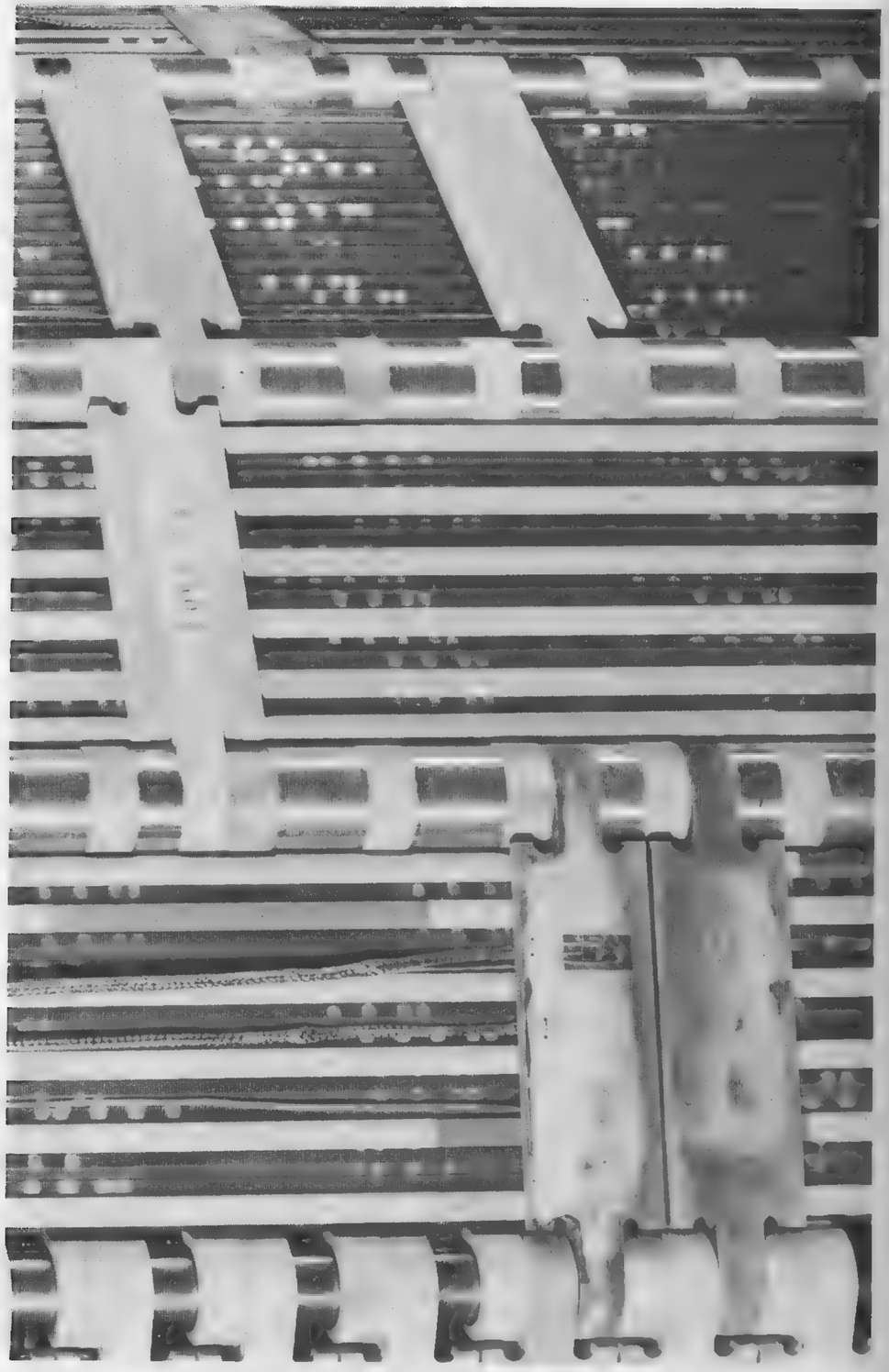


FIGURE 6 VIEW OF OUTSIDE OF TORY IIA CORE

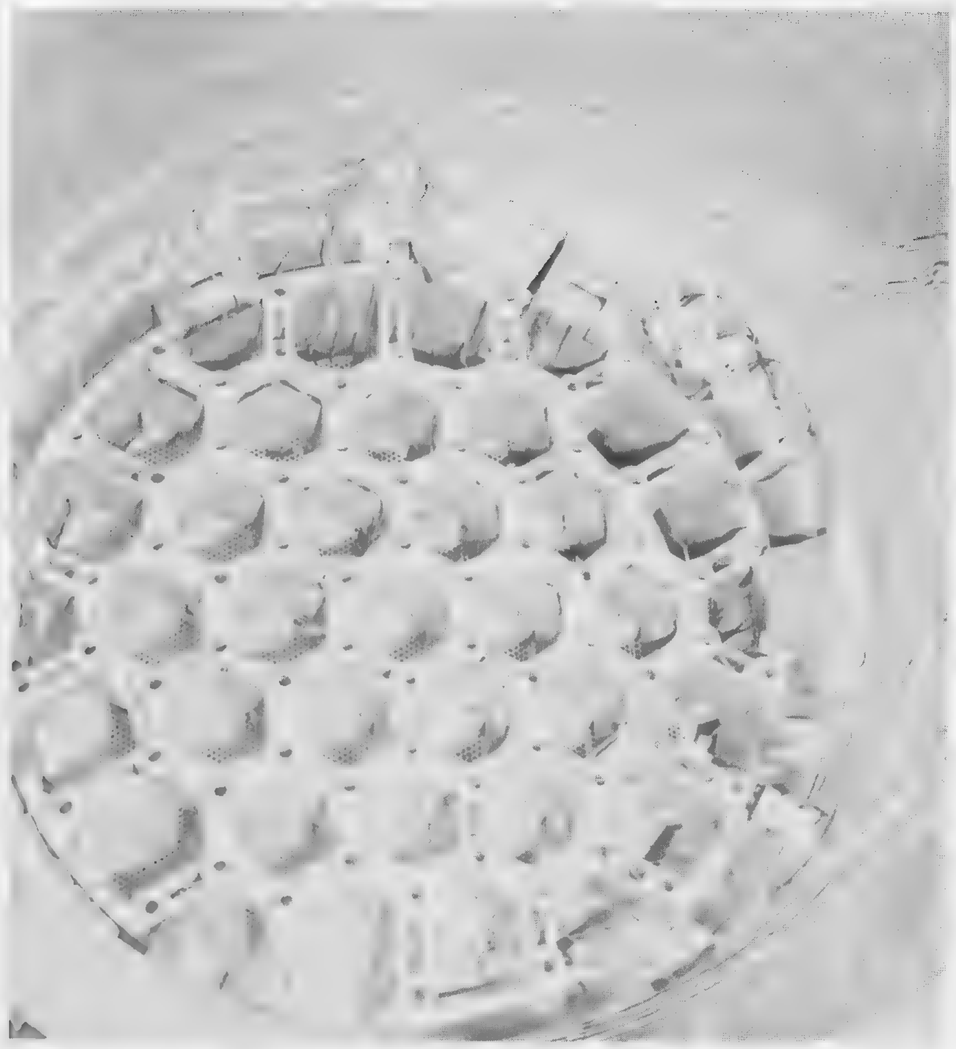


FIGURE 7 INLET END TORY IIA CORE

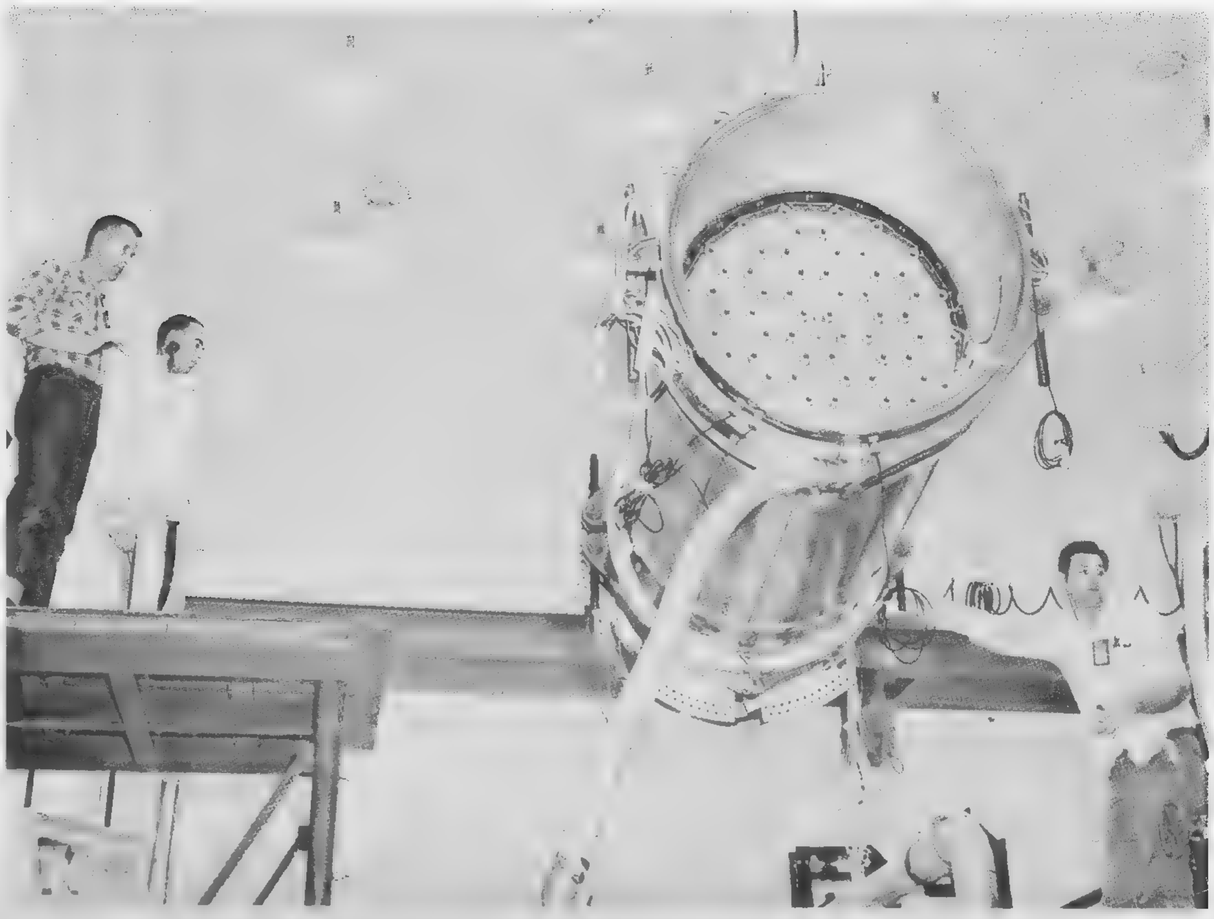


FIGURE 8 EXIT END OF FULLY ASSEMBLED TORY IIA CORE IN PRESSURE VESSEL

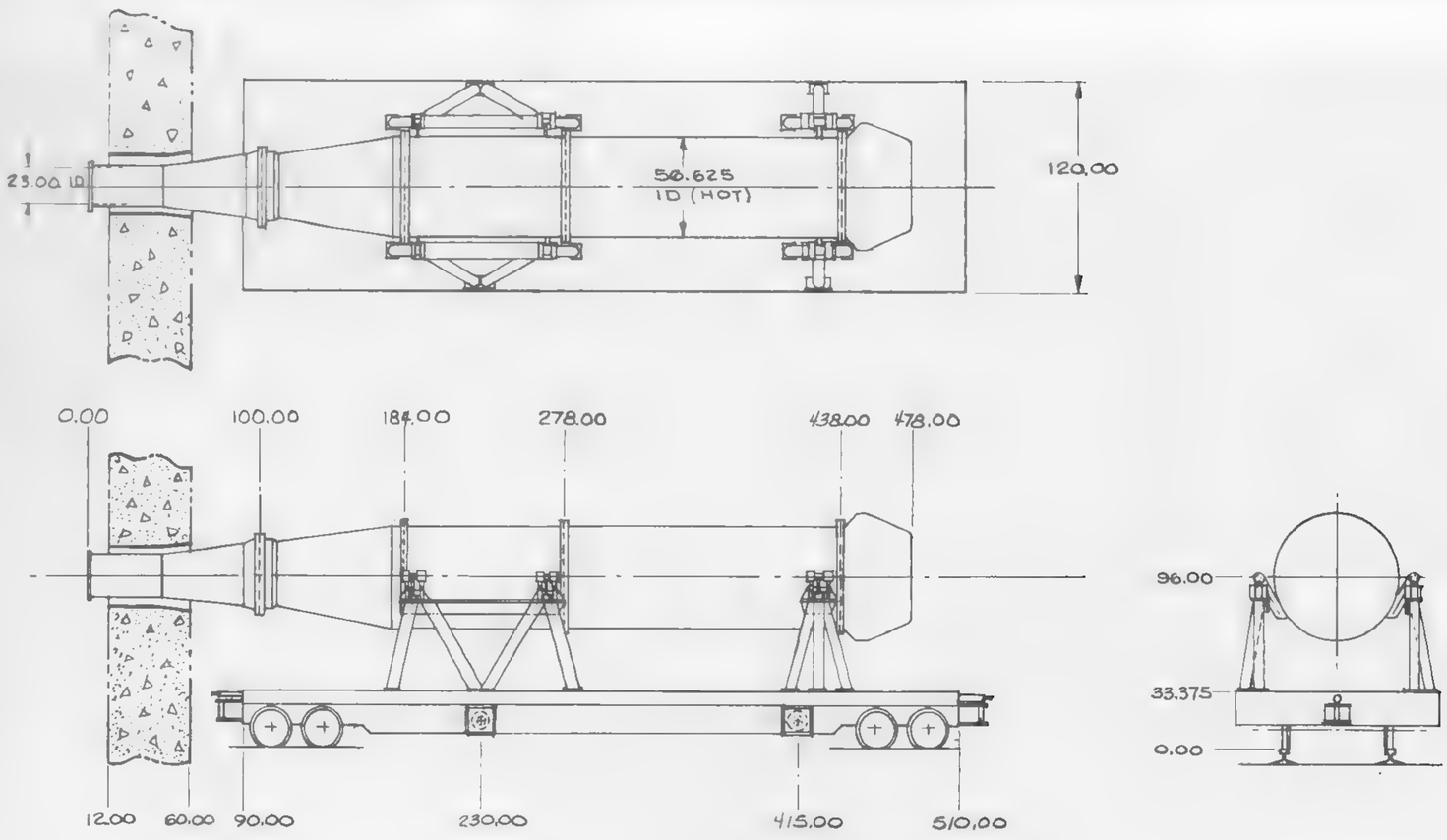


FIGURE 9 TORY IIC TEST VEHICLE

the reactor is being made of Hastelloy C. The missile airframe requirements are similar to those for supersonic aircraft. Metal temperatures will be in the vicinity of 1000°F. Radiation damage is not a problem for metallic structures but radiation heating in the vicinity of the reactor will require cooling. Electronic components will require radiation shielding.

The Tory II-A reactor has been designed so that ceramic elements are not placed in tension due to mechanical loads. However, thermal stresses are quite large and require close attention. Metallic structural elements such as R-235 and Rene 41 are adequate for internal structures if cooled properly. The fabrication of the R-235 tension tubes proved to be difficult and require very close attention to heat treatment. Refractory metals such as molybdenum and niobium are required at the exit end of the reactor. Since these baseplates see temperatures in excess of 2000°F in air moving at Mach 0.5 and at several hundred psi, oxidation must be prevented by means of coatings.

Holding onto a white hot object which sustains pressure drops amounting to loads of several hundred thousands of pounds while subjected to random accelerations of several g's due to flight loads has presented many interesting materials problems. It is becoming apparent that these problems can be overcome with proper design and proper use of materials.

MATERIAL REQUIREMENTS FOR NUCLEAR ROCKETS

Donald P. MacMillan
Staff Member
University of California
Los Alamos Scientific Laboratory
Los Alamos, New Mexico

ABSTRACT

The simplest type of nuclear rocket engine is basically a solid to gas heat exchanger. Since the specific impulse developed by the working fluid increases with temperature, the emphasis in development work is directed toward utilization of materials of the highest melting points available. Because, in addition, the specific impulse decreases with the average molecular weight of the working fluid ejected, useful propellants are principally hydrogen, or a compound which pyrolyzes to give largely hydrogen. Therefore material problems consist mainly of study of the properties of refractory materials and of their compatibility with one another and with hydrogen under the environmental conditions obtaining in the rocket reactor.

The material problems most unique to the Rover program (development of nuclear powered rocket engines) are principally in the area of fuel element design. Since the nuclear rocket engine is first of all a reactor, the neutron absorption of materials must be small.

Among the important non-nuclear characteristics of fuel element materials is retention of strength at high temperature, resistance to thermal shock and thermal stress, and capability of sustaining a high strain rate. The

bulk power density of nuclear rocket engines must be of the order of 100 MW per cu ft. This demands good thermal conductivity if excessive thermal gradients are to be avoided.

GENERAL REQUIREMENTS

The Rover Project is currently aimed at development of a fission powered rocket engine in which energy is generated in solid fuel elements and transferred to a gaseous working fluid. It follows that the fuel elements must withstand even higher temperature than the effluent gas. This is in marked contrast to the chemical rocket engine in which the reaction chamber and nozzle throat may, if desired, be maintained at a temperature substantially lower than the working fluid because the heat is generated directly in the gas. Since the specific impulse produced by a rocket engine is roughly proportional to the square root of absolute temperature to which the working fluid is heated, it is desirable to operate at the highest temperature that the materials of construction will tolerate. The Rover rocket reactor must (a) satisfy the criteria of a nuclear reactor, (b) be mechanically sound while withstanding corrosion and erosion by propellant gas at the highest temperature possible for the required operating life. Material problems arise in connection with all parts of a fission powered rocket reactor, i. e. fuel elements, structural materials, control rods, moderator, reflector, etc. However, the most critical components are the fuel elements and most of what follows will be concerned with the problems of fuel elements.

NEUTRONIC REQUIREMENTS

A cardinal principle of reactor design is that more neutrons must be produced than are lost by absorption in core materials and by leakage out of the core. It is somewhat more difficult to satisfy these requirements in small reactors than in very large ones. However, in any case, materials of construction chosen must have tolerable neutron absorption

and excessive amounts of highly absorbing materials must be avoided. It is customary to distinguish between the thermal-neutron-absorption cross section of a material and the resonance-absorption integral, which is a measure of the absorption of epithermal and higher-energy neutrons. To take one extreme of the materials whose high temperature structural strength is adequate, the thermal-neutron-absorption cross section of carbon is very small (0.0045 barns), and the resonance-absorption integral is zero barns. Such a material, which is also a good moderator, can readily be used in a homogeneous reactor design. On the other hand, tungsten, the highest melting metal available, is attractive as a fuel element substrate material. However, the thermal neutron absorption cross section of the naturally occurring mixture of isotopes is 19 barns and the resonance absorption integral about 450 barns. This places some restrictions on design of a reactor with tungsten fuel elements.

The core of a reactor must of course contain fissionable material. In principle, one has the choice of homogeneous or inhomogeneous loading of a reactor and there are advantages to both types of design. In any case, one of the principal problems is of so containing the fissionable material that an excessive amount is not lost during the life of the reactor. Metallic uranium and plutonium, whose melting points are 1132 and 639°C respectively, melt far below the operating temperature of a rocket reactor and cannot be contained in the elementary form at temperatures of interest. Uranium compounds are not among the most refractory materials known and their vapor pressure is high enough to make less attractive some fuel elements of otherwise attractive design.

Let us consider the problems of incorporating uranium into a tungsten fuel element. Uranium is not very soluble in tungsten. Of the uranium compounds that might be used, uranium carbide has the disadvantage that it reacts with tungsten to form a liquid phase near 2500°C. Uranium dioxide, although it does not react with tungsten, has a vapor pressure so high at the temperatures of interest that it would have to be confined to prevent subsequent loss of fissionable material.

Kiwi-A, the first Los Alamos reactor, employed graphite fuel elements made by Group CMB-6 of the Los Alamos Scientific Laboratory. Graphite fuel elements can be made by several different methods. A modest concentration of uranium can be introduced into an existing graphite by solution impregnation although it is difficult to obtain uniformity of loading by this means. It is likely to be more satisfactory to add a uranium compound such as UO_2 to the "green mix" from which the graphite is formed. The uranium oxide is then converted to carbides during the graphitization process and the uniformity of dispersion of the uranium can be ascertained by radiography.

POWER DENSITY

There are many and extremely interesting proposals for propulsion in space, among which is, for example, ion propulsion. It may be possible to achieve an extremely large specific impulse, like 10,000, by such schemes, with consequent great economies in reaction fluid requirements. Such devices, however, are incapable of the enormous power density required to produce acceleration in excess of 1.0 g required for ground take-off of a rocket. The bulk power density of nuclear rocket engines for ground take-off must be of the order of 100 mw/cu ft, i.e. 3.5 kw/cu cm. The problem of rocket reactor design therefore involves power density one or more orders of magnitude higher than encountered even in ETR and MTR. The impossibility of interposing an electrical link between reactor and any kind of electric propulsion system is quite obvious when one considers that electric generating equipment commonly weighs of the order of one ton per megawatt. The nuclear rocket reactor on the other hand does not suffer from lack of available power but is limited by the amount of reaction fluid which can be carried in the vehicle.

As a result of the high power density in nuclear rocket reactors, the thermal conductivity of fuel elements must be good in order to carry the heat from the interior of a fuel element to the heat transfer surface if enormous temperature gradients in the fuel element are to be avoided.

As an illustration of this, consider a zirconium carbide fuel element. The melting point of ZrC is about 3500°C, which appears attractive. Let us suppose, however, that the fuel element needs to be 1/8 inch thick and must contain 20 mol percent UC. To begin with, the melting point of UC is only 2350°C. The ZrC and UC are mutually soluble in the solid state and we can crudely estimate by proportion that the melting point of the UC-ZrC would be about 3230°C. Since the bulk power density of the reactor must be about 100 mw/ft^3, the heat flux through the fuel element surface will be approximately 2×10^6 Btu/hr/ft^2. The temperature difference between centerline and surface of a flat, semi-infinite plate is given by

$$\Delta T = Qt^2/8k$$

where Q is the bulk power generation, t is the plate thickness and k the thermal conductivity. For the sake of illustration, the thermal conductivity of the fuel element material will be taken to be 10 Btu/hr/ft/°F. This leads to a temperature difference between centerline and surface of 250°C and therefore to a surface temperature of 2980°C.

RADIATION DAMAGE

The core material in a nuclear rocket reactor is exposed to a radiation field substantially greater than encountered in any other reactor. However, the operating life of the rocket reactor is short, with the result that the integrated lifetime flux, nvt, is at least one and perhaps two orders of magnitude less than in ETR. Fortunately, radiation damage to materials tends to anneal out to an increasing degree as temperature is raised. For example, there has been a great deal of study of radiation damage to graphite in reactors such as those at Hanford and it is found that the accumulated damage decreases markedly when the temperature of irradiated graphite is raised to temperatures which are encountered in a graphite cored rocket reactor. Radiation damage problems in the core of rocket reactors may hopefully be expected to be less severe than in reactors operating at more modest temperatures.

REFRACTORY MATERIALS

The number of materials from which the designer may choose in making a fuel element decreases rapidly with increasing temperature at which the reactor core must operate. This is illustrated by Figure 1 which shows in a general way the number of materials remaining solid above any given temperature. It should be noted that there are only seven elements melting above 2500°C, of which two, rhenium and osmium, are too rare to be of much service. It is notable that most of the materials melting above 2500°C involve compounds of the transition metals of groups IV, V, and VI, in the periodic table and that these compounds are principally carbides, nitrides, borides, and oxides. Clearly these are

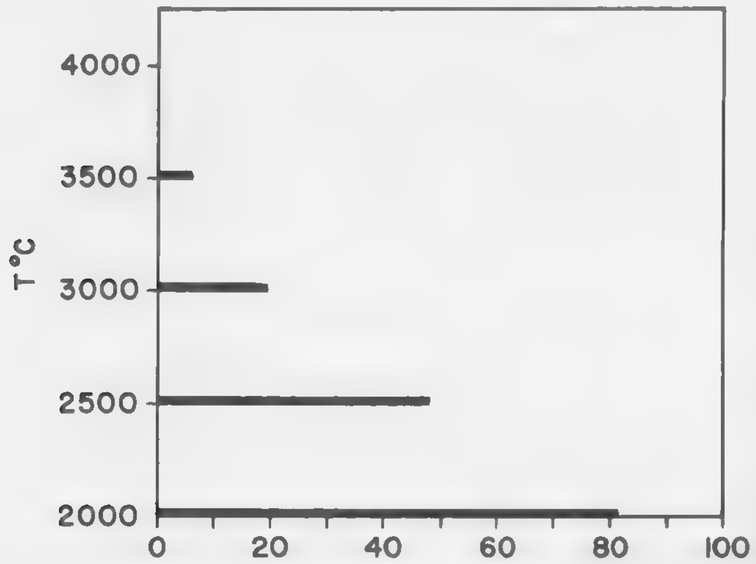


FIGURE 1 NUMBER OF ELEMENTS AND BINARY COMPOUNDS WHOSE MELTING POINT IS GREATER THAN T °C

materials whose properties and fabrication are less well known and which are less "well behaved" than the common structural metals. As a consequence it will usually be found that the employment of one of them in design involves more than merely "plugging in" a high melting material in place of some familiar material such as Inconel X. For purposes of considering the properties of the high temperature materials, one may divide them into three classes:

(a) Refractory metals W, Ta, Mo, Nb.
(b) "Ceramics" such as the oxides, borides, carbides, nitrides, and silicides of transition metals of group IV, V, and VI.
(c) Graphite.

MECHANICAL PROPERTIES

The properties of these three groups of material differ sharply. While design can minimize the strength required of a fuel element material, the mechanical characteristics of the material have a large effect on how it can be used. Like the more familiar metals, refractory metals are characterized by high tensile strength at room temperature, and by progressive loss of strength as temperature is raised, with the result that long before the melting point is reached they become very soft. Graphite, weak compared to structural metals at "ordinary" temperatures, retains its strength to temperatures above 2700°C. Indeed it has the interesting property of increasing in strength with temperature to about 2500 to 2600°C while it is almost twice as strong as at room temperature. At this temperature its strength is of the same order as that of tungsten, the most refractory of the common metals. The resistance of graphite to thermal stress and thermal shock has been taken advantage of for many years in the electro metal industry where graphite electrodes have been used for arc melting of metals. The third group of materials, often called "ceramics", are interstitial compounds of transition metals in groups IV, V, and VI of the periodic table. In these compounds the small non-metallic atom which may be boron, carbon, or nitrogen, occupies interstices of the metal lattice. These materials include materials of the very highest melting point. Unfortunately, as a group they are "brittle" and will not tolerate thermal shock or high rates of strain, with the result that they are difficult to fabricate and present discouraging problems in design.

Unlike metals, which generally exhibit fairly definite strength, the strength properties of graphite must be regarded

as having large statistical variation. The design engineer faced with employing graphite under demanding conditions will feel obliged to determine e. g. the standard deviation of tensile strength, which seems unlikely to be less than five or ten percent under the best conditions and is commonly greater. The variation from piece to piece and lot to lot obviously can be of greater magnitude.

THERMAL STRESS RESISTANCE

Since the life required of a nuclear rocket reactor is measured in minutes rather than in hundreds or thousands of hours and because, in the interest of performance, temperature is pushed to the point where the materials become plastic, it is the creep properties of materials which are of the greatest importance rather than tensile or compressive strength. Comparatively little is known about the mechanical properties of the very refractory materials useful for fuel elements. It is generally true that tolerance of large temperature gradients may be crudely measured by the expressi

$$M = k \times s/\alpha E$$

where M is a measure of the thermal stress resistance, s is tensile strength, α is the thermal expansion coefficient and E is Young's modulus. (Table I.) It is evident that the thermal stress resistance of metals is by far the best available, while the interstitial compounds are the poorest, graphite being intermediate. Cleverness in design can of course be employed to reduce the severity of thermal stresses. For example, if a way could be found to make use of a TaC fuel element a few thousandths of an inch thick, thermal stresses could be limited to a trivial amount. The characteristic brittleness of materials of this class, however, make achievement of such designs difficult.

CORROSION

Corrosion becomes an increasing problem as temperatu is raised. In design, the choice of materials, already limit is further constrained by problems of compatibility of the

TABLE I

THERMAL STRESS RESISTANCE

Material	Thermal Conductivity k BTU/hr/ft^2/in.	Tensile Strength s lbs/in.^{2}	Young's Modulus E lbs/in.^{2} x 10^{-7}	Linear Expansion Coefficient α 10^6/°F	Figure of Merit $\frac{ks}{E\alpha}$
TaC	154 (77°F)	4,000 (71°F)	4.15	3.57 (71-1100°F)	4.2×10^3
TiC	119 (77°F)	8,000 (2200°F)	4.5	4.12 (71-1100°F)	5.1×10^3
ZrC	142 (77°F)	15,350 (2200°F)	7.0	3.74 (71-1100°F)	8.6×10^3
Graphite (H4IM)	264*(2900°F)	1,500 (2900°F)	0.17**	3.3 (77-4500°F)	7.1×10^4
Mo	768 (1600°F)	92,000 (1600°F)	4.0 (1600°F)	3.06 (77-1600°F)	5.8×10^5

* All graphite data are perpendicular to the grain.
** Estimated from room temperature value.

structural material with the "working fluid." Because the specific impulse of a rocket engine is roughly proportional to $M^{-1/2}$, where M is the mean molecular weight of the gas entering the nozzle, the working fluid of choice for a nuclear rocket is hydrogen. The molecular weight of hydrogen is about one tenth that of the gases produced by combustion of chemical rocket fuels and hence the specific impulse produced at a given temperature is about a factor of three higher, a very great advantage. The corrosion of graphite by oxidizing atmospheres at high temperatures is well known but it is perhaps not as well known that it is also corroded by hydrogen at temperatures above about 1400°C as shown in Figure 2. The corrosion becomes appreciable at about 1500°C and increases rapidly with rising



FIGURE 2 SAMPLES 2 AND 3 WERE EXPOSED TO HYDROGEN AT ABOUT 10 ATMOSPHERES AND A FLOW RATE OF THE ORDER OF 50,000 LBS FT^{-2} HR^{-1}. SAMPLES 1 AND 4 WERE NOT TESTED.

temperature. Figure 3 shows the strong dependence of corrosion rate on temperature for a typical graphite in hydrogen under flow conditions such as might be reasonable in a rocket engine.

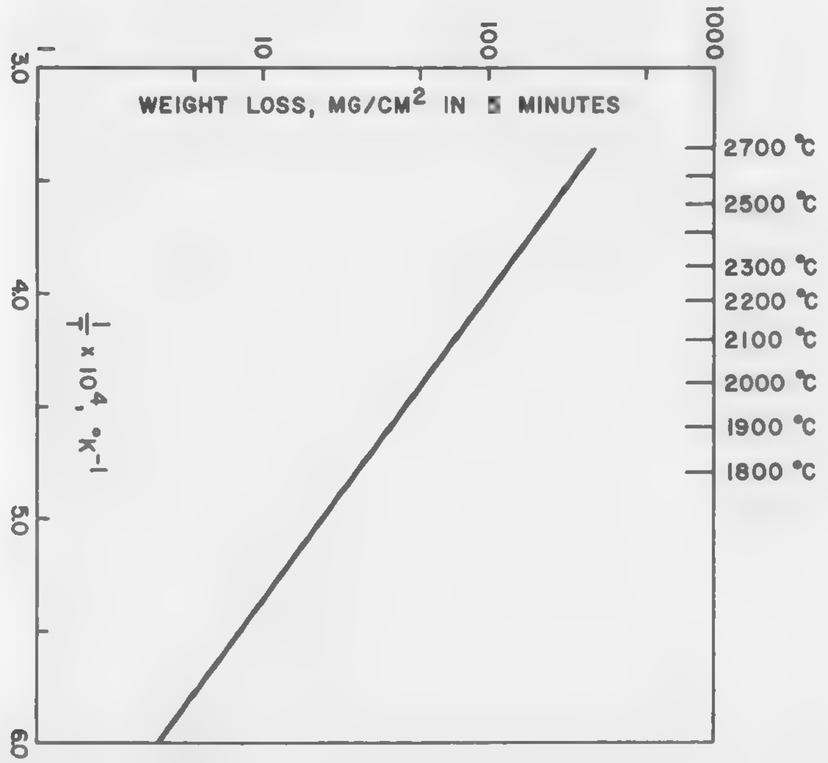


FIGURE 3 CORROSION OF A GRAPHITE GAS PASSAGE BY HYDROGEN AT A FLOW RATE OF 5×10^4 LBS FT^{-2} HR^{-1}

The vulnerability of graphite to corrosion has led to studies of the mechanisms of corrosion and to efforts to develop coatings of refractory materials. The metallic carbides of the transition metals groups IV, V, or VI are among the most refractory materials, and numerous experimental methods of applying them to graphite have been employed. Difficulties familiar from lower temperature fields are encountered such as problems of attaining perfection of coating and then insuring perfection by some method of inspection. This, as any who have met the problem well know,

is not easy. Another major problem encountered in development of a successful coating is that of securing adherence under thermal shock and thermal cycling, particularly in view of the fact that the graphite and coating usually have different thermal expansion coefficients.

ENVIRONMENTAL TESTING

Environmental testing of materials under conditions simulating all but the radiation field inherent in the rocket reactor can usually be accomplished using electric heating. Materials under test can be given a total irradiation equaling that expected in a rocket reactor by irradiation in a reactor such as MTR or ETR. However, even such reactors as these fall short of the dose rate of a rocket reactor by one or more orders of magnitude.

The final test of performance of materials under environmental conditions is to carry out material tests in the rocket reactors themselves. This necessitates recovery of samples from the reactor after completion of the test. To accomplish this, a large hot cell has been built at the Nevada Test Site where these reactor tests are carried out. After completion of testing, the reactor, which is mounted on a specially designed railroad flatcar, is brought to the disassembly building. The hot cell as seen from the large entrance door is shown in Figure 4. Equipment includes a high capacity overhead manipulator carried on a bridge crane (not yet installed when the picture was made), two General Mills side wall manipulators and several small manipulators such as the Argonne Model 8. The latter, of course, are intended for only such things as repair of the larger manipulators and handling small pieces of material at a window. The hot cell is overlooked by several windows from any one of which the larger manipulators can be operated. After gross disassembly of the reactor has been accomplished in the large hot cell, examination of parts of the reactor can be continued in detail in two smaller hot cells in the building, where, if desired, small samples can be cut out for further examination in the hot cells at Los Alamos.



FIGURE 4 HOT CELL FOR DISASSEMBLY OF ROVER TEST REACTORS AT THE A. E. C. NEVADA TEST SITE, AS SEEN FROM THE ENTRANCE DOOR

SLIDING CONTACTS AND FRICTION PHENOMENA IN SPACE

F. J. Clauss, Staff Scientist
C. F. O'Hara, Senior Scientist
S. P. Drake, Lab Analyst
F. B. Cooke, Associate Scientist
Lockheed Missiles and Space Company
Sunnyvale, California

ABSTRACT

Problems in the operation of such parts as gears, bearings, and sliding electrical contacts that result from the environments to which spacecraft are exposed will be reviewed, with special emphasis on obtaining long-time reliability under orbital conditions together with minimum weight and size. The advantages and limitations of various classes of lubricants and self-lubricating materials for spacecraft applications are reviewed, and new data from current experimental studies are presented.

INTRODUCTION

Space flight is now an established reality, and advanced systems are being designed to perform such complicated missions as reconnaissance and sentry duty to detect the launching of ballistic missiles from any point on earth. Manned space flight and space exploration are other examples of advanced spacecraft objectives. These systems require more complexity, better reliability, and longer operation than the early satellites launched into orbit. One factor that has become increasingly important in meeting these requirements is the behavior of materials in space.

One of the major material problem areas for advanced spacecraft systems is that of friction and wear of rubbing or

sliding surfaces as encountered in the operation of gears, bearings, and electrical contacts used in various spacecraft mechanisms. Lubrication is needed to reduce frictional drag and minimize the power required to drive the mechanisms. Inadequate lubrication results in excessive wear and can be the limiting factor in the lifetime of an entire system. Among the special problems that complicate the problem of providing adequate lubrication in space are the very high vacuum that exists in space, temperature extremes, and radiation.

The difficulties in providing lubrication for spacecraft mechanisms can be met in several ways. The effects of operation under vacuum conditions can be avoided, for example, by enclosing the moving parts within hermetically sealed containers. Where necessary, forced-feed systems can be used so that lubricant lost by evaporation in the vacuum of space is periodically replenished from a reservoir. These and other stratagems are often impractical, however, and at best have the disadvantage of increasing the weight, size, and complexity of the spacecraft systems. Their use should be restricted, therefore, to those cases where they are the only feasible means for providing lubrication.

A much better approach lies in the application of lubricants and self-lubricating materials that themselves provide a reliable and straightforward solution to the problems of space lubrication. Unfortunately, very little information exists either on the implications of the space environment for the lubrication problem or on the behavior of lubricants and self-lubricating materials under space environment conditions. The purposes of this paper are, accordingly, to discuss the problems that may be anticipated in providing satisfactory lubrication for mechanisms subjected to the influence of the space environment and to summarize available information on the applicability of various lubricants and self-lubricating materials to solve such problems.

ENVIRONMENTAL CONDITIONS THAT AFFECT THE LUBRICATION OF SPACECRAFT

This paper is primarily concerned with the use of lubricants and self-lubricating materials for long periods under orbital conditions in space or in space probes. Before leaving the earth environment, however, mechanisms are subjected to a variety of other environmental conditions. These too must be considered, or the spacecraft may never be successfully placed in space. Some of these conditions are imposed a second time on vehicles that re-enter the earth's atmosphere. In order to insure that parts operate reliably for the duration of the vehicle mission, therefore, all of the environmental conditions must be considered. These include:

- Ground Activities
  - Operation for test and checkout
  - Handling
  - Transportation
  - Storage
  - Exposure to the elements
- Short-time Operation during Launch, Ascent, and Re-entry
  - Acceleration and shock
  - Vibration
  - Temperature extremes
  - Contact with reactive fuels and oxidizers
- Long-Time Operation in Orbit
  - Ultrahigh vacuum
  - Temperature extremes
  - Zero gravity
  - Radiation

Ground Activities

Assembled mechanisms used in spacecraft and missiles are repeatedly tested on the ground prior to actual launch during the checking out of various components and entire

systems. As a result, parts that will operate for less than a minute during the launch and ascent phases can accumulate as much as several hundred hours of test operation prior to the time of launching. Lubricants selected for use with these parts under the vacuum conditions in space will therefore have to operate for a considerable period under normal atmospheric conditions. (In some instances, mechanisms that are sensitive to prolonged ground operation must be replaced by fresh units prior to launch.)

Necessary handling and transportation of delicate mechanisms involve an ever-present potential for damage from major shocks and vibration. Dropping a part on a concrete floor, for example, can be more injurious than the effects of actual launching. Handling and transportation by rail can cause shocks of as much as 30 g and, without special handling and packaging, such damage as brinell marks in ball and roller bearings can result.

Inadequate protection of parts during storage or while standing at launch sites can render them ineffective by allowing exposure to the elements with resulting corrosion, contamination, or changes in the lubricants. Elements and conditions that contribute to this hazard, and which are generally found at launching sites, include high-humidity atmospheres, mist, fog, water, salt, sand and dust.

Materials used for gears and bearings should be made of corrosion-resistant materials or protected by suitable films of oils, greases, or other coatings. Seals should be provided around joining surfaces or couplings to exclude minute particles of dirt. These precautions are particularly important for parts mounted on the exterior of a vehicle since they are most subject to weathering.

Short-Time Operation During Launch, Ascent, and Re-Entry

Heavy shock and vibration loads that occur during the short-time periods of launch, ascent, and re-entry can cause brinell marks in ball and roller bearings. The rotors of most fractional horsepower motors are light enough so that

brinelling does not appear to be a real problem with such parts. However, bearings that support heavy loads and which are stationary during launch and ascent are most susceptible to this type of damage. Two methods may be used to prevent brinell marks being caused by heavy loads. One is to rotate the shafts and bearings by having the mechanism in operation during the launch phase. The other provides for blocking the load so that it is not supported on the bearings during the launch phase and subsequently removing the blocks after the vehicle is in orbit.

Since high temperatures are generated by fuel burning and by aerodynamic heating, certain bearings (such as those used on control surfaces) and other parts must be designed to withstand high temperatures. At the other extreme, the use of cryogenic fluids for propulsion (e. g., liquid hydrogen, fluorine, and oxygen in conventional types of power plants and liquid helium in nuclear power plants) means that pumps, valves, and other moving parts will require the maintenance of lubrication at very low temperatures (e. g., below 100°K). Since the fluids used for propulsion are very reactive and include the strongest oxidizers known, lubricants which might come into contact with such fluids must be extremely inert.

Long-Time Operation in Orbit

Satellites that must operate in orbit and space probes are subjected to such special conditions as ultrahigh vacuum, temperature extremes, zero gravity, and radiation. Certain parts used in such satellites must operate in the hard vacuum of space, which is on the order of 10^{-9} mm Hg, more or less, depending upon the orbital altitude.* These include bearings, gears, and sliding electrical contacts on antennas, solar-cell assemblies, or other exposed gear. Rotating parts inside certain electronic tubes also must operate in vacuum. The special problems created by vacuum include

* At an orbital altitude of 500 miles, for example, the pressure is between 10^{-9} and 10^{-10} mm Hg.

higher evaporation rates of oils and greases, oil creepage along surfaces, and cold-welding of metals that are in contact with each other.

Not all parts are exposed to the hard vacuum of space. Some can be hermetically sealed in leakproof containers, and others protected by labyrinth or other types of seal. In many cases, however, sealing parts in containers is impractical or increases the weight, size, and complexity of the mechanism. For this reason, there is considerable interest in lubricants and self-lubricating materials that are themselves capable of operation in vacuum, thus eliminating the need for sealed containers.

Although most payloads on satellites and space probes are maintained near room temperature, temperatures of several hundred degrees will be experienced around electric motors that operate continuously; such temperatures will markedly accelerate evaporation under vacuum conditions. Parts that are outside the skin of a spacecraft, such as bearings on solar cell arrays, will experience wider orbital temperature fluctuations than those inside, and their low temperatures may be about -129°C (-200°F) when the satellite is passing the shadow side of the earth. Oils selected for such use must not freeze or become too viscous under such conditions, nor must they become too thin or volatile at high temperatures when directly exposed to the sun. For spacecraft and satellites with secondary propulsion systems, temperature extremes can include the high temperatures associated with combustion and the low temperatures associated with cryogenic fuels and oxidizers.

Zero gravity is an item on the credit side, since it means that, once in orbit, bearings need not support any structural loads. Bearing loads will be reduced to levels required by inertial loads associated with accelerating and decelerating mechanisms, the effects of unbalanced dynamic forces, and the centrifugal forces of balls against races in rotating ball bearings. The reduced bearing loads mean less wear. On the other hand, gravity-type feed systems for lubricants are obviously ineffective.

Radiation includes the penetrating Van Allen radiation and solar corpuscular radiation that exist in space, supplemented by nuclear radiation that would result from use of a reactor power source. Both the materials used for gears and bearings and any lubricants used with them must resist such radiation.

HYDRODYNAMIC AND BOUNDARY LUBRICATION

Mechanisms for spacecraft can operate under either hydrodynamic conditions or boundary conditions of lubrication, or under mixed hydrodynamic and boundary conditions.

Hydrodynamic Lubrication

Hydrodynamic lubrication is a type of lubrication in which the rubbing surfaces are separated by a continuous and relatively thick film of a gas such as air or a liquid such as oil. The fluid carries the load or weight of the free member of the rubbing pair and separates it from the stationary member. It also provides a medium of very low shear strength or viscosity. The resistance to relative motion between surfaces provided with hydrodynamic lubrication is very low, due to the viscosity of the fluid. The coefficients of friction are generally less than 0.001.

Hydrodynamic lubrication provides minimum friction, and this capability has been responsible for its extensive use with bearings for guidance and control systems of missiles and spacecraft that can be enclosed in sealed units. Hydrodynamic lubrication is more a matter of mechanical design than material selection and is not further discussed in this paper.

Boundary Lubrication

Full hydrodynamic lubrication cannot always be realized in practice, and it is therefore necessary to consider the various aspects of boundary lubrication. The nature of boundary lubrication, the mechanism of friction and wear

under boundary lubrication conditions, and the effects of surface films and their removal in vacuum are discussed in the following sections.

Nature of Boundary Lubrication

Most moving parts with fluid lubrication operate under conditions of boundary lubrication in which there is at least a partial breakage of the continuous film so that the surfaces of moving solids come into contact. This occurs when the speed or the fluid pressure between the surfaces becomes too low to support the bearing load, causing the hydrodynamic film to be squeezed out or broken or to become so thin that its thickness is less than the height of the surface irregularities. Some of the asperities -- the high points on even the smoothest surface -- then begin to rub on one another; the coefficient of friction rises; and surface wear occurs.

Modern theories of boundary lubrication interpret frictional resistance as the net result of the effects of two concurrent conditions, namely, the shearing of welded junctions formed between points of contact and the ploughing out of the softer material to an appreciable depth below the surface by the harder material riding over it. For hard materials in contact with one another, analysis indicates that the ploughing term is relatively small and that friction is largely due to the shearing of the welded junctions.

Three important points in the adhesion theory of friction and wear, that is, the welded junction theory, are as follows:

- The area of true contact is only a small fraction of the apparent contact area.
- High localized temperatures are generated at the points of contact by frictional heating.
- The two surfaces interact with each other to an extent that depends upon the materials themselves and the presence of surface films.

Area of true contact - When clean metal surfaces are placed together, they touch only where the asperities or high

spots meet, and the real area of contact is much smaller than the apparent area. The greater the force pressing the surfaces together, the more the asperities are crushed down and suffer plastic deformation. This action increases both the number and size of the contacts involved in supporting the load so that the area of real contact increases.

Surface temperatures of rubbing solids - When solids slide over one another, extremely high surface temperatures are generated even under moderate conditions of load and speed. The high temperatures are confined to very thin surface layers at the contacting points and are of very brief duration. For example, for a constantan cylinder sliding on a steel surface under a load of 4.1 lb and a sliding speed of 120 in./sec, temperature flashes of 1000°C (1832°F) were measured that lasted for less than 10^{-4} sec (Ref. 1, p. 41).

Surface temperatures produced by frictional heating increase with the sliding speed and the load. The poorer the thermal conductivity of the materials, the higher the temperatures that are generated. Even under the most severe conditions, however, surface temperatures cannot generally exceed the melting point of the bodies. Lubrication reduces the heating, but high temperatures are generated at the points of intimate contact even in the presence of lubricant films.

Interaction of surfaces - Sliding between metal surfaces is not a continuous, smooth process but often proceeds in a series of intermittent jerks. The friction rises to a maximum during the "stick" and falls rapidly during the "slip," and there are corresponding changes in the area of contact and the surface temperature. Experiments indicate that, under the intense pressure acting at the summits of the surface irregularities, localized adhesion or welding between the metal surface takes place. The occurrence of this condition is undoubtedly aided by the frictional heating. The metallic junctions that are formed must be sheared if the surfaces are to slide past one another, and the force required to shear the junctions and permit sliding is proportional to the product of the shear strength of the junctions and the area of real contact.

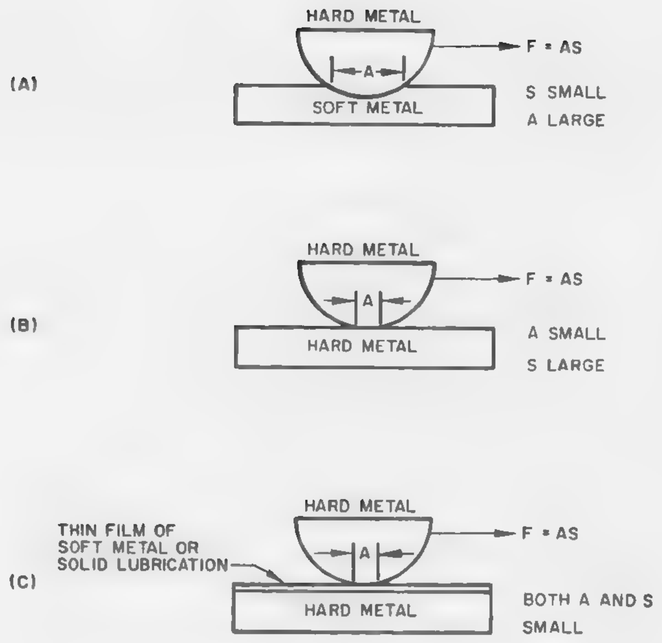


FIGURE 1 LUBRICATION OF SOLIDS BY THIN FILMS

Figure 1 illustrates, in simple form, the conditions that exist during boundary lubrication. The first example represents a hard body riding in contact with a soft one. The hard body presses into the soft one so that the area of real contact is large. Even though the strength of the junctions formed with the soft metal is low, the frictional force F, which equals the product of the shear strength S and the area A of the welded junctions, is relatively high. For the second case indicating two hard bodies in contact with one another, the area of real contact is small, but the strength of the junctions formed is large so that again the frictional force is relatively high. The ideal situation is that shown in Figure 1C. Here, a film of soft material with a low shear strength is placed between two hard bodies. The hard substrate supports the load and keeps the contact area small while the film of soft metal reduces the junction strength. These two factors thus combine their effects to reduce the frictional force.

Of course, the oxide films that are normally present on metal surfaces are not the most efficient boundary lubricants. Films of low shear strength can be provided by using laminar

solids, such as molybdenum disulfide, which have low shear strength along certain crystallographic planes, or by using soft metals such as silver, gold, and lead which have low shear strength in all directions. Boundary lubrication by oils, greases, and liquid metals accomplish the same purpose but they are not tightly bonded to the surface. Duplex bearing alloys, such as copper-lead, that contain hard and soft constituents in their metallurgical structure function by much the same principle; that is, the hard portions of the structure support the load and the lubricant is fed to the surface from the areas containing the soft constituent. A variation on this same idea is to rule or knurl a grid into the surface of a hard metal and then smear a soft metal into the indentations. This permits combinations of hard and soft metals that cannot be melted and cast together and provides storage capacity for the soft constituent.

Effect of Surface Films and Their Removal in Vacuum

Adsorbed or chemisorbed gas films, such as oxides, are normally present on even the cleanest metal surfaces in the normal atmosphere. These films prevent bare metal-to-metal contact and the formation of strong welded junctions so that the coefficient of friction is less than if bare metal-to metal contact were obtained.

Parts that are exposed to the hard vacuum of outer space will operate at pressures on the order of 10^{-9} mm Hg (more or less, depending upon the altitude). Surface films of adsorbed or chemisorbed gases that are removed by wear or by sublimation into space will not reform so that the films present on even the cleanest surfaces in the normal earth atmosphere will vanish within some time after being put into orbit. Under these conditions, gross-seizure or cold-welding can occur between the surfaces when they are brought together under even very slight contact forces. This phenomenon has been illustrated by laboratory experiments described in Ref. 1, pp. 145-149.

In one set of experiments, clean nickel surfaces prepared in air had coefficients of friction of about 1.4. The surfaces were then heated to 1000°C (1832°F) in vacuum to remove

contaminant films. On cooling in vacuum to room temperature, the coefficient of friction of the degassed surfaces readily reached a value of 9. Admitting air or a trace of oxygen reduced the friction, but hydrogen had no measurable effect. On surfaces that were even more thoroughly degassed, large-scale seizure occurred on contact. Separation of these surfaces was possible only by prying them apart, and the friction was too high to be measured.

Friction and Wear of Spacecraft Components

When adequate lubrication is not provided, friction and wear become important in limiting the lifetime of spacecraft components. In mechanical components such as ball bearings, the points of contact between the balls, races, and retainers become welded junctions; these are torn apart and reformed by continued operation, and the ball bearings eventually become jammed by the accumulation of wear debris. Gear teeth are worn away by the same process of metal plucking that occurs as small welded junctions are alternately formed and torn apart, so that backlash increases to the point where the device becomes useless. Cams and followers, as well as reset and positioning mechanisms, are rendered inoperable by excessive drag or "hangup" that accompanies wear in the absence of lubrication.

Not only mechanical failures, but electrical failures as well occur as a result of friction and wear. For example, brushes on D. C. motors are worn down by rubbing against commutator rings. In a slip ring assembly, wear between the contacting brushes and ring increases electrical background noise that obscures signals. This last is an acute problem in spacecraft systems, where the background noise in telemetered signals must be held to a minimum. A compromise must be made between having good metal to metal contact in order to insure good electrical continuity across the contact and, at the same time, reducing metal to metal contact in order to reduce wear. In some applications on spacecraft, a slip ring is eliminated by conducting current through a rotating bearing. This means that the lubricant interposed between the sliding or rolling surfaces must be a good electrical conductor rather than an insulator.

In most instances it is possible to select lubricants or self-lubricating materials that satisfy the requirements. As rubbing speeds increase and as greater requirements are placed on lifetime and reliability, however, the selection of proper lubricants or self-lubricating materials becomes more important as well as more difficult. Such selection requires knowledge of the advantages and disadvantages of the various lubricants and self-lubricating materials available and of their potential for use under space conditions. In the following sections, some information obtained from current research programs on the operation of lubricants under space conditions of vacuum is presented, along with comments on the stability of the lubricants under space radiation conditions.

OILS AND GREASES

Oils and greases are the most widely available and most commonly used type of lubrication. Their use offers the following advantages:

- o Ease of initial application and renewal.
- o Wide range of properties available to meet specific needs.
- o Ability to remove frictional heat from moving parts.
- o Protection of metal surfaces against rusting and other types of corrosion.
- o Sealing against dust particles, sand, and other foreign matter.
- o Lower cost than other types of lubrication.

For use under spacecraft conditions, oils and greases may be limited by the following factors:

- o Inability to operate at extreme temperatures (either high or low) and over extended temperature ranges.
- o Evaporation, which is accelerated by vacuum operation.

- o Creepage or migration over surfaces and away from the parts they are intended to lubricate.
- o Radiation stability.

Use Under Vacuum Conditions

Table I presents some data that compares the lifetimes provided by oils used to lubricate ball bearings operating in vacuum with the lifetimes provided by the same oils under the same conditions but in air. All four oils were providing lubrication in air after about 9500 hrs. (13 months) of operation, whereas in vacuum three of the four oils resulted in failures in 3335 hours (approximately 4.5 months), or less, and only one oil was still providing lubrication in vacuum after 8939 hours (slightly more than 1 year). Failures have been due to loss of the oil by evaporation, even though the bearings that were used were of the double-shielded type. The only lubricant in this series of tests that operated successfully under vacuum conditions was a mineral oil, which has the very low vapor pressure of 10^{-9} to 10^{-10} mm Hg at room temperature. The disadvantage of this oil is that it is very viscous and does not provide a low running torque at the test temperature used in these tests.

Table II presents additional data on the performance of several of the many oils and greases that have been evaluated in the program being conducted at the Lockheed Missiles and Space Company. In these tests, the oil or grease has been evaluated with R3-size ball bearings (3/16-in. i.d. by 1/2-in. o.d.). Some bearings tested had steel ribbon-type retainers, and others had machined Synthane retainers. All bearings were of the deep-groove radial type with double shields. The bearings with steel ribbon-type retainers were run-in in air for 16 hrs at 8000 rpm with the lubricant supplied by the bearing manufacturer. They were then cleaned ultrasonically and relubricated with the test oil or grease. Bearings with machined Synthane retainers were vacuum-impregnated with the oil under study.

The bearings were installed on small induction motors that were mounted inside vacuum chambers for testing. Both bearings on any one motor received the same lubricant. The

TABLE I

COMPARISON OF LUBRICATING LIFETIMES PROVIDED ON BALL BEARINGS BY SEVERAL OILS FOR OPERATION IN AIR AND IN VACUUM

Lubricant	Operation	Average Weight of Lubricant per Bearing (milligrams)	Lifetime
Low vapor pressure mineral oil	Air	50.4	Still running after 9527 hours
	Vacuum	53.8	Still running after 8939 hours
Silicone oil, distilled to remove volatiles	Air	53.6	Still running after 9491 hours
	Vacuum	61.8	Failed after 3335 hours
Polyphenyl ether	Air	61.2	Still running after 9526 hours
	Vacuum	70.7	Failed after 2476 hours
Silane	Air	31.0	Still running after 9505 hours
	Vacuum	43.4	Failed after 1367 hours

Test conditions: Speed: 8000 rpm (continuous)
Ball bearings: R3 size (0.1875-in. bore x 0.500-in. o.d.), 440C stainless steel, Synthane retainers, double shielded
Vacuum: 10^{-7} to 10^{-8} mm Hg
Temperature: 110-190°F

TABLE II

LUBRICATING LIFETIMES PROVIDED BY OILS AND GREASES ON BALL BEARINGS OPERATING IN VACUUM

Lubricant	Bearing Type	Average Weight of Lubricant per Bearing (mg)	Temp. of Bearing Housing (°F)	Coast Time (min:sec)	Life-time (hrs)	Remarks
Chloromethylphenyl silicone oil + lithium base soap	1	96.0	132-220	1:53 after 2233 hrs 2:16 5013 2:35 6983 1:42 9420	9612	Grease decomposed to heavy residue
Chloromethylphenyl silicone oil	2	29.4	130-210	10:20 after 3180 hrs 9:55 4000 4:13 4299	4574	Weight loss indicates 80-90% of lubricant was lost
	4	24.4	145-190	3:10 after 2452 hrs 4:23 4741 5:0 6238	> 6425	Still running
Chloromethylphenyl silicone oil, stripped	3	61.8	160-200	9:14 after 1580 hrs 10:15 2362 9:17 3150	3335	
Low vapor pressure silicone oil (vacuum diffusion pump oil)	4	24.8	140-180	9:2 after 461 hrs 7:55 1757 3:35 2527	2603	
Low vapor pressure mineral oil	3	53.8	167-200	0:16 after 1313 hrs 0:15 4990 0:18 8610	9527	Still running

Bearing types: 1 = 440C stainless steel, ribbon retainers
2 = 52100 chrome steel, ribbon retainers
3 = 440C stainless steel, Synthane retainers
4 = 52100 chrome steel, Synthane retainers

Test conditions: Speed: 8000 rpm (continuous)
Ball bearings: R 3 size, double shielded
Vacuum: 10^{-7} to 10^{-8} mm Hg

radial load on each set of bearings was that provided by the weight of the motor rotor. It was 5.65 oz, divided between the two bearings.

For the test, four motors were usually operated simultaneously in each vacuum chamber. The motors were of the a-c induction type and rated at 0.01 hp. Their normal operating characteristics were as follows: 115 v, 0.3 amp, 400-cps power input, and 8000-rpm synchronous speed. Shafts had been machined to 3/16-in. diameter, and the bearing housings were opened up to expose the bearings more readily to the vacuum.

In the absence of convection cooling, the stator windings overheated when the motors were operated above 100 v in vacuum. This caused excessive outgassing and breakdown of the varnish insulation which, in turn, short-circuited the stator windings. For operation in vacuum, therefore, the motor voltage was reduced to a range of 70 to 90 v in order to minimize the heat generated in the stator windings.

Temperatures were measured with iron-constantan thermocouples attached to the bearing housings. Temperatures as high as 220°F were reached in the early parts of some tests while the motors were operated at near 115 v. Operation at this voltage was accompanied by excessive stator temperatures and insulation breakdown; hence, subsequent operation was conducted at a reduced voltage to keep the temperatures of the bearing housings below 180°F.

The current drawn by the motors was generally in the range from 0.1 to 0.2 amp. Motor speed was 7850 to 8000 rpm and was measured with a Strobotac unit. The motor current was monitored by a milliammeter placed in the circuit of each motor, and an increase in bearing torque was reflected by an increase in current. When a motor stalled because of bearing failure, the current increased by a factor of two or more, causing a fuse in the circuit to blow, automatically cutting off power to the motor and its associated timer.

After a set of motors was operated for several hours in air to insure satisfactory performance, the vacuum chamber was settled in place and the system evacuated. For tests with oils and greases, the vacuum systems employed oil-diffusion pumps and liquid-nitrogen traps. Vacuum during operation range from 10^{-6} to 3×10^{-8} mm Hg. The power to each motor was cut off periodically, and the time required for coasting from 8000 rpm to full stop was measured. This coast time was determined in order to obtain an indication of the running torque of the bearings.

Of the oils and greases tested to date, the longest run has been achieved with ball bearings lubricated with a grease consisting of a chloromethylphenyl silicone oil in a lithium base soap, which operated for 9612 hours (slightly more than 13 months) before failure. The same chloromethylphenyl silicone oil used as an oil (i.e., without the lithium base soap) is still lubricating another set of bearings that have operated for 6425 hours. This oil has performed better when it is vacuum impregnated into the Synthane retainers of bearings than when it is added to ball bearings having ribbon retainers.

Several attempts have been made to improve performance by using oils that have low vapor pressures. In one test, the chloromethylphenyl silicone oil was molecularly distilled to remove the 50% more volatile fraction, and the residue was tried in the expectation that the less volatile fraction might lubricate in vacuum for a longer period. The results cited in Table II indicate that the stripped oil performed poorer than the undistilled oil, contrary to the expectations, indicating that the lubricity of the oil had been decreased by the distillation. A low vapor pressure silicone oil, of the type used in vacuum oil diffusion pumps, also gave relatively poor performance. On the other hand, bearings lubricated with a low vapor pressure mineral oil are still running after 9527 hours (about 13 months).

A great number of other oils and greases have been and are being evaluated in the program at LMSC. Many of these have operated successfully for over 3000 hours under the test conditions, whereas many others have failed in less than 1000 hours. Only a small number of tests have been

conducted to date on any one oil or grease, and additional tests are necessary before reliable statistics can be established.

LAMINAR SOLIDS

Many inorganic solids have a slippery feel. Graphite is the classic example of such a solid; its lubricating qualities are well known, and it is widely used to lubricate fine mechanisms.

Part of the explanation for the slipperiness and lubricating qualities of these solids lies in their type of crystal structure. Generally, they have crystal structures in which the atoms are closely packed on widely separated planes, giving rise to their classification as "laminar solids". The interatomic forces that hold such a structure together are accordingly strong between neighboring atoms lying in the same plane but are weak between atoms lying in different planes. As a result, the planes can slide over one another with relative ease and without breaking down or being penetrated by surface asperities, and the solids can function as lubricants.

Not all laminar solids are effective lubricants. Moreover, their lubricating effectiveness varies with such service conditions as humidity and temperature and may be contingent upon the presence of certain adsorbed materials. No one laminar solid surpasses all others for all service conditions, and the choice of a solid lubricant depends upon the particular application.

For many applications, the most widely used solid lubricants are either graphite or molybdenum disulfide (MoS_2), or a combination of the two. Graphite does not lubricate in a vacuum, and it is therefore unsuited for many spacecraft applications. Molybdenum disulfide appears more promising since its coefficient of friction is only about one-half that of graphite and, unlike graphite, it is an effective lubricant in vacuum. At temperatures above roughly 500 to 750°F lead monoxide (PbO) appears superior to molybdenum disulfide.

The use of solid lubricants involves both the choice of the solid lubricant and the determination of the best way to use it. Laminar solids are used as lubricants in the following ways:

- Loose powders or dispersions in volatile carriers
- Burnished films (i.e., films formed by rubbing the solid powders onto the surface to be lubricated)
- Bonded films
- Oil and grease additives
- Impregnants into porous solids

Lubrication by films of laminar solids can be particularly advantageous under the following circumstances.

High loads - Extreme pressure causes fluid lubricants to be squeezed out from between the surfaces. With laminar solids, shearing takes place more easily when loads are high, so that laminar solids are well suited to extreme pressure lubrication.

Low speeds - At low sliding velocities, the asperities on mating surfaces tend to penetrate the lubricating films provided by fluid lubricants, so that stick-slip action and cold-welding occur.

Extreme operating temperatures - Oils and greases are subject to thermal decomposition at elevated temperatures. Their viscosity varies widely with temperature, and they become viscous or solid at low temperatures. Laminar solids have better thermal stability and do not become viscous at low temperatures or "thin out" at elevated temperatures, so that they provide a wider service temperature range.

Dirty or abrasive environments - The tacky surfaces of oils and greases tend to collect particles so that the lubricant can act more as a grinding compound. Laminar solids may, therefore, be better in dusty applications where complete sealing is impractical.

Fretting likely - Vibration in many machine joints can cause fretting wear, even though there is no apparent motion between the parts.

Inaccessible parts after assembly - In complex mechanisms for which relubrication by oils or greases is not feasible, bonded films of laminar solids can often furnish permanent, in-place lubrication.

Simplified design - Designs can be simplified and costs reduced by eliminating machined oil passages, oil cups and other reservoirs, filters, and recirculating pumps.

Inadequate or unreliable maintenance - One may not wish to rely on mechanisms to pump or recirculate lubricating oils.

Intermittent action with long periods of part disuse - Oils and greases may be inadequate where a part is subjected to intermittent action and long idle periods.

Avoiding reaction with environment - Environments such as fuels, solvents, and liquid oxygen (LOX) are reactive with oils and greases, whereas laminar solid lubricants can be used that are unreactive in contact with such environments.

Stability under nuclear radiation - The radiation stability of laminar solids is many orders greater than that of oils and greases.

Lubrication by films of solid lubricants has the following disadvantages.

Nonrenewable - When the lifetime of a bonded film is exhausted, the coating is nonrenewable unless the mechanism is disassembled and the coated part is reprocessed. Service lifetimes should be accurately determined beforehand by simulated or actual wear tests.

Noncooling - Unlike lubrication with oils, the solid film lubricants cannot carry away any heat generated during operation of the part.

Close control of processing variables - The precoating surface treatment needs close control if best service is to be obtained. For example, surfaces must be mechanically roughened or chemically etched to an optimum finish and must be thoroughly cleaned. Some of the effects of processing are discussed in later paragraphs.

Restrictive coating-application methods - The coating-application methods limit design; for example, holes of small inside diameter are hard to coat by spraying, tumbling, or brushing, and must be dipped; blind holes may require special injection jigs, even vacuum coating.

Use of Bonded Molybdenum Disulfide Films on Ball Bearings under Vacuum Conditions

A number of commercial bonded molybdenum disulfide films have been evaluated under vacuum conditions in the research program being conducted at LMSC.* Table III lists results obtained from tests conducted in an identical manner to the procedure for evaluating oils and greases, as described above. Results are also listed for a series of start-stop-reverse tests. In these tests, the motors were operated continuously for 52 min at 8000 rpm in one direction, then allowed to coast to stop and to remain idle during the succeeding period of 8 min. The motors were then operated for another 52 min at 8000 rpm in the opposite direction, again allowed to coast to stop and to remain idle during an 8-min period. The sequence was then repeated with operation of the motors in the original direction.

Preliminary runs had indicated that crown-type retainers were unsatisfactory, so all subsequent tests with MoS_2 films were conducted with ball bearings having ribbon-type retainers of pressed steel. The MoS_2 films were applied before assembly, and the coated parts were subsequently assembled. Best results were obtained with the MoS_2 films applied to the races and retainers only, leaving the balls uncoated.

Bearings with MoS_2 films are initially very rough and have high torques. It is necessary first to run in these

---

*In practically all cases, the performance of bonded films was superior to that of a burnished film formed from loose MoS_2 powder, which failed after only 31 hours.

TABLE III

LIFETIME OF BALL BEARINGS LUBRICATED WITH BONDED FILMS OF MOLYBDENUM DISULFIDE, MoS_2

Lubricant	Application of MoS_2 Coating	Operation	Lifetime
MoS_2, bonded with sodium silicate	Races and retainers	Unidirectional	2213 hrs to failure 1862 hrs to failure 1796 hrs to failure 1957 hrs (average) to failure
		Start-stop-reverse	772 hrs to failure (669 hrs at 8000 rpm)
MoS_2 bonded with low-temperature curing ceramic	Races and retainers	Unidirectional	157 hrs to failure
	Races, retainers, and balls	"	27 hrs to failure

Test conditions: Speed: 8000 rpm
Ball Bearings: R3 size, 440 C stainless steel, unshielded
Vacuum: 10^{-7} to 10^{-8} mm Hg
Temperature: 140 to 180°F

bearings by operating them very slowly and blowing out the particles of coating that flake off, then operating them somewhat faster and again blowing out loosened debris. This procedure is repeated several times until a constant, low torque value is obtained and the bearings run smoothly.

The longest life obtained to date with an MoS_2 film has been with a film bonded with sodium silicate. One pair of ball bearings coated with this film ran as long as 2213 hr in vacuum at 8000 rpm before failure. Coast times for these bearings were relatively long, indicating low running torque. Tests under start-stop-reverse conditions had only about one-third the life of those run under continuous unidirectional operation.

Although bearing lifetimes obtained in the LMSC studies with bonded MoS_2 films are less than those obtained with oils and greases, the MoS_2 films have several other virtues that should be considered. Since they are nonvolatile, their lifetimes are not likely to be markedly sensitive to increases in temperature whereas oils and greases can be expected to volatilize at significantly greater rates with increasing temperature.* Also, the MoS_2 films are not likely to become viscous when used at low temperatures. If radiation from a nearby nuclear power source becomes an important consideration, MoS_2 films, especially those bonded with an inorganic binder like sodium silicate, may be particularly suitable since they are very resistant to radiation.

Use of Molybdenum Disulfide Impregnated Electrical Contacts

Table IV presents the results of one group of tests on electrical slip ring assemblies that were operated for a short time in air and then in vacuum. In this application, the electrical noise generated by the contacts is the limiting factor in the performance.

*A temperature increase of about 28°C (50°F), for example, can double or quadruple the vapor pressure of many oils.

TABLE IV

RESULTS OF NOISE MEASUREMENTS WITH VARIOUS COMBINATIONS OF BRUSH AND SLIP RING MATERIALS

		Average Noise (microvolts)			
Slip Ring Material		Silver		Rhodium-plated Silver	
Brush Material		80% Ag + 20% Graphite	88% Ag + 12% MoS_2	80% Ag + 20% Graphite	88% Ag + 12% MoS_2
Time	0	10	50	40	10
	22 hrs in air	10	80	10	50
	30 hrs in vacuum	100	10	150	10
	200 hrs in vacuum	1500	10	2500	10

Test conditions: Slip rings, 2.25-in. dia x 0.1875-in. wide rotating at 17.8 rpm
Brushes, 0.116-in. x 0.184 in. (27,180 circular mils of apparent contact area)
Brush force, 103 grams (4 mg per circular mil)
Current, 32 milliamps per brush (1.2 microamp per circular mil of apparent contact area)
Vacuum, 4×10^{-7} mm Hg (approx.)
Average noise is the voltage drop that can be accurately reproduced on an 8-cycle per sec bandwidth.

The silver brushes impregnated with graphite performed well in air, but resulted in excessive noise that increased in amount as the unit was operated in vacuum. Molybdenum disulfide impregnated brushes, on the other hand, were more effective in vacuum than in air, and considerably outperformed the graphite impregnated brushes under vacuum conditions.

The electrical noise generated by the brushes increases with the current conducted across the sliding interface, as shown by the data in Table V. These data were obtained under the same test conditions as the data in Table IV, except that one set of brushes had conducted 32 milliamps for 100 hrs and the other set of brushes had run for 100 hrs with no current. At the end of 100 hrs, the noise was measured at several levels of current. The data in Table V are for 98% Ag:12% MoS_2 brushes on silver rings. The data in Table V also show that brushes that had carried current for 100 hrs were noisier than those that had operated without any current.

SOFT METALS

Soft metals with low shear strength, such as silver and gold, can be used as thin films over hard substrates to provide lubrication. The theory behind their use is similar to that described earlier; that is, the hard substrate keeps the area of real contact between the mating parts small, and the films of low shear strength reduce the formation of strong, welded junctions.

Among the advantages of soft metals are excellent vacuum stability (except for metals such as zinc and cadmium, which have relatively high vapor pressures); excellent radiation stability; good chemical stability; and excellent high-temperature stability. The fact that soft metals conduct an electric current can also be an advantage; in one application, for example, the use of silver films to lubricate ball bearings eliminated the need for a slip ring by allowing the current to be conducted directly through the bearing elements.

TABLE V

VARIATION OF NOISE WITH CURRENT LEVEL AND TIME OF PASSING CURRENT

Current, milliamps per brush	Average Noise (microvolts) After 100 hrs with 32 ma/brush	After 100 hrs with no current
10	10	5
50	12	10
100	30	15
200	70	20

Test conditions: Same as for Table IV
Brush: 88% Ag; 12% MoS_2
Ring: Silver

Except for certain extreme conditions, the friction and wear of soft metals is greater than that with other types of lubrication. Also, the use of soft metal films on parts such as ball bearings requires special handling that complicates installations and restricts designs.

Soft metals can be used in the form of thin films that are initially deposited on a hard substrate by such processes as vacuum deposition, chemical plating, and mechanical burnishing. Another technique for forming the lubricating film of soft metal is to impregnate the soft metal into a hard porous substrate from which it can be fed to the surface. Hard powder metallurgy compacts that have been infiltrated with a soft metal such as silver offer the advantage of providing a reservoir from which additional soft metal can be fed to the surface to renew surface films as they are worn away. The porous body can be made of a nonmetallic material to minimize its tendency to weld to a mating metallic surface. A similar technique is to knurl or machine indentations or other cavities into a surface and smear the soft metal into them.

Use of Soft Metal Under Film Vacuum Conditions

The use of soft metal films to provide lubrication under vacuum conditions was described in the literature over 20 years ago. Soft metals were found quite satisfactory for lubricating the ball bearings in rotating-anode x-ray tubes. Such bearings are small (on the order of 3/16-inch bore), are subject to light loads, and are heated during x-ray generation to temperatures estimated as ranging from 400 to 1100°F. Speeds are on the order of several thousand rpm, and the vacuum is in the range of 10^{-6} to 10^{-8} mm Hg.

Apiezon oil and grease, and other low-vapor pressure oils used in vacuum diffusion pumps were unsatisfactory because they migrated during tube operation and covered the face of the anode target with a thin film of lubricant. Thin films of barium evaporated from a hot film on the ball bearings of tool steel* produced several improvements, as compared to dry, unlubricated bearings. The speed increased from 3100 to 3650 rpm; the coast time (time for bearings to slow down and come to rest after motor was turned off) increased from 12 sec to 8 min; and the noise level dropped from 87 to 68 db. The films were said to be permanent for hundreds of hours of rotation at room temperature (i. e., provided the tube was not generating x-rays) and for at least 50 to 100 hrs of rotation at the elevated temperatures during x-ray generation.

Additional metals tried on the tool steel ball bearings included zinc, magnesium, strontium, calcium, silver, gold, copper, iron, nickel, cobalt, platinum, and chromium. Some of these gave results similar to those with barium, but none gave better results, and a number of them were poorer.

One of the leading manufacturers of rotating anode x-ray tubes currently uses silver films deposited by a proprietary technique on the balls of the ball bearings used for rotating-anode x-ray tubes. Three types of ball bearings are used to facilitate assembly and to allow for thermal expansion

*High speed tungsten-cobalt-chromium steel.

and contraction during operation: bearings with split inner races; angular contact bearings that are spring-loaded axially; and bearings with flat outer races. Under operating conditions, the silver-coated ball bearings have minimum lifetimes of 1000 hours and have attained lifetimes of 10,000 hours or more.

Gold-plated ball bearings are also being studied for use in vacuum by several research laboratories in the country. Preliminary results show that they are also promising for use under space conditions.

PLASTICS

Plastics have been found very useful in many applications involving friction and wear, such as gears, bearings, cams, and rollers. Nylon, for example, has long been used to provide quiet-running gears that require little attention, and Teflon has been used for sleeve bearings that operate dry with little friction. Plastic gears and bearings generally operate dry, though a few drops of oil applied initially improve their performance.

The form in which the plastic is used can be varied to meet specific needs, and many specialty grades and techniques are available that overcome some of the general disadvantages of plastics, thus allowing full use of their special properties. In many applications, plastics can be used in pure bulk form, as in the case of cast, molded, pressed and sintered, or machined articles. In other applications, bulk plastics incorporate various fillers that improve their frictional and mechanical properties. In still other uses, plastics are used in the form of thin films or as impregnants in porous solids.

A complete discussion of the various plastics and their specialty forms is beyond the scope and limitations of this paper. However, the following sections discuss some of the general advantages and disadvantages that plastics have for applications involving friction and wear.

Advantages of plastics include the following:

Self-Lubrication. Most plastics have good friction characteristics, even when run dry. Self-lubrication can be improved by adding fillers such as MoS_2. Porous plastic bodies can be impregnated with oils to provide lubrication, as in ball-bearing retainers of Synthane (a porous paper-base phenolic composition). In other cases, a plastic such as Teflon that has outstanding anti-friction properties can be impregnated into a porous metal to provide lubrication. These characteristics of self-lubrication can be used to advantage where relubrication is difficult, where operation is intermittent with long idle periods, or where temperatures are too low for oils and greases to be effective (e.g., cryogenic applications).

Cold-Welding Tendencies. Plastics can be selected that have little tendency to "stick" or cold-weld to metals, even under ultrahigh vacuum. The anti-sticking characteristics of Teflon to metal are well known and, in fact, they are a positive disadvantage at times when bonding a film of Teflon to a metal is desired in order to form an inert film or take advantage of some other Teflon properties.

Vibration Absorption. Plastics have a good capacity for absorbing vibration and, therefore, provide quiet running with minimum noise and vibration. This characteristic is well-known in the case of gear trains of nylon.

Impact Resistance. Some of the plastics have very good impact strength. They can deform elastically to absorb shock and vibration so that, during the launch phase of spacecraft, there is less danger of brinelling with ball bearings using plastic balls than with those using steel balls. This characteristic has been used to advantage in several applications of ball bearings for armored-vehicle turrets. Reference 2 reports on the successful replacement of steel balls in the main bearing assembly of the U.S. Army T-92 light tank with 1-in. diameter plastic balls. This bearing is 90 in. in diameter, supports the weight of the main turret and gun cupolas, and absorbs gun recoil and acceleration forces during high-speed travel over rough terrain. Another application of plastic bearings reported in Ref. 2 was their

use in the gun mount of an LVT-5 landing vehicle. These bearings were 10 in. in diameter and carried a full complement of balls. Load-carrying plastic balls of 0.406-in. diameter alternated with spacer or idler balls of 0.394-in. diameter. These bearings survived recoil and other heavy loads without appreciable signs of wear or brinelling.

Density. Plastics have lower densities than most metals so that plastic parts can be lighter in weight. The densities of plastics are as low as 1/6 or 1/7 that of steel or about half that of magnesium.

Tolerances. Tolerances are less critical for plastics than for steel in such parts as balls, bearing races, and gear teeth. Plastics deform more readily to meet the needs of poorer tolerances and of less accurate mounting and alignment.

Machinability. Plastics have good machinability and can be molded to close tolerances. They also have good dimensional stability. There are exceptions, however, where moisture absorption occurs, as in the case of molded nylon.

Contamination. Contamination by dust and wear debris is less of a problem with plastics than with metals. Plastics have less tendency than oils and greases to attract dust. The plastics themselves are abrasion resistant, and they allow contaminants to be embedded into them, thus preventing scoring of the mating part. This property makes sealing against contamination less critical with plastic components than with those fabricated from metal.

Corrosion. Plastics are relatively inert and free from corrosion, such as that which might be caused by humidity, fog, or other moisture prevailing in the atmosphere at launching sites, or that might be caused by contact with acids or other normally reactive chemicals.

Compatibility. Plastics are compatible with oils, greases, and many chemicals so that such materials can be added for lubrication or to protect other parts against corrosion without harming the plastic components with which they come into contact.

Durability. Plastics have low wear rates and outlast metals in many applications.

Cryogenic Temperatures. Plastics such as Teflon retain their useful mechanical properties as well as their friction and wear characteristics at cryogenic temperatures, which are below those at which oils and greases become too viscous for use.

Vacuum. Plastics are generally less volatile than oils and greases so that they are more stable under vacuum conditions.

Creepage. Self-lubricating plastics are useful in instrument mechanisms and other devices where oils and greases creep away from the bearings or other parts needing lubrication.

Plastics suffer certain disadvantages for applications involving friction and wear when compared to metals. It would be improper to generalize too widely here, since disadvantages are not always common from one plastic to the next. Also, many specialty grades and techniques are available that overcome some of the disadvantages.

Thermal Conductivity. The thermal conductivity of plastics is much lower than that of metals. Consequently, they are less able to dissipate frictional heating generated at rubbing interfaces so that plastic parts run hotter than similar parts made of steel. For use at high speeds, it may therefore be necessary to use the plastic in the form of a thin film over a metal substrate so that the metal can conduct the frictional heat away more efficiently. Other techniques for accomplishing the same purpose include the use of metal fibers as fillers and of metal backing screens.

Thermal Expansion. Plastics have high rates of thermal expansion. Their coefficients of thermal expansion are ten times or more that of steel.

Temperature Resistance. Bulk plastics cannot be used at as high temperatures as can steels. They soften with heat and generally should not be used above 200 to 300°F. Teflon, the most heat-resistant of the plastics, melts at 620°F and

cannot be used in pure bulk form at temperatures approaching this level.

Operating Speeds. As a consequence of the foregoing limitations, the use of plastics is restricted to lower speeds than those at which steels can be used.

Structural Strength. Plastics are weaker than steels so that the load-carrying capacity of plastic gears and bearings is less than for the same size steel part. Since plastics are strong enough for the lightly loaded applications common to spacecraft systems, however, this is not a major objection to their use under the proper conditions.

Radiation Stability. The radiation stability of plastics is poorer than for metals.

CERAMICS AND CERMETS

Ceramics and cermets are essentially hard, brittle materials, such as sapphire, glass, cemented carbides, fully dense oxides, bonded oxides, and Pyroceram. *

Advantages offered by these materials include the following:

- o Hardness - These materials are extremely hard and have generally good wear resistance.
- o High-temperature stability - These materials retain their hardness and strength to higher temperatures than do metal alloys.
- o Chemical stability - Resistance to oxidation at elevated temperatures is excellent in most cases. Resistance to corrosion and compatibility with LOX are also generally good.
- o Dimensional stability - These materials are dimensionally stable and can be precision finished to high accuracies and excellent surface finishes.

---

* Corning Glass Works' trademark for its crystalline materials made from glass.

- o Minimum tendency to cold weld - These materials have little tendency to cold weld to metals, even under hard vacuum conditions.

Disadvantages of the ceramics and cermets generally include the following:

- o Brittleness - These materials are less ductile than most metal alloys and are more sensitive to damage by shock and vibration. Shock loading to protect them against impact and vibration during the launch and ascent phases may be necessary for spacecraft applications.
- o Low load-carrying ability - The load carrying capability for some of these materials is less than that of steel.
- o Catastrophic failures - Failures of parts such as gears and bearings made of the ceramics and cermets are often catastrophic, resulting in complete destruction of the part.
- o Load and speed limitations - Because of the first three limitations, the use of ceramics and cermets is generally restricted to low speeds and light loads.

The ceramics and cermets appear to have their most promising applications in the following areas:

- o High-temperature rubbing seals and bearings - Where temperatures are too high to provide an effective lubricant, unlubricated rubbing surfaces of the ceramics and cermets (either in contact with themselves or against metal alloys) appear useful, although lifetimes may be limited.
- o Gas lubricated bearings - Because of their ability to be precision machined to high accuracies and fine finishes, ceramics and cermets are useful for parts of gas lubricated bearings. Their high-temperature stability extends their operating range.
- o Instrument bearings - Jewel bearings of sapphire have long been used in precision instruments where loads and speeds are negligible.

BIBLIOGRAPHY

1. Bowden, F. P., and D. Tabor, The Friction and Lubrication of Solids, Oxford University Press, London, 1954.

2. Montalbano, Joseph E., "Plastic Ball and Roller Bearings," Machine Design, Vol. 30, No. 16, pp. 96-99, August 7, 1958.

PROBLEMS OF THERMAL CONTROL SURFACES IN THE SPACE ENVIRONMENT

R. E. Gaumer
Head, Thermophysics Research
Lockheed Missiles & Space Company
Palo Alto, California

ABSTRACT

The necessity for thermal control surfaces for space vehicles, the ranges of temperature required for component control, the degree of tolerances allowable for individual component temperature control, and the connection between present day materials research for advanced applications and problems of spacecraft thermal control will be discussed.

The principles of "passive" thermal control of radiant energy will be mentioned in sufficient detail to allow division of all passive thermal control materials into four types of control surfaces. Several specific examples of materials employed for each type of thermal control surface will be given, together with data pertaining to the pertinent themophysical properties of these materials. Consideration will be given to both coatings and metallic substrata, including the presently used aluminum, magnesium, and beryllium alloy substrata.

The effects of the total environment upon material characteristics and thermal characteristics will be discussed in sufficient detail to indicate adequacy of presently available materials or to indicate necessary directions of materials development work. The total environment of a space vehicle is arbitrarily classified as pre-launch and post-launch phases. The pre-launch phase includes corrosion, oxidation, contamination, handling difficulties, etc.

The post-launch environment will be discussed as including the ascent phase and such orbital environmental phenomena as ultra-violet effects, vacuum volatization, thermal cycling effects and surface erosion phenomena. An effort will be made to discriminate between environmental effects which are important as to their effects upon materials and those which are, relatively, second order effects.

A review will be given which indicates the degree to which stable, reliable substrata and coatings of the four basic types exist in the industry today, with recent data appended as justification for the statements made. Considerations of weight, cost and reliability will be mentioned, as well as the radiation characteristics and thermophysical properties of the materials discussed.

Finally, an effort will be made to indicate those areas of material science and technology in which further research and development effort appears to be necessary in order to achieve adequate stable and reliable materials for spacecraft thermal control. The criteria for adequacy are the various parameters discussed earlier in the paper.

The designers of today's spacecraft are concerned with the maintenance of prespecified temperatures of individual components within the satellite, missile, space probe or other form of spacecraft. Most components are required to remain at a certain specified temperature, plus or minus an allowable tolerance for satisfactory component performance in orbit. Since it is extremely costly in terms of weight, power, and money to supply internal heating or cooling capabilities, it becomes necessary to regulate the local external temperatures of the skin of the space vehicle. Then, in turn, internal temperatures are regulated by suitable choice of thermal impedances between the exterior and interior of the spacecraft. Although localized methods of heating or cooling are occasionally used, the most typical requirement involves a choice of material suitable for maintaining the external temperature of the skin at the proper

space-time average equilibrium temperature. One must also take into account energy generated and dissipated internally, usually by electronic gear. The greatest single source of energy useful for thermal purposes is the energy emanating from the sun. In addition to absorbing electrical and solar energy, the spacecraft also radiates energy to what essentially constitutes an infinite sink; i. e., to an enclosure maintained at $\sim 4^{\circ}K$.

The variety of temperature tolerances and, indeed, of temperature limits of individual components of spacecraft varies widely throughout the temperature spectrum. Cryogenic payload or fuel components must be maintained at temperatures in the range of $20^{\circ}K$. The auxiliary power conversion units frequently operate in the range of $1000^{\circ}K$. Between these limits a broad range of equipment temperatures exist as indicated in Figure 1. An effort has been made in Figure 1 to indicate by means of the width or narrowness of the bars the allowable tolerances for temperatures of individual components. Electronic equipment, manned

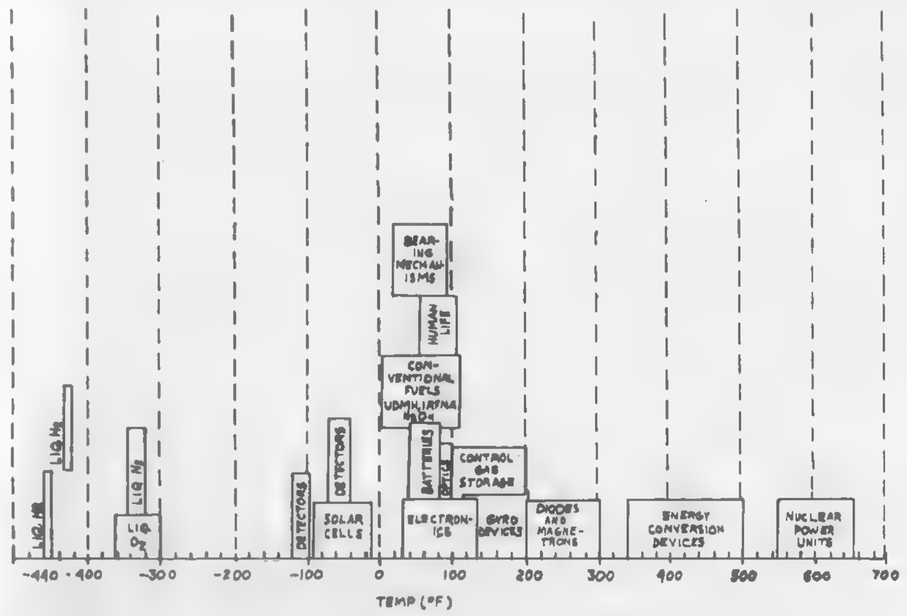


FIGURE 1 COMPONENT TEMPERATURE TOLERANCES

spacecraft, and most other essentially terrestrial phenomena must be maintained within a band of 20-60°C for proper operation in the space environment.

Certain critical optical components need to have temperature control maintained to within a fractional part of a degree in order to insure proper resolution in orbital situations. Optical components are particularly sensitive, since the ultimate criteria of adequate performance is optical resolution which is, in turn, affected by any geometrical displacement of the optical lens or mirror system. Differential thermal expansion phenomena must be carefully controlled in order to avoid such critical geometrical disturbances.

The necessity for nearly absolute reliability of materials and components which are used in the construction of spacecraft becomes evident when one considers the multimillion dollar price tag of many satellites. It is imperative that all materials be nearly completely stable for the period of operation prespecified for the particular mission. Extremely low weight, a high strength-to-weight ratio, high tolerance against orbital contamination or oxidation and many other considerations must be included in the choice of materials which may be utilized for thermal control of spacecraft. The necessity for producing materials which possess the fundamental physical characteristics necessary for adequate thermal control and which simultaneously possess the desirable characteristics of low weight, reasonable cost, and high stability in space environments has given a tremendous impetus to the development of new materials which are potentially useful in space flight concepts.

Re-entry considerations, in particular (which are characterized by high heat flux, high temperature, and relatively high aerodynamic shear phenomena) have led to a considerable emphasis on the development of refractory metals and refractory oxides which probably will possess the desired characteristic stability and proper thermal radiation characteristics throughout their useful lifetime. Such materials as beryllium, tantalum, titanium, and the super alloys, have become commonplace in the satellite industry of today, as a result of the above considerations.

As mentioned above, the usual method of temperature regulation in spacecraft is by means of "passive" thermal control, since "active" thermal control is usually quite costly in terms of both weight and power. Without going into elaborate details, the principles of passive thermal control of radiant energy involve selective reflections and emissions of electromagnetic energy. The sun constitutes the sole source of radiant energy for a spacecraft, other than internally generated electrical power. Materials exhibit vastly different characteristics as to their absorption of solar energy and their consequent emission of temperature-characteristic radiant energy. The coefficient of absorption of solar energy is commonly characterized by α_s (solar absorptance). Solar energy exists primarily in the wavelength range 2,000-18,000 Å. The coefficient of emission of radiant energy, characteristic of the equilibrium temperature of the radiator, is commonly designated by ϵ (infra-red emittance). Room temperature characteristic infra-red energy is in the 100,000 Å range. The ratio α_s/ϵ may be considered to be a measure of that amount of energy stored by the receiving surface and, consequently, of the equilibrium temperature of the receiver.

$$(\overline{T}_o)^4 = C_1 \frac{\alpha_s}{\epsilon} + C_2 \frac{P_i}{\epsilon} + C_3 \qquad (1)$$

where P_i = internally generated power.

An obvious interpretation of Eq. (1) shows that as $\alpha_s \to 1$, most of the available solar energy is absorbed by satellite, with consequent high equilibrium temperature. As $\epsilon \to 1$, a large proportion of the stored energy, characteristic of the temperature of the spacecraft surface, is radiated and lost to the space environment with consequent low equilibrium temperature. A high ratio α_s/ϵ corresponds to a relatively high space-time orbital average equilibrium temperature of the receiving surface, whereas a low value α_s/ϵ corresponds to a low space-time orbital average equilibrium temperature of the receiving surface. Materials are available which exhibit α_s/ϵ ratios ranging from approximately 40 to approximately 0.2. For some orbits, these ratios correspond to approximately 700°C and approximately -100°C,

respectively. Materials characterized by very high α_s/ϵ ratio are called solar absorbers. Materials characterized by very low α_s/ϵ ratios are called solar reflectors. Materials characterized by α_s/ϵ approximately equal to one are divided into two categories; α_s/ϵ = 0.9/0.9 is called a flat absorber, whereas α_s/ϵ approximately 0.2/0.2 is called a flat reflector. Figure 2 presents a table of materials characteristic of the above mentioned four classes of thermal control materials. The best examples of the individual classes are:

1) solar absorbers; "Tabor" surfaces and highly polished metals
2) solar reflectors; white paint, white ceramics
3) flat absorbers; black paint, black electrodeposited coatings
4) solar reflectors; metallic pigmented paints.

It may be evident from the above discussion that the majority of thermal control materials are of the type of coatings or film forming materials which are applied to

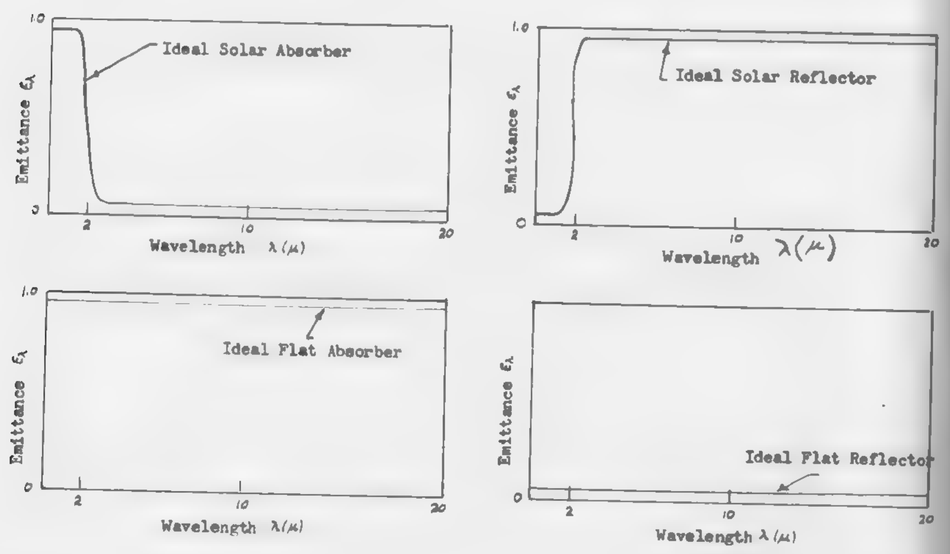


FIGURE 2 REPRESENTATIVE SPECTRAL EMITTANCE CURVES OF THE FOUR IDEAL SURFACES

the basic structural materials. Electrical conductors require a thickness of a few micro-inches for optical and infrared opacity, while dielectrics normally require several thousandths of an inch thickness for opacity.

Considerations which dictate choice of the basic structural materials are usually the strength-to-weight ratio, availability, and cost; these have led to a choice of aluminum, magnesium and beryllium alloy substrata for most space vehicles. Hence, it becomes necessary to develop adequate coatings for application to these specific substrata. Customarily, a mosaic of satisfactory thermal control coating materials is designed whose area-weighted average value of α_s/ϵ is satisfactory from a design point of view. These mosaic materials to be coated upon the basic skin substratum must, of course, be compatible with the substratum if they are to perform reliably throughout the satellite lifetime. They must also be reasonably stable and durable in production and application situations. Other considerations affecting the choice of materials for thermal control of spacecraft are the pertinent thermophysical characteristics such as thermal conductivity, thermal diffusivity, and specific heat. These parameters obviously affect the rate of heat transfer and of heat storage of components. Needless to say heat transfer rate is an important factor since the average satellite goes into and out of the sun about once every hour.

Thus the first step in the selection of materials for spacecraft thermal control involves the specification of a material with desired values of α_s, ϵ, K, C_p, α, and ρ. It now becomes necessary to consider the effects of the total environment to which the space vehicle will be exposed upon the stability and reliability of pertinent physical and thermal characteristics. The total environment of the space vehicle may be arbitrarily classified into pre-launch and post-launch phases. The pre-launch environmental phase includes the terrestrial phenomena of corrosion, oxidation, contamination, handling problems, fingerprinting, humidity control, etc. Although the pre-launch environmental phase is rather more prosaic than the orbital phase, it is no less significant in its effects upon the thermal

radiation characteristics of materials. For instance, the effect of fingerprinting a gold plated thermal control surface is to change the α_s/ϵ ratio from ~ 8 to ~ 0.8 with a resultant loss of thermal control in any black box immediately adjacent to the external thermal control panel. The quest for materials which are stable to all environmental phenomena leads immediately to the consideration of substances with extremely high binding energies. These materials tend to be less affected by ordinary low-energy phenomena than do the more unstable materials, such as organics.

The post-launch phase of the space environment can be divided into an ascent phase, an orbital phase, and a re-entry phase. The ascent phase, for unprotected vehicles, is characterized by exposure to relatively high (approximately 500°C) temperatures during the period of ascent, high aerodynamic heating rates, high aerodynamic shear and lateral and longitudinal vibrations of approximately 10 g's. The ascent phase is particularly severe upon the class of materials characterized as solar reflectors; i. e., white paints which tend to darken and turn brown. Ceramics and adhesive-bonded materials tend to suffer loss of adhesion as a result of severe vibrations encountered during the ascent phase.

The orbital phase of the post-launch environment is characterized by such phenomena as a high level of ultra-violet energy, Van Allen belt effects, vacuum volatilization, thermal cycling effects, surface erosion phenomena, and high energy particulate radiation.

It has been established during the course of the program existing at LMSC that ascent heating, ultra-violet degradation and Van Allen belt radiation are the most severe space environmental effects in terms of environmental degradation of materials for thermal control. Such phenomena as surface erosion due to sputtering or micrometeorites have definitely been shown to be second order in terms of satellite thermal design for one year's lifetime. The effect of ultra-violet radiation is generally to cause the α_s/ϵ ratio of nearly everything to approach $\alpha_s/\epsilon \simeq 0.9/0.9 = 1$; in short, to reduce everything to an average temperature characteristic of α_s/ϵ ratio = 1. Thermal cycling as a result of orbital

temperature fluctuations is important in an indirect way in that it causes loss of adhesion between the basic substratum and the coating materials used for thermal control. Vacuum volatilization and subsequent loss of the materials is second-order in importance except where organic materials of relatively high vapor pressures have been employed for thermal control. Every effort is made to design the thermal control surfaces for space vehicles without use of any organic material characterized by high vapor pressure and low binding energy. Although by no means everything is known about the effect of the total environment upon the stability of materials chosen for thermal control of spacecraft, certain generalizations can safely be offered at this time based upon the past two years research program, the aim of which is to provide thermally satisfactory and reliable materials.

The class solar absorbers (high α_s/ϵ) ratio is particularly susceptible to damage during the pre-launch environment. Oxidation and corrosion are the two worst enemies of these highly reflecting surfaces. Every effort must be made to provide satisfactory protection for gold-plated or highly polished surfaces during the pre-launch period.

After having been launched the materials comprising the class solar absorbers are reasonably safe from degradation in the space environment, due to the relatively high binding energies of the components involved. The type of materials used as solar reflectors are white paints, white ceramics, and certain types of anodized metal surfaces and are relatively durable in the pre-launch environment but extremely susceptible to ultra-violet damage and Van Allen belt radiation degradation while in orbit.

Tests performed at LMSC indicate that degradation of the α_s/ϵ ratio (and subsequently of the temperature of internal components) of 30-80% in a one-year exposure to average orbital high energy radiation conditions for solar reflecting materials. Figure 3 illustrates the type of degradation that may be expected due to ultra-violet damage. Although a reasonable understanding exists insofar as most specific environmental effects on most specific materials are concerned, the precise mechanism by which ultra-violet

electromagnetic energy causes degradation of various coating materials used for thermal control is not well known at this time. It is supposed that the bulk of the ultra-violet degradation of optical performance of paints results from two separate mechanisms. One mechanism, the formation of color or impurity centers, appears to affect the pigmenting material in a paint or coating material whereas a breakdown of the vehicle which holds the pigment together and in contact with the substratum is presumed to be associated with chemical cross-linking or scission phenomena. Although materials have been developed to date which appear to exhibit satisfactory resistance to the ultra-violet and Van Allen belt radiation phenomena in orbit, these have been largely developed by a "cookbook" philosophy. It seems unlikely that completely satisfactory thermal control coatings and materials can be developed until an adequate phenomenalistic explanation of the mechanism of degradation can be developed. Research efforts are underway at LMSC in order to provide such an understanding.

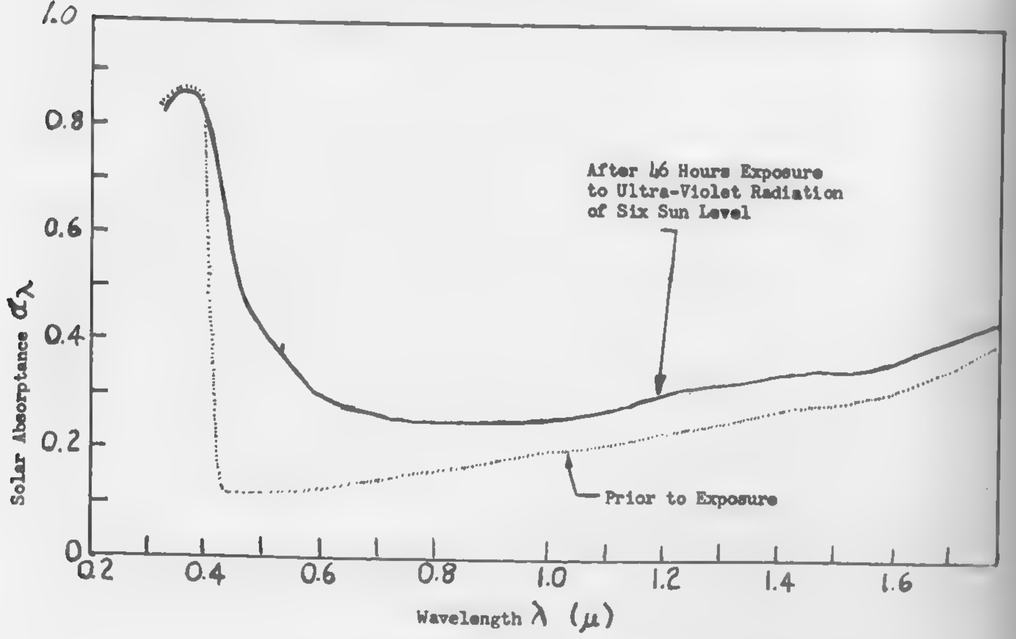


FIGURE 3 SPECTRAL ABSORPTANCE α_λ VERSUS WAVELENGTH FOR TiO_2-PIGMENTED EPOXY-BASE PAINT

In terms of the four basic types of thermal control surfaces useful in spacecraft thermal control Figure 4 gives an indication of the degree of perfection which has been obtained in these four basic types of radiation controlling materials. As is obvious from Figure 4, reasonably satisfactory flat absorbers and flat reflectors exist today. In the areas of solar absorbers and solar reflectors, a considerable amount of research remains necessary, both in order to optimize the α_s/ϵ ratios of the surfaces under consideration and in order to develop adequate stability and reliability for a time of at least one year's orbital lifetime. When one begins to consider the type of thermal control surface necessary for space probes, lunar landings and so on, which are characterized by extremely high or by extremely low heat fluxes and by extra-terrestrial environmental phenomena which are poorly understood, then the challenges to materials research necessary in order to develop adequate materials for thermal control of spacecraft become evident.

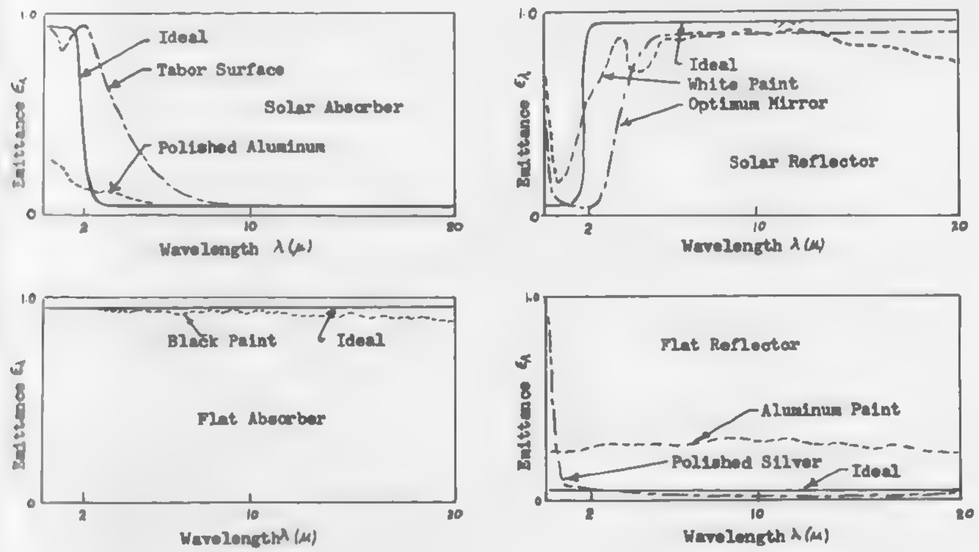


FIGURE 4 PRACTICAL VS IDEAL THERMAL CONTROL SURFACE TYPES

In conclusion a few remarks are given as to those areas of materials research and development which appear to need further attention in order to satisfy present requirements for thermal control of spacecraft. The items listed below are by no means of equivalent importance; however, there exists a pronounced need for the materials described at the present time.

- o High-temperature Adhesives - A need exists for an adhesive bonding agent which is capable of maintaining minimal shear strength while bonding foil type thermal control surfaces to basic magnesium and aluminum substrata. These adhesives must be capable of withstanding temperatures of up to 1000°F on a short time (3-5 minutes) basis. Aerodynamic shear and vibration will be experienced simultaneously with the thermal pulse. Such an adhesive must also be capable of withstanding all orbital environmental phenomena described above.

- o Controlled Ablators - Ablative materials for spacecraft re-entry are required where controlling physical parameters are sufficiently well understood so that calculations of weight loss as a function of re-entry heat flux can be reliably performed.

- o Solar Absorptance Coating for Magnesium Thorium Alloys - The corrosion and oxidation resistance of presently employed Mg-Th alloys such as HM21A and AZ-31 is such that it is impossible to utilize the radiation characteristics of the substratum for a solar absorber thermal control surface. Some methods of plating such as electrodeposition or vacuum deposition of a stable, durable material with intrinsically high α_s/ϵ ratio onto the basic skin alloy would be extremely useful to the industry.

- o Self-thermostatic Materials - A material which would vary its radiation characteristics as a function of temperature in such a fashion as to maintain a prespecified equilibrium temperature

or narrow band of temperatures is urgently needed. The availability of such a self-thermostatic material would solve 90% of the problems which presently confront thermal designers of spacecraft. Some possibilities for self-thermostatic thermal control materials are semi-conductors, ferromagnetic materials, ferro-electric materials, and such compounds which exhibit pronouncedly temperature sensitive phase transitions. Another possibility is the use of a photo-thermotropic substance which will vary the characteristic orientations of submolecular sized particles in a manner controllable by thermal adjustment. Research is underway in all of these areas under the sponsorship of LMSC.

- o Solar Reflecting White Paint - The goal of development work for solar reflectors is the accomplishment of α_s/ϵ ratio of approximately 0.1. Such an α_s/ϵ ratio will result in an orbital equilibrium temperature of approximately -200°F, which is suitable for infrared detection packages. Presently attainable white paints have α_s/ϵ ratios only slightly less than 0.2. It is necessary that such a paint be resistant to ascent aerodynamic heating, orbital ultra-violet irradiation, and high energy particulate radiation. Furthermore, due to practical considerations, it should be possible to apply such a paint by ordinary spraying procedures without the necessity for elevated temperature curing cycles.

- o Practical Tabor Coatings - Tabor coatings having characteristic α_s/ϵ values of 40 are attainable in the research laboratories, but, to date, all attempts to utilize such coatings on the substrata available for spacecraft and under the rather severe environmental conditions to which such coatings would be exposed in space applications have been unsuccessful.

- High-temperature Radiative Coating - For re-entry and space probe utilization, as well as for application to nuclear and other auxiliary power units, a very great need exists for a material with emittance ≥ 0.95. It should be pointed out that this minimal emittance has to exist at the operative temperature which is usually in the vicinity of $1000^{\circ}F$. Consequently, such a coating material must be stable in every sense of the word at elevated temperatures. Further research and development effort in the materials sciences can be inferred from consideration of Table I and subsequent contrast with Figure 2.

TABLE I

RADIATION CHARACTERISTICS OF MATERIALS

Material	α_s	ϵ	α_s/ϵ
Aluminum	0.387	0.027	14.35
Gold Plated on Stainless Steel	0.301	0.028	10.77
Gold over Titanium with Resin Undercoat	0.300	0.033	9.10
Gold, Vacuum Deposited	0.282	0.034	8.29
Aluminum Foil - Dull Side	0.223	0.030	7.43
Beryllium	0.444	0.063	7.04
Aluminum Foil	0.218	0.032	6.81
Aluminum Foil Type	0.238	0.043	5.54
Aluminum Foil - Shiny Side	0.192	0.036	5.33
Inconel X Foil	0.624	0.143	4.36
Aluminum	0.218	0.051	4.28
Molybdenum Slug	0.480	0.122	3.94
Chrome - Aluminized Mylar	0.247	0.085	2.90
Carbon Black Pigment	0.908	0.780	1.16
Five Mils of Rokide C	0.898	0.789	1.14
Dull Black Micobond	0.936	0.844	1.11
Aluminum, Sandblasted, 120 Size Grit	0.600	0.410	1.50
Electroless Nickel	0.450	0.170	2.60
Dow 17 on Magnesium	0.53-0.72	0.50-0.82	0.95

ϵ = total hemispherical emittance at $500^{\circ}R$

α_s = solar absorptance, extraterrestrial

TABLE I (continued)

Material	α_s	ϵ	α_s/ϵ
Epoxy Paint, Skyspar (untinted white)	0.260	0.860	0.30
Kemacryl Lacquer (white)	0.260	0.750	0.35
Five Mils of Silica Oxide on Magnesium	0.210	0.830	0.25
Cermet (ceramic containing sintered metal)	0.650	0.580	1.10
Lithiated Aluminum Silicate Inorganic Paint	0.180	0.870	0.21
QMV Beryllium Alloy			
Rolled Plate, Chem. Milled	0.480	0.110	4.40
Rolled Plate, Chem. Milled, Chem. Polished	0.500	0.090	5.60
Fuller Gloss White Silicone	0.300	0.810	0.37
Fuller Flat Black Silicone	0.890	0.810	1.10
Fuller Aluminum Silicone	0.230	0.200	1.20
Dull Black Micabond Vinyl (Phenolic) Paint	0.930	0.840	1.10
Kemacryl Lacquer (black)	0.940	0.830	1.10
Aluminum Coated with SiO	0.510	0.700	0.73
Pure Tantalum	0.442	0.081	5.46
Rene 41, Vapor Honed and Buffed	0.398	0.103	3.86
White Porcelain Enamel	0.256	0.828	0.31
Production Dow 15 on HM21A Magnesium	0.359	0.030	11.98

ϵ = total hemispherical emittance at 500°R
α_s = solar absorptance, extraterrestrial

RE-ENTRY ENVIRONMENT

Jackson R. Stalder
Vidya, Incorporated
Palo Alto, California

ABSTRACT

The primary problems which are encountered during entry of vehicles into the atmosphere of the earth and of other planets are discussed from the viewpoint of definition of the environment which must be withstood by the vehicles.

Trajectory characteristics are discussed for ballistic vehicles, and the effect of the utilization of lift as a means of decreasing deceleration forces is examined.

Major aspects of aerodynamic heating are discussed including the relative magnitudes of convective and radiative heating. Heating rates for typical re-entry vehicles are shown.

The several types of thermal design for coping with the heating problem are discussed, and the major advantages and disadvantages of each are briefly mentioned.

INTRODUCTION

The problem of controlled entry into the earth's atmosphere has, for the past 10 years, received an unprecedented amount of attention from the engineering and scientific community. By reason of the large effort which has been exerted on this problem, ballistic missiles are now commonplace, and the problem of designing re-entry capsules for ballistic or satellite orbits has been placed on engineering basis.

Recent national decision to expedite the attainment of manned space travel has now focused attention on entry from lunar and planetary orbits. The increase in entry velocity resulting from extra-terrestrial entry as compared with entry from earth orbits has raised problems which are not yet amenable to routine engineering solution. The present aerodynamic and thermodynamic problems lie largely in the fields of advanced physical and chemical research and include extremely complex questions concerning the non-equilibrium chemistry and physical properties of air which is heated, almost instantaneously to temperatures of many thousands of degrees. Most of the problems are so complex as to defy analytic solution; consequently, extensive experimentation is in progress. It is worth noting that the problems encountered in development of the test equipment are comparable in magnitude to the flight problems which will be solved in the test apparatus.

It is the purpose of this paper to discuss the primary problems which are encountered during entry of vehicles into the atmosphere of the earth and of other planets from the viewpoint of defining the environment which must be withstood by the vehicle.

TRAJECTORY CHARACTERISTICS

All of the re-entry problems arise because of the tremendous amount of kinetic energy which must be dissipated as the vehicle decelerates from its maximum orbital speed to its impact, or landing, speed. The kinetic energy which, somehow, must be dissipated is shown in Figure 1 as a function of the vehicle speed at entry into the sensible atmosphere. Also indicated in this figure are the amounts of heat absorbed by the vaporization of several materials from the solid state to the gaseous state. Figure 1 shows, for example, that entry from a minimum speed lunar or planetary orbit would completely consume a carbon heat shield if all of the kinetic energy were dissipated by vaporizing the heat-shield material.

In view of this, the obvious course to follow is to devise configurations and trajectories which allow the vehicle's

kinetic energy to be dissipated, not by heating the structure, but by delivering this energy to the surrounding atmosphere. To this end, a great deal of study has been directed over the past decade.

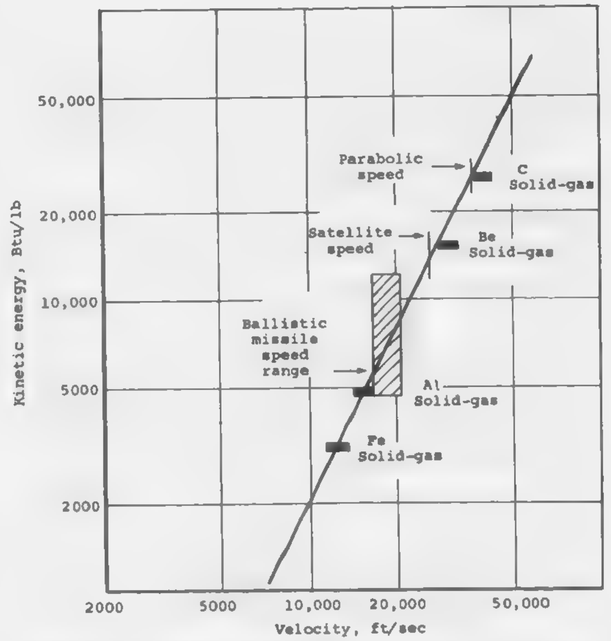


FIGURE 1 KINETIC ENERGY OF RE-ENTRY VEHICLES

Considering first the case of ballistic re-entry, that is, re-entry of vehicles which do not employ lift forces, these trajectories were prior to 1952, studied primarily by performing detailed machine calculations employing one of several detailed model atmospheres.

Generally, gravitational forces were included in the motion equations, and account was taken of the variation of vehicle drag coefficient with Reynolds and Mach numbers. These computations were of limited value, since it was not possible to draw general conclusions concerning the trajectory because of the specialized assumptions that were made concerning vehicle configuration and entry conditions of speed, angle, etc.

In 1952, a drastic simplification of the ballistic re-entry problem was effected by Allen and Eggers of the Ames Research Center.[1] The simplification was a result of an

approximate analytic solution to the problem of determining the motion and heating of ballistic vehicles entering the earth's atmosphere. The solution was accomplished by the recognition of several facts:

1. The variation of atmospheric density with altitude could, in the altitude range of interest, be represented very closely by an exponential function of form

$$\rho = \rho_o e^{-\beta y} \qquad (1)$$

This relationship is compared with the standard ARDC atmosphere in Figure 2.

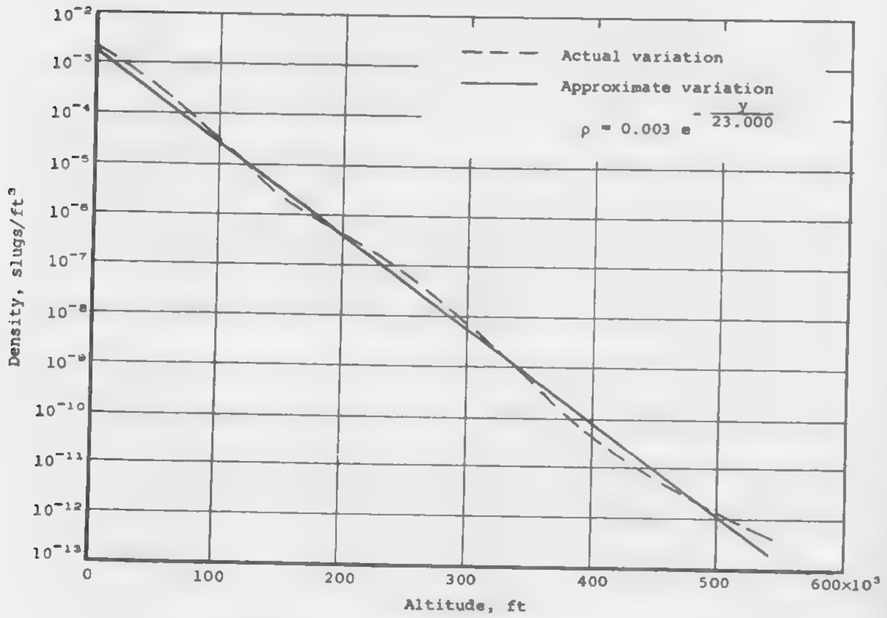


FIGURE 2 VARIATION OF DENSITY WITH ALTITUDE

2. The total drag coefficient of a given ballistic vehicle could, to a fair approximation, be considered to be constant in the speed and altitude range of interest.

3. Gravity had a negligible effect on the vehicle motion.

These observations, which permitted closed solution of the vehicle motion to be obtained, led immediately to a considerable advance in our understanding of the motion, especially--and to a lesser extent, the heating of ballistic re-entry vehicles. The major conclusions of this early work can be summarized as follows:

1. The maximum deceleration of a missile is independent of its mass, size, and shape and is determined only by the entry speed and flight-path angle. The independence of mass and size is shown in Figure 3, taken from Reference 2, which shows the deceleration histories of a series of spherical bodies undergoing vertical descent into the atmosphere. It can be seen that the maximum deceleration of all the spheres is the same--only the altitude at which this deceleration is experienced is changed.

2. For missiles of conventional mass and size, heat transfer to the missile could be minimized by employing a blunt shape with a high-pressure drag compared to friction drag. Thus, the kinetic energy of the missile could be dissipated to the atmosphere by generation of a strong bow shock wave rather than delivered to the missile through skin friction.

The analysis led immediately to the employment of the now-familiar blunt shapes for ballistic missile nose cones rather than the relatively slender shapes which had previously been considered.

More exact analyses have subsequently been made, [3-6] which account for additional forces acting to perturb the vehicle motion. These forces are: gravity forces, centrifugal force, lift force, vertical acceleration, and vertical component of drag. These forces, which are of little importance for the case of relatively steep angle re-entry of ballistic missiles become of paramount importance for other types of re-entry vehicles.

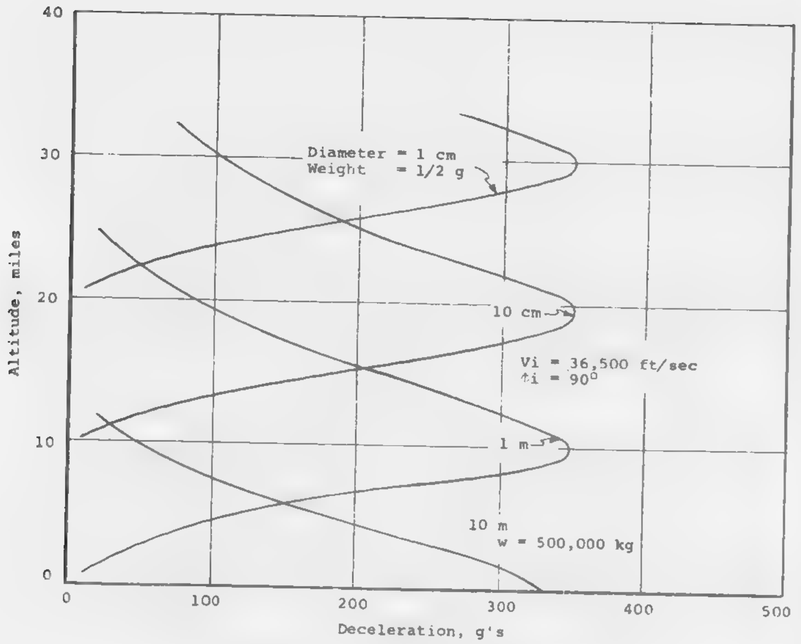


FIGURE 3 DECELERATION OF SPHERES

Probably, the most general analysis available is that of Chapman.[3] This analysis accounts for the forces cited in the preceding paragraph and is applicable to ballistic, glide, skip, satellite, and escape vehicles. In addition, the method developed can be used to compute trajectories during which the lift or drag is changed or programed during descent, and is generalized for computation of conditions for re-entry into planets other than earth.

Figure 4, taken from Reference 3, shows the types of trajectories to which Chapman's analysis can be applied. (As a matter of historical interest, it should be observed that gliding and skipping trajectories were considered as early as 1933 by Sanger, [7] in connection with the design of long-range rocket-powered vehicles.)

Three assumptions are made initially in Chapman's analysis. These are:

1. Atmosphere and planet are spherically symmetrical.
2. The variation of atmospheric density with altitude can be represented as an exponential function.

3. The peripheral velocity of the planet is small compared with the vehicle velocity.

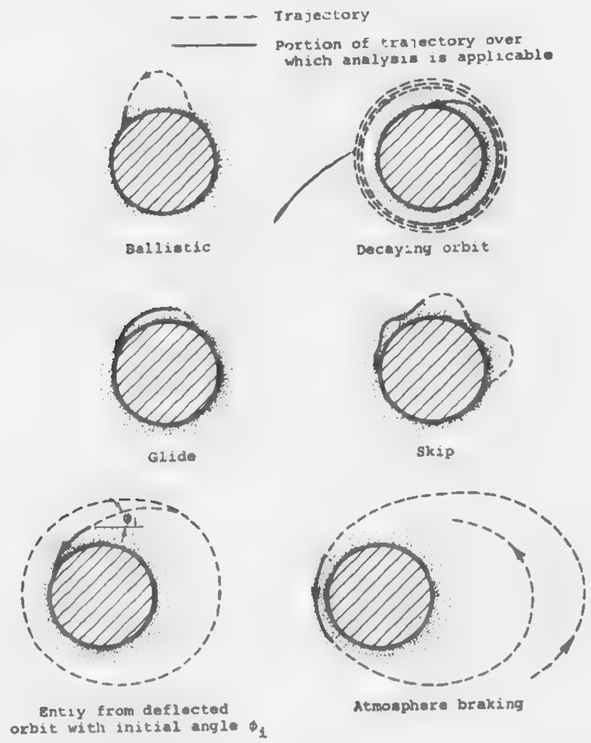


FIGURE 4 TRAJECTORIES COVERED BY CHAPMAN'S ANALYSIS

With these assumptions, a pair of motion equations result for the tangential and vertical velocity components of the vehicle,

$$\frac{du}{dt} = - \frac{\bar{\rho}_o e^{-\beta y} u^2}{2 \left(\frac{m}{C_D A}\right)} \cos \phi \qquad (2)$$

$$- \frac{1}{g} \frac{dV}{dt} = 1 - u^{-2} + \frac{\bar{\rho}\phi}{2} \frac{C_D A r \bar{u}^2 e^{-\beta y}}{m \cos^2 \phi} \left(\sin \phi - \frac{L}{D} \cos \phi\right) \qquad (3)$$

In brief, the pair of motion equations are reduced to a single equation by introducing a new dimensionless dependent variable Z, defined by,

$$Z = \frac{\bar{\rho}_o}{2\left(\frac{m}{C_D A}\right)} \sqrt{\frac{r}{\beta}}\, \bar{u} e^{-\beta y}$$

which results in a single nonlinear equation,

$$u \frac{d}{d\bar{u}}\left(\frac{dZ}{d\bar{u}} - \frac{Z}{\bar{u}}\right) - \frac{1-\bar{u}^2}{\bar{u}Z} \cos^4\phi + \sqrt{\beta r}\,\frac{L}{D}\cos^3\phi = 0 \quad (4)$$

The two necessary boundary conditions depend upon the type of trajectory considered. For example, entry from a decaying satellite orbit leads to,

$$Z_i(1) = 0 \qquad Z_i'(1) = 0$$

One Z function would then be required for each value of the parameter $\sqrt{\beta r}(L/D)$ appearing in Equation (4).

The reader is referred to Chapman's original paper for other details of the analysis. However, it can be stated that most of the aerodynamic and thermodynamic functions of interest such as:

Acceleration
Dynamic pressure
Free-stream Reynolds number
Laminar heating rate
Turbulent heating rate

can be obtained in terms of the Z function.

Utilizing the results of Chapman, it is possible to examine the general characteristics of the trajectories of a number of vehicles and to determine the environment which will be encountered.

DECELERATION

The magnitude of the vehicle deceleration is of interest in connection with the structural design of the re-entry vehicle and is, of course, of overwhelming importance in the design of manned re-entry vehicles. Since, as previously

shown, the maximum deceleration of a purely ballistic vehicle is controlled solely by the initial entry speed and flight-path angle, one is led, in the design of manned vehicles, to examine the effect of lift on the maximum deceleration encountered.

The effect of lift-drag ratio on horizontal deceleration during a decaying orbital entry into earth's atmosphere is shown in Figure 5. The very large effect of even small

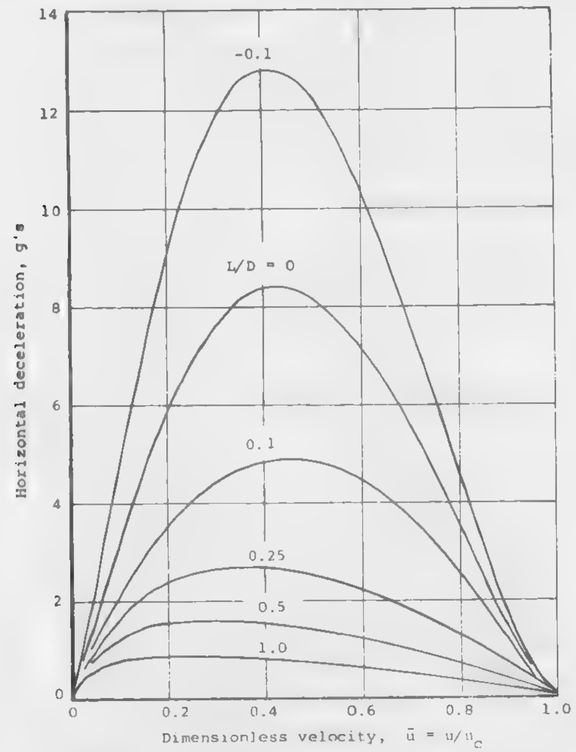


FIGURE 5 EFFECT OF L/D ON DECELERATION

lift-drag ratio is apparent as is the fact that maximum deceleration occurs at about 0.4 times orbital velocity, or slightly over 10,000 feet per second, for earth's re-entry. Figure 6 shows the maximum deceleration in earth g's and duration of entry for several values of lift-drag ratio for the case of decaying orbital entry into the atmospheres of Mars, Venus, Earth, and Jupiter. Also shown is a band representing human tolerance to deceleration. The strong effect of even small lift-drag ratio in altering deceleration is again apparent.

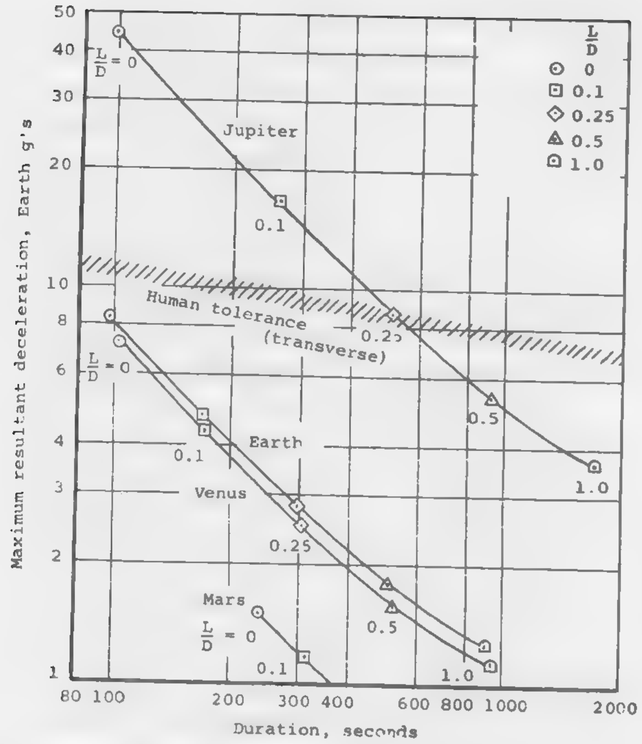


FIGURE 6 DECELERATION IN PLANETARY ATMOSPHERES

AERODYNAMIC HEATING

The heating of re-entry vehicles is the one subject which has received, by far, the most attention during the past decade since concentrated attention was given to re-entry problems. The first rudimentary calculations of convective heat transfer to re-entry bodies led to computed heat-transfer rates far in excess of those which had been previously dealt with in industrial applications. For the past 10 years, intensive work has been going on in an effort to refine and extend the early calculations. The present status of heating calculations is far from satisfactory for very high-speed re-entry such as would occur, for example, from a planetary orbit. For these cases, there are serious unanswered questions regarding the effects of dissociation and ionization of the air surrounding the vehicle on the convective heat transfer. In addition, excitation of atoms and molecules causes the air to become incandescent and radiative heat transfer becomes important--for certain conditions, overshadowing the importance of convective heating.

Many summary papers have been written on heat transfer to re-entry vehicles,[8-16] and the reader is referred to these for details of computational methods. In what follows only the major aspects of the effect of body configuration and type of trajectory employed will be discussed in terms of the environmental condition which must be withstood by the re-entry vehicle.

To display the range of heating rates encountered, Figure 7 shows the heat pulses, for several types of ballistic vehicles, due to convective heating at the stagnation point.

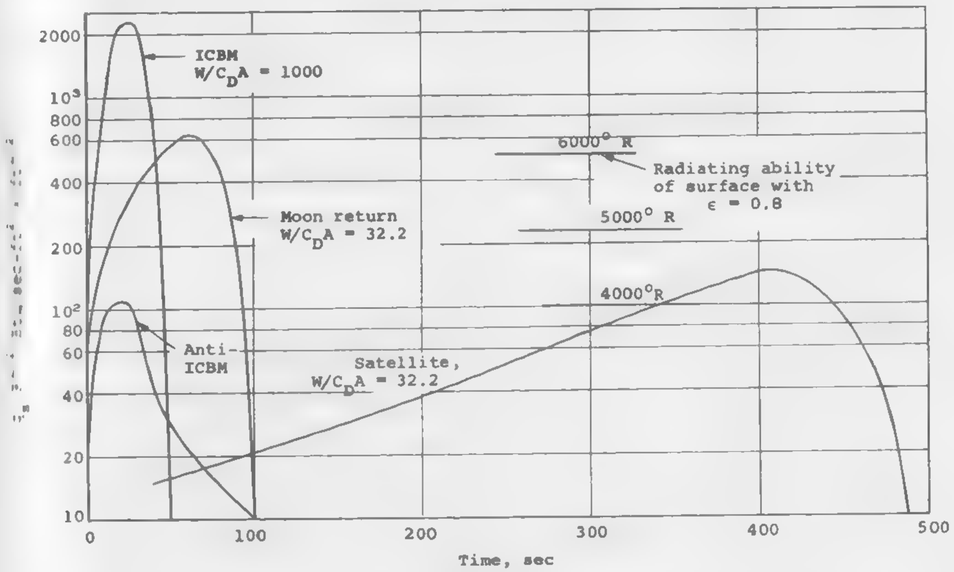


FIGURE 7 STAGNATION POINT HEAT PULSE FOR BALLISTIC VEHICLES

Also shown is the maximum radiating ability of a high-emissivity surface. From this figure, it is clearly apparent that a heavy ICBM or a relatively light non-lifting moon-return vehicle would be unable to re-radiate the incoming heat. Note that the ordinate in this figure is $\dot{q}_s R^{1/2}$, implying that heating rate can be reduced by employing a large nose radius. This, of course, is the primary reason for the relatively flat face of the familiar Mercury capsule.

The effects of altitude and velocity on stagnation-point heating rates are shown in Figure 8, taken from Reference 17, for a 2-foot-diameter sphere. The increasing importance

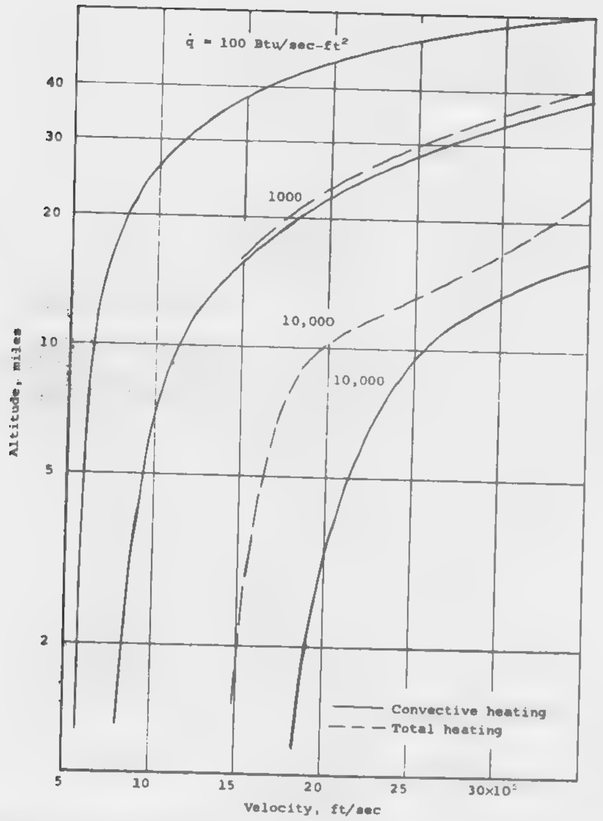


FIGURE 8 HEAT FLUX MAP FOR STAGNATION POINT OF 2-FOOT SPHERE

of radiative heat transfer as velocity increases is noticeable. This effect is shown again in Figure 9, taken from Reference 1. This figure is again an altitude-velocity map and shown on it are two trajectories, the first of a typical ICBM with a drag parameter, W/C_DA, of 400 and the second, a Mars probe with a W/C_DA of 50. In each case, the nose radius is assumed to be 1 foot. Crossing the lower right-hand corner of this figure is a line which is the altitude-velocity contour where the radiative heat transfer is just equal to the convective heat-transfer--radiation becoming more important at the higher speeds and densities. It can be seen that the Mars probe trajectory falls below this line indicating that radiation heating will be important for this vehicle. Likewise, it can be seen that the ICBM trajectory is well above the contour, indicating that radiation heating of this vehicle will be of small magnitude.

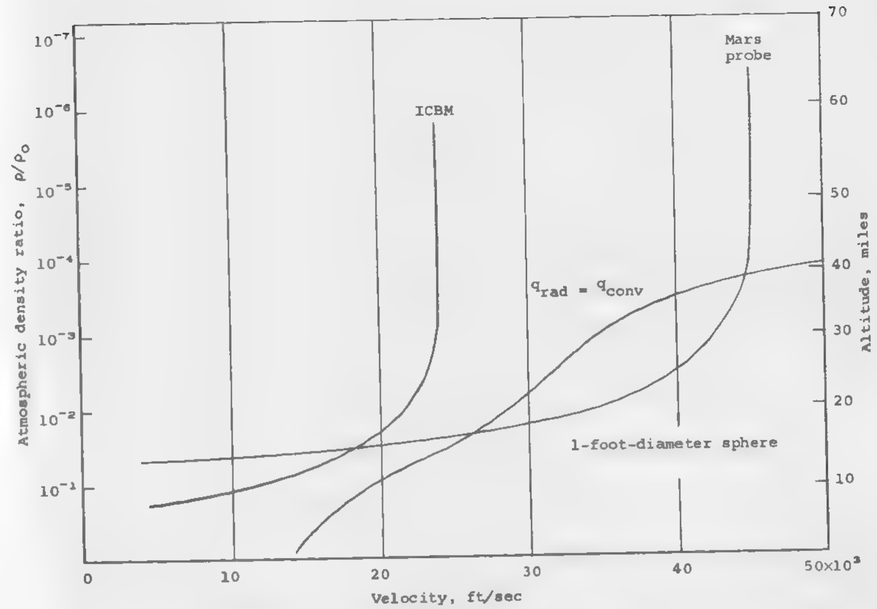


FIGURE 9 ALTITUDE-VELOCITY MAP

As with deceleration the use of a small amount of lift has a considerable effect upon heating rate. For entry into the earth's atmosphere, the maximum radiation-equilibrium temperature at the stagnation point for vehicles of differing drag parameter, W/C_DA, is shown in Figure 10 taken from Reference 3 for several values of L/D. In this figure, the

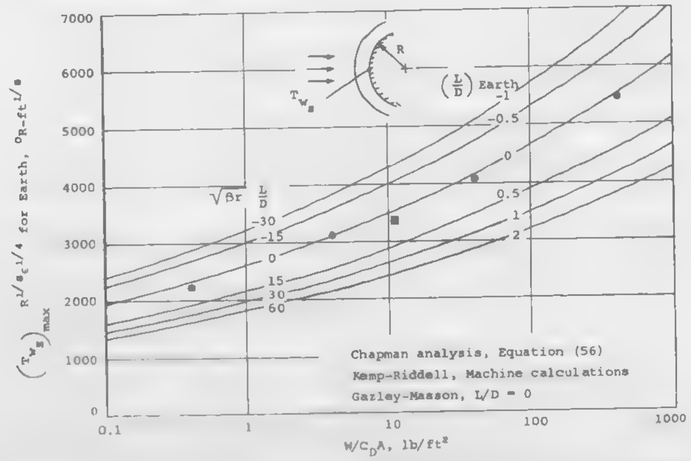


FIGURE 10 RADIATION-EQUILIBRIUM TEMPERATURE FOR SPHERES

values shown for the ordinate $(T_{WS})_{max} R^{1/8} \epsilon^{1/4}$, are surface temperature in degrees Rankine for a nose radius of 1 foot and for a surface emissivity of unit. For decaying orbital entry into planetary atmospheres, Figure 11, also taken from Reference 3, shows the effect of lift on maximum surface temperature for entry into the atmospheres of Jupiter, Venus, and Mars in addition to earth. From this figure, it is clear that there would be little prospect of utilizing radiation cooling for a vehicle designed to land on Jupiter. It is interesting to note that, for all planets, the optimum L/D for minimum surface temperature is close to unity.

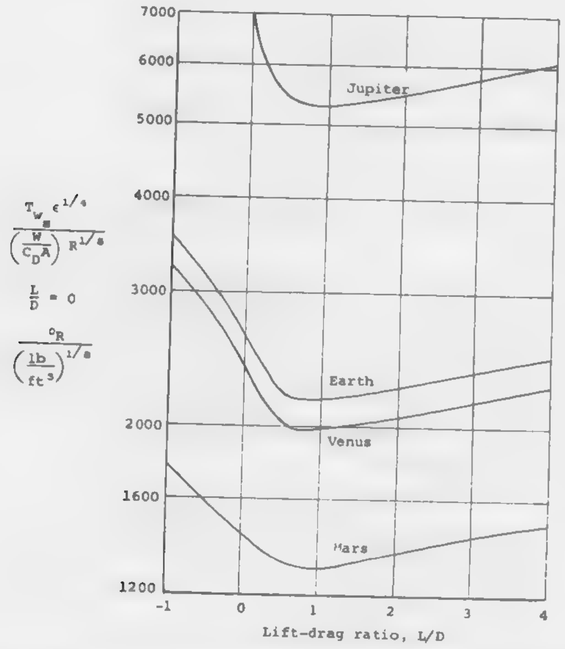


FIGURE 11 EFFECT OF L/D ON RADIATION EQUILIBRIUM TEMPERATURE FOR PLANETARY RE-ENTRY

Three major types of thermal design have been employed to meet the varying heat-transfer conditions during re-entry along different trajectories. These are:

1. Heat-sink cooling
2. Ablative cooling
3. Radiation cooling

In order, these types of cooling are useful for:

1. Heat pulses of moderate magnitude and short duration
2. Heat pulses of large magnitude and short duration or moderate magnitude and long duration
3. Heat pulses of low magnitude and long duration

Each of the methods has advantages and disadvantages which are discussed separately below.

HEAT-SINK COOLING

Heat-sink cooling involves the storage of heat in a material which does not undergo a phase change. The total amount of heat which can be stored is then limited by the melting or sublimation temperature of the material, its specific heat and the temperature distribution in the material.

An ideal heat-sink material would be characterized by:

1. High melting or sublimation temperature
2. High thermal conductivity
3. High specific heat
4. High ductility
5. Low coefficient of thermal expansion
6. High oxidation resistance

This type of cooling is characterized by the solid copper nose cone of early ICBM's of moderate $W/C_D A$. This design was chosen because the characteristics of the nose cone material were well known and because its thermal behavior could be predicted to an accuracy equal to the accuracy with which the aerodynamic heating could be predicted. The use of copper led to very heavy construction; nevertheless, it was felt that the weight penalty was overshadowed by predictability of operation and the fact that the nose-cone geometry remained constant.

Later designs employed materials such as beryllium and graphite which were able to store much more heat than copper per pound of material.

A comparison of the heat-storage ability of copper, beryllium, and graphite is shown in Figure 12, taken from Reference 18. These computations were made for the stagnation point of a 5-foot hemisphere for a typical ICBM entry

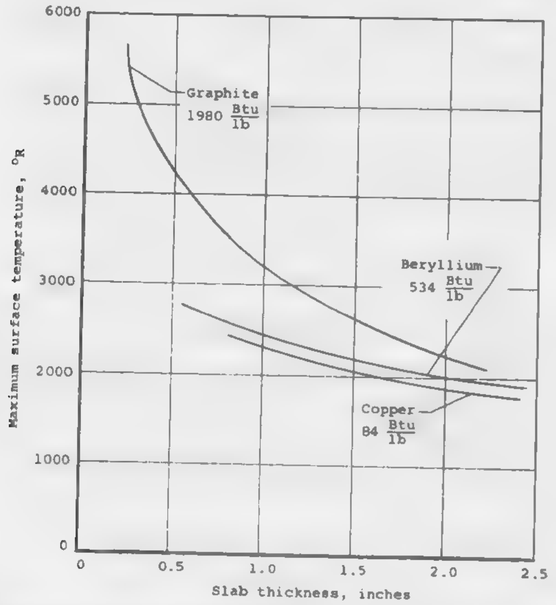


FIGURE 12 EFFECT OF SLAB THICKNESS ON MAXIMUM SURFACE TEMPERATURE

speed of 23,000 feet per second and a drag parameter, W/C_DA of 345. The amount of heat absorbed per unit weight of material is noted on each curve at the surface temperature corresponding to 75% of the melting or sublimation temperature. It can be seen that both graphite and beryllium are greatly superior to copper as heat-sink materials from a weight standpoint. Graphite is especially attractive, weighing only about 1/24 as much as copper. Beryllium weighs less than 1/6 as much as copper.

ABLATIVE COOLING

The best method presently known for protecting a vehicle from the intense aerodynamic heating of re-entry into the atmosphere is by means of ablative cooling. In this type of cooling system, the exterior surface material of the vehicle protects the interior by both absorbing and blocking the incoming heat. The heat is absorbed by the surface material

through its sensible heat capacities and its latent heats of phase change. Sensible heat is absorbed by the material in all three phases: solid, liquid, and gaseous. The phase changes, in some cases, may occur as the result of pyrolysis where the long chemical chains of a solid or liquid organic compound are decomposed into smaller molecules. The incoming heat is blocked from entering the vehicle by the material through its action as an insulator or by its injection as a gas into the boundary layer. A good ablator will possess a low thermal conductivity so that the penetration of heat is confined to the region immediately behind the surface. The efflux of the gaseous products of ablation reduces the incoming heat-transfer rates by reducing the velocity gradients in the boundary layer and by absorbing some sensible heat there. There may be adverse effects of the introduction of the gaseous products of ablation into the boundary layer because of the possibility of combustion and of endothermic release of chemical energy occurring there. The latter aspect has been studied in References 17 and 18 and, in general, the blockage of heat due to the efflux of gas at the surface exceeds the additional heat transfer caused by the combustion. In fact, the occurrence of combustion may even help in the blockage of the incoming heat if the products of combustion have a much lower molecular weight than the original gaseous products of ablation.

The types of materials used as ablators may be homogeneous substances, such as solid slabs of Teflon, nylon, quartz, or a mixture of two or more materials, such as a reinforced plastic. The latter usually contains fibers that are either woven or felted into sheets. These sheets are stacked, and the entire stack is molded into a single mass through the use of a binder. The fibers can be made of such materials as glass, refrasil, quartz, carbon, and nylon. The most commonly used binder is a phenolic plastic which may constitute between 10% and 30% by weight of the final material. The behavior of the reinforced plastics as ablators not only depends on the composition and proportions of the fibers and binder, but on the orientation of the fibers with respect to the surface. Fibers that are normal to the surface channel the gaseous products of the pyrolyzed binder to the surface and increase the effectiveness of the gaseous

products to absorb and block the incoming heat. Fibers laid parallel to the surface tent to block the gaseous binder from emerging from the surface and pockets of gas form below the surface. This trapped gas, in time, blows off the enveloping fibers resulting in a loss of material without an absorption of heat. In the latter case, the effectiveness of the ablation process also is reduced further because the gaseous products do not emerge uniformly and continuously.

From the preceding discussion, it is apparent that the process of ablation is rather complex. Within the solid, heat balances occur between heat conduction, sensible heat storage, and heat absorption by chemical and phase changes. The nonhomogeneous and nonisotropic character of materials affect the heat-conduction properties of these materials. A similar balance between the heat-transfer processes occurs in the molten region, if any exists. In the gaseous boundary layer all of the chemical effects noted previously in the convective heat-transfer section occur, with additional complications introduced by the presence of the gaseous ablation products. Most of the knowledge available concerning the ablation mechanism has been based on highly idealized models of the behavior of these processes, References 19 to 22. A great deal of experimentation will be required before a complete understanding will be obtained of the actual ablation mechanisms of materials subjected to various environments.

Because of its high cooling effectiveness per unit weight, ablative cooling is currently being extensively employed in design of both ballistic and lifting vehicles. Effective heats of ablation may range, typically, from 2000 to 5000 BTU per pound. A serious disadvantage of ablative cooling is, of course, the change in vehicle geometry which results as the material is consumed. This effect is especially deleterious when small geometry changes are important, such as the leading edge of winged vehicles designed to land at relatively low speed.

It should also be pointed out that the heat-blockage effect which results from the efflux of gas from the surface primarily reduces convective heating only and would be

expected to have no or little blocking effect on radiative heat transfer. This is a problem of great interest to designers of vehicles which have trajectories where radiative heat transfer is important and at this time requires intensive study.

RADIATION COOLING

In theory, the simplest type of cooling is radiation cooling. In this system, the incoming convective and radiative heat is re-radiated by the surface of the vehicle. Since no incoming heat is stored or blocked, the skin of the vehicle rises in temperature to an equilibrium temperature where the re-radiated energy is just equal to the sum of the incoming convective and radiative heat. It is worth pointing out that, for re-entry speeds, the reduction in convective heating which results from the decreasing driving temperature potential as the surface temperature is increased is negligible. This can easily be seen from the values of the stagnation gas enthalpy and the gas enthalpy at the surface temperature. The stagnation enthalpy corresponding to a flight speed of 36,000 feet per second is about 26,000 Btu per pound. The surface enthalpy at, say, 4000°F is about 1300 Btu per pound. The convective heat-transfer rate is proportional to the enthalpy difference $(i_s - i_w)$. Thus, for a surface temperature of 4000°F, the convective heating is reduced by less than 4% from the value it would have if the surface temperature were maintained at 0°F.

The use of refractory metals is common in the design of radiation-cooled structures. These materials, however, typified by molybdenum, suffer from low-oxidation resistance at elevated temperatures. Hence, their surfaces must be coated with an oxidation-resistant coating. This procedure is difficult to accomplish in practice, since a few pinholes through the coating could, conceivably, lead to catastrophic structural failure due to oxidation erosion. For this reason, work is currently being pursued on all-ceramic materials, typically oxides, which do not suffer this drawback. Fabrication, ductility, weight, and attachment problems are severe, however, and will require intensive research to overcome.

BIBLIOGRAPHY

1. Allen, H. J. and A. J. Eggers, Jr.: A Study of the Motion and Aerodynamic Heating of Ballistic Missiles Entering the Earth's Atmosphere at High Supersonic Speeds. NACA Rept. 1381, 1958.

2. Allen, H. J.: Problems in Atmosphere Entry from Parabolic Orbits. Paper presented at the National Conference on Aeronautical and Space Sciences, Nagoya, Japan, Nov. 8, 9, 1960.

3. Chapman, D. R.: An Approximate Analytical Method for Studying Entry into Planetary Atmospheres. NACA Tn 4276, 1958.

4. Sanger, E. and J. Bredt,: A Rocket Drive for Long-Range Bombers, Deutsche Luftfahrtforschung. UM 3538, 1944.

5. Gazley, Carl, J.: Deceleration and Heating of a Body Entering a Planetary Atmosphere from Space. Rand Rept. P-955, 1957.

6. Eggers, A. J., Jr., H. J. Allen and S. E. Neice.: A Comparative Analysis of the Performance of Long-Range Hypervelocity Vehicles. NACA Tn 4046, 1957.

7. Sanger, E.: Raketen-Flugtechnik, R. Oldenbourg, 1933.

8. Goodwin, Glen and M. O. Creager.: The Design of Hypersonic Gliders for Minimum Cooling. Paper presented at IAS Summer Meeting, July 8, 10, 1958.

9. Rubesin, M. W.: A Modified Reynolds Analogy for the Compressible Turbulent Boundary Layer on a Flat Plate. NACA Tn 2917, 1953.

10. Seiff, A.: Examination of the Existing Data on the Heat Transfer of Turbulent Boundary Layers at Supersonic Speeds from the Point of View of Reynolds Analogy, NACA Tn 3284, 1954.

Transfer with Dissociated Air. Jour. Aero. Sci., vol. 25, no. 2, 1958.

12. Fay, J. A. and F. R. Riddell: Theory of Stagnation Point Heat Transfer in Dissociated Air. Jour. Aero. Sci., vol. 25, no. 2, 1958.

13. Rose, P. H. and W. I. Stark: Stagnation Point Heat Transfer Measurements in Dissociated Air. Jour. Aero. Sci., vol. 25, no. 2, 1958.

14. Van Driest, E. R.: The Problem of Aerodynamic Heating. Aero. Eng. Rev., Oct. 1956.

15. Kivel, Bennett: Radiation Heat Transfer during Re-Entry. ASME Paper 61-WA-264, Aug. 31, 1961.

16. Adams, Mac C.: A Look at the Heat-Transfer Problem at Super Satellite Speeds. Avco Rept. AMP 53, Dec. 1960.

17. Wood, R. M.: Atmospheric Entry. Douglas Aircraft Co. Engineering Paper No. 1246.

18. Stalder, J. R.: The Useful Heat Capacity of Several Materials for Ballistic Nose-Cone Construction. NACA Tn 4141, Nov. 1957.

19. Sutton, G.: The Hydrodynamics and Heat Conduction of a Melting Solid. Jour. Aero. Sci., vol. 25, no. 1, 1958.

20. Bethe, H. A. and M. C. Adams,: A Theory of the Ablation of Glossy Materials. Jour. Aero. Sci., vol. 26, no. 6, 1959.

21. Lees, L.: Similarity Parameters for Surface Melting of a Blunt Body in a High Velocity Gas Stream. Jour. Amer. Rocket Soc., vol. 29, no. 5, 1959.

22. Roberts, L.: Stagnation Point Shielding by Melting and Vaporization. NASA Rept. 10, Apr. 1959.

PYROLYTIC MATERIALS FOR RE-ENTRY APPLICATIONS

Daniel Schiff
Director, Research and Development
High Temperature Materials, Inc.
Boston, Massachusetts

ABSTRACT

A general description of pyrolytic materials and their processing is given. The behavior of anisotropic pyrolytic materials to thermal, oxidation and other environmental conditions is discussed for re-entry space vehicles with peak temperatures from 4000°F to 6000°F. The materials response is evaluated for transient heating conditions of ballistic missiles and for the quasi-steady state heating of lift and drag type re-entry vehicle. The results of analytical studies on varying physical properties such as the anisotropy in thermal conductivity are discussed.

The characteristics of pyrolytic graphite and pyrolytic boron nitride are presented and their anisotropic thermal and mechanical properties correlated with their structures. Property data for pyrolytic graphite and pyrolytic boron nitride is reviewed as a function of temperature and compared with other materials of interest. The residual stresses present in these anisotropic materials are discussed and their effects on design and process considerations are presented.

The effect of minor alloy additions is reviewed with reference to the type of additive, the changes in physical properties, and the effects on their response to re-entry environments.

Production methods are outlined for the purpose of demonstrating the applications of these materials to various shapes and their fabrication into different components and sizes. Conclusions are drawn that the use of pyrolytic materials can improve the performance of present re-entry vehicles and examples are given of the expected performance of systems utilizing pyrolytic materials.

INTRODUCTION

During re-entry of a space vehicle through the atmosphere, the heat generated at leading surfaces must be either absorbed or rejected in one fashion or another. The first generation of re-entry vehicles have been exposed to high heat fluxes for short exposure times on the order of minutes. To meet re-entry conditions, heat shields composed of ablative materials, insulative or absorptive materials and their combination have been used successfully. Further gains in this area will be obtained through the development of more efficient or lighter structures which will increase payloads or the range of a vehicle.

Today the designer is faced with a more difficult task, that of providing a heat shield for controlled re-entry or glide vehicles which will be exposed to lower heat fluxes but for considerably longer times, of an hour and longer. For this application insulating structures are required and materials selection becomes a prime concern.

The desired materials properties are a high melting or sublimation point, a high strength to weight ratio at high temperatures and a high resistance to oxidation. In addition, a low thermal conductivity and a high surface emissivity are required to minimize internal cooling requirements.

The anisotropic materials to be discussed, pyrolytic graphite and boron nitride, are expected to meet the requirements of a refractory material for re-entry applications.

The melting point or sublimation temperatures of these materials are well over 5000°F. Their strength to weight ratio in the region of 4000°F to 5000°F increases to values in excess of 500,000 inches; pyrolytic graphite whose strength properties have been accurately determined is far stronger in this temperature range than any other known material. The oxidation resistance of pyrolytic graphite at temperatures in the 4000°F to 5000°F range must be considered excellent since at these temperatures other refractory materials have already failed by one mechanism or another. Theoretical analyses supported by standard property measurements have revealed that only a nominal and tolerable amount of pyrolytic graphite would be oxidized at temperatures over 4000°F for periods of one hour and longer. Preliminary data on boron nitride indicates that this material has an oxidation rate some ten times lower than that of pyrolytic graphite.

Pyrolytic materials will also perform more efficiently because of their anisotropic properties. The anistropy is derived from a highly oriented crystal structure which possesses marked directional properties. For example, pyrolytic graphite, which possesses the graphite hexagonal layer plane structure, has a thermal conductivity ratio in orthogonal directions which is in the range of 200 to 1. The material is an excellent thermal insulator normal to the surface, while it is also an excellent heat conductor parallel to the surface. In comparison, normal graphites composed of anisotropic crystals which have a limited degree of orientation may have a thermal conductivity ratio from 2 to 3 in some cases.

In an insulating refractory system a low thermal conductivity in a direction normal to the re-entry body surface can result in high surface temperatures. With anisotropic pyrolytic materials, under the same heat flux conditions, lower temperatures are possible because of the high thermal conductivity of the materials in the direction parallel to the surface. The thermal conductivity in this direction which is comparable to that of the best known conductors increases the radiating surface area of leading re-entry surfaces and consequently increases the percent heat which is re-radiated.

PROCESSING OF PYROLYTIC MATERIALS

The pyrolytic materials produced for re-entry applications are pyrolytic graphite and boron nitride, and some alloys of these materials. High temperature gas phase reactions are employed for the processing of these materials and it is the process used which leads to their formation with a high degree of crystal orientation. In practice the process is carried out by passing the vapors of a compound, such as a hydrocarbon for pyrolytic graphite, over a surface maintained at elevated temperature. The compound is decomposed at the hot surface where graphite or boron nitride crystals nucleate and grow in a preferred direction. In this fashion bulk material is built up on a mandrel or mold from which it can be separated.

The structure of pyrolytic graphite is shown in Figure 1. This is a typical photomicrograph which through polarization shows a close knit structure of elongated crystals which have hexagonal layer planes parallel to the deposition surface. In comparison normal graphite has a disoriented crystal and void structure as shown in Figure 2. The structure of boron nitride which is nearly identical to that of pyrolytic graphite because of the similarity in their crystal structure, is shown in Figure 3.

Alloys of pyrolytic graphite have been produced by the addition of substitutional and interplanar foreign atoms to the lattice. These additions are made to change some of the mechanical, thermal or electrical characteristics of pyrolytic graphite while retaining the basic properties of the material. The crystal structure and microstructure of the alloys are similar to the normal structures shown above. Additions of boron, tungsten, niobium and molybdenum in concentrations less than a few percent were made and property changes which were obtained will be discussed in another section. Alloys of boron nitride are also being developed.

These pyrolytic materials have been produced in a variety of sizes and shapes for use in a number of applications. Spherical particles of 200 micron diameter have



FIGURE 1 PYROLYTIC GRAPHITE POLARIZED
200X

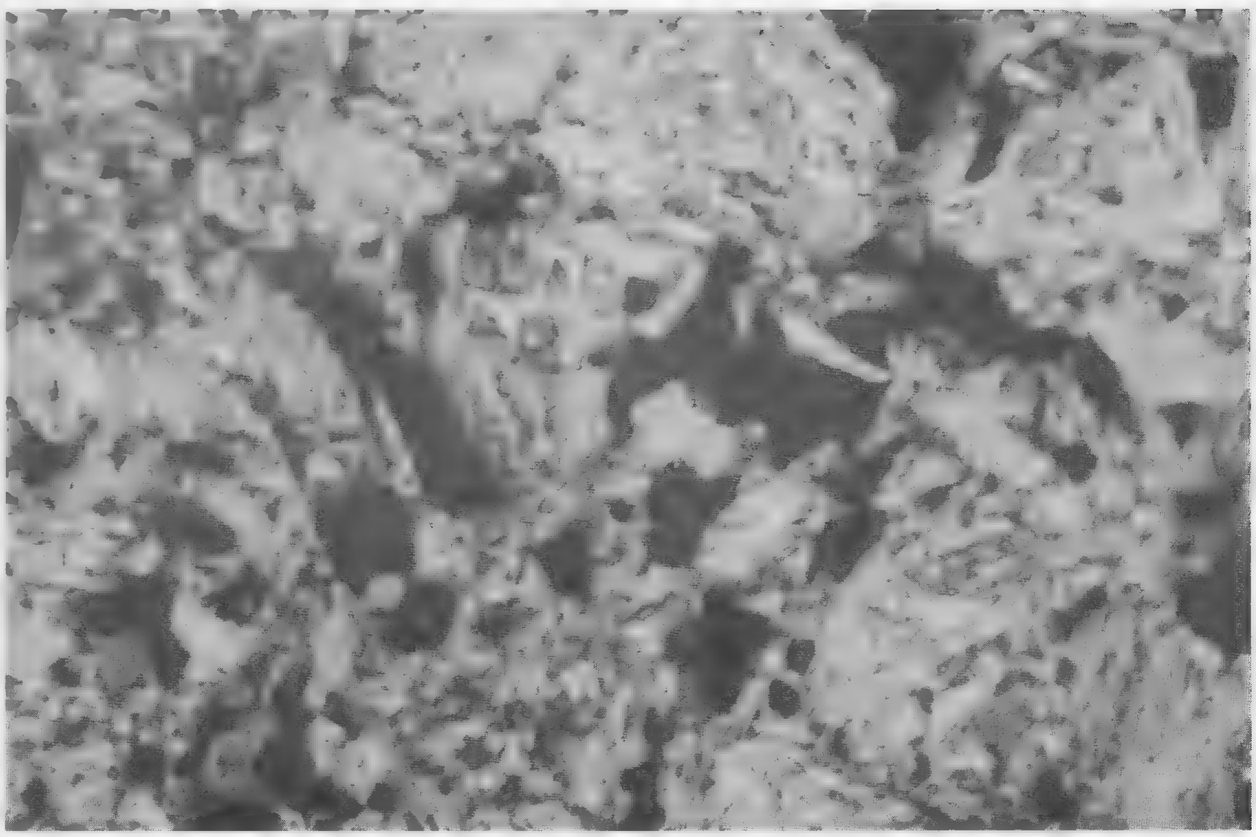


FIGURE 2 COMMERCIAL GRAPHITE
200X



FIGURE 3 BORON NITRIDE POLARIZED 200X

been coated with uniform layers of pyrolytic graphite and free standing pyrolytic graphite shapes the size of a man have been produced. The size component which can be made is limited only by the size of the process equipment which can be fabricated. Where this size becomes impractical pyrolytic graphite structures can be constructed from building blocks by joining and brazing techniques which have been developed. Figures 4 and 5 show different pyrolytic graphite shapes which have been produced. Figure 6 shows a boron nitride six inch hemisphere and Figure 7 a coating of boron nitride on pyrolytic graphite which demonstrates the feasibility of combining these materials to utilize the best properties of each.

PROPERTIES

The properties of anisotropic pyrolytic materials are similar in many respects. Their directional properties are important characteristics which determine their behavior under various conditions. All of the thermal properties except specific heat are directional and the mechanical as well as the electrical properties are also highly anisotropic.

The following table (Table I) presents some of the average properties of pyrolytic graphite, boron pyralloy which is a pyrolytic graphite with less than 2% boron, and boralloy, a boron nitride compound. The crystal structures are nearly identical and their lattice constants are in the same range of values. The sublimation temperatures are values reported in the literature. However, the sublimation temperature which is determined from vapor pressure curves may be higher for the highly oriented and high purity boron nitride produced pyrolytically. The densities which are close to their theoretical values are also nearly the same for all of the materials. Variations in the densities are solely dependent on the process parameters used. Values of the Young's modulus are also nearly the same, and the small difference which exists is probably within the range of values obtained in a single material. The directionality in the electrical properties is seen in the difference between the "a" and "c" electrical resistivities of pyrolytic graphite

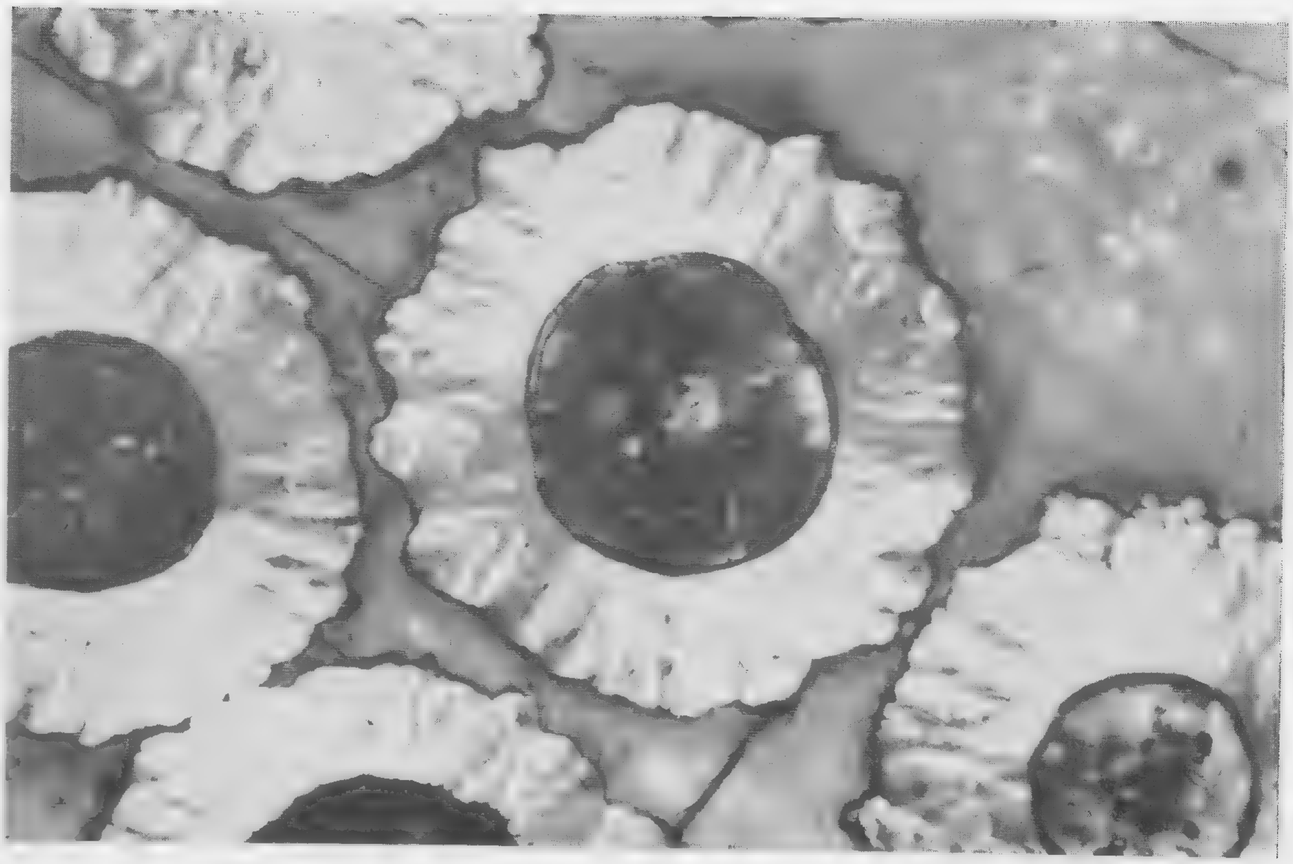


FIGURE 4 200 MICRON PARTICLES COATED WITH PYROLYTIC GRAPHITE POLARIZED 200X



FIGURE 5 PYROLYTIC GRAPHITE COMPONENT

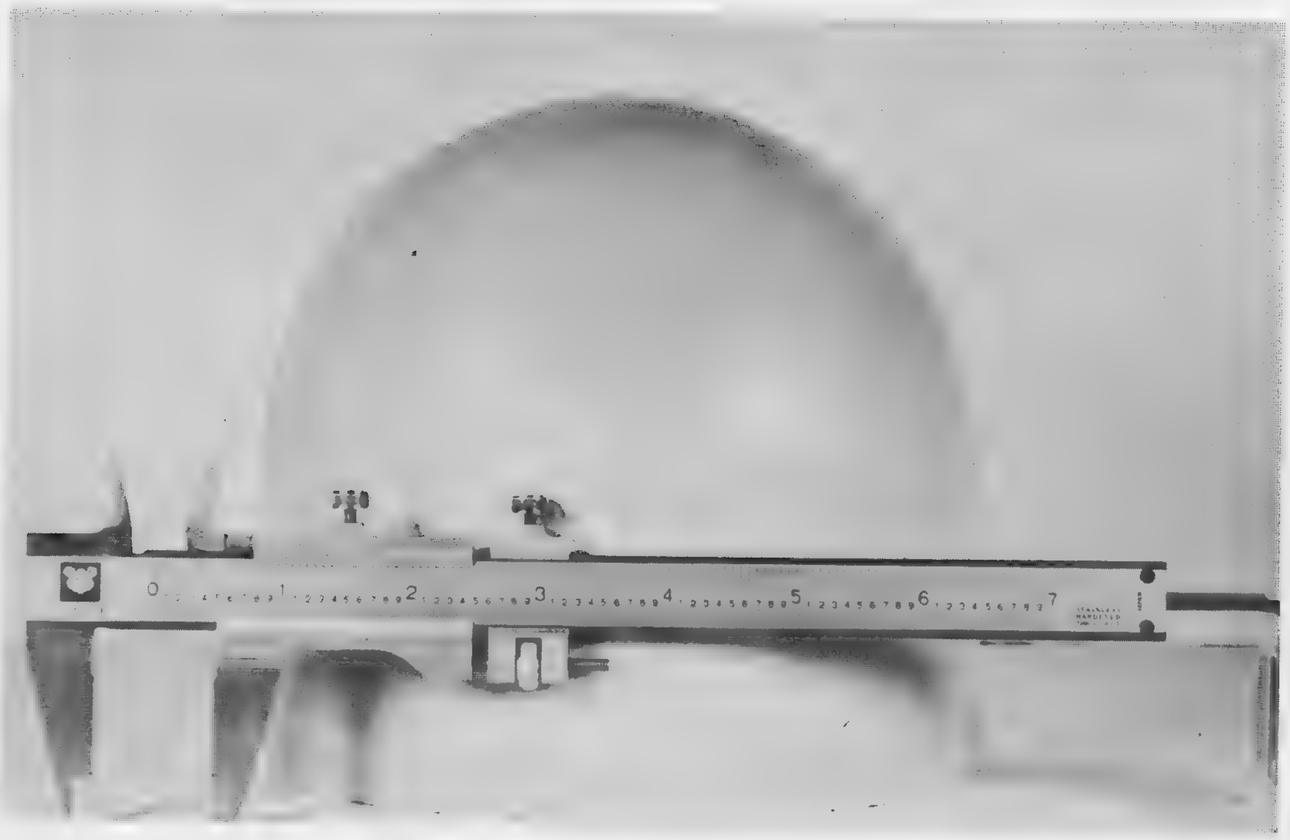


FIGURE 6 BORON NITRIDE 6 INCH HEMISPHERE



FIGURE 7 BORON NITRIDE COATING ON PYROLYTIC GRAPHITE

TABLE I

	Pyrolytic Graphite	Boron Pyralloy	Boralloy
Composition	C	C + < 2% B	BN
Structure	Hex.	Hex.	Hex.
Lattice Const. C/2	3.35-3.42	3.35-3.42	3.36
M. P. Subl.	6600°F	6600°F	5430°F
Density	220-223	220-223	200-220
Young's Modulus	$4.26(10)^6$	$4.6(10)^6$	$4.4(10)^6$
Resistivity (ohm-cm)			
"a"	0.0005	0.00025	$< 10^6$
"c"	0.55	0.02	$< 10^6$
Bend Strength "c" (psi)	23,000	35,000	27,500

and its boron alloy. The lower "c" direction resistivity of boron pyralloy is due to the presence of boron in the lattice which increases the conductivity by increasing the number of positive holes in the solid. In comparison, boron nitride is an excellent electrical insulator in both directions. The average bend strength values given in this table show the increase obtained by boron additions to pyrolytic graphite and the relative strength of boron nitride.

Thermal Conductivity

The thermal conductivities of pyrolytic materials in the direction parallel to the deposition surface as a function of temperature are seen in Figure 8. The thermal conductivity of pyrolytic graphite in this direction is of a magnitude equal to that of an excellent conductor. Boron pyralloy has a lower conductivity at low temperatures which increases and approaches that of pyrolytic graphite as the temperature increases. The electrical insulator boron nitride is seen to have a relatively high thermal conductivity in this direction; it has a conductivity approximately half that of boron pyralloy and only 25% less than that of tungsten. Preliminary measurements indicate that the a-axis or layer plane thermal conductivity of pyrolytic graphite with small W concentrations has increased threefold.

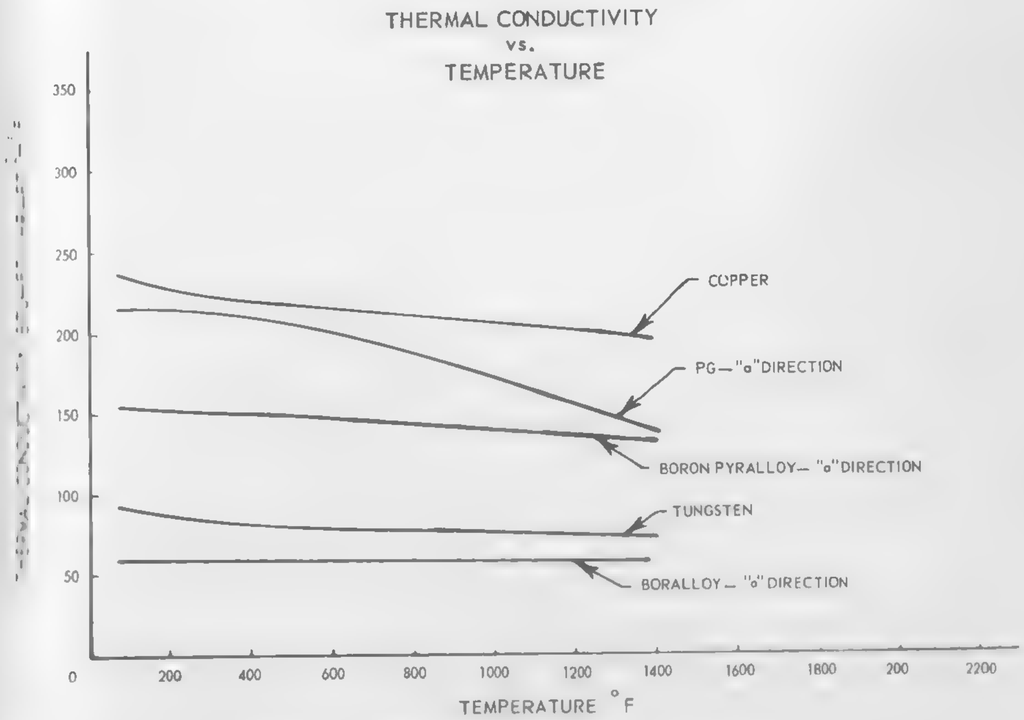


FIGURE 8 THERMAL CONDUCTIVITY "a" DIRECTION

The corresponding "c" axis thermal conductivities are presented in Figure 9. Pyrolytic graphite and boron pyralloy have nearly equal conductivities while boron nitride has a lower conductivity. The thermal conductivities of pyrolytic materials in this direction are comparable to and even lower than the conductivities of the most refractory metal oxides. Thermal measurements on other pyrolytic graphite alloys produced are presently being made.

Thermal conductivity measurements on pyrolytic graphite have been made by several laboratories. Figure10 shows the combined results for the "a" and "c" direction thermal conductivities of pyrolytic graphite to nearly 5000°F.

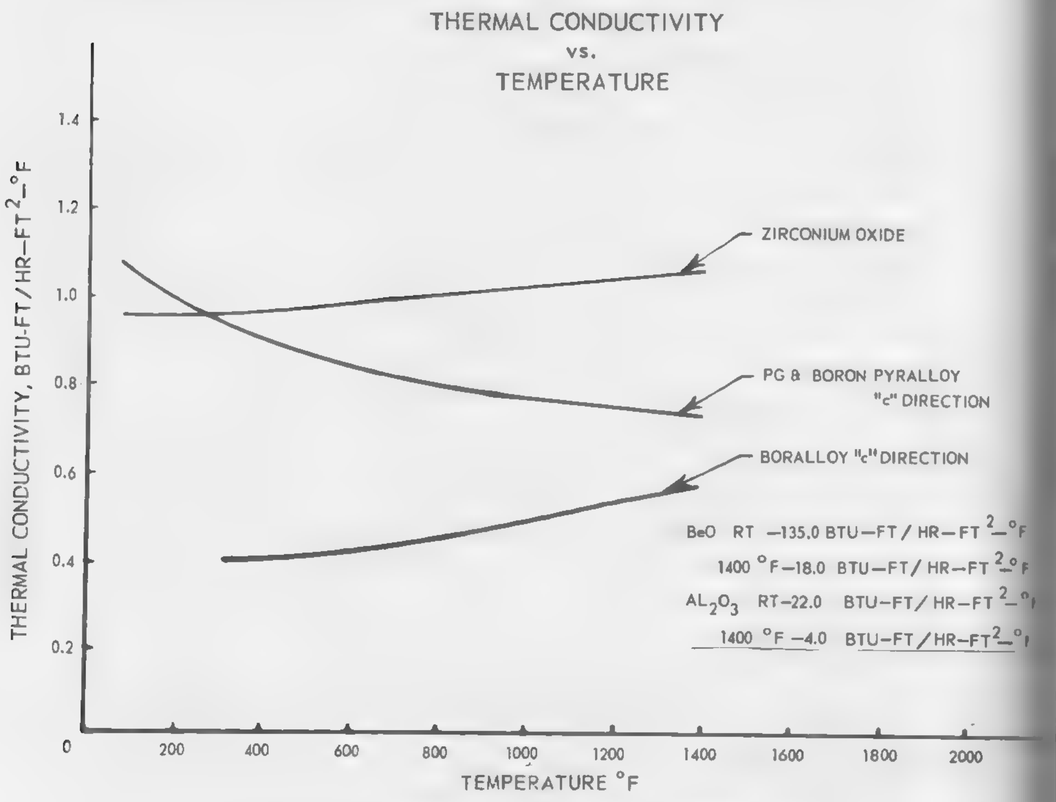


FIGURE 9 THERMAL CONDUCTIVITY "c" DIRECTION

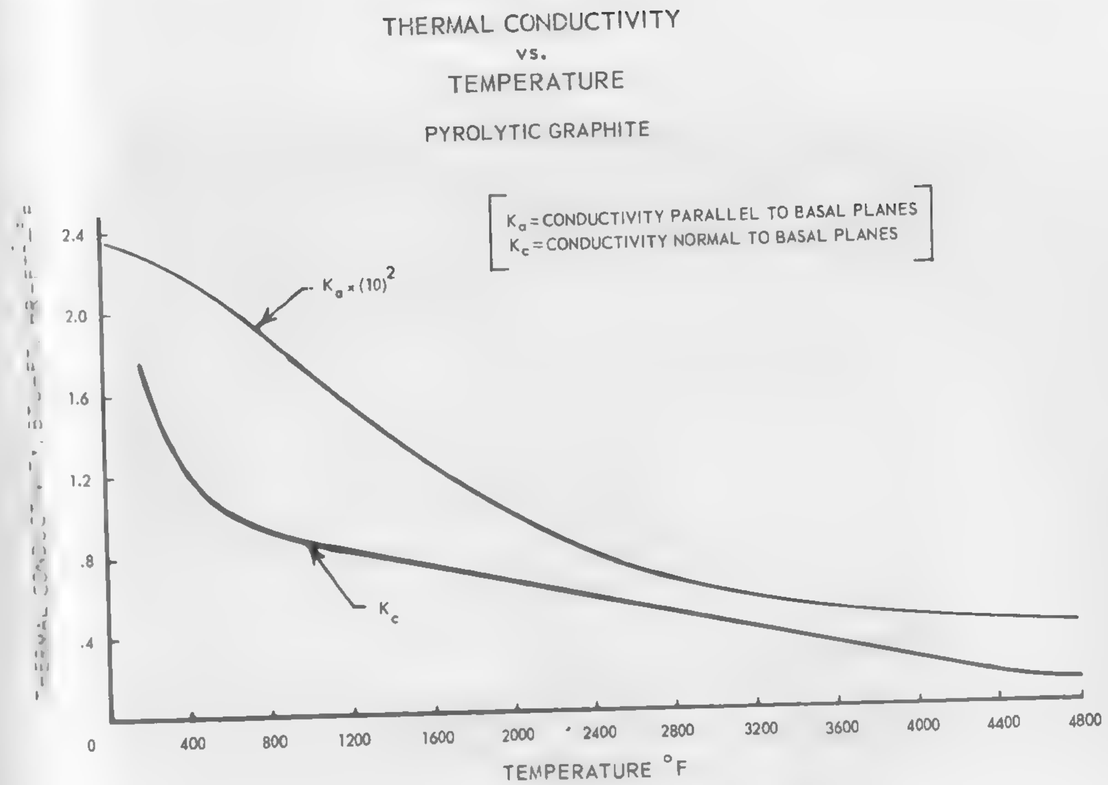


FIGURE 10 THERMAL CONDUCTIVITY "a" AND "c" DIRECTION

The insulating properties of pyrolytic graphite in the "c" direction are seen to improve continuously to very high temperatures. The "a" direction conductivity decreases approximately 50% from room temperature to the region of 1700°F and is seen to approach an asymptotic value in the temperature range from 3000°F to 5000°F.

The thermal conductivities of pyrolytic materials define these materials as excellent heat conductors in the direction parallel to the deposition surface and as excellent insulators in the perpendicular direction. The merits of pyrolytic materials for use as heat shields on re-entry bodies was discussed above. The magnitude of the thermal conductivity ratio in parallel directions is visualized in the simple torch test shown in Figure 11.



FIGURE 11 FLAME TEST
Top - Graphite; Bottom - Pyrolytic Graphite

Tensile Strength

The tensile strength of pyrolytic graphite in the "a" direction as a function of temperature together with the tensile strengths of other refractory materials is shown in Figure 12. The increase in the tensile strength of graphite and pyrolytic graphite with temperature is one of the unique properties of these materials. Other refractory materials decrease in strength and in the temperature range from 3000°F to 5000°F become useless as structural materials. On a strength to weight basis the difference in the strength properties of pyrolytic graphite and other materials is even greater. The tensile strength of boron nitride and boron pyralloy at room temperature are also listed. Their strengths as a function of temperature have not yet been measured.

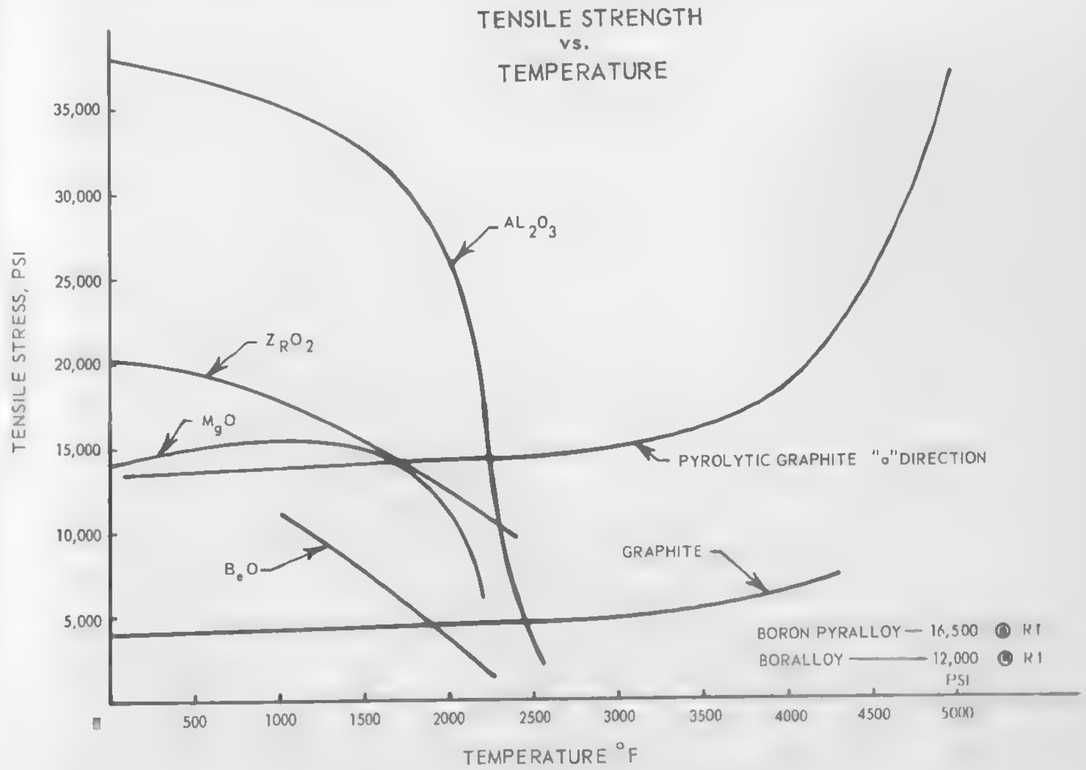


FIGURE 12 TENSILE STRENGTH "a" DIRECTION

The strength of pyrolytic graphite shown in the last figure is an average for as-deposited materials. Figure 13 presents the upper and lower limit for the tensile strength of pyrolytic graphite in the layer plane direction. The increase in strength to a value approaching 100,000 psi at 5000°F was obtained by annealing the material at temperatures higher than their processing temperatures. The annealing temperatures used were in the range of 4500°F to over 5000°F.

The "c" direction tensile strength of pyrolytic graphite is lower than its "a" direction strength by a factor of 5 to 10. The magnitude of the difference has not been determined accurately because of the inaccuracy of the results obtained. The inaccuracy stems from use of relatively small testing samples which can only be obtained across the thickness of pyrolytic graphite plates. A second, perhaps more important factor, is the damage which may result on the surface of test specimens during their preparation. Pyrolytic graphite contains residual stresses due to its anisotropic thermal expansion and these stresses can be relieved through partial delamination along basal planes when sections of the material are removed from relatively large areas. The measurements made to date therefore appear to reflect the state of a test sample instead of being representative of the bulk strength of the material. The "c" direction tensile strength of pyrolytic graphite determined by present technique lies in the range of 100 to 1500 psi.

The alloying of pyrolytic graphite was investigated as a means of increasing its apparent "c" direction tensile strength. Preliminary data obtained by the same testing technique indicates that tungsten and molybdenum in concentrations less than 1% have increased the "c" direction strength by 50 to 90%.

A considerable amount of work has been done in analyzing the magnitude of the stresses which are developed in pyrolytic graphite during rapid heating to very high temperatures. As will be shown later, for re-entry applications, the stresses developed are well within the maximum allowable stresses for the material.

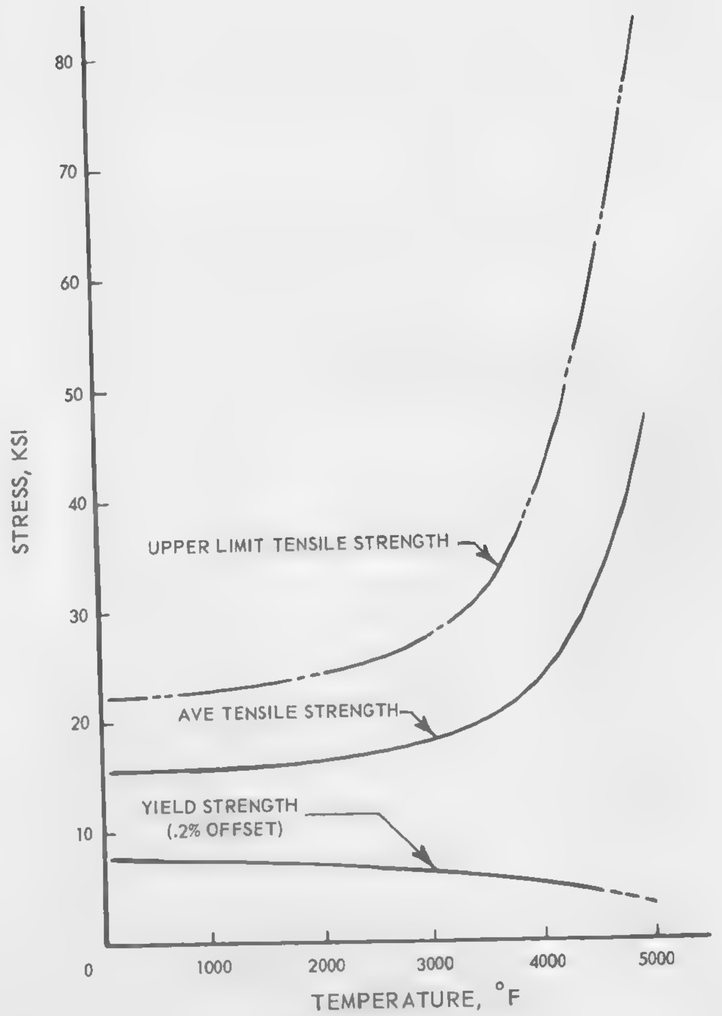


FIGURE 13 TENSILE STRENGTH PYROLYTIC GRAPHITE "a" DIRECTION

Oxidation Resistance

The oxidation rate of pyrolytic materials was measured at atmospheric pressure in an atmosphere of dry air. The velocity of the air flowing over the materials was maintained at approximately twenty feet per minute. The oxidation results presented are preliminary and limited in scope. Such factors as air stream velocity, oxygen pressure, time of temperature, and others are not highly reproducible at the present time. The data which is presented in Figure 14 is significant however, on a merit and comparison basis.

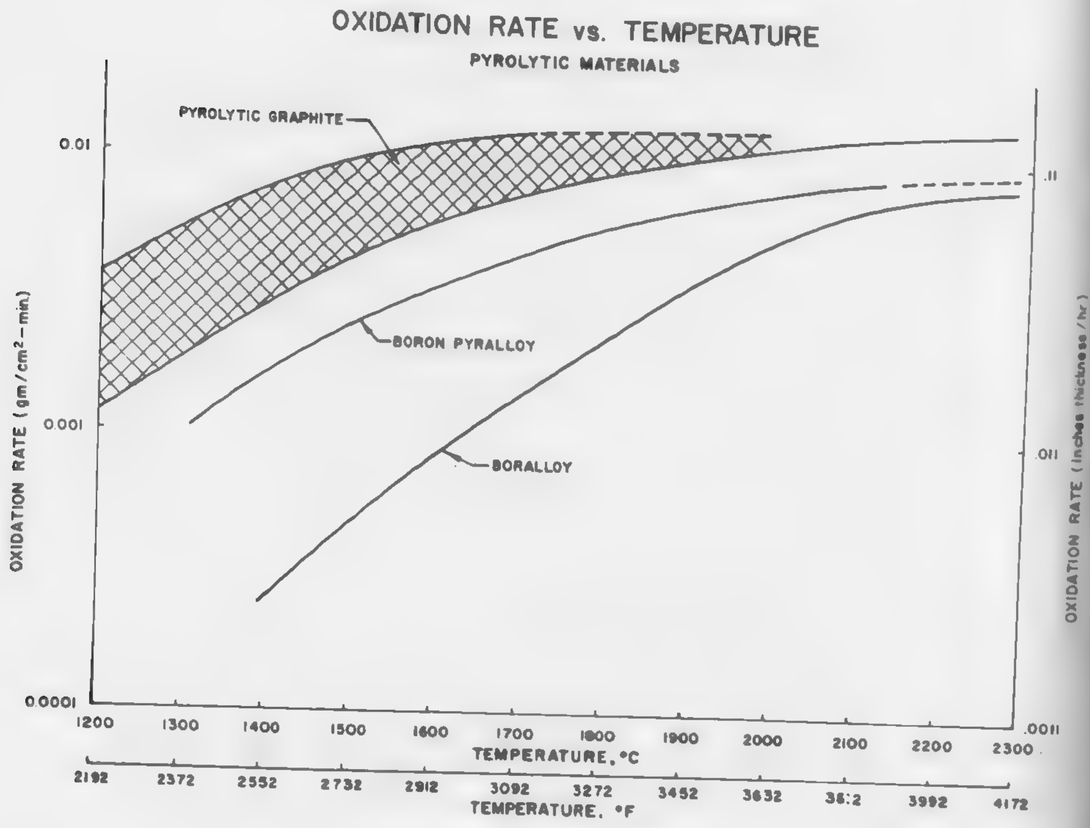


FIGURE 14 OXIDATION RESISTANCE

A scatter area is seen for the oxidation rate of pyrolytic graphite. The variation in the oxidation rate at the lower temperatures for this material reflects the use of materials produced under different sets of process conditions, and it may also reflect the scatter obtained from one sample to the next. Generally for all materials the reproducibility increased as the temperature increased. The reaction mechanism which becomes diffusion controlled at high temperatures may account for the increased accuracy obtained.

Of the materials tested pyrolytic boron nitride oxidizes at the lowest rate. In terms of mils per hour its oxidation rate is approximately 10 mils per hour at 3000°F and below 80 to 90 mils per hour in the temperature range from 4000°F to 4200°F. The oxidation rates at a temperature in the region of 2200°F are considered low for all materials tested. Pyrolytic graphite oxidized at a rate which is less than 15 mils per hour at 2200°F while boron nitride oxidized at a rate less than 1 mil per hour. Boron pyralloy which in this case contains 0.73% boron is seen to oxidize at an intermediate rate.

The results generally show the relative oxidation rates of pyrolytic materials but they do not necessarily predict their performance in low pressure, long time re-entry environments.

As previously shown, it is possible to combine these materials by producing coatings of one material on another. The processing technique also makes it possible to form graded compositions so that the surface of a component may have the most desirable material properties.

During glide re-entry where peak temperatures are maintained for relatively short periods of time it may be advantageous to use pyrolytic boron nitride which has a much lower oxidation rate over a wide temperature range.

Specific Heat and Emissivity

The specific heat of pyrolytic graphite as a function of temperature is shown in Figure 15. The specific heat is

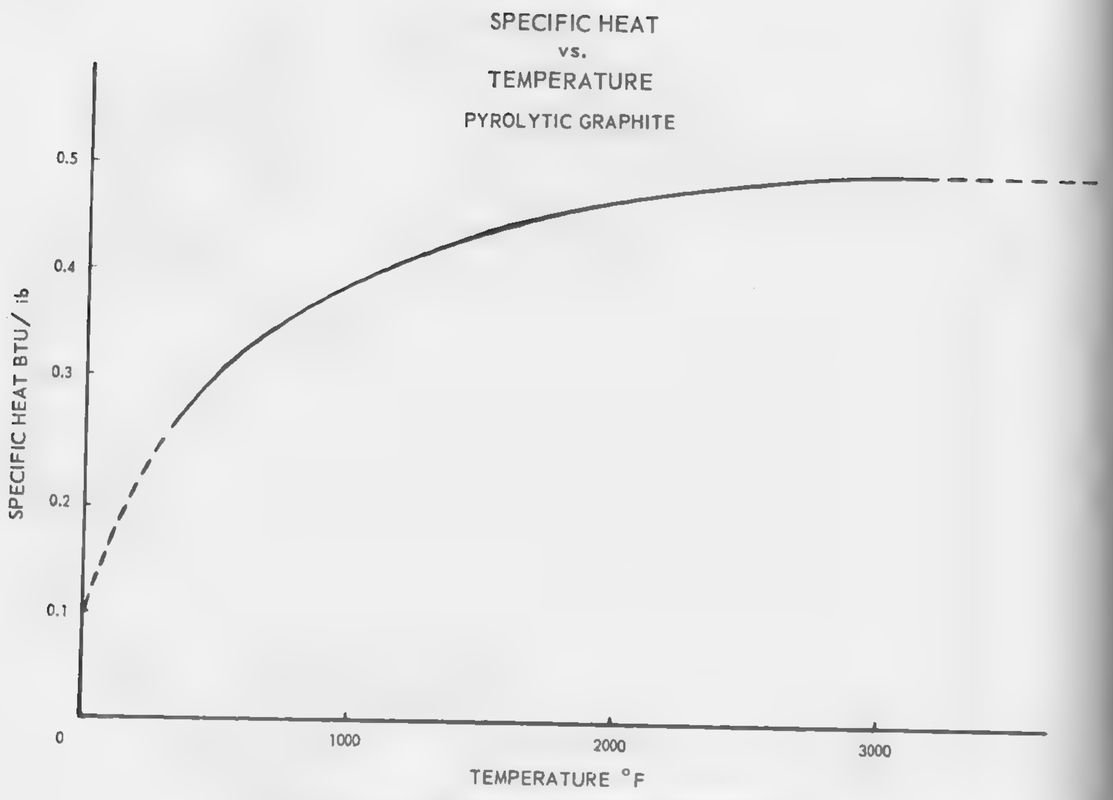


FIGURE 15 SPECIFIC HEAT OF PYROLYTIC GRAPHITE

seen to increase to its maximum value in the temperature range from 2500°F to 3000°F.

The emissivity as a function of temperature is seen in Figure 16. As is well known high emissivities are important for refractory insulating materials which are used as re-entry heat shields. The emissivity of pyrolytic graphite is sufficiently high for it to act as a good radiator during re-entry. A shell of the material will also radiate a greater percent of the heat input because of the high conductivity parallel to the surface, which effectively increases the radiating surface area.

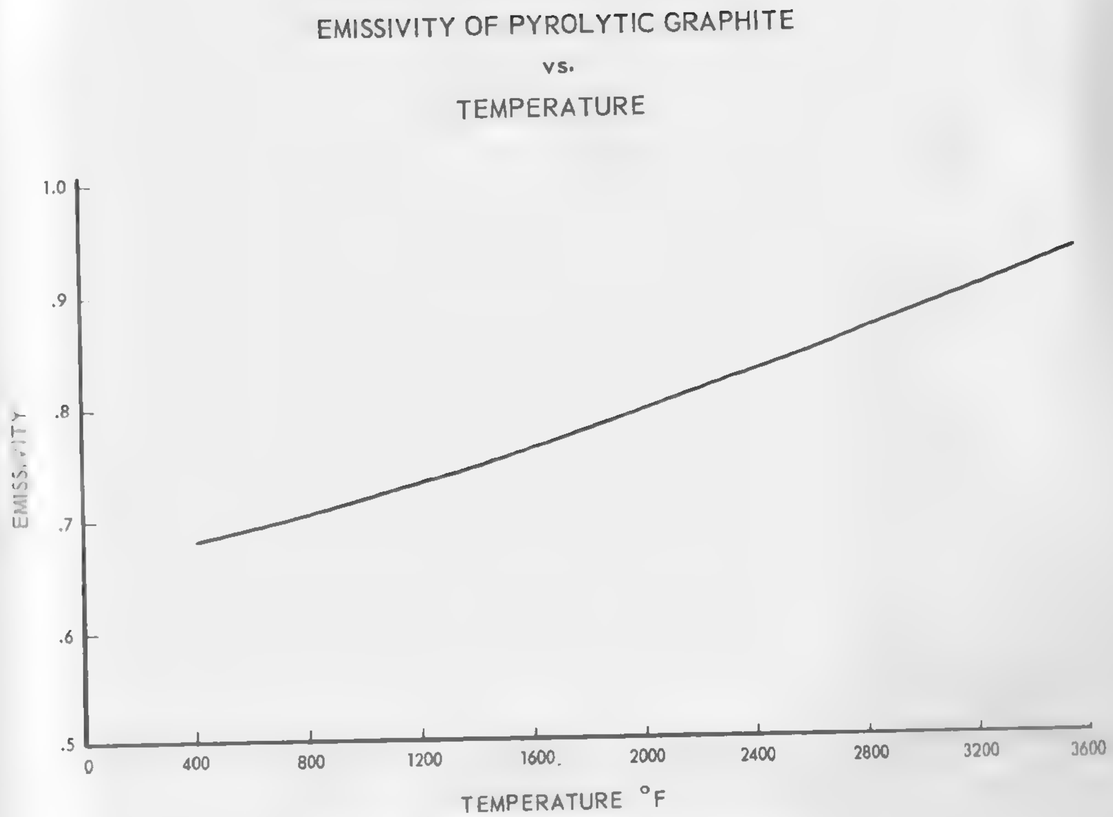


FIGURE 16 EMISSIVITY OF PYROLYTIC GRAPHITE

Thermal Expansion

The anisotropic thermal expansions of pyrolytic graphite and other pyrolytic materials are important quantities which lead to residual stresses in these materials during their cool down from process temperatures. The quantities are also important for the determination of the thermal stresses developed during a subsequent rapid heating to very high temperatures. Figures 17 and 18 present the "a" and "c" direction thermal expansion coefficients of pyrolytic graphite as a function of temperature. The dotted portion of the curves are preliminary data. In the "a" direction pyrolytic graphite initially contracts on heating above room temperature. As a function of temperature the expansion coefficients are nearly linear and a ten to one ratio exists between the "c" and "a" direction coefficients.

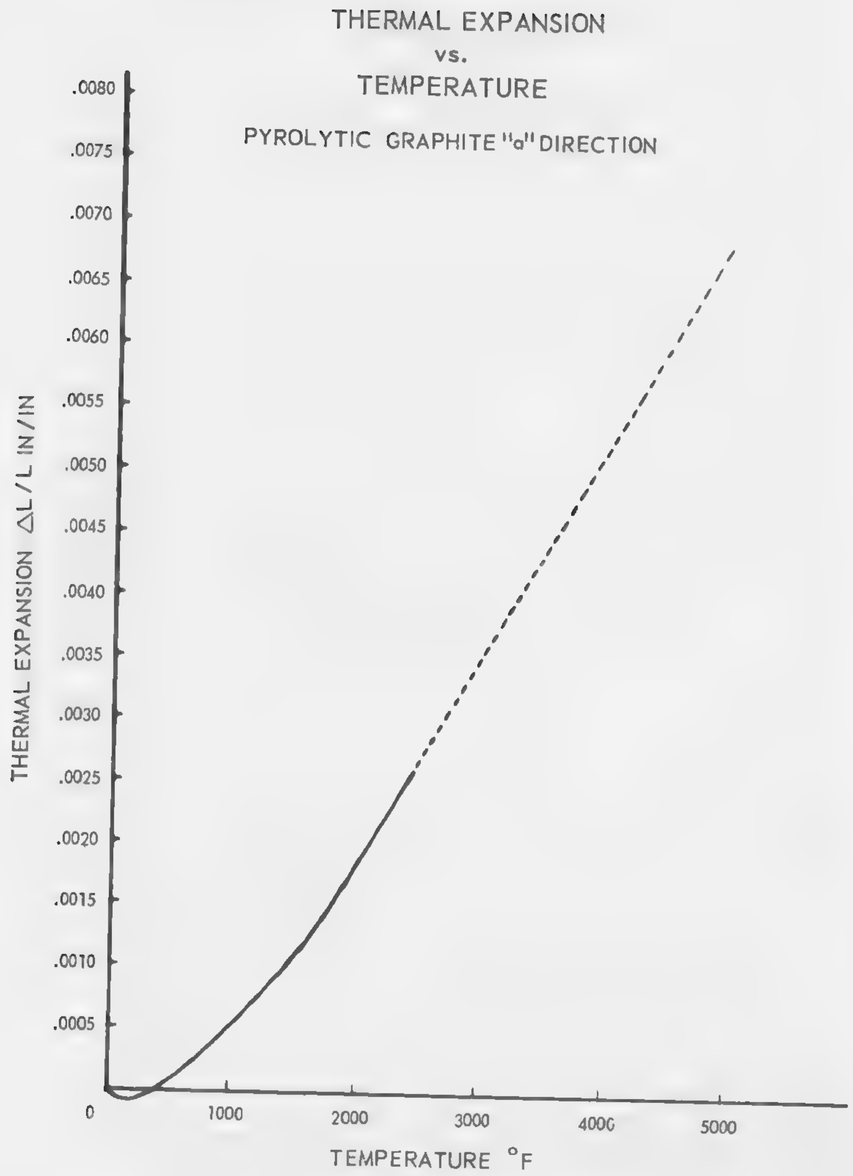


FIGURE 17 THERMAL EXPANSION "a" DIRECTION

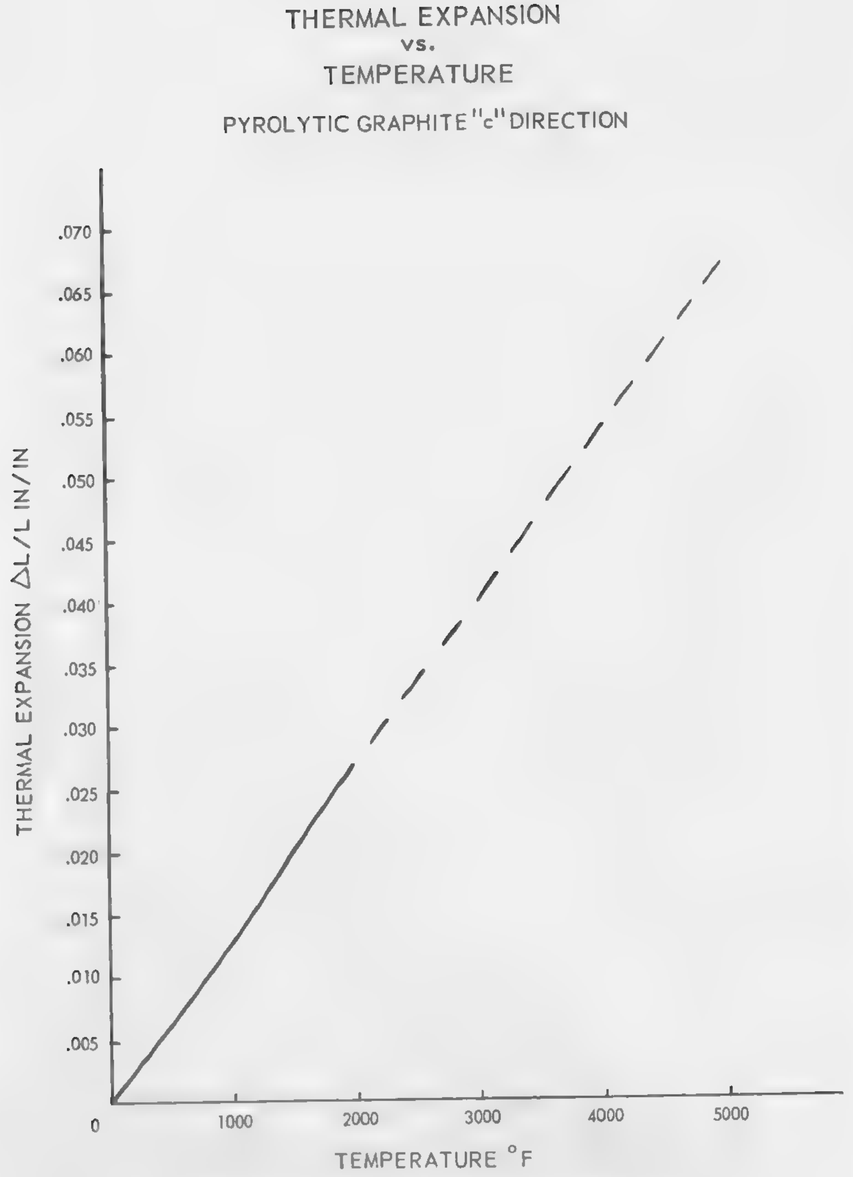


FIGURE 18 THERMAL EXPANSION "c" DIRECTION

The anisotropic residual stresses in pyrolytic graphite components can be calculated for particular shapes. For a cylindrical geometry the residual stresses become a simple function of the thickness to radius ratio where they are tangential tension and longitudinal compression on the inside surface, and tangential compression and longitudinal tension on the outside surface. The largest stress predicted by anisotropy alone is the tangential stress which increases with increasing thickness to radius ratio.

Other factors also contribute to the residual stress pattern. During processing, variable lattice transformation or "growth" takes place in the material due to an annealing effect. The "growth" is one which takes place as a function of time at process temperatures. The initial material deposited is at temperature considerably longer than the last material deposited and the change in lattice spacing across the thickness produces residual stresses. The residual stresses due to the "growth" phenomena are opposite in sign to the reference anisotropic tangential stress, and are of the same sign in the longitudinal direction.

Also, in some cases, because of the insulating qualities of pyrolytic graphite the first material deposited is produced at a higher temperature. This effective decreasing deposition temperature with thickness also contributes to the internal stress pattern.

A further factor to consider is the role of the mandrel. The commercial graphite normally used does not undergo dimensional changes during processing and therefore can act to constrain the pyrolytic deposit. The amount of constraint which produces residual stresses will vary with mandrel design and type used.

The residual stress pattern in pyrolytic graphite is, therefore, due to the anisotropy of the material and to what may be labeled process stresses. The process stresses may be minimized or increased to a maximum through control of the associated factors. These latter stresses can also be reduced to a minimum or to a desired level by

fast annealing of the material at a temperature slightly higher than the process temperature used.

In the final analysis it is possible, through control of the factors influencing the residual stresses in pyrolytic materials, to produce the most favorable stress pattern for a given application.

DISCUSSION

For re-entry heat shield applications the properties of pyrolytic materials should make them particularly advantageous. Pyrolytic graphite is known to be the highest temperature structural material available. For operation in the temperature range from 3000°F to over 5000°F it is the only material presently useful, except perhaps alloys of pyrolytic graphite, boron nitride and commercial graphite. On a strength to weight basis pyrolytic graphite would provide the lightest structure possible for very high temperature applications. Such an application might be "hot structure" control surface where strength requirements are very important. The oxidation resistance of pyrolytic graphite for ballistic re-entry is known to be satisfactory. The other pyrolytic material produced, Boron Pyralloy and Boron Nitride, have oxidation resistances superior to pyrolytic graphite. For long time re-entry application the lower oxidation rate of boron nitride and boron pyralloy at temperatures on the order of 4000°F should be advantageous, but the lower oxidation rate of these materials over a wide temperature region may be their most pertinent feature.

A comparison of the oxidation less during glide re-entry of commercial graphite and pyrolytic graphite has been made. This excellent analysis by Nolan and Scala shows the superiority of pyrolytic graphite in the temperature environment to over 4000°F. The oxidation resistance of pyrolytic graphite is considered excellent and is attributed in part to its higher transition temperature. That is, the temperature where the oxidation reaction changes from a rate process to a diffusion controlled process. In this respect the lower oxidation rate of pyrolytic boron nitride and boron pyralloy over the

same temperature range makes them superior materials for this application.

The high temperature strength of pyrolytic boron nitride has not yet been determined as a function of temperature. In view of its similarity in crystal structure to pyrolytic graphite there is reason to believe that its strength will increase with temperature. In any event, boron nitride or boron pyralloy could be used as surface layers on pyrolytic graphite and a re-entry material developed which has optimum strength and oxidation resistance.

The high thermal conductivity of pyrolytic materials in the direction parallel to their surface is specially advantageous for re-entry since it serves to distribute the heat input over a larger surface area. The outer surface of a shell of pyrolytic materials will operate at a sufficiently high temperature for it to reject a high percent of the heat input. The emissivity of pyrolytic graphite is high at elevated temperatures and pyrolytic boron nitride has an emissivity only some 10 to 15% lower.

The thermal conductivity in the direction normal to the surface of pyrolytic graphite is sufficiently low for practical thicknesses of the material to serve as an effective heat shield. Boron nitride has a still lower thermal conductivity than pyrolytic graphite and would lessen material weight for this purpose. The temperature profile of a pyrolytic graphite ballistic nose cap has been analytically determined. Environmental or rocket tests have also been performed on the same nose section and the resulting temperature profiles were found to be in agreement. The results obtained which are still confidential lend support to the analytical approach as a means of determining the temperature profile under different sets of conditions.

For re-entry glide vehicles instantaneous peak surface temperatures and temperature profiles across leading pyrolytic graphite surfaces have been determined.[1] The results obtained which are dependent on design and other factors are most significant for our purpose in showing up the insulating qualities of pyrolytic graphite. Where peak temperatures in the range of 3600°F to 3800°F were determined

after approximately 17 minutes of re-entry, a commercial graphite sustained a maximum temperature gradient of the order of 300°F/in. In comparison pyrolytic graphite sustained a gradient of the order of 7000°F/in.

The use of pyrolytic graphite can, therefore, result in low internal surface temperatures and this can be accomplished with nominal thicknesses of the material.

Re-entry vehicles will be subjected to a wide range of heating conditions, and for each application a particular system will be the most efficient. Promising systems such as the Bell Aerosystem's Double Wall concept[2] and Chance Vought's Thermosorb System[3] which are presently being developed, will impose a minimum weight penalty, and will maintain interior surfaces at temperatures no greater than 200°F. These systems will be able to operate at temperatures on the order of 2500°F, and through further development the limit may be increased to 3500°F. In the final analyses, the operational limit of glide re-entry systems is determined primarily by the external heat shield material utilized.[4]

The use of pyrolytic materials as heat shields offers a means of extending the operational limit of a system to surface temperatures in the range of 4000°F to 5000°F and over. Preliminary calculations of a heat shield system composed of pyrolytic materials has revealed that such a system will be most efficient where high heat fluxes and high temperatures are encountered. The use of pyrolytic materials should in effect widen the re-entry corridor available to glide re-entry vehicles.

The development of pyrolytic materials is continuing and significant property improvements are anticipated. In the near future it is expected that it will be possible to tailor the properties of these materials for a specific application.

BIBLIOGRAPHY

1. Scala, S. M. and E. J. Nolan, "The Aerothermodynamic Behavior of Pyrolytic Graphite During Sustained Hypersonic Flight," G. E. R61SD051, March, 1961.

2. Guyton, R., "High Temperature Composite Structural Configurations: Radiative Thermal Protection Systems for 2500-4500°F Operation," AFOSR Conference on Aerodynamically Heated Structures, July 25-26, 1961.

3. Dickson, J., "Thermal Protection with a Temperature Capability to 2500°F for Cool Structures," AFOSR Conference on Aerodynamically Heated Structures," July 25-26, 1961.

4. King, J., "Thermally Integrated Structure: A Review of Low-Intensity Cooling Systems for Thermally Protected Air Frames," AFOSR Conference on Aerodynamically Heated Structures, July 25-26, 1961.

MATERIALS PROBLEM AREAS PECULIAR TO SUPERSONIC AIRCRAFT

Nicholas J. Hoff
Head of Department of Aeronautics
and Astronautics
Stanford University
Stanford, California

ABSTRACT

The only radically new phenomena influencing the selection, development and evaluation of materials for supersonic aircraft are the aerodynamic heating of the structure by the high-speed air flow and the consequent high temperatures at which the materials must operate. Information is presented on aerodynamic heating and on the effect of high temperatures on the behavior of materials and structures.

INTRODUCTION

Concern over the best possible selection of aircraft materials is as old as aeronautics. To prove this point, it might be worthwhile to quote from a letter in which Orville Wright described problems of this kind he and his brother, Wilbur, had to solve at the turn of the century[1*]

> "For most of our aeroplane work we preferred the light white spruce of West Virginia. In the tests we made years ago we found that an inch-square piece of the white spruce was not as strong as the inch-square piece of the heavier spruce. The strengths were approximately in proportion to the

---

* References at the end of the paper.

weights; but we figured that we would get a slightly increased strength with the light spruce because, with the same weight, the cross section would be greater."

Clearly here are the beginnings of scientific materials selection and optimal design. Of course, the basic material of the Wright planes was wood, but this was not true of all the early planes. Indeed, Langley's aerodrome (the early name for the airplane) was built of steel in 1903; the wing of Brequet's 1910 model in France had a single spar consisting of a large-diameter steel tube; and in 1912 H. Reissner built a metal monoplane in Germany whose wing was constructed of corrugated aluminum sheet without any fabric covering.[2]

The basic problems of materials selection the designers of airplanes had to face at the beginning of the century were essentially the same as those encountered today in connection with subsonic aircraft although the relative importance of the phenomena involved has changed vastly, as for instance in the case of fatigue. A significantly new phenomenon arose only recently when airplanes began to fly at supersonic speeds; it is usually called aerodynamic heating in this country and kinetic heating in Great Britain.

AERODYNAMIC HEATING

The heating effect of air on bodies traveling through it at high speed has been observed, although not recognized, by man for thousands of years as he looked at the shooting stars passing across the sky in the late summer. These meteorites become visible after they enter the atmosphere of the earth because the pressure and friction of the air raise their temperature to a level where their surface begins to radiate light and to burn. Nevertheless most persons find it hard to accept the fact that a high-speed airstream heats a stationary body submerged in it. Their personal experience has been that a breeze on a hot day cools them.

The apparent contradiction has its explanation in the opposing effects of two physical phenomena which take place at the same time. The heat generated by the airstream increases rapidly with the speed of flow; it is so small at the velocity of the breeze that it cannot even be measured with ordinary thermometers. It becomes noticeable at 400 or 500 miles per hour and attains its full importance only at supersonic speeds. On the other hand, the human skin is cooled mostly by evaporation. On a calm, warm summer day the layer of air closest to the skin soon becomes saturated with vapor and prevents further evaporation. When a fresh breeze carries away this layer and replaces it with air of low humidity content, evaporation can continue and one experiences relief.

The heating effect of the air stream is thus not noticeable to man in his ordinary life while the cooling effect gives him a pleasant sensation in the summer. The conditions are reversed with the airplane where the cooling effect is absent in the conventional design but the heating effect is likely to cause a great deal of trouble at high speeds. However, evaporative cooling has been used in jet engines by introducing the liquid propellant into the combustion chamber through a porous metal wall, and it has been suggested for the cooling of the bow of the fuselage and of the leading edges of the wings of airplanes flying at supersonic speeds.

It should be useful to quote here a few formulas from the literature[3] and to give a few numerical values defining aerodynamic heating in a quantitative manner. At the leading edge of the wing the relative velocity of the air with respect to the airplane is reduced to zero at the so-called stagnation point. Hence the entire kinetic energy of the flow is transformed into heat energy. The temperature of the air at this point is known as the stagnation temperature T_s. It can be computed from the formula

$$T_s = T\left[1 + (M^2/5)\right] \qquad (1)$$

Here T is the ambient temperature of the air in degrees

absolute and M is the Mach number of flight defined as the ratio of the flight velocity to the velocity of sound corresponding to the ambient conditions.

Let us assume that the flight takes place at a Mach number of 3 at an elevation of 50,000 ft. At that height the standard temperature is $-67.6^{\circ}F$, which is $392^{\circ}R$. Substitution in Eq. 1 yields

$$T_s = 392\left[1 + (9/5)\right] = 1098^{\circ}R = 638.4^{\circ}F \quad .$$

This is the temperature the leading edge of the wing would attain in the absence of cooling. The maximum possible temperature for the surface of the wing further downstream is known as the adiabatic wall temperature T_a. The rise from the ambient temperature to the adiabatic wall temperature is only 85% of the rise from the ambient temperature to the stagnation temperature. Hence in the present example $T_a = 392 + (0.85)(706) = 992^{\circ}R = 532^{\circ}F$. This is true when the flow in the boundary layer is laminar, that is smooth. When the boundary layer flow is turbulent, the rise to the adiabatic wall temperature is 90% of that of the stagnation temperature.

One of the most significant features of Eq. 1 is the appearance of the speed of flight raised to the second power. This indicates that the temperature increases very rapidly when the flight speed is increased. Indeed, the stagnation temperature given by the formula is $3214^{\circ}R \simeq 2754^{\circ}F$ when the flight takes place at the same elevation but at a Mach number of 6. Above this temperature the properties of the air begin to change to such an extent that Eq. 1 should not be used at speeds significantly exceeding M = 6.

Incidentally, it is useful to note that the speed of sound v_s in the atmosphere depends only on the ambient temperature in accordance with the formula

$$v_s = 49.1\sqrt{T} \qquad (2)$$

where v_s is given in feet per second and the temperature T

must be substituted in degrees Rankine. Hence at 50,000 ft we obtain

$$v_s = 49.1\sqrt{392} = 970 \text{ ft/sec} = 660 \text{ mi/hr} \quad .$$

The heating rate experienced by the wing can be calculated from the Crocco formula valid for laminar boundary layer flow:

$$q = 0.3(k/x)\sqrt{R}(T_a - T_w) \quad . \qquad (3)$$

In this formula q is the heating rate in Btu per square foot per unit time, k is the conductivity of the air, T_a is the adiabatic wall temperature defined earlier, T_w is the temperature of the surface of the wing, and R is the local Reynolds number defined as

$$R = ux\rho/\mu \quad . \qquad (4)$$

In this equation x is the distance of the point where the heating rate is sought from the leading edge of the wing, and u, ρ and μ are the local flow velocity, the density and the viscosity of the air at the distance x, all these quantities measured in the flow just outside the boundary layer.

If the wing of the airplane is thin and is flying at a small angle of attack, evaluation of the flow quantities and substitution in Eq. 3 lead to

$$q = 70 \quad \text{Btu per square foot per minute}$$

at a distance x = 1 ft from the leading edge, provided the wall temperature is $-67.6^{\circ}F$ initially. It follows from Eqs. 3 and 4 that the heating rate varies with x in inverse proportion to $\sqrt{x}$. This is true only for heating by the laminar boundary layer; in the case of the turbulent boundary layer q is inversely proportional to the fifth root of x. Moreover, the heat transmitted to the wall is much greater in the turbulent layer than in the laminar one because of the more rapid mixing of the particles in the flow. In the present example, for instance, calculations show that turbulent heating has about 8 times the intensity of laminar heating at a distance of 1 foot from the leading edge.

Since the specific heat of aluminum alloys is about 0.23 Btu/lb°F, the heat capacity of a plate of one square foot area and 1/8 in. thickness weighing about 1.8 lb/ft^2 is about 0.414 Btu /°F. Hence under the stated conditions of flight the temperature of such a wing cover plate would rise about 170°F every minute under the effect of aerodynamic heating of an intensity of 70 Btu per square foot per minute. The rate would be about 8 times higher if the boundary layer were to become turbulent. Fortunately, these high heating rates prevail only as long as the wing is cold. When it gets hot, the difference $T_a - T_w$ in Eq. 3 becomes smaller and eventually approaches zero. This is in agreement with the earlier statement that the maximum possible temperature of the wall is T_a.

DETERIORATION OF THE PROPERTIES OF MATERIALS

It is unnecessary to explain to this audience how the mechanical properties of the materials of construction deteriorate when the structure is exposed to high temperatures for prolonged periods of time. It might be mentioned, however, that the elastic limit, the yield stress and the ultimate stress are all important in determining the load-carryin capacity of the structure. In addition, the rigidity of the structure characterized by Young's modulus E and the shear modulus G plays a significant role not only in the determination of the buckling loads but also in the evaluation of the deformations of the structure. Maximum deformations under static loads can in some cases represent the conditions governing the design of the structure or the selection of its material of construction. More often the dynamic behavior establishes the critical condition. A decrease in the values of E and G modifies the response of the structure to dynamic loads and reduces the maximum speed at which the airplane can fly without danger of flutter.

Since the end of World War II a very large amount of information has been collected on the effect of loads applied repeatedly to the elements of aircraft structures. It is well known that comparatively small loads can cause failure

if they occur a large number of times; this phenomenon is known as fatigue. However, the empirical fatigue curves must be established anew for each material to be used in the construction of an airplane, and unfortunately there is no reliable method available for the prediction of fatigue failure under varying load amplitudes from data collected in fatigue tests carried out at constant load amplitudes. Thus the task of predicting the probable lifetime of an airplane is very difficult at the present time. When the new parameter temperature is introduced into the problem in consequence of aerodynamic heating, the magnitude of the task becomes so overwhelming that one expert has stated that it will be economically impossible to guarantee the fatigue lifetime of the supersonic transport. A better fundamental understanding of the fatigue phenomenon is therefore urgently needed but is not yet in sight.

An entirely new material property to the aeronautical engineer is the emissivity ϵ which is equal to the absorptivity α . The latter is defined as the ratio of the radiant energy absorbed by a surface to the total radiant energy impinging on the surface. The emissivity and the absorptivity, in general, are functions of the wave length of the radiation and of the temperature of the surface. The ideal black body is defined as one characterized by $\alpha = \epsilon = 1$.

The importance of these concepts to the aeronautical engineer is that a supersonic aeroplane is cooled by the heat lost through radiation, and that the cooling effect increases very rapidly with the temperature of the surface. The Stefan-Boltzman law states that the radiant energy q departing per second from a surface of one foot square is in Btu

$$q = 0.48 \epsilon \, (T_w/1000)^4 \qquad (5)$$

where ϵ is the emissivity and T_w is the surface temperature in degrees Rankine.

When an airplane has been flying for a sufficiently long time at a constant altitude at a constant velocity, it has reached thermal equilibrium. This means that the heat

lost from one square foot of its wing surface in accordance with Eq. 5 must be equal to the heat gained through aerodynamic heating in accordance with Eq. 3. By equating the two expressions one can calculate the surface temperature T_w. This will be found to differ only slightly from the adiabatic wall temperature when the airplane is flying at an elevation of 50,000 ft at a speed corresponding to M = 3, but the decrease in temperature due to radiation is of the order of magnitude of 50% of the adiabatic wall temperature when the flight takes place at an elevation of 200,000 ft at M = 6. In the latter case the relief in temperature is very sensitive to the exact value of the emissivity ϵ. As manned re-entry from an orbit may take place most auspiciously in a high-speed glide vehicle and since such a vehicle must fly very high and very fast, the study of the variations in the value of the emissivity with exposure to high temperature is beoming an important task for the materials expert.

THERMAL STRESSES

If a bar, initially at a temperature T_o, whose length is L_o is heated to a temperature $T_1 = T_o + \Delta T$, its length increases to

$$L = L_o(1 + \alpha \Delta T) = L_o + \Delta L_T \qquad (6)$$

where α is the coefficient of (linear) thermal expansion and ΔL_T is the increment in length in consequence of heating. If the bar is part of a structure containing relatively rigid elements whose length does not change while the selected bar is being heated, these elements exert compressive forces on the bar in order to prevent its expansion. Since the shortening of a bar of length L_o and cross-sectional area A under the action of a compressive force P is

$$\Delta L_P = PL_o/EA = \sigma_T L_o/E \qquad (7)$$

where ΔL_P is the shortening caused by the force P, E is Young's modulus of elasticity and $\sigma_T = P/A$ is the compressive stress in the bar, the length of the heated remains unchanged if

$$\Delta L_P = \Delta L_T \quad .$$

This is the condition from which the stress σ_T can be computed. Substitution from Eqs. 6 and 7 yields

$$\sigma_T L_o/E = L_o \alpha \Delta T \quad .$$

Solution for σ_T leads to the formula

$$\sigma_T = \alpha E \Delta T \quad . \qquad (8)$$

The stress σ_T is called the thermal stress in the bar.

According to Eq. 8 the thermal stress is proportional to the rise in temperature and to the product of the material constants α and E. If this product is small, the structure will not experience high thermal stresses. But the designer wants high values of Young's modulus for rigidity and for resistance to buckling; hence α should be as small as possible. Typical values of αE are in pounds per square inch per degree Fahrenheit:

Iron:	200
Aluminum:	140
Magnesium:	90

This means that a rise in temperature amounting to 100°F causes a thermal stress of 14,000 psi in an aluminum bar under the conditions mentioned. Hence in supersonic aircraft and missiles where temperature differences of several hundred degrees Fahrenheit can occur, the danger of high thermal stresses is very real.

Unfortunately the materials specialist does not seem to have much of an opportunity to reduce the coefficient of thermal expansion α. Thus the structural designer must seek arrangements in which thermal expansion is possible, at least in part. When the thermal expansion can be accommodated in part, ΔL_P need only be equal to a fraction of ΔL_T, and the thermal stress is reduced. When there is no restraint to expansion, there cannot be any thermal stress in a uniformly heated bar.

Of course, in the wing and fuselage structure of aircraft the situation is much more complex and the thermal stress is less than that given by Eq. 8. As a matter of fact the purpose of thermal stress analysis[4] is exactly to determine the proper multipliers of $\alpha E \Delta T$. However, with rapidly varying temperatures the thermal stress often amounts to 70 to 80% of the value given by Eq. 8 and the formula is useful because it indicates, in a very simple manner, the maximum possible values of the thermal stress.

As ductile metals generally become more ductile when the temperature rises, structural elements made of them are not very likely to fracture while the airplane structure is being heated by the supersonic airstream. They are more likely to crack during a cooling period while the airplane is cruising at subsonic speeds following a dash in the supersonic range. Similarly cracks are likely to form in structural parts made of refractory materials whose ductility is low. The appearance of cracks is facilitated by high temperature gradients. These can be avoided, or at least reduced, if materials with good thermal conductivity and good thermal diffusivity are employed.

Finally it should be mentioned that the resistance of a thin or slender structural element to buckling is proportional to the modulus E, as can be seen from the oldest buckling formula which is due to Euler:

$$P_{cr} = \pi^2 EI/L^2 \quad . \qquad (9)$$

Here P_{cr} is the buckling load, E is Young's modulus, I is the moment of inertia of the cross section of the column, and L is the length of the column. Since the thermal stress is also proportional to E (see Eq. 8), Young's modulus is canceled when the critical value of the rise in temperature ΔT_{cr} is sought and the only physical constant entering the formula is the coefficient of thermal expansion α.

CREEP

A physical phenomenon which has been known for over a hundred years but has only lately attracted much attention

is the phenomenon of creep. By this term is meant the continued increase with time in the length of a bar that is subjected to a constant tensile load. Annealed copper and lead creep noticeably at room temperature under moderate loads but the creep phenomenon is not observed in everyday life with our structures built of steel and aluminum alloys. This does not imply that creep is a rare phenomenon; it only proves that earlier generations of engineers had the common sense of selecting as structural materials those metals that maintain their dimensions constant at ordinary temperatures.

The dependence of the rate of change in the length of a tensile creep specimen, the creep rate, on the temperature and the applied stress has been the subject of many theoretical and experimental investigations in the last thirty odd years. In spite of much progress made, theory and experiment are still far apart and the designer of structures must rely on empirical data in his work. Particular problems for whose solution we are still groping in the dark are the effect on the creep rate of a change in the applied load in course of the creep test, and the generalization of one-dimensional creep test results to creep under triaxial states of stress.[5]

The urgency now existing for acquiring a better understanding of creep phenomena is of course caused by the high temperatures at which nuclear power plants and hypersonic airplanes and missiles have to operate. There is a significant difference, however, between these two applications. In the case of nuclear power plants, at least when they are built on the ground, safe operation and relatively long life are prime requirements. For this reason the allowable creep rates are low. Somewhat higher rates will be permissible with the supersonic transport airplane. The situation is quite different in the case of the nose cone of a ballistic missile which may re-enter the atmosphere at a Mach number of 25 and may be subjected to high stresses and extreme aerodynamic heating for only ten or twenty seconds. Such a missile is built for a single flight; if it creeps at the rate of several hundred percent per hour under the extreme conditions, the duration of these conditions is just not enough to change the shape of the structure sufficiently to cause trouble. Intermediate between the Mach number 3 transport and the ballistic nose cone is the

hypersonic glider used as a shuttle vehicle between an orbiting space station and the ground. Such a glider may be operating at very high temperatures for 15 to 30 minutes; it will also be required to make repeated trips to the space station and back.

Since the creep rate of metals is a highly non-linear function of the applied stress, unusual phenomena of great theoretical and practical interest can be predicted and observed with structural elements under conditions when the material is subject to creep. Only two of these will be mentioned here, namely creep fracture in tension and creep buckling.

When the uniaxial creep law is

$$\dot{\epsilon} = (\sigma/\lambda)^n \tag{10}$$

where $\dot{\epsilon}$ is the creep rate, σ the applied stress, and λ and n are constants, simple theoretical considerations show that a tensile test specimen must fracture in a finite time t_{cr}. This time is given by the equation

$$t_{cr} = 1/n\dot{\epsilon}_i \tag{11}$$

where n is the exponent in the creep law of Eq. 10 and $\dot{\epsilon}_i$ is the creep rate at the beginning of the test. This theoretical formula was derived in 1953;[6] it was modified to hold for various other creep laws in 1958.[7]

The behavior of a column whose material creeps is equally interesting. Any initial deviation from the perfect theoretical conditions is exaggerated by the creep deformations. When n is greater than unity in the creep law of Eq. 10, the column buckles in a finite time even though the compressive force P is less than Euler's critical load P_E. When n = 3 the critical time is given by the formula[8]

$$t_{cr} = \frac{1}{3} \frac{\epsilon_E - \epsilon_o}{\dot{\epsilon}_i} \log \frac{2r}{a_i} \tag{12}$$

where a_i is the amplitude of the sinusoidal initial deviations

of the center line of the column from the line along which the compressive load P is acting, r is the radius of gyration of the cross section of the column, $\dot{\epsilon}_i$ is the initial creep rate under the uniform stress P/A (where A is the cross-sectional area of the column), ϵ_E is the elastic strain corresponding to Euler's buckling formula

$$\epsilon_E = \pi^2/(L/r)^2 \tag{13}$$

and ϵ_o is the elastic strain corresponding to the applied load

$$\epsilon_o = P/EA \tag{14}$$

The creep buckling formulas published in the literature are based on empirical creep laws derived from experimental data. It will certainly be possible to improve them as soon as materials experts furnish the applied mechanics man with more complete information on the behavior of materials in creep.

BIBLIOGRAPHY

1. The Papers of Wilbur and Orville Wright, edited by Marvin W. McFarland, McGraw-Hill Book Co., New York 1953, vol. 2, p. 1106.

2. A Short History of the Development of Airplane Structures, by Nicholas J. Hoff, American Scientist, vol. 34, No. 2, p. 212, April 1946.

3. Thermal Conditions Associated with Aircraft in Flight, by Martin Bloom, WADC Technical Report 55-169, Wright Air Development Center, Wright Field, Ohio, March 1956.

4. Theory of Thermal Stresses, by Bruno A. Boley and Jerome H. Weiner, John Wiley and Sons, New York, N. Y., 1960.

5. Mechanics Applied to Creep Testing, by Nicholas J. Hoff, The William M. Murray Lecture 1958, Proceedings of the Society for Experimental Stress Analysis, vol. 17, No. 2, p. 1, December 1959.

6. The Necking and the Rupture of Rods Subjected to Constant Tensile Loads, by Nicholas J. Hoff, Journal of Applied Mechanics, vol. 20, No. 1, p. 105, March 1953.

7. Structures and Materials for Finite Lifetime, by Nicholas J. Hoff, Advances in Aeronautical Sciences, Proceedings of the First International Congress in the Aeronautical Sciences, Madrid, 1958, Pergamon Press, London, 1959 p. 928.

8. A Survey of the Theories of Creep Buckling, by Nicholas J. Hoff, Proceedings of the Third U.S. National Congress of Applied Mechanics, The American Society of Mechanical Engineers, New York, 1958, p. 29.

SOME MATERIALS AND STRUCTURES PROBLEMS ASSOCIATED WITH DESIGNING B-58 TYPE STRUCTURE FOR SUPERSONIC CRUISE CAPABILITY

W. D. Buntin
Senior Structures Engineer
General Dynamics/Fort Worth
Fort Worth, Texas

ABSTRACT

The general problem areas in choosing materials and designing structures for sustained supersonic flight are summarized. The results of a study of the effects of normal operating conditions at Mach 2.4 on the wing structure of a B-58 type delta wing aircraft are presented. The type of structure considered for this detailed study was sandwich construction consisting of aluminum alloy skins and fiberglass honeycomb core similar to that used in B-58 aircraft. The problem areas considered include maximum load requirements, fatigue, creep, and thermal load effects. Tests of both materials and full scale components in each of these areas are described. Test results and analysis results are presented which show the capability of aluminum sandwich construction for sustained supersonic flight.

Some consideration is given to the requirements for sustained Mach 3 flight. The uses of titanium as a structural material are briefly discussed. Such discussion includes the use of titanium brazed sandwich construction.

INTRODUCTION

Supersonic flight has created new problems in the design of aircraft structures. Most of these problems are the result of aerodynamic heating and its resultant effect on the structure. In addition, there is increasing concern about sonic fatigue, caused by the use of jet engines with enough thrust to push aircraft to supersonic speeds. Maximum range for efficient operation at supersonic speeds necessitates aerodynamically smooth surfaces throughout each flight. Other problems that must be considered include reliability, ease of maintenance and repair, and cost.

These problems face the designer of supersonic airplanes in making a selection of suitable materials and in choosing the most satisfactory type of construction. Choice of material and type of construction must be considered with respect to each other. The importance of minimum weight is increased as the demands for greater performance are increased. All of these problems had to be faced in the design of the B-58 bomber. The resulting wing panel design consisted of aluminum sheets bonded to fiberglass honeycomb core to form the now familiar sandwich type of construction.

The capability of the B-58 to fly at supersonic speeds is well known. Not so well known is the capability of the B-58 type structure for flight for prolonged periods at speeds up to Mach 2.0. Even more significant is the fact that, with certain modifications, capability for continuous cruise at Mach 2.4 can be provided in this type structure. The intent of this paper is to discuss some of the problems that were studied to determine the capability of the type of wing structure used in the B-58 for prolonged service at Mach 2.4. Many of the problems that had to be faced are generally applicable to the design of any supersonic airplane. Some of these problems and their solutions will be emphasized.

In looking beyond the supersonic speed of Mach 2.4, aerodynamic heating becomes more and more significant to the structure. As temperatures go higher, new and different materials must be considered. The use of titanium for Mach 3.0 structure looks promising and some of the aspects of this problem will be discussed briefly.

CRITERIA AND ENVIRONMENT FOR SUPERSONIC FLIGHT

The basic requirements of airplane structures are adequate static and fatigue strength and the ability to resist deformations which would impair operations. In other words, the structure must not fail and it must retain its basic shape. These requirements exist throughout the service life of the vehicle.

Aerodynamic heating begins to be significant at speeds of Mach 2.0 and beyond. This heating affects the ability of the structure to meet each of the basic requirements above. The structure can be called upon to withstand the repetitive effects of minimum temperatures well below $0^{o}F$ and maximum temperatures several hundred degrees above $0^{o}F$, depending upon the speed attained. To better appreciate temperatures associated with supersonic speeds, consider the plot of Mach number versus adiabatic wall temperature shown in Figure 1.

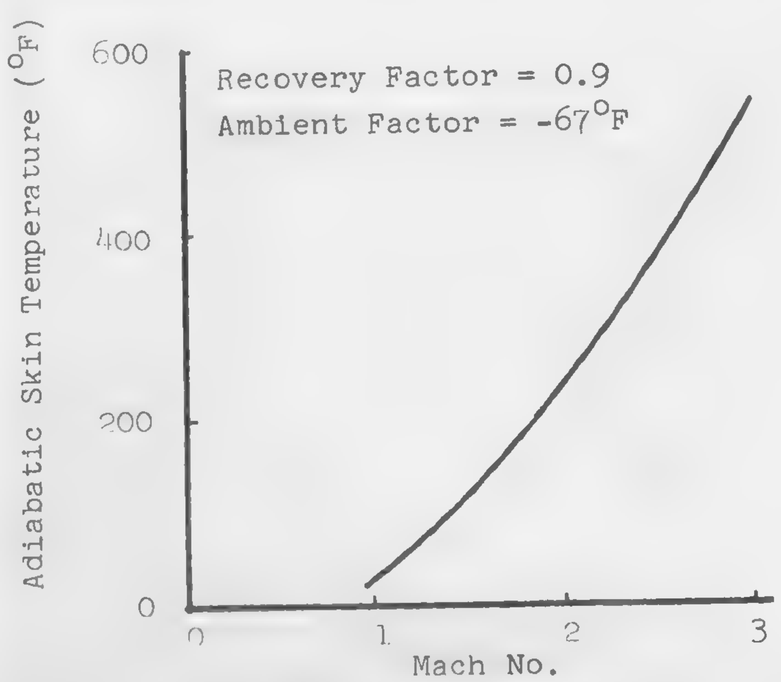


FIGURE 1 ADIABATIC WALL TEMP. VS MACH NO.

Methods for calculating these temperatures are discussed in Reference 1. The design problem becomes one of determining the effects of such heating on the structure. The problem is further complicated because these effects are time dependent.

If aerodynamic heating significantly affects the strength of a structure, the other environmental factors become more important as compared to the subsonic case. For example, cyclic loads due to gusts and maneuvers will cause more fatigue damage in a given structure if the fatigue strength has been degraded due to exposure at elevated temperature. Steady-state loads and cyclic loads that occur at elevated temperature can cause cumulative creep. Another factor to be accounted for in most cases is thermal stress. Each of these effects must be considered in relation to each other. It is further evident that the ability of the structure to resist cumulative fatigue, cumulative creep, and strength degradation depends upon the time of exposure to elevated temperatures as well as the loads that occur during this time.

DESCRIPTION OF THE TYPE OF WING PANELS IN THE B-58

The B-58 was conceived as a delta wing bomber with requirements to fly at speeds up to Mach 2.0. The general structural arrangement of the airplane is shown in Figure 2.

The wing is a multispar design and serves as a fuel tank. The temperature design requirements for the structure were at 260°F. This temperature represents the calculated adiabatic wall temperature at Mach 2.0 on an Air Force ambient hot day at 36,000 feet altitude. Standard day temperatures are lower. The minimum temperature requirement for structural design was -67°F. This represents a lower limit of temperatures that occur during subsonic cruise at high altitudes. The requirements for aerodynamically smooth surfaces and insulation of fuel in the wing against heating had a great deal to do with the type of construction selected for the wing panel design. These panels also had to resist an internal wing pressure of 20 psi.

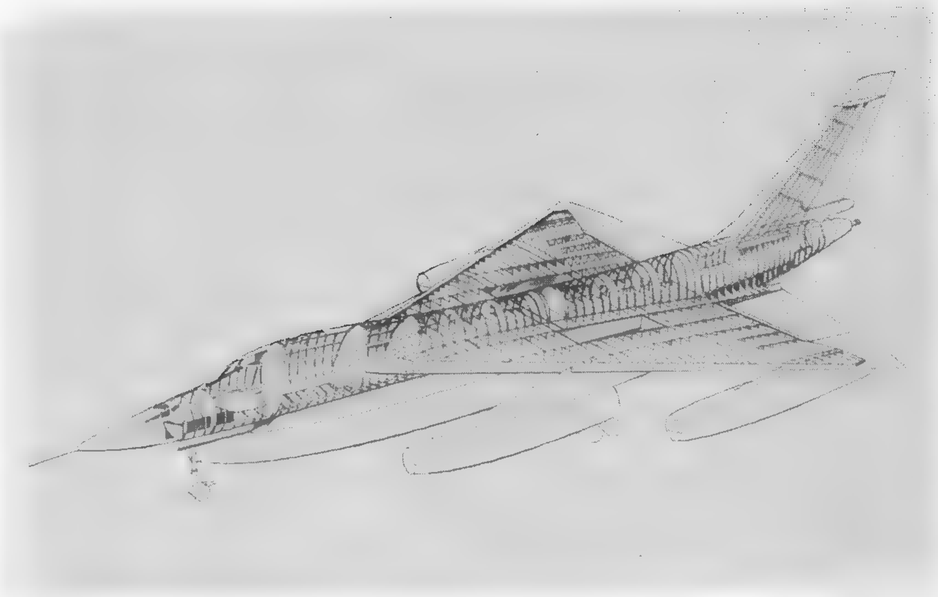


FIGURE 2 B-58 GENERAL STRUCTURAL ARRANGEMENT

All of these requirements were in addition to that of acting as primary load carrying members for air loads.

Aluminum sandwich construction with fiberglass honeycomb core met each of these requirements and provided very favorable strength to weight ratios as wing surface panels. A very extensive development program was carried out beginning with small specimen tests and progressing through tests of large compression panels. Finally, large splice panels and box beams were built and tested. This program established tooling and shop production techniques as well as design allowable stresses for this type of construction.

Two different aluminum alloys were selected for manufacturing the wing sandwich panels. The skins were 2024-T86 and the internal grids, or slugs, are 7075-T6. The 2024-T86 material has good strength for relatively low weight at the elevated temperature design condition of 260°F. The wing

panels are relatively flat and forming was no problem. The 7075-T6 material used for the slugs is capable of withstanding the temperatures expected inside the wing panels and was readily available in the thick plates needed for large panels. In addition, extensive use of aluminum in the aircraft industry had shown both of these alloys to be reliable and practical materials.

Figure 3 shows one of the larger wing panels and its location on the B-58 wing surface. The sections indicate the boundary conditions around the panel.

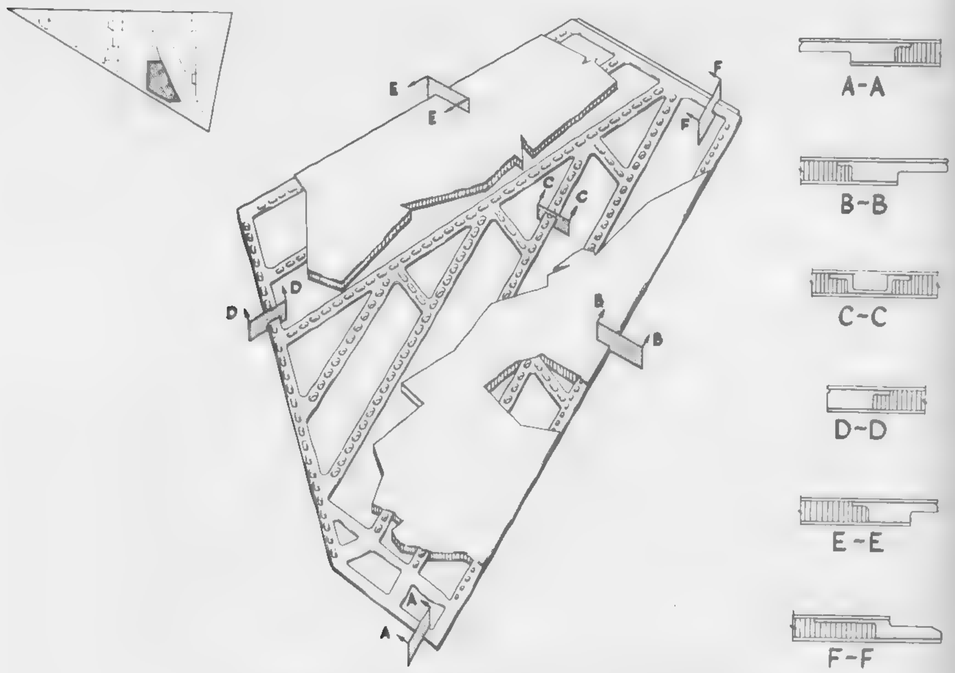


FIGURE 3 B-58 UPPER SURFACE WING PANEL

All surface panels over the wing were designed to the same over-all thickness of 0.580 inches to simplify manufacture and assembly. The skin thicknesses required varied with required wing strength at the various locations. This was accounted for by varying the thickness of the core. This is a very brief description of the wing panels in use today on the B-58. A more detailed description can be found in Reference 2.

CONSIDERATION OF B-58 TYPE WING PANELS FOR SUPERSONIC CRUISE

It was natural to study this type of structure for extended supersonic flight capability. The first step in this study was to determine the capability of the materials for prolonged use in elevated temperature environments. Equilibrium temperatures were calculated in the covering panels of a delta wing of the B-58 type. Three plots of these temperatures are shown in Figure 4.

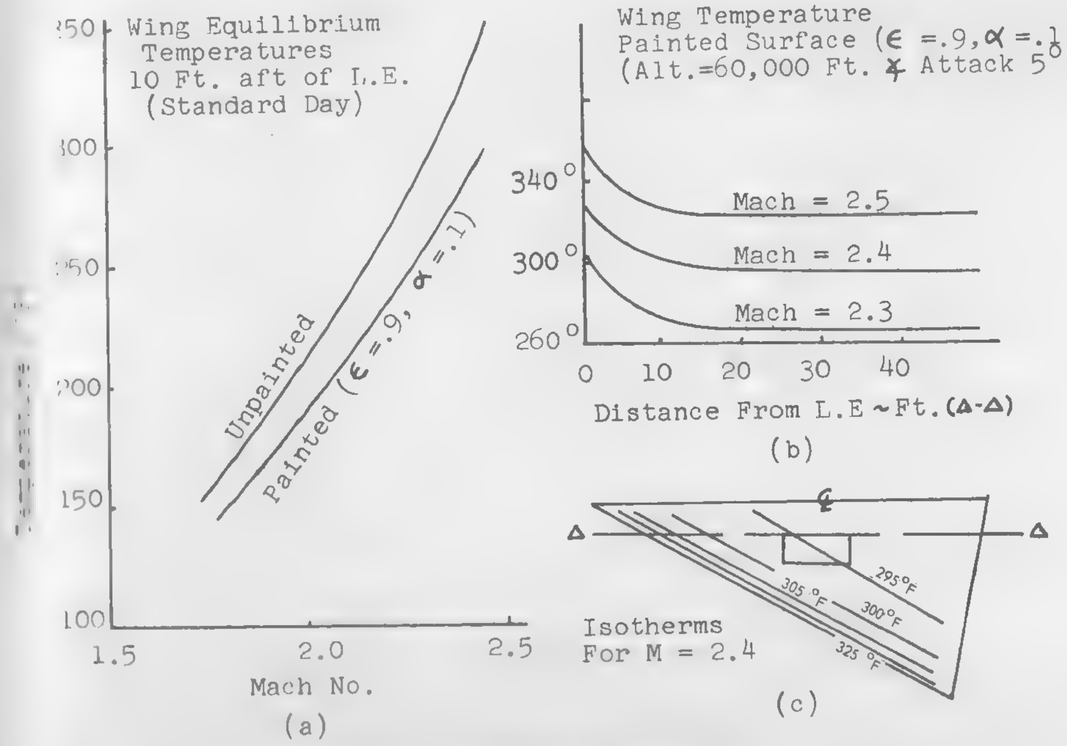


FIGURE 4 TEMPERATURE VS MACH NO.

The reduction in skin temperature made possible by coating the wing surface with a paint is shown in Figure 4(a). Such a paint has the capability of effectively reflecting solar heat and emitting heat caused by air friction. The plots in Figure 4 indicated that the 2024-T86 aluminum alloy would be required to withstand accumulated exposures at 300-325°F for service at Mach 2.4. The exception to this is the leading edge where high temperatures develop. The design of a leading edge would have to take this into account. The effect of Mach 2.4 temperatures on the materials that make up the wing sandwich panels was determined. The materials investigated included the aluminum alloys, 2024-T86 and 7075-T6, the fiberglass honeycomb core, and the adhesives.

Analysis of available data indicated that the strength of 2024 aluminum alloy at 300-325°F is 78-88% of its initial room temperature strength, depending upon the length of exposure. Consider the data shown in Figure 5.

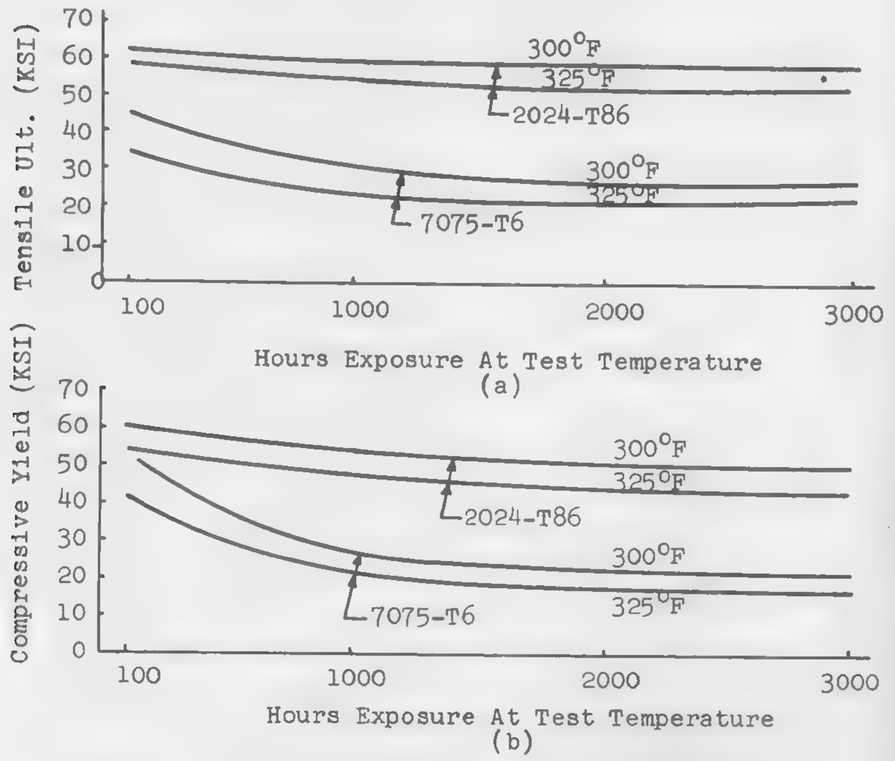


FIGURE 5 ALUMINUM ALLOYS AT ELEVATED TEMPERATURES

Careful examination of the data shows that both 2024-T86 and 7075-T6 aluminum alloys lose strength more rapidly during the initial portion of the high temperature exposure period, at least for the temperatures shown. Of the two materials, 7075-T6 is more susceptible to strength degradation. This immediately suggested that composite panels would retain good strength somewhere between that of the 2024-T86 material and the 7075-T6 material. This strength would also depend upon the ability of the other materials, the adhesives and the honeycomb core, to retain sufficient strength to develop the skins.

Tests were run which showed that the adhesives and the honeycomb core do have the required strengths after prolonged exposure to high temperatures. Results of these tests are presented in Figure 6.

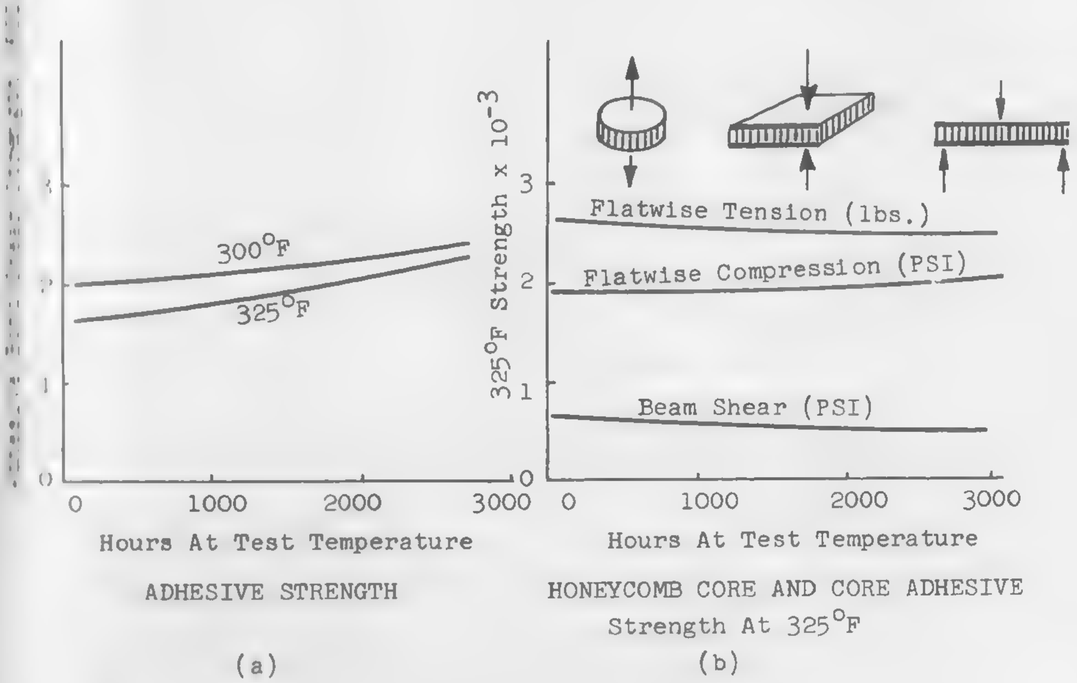


FIGURE 6

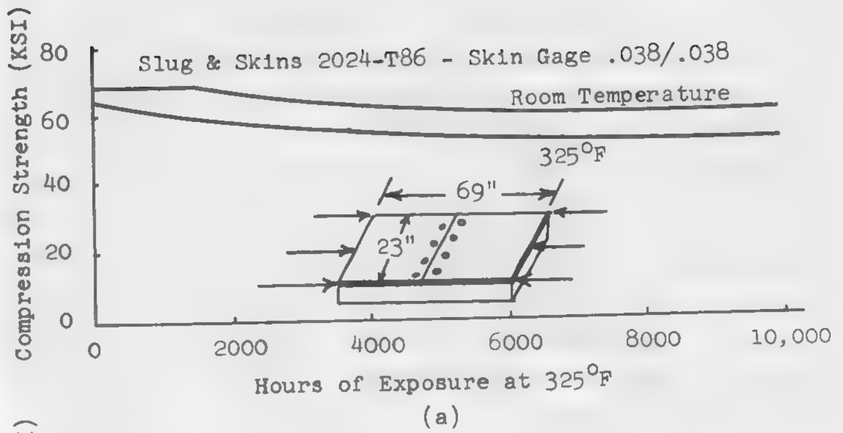
The metal data, and the adhesive data, and the honeycomb core data showed that the composite panel would retain good strength when used in 300-325°F environments.

Analysis of the metals data pointed out a significant fact. Though good strength could be expected as originally designed, the strength of the B-58 type wing panels could be improved by replacing the 7075-T6 slug material with 2024-T86. During the past 2 to 3 years, aluminum companies have built up the necessary facilities to produce 2024-T86 in plates of the required widths and thicknesses. General Dynamics/Fort Worth has developed methods for forming and machining 2024-T86 plates to be used in sandwich panel construction. As a result, wing panels can be fabricated using 2024-T86 slugs with no change in existing tooling.

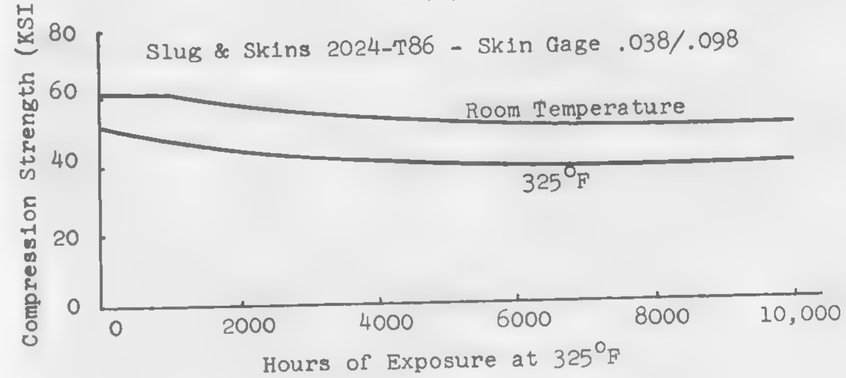
In order to verify predicted composite panel strengths, several full scale panels were built. These panels were built using 2024-T86 material for both skins and slug. The panels were put into an oven at 325°F and allowed to remain varying lengths of time. These panels were tested to confirm the high strengths indicated by the material data. The curves shown in Figure 7 are based on these test results.

The curves in Figure 7 show wing sandwich panel compressive strengths for room temperature in addition to the elevated temperature for 325°F. It will be shown later that room temperature strengths actually set the design for a B-58 type delta wing structure.

At this point in the study, the tests and analytical work had made it possible to establish design allowable stresses for wing panels subjected to the conditions of continuous cruise at Mach 2.4. Such design allowables are reduced below those achieved in the laboratory tests to allow for manufacturing variations. For example, the 325°F design allowable for a 0.038/0.098 wing sandwich panel after 10,000 hours exposure to 325°F has been set as 34,500 psi.



(a)



(b)

FIGURE 7 ALUMINUM SANDWICH PANEL STRENGTH

CONSIDERATIONS FOR CREEP AND FATIGUE

Having established static strengths compatible with Mach 2.4 cruise environments, the design studies turned to creep and fatigue considerations. Creep resistance is a measure of time dependent deformation. The available material data concerning creep for 2024-T86 material at 300-325°F indicated that for predicted wing stress levels excessive creep would not occur. The amount of creep would depend, of course, upon the total time under load at the elevated temperature. One of the big problems in investigating creep possibilities is in obtaining data applicable to the specific conditions at hand. The only alternate in many cases is to resort to extrapolation procedures. Rather than rely completely on such analytical evaluations, a creep test was begun on a full scale panel. The test temperature

was selected as 325°F. The sustained load produces a compression stress in the panel of 17,500 psi. The stress level is representative of the higher steady state stresses expected to occur in the wing of a supersonic cruise airplane. The test is still in progress. After 7500 hours exposure, the creep deformation was less than .1%.

The fatigue strengths of the aluminum alloys that have been discussed also deteriorate with exposure to high temperature. Consider the data plotted in Figure 8.

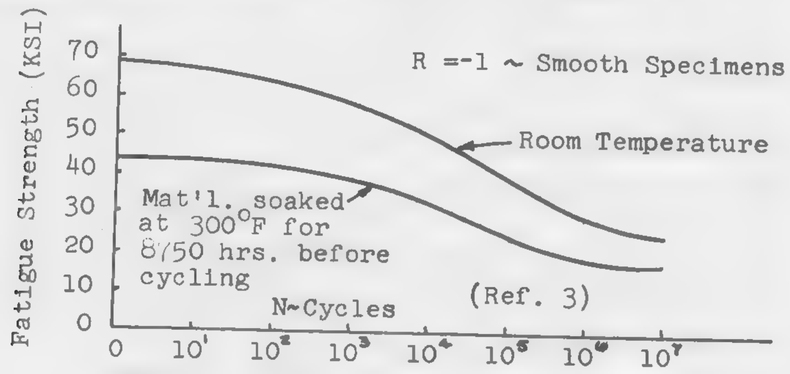


FIGURE 8 2024 ALUMINUM ALLOY FATIGUE STRENGTH

It is informative to look at this data when plotted in terms of fatigue strength as a percentage of tension ultimate versus cycles to failure. This was done in Figure 9.

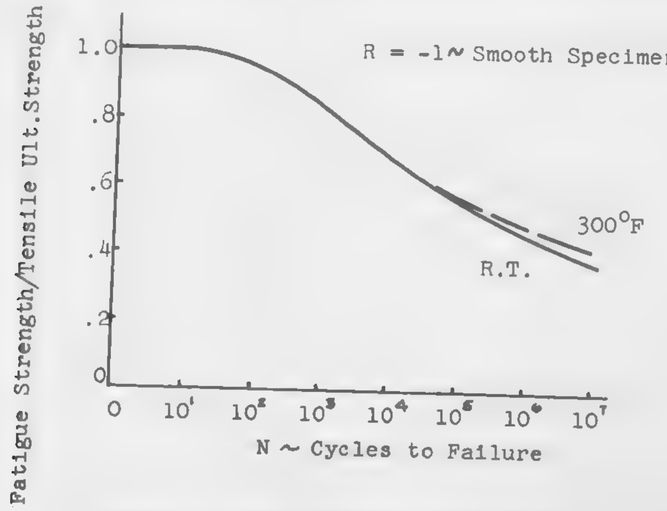


FIGURE 9 2024 ALUMINUM ALLOY FATIGUE DATA

Plotted in this manner, the data indicates that the loss in fatigue strength due to exposure at high temperatures is no greater than the proportionate loss in tensile ultimate strengths. The fatigue data discussed above pertains to smooth specimens. Very little data has been found concerning notched fatigue strength of 2024-T86 aluminum alloy at elevated temperatures. What data is available indicates that the proportionate loss of fatigue strength will be less for the notched specimens than for the unnotched specimens at temperatures in the 300-325°F range. If such proves to be true, then a design based on properties obtained after exposure to elevated temperatures would be less likely to experience a fatigue failure than a design involving no elevated temperature exposure. This assumes similar service spectra.

Summarizing to this point, the following conclusions could be drawn concerning the use of aluminum alloy sandwich panels for wing covering on a Mach 2.4 airplane.

1. The panels could be used efficiently for prolonged service in the temperature ranges of 300-325°F.

2. Design allowables could be set for both room temperature and elevated temperature strengths to include the effects of 10,000-hours exposure to 300-325°F.

3. Tests had indicated that excessive creep would not occur during 10,000 hours at service temperatures up to 325°F.

4. Fatigue data concerning the effects of elevated temperature on material fatigue strengths indicated that good fatigue resistance could be expected in composite panels.

ANALYSIS OF THE EFFECTS OF MACH 2.4 CRUISE ON B-58 TYPE WING PANEL CONSTRUCTION

Once the various strengths of the B-58 type wing panels had been defined, the next logical step was to investigate specific usage. It has been pointed out that by changing the internal grid in the present B-58 wing panels to 2024-T86 materials, the structure is capable of prolonged service at Mach 2.4. The actual length of service could only be established by analysis and tests. A typical flight profile was established and the associated environment was determined. This environment included both flight air loads and thermal loads. An analysis of the effects of such loads was carried out.

FLIGHT PROFILE

Several flight profiles involving Mach 2.4 cruise were investigated. The specific detail of any given profile depends upon usage. For example, military usage would probably involve faster acceleration to cruise altitude and longer flights than supersonic transport operations. The flight profile shown in Figure 10 was selected for detailed analysis in that it creates most of the problems that occur in Mach 2.4 cruise operations.

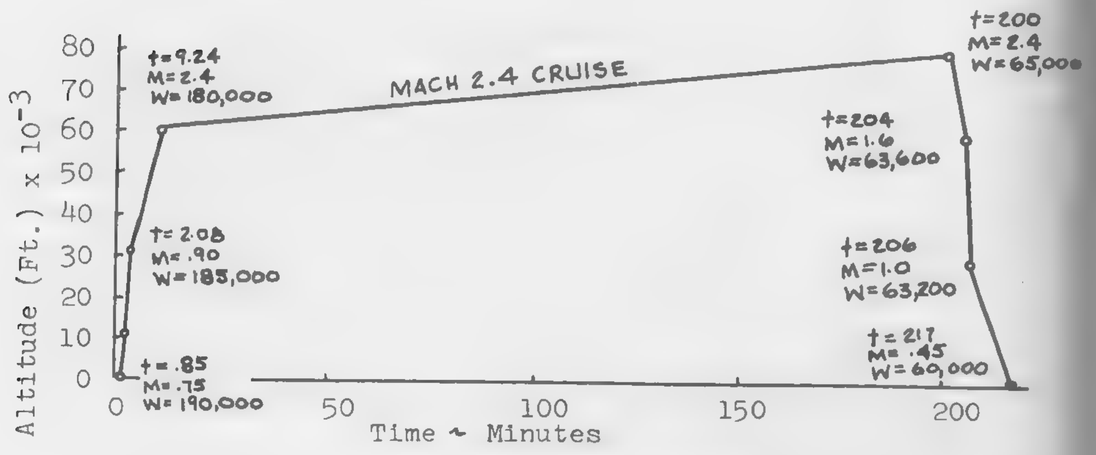


FIGURE 10 MACH 2.4 FLIGHT PROFILE

Such a profile can be divided into three phases: ascent, cruise, and descent. Each phase imposes a different requirement on the structure in terms of strength degradation, creep, and fatigue.

WING PANEL TEMPERATURES

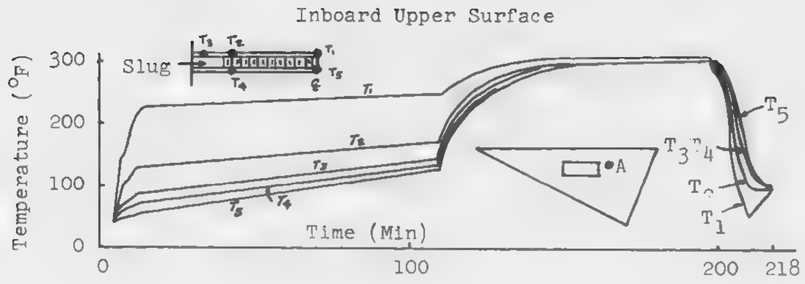
The first step in analyzing the effects of this profile was to predict the associated temperature developed in the structure. Two locations on the wing surface, designated A and B, were studied. One point, B, was located near the leading edge and the other, A, inboard at the span station where strength requirements would be highest.

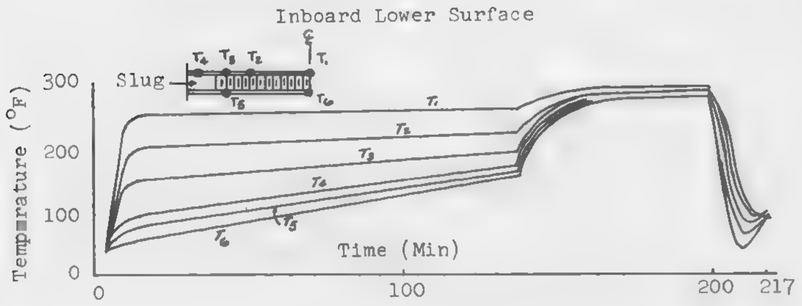
Transient temperatures were calculated at these two points for both upper and lower wing surfaces. These calculated temperatures were based on the following conditions:

1) Take off temperature of 40°F
2) Air Research Development Command atmosphere
3) Turbulent heat transfer
4) Programmed fuel consumption
5) Solar radiation on wing upper surface
6) External surfaces painted white.

The transient temperatures calculated for points A and B are shown in Figure 11.

These temperature profiles point to several things. For the type of wing used as an integral fuel tank, the wing fuel acts as a heat sink and the structure is at temperatures lower than the adiabatic wall temperatures for a significant part of the time. In addition, the temperatures change throughout the flight. This means that strength deterioration is actually dependent on exposure to at least two different temperatures. A considerable temperature differential exists in the structure which causes thermal stresses during acceleration and the first part of the cruise condition. The same is true for the deceleration phase. The thermal stresses will be discussed later.





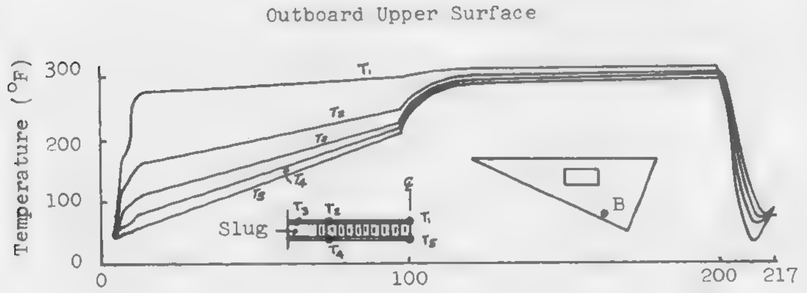


FIGURE 11 WING TEMPERATURES

These temperature curves show the amount of time at elevated temperature for each mission. Design allowables will be set on the basis of time at elevated temperature. Since at least two levels of elevated temperature are indicated, a technique for determining the effects of a temperature-time variation is needed. Such techniques are discussed in Reference 4. Actually the panel tests indicated that there would be little difference between design allowables based upon 5000-hours exposure and 10,000 hours. The analyses which follow assume 10,000-hour exposure allowables and are probably conservative from that standpoint.

WING PANEL STRESSES DUE TO FLIGHT LOADS AND TEMPERATURE

The next step in the analysis was to estimate stresses due to flight loads consistent with the gross weights and Mach numbers shown on the flight profile. The stresses will depend on the design criteria for the airplane. A delta wing type assumed in this study is most critical structurally in the transonic zone flight. This is illustrated by the plot of wing root bending moment versus Mach number for several gross weights and load factors shown in Figure 12.

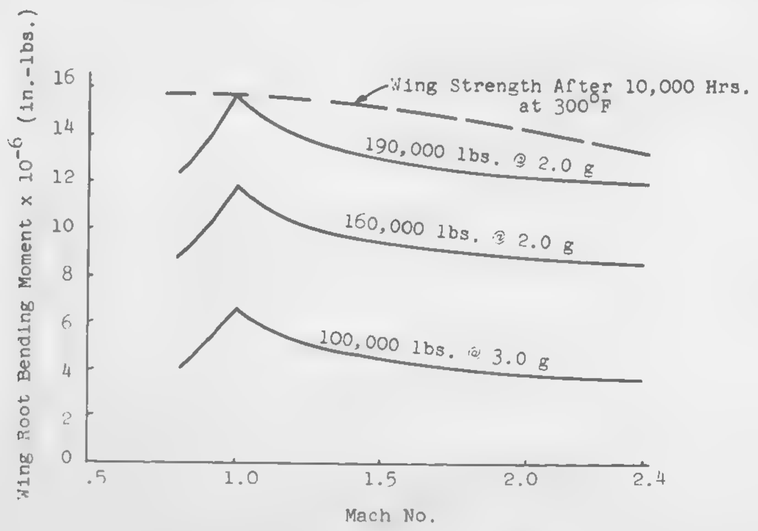


FIGURE 12 REQUIRED WING STRENGTH

The shape of these curves shown in Figure 12 have been well established by flight test data obtained from the B-58 flight test program. The numerical values were calculated using unit air load data from the B-58 program and inertias for the wing structure and engines estimated to be most appropriate. The design criteria selected for these studies was that the airplane should be able to develop a limit load factor of 2.0 at 190,000 pounds gross weight at Mach 1.0. This point is shown on the top curve in Figure 12. The curves show that as Mach number increases above 1.0, the wing strength required is progressively less. This is attributed to an inboard shift of the aerodynamic center of pressure on the wing. The allowable wing strength is shown to decrease also. However, it is significant that the allowable wing strength decreases at a much slower rate than the required wing strength. Thus, at Mach 2.4 the wing would have considerable reserve strength inherent in its design. Such moment curves developed at the various wing span stations provide the means of calculating stresses in wing panels for a given nW (load factor x gross weight).

Aerodynamic heating associated with the Mach 2.4 flight profile will cause thermal stresses in the wing panels. Such thermal stresses are primarily the result of differential temperatures between the outer skin, the internal grid, and the inner skin. The magnitude of the thermal stresses were calculated at the wing points A and B selected for analysis. These calculations were made by conventional elastic methods considering the predicted temperatures and typical wing sandwich panel geometry.

Analysis results showed that the inboard point A was critical in terms of both flight load stresses and thermal stresses. The calculated stresses for this point for both upper and lower surfaces are shown in Figure 13.

In addition to the steady state and thermal stresses, transient loads will create additional stresses which must be considered. Such loads occur as the result of gusts and maneuvers. Gust and maneuver loading spectra predicted for the wing point A as a result of 10,000 hours of flight according to the Mach 2.4 profile are shown in Figure 14.

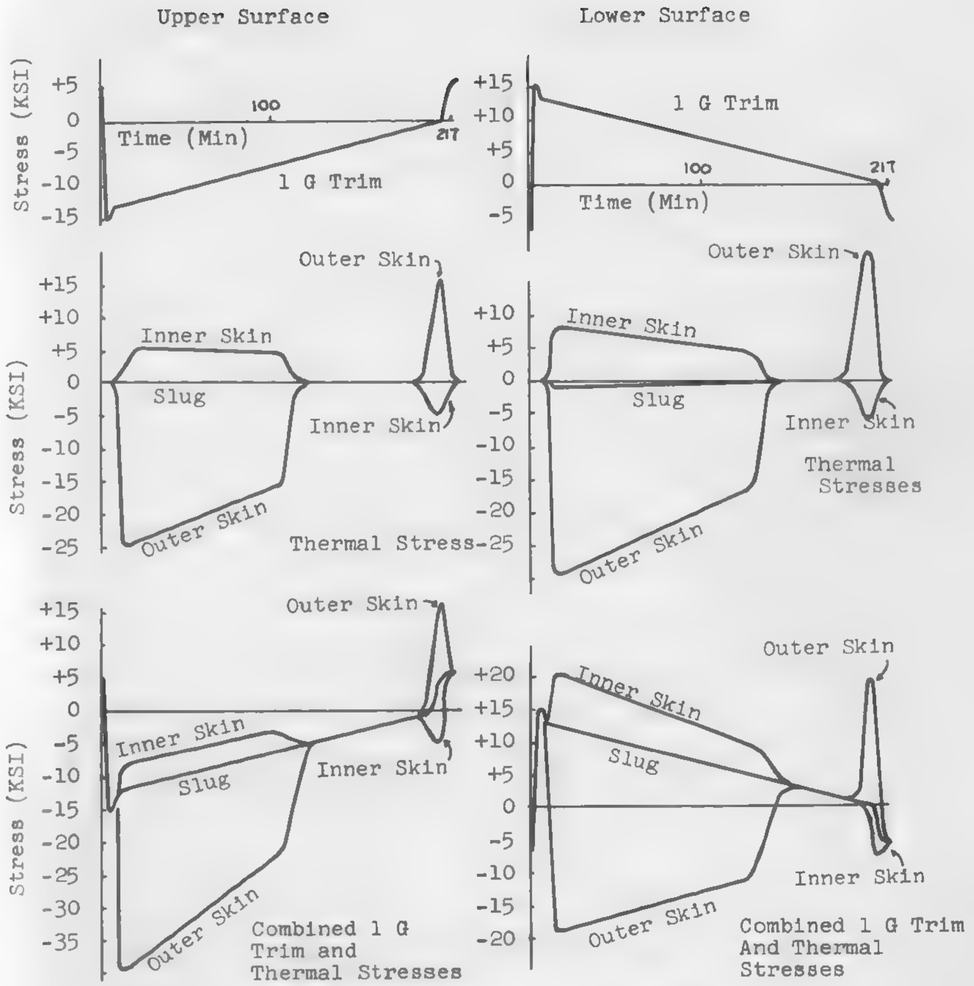


FIGURE 13 CALCULATED WING STRESSES

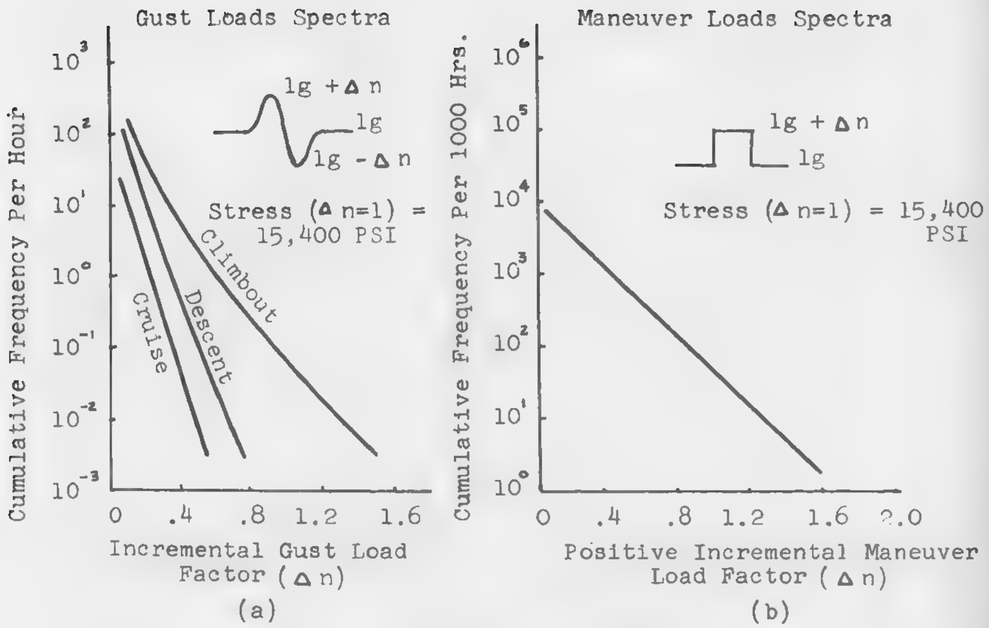


FIGURE 14 ESTIMATED GUST AND MANEUVER LOADS SPECTRA

The gust spectra were estimated using response characteristics of a delta wing to random turbulence as determined in the B-58A fatigue certification program. For convenience, the cyclic gust loads are expressed in terms of the estimated 1.0 g stress at wing point A for a 190,000 pound airplane flying at Mach 1.0. The maneuver spectrum was based on MIL-A-8866 (ASG). It is also expressed in terms of the 1.0 g stress at wing point A for the 190,000 pounds Mach 1.0 condition.

EFFECTS OF WING STRESSES ON THE STRUCTURES

Having defined the stresses that would occur, the next step was to determine the effect of such stresses on the wing panel structure. Analyses of the critical wing point A for both the upper and lower surfaces considered strength degradation, creep and fatigue. Strength degradation as service accumulates has been discussed in establishing design allowables. This factor was taken into consideration in considering creep and fatigue.

The creep analyses were based upon available creep data extrapolated to meet the conditions of the problem. Relaxation of thermal stresses due to creep is predicted to occur early in the life of the upper wing panels. Subsequent flights should experience essentially an unchanging pattern. Such relaxation is expected to be less than 5000 psi in the outer skin of the upper surface panels. No relaxation is expected to occur in the lower panel due to the combination of relatively low temperatures and stresses. The maximum permanent strain due to creep is predicted to be less than .1% for 10,000 hours of Mach 2.4 operations. It is significant from the creep standpoint that the wing stresses are lowest when temperatures are high. In other words, the fuel in the wing effectively serves as a heat sink during initial cruise when stresses are highest. These indications of negligible creep are strengthened by the full size wing creep test still in progress which was mentioned earlier.

Fatigue is most significant in the lower surface or tension side of the wing. The fatigue analyses were based upon a conservative approach which accounted for material degradation and existing material fatigue strength data. Analysis predicted trouble free service life in excess of 15,000 hours for the assumed design. The integrity of a wing sandwich panel in resisting fatigue has been amply demonstrated in the B-58A fatigue certification program.

TEST PROGRAM

To further investigate the effects of sustained Mach 2.4 flight on aluminum wing sandwich panels with honeycomb core, a test program was established. The objectives of the test program were to produce realistic temperatures and loads in full scale wing panels as a function of time to simulate repeated Mach 2.4 missions.

The load-temperature-time profiles to be applied to the test specimen are shown in Figure 15. The temperature profile and Test Load Block I simulate the environments and loads corresponding to one flight. These temperature-load profiles will be applied 2770 times to the test specimen

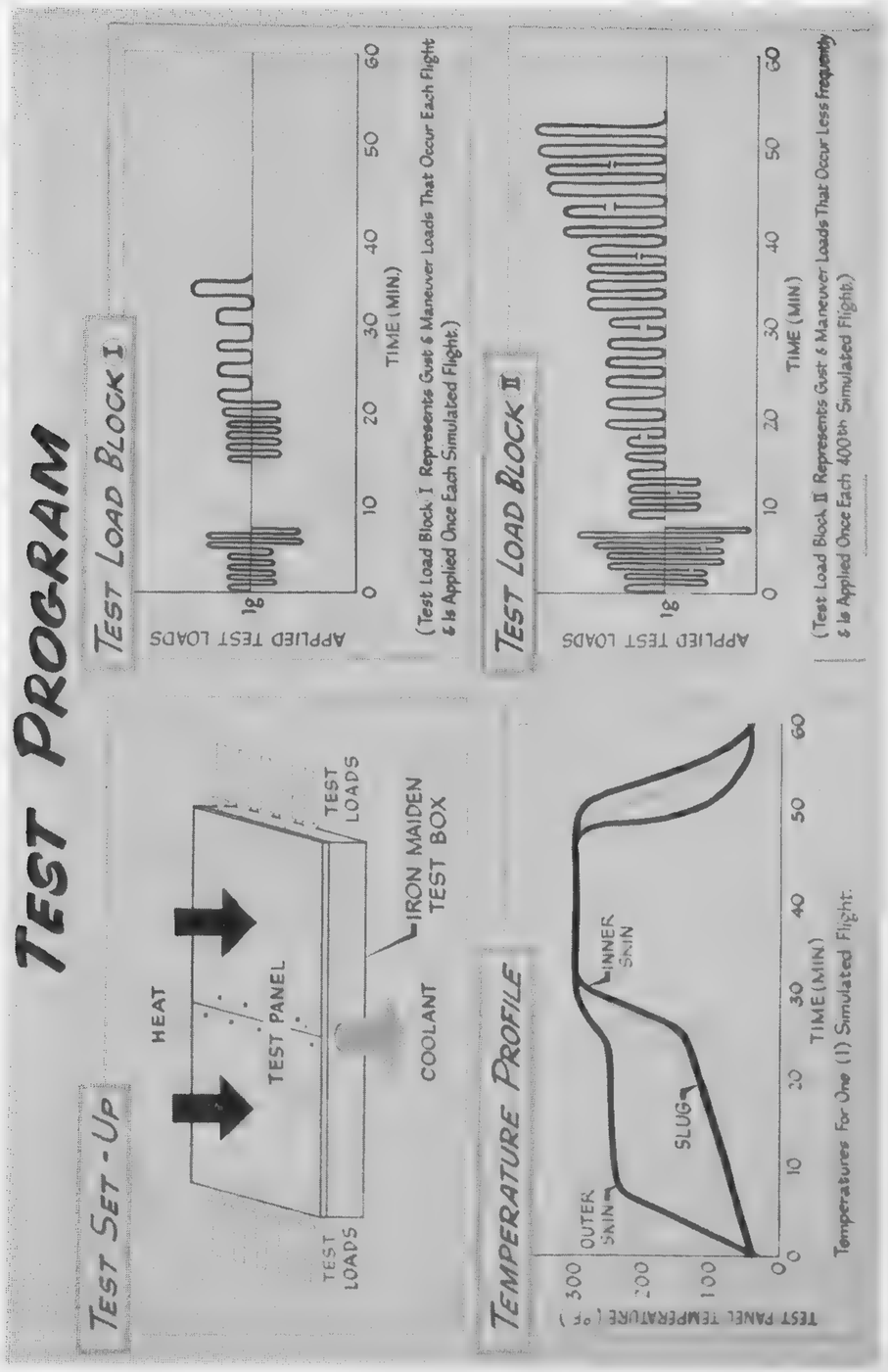


FIGURE 15

simulating 10,000 hours of Mach 2.4 flight. Test Load Block II will be substituted for I every 400th application in order to account for the higher loads that occur periodically.

The first test being run produces the upper wing surface condition. Should it be desirable to test wing panels representing the lower surface condition, this can be readily accomplished. Currently simulated flights have been applied to the first test wing panel. The results of these wing panel tests will be correlated with analyses results to show further the capability of the type of wing sandwich panels used in the B-58 for long service at sustained supersonic speeds.

SUMMARY

The study which has been discussed inevitably leads to the following conclusions:

The 2024-T86 aluminum alloy has excellent strength at 300-325°F after long exposure.

Tests of large sandwich panels have shown excellent strength after 10,000-hours exposure at 325°F.

The 2024-T86 aluminum alloy can be expected to have good fatigue resistance at 300°F.

Aluminum sandwich panels bonded with fiberglass honeycomb core can be used effectively for prolonged service at Mach 2.4.

The study included many other items that are beyond the scope of this paper. Sonic fatigue, panel flutter, tear resistance, and maintainability problems - all are found to be solved satisfactorily by this type of construction. The various problems which this study encountered should be mentioned. A great deal of testing had to be accomplished and most of the testing involved time. Testing will continue to be the primary tool in investigations of this sort. At present, there are no reliable short cuts in obtaining the effects of long hours of exposure on both materials and

built-up structure. The analytical work pointed up a lack of sufficient data for design purposes. What data is available is satisfactory in making material comparisons, but is inadequate for detail design. This is particularly true concerning creep and fatigue. Therefore, the designer is greatly interested in extrapolation techniques that are effective and can be used without materially penalizing his design. There is also the requirement for methods that determine the interaction effects of creep, fatigue, and thermal stress. For example, most material data showing elevated temperature exposure effects on mechanical properties is obtained with no load applied to the specimen. The question is asked whether tensile ultimate, for example, would have been the same had a constant load been applied throughout the exposure. Another way of stating this question is what are the effects of creep on mechanical properties. Until the answers to these questions are provided in the form of working tools, testing has to continue to be the designer's primary tool.

CONSIDERATIONS IN DESIGNING FOR MACH 3.0 REQUIREMENTS

A number of investigators have discussed consideration of various materials and types of construction that might be suitable for Mach 3.0 transport design requirements. Such discussions are included in Reference 5 and Reference 6. The temperatures associated with Mach 3.0 flight are generally agreed to be in the 500°F range. In all probability, materials such as titanium alloys and stainless steels will be required for the major part of the aircraft structure. From the standpoint of structural efficiency, several of the titanium alloys look attractive. Compared to steel, material merit indices which provide comparative weights for the various strengths of the two materials show titanium to advantage. Two simple ratios are plotted against test temperature in Figure 16 for Ti-4Al-3Mo-1V and PH 15-7 Mo (RH950) stainless steel.

The data used in plotting the stainless steel curves was taken from Reference 8. The data for the titanium alloy

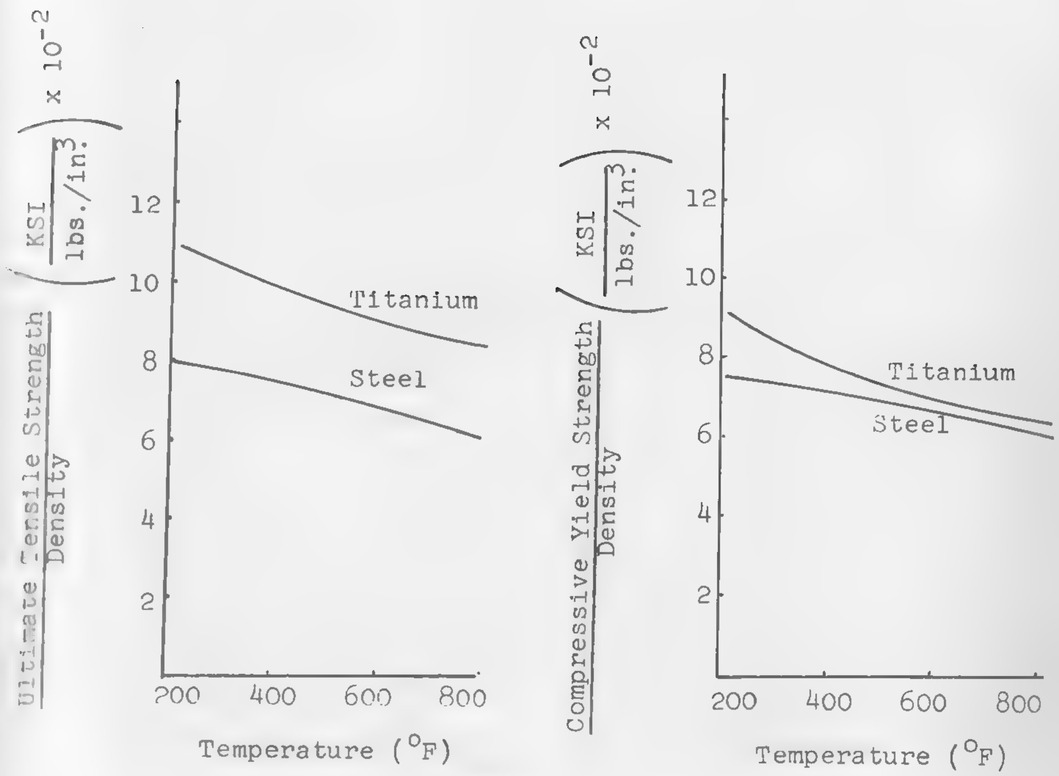


FIGURE 16

curves is proposed for inclusion in Reference 8. Compression yield data has been included since it is particularly significant in sandwich type construction. The relative potential for thermal stress is of particular interest. Here practically all of the titanium alloys show up to greater advantage than the stainless steels. Comparisons concerning direct stiffness have nearly always given steel the advantage. Stiffness is of considerable importance concerning aeroelastic effects of wings, for example. However, one of the later titanium alloys being developed shows increased stiffness sufficient to overcome the advantage of steel. This titanium alloy is Ti-8Al-1Mo-1V. Comparative stiffness ratios are shown in Table I for Ti-8Al-1Mo-1V and PH 15-7 Mo (RH950) stainless steel.

This titanium alloy is also said to have excellent resistance to creep and preliminary vendor data shows good fatigue strength.

Table I

COMPARATIVE STIFFNESS RATIOS

Material	$\frac{\text{Elastic Modulus}}{\text{Density}}$ $\left(\frac{\text{psi} \times 10^{-6}}{\text{lbs/in}^3}\right)$	
	R. T.	700°F
Ti-8Al-1Mo-1V	122.5	105.5
PH 15-7 Mo (RH950)	104.6	92.0

One of the objections voiced against the use of titanium sheets has come from the shop. Considerable difficulty has been experienced in the past in forming and fabricating titanium sheet material. However, titanium development programs such as that discussed in Reference 9 have produced very valuable information concerning formability, weldability, and practical manufacturing processes. Today it is believed that titanium can be fabricated quite readily.

Titanium alloys can be used for practically all types of construction including brazed sandwich, built-up welded construction, and the more conventional plate-stringer type of construction. The specific alloy chosen depends upon the type of construction in each case. General Dynamics/Fort Worth has done considerable investigation into the possibilities of brazed titanium sandwich construction. This titanium sandwich panel research and development program is reported in Reference 10. Procedures for brazing were developed and fabrication limitations were established. Several brazed production-size sandwich panel designs were fabricated and tested. The titanium alloy used for these panels was Ti-5Al-2.75Cr-1.25Fe (RS140). Test of these panels showed that they possessed excellent structural efficiency at temperatures from -67°F to 800°F. Strength-to-weight ratios of brazed titanium sandwich panels exceeds those of stainless steel sandwich construction used in the B-58 by a factor of approximately 1.5. These RS140 panels have also been subjected to sonic environments in both the

siren chamber and as a part of the B-58 sonic fatigue test. This B-58 tie down test consisted of 10 hours of maximum afterburner operation which developed sound levels as high as 170 decibels. No failures occurred in the panels. Exposure to 600°F for 500 hours had no effect on the panel strengths or elongation.

A very limited program where Ti-8Al-1V-1Mo sheets were brazed to Ti-6Al-4V core has been completed. Two twelve-inch-square sandwich panels were produced. Column compression specimens (2"x3") cut from these panels showed room temperature strengths of 170,000 psi and 1000°F strengths of 105,000 psi. Room temperature strength after 100 hours at 1000°F was 176,800 psi and 1000°F strength after 100 hours at 1000°F was 105,000 psi. After 50 hours in salt spray, room temperature strengths were not affected. Panels brazed using Ti-8Al-1V-1Mo will produce significant weight savings while minimizing stiffness differences compared to stainless steel sandwich panels.

Regardless of the type of construction and materials chosen for design of Mach 3.0 transport aircraft, an extensive development program is indicated. Such a program must begin with material and proceed through design, fabrication, and tests of full scale structure. A great deal of the testing will be dependent upon time. The problems are not insurmountable and, in fact, are reasonably well defined. However, as opposed to the Mach 2.0-2.4 case, the solution to many of the design and fabrication problems for Mach 3.0 flight are still in the future.

ACKNOWLEDGEMENT

Much of this paper is based upon work done by Messrs. L. M. Smith, C. H. Mooney, Jr., H. H. Hotchkiss, and R. G. Brown. The author is grateful for their support and encouragement.

BIBLIOGRAPHY

1. Gerard, G., "Life Expectancy of Aircraft Under Elevated Temperature Conditions", WADC TR 53-493, October, 1953.

2. Smith, L. M., and C. W. Rogers: Bonded Bomber - B-58. SAE Paper 420B, National Aeronautics and Space Engineering and Manufacturing Meeting, Los Angeles, California, October, 1961.

3. Rand Report R-104, August, 1948.

4. Brownfield, C. D., and D. M. Badger: Effects of Temperature-Time-Stress Histories on the Mechanical Properties of Aircraft Structural Metallic Materials, Part II. Stressed Exposure of 7075-T6. WADC Technical Report 56-585, September, 1960.

5. Staff at Langley Research Center: The Supersonic Transport - A Technical Summary. NASA TN D-423, June, 1960.

6. Schafer, W. H., G. Foelsch and F. W. Krohn: Summary - Titanium as a Structural Material for Supersonic Cruise Vehicles. General Dynamics/ Convair ERR-SD-084, September, 1960.

7. Howard, H. B.: Merit Indices for Structural Materials. Agard Report 105, 1957.

8. MIL-HDBK-5. Strength of Metal Aircraft Elements. March, 1959.

9. Alesch, C. W. and S. R. Carpenter: Titanium Development Program. ASD TR 61-7-576, May, 1961.

10. Johnson, W. E. and others: Titanium Sandwich Panel Research and Development. AMC TR 59-7-618, November, 1959.

THE USE OF PRECIPITATION HARDENING STAINLESS STEELS IN SUPERSONIC AIRCRAFT

L. P. Spalding
Section Head, Materials
North American Aviation, Inc.
Los Angeles, California

ABSTRACT

Some applications of precipitation hardening stainless steels in the XB-70 supersonic airplane are described. Problems were encountered in the development of a brazing alloy and process compatible with optimum heat treatment response of the steel, embrittlement of heat treated fusion welds under simulated service exposure, corrosion resistance, and crack propagation. Rolled bar, thick plate and extruded shapes exhibited erratic and frequently poor transverse ductility. The metallurgical background of these problems is discussed in this paper.

The XB-70 airplane is designed to cruise at 2000 mph at an altitude of 70,000 ft. This high performance results in structure temperatures of 450-630°F, which preclude the use of conventional light alloy construction. Early in the design studies attention was focussed on titanium and steel alloys, particularly the precipitation hardening stainless steels. PH steels were ultimately selected for some 70% of the structure, on the basis of high strength, corrosion resistance, ability to be brazed and welded, and also availability and cost. As a matter of information, H-11 type steel and titanium alloys make up most of the remaining structure; however, they will not be discussed here.

Preliminary studies emphasized the outstanding structural efficiency of sandwich construction. Honeycomb type

sandwich provided the added feature of adequate fuel insulation with no weight penalty. Brazing was required to join the honeycomb sandwich components: adhesive bonding would not withstand the temperatures. Welding was chosen as the primary means of joining structural elements since it provided better efficiency than mechanical joints. Also, welding provided a method of sealing for fuel containment: organic sealants in mechanical joints could not tolerate the operating temperatures.

The total airframe requirements encompass the range from 0.001 in. foil for honeycomb sandwich core through sheet, plate and rolled or extruded bar to forged billets 4 in. x 22 in. x 72 in. Because of anticipated complications in welding and heat treatment it was desired that a single PH alloy be used. However, the ultimate choice was PH15-7 Mo alloy for foil, sheet, thin plate and extrusions, and 355 alloy for heavy plate and extrusions, bar and billets. Important factors in these selections were strength, ductility and corrosion resistance.

HONEYCOMB SANDWICH BRAZING

Since high strength and creep resistance at 630°F are required of the brazed joints it appeared obvious that an alloy with a high melting temperature should be superior to a low melting alloy. It was evident that the liquidus temperature of the brazing alloy must be compatible with a temperature used during the heat treatment of the PH steel, otherwise either a poor bond or inferior steel properties would result. The PH steels are generally supplied in a 1950°F annealed condition for stability and ease of fabrication. They must be conditioned for a short time at about 1700°F in order to effect subsequent transformation hardening. Transformation is accomplished by a sub-zero treatment at -100°F for 8 hr. The final step, 900-1050°F for 1 hr., is a precipitation hardening treatment, which also tempers the martensite formed during the prior transformation. This gives the so-called RH treatment for PH15-7Mo. The processing of 355 alloy is similar in principle, with slightly different times and temperatures for optimum

properties. Based on these considerations, a brazing temperature close to the 1700°F conditioning treatment was decided upon. Several silver-base alloys seemed to fit the requirements.

Laboratory tests of an 85silver-15manganese alloy, which had been suggested by other investigators, revealed serious crevice corrosion (Figure 1). The brazed sandwich actually fell apart after a few hours exposure to salt spray or in a humidity cabinet. This alloy was abandoned.

Sterling silver (92.5Ag-7.5Cu) with 0.2 lithium added for fluxing and fluidity was tried next. The alloy had a brazing temperature of 1625°F and gave lap shear strengths of 18,000 psi at room temperature and 13,000 psi at 500°F. It was not subject to corrosion. The alloy flowed well, giving good core-to-face-sheet fillets. It also filled the capillary crevices along the core nodes (Figure 2) providing 40% higher core shear strength than that achieved without node flow of the brazing alloy.

As mentioned earlier, one feature of the honeycomb sandwich construction was its heat insulating ability. Unfortunately, node flow of the braze alloy, with its high thermal conductivity, seriously lowered the insulating value. The design target was 3.7 BTU/hr./sq.ft./°F for a sandwich thickness of one inch, while the sterling-lithium alloy gave a value of 5.2 (same units). At this point some consideration was given to restricting node flow by artificially contaminating the foil surface, but this scheme was soon abandoned because the process was not reproducible and because of the loss in core shear strength.

Other brazing alloy systems were tried. The nickel-chromium-silicon-boron type diffused rapidly into the core foil, causing embrittlement and loss of heat treat response. A 62.5Ag-32.5Cu-5.0Ni alloy looked promising, but lacked the desirable node flow characteristic.

The next approach tried was to decrease the conductivity of the sterling-lithium brazing alloy by alloy additions. Reasoning from the analogy between thermal and electrical conductivity, and having scattered data on the latter property,



FIGURE 1a HONEYCOMB BRAZED WITH 85 Ag-15 Mn ALLOY
200X



FIGURE 1b CREVICE CORROSION OF 85 Ag-15 Mn BRAZEMENT
140X

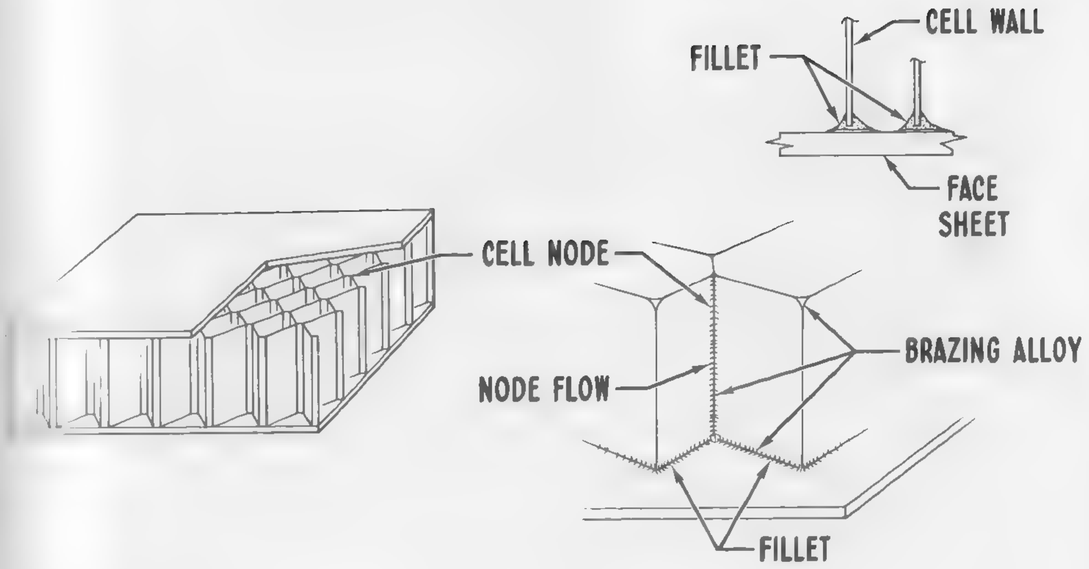


FIGURE 2 BRAZE ALLOY FLOW CHARACTERISTICS

it appeared that a number of additives should be effective. Among these were: phosphorus, tin, antimony, manganese, selenium, tellurium, indium and palladium. Effects of the additives on strength and brazing temperature, as well as conductivity, had to be considered (Figure 3). Some additives were discarded after early trials, since their alloys were too brittle to roll into foil. Effort was concentrated on tin, manganese, indium and palladium, and combinations of these. Table I gives the composition, calculated thermal conductance, and approximate brazing temperature for 15 experimental alloys. (Note that the conductance tabulated here is for the brazing alloy itself, not for a sandwich, and is in different units than for sandwich conductivity.)

Concurrent tests were run to check diffusion or intermetallic alloying of the braze alloy with the base metal, and corrosion and oxidation resistance. With a few exceptions, such as segregation in tin alloys and crevice corrosion with 5% manganese, all the experimental alloys were satisfactory in these tests. Considerations of brazing temperature, flow characteristics, and workability led to

TABLE I

CHARACTERISTICS OF
EXPERIMENTAL BRAZING ALLOYS

Alloy No.	Nominal Composition Ag	Cu	Li	Other	Thermal Conductivity (Cal/cm²/sec/°C/cm)	Approx. Brazing Temp. (°F)
1	92.3	7.5	0.2	--	0.370	1620
2	90.3	7.5	0.2	2Mn	0.159	1625
3	89.8	6.5	0.2	3.5Mn	0.105	1630
4	88.8	6.0	0.2	5Mn	0.095	1635
5	90.3	7.5	0.2	2Sn	0.133	1605
6	89.3	7.5	0.2	3Sn	0.108	1595
7	88.3	7.5	0.2	4Sn	0.093	1585
8	88.3	7.5	0.2	2Sn-2Mn	0.080	1605
9	89.5	7.5	0.2	2Sn-0.8Pd	0.161	1625
10	88.1	7.5	0.2	3Sn-1.2Pd	0.137	1620
11	86.7	7.5	0.2	4Sn-1.6Pd	0.118	1620
12	89.3	7.5	0.2	3In	0.159	1595
13	86.8	7.5	0.2	5.5In	0.142	1575
14	84.3	7.5	0.2	8In	0.116	1540
15	88.1	7.5	0.2	3In-1.2Pd	0.167	1620
16	84.6	7.5	0.2	5.5In-2.2Pd	0.134	1620

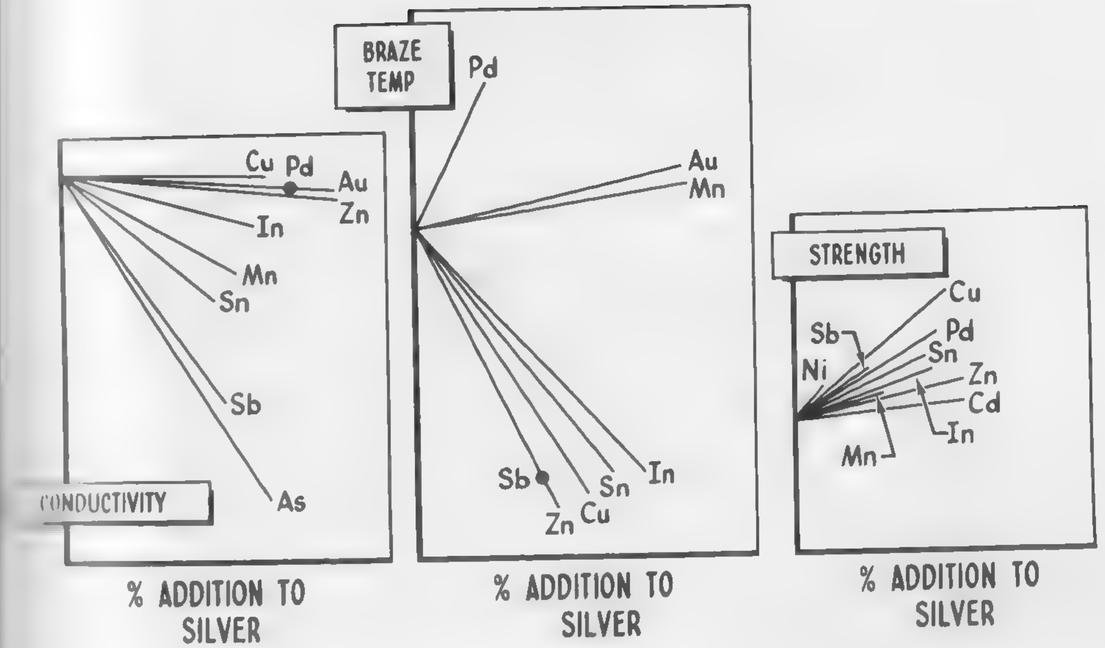


FIGURE 3 ALLOYING FOR LOW THERMAL CONDUCTIVITY

the selection of an alloy containing 84.6Ag-7.5Cr-5.5In-2.2Pd-0.2Li (No. 16 in Table I). In this composition the indium is primarily responsible for reducing thermal conductivity, while palladium counteracts the melting temperature lowering of the indium. When tested in a honeycomb sandwich one inch thick, a thermal conductivity of 3.0 BTU/hr./sq. ft./°F was achieved -- well below the target of 3.7.

The low thermal conductivity alloy developed from this work had characteristics similar to the sterling-lithium alloy, with a brazing temperature of 1625°F. At this and higher temperatures, both alloys were quite fluid, but satisfactory for parts brazed flat. On curved parts there was a tendency toward gross drainage to the low points, and braze alloy starvation in the higher areas. To overcome this condition, the low thermal conductivity braze alloy was infiltrated into a matrix of powdered nickel, in the ratio of 80% braze alloy-20% nickel, and subsequently rolled to foil. The nickel acts much as a sponge, retaining the braze alloy in place through capillary action. In addition to solving the

flow problem, this modification permitted the use of higher brazing temperatures, up to 1730°F, which afforded advantages in heat treatment as described later.

WELD DUCTILITY

In the fabrication of the XB-70 airframe two general applications of fusion welding are employed on the PH steels. In both cases the tungsten electrode, inert gas shielded arc (TIG) process is used. The larger assemblies and subassemblies, already in the heat treated condition, are welded together, and the resulting welds are left in the annealed condition, since heat treatment is precluded by the size and complexity of the assemblies. These welds have been made with WPH15-7Mo filler metal, a modification of the basic PH15-7Mo analysis with carbon and chromium on the low side to minimize delta ferrite formation. The welds show good ductility and, while their strength is low, compensation is effected by thickening the members in the vicinity of the joints. Some weld cracking was encountered with the WPH15-7Mo filler wire.

In other cases, elements of honeycomb sandwich panels (such as spliced face sheets and attaching members) are joined by welding prior to the brazing and heat treatment of the panels. These heat treated welds fall into two categories: thin sheet (less than 0.020 in.) welded without filler wire, and heavier gauges welded with filler metal additions. The latter category will be discussed here.

A series of tests was run with the WPH15-7Mo wire recommended by the steel producer, with results as given in the upper portion of Table II. This shows that the parent metal responded satisfactorily to both the standard RH 950 heat treatment and to the then-used brazing cycle heat treatment: 1625°F 15 min., cool to 1000°F 45 min., cool to R.T., -100°F 5 hrs., 950°F 8 hrs. (subsequently referred to as BCHT). The welded specimens showed marginal ductility for the RH 950 treatment while the BCHT gave low strength and unacceptable embrittlement. Exposure of specimens to 700°F for 100 hrs. resulted in appreciable

TABLE II

EFFECT OF HEAT TREATMENT AND TEMPERATURE EXPOSURE ON WPH15-7Mo WELDS

Heat Treatment and Exposure Conditions	Parent Metal Properties Ult. Str. (KSI)	Parent Metal Properties Elong. (2 in.)	Welded Properties Ult. Str. (KSI)	Welded Properties Elong. (1/2 in.)
RH 950*	236	8.1	228	4.0
Room Temp. BCHT**	226	7.5	190	1.9
Room Temp. RH 950 700°F - 100 hr.	244	6.5	222	2.2
BCHT 700°F - 100 hr.	240	4.0	174	1.8
Mod. BCHT***	216	7.3	209	9.7
Room Temp. Mod. BCHT 650°F - 1000 hr.	229	7.2	221	3.5

* 1710°F 20 min. -AC to RT- -100°F 8 hrs. -950°F 1 hr.
** 1625°F 25 min. -FC to 1000°F 45 min. -AC to RT- -100°F 5 hrs. -950°F 8 hrs.
*** 1730°F 20 min. -FC to 1000°F 30 min. -AC to RT- -100°F 3 hrs. -1050°F 1 hr.

loss of ductility in the parent material, and further embrittlement and strength loss in the welded specimens.

Two parallel courses were pursued to solve this problem. Since delta ferrite was suspected as a major contributor to the observed low ductility, it was postulated that a higher conditioning treatment and faster cooling would favor austenite retention, with a lessening of delta ferrite and other transformation products. Therefore the heat treat (and brazing) cycle was modified by increasing the conditioning temperature from 1625°F to 1730°F. This was made possible by the brazing alloy modifications described previously. In addition, the cooling time from the brazing temperature to 1000°F was decreased through equipment and processing changes. Finally, the precipitation aging temperature was increased from 950°F to 1050°F. This last change results in overaging, which was expected to provide greater stability and less tendency toward embrittlement on elevated temperature exposure. The increase in aging temperature resulted in lowering the strength level about 10% in both parent metal and welds. The loss was accepted as a means of achieving adequate ductility: it was further justified by the results of crack propagation tests to be described later.

The results of these heat treatment modifications, taken simultaneously, are shown in the lower part of Table II. It is seen that good ductility was obtained in both parent metal and welds (made with WPH15-7Mo filler wire) at room temperature. Parent metal ductility was unaffected by elevated temperature exposure, but the welded specimens still showed a pronounced drop. All specimens showed a significant strength increase on aging, indicating that full stability had not been achieved even with the higher aging treatment. (Note that in comparison with the earlier tests a longer exposure time at a slightly lower temperature was used. This was felt to be more representative of service exposure.)

Since the ductility of welds exposed to elevated temperature was still unsatisfactory, filler metals of different compositions were tried. One abortive attempt may be

mentioned first. Nitrogen gas was added to the argon or helium shielding gas normally used in TIG welding with the idea of stabilizing the austenite in the weld deposit and thereby promoting ductility. This did not work.

Several modifications of the basic 15-7 analysis were tried as filler wires. These modifications incorporated low carbon for better thermal stability and corrosion resistance. Others involved changes in the chromium and nickel content to alter the austenite-ferrite balance. Molybdenum was omitted in some analyses, with the thought that this might reduce weld cracking tendencies.

All test specimens were processed in accordance with the modified brazing cycle treatment developed in the previously described test series. Mechanical properties at room temperature and after elevated temperature exposure are given in Table III. These data clearly show the benefits in improved stability and ductility which derive from a low carbon level. The 13-8 and 13-9 analyses appear to be somewhat superior to the 15-7 types.

TABLE III

COMPARISON OF FILLER MATERIALS

Filler Wire Type	Room Temp. Ult. Str. (KSI)	Room Temp. Elong. (1/2 in.)	650°F - 1000 hrs. Ult. Str. (KSI)	650°F - 1000 hrs. Elong. (1/2 in.)
WPH15-7Mo (.07C)*	209	9.7	221	3.5
WPH15-7 (.02C)	203	8.3	216	6.7
WPH13-9 (.04C)	210	8.5	225	7.0
PH13-8Mo (.03C)	210	13.0	222	10.4

* Included from Table II for comparison.

Some evidence had been gathered earlier which indicated that stress corrosion of heat treated welds might be a problem. Accordingly, a series of stress corrosion tests was run, using the same filler wires which had been checked for weld ductility. Specimens were approximately 1 in. x 8 in. with a transverse weld bead ground flush. The modified braze cycle heat treatment was used. Specimens were loaded in beam flexure to 80% of the yield strength and exposed to 20% salt spray. Figure 4 depicts the results.

These data show that molybdenum definitely promotes stress corrosion resistance. In the only case where a direct comparison is possible (that of the 13-9 analysis) low carbon is also seen to improve the stress corrosion behavior, as might be expected. Based on these findings, the low carbon PH13-8Mo composition filler wire has been

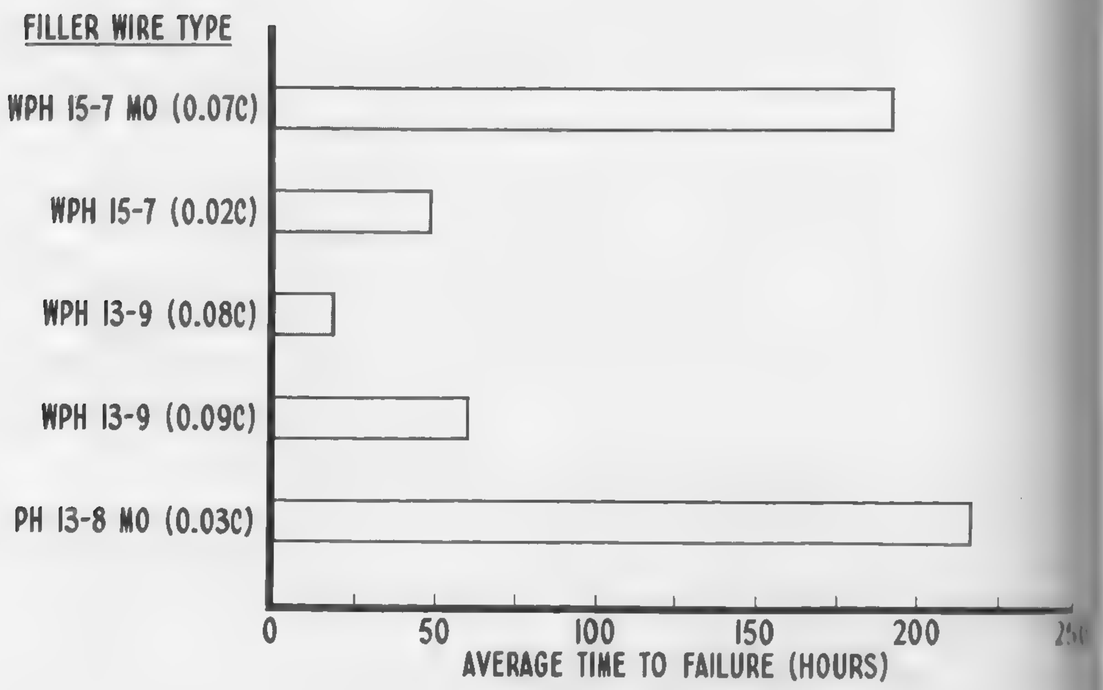


FIGURE 4 STRESS CORROSION OF WELDS

adopted for welding PH15-7Mo steel. This filler wire also essentially eliminated the weld cracking problem which had been encountered with WPH15-7Mo wire.

CRACK PROPAGATION

Numerous catastrophic failures of high strength steel structures -- particularly pressure vessels -- have been attributed to propagation of cracks emanating from small defects in the structure or material. This phenomenon is characterized by the explosive extension of a pre-existing crack under net area stresses which are significantly below the strength of the material. Crack propagation, or the analogous property of tear resistance, has been extensively studied, notably by Irwin and Kies, who have developed theories and criteria applicable to the observed behavior. The two commonly accepted measures of tear resistance are the parameters G_c and K_c, defined respectively as the critical crack extension force and the fracture toughness. G_c may be calculated from the expression:

$$G_c = \frac{\pi F^2 l_{cr}}{E} \left[\frac{y^4 + 2}{(y^4 + y^2 - 2)^2} \right] \qquad (1)$$

where

G_c = critical crack extension force (in. -lbs. /in. ^{2})
F = gross area stress (psi)
l_{cr} = crack length immediately prior to exposive growth (in.)
E = Young's modulus (psi)
y = l_{cr}/W
W = specimen width (in.).

The parameter K_c may be calculated from the relation:

$$K_c^2 = E \times G_c \qquad (2)$$

where

K_c = fracture toughness (psi-$\sqrt{\text{in.}}$).

Alternatively, K_c may be calculated by the procedure described in Ref. 1, and G_c then derived from the above relation.

It is possible to obtain useful comparative G_c and K_c data by means of small center-notched or edge-notched sheet specimens subjected to slowly increasing tensile load (Ref. 1). More critical comparisons may be obtained by the use of wider specimens. However, most investigators agree that rather elaborate specimens and loading conditions are necessary to derive reliable data on crack propagation for specific design applications.

Preliminary tests had shown that the tear resistance of PH15-7Mo sheet at high strength levels might not provide satisfactory performance. Two types of tests were run to verify this point and to determine the effect of different heat treatments on crack propagation. In one series of tests, specimens 10 in. wide x 18 in. long x 0.050 to 0.063 in. thick were used with a variety of heat treatments. A central notch made with saw cuts approximately 0.5 in. long and 0.009 in. wide was slightly extended in length by fatiguing the specimens until small cracks developed at each end. The original crack lengths varied from 0.52 in. to 0.57 in. Specimens were subjected to slowly increasing tension load up to the point of rapid crack propagation, where the maximum load was measured, along with the crack length at that time. Calculations of K_c and G_c made according to the procedure of Ref. 1 are presented in Table IV.

A second test series employed repeated load tests of specimens 18 in. wide x 36 in. long x 0.050 in. thick, with centrally located saw cuts 0.009 in. x varying length. These were subjected to cyclic tension loads of either constant magnitude or spectrum type, representing airplane life. The data obtained from these tests were: (1) rate of crack growth, or simply total life in cycles or hours, and (2) critical crack length.

As an example, Figure 5 shows the crack growth rate vs load cycles at a stress level of 67,500 psi for PH15-7Mo with the RH 950 and RH 1050 (corresponds to brazing cycle)

TABLE IV

CRACK PROPAGATION TEST DATA

Heat Treat	Tensile Data Ult.	Yld.	Elong.	Crack Length (in.)	Max. Stress (KSI)	K_c (KSI$\sqrt{\text{in.}}$)	G_c (in.-lbs./sq.in.)
RH 850	232	207	7.7	1.40	39.4	58.7	121
RH 950	238	218	5.2	1.50	49.9	77.5	210
RH 1100	198	193	7.0	2.18	89.8	181	1140
BCHT 1050	212	201	6.5	2.22	67.1	133	620
Weld + RH 1100	193	189	4.3	1.67	72.9	126	558

Tabulated values are averages of 3 to 6 tests.

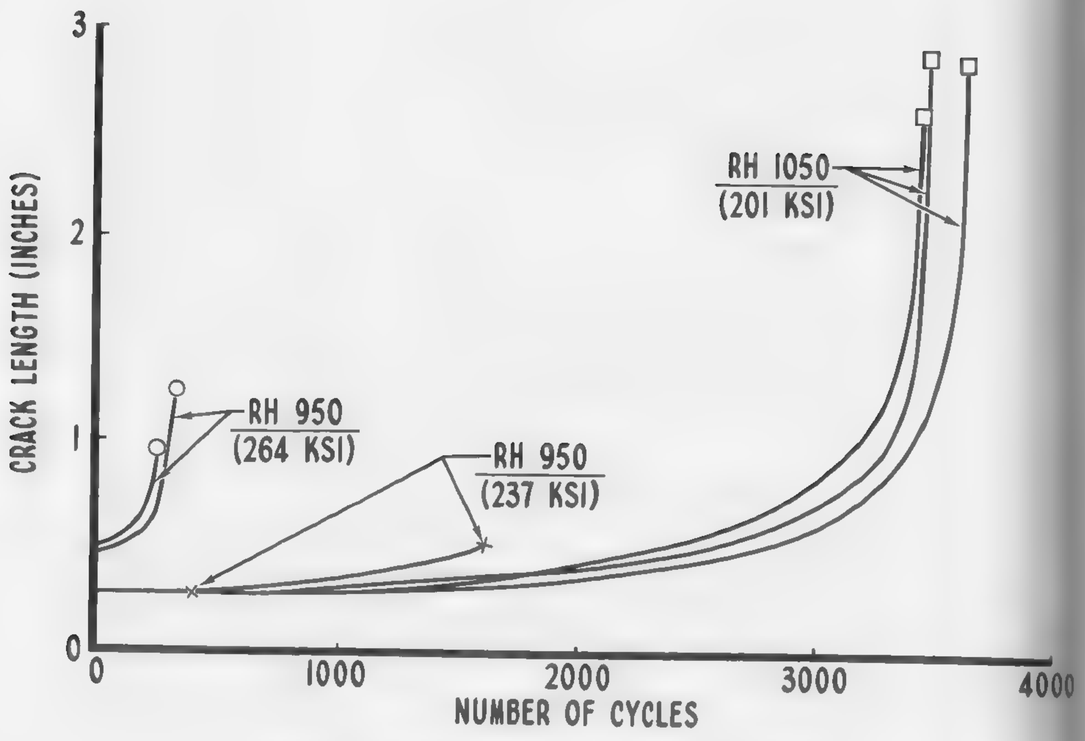


FIGURE 5 CRACK PROPAGATION VS HEAT TREATMENT

heat treatments. Combining these results with data from other tests using different cyclic load levels, the curves of Figure 6 were constructed to show the critical crack length as a function of applied stress (expressed as percent of ultimate strength). From these, average values of G_c and K_c were 228 and 81,000 respectively, while for the RH 1050 treatment they were 635 and 134,000. These values agree very well with those obtained from the static tests (Table IV) and may be compared with those for 2024 aluminum alloy (G_c = 455, K_c = 67,500) and 6Al-4V titanium alloy (G_c = 403, K_c = 83,000). Both of these alloys are considered very good from a tear resistance standpoint. The superiority of the RH 1050 heat treatment from a crack propagation standpoint is clearly demonstrated, and the earlier decision to modify the heat treat cycle for better weld ductility is thus reinforced by these results.

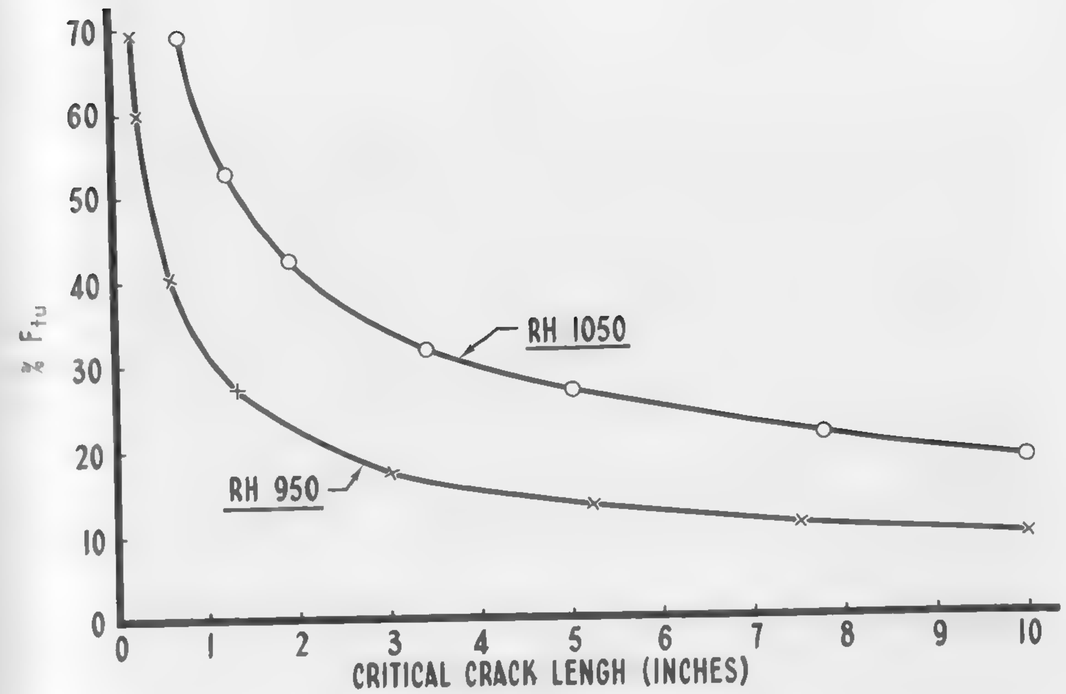


FIGURE 6 CRACK LENGTH VS STRESS

HEAVY STRUCTURAL MEMBERS

The normal microstructure of PH15-7Mo is characterized by the existence of segregated delta ferrite in amounts ranging from 15 to 25%. During hot working the delta ferrite is elongated, often producing a banded structure (Figure 7). When tested in a direction perpendicular to the bands, these structures exhibit poor ductility. In thin members (e. g. sheet) this low ductility is of little concern, since loading transverse to the surface rarely occurs. However, parts machined from heavier stock may often be loaded across the banded structure, in the so-called short transverse direction.

It was believed that sufficient, multi-directional hot working might break up the delta ferrite structures, resulting in acceptable multi-directional ductility. Some tests of extrusions produced with varying extrusion ratios which illustrate this effect are presented in Figure 8. From these and other data it was concluded that an extrusion ratio of

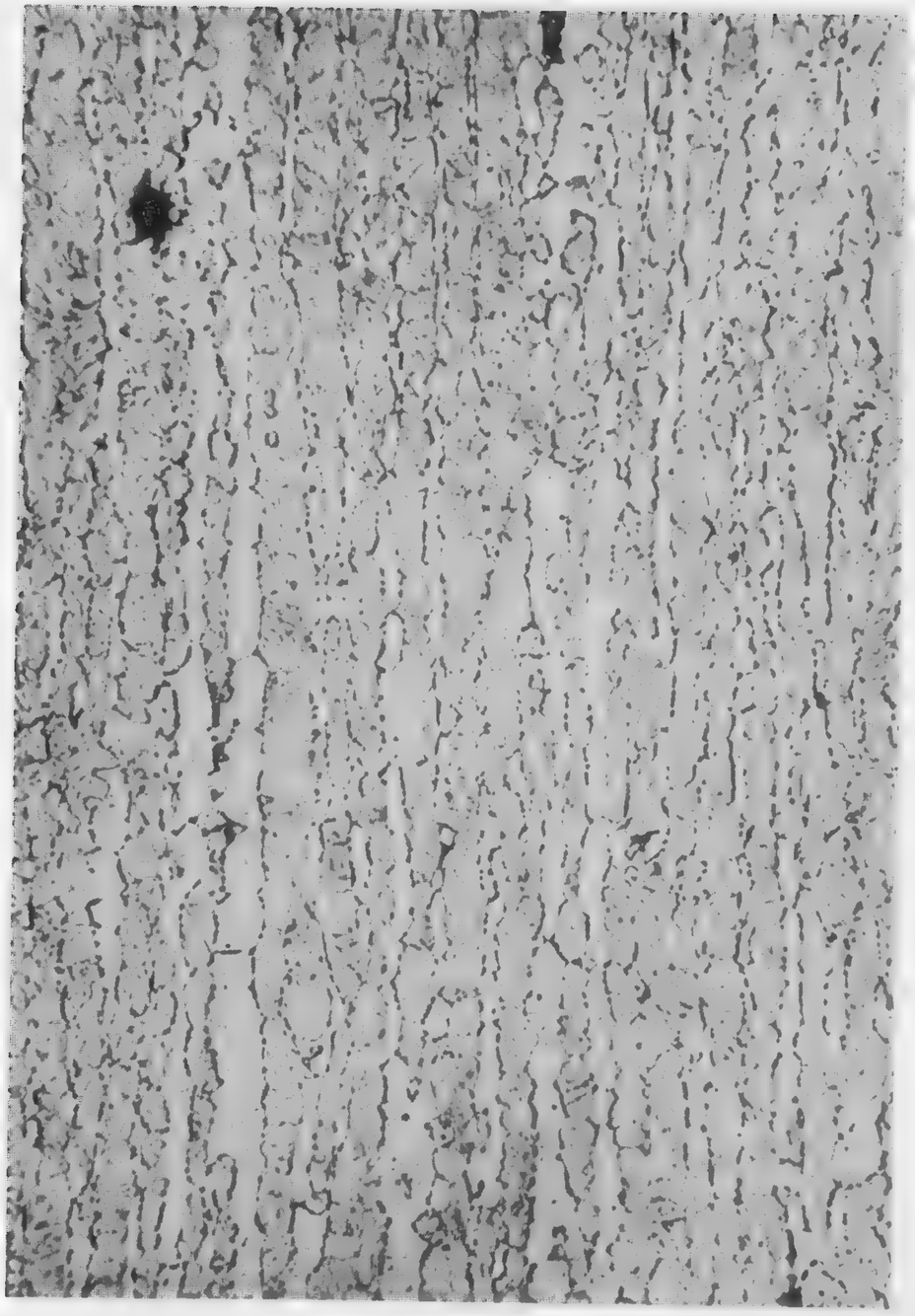


FIGURE 7 DELTA FERRITE BANDS IN PH15-7 Mo
250X

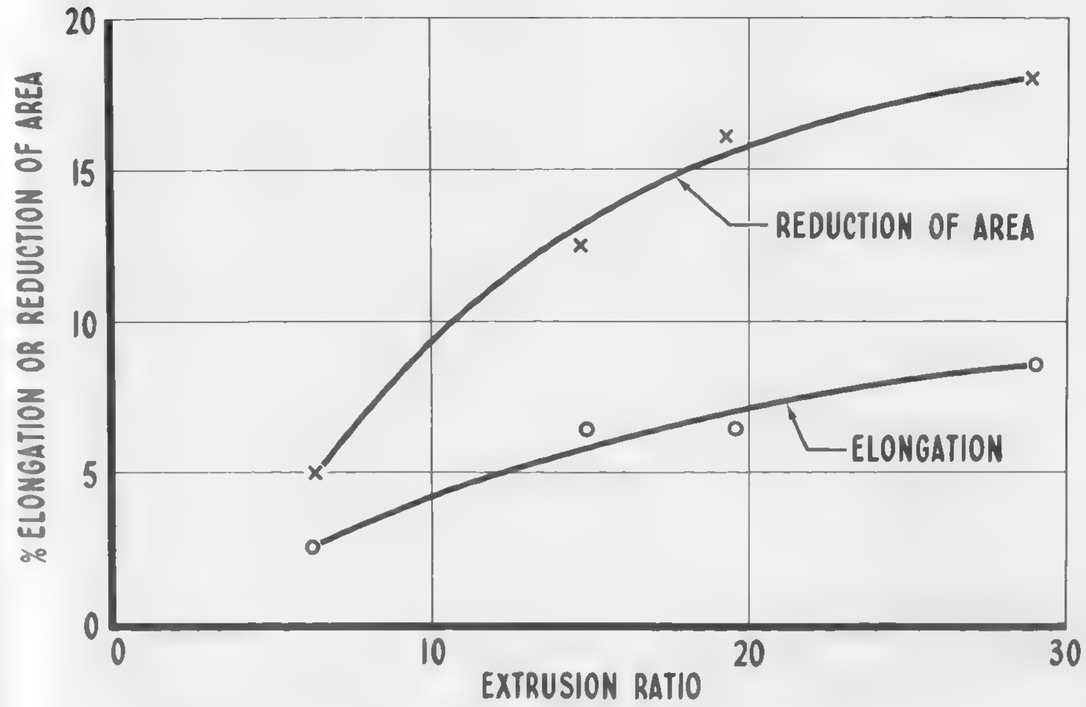


FIGURE 8 EFFECT OF EXTRUSION RATIO ON TRANSVERSE DUCTILITY

20:1 or greater would produce satisfactory material, and this criterion has been used on some of the smaller extrusions.

There were other requirements for extrusions with cross sections as large as 15 sq. in. The starting billets and extrusion presses required for a 20:1 extrusion ratio in such sizes eliminated all but one possible source. It was decided not to risk single source procurement, especially since there was no assurance of acceptable properties in such large sizes, even with the high extrusion ratio. Also, there were requirements for rolled rectangular bars (as an alternate to some extruded sections), heavy plate, and forged billets with cross sections up to 90 sq. in. and lengths up to 6 ft. or more. These could not be supplied in PH15-7Mo with satisfactory properties.

By virtue of its composition, 355 alloy is essentially free of delta ferrite and was expected to show adequate short

TABLE V

PROPERTIES OF 355 ALLOY BARS AND BILLETS

Size (in.)	Direc-tion*	Ult. (KSI)	Yld. (KSI)	Elong. (2 in.) (%)	Red. of Area (%)
Specification Requirement**	L	195	165	10.0	35.0
	LT	195	165	8.0	10.0
	ST	195	165	5.0	5.0
5-1/4 x 12 x ?	L	206	179	12.0	45.0
	LT	207	185	10.0	40.5
	ST	199	170	11.5	21.5
4-1/2 x 11 x 63	LT	196	172	14.5	35.0
	ST	199	169	9.0	14.0
5 x 18-3/8 x 96	L	220	188	19.0	42.0
	LT	212	179	15.0	26.0
	ST	198	167	6.5	10.0
3 x 7 x 64	L	209	181	17.0	49.5
	LT	208	172	15.0	34.3
	ST	207	174	6.5	7.0
4-1/2 x 17-1/4 x 18	L	226	196	18.0	47.0
	LT	214	180	13.0	33.0
	ST	203	170	5.5	7.0
3 x 21-1/2 x 24	L	204	168	6.0	6.5
	ST	200	171	4.5	4.0
4 x 22 x 66	L	222	191	17.5	51.5
	LT	206	175	10.5	20.0
	ST	198	172	2.0	2.5
4-1/4 x 13 x 20	LT	208	170	16.0	28.5
	ST	200	174	2.0	3.0

* L = Longitudinal; LT = Long transverse; ST = Short transverse.

** Minimum properties for standard SCT treatment (1710°F rapid cool, -100°F 3 hrs., 900°F 3 hrs.)

transverse ductility in the desired sections. A large number of rolled and forged bars and billets in 355 alloy were procured and tested. Representative results are shown in Table V. It is seen that all samples met the specified strength requirements. Three samples easily passed the ductility requirements, two were marginally acceptable, and three clearly failed. The 40% rejection rate represented by the above tests presents obvious problems for both the producer and buyer. It was possible to use a few of the rejectable billets for machined parts which were not subject to transverse loading, but the remainder was unusable.

Bars, billets and forgings in 355 alloy are normally given a 1950°F anneal, followed by water quenching. Austenite stability is frequently so great, particularly if high finishing temperatures are used, that the normal processing sequence of 1710°F austenite conditioning followed by subzero treatment and aging may not result in complete transformation. According to Becht (Ref. 2) this retained austenite is responsible for low strength and ductility, and he has proposed an intermediate treatment to destabilize the austenite. This utilizes 3 hrs. at 1300-1500°F to effect carbide precipitation prior to the 1710°F and subsequent processing. Another treatment involves 1950°F WQ, equalize at 1600°F WQ, -95°F 3 hrs., 1070°F 3 hrs. to accomplish the same purpose and also provide good machinability. This latter pre-treatment has also given evidence of providing better strength after final heat treatment, allowing a 900°F final temper rather than the conventional 850°F, which should also help to improve ductility.

Becht has also discussed (Ref. 2) the effect of ingot size and solidification rate as a factor in the segregation of retained austenite. His data show that with larger ingots the equalizing treatment is not successful, but consumable electrode melting (under inert atmosphere) results in good strength and ductility in finished, heat treated billets.

The majority of billets purchased have been made from consumable electrode melts and have included one of the equalizing treatments in their conditioning. Still, we observed many cases of poor ductility, as evidenced by

Table V, although strengths were uniformly high. In contrast, Becht's study of retained austenite showed large drops in strength as well as ductility. Thus there is an unexplained difference in the two investigations.

In relation to the above discussion of ingot size and hot working schedules, the producer has suggested that heavy unidirectional working as required, for example, by the 3 in. x 21-1/2 in. cross section, is conducive to poor short transverse ductility. Accordingly, a size limitation of 50 sq. in. and a width-to-thickness ratio of 2 to 1 maximum has been proposed for guaranteed properties. This is an unsatisfactory situation, since it means the widest available billet is 10 in., and a 5 in. x 10 in. billet would have to be procured for a 3 in. x 10 in. size requirement.

The martensitic PH steel, 17-4PH, was tried as an alternate to the 355 alloy. The producer felt that acceptable properties, as exemplified by the "Requirements" given in Table VI could be obtained. However, the tabulated results, which are representative of a fair number of billets, again show erratic behavior and a high percentage of rejections. This producer has subsequently suggested a 6 in. x 6 in. maximum section for "guaranteed" properties, without reference to width-thickness ratios.

The 17-4 billets were produced from conventional electric furnace melted ingots. Vacuum melting was suggested as a means of improving the transverse ductility, but the producer claims that limited trials showed no significant improvement. (Note that vacuum melting of 355 alloy is not feasible because of the appreciable nitrogen required in the analysis.)

At present there are two apparent solutions to the problem of low short transverse ductility in large PH steel billets. One is to procure excess quantities and discard the unsatisfactory material. This procedure has been followed to date. The other approach is to design the required structural members as built-up weldments, to be made from smaller and lighter sections whose properties are satisfactory. To accommodate the different design allowables associated with welds, some redesign of specific parts might be required.

TABLE VI

PROPERTIES OF 17-4PH FORGED BILLETS

Size (in.)	Direction*	Ult. (KSI)	Yld. (KSI)	Elong. (2 in.) (%)	Red. of Area (%)
Specification Requirement**	L	190	170	10.0	35.0
	LT	190	170	5.0	10.0
	ST	190	170	5.0	10.0
3-3/8 x 13 x 168	L	196	185	15.0	46.0
	ST	191	170	8.0	13.5
4 x 22 x ?	LT	198	175	13.0	38.5
	ST	196	171	11.0	10.0
2-1/2 x 10 x 251	L	211	184	14.5	48.5
	LT	209	183	10.0	30.5
	ST	***	***	***	***
3 x 11-1/2 x 99	LT	192	174	13.0	42.0
	ST	185	171	3.0	5.5
5 x 10 x 96	L	197	178	12.5	35.0
	LT	197	172	10.5	23.0
	ST	192	171	2.0	2.5

* L = Longitudinal; LT = Long transverse; ST = Short transverse.

** Minimum properties after 1900°F solution treatment and 950°F temper.

*** Billet too thin to obtain short transverse tests.

We believe that the right combination of metallurgical factors should solve the problem of low ductility. Changes to the basic analyses in the direction of low carbon and low delta ferrite, possibly combined with vacuum or consumable electrode melting for cleanliness are suggested. Further studies leading to control of ingot breakdown and subsequent hot working schedules are in order. More work on heat treat modifications may be helpful. All of these approaches have been discussed with the producers, and some experimental work is in progress. Such work is costly and time-consuming, and it is difficult to support against an experimental aircraft program. Continued procurement of airplanes as a production type would warrant the necessary effort along the paths outlined above.

In concluding this account of our experiences, we feel that much has been accomplished in the development and application of PH steels through the efforts of the producers and North American, working together on the XB-70 program. Although much still remains to be learned about these interesting and complex steels, answers to a number of difficult metallurgical problems have been obtained, assuring the successful construction and scheduled flight of the XB-70.

BIBLIOGRAPHY

1. Anon. Fracture Testing of High-Strength Sheet Materials. ASTM Bulletin, No. 243, pp. 29-40, Jan. 1960.

2. Becht, E. F. comments on: Retained Austenite in Precipitation Hardening Stainless Steels. Transactions of the Am. Soc. for Metals, Vol. 52, pp. 443-449, 1960.

MATERIALS FOR THE SUPERSONIC TRANSPORT

Paul H. Denke
Technical Assistant, Strength Section
Transport Aircraft Division
Douglas Aircraft Company, Inc.
Long Beach, California

ABSTRACT

The supersonic transport will be designed to meet a set of requirements which impose severe limitations upon the choice of materials for major structural components. These requirements include operation at high speed (3 to 4 times the speed of sound), and high altitudes (around 70,000 feet), for long periods of service (30,000 to 40,000 hours). Passenger safety and the need for a high level of structural efficiency must be taken into account. These considerations and others combine to complicate the selection of materials.

Central among the problems concerning materials are elevated temperature effects, including short-time mechanical property degradation, long-time instability, and creep. Fatigue, stress corrosion, notch resistance and other problems must be considered. The use of aluminum, the traditional metal for civil transports, will be discontinued probably in favor of titanium or steel alloys.

The paper discusses the requirements, the problems, the approach to the problems, the compromises involved, and some of the candidate alloys currently under consideration.

INTRODUCTION

The supersonic transport program is emerging from the initial phases of planning and evaluation. After studying various aspects of the problem, the Department of Defense, NASA, and FAA have issued a joint report concluding that the project is technically feasible. FAA has published a preliminary study of standards for airworthiness, operations and maintenance. A number of airframe companies are actively engaged in advanced studies, and Congress has appropriated funds for research in the fields of structures and propulsion necessary to support a full-scale design effort.

One of the basic structural problems concerns the selection of materials for major airframe components. The proper choice of materials is important to the success of the project. Fortunately a sufficient number of promising alloys are available to ensure that a satisfactory choice can be made. Nevertheless, the design of the aircraft involves a number of unique and severe requirements which must be given careful consideration.

What makes the choice of materials especially significant is the fact that the use of aluminum, the traditional metal for civil transports, will be discontinued in favor of stainless steel, titanium alloy, or some other metal which is relatively new and untried as far as airframe applications are concerned. Practically all commercial aviation experience, over a period of 30 years, has been based on aluminum alloy as the principal airframe material. This period encompasses three or four generations of transport aircraft and half the history of aviation since the first heavier-than-air flight. During this time the most venturesome experiments with materials consisted of comparatively minor improvements in the alloy. Even with this conservative approach, the operating experience was not entirely trouble-free. The change to other metals, therefore, is a possible source of difficulty. The difficulty can be avoided through a realistic research and development program that can evaluate metals and eliminate those which are not satisfactory.

The purpose of this paper, therefore, is to bring some of the important material problems to the attention of people who are well informed in the field, in order to secure the benefits of increased exchange of information. No attempt is made to draw final conclusions about the choice of materials, except in certain obvious instances. The data which are presented are intended to illustrate the problems, not to support conclusions about materials selection.

THE SUPERSONIC TRANSPORT

Figure 1 shows a possible configuration of the airplane. This design represents one stage of the development program described in Reference 1. The configuration incorporates a thin, low aspect ratio-delta wing, a delta-shaped canard control surface, and a pod containing four turbofan engines located below the wing. The fuselage is pressurized for high altitude operation, and fuel is carried under pressure in the wing.

DESIGN REQUIREMENTS

A typical mission profile is given in Figure 2. The figure shows the planned cruise altitude of 60,000 to 70,000 feet, and cruise Mach number of 3.0. At these altitudes, Mach 3 corresponds to a true airspeed of about 2,000 miles per hour. This speed represents a lower limit. Mach numbers of 3.5 and higher are being considered.

Figure 3 shows the structural temperatures that result from Mach 3 cruise. The figure shows that surface temperatures on the order of 450-600°F will exist during most of the flight.

Figure 4 shows the dependence of wing surface temperature at a point two feet aft of the leading edge on Mach number. The figure shows that temperatures increase rapidly with speed. At Mach 4 the surface temperatures are on the order of 900°F. The Mach number finally chosen for design cruise therefore has a critical influence on the material selection problem.



FIGURE 1 A SUPERSONIC TRANSPORT CONFIGURATION

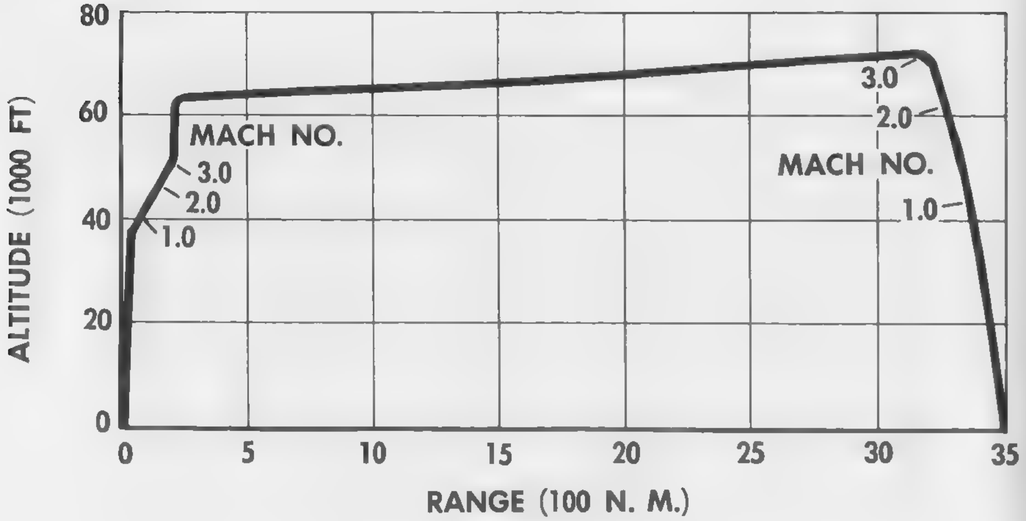


FIGURE 2 MISSION PROFILE

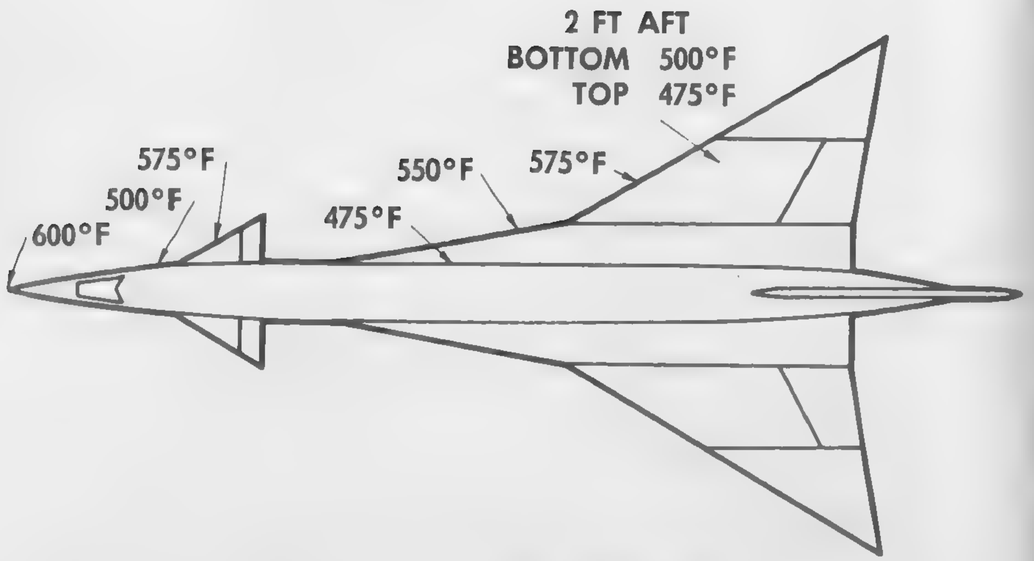


FIGURE 3 STRUCTURAL TEMPERATURES

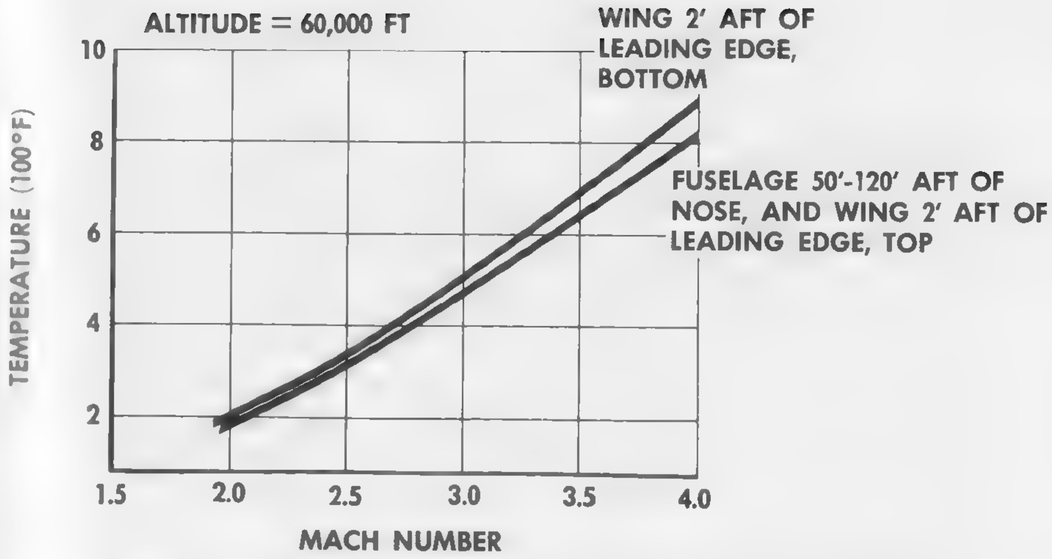


FIGURE 4 DEPENDENCE OF STRUCTURAL TEMPERATURE ON MACH NUMBER

The supersonic transport is to be designed for a service life of 30,000 to 40,000 hours. In operation, these figures correspond to a useful life of 10 to 13 years, on the basis of 3,000 hours per year utilization. A service period of this duration is necessary to make the project commercially feasible. The fact that the structure must sustain load at elevated temperature for long periods of time has an important influence on the choice of material.

The considerations of civil operation impose other significant requirements. Passenger safety is paramount; therefore, the metal must have the quality of reliability, as represented by fatigue resistance, notch resistance, etc. On the other hand, the need for profitable operation requires a highly efficient structure. Consequently, a material of high strength to weight ratio is necessary.

The low aspect ratio wing represents unconventional structure compared to the high aspect ratio wing of the subsonic jet transport. The low aspect ratio will tend to introduce an important degree of biaxiality of stress and, therefore, the significance of this effect will be emphasized.

Future growth is an important consideration. The airplane will be expected to be capable of growth in size, weight, and speed. With respect to material selection, the important consideration is growth in speed, because of the accompanying increase in temperature. One way of allowing for this possibility is to design in such a way that a material with higher temperature capability can be substituted for a lower temperature material with minimum difficulty.

The schedule has an important bearing on choice of materials. Reference 2 estimates the date of type certification as 1970 or 1971. This schedule allows a minimum amount of time for selection of materials. Consequently, the widespread structural use of experimental alloys, reinforced plastic and filament wound construction, for which little airframe technology exists, is probably ruled out.

THE PROBLEMS OF MATERIAL SELECTION

Elevated temperature effects are central among the problems. These effects include short-time mechanical property degradation, long-time instability, and creep. In addition, problems like fatigue and corrosion can be aggravated at elevated temperature.

SHORT-TIME PROPERTIES

Short-time material property degradation presents a problem because structural efficiency is affected. However, the problem is clear-cut and the data necessary for its solution are not hard to obtain. Figure 5 shows the general dependence of short-time strength on temperature. The index of strength plotted as ordinate, the ratio of tensile ultimate to density, provides a measure of relative structural efficiency. The figure shows the general downward trend of strength with temperature, the fact that steel and titanium alloys are competitive, and the reason why aluminum is not considered for the Mach 3 transport. The term "short-time", as used here, means that the specimen is heated and tested in less than half an hour.

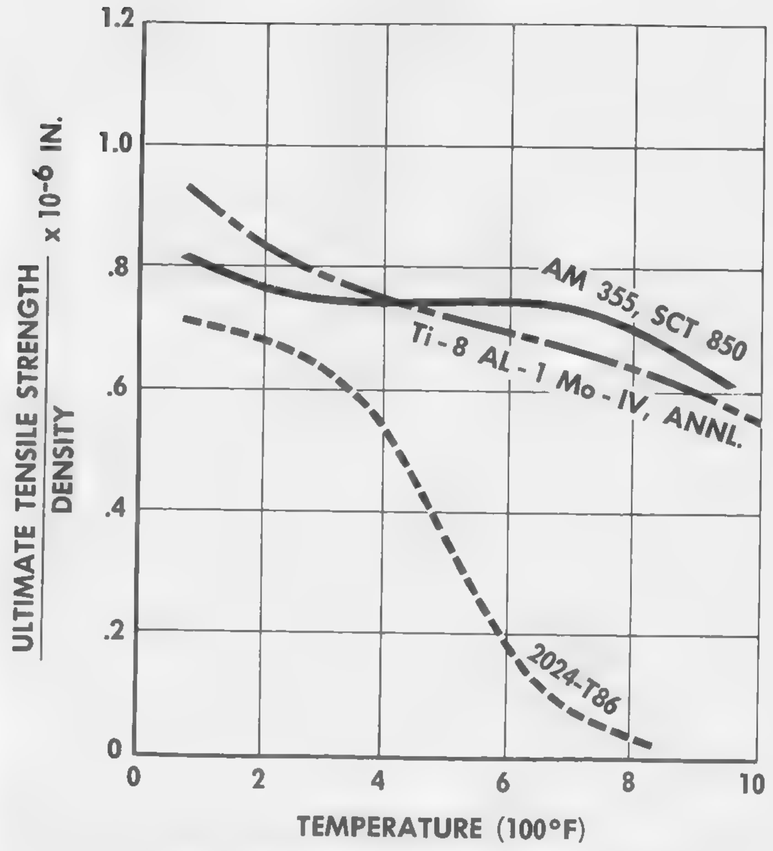


FIGURE 5 DEPENDENCE OF SHORT TIME STRENGTH ON TEMPERATURE

Data of the kind shown in Figure 5 are required for all materials considered for the Mach 3 transport. Similar short-time data are required for tensile yield, compressive yield, elongation and Young's modulus. Data should be plotted in conventional form and in parametric form to show structural efficiency.

LONG-TIME PROPERTIES

The determination of short-time properties at elevated temperature represents a significant, but not a very difficult problem. The determination of long-time properties, to 30,000 hours, is not only significant, but also difficult for several reasons. First, the introduction of temperature introduces two new variables, temperature itself and time.

The additional variables mean that many more tests must be run to allow for various possible combinations of stress, temperature and time. Second, long-time tests are expensive because they tie up testing equipment for long periods. Third, very long-time tests are hard to fit into the schedule. Thirty thousand hours testing time is 3.5 years if the test is run without interruption. Getting the results of such tests soon enough to be of use is a problem, yet some of this work must be done, because the information can be obtained no other way.

The simplest type of long-time test is performed at temperature under no load. Figure 6 shows the effect of exposure to elevated temperature on the room temperature sharp notch strength of the titanium alloy 13V-11Cr-3Al. The data were obtained at NASA.[3] The ASTM edge-notch specimen, which is a tensile coupon with sharp edge notches, was used in these tests. The ultimate strength of the specimen provides a measure of the material's ability to support load in the presence of a stress raiser.[4] This property, which is of great significance in design, is discussed in

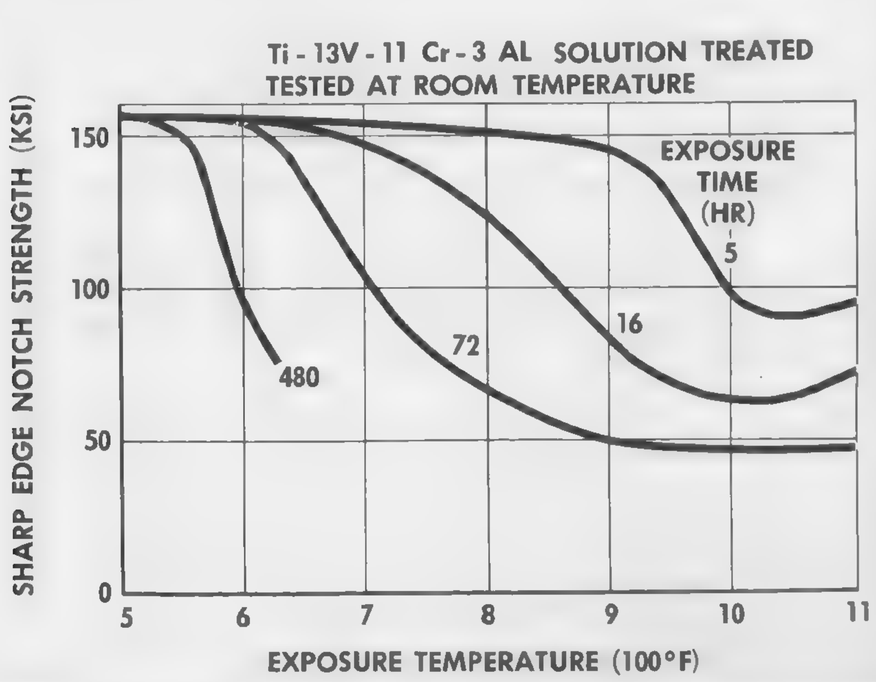


FIGURE 6 EFFECT OF EXPOSURE TO ELEVATED TEMPERATURE ON NOTCH STRENGTH

more detail in a later section. The figure shows that exposure at elevated temperature has a pronounced effect in reducing the notch strength of this alloy, and that the amount of reduction increases with time. After 480 hours at 600°F the notch strength has deteriorated to 61% of its initial value. What the notch strength would be after 30,000 hours is a matter for speculation. This example emphasizes the importance of long-time data.

Very little long-time data are available but more will be forthcoming as the result of several programs currently in progress or about to be initiated. Some of these programs are described in a later section.

A second type of test involves holding for long times under stress and elevated temperature, followed by short-time tensile testing to failure. Creep data can be obtained, but the principle purpose is to determine the effect of long-time exposure to load and temperature on short-time properties. Figure 7 shows the results of some tests conducted at the University of Michigan.[5] The material was the super-alloy Rene 41. The exposure conditions were 650°F and 40,000 psi for 1000 hours. The effect of exposure on the tensile ultimate and yield strengths was not severe, but the loss in ductility was appreciable, especially at the lower test temperatures.

CREEP

Much more creep data must be obtained for the candidate materials. Most of the existing data are for 1000 hours or less, and much of it is for temperatures above 600°F. Figure 8, which is typical of the existing data, shows creep rupture and creep yield information for PH15-7 Mo, RH950. The figure indicates that for periods of time less than 1000 hours, creep at 600°F is no problem for this alloy.

The top priority creep problem is to determine whether or not creep will have any significance in the design of the Supersonic Transport. Before this determination can be made, the following information must be obtained: First, how much creep can be allowed in the structure of the SST?

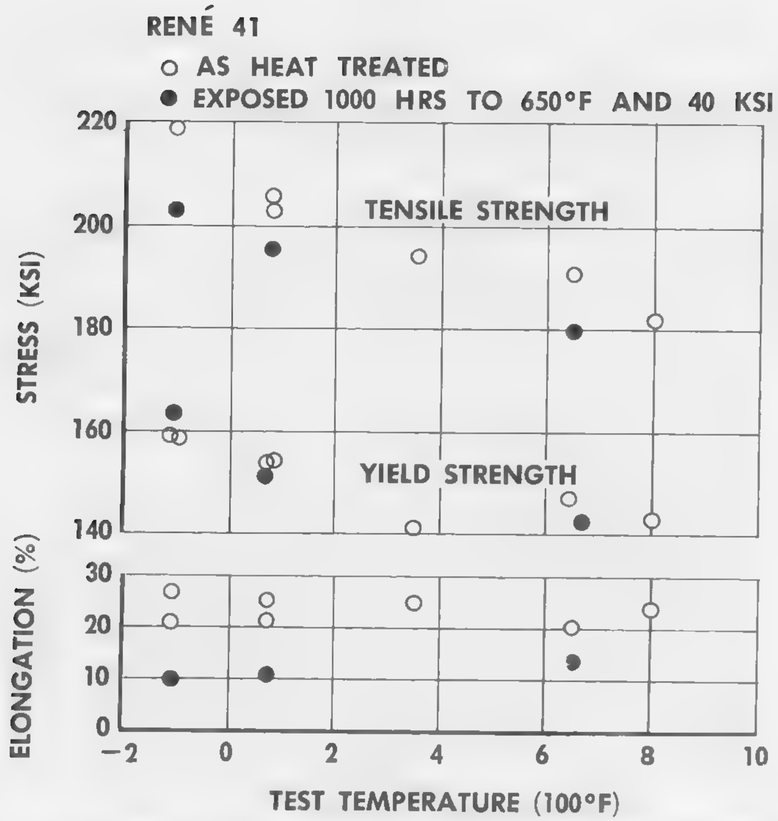


FIGURE 7 EFFECT OF EXPOSURE TO ELEVATED TEMPERATURE AND STRESS ON SHORT TIME STRENGTH AND ELONGATION (TRANSVERSE)

This information must be supplied by the licensing agencies and the designers; second, what will be the cruise Mach number for the SST? third, what are the creep characteristics of the candidate materials? This information must include creep strain and creep rupture data for temperatures down to 500°F for periods of time to 30,000 hours.

PREDICTIONS OF THERMAL EFFECTS

Means for predicting the long-time effects of elevated temperature on material stability and deformation are required. The means can take the form either of empirical analysis or accelerated test.

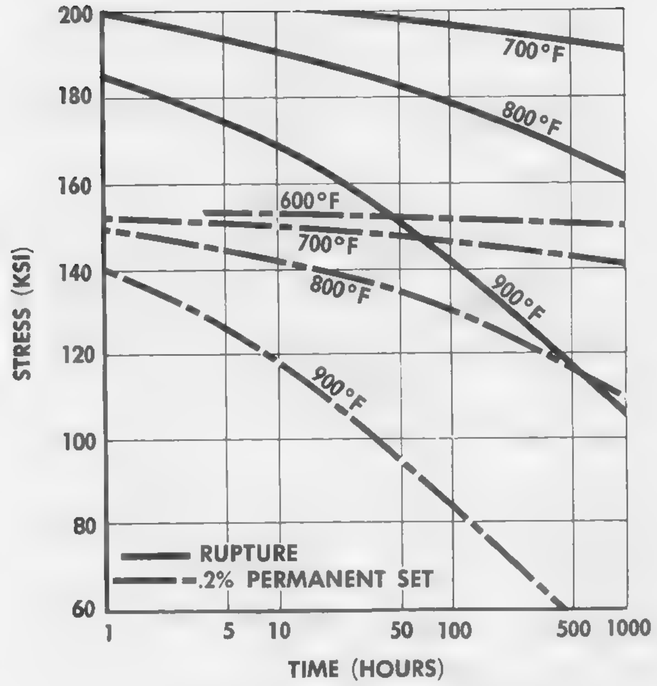


FIGURE 8 TENSILE CREEP OF PH15-7 Mo, RH 950

Very few efforts have been made analytically to predict the stability of material mechanical properties, probably because of the complex physical and chemical processes at work in the polycrystalline alloys during exposure to heat and stress. Unfortunately, these same processes influence creep. This fact helps to explain why no completely adequate means has been found for extrapolating creep data or predicting creep under varying conditions of stress and temperature.

The methods that have been proposed for computing cumulative creep strain under variable conditions of load and temperature include the following: the time-hardening rule; the strain-hardening rule; and the life-fraction rule. These rules are simple procedures for cumulating creep strain on the basis of experimental curves of creep strain versus time for constant stress and temperature. The applicability to 2024-T3 aluminum alloy was investigated by the NASA.[6] A typical result is shown in Figure 9. The data were obtained by applying a program of stress to a tensile specimen of 2024-T3 at 400°F. The stress program is

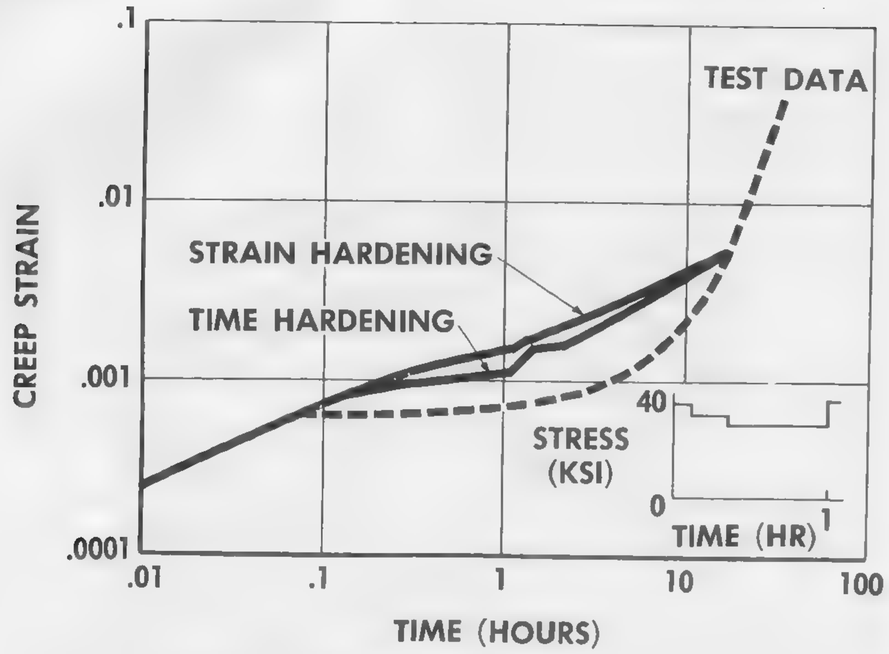


FIGURE 9 COMPARISON OF STRAIN HARDENING AND TIME HARDENING RULES WITH TEST RESULTS

shown in the lower right-hand corner of the figure. Some rather large discrepancies are indicated between the test results and the strain-hardening and time-hardening rules. These discrepancies are attributed to the effects of creep-recovery not accounted for by the formulas. Although the material studied is not applicable to the SST, the results suggest that better methods of computing cumulative creep strains are necessary.

If the materials selected for the SST creep appreciably under design conditions, then the cumulative creep problem will be important not only for the purpose of estimating total creep strain, but also because a number of allied problems are involved. For instance, the calculation of the stress distribution in a statically indeterminate wing structure would depend on the cumulative creep strain. This factor also enters the problem of predicting creep buckling.

FATIGUE

Figure 10 shows the effect of temperature on fatigue life for PH15-7 Mo. The data are from Reference 7. The specimens were tensile coupons containing central circular holes. The figure shows appreciable decreases of fatigue life with temperature. The temperatures shown are somewhat above the range of interest; however, other materials may show pronounced effects in the 600°F. range.

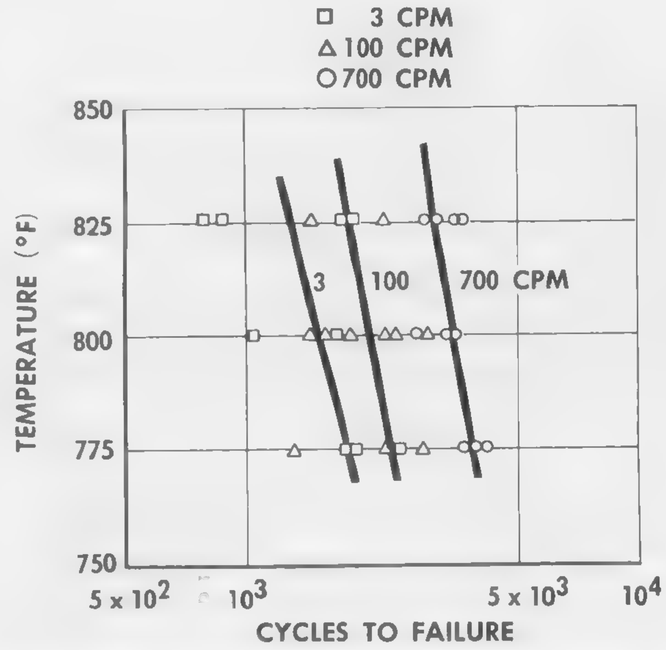


FIGURE 10 EFFECT OF TEMPERATURE ON FATIGUE LIFE OF PH15-7 Mo

Figure 10 illustrates another effect of importance: the dependence of fatigue life on frequency of load application at elevated temperature. Stated another way, the figure shows the conjoint effects of fatigue and creep. The specimens tested at lower frequencies failed at fewer cycles for the same stress level, because longer running times and longer exposures to elevated temperature were involved.

These results suggest that frequency sensitive materials may have to be tested at the actual rate of load application. In such cases, tests would last up to 30,000 hours or more.

A means is required, therefore, of obtaining meaningful fatigue data from accelerated tests, in the event that the fatigue characteristics of the material under consideration should be sensitive to loading frequency. A satisfactory means of predicting structural life on the basis of such data also must be found. The prediction technique may have to account for an additional variable, atmospheric ozone, which at 70,000 feet may be sufficiently concentrated to affect the fatigue resistance of certain alloys.

CUMULATIVE FATIGUE DAMAGE

A means of computing cumulative fatigue damage under combined random spectrums of load and temperature must be available. The problem never has been solved completely even for the room temperature case. The Palmgren-Miner rule has been used extensively for prediction purposes, sometimes with inconsistent results. However, precise answers are not expected, since fatigue is a statistical process. Nevertheless, cases are known in which the errors resulting from applying the rule are much larger than can be attributed to statistical variation.

For example, Figure 11 shows the results of fatigue tests run at the NACA on unnotched aluminum 7075-T6 tensile coupons.[8] Two step tests were run in which cycles of stress at one level were followed by cycles at a different level to failure. The ordinate of Figure 11 is the cycle ratio at the first stress level, while the abscissa is the cycle ratio at the second level. Here the term "cycle ratio" means the ratio of the number of cycles run at a given stress level to the fatigue life at that level. If Miner's rule were correct, the test points would lie on the diagonal dotted line. The curves show results for the two cases of low stress followed by high stress, and the reverse. Large systematic departures from Miner's rule are evident. When a small number of cycles of high stress are applied first, the effect is to prolong the life at subsequent cycles of low stress.

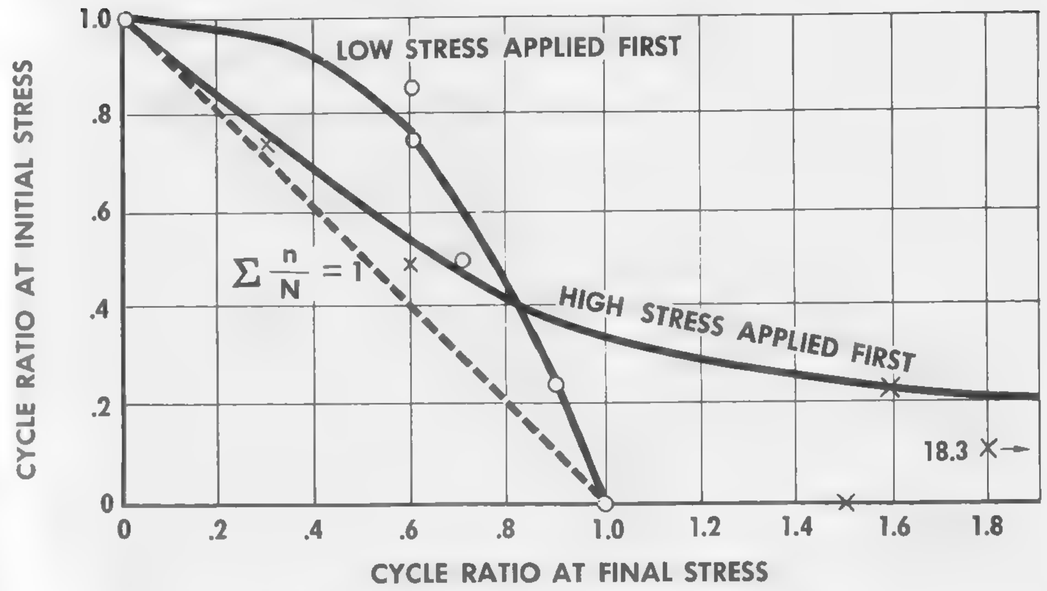


FIGURE 11 RESULTS OF TWO-LEVEL FATIGUE TESTS ON 7075-T6

The improvement in life resulting from large tensile prestresses is attributed to the development of compressive residual stresses in the region of notches or other stress raisers following the preload. If the hypothesis is correct, then compressive preloads might have an adverse effect. Heywood[9] has shown that such an effect does exist. In his tests, compressive preloads were found to reduce fatigue life in one case by a factor of 20. Templin also demonstrates this effect.

Evidently the problem of cumulative damage prediction is sufficiently unresolved so that further study is justified, even for the room temperature case. The addition of elevated temperature as a variable complicates the picture. Cumulative damage prediction, therefore, is a problem in the design of the SST.

FATIGUE UNDER BIAXIAL STRESS

Not a great deal of experimental or theoretical study has been devoted to fatigue under biaxial stress, yet this condition generally exists in the airframe structure. The fuselage

skin of the SST will be subjected to biaxial stresses because cabin pressure imposes circumferential and longitudinal stresses in the ratio of two to one, while other loads contribute tensile stresses in both directions in addition to shear. The problem is more urgent than it was for the subsonic jet transport, because passengers and crew cannot be exposed to the environment at 70,000 feet even with emergency oxygen equipment.

The wing skin also will be in a biaxial stress state because of the low aspect ratio, which makes the wing behave more like a plate than a beam, and the fact that wing fuel tanks must be pressurized to reduce boil-off.

Some evidence exists to support the octahedral stress hypothesis for biaxial fatigue.[11] However, further work should be done for the candidate metals. Information on the effect of biaxiality is needed.

One difficulty is the preparation of a suitable specimen. Round tubes at first appear to offer a satisfactory solution, because tubes can be pressurized and loaded to produce various conditions of stress. Unfortunately, information on sheet materials is required, and tubes made by welding sheets bent into tubular shapes do not possess the characteristic sheet material properties. The same objection naturally applies to tubes machined from bar stock.

A possible solution is shown in Figure 12. The specimen is in the shape of a cross. The material at the intersection of the two arms can be loaded biaxially. Here the problem is to proportion the specimen in such a way as to produce a condition of stress which is known, free of steep gradients, and maximum in the center. The development of a specimen of this kind is described in Reference 12.

CORROSION

For structural efficiency, the heavier metals must be worked to higher stresses. Since steel is three times heavier than aluminum, it must be worked to roughly three times the stress. Titanium is intermediate. In an applica-

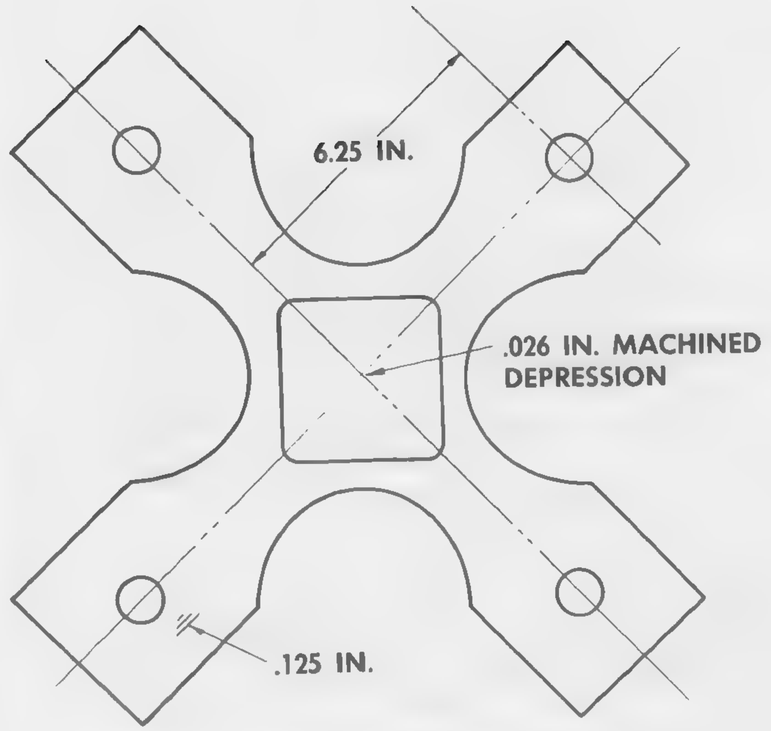


FIGURE 12 BIAXIAL TENSILE SPECIMEN (Reference 12)

tion where the load to be carried is fixed, the use of steel or titanium sheet thus will lead to thinner gauges than would the use of aluminum. In such applications, equal amounts of corrosion are more critical for the heavier metals because a greater percentage of the thickness is lost.

Paints, claddings and similar means can be considered for protecting the surface. However, the designer would prefer to avoid such means, if possible.

The relative resistance to corrosion and oxidation of the candidate metals can be and is being evaluated by test. To be acceptable, the loss in strength from corrosion during the life of the aircraft should be negligible.

STRESS CORROSION, HYDROGEN EMBRITTLEMENT, ETC.

A number of phenomena involve the weakening of metals by chemical agents through mechanisms which are distinguished from the action of simple corrosion. Stress corrosion is damage under the combined action of chemical attack and stress. Hydrogen embrittlement is damage resulting from the entrance of hydrogen atoms interstitially into the crystalline lattice; the hydrogen may be brought into contact with the metal in the form of atmospheric moisture or during a plating process. Recently the possibility that salt may have an embrittling effect on titanium at elevated temperature has been noted.

Time is a factor in these effects since chemical action is not instantaneous. Often a part will perform its function satisfactorily under conditions of high stress only to fail later under comparatively moderate loading.

Figure 13 shows some results obtained on cracked tensile specimens held at steady stress in an environment of distilled water.[13] After a period of time, failure occurred. The type of initial crack is shown in the lower left-hand corner of the figure. The results show that the amount of stress the part can sustain over a protracted period decreases with the initial size of the crack and with the duration of the period. The exact mechanism of failure and the role played by the water are not entirely understood, but one fact is clear: the higher the stress, the shorter the life.

Effects of this kind are cause for concern in the materials selection problem. Because of the need for structural efficiency, a tendency can be observed through successive generations of aircraft to develop more and more of the potential strength of the component materials. Indications are that the SST may continue this trend. Unfortunately, the time-dependent effects discussed in this section become more severe as stress levels increase. Due consideration should be given, therefore, to the relative abilities of the candidate metals to resist this class of time dependent environmentally influenced effects, which includes stress corrosion and hydrogen embrittlement.

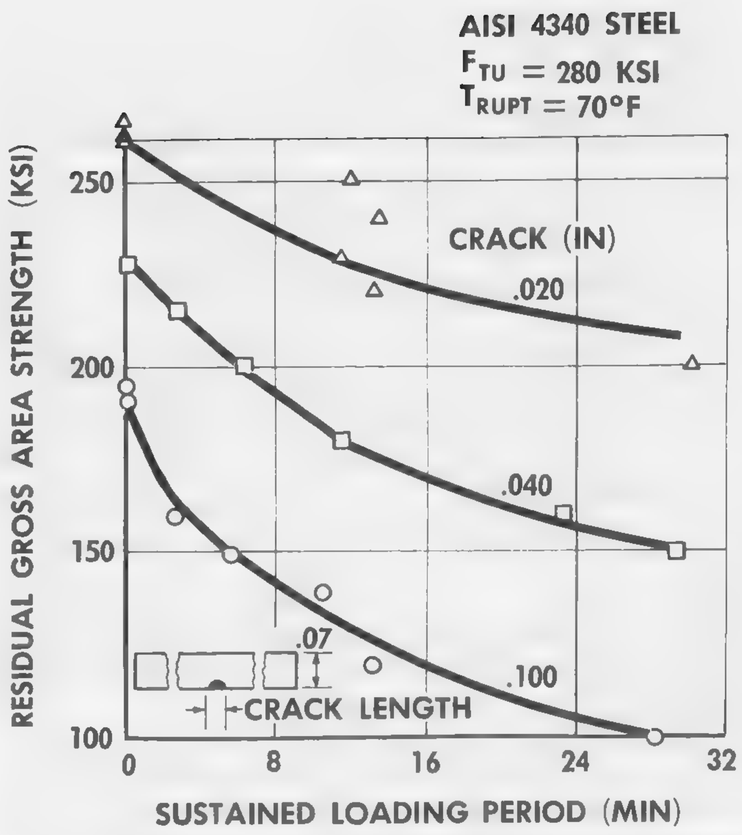


FIGURE 13 EFFECT OF DISTILLED WATER ENVIRONMENT ON RESIDUAL STRENGTHS OF MICRO-CRACKED STEEL PANELS

In planning tests to study these effects, consideration should be given to the possibility that certain parts may be loaded for longer periods than 30,000 to 40,000 hours, which represent flight time. Lugs with interference fit pins, to cite one example, are loaded continuously.

The NASA Special Committee on Materials Research for Supersonic Transports has studied the problem of stress corrosion, and made recommendations for standardizing the test specimen and procedure. The specimen is a strip 1" x .025" x approximately 5". The strip is inserted in a simple slotted fixture in a bent position such that the maximum stress is a prescribed fraction of the 2% yield strength. Salt spray environments are introduced. Procedures for inspection and stress calculation are described.[14]

NOTCH RESISTANCE

In selecting materials, the designer must consider the possibility that at some stage the metal will develop small notches or imperfections. These imperfections can be introduced during production of the material, fabrication of the aircraft, or actual operation; they can take the form of nicks, scratches, cracks, etc. The existence of such stress-raisers is undesirable but inevitable; their presence weakens the metal.

Notch resistance is the term given to the property which measures the ability of a material to carry load in the presence of a stress raiser. The terms "fracture toughness", "crack strength" and "residual strength" refer basically to the same material property.

Materials vary in notch resistance. In tough materials, the presence of a notch may have hardly any effect. In brittle materials, the presence of a small notch can reduce the strength almost to zero.

Figure 14 demonstrates the property. The figure shows the results of tests on tensile coupons containing centrally located cracks or saw cuts. The ratio of gross section stress to ultimate strength is plotted as a function of the ratio of crack length to panel width. As an aid in interpreting the figure, the following points should be kept in mind:

1. When the crack length is zero, the gross section stress is equal to the ultimate tensile strength.

2. When the crack length is equal to the panel width, the gross section stress is zero.

3. A perfectly notch resistant material would be represented approximately by the diagonal straight line, since the gross section stress would be proportional to the net remaining section.

4. A material having zero notch resistance would be represented by the coordinate axes, since the gross section stress would be zero even for very small cracks.

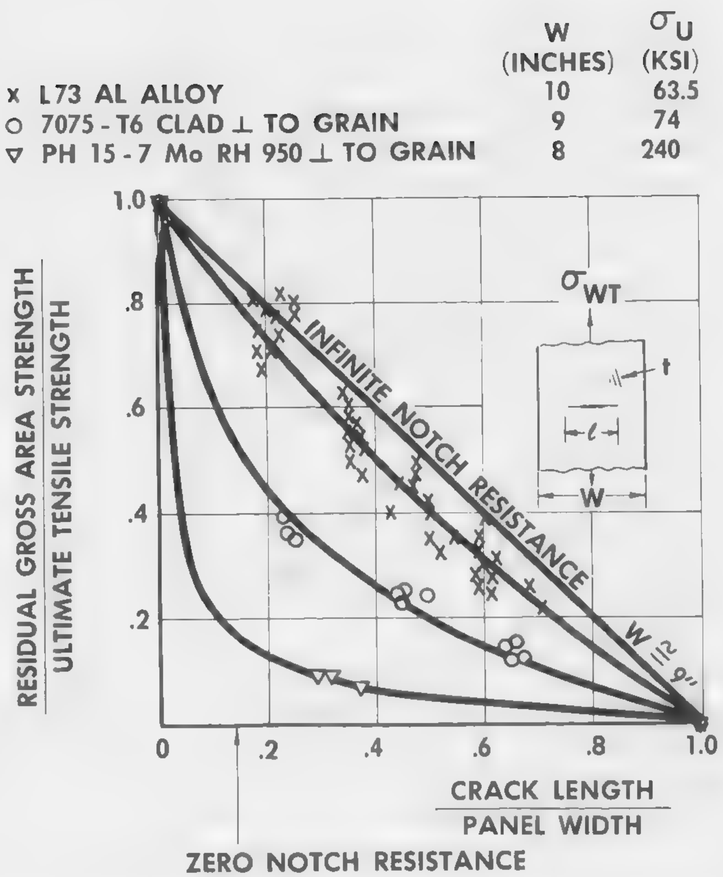


FIGURE 14 NOTCH RESISTANCE OF CENTRALLY CRACKED TENSILE SPECIMENS

Data for three alloys are plotted. For all the metals the points (0, 1) and (1, 0) are considered data points for reasons 1 and 2, cited above. To facilitate the interpretation, curves have been faired through the data. Evidently the aluminum alloy L73 (a British alloy) is very notch resistant since the data points fall close to the diagonal straight line.[15] The stainless steel PH15-7Mo RH950 is quite notch sensitive.[16] When 30% of the section is cracked, 90% of the strength is lost. The aluminum 7075-T6 is intermediate.[17]

The figure shows that metals vary greatly in notch resistance. Methods for measuring and analyzing this important property are necessary so that comparisons among different metals with respect to notch resistance can be made.

Figure 14 showed how notch strength varied with crack length and material when panel width was held constant. Figure 15 shows the dependence upon panel width. For .040 7075-T6 aluminum, data points are shown for 9 in. and 20 in. wide panels. The 9 in. panels appear to be more notch resistant. Actually the material is the same in both cases and the notch resistant property of the material remains constant. The apparent dependence of notch resistance on panel width is accounted for by the formulas given in a subsequent section. The figure also indicates that accurate notch resistance data cannot be obtained from very narrow panels.

Notch strength also depends upon sheet thickness, grain direction, and temperature.

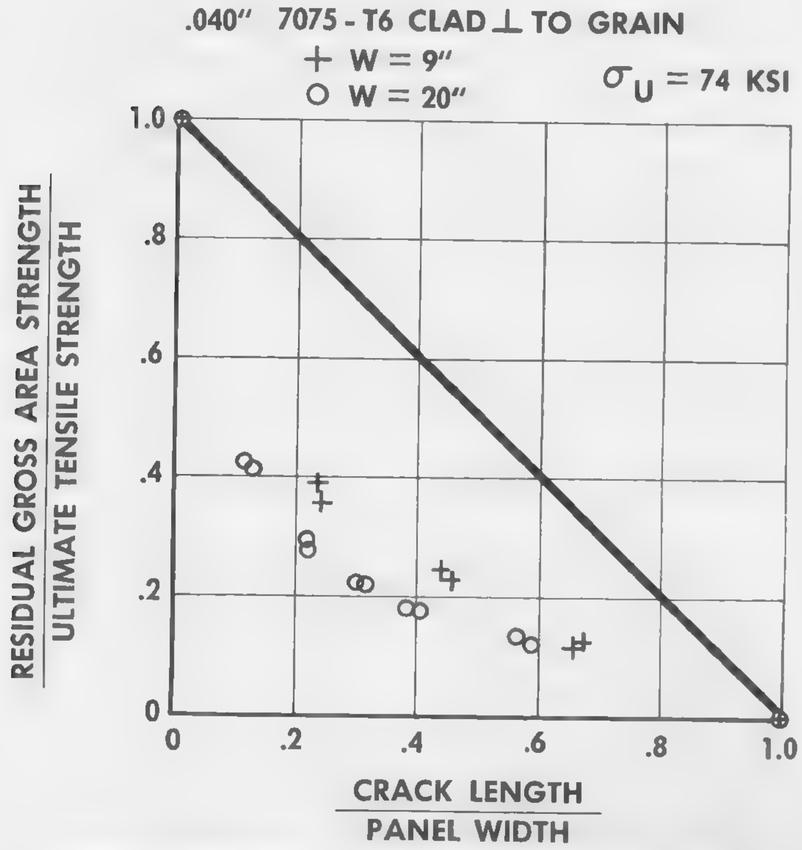


FIGURE 15 DEPENDENCE OF NOTCH RESISTANCE ON PANEL WIDTH

MEASUREMENT OF NOTCH RESISTANCE

The measurement of notch resistance is somewhat handicapped by the large number of variables involved, and the fact that the property is not precisely defined. However, in these respects the situation is not much worse than already exists with regard to the measurement of ductility, or even ultimate tensile strength, neither of which are simple properties. The way to obtain meaningful data is to establish a standardized test. Such standardization is urgent because the property is very significant in design.

Accordingly the NASA Special Committee on Research for Supersonic Transports has recommended procedures for notch testing.[14] Three specimens are recommended: two for preliminary "screening" and a third for more careful "follow-on" studies.

One of the screening specimens is of the edge-notch type already tentatively recommended by the ASTM Committee on Fracture Testing of High-Strength Sheet Materials.[4] The specimen, shown in Figure 16, is tested in tension. This specimen is expected to be suitable for detecting materials which are very notch sensitive.

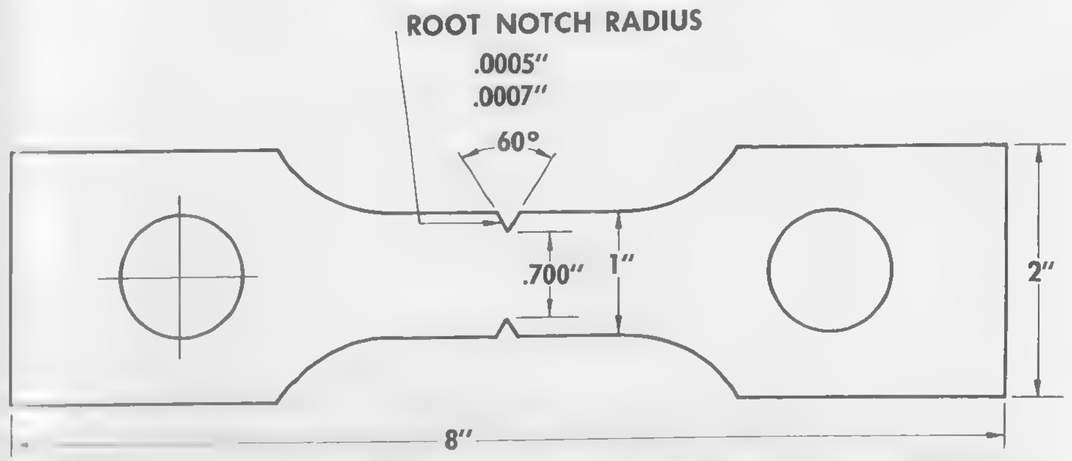


FIGURE 16 EDGE NOTCH SPECIMEN

The other screening specimen is a tensile coupon about 1.5 in. wide containing a central fatigue crack. This specimen is believed capable of giving a greater degree of discrimination of notch resistance because the fatigue crack is a more severe stress raiser than the edge notch. Also, the specimen realistically represents a condition of great concern to the designer: the fatigue cracked panel.

The follow-on specimen, shown in Figure 17, is intended to give precise notch strength data at a reasonable cost. As Figure 14 illustrates, wide panels are necessary to give good notch strength data. The specimen of Figure 17 is believed to be a satisfactory compromise.

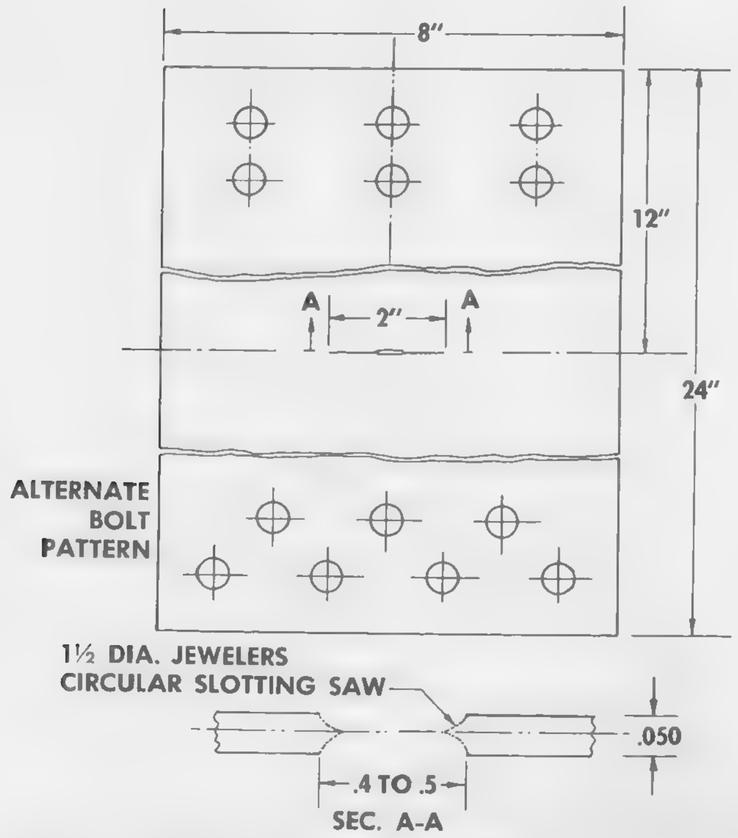


FIGURE 17 FATIGUE CRACKED NOTCH STRENGTH FOLLOW-ON SPECIMEN

ANALYSIS OF NOTCH STRENGTH DATA

A means of notch strength data reduction is required to provide a numerical measure of notch resistance. The subsequent discussion concerns data reduction methods for tensile coupons containing central fatigue cracks.

The most straightforward procedure is to report the ratio of the net section stress to the ultimate tensile strength, σ_n/σ_u. The net section stress is given by

$$\sigma_n = \frac{\sigma}{(1 - 1/w)} \qquad (1)$$

where σ is the gross section stress, l is the crack length, and w is the panel width, as shown in Figure 14. This procedure is satisfactory provided all data to be used for comparisons among materials are obtained from geometrically identical specimens, such as the 8 in. panel described in the preceding section. Otherwise, the ratio σ_n/σ_u cannot be used for comparison because it depends on many things, including crack length.

For example σ_n/σ_u for the PH15-7Mo data shown in Figure 14 is approximately 0.1/0.7 = 0.14. But if panels with very small cracks were tested, the ratio would be much closer to 1, because in the limiting case of zero crack length the ratio σ_n/σ_u is unity.

A method of data correlation which accounts at least for the effects of panel width and crack length is required. The method also should account for the zone of plasticity which develops at the end of the crack.

The Griffith-Irwin expression for gross section notch strength for a centrally cracked coupon is

$$\sigma = K_c \left[w \tan \left(\frac{\pi a}{w} + \frac{K_c^2}{2w\sigma_{ys}^2} \right) \right]^{-2} \qquad (2)$$

where a is half the crack length, σ_{ys} is the 0.2% yield strength and K_c is the fracture toughness constant.[4] This equation is based on an approximate elastic distribution of stress at the end of the crack, with a correction for plasticity.

In order to provide a general idea of the character of Eq. 2, it has been used to compute values of the ratio σ/σ_u as a function of 1/w and K_c for 9 in. panels of a hypothetical material having the properties σ_{ys} = 60 KSI, σ_u = 90 KSI. The results are shown in Figure 18. The figure shows that the curves in general do not pass through the points $\sigma/\sigma_u = 1$, 1/w = 0, or $\sigma/\sigma_u = 0$, 1/w = 1, nor do they approach the diagonal dotted line representing very tough materials. As K_c increases, the curves fall back on themselves until the curve corresponding to K_c = 318 KSI$\sqrt{\text{in.}}$ coincides with the origin. As a result, K_c is a double-valued function of σ/σ_u and 1/w. However the fracture toughness formulas are not intended to apply to the more ductile materials (large K_c) for which yielding is general over the entire cross section at the time of failure.

Figure 19 shows how Eq. 2 compares with test results obtained on 7075-T6 clad specimens 9 in. and 20 in. in width. The value K_c = 50.5 KSI$\sqrt{\text{in.}}$ was obtained by requiring the curve for w = 9 in. to pass through the point indicated by the circle, which represents a conservative value for the test results on 9 in. panels for crack lengths equal to one quarter of the panel width.

An approximate expression for notch strength based on an assumed plastic stress distribution at the end of the crack combined with an elastic distribution beyond the plastic zone has been given in Reference 16. The expression, based partly on the work of Crichlow,[17] is

$$\frac{\sigma}{\sigma_u} = \frac{1 - 1/w}{1 + 31/R_p} \qquad (3)$$

where R_p is a constant called the plastic zone notch resistance factor. From Eq. 3, R_p can be shown to be equal to the length of a crack in an infinitely wide sheet for which the residual notch strength is equal to one half the ultimate.

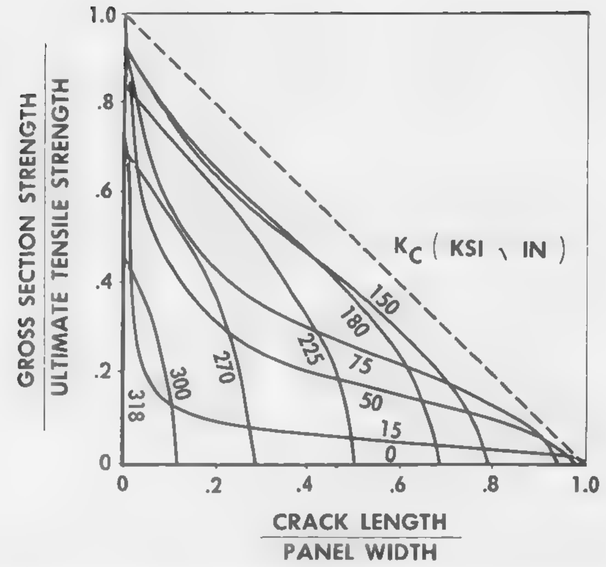


FIGURE 18 CHARACTER OF THE FRACTURE TOUGHNESS FORMULA

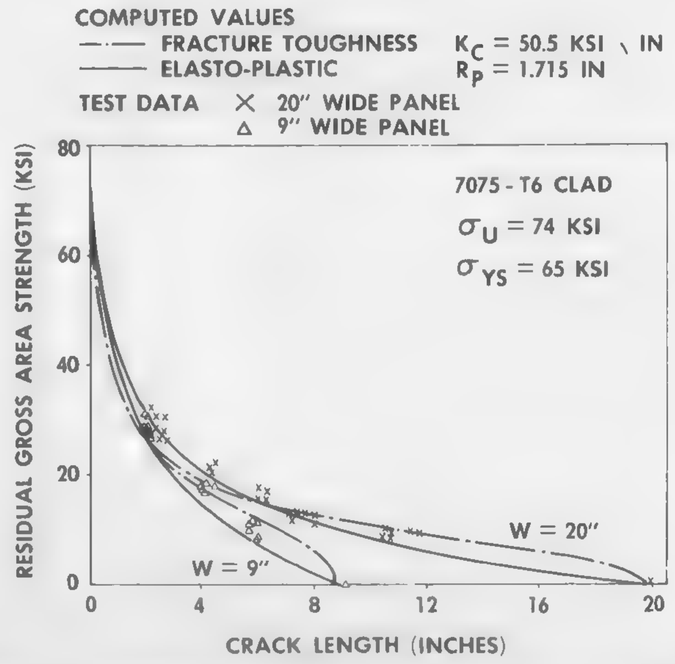


FIGURE 19 COMPARISON OF NOTCH STRENGTH FORMULAS WITH TEST RESULTS FOR 7075 T-6 CLAD ALUMINUM ALLOY

Figure 20 is a graph of Eq. 3 for 9 in. panels. Comparison of Figures 14 and 20 shows that Eq. 3 has the correct character. Also large values of R_p represent tough materials and small values represent brittle materials.

Figure 19 shows the comparison between Eq. 3 and the data for the 7075-T6 clad specimens.

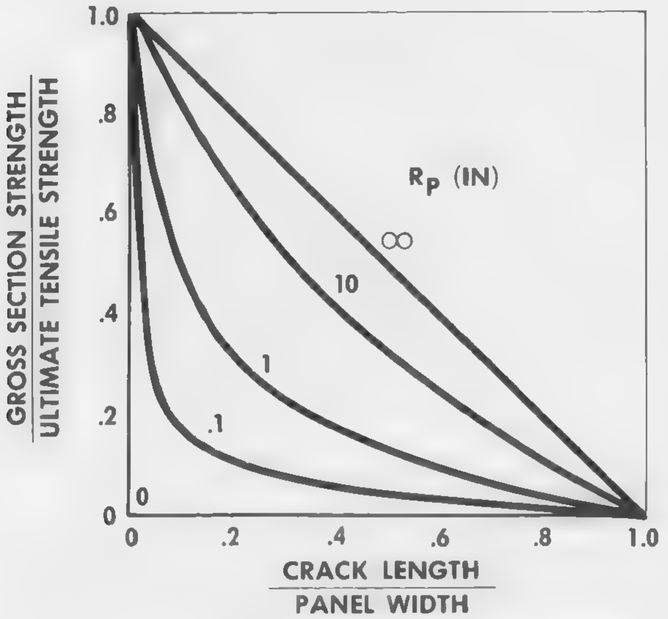


FIGURE 20 CHARACTER OF THE ELASTO-PLASTIC FORMULA

In general no relation can be derived between the parameters K_c and R_p because Eqs. 2 and 3 are quite different. However the two equations assume almost the same form for infinitely wide panels as follows:

Fracture Toughness:

$$\frac{\sigma}{\sigma_u} = \left(\frac{\sigma_u^2}{2\sigma_{ys}^2} + \frac{\pi}{2} \frac{\sigma_u^2}{K_c^2} 1 \right)^{-1/2} \qquad (4)$$

Elastoplastic:

$$\frac{\sigma}{\sigma_u} = \left(1 + \frac{3}{R_p} 1 \right)^{-1/2} \qquad (5)$$

The formulas still do not have quite the same form because the fracture toughness formula give $\sigma = \sqrt{2}\sigma_{ys}$ instead of $\sigma = \sigma_u$ for 1 = 0.

In the case where $\sigma_u = \sqrt{2}\sigma_{ys}$ the equations have the same form and the following relation can be derived:

$$K_c = \sigma_u \sqrt{\frac{\pi}{6} R_p} \qquad (6)$$

It is interesting to note that in a sense K_c is an absolute measure of notch resistance while R_p is a relative measure. Consider two very wide panels composed of materials differing in ultimate tensile strengths. Suppose nevertheless that the ratio σ/σ_u is the same for both panels when each contains a one inch crack. In this case the materials could be said to have the same relative notch resistance, although the panel composed of the stronger material would have greater absolute strength. Calculation would show R_p to be the same for the two materials while the K_c's would differ in the ratio of the ultimate strengths. This difference between the two parameters is demonstrated by the presence of the ultimate tensile strength σ_u in Eq. 6.

ADDITIONAL RESEARCH ON NOTCH RESISTANCE

Further study is necessary to clarify the dependence of notch strength on notch acuity, notch size, coupon width, thickness and temperature. Specimens should be standardized and data reduction procedures improved. The notch resistance properties of the candidate alloys should be established. Final determination of notch resistance should be made on the basis of fatigue cracked panels.

CRACK PROPAGATION

The determination of crack propagation rates for the candidate materials is of some significance. Materials having high rates of crack propagation under cyclic load are less desirable than those in which cracks grow more slowly.

Crack rate data can be obtained from centrally notched specimens of the type discussed in the preceding section. Loads can be applied according to standard fatigue testing procedures. References 16 and 18 discuss methods of testing and crack rate measurement.

Figure 21 shows a typical curve of crack length versus number of cycles. The test was performed on a centrally notched coupon of AM 355 steel.[16] Note that the slope of the curve increases with the number of cycles; and that the curve is essentially vertical at the time of failure. At this

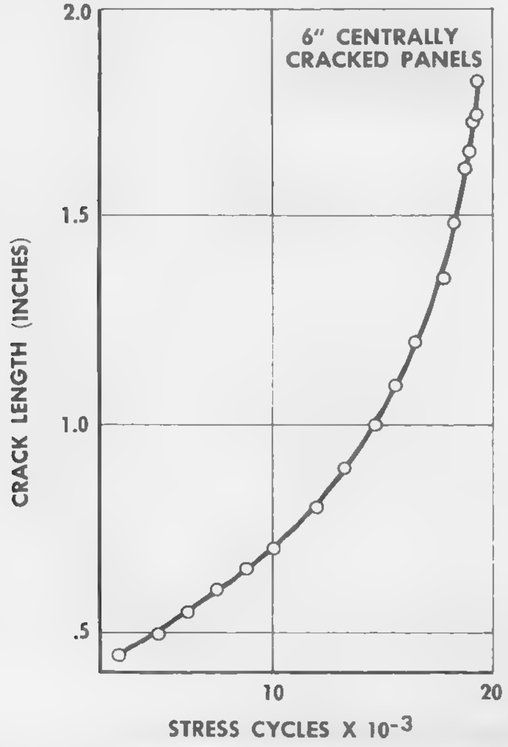


FIGURE 21 CRACK PROPAGATION CURVE FOR AM 355 STEEL

time the crack has also reached its critical length, which is the length at which fast fracture occurs under the maximum cyclic stress.

In many studies of rate of crack propagation, the rate dl/dn is plotted against the Paris-Anderson parameter $\sigma\sqrt{a}\alpha$ where σ is the maximum stress in the fatigue cycle, a is the half crack length, and α is a correction for panel width.[18] This parameter is based on the elastic distribution of stress at the crack tip. Tests indicate that correlation exists between $\sigma\sqrt{a}\alpha$ and the crack rate.

However, a glance at Figure 21 suggests that perhaps another factor should enter the crack rate parameter. This factor, the critical crack length l_c, is suggested because the rate of cracking becomes very large (essentially infinite) when the crack approaches the critical length. Since the critical crack length exerts such an important influence on the crack rate at the end of the process, it seems probable that the proximity of the crack length to l_c should influence the crack rate prior to failure. Accordingly the suggestion was made in Reference 16 that the expression for crack rate might take the form

$$\frac{dl}{dn} = \mu \frac{1}{1 - l_c} \qquad (7)$$

where μ is a parameter, called the mean crack rate, that depends on stress level. In this expression dl/dn becomes large when l approaches l_c.

The later stages of fatigue crack propagation appear to be much more predictable than the nucleation phase, so that the prospects of finding suitable means of predicting crack rates seem favorable. In fact considerable progress has been made. A reliable parameter for comparing crack rates or different materials is needed.

OTHER CONSIDERATIONS

The preceding discussion has touched on a number of material selection problems, including some of the most

important; however others of equal significance remain. The remaining problems, some of which influence fabrication and economics more than performance of the aircraft, include weldability, brazeability, machinability, formability, and producibility. The term producibility is intended to reflect the cost of producing the alloy.

APPROACH TO THE PROBLEMS

An extensive materials research effort on sheet alloys for the supersonic transport is in progress. The governmental agencies already participating include the Langley and Lewis Research Centers of NASA and the Aeronautical Systems Division, USAF. Universities and private institutions also are contributing. The work in progress includes studies of long time stability to 30,000 hours at temperatures around 600°F, sharp notch properties, fatigue, crack propagation, stress corrosion, etc. Titaniums, stainless steels and super alloys are being investigated. The NASA Special Committee on Materials Research for Supersonic Transports, appointed in April 1961, is serving as a recommendatory body with respect to the research.

THE COMPROMISES

One of the more important compromises is between strength and notch resistance. Metals often become less notch resistant as they are strengthened through alloying, heat treating and working. The titanium alloy B120VCA is an excellent example; annealled it is one of the most notch resistant metals, heat treated above 200 KSI it is notch sensitive. The compromise is important because it involves structural efficiency on the one hand and structural reliability on the other.

The ideal solution is to find a metal that is outstanding in both strength and notch resistance. If this approach is not entirely successful, the "fail safe" concept provides an alternative. The metal is chosen principally on the basis of strength, and additional reliability is provided by designing

a multiple loadpath structure. In such a structure alternate loadpaths are available should an emergency arise involving loss of a member.

The fail-safe concept is valuable in design. In a sense metals as well as structures can be said to have fail-safe characteristics to some degree. Thus, a stress-raiser in a ductile material may not be serious because the ductility can permit the overloaded fibers to yield and redistribute stress to adjacent areas. Such a metal possesses an internal structure which is fail-safe.

The metals finally chosen should have some fail-safe characteristics of their own, in the form of notch resistance. The entire burden of reliability should not be placed on structural design.

A second compromise involves future growth. Later versions of the aircraft may be expected to perform at increased speeds and temperatures. Unfortunately, the alloys available for applications above Mach 4 are heavier and less efficient than the metals suitable for the Mach 3 to 3.5 range. Thus, the compromise is between present efficiency and future performance.

A third compromise involves the schedule. Some alloys still in the developmental stage have very promising properties. Unfortunately, the technology for producing, machining, forming and joining these alloys is rudimentary or non-existent. Developing the necessary technology would result in delay. The designer is unlikely to select a highly experimental alloy for this reason, but he may decide to choose a metal relatively less developed than others now available. The compromise is between the prospect of increased efficiency and the possibility of schedule slippage.

These compromises and many others will have to be resolved.

THE CANDIDATE METALS

Steels, titaniums and super alloys are being considered. The following alloys are among the most promising:

Steels:	PH15-7Mo, AM350, AM355
Titaniums:	6A1-4V, 4A1-3Mo-1V, RC140, 8A1-1Mo-1V
Super Alloys:	Rene 41, A286, Inconel W, Waspalloy, C605, D979, N155, V36, Inco 718, Inco 901

Several of these metals have outstanding properties and could be suitable in the SST application.

CONCLUSION

A number of material selection problems face the designer. These problems are important, and the success of the SST program depends to some degree on finding satisfactory solutions. However, several promising candidate alloys are available. The research programs now in progress and about to be initiated should provide the necessary basis for making a proper choice.

BIBLIOGRAPHY

1. Douglas Aircraft Company, Inc., "Douglas Supersonic Transport System, Technical Features," 1961.

2. DOD, NASA, FAA; "Commercial Supersonic Transport Report," June 1961.

3. Brown, W. F. Jr., G. B. Espey, and M. H. Jones, "Considerations in Selection of Wing and Fuselage Sheet Materials for Trisonic Transports," Society of Automative Engineers, Paper No. 341 D, 1961.

4. "Fracture Testing of High-Strength Sheet Materials: A Report of a Special ASTM Committee," ASTM Bulletin, January 1960.

5. Rowe, J. P., T. M. Scoonover, and J. W. Freeman, "Results of Screening Tests on Rene' 41 Alloy for Possible Use in the Airframe of a Trisonic Transport," The University of Michigan, College of Engineering, June 30, 1961.

6. Berkovits, A., "Investigation of Three Analytical Hypotheses for Determining Material Creep Behavior Under Varied Loads, with an Application to 2024-T3 Aluminum-Alloy Sheet in Tension at 400°F," NASA TN D-799, May 1961.

7. Douglas Aircraft Company, Inc., "Investigation of Thermal Effects on Structural Fatigue," WADD TR 60-410, Part II, 1961.

8. Grover, H. J., S. M. Bishop, and L. R. Jackson, "Fatigue Strengths of Aircraft Materials Axial-Load Fatigue Tests on Unnotched Sheet Specimens of 24S-T3 and 75S-T6 Aluminum Alloys and of SAE 4130 Steel," NACA TN 2324, March 1951.

9. Heywood, R. B., "The Effect of High Loads on Fatigue," Proceedings of the Colloquium on Fatigue, Stockholm, May 25, 27, 1955.

10. Templin, R. L., "Fatigue of Aluminum," H. W. Gillett Memorial Lecture, American Society for Testing Materials, 1954.

11. Sines, G., and J. L. Waisman, "Metal Fatigue," McGraw-Hill Book Company, Inc., 1959.

12. Terry, E. L., and J. H. Best, "Development of Methods for Obtaining Materials Design Data on High Strength Alloys for Rocket Case Applications," Third Progress Report, Contract No. AF 33(616)-7720, September 1961.

13. Yen, C. S., and S. L. Pendleberry, "Fracture Strength of High-Strength Steels Containing Shallow Cracks," Douglas Aircraft Company, Inc., Engineering Paper No. 1205.

14. NASA Special Committee on Materials Research for Supersonic Transports, Minutes of Third Meeting, September 19, 20, 1961.

15. Wells, A. A., "Unstable Crack Propagation in Metals: Cleavage and Fast Fracture," Crack Propagation Symposium, College of Aeronautics, Cranfield, September 26, 28, 1961.

16. Christensen, R. H., and P. H. Denke, "Crack Strength and Crack Propagation Characteristics of High Strength Metals," ASD TR 61-207, May 1961.

17. Crichlow, Walter J., "The Ultimate Strength of Damaged Structure Analysis Methods with Correlating Test Data," from "Full Scale Testing of Aircraft Structures," Pergamon Press, New York, 1960.

18. Donaldson, D. R., and W. E. Anderson, "Crack Propagation Behaviour of Some Airframe Materials," Crack Propagation Symposium, College of Aeronautics, Cranfield, September 26, 28, 1961.

HISTORY AND RECENT DEVELOPMENTS IN DIRECT ENERGY CONVERSION SYSTEMS

Paul H. Egli
U.S. Naval Research Laboratory
Washington, D.C.

ABSTRACT

Improved power sources and energy conversion systems are an important long range national problem and of immediate military importance. Various direct conversion processes appear promising for the solution of some of these problems. In thermoelectricity, progress in materials has been good, but much remains to be done. Even at this stage a number of valuable thermoelectric devices can be constructed, particularly cooling devices ranging from small modules for temperature control of electronic parts to submarine air conditioning, and small size power generators for various remote locations including long lived satellite missions. Thermionic emission offers light weight power generators for large power supplies for relatively short missions. Magnetohydrodynamics is confronted with imposing problems associated with the high temperature requirements for operation of more than a few minutes duration. Important improvements are in sight, and continued progress is imperative to provide high density power sources for advanced weapon systems. Photoelectric processes show good improvements toward the goals of lower costs and performance in severe environments. Fuel cells offer exciting possibilities for uses ranging from the main power source for submarines to the auxiliary power on short time space missions.

INTRODUCTION

Improved power source and energy conversion systems represent one of the most important long range scientific problems facing the Nation. A rapidly increasing population and an increasing per capita usage of energy, coupled with declining fuel reserves, poses a problem of serious proportions. Space exploration consumes energy at fantastic rates, and the race for space domination will unquestionably be won by the nation which can best provide the energy requirements.

The military services have difficult, immediate problems which require new power systems, and part of the efforts to solve these problems is represented by the research and development program on direct energy conversion.

The military needs for improved power sources can be classified in four general categories. One area of requirement is for Flight Vehicle Auxiliary Power. This includes electric generators for high performance aircraft, power for missile guidance and for satellites. A second area of needs is power sources for Remote Locations. This includes such applications as arctic weather stations, field communications, navigation aids, and deep sea power sources for sonar detection systems. A third area of requirements is for Vehicle Propulsion and Auxiliary Power. This includes land vehicles such as tanks and for ships, particularly submarines. The fourth area of needs is for what might be called Advanced Weapons and includes such things as radiation weapons and ion rockets.

Each of these areas of application requires different characteristics. For flight vehicle auxiliary power sources, the need is for reliability and light weight. The number of watts per pound delivered by the system is more important than efficiency per se. For remote locations, unattended long-lived reliability is the dominating criterion with size, weight, and silence important in some applications. For vehicle propulsion there are a number of requirements including efficiency, size, weight, reliability, freedom from maintenance, performance with a varying load, and silence.

For advanced weapons it is energy density that is the dominating requirement. In some instances a power source substantially better than anything on the horizon must be developed for the weapon system to become practical.

The current Energy Conversion program is concerned primarily with better ways of utilizing nuclear energy. For any particular application, however, it is necessary to consider each possible combination of primary energy source and conversion process. Concerning the development of sources of energy, nothing can be done about solar energy except to design more efficient collectors. Chemical energy as a source of heat deserves more attention than it is now receiving. Data concerning the heat generated from exotic fuels will presumably be collected from the program on rocket propulsion. Regardless of the fuel, however, the nature of direct conversion devices requires combustion chambers with uniform temperatures. More attention should be directed toward this problem by exploring such avenues as catalytic burning of conventional fuels. Concerning electro-chemical power sources, a substantial development program has recently been launched. It is reasonable to expect substantial improvements in battery reliability within the next two or three years and appreciable improvement in energy density within the decade. Concerning nuclear energy, the need for increased availability of isotopes and for improved high temperature reactor designs will be discussed in connection with the individual conversion processes.

The Conversion Systems are discussed under five headings of which four are direct conversion processes. That is, they do not employ a working fluid which produces mechanical work which in turn must be converted to electricity. Before describing the individual processes, it is appropriate to note that with some exceptions with respect to magnetohydrodynamics, all of the advanced conversion processes have a number of characteristics in common. Some of these characteristics are advantages and some create problems that must be solved in order to use these power sources effectively. (1) All produce Direct Current at low voltage. Compact, efficient power systems thus require the development of improved DC to AC inverters and AC to DC converters.

(2) Part load efficiency poses a problem which requires the development of improved regulation systems. (3) All of the direct conversion processes are static so that the power sources will be relatively silent. (4) A generator of any substantial size will be composed of a large number of small modules. The redundancy of many small elements and the absence of moving parts is the basis for expecting low maintenance, long-lived reliability. (5) Finally, the efficiency is essentially independent of size, and this has several important implications. Compact power plants can be built without the loss of efficiency that is inevitable with mechanical devices. There is thus no advantage to distribution from central generators; individual generators can be installed at the site where the power is needed. Recognition of these characteristics and solutions to these common problems will have a large bearing on the success of direct conversion power sources; and additional attention should be directed toward these problems.

THERMOELECTRICITY

Thermoelectricity has a long history. It was discovered in 1822, and efficiencies as high as 3% could be obtained in 1850. This was a higher efficiency than was obtained by the steam engines of that day. The scientists involved took a wrong turn, however, and no further progress was made, except that thermocouples have been widely used to measure temperature. The process is superficially very simple. Heat forces an electric current to flow from the hot to the cold end of any conductive material just as an electric current carries along some heat as it moves through a conductor. Thus, the same process can be adapted for use either as a power generator or as a heat pump to produce refrigeration, and both applications appear promising.

The first problem has been and is to develop efficient materials, and nearly all of the effort has been devoted toward this goal. The properties that are necessary represent a compromise between a number of conflicting requirements. Higher voltages are developed by insulator materials with a small number of free electrons. High conductivity is required, however, so that the current developed is not

dissipated in resistance heating. And finally a low thermal conduction by lattice vibrations is necessary to minimize the flow of heat which produces no work. The materials which best meet these qualifications are intermediate between semiconductors and semi-metals and extensive efforts have been made to develop guide-lines which help predict the most likely chemical compounds. The problem is complicated by the fact that no single material can be expected to operate well over a wide temperature range. Since a wide temperature range is required for a reasonable Carnot efficiency, several materials must be used in a single couple.

Details of materials developments are discussed in a subsequent paper by Rosi. Briefly, progress has been encouraging. A summary of some of the newer materials is given in Figures 1 and 2. Among other materials developed even more recently are the silicon-germanium alloys by Abeles at RCA and bismuth-antimony for cooling at cryogenic temperatures by Wolfe at Bell Telephone Laboratories.

Much remains to be done in materials research, however. Some of the most obvious of fundamental approaches have received very little attention. Little has been done for example toward learning more about thermal conduction processes. Few serious efforts have been made to determine whether electronic conduction by inner electron shells can be made useful. Inhomogeneous systems remain largely a mystery. Anisotropy in different lattice directions has been overlooked in many systems and semi-metals have been virtually ignored. Until these and other factors are understood, materials research must be regarded as in an early stage. Nevertheless, even with today's materials, a family of useful devices can be achieved.

POWER GENERATION

At this early stage in thermoelectric-hardware development, most of the effort both in commercial and military applications has been directed toward small, special-purpose generators. A generator producing a few watts is highly successful as a power source for remote controls in oil fields, and a generator in the hundred-watt range is being

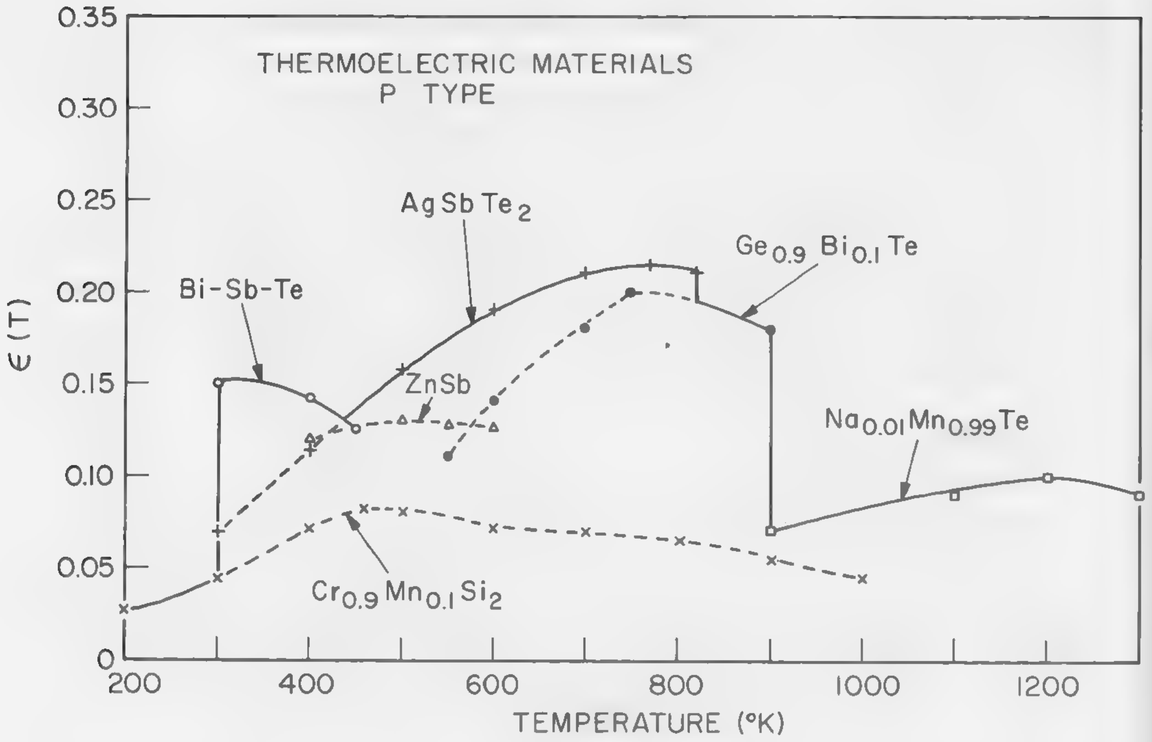


FIGURE 1

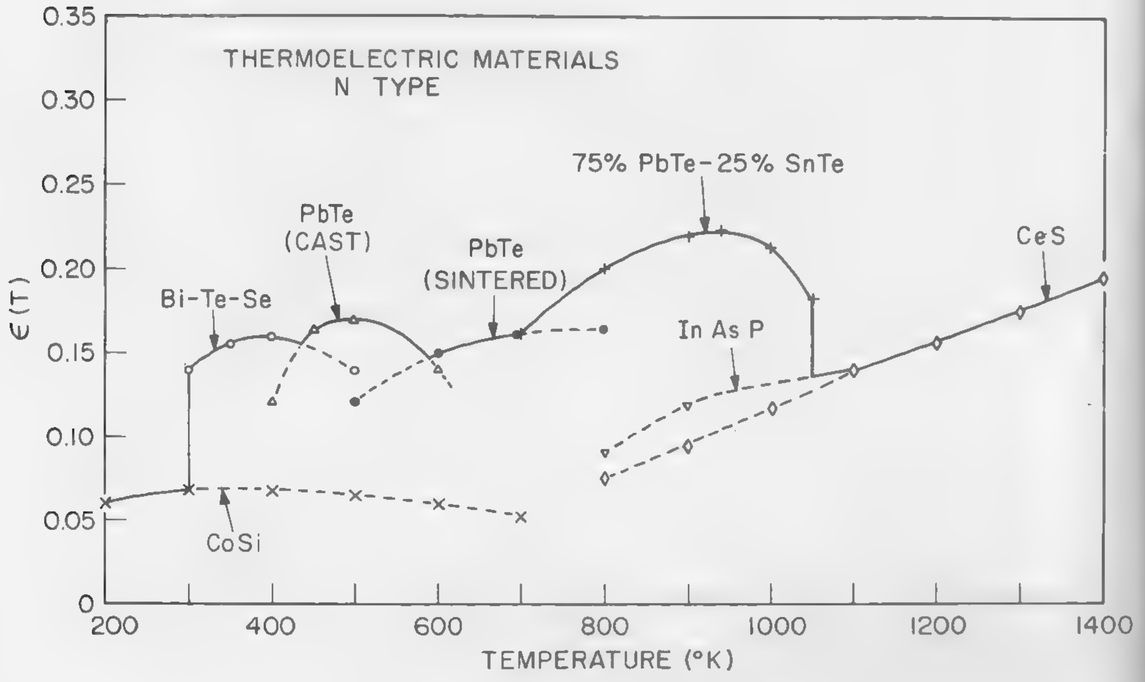


FIGURE 2

employed for cathodic protection of large pipe lines. A military counterpart in this size range is the portable power supply for combat field communications (Figure 3). Two companies have delivered such devices to the Navy; each burns gasoline or propane and produces 250 watts from a package approximately one cubic foot in size and weighing about 40 pounds, exclusive of fuel tanks. A number of smaller generators are nearing completion, some heated by fossile fuel and some by isotopes. Coast Guard buoy lights and arctic weather stations are typical applications. Figure 4 shows a design intended for deep submergence, such as is required for sonobuoys.

Thermoelectric devices promise to be particularly valuable for satellite power supplies. The SNAP program of the AEC is the most familiar effort in this direction, but a number of other approaches deserve attention. Figure 5 shows a design for a thermoelectric panel using unfocused solar radiation. It is much lighter and less expensive than silicon solar cells, but less efficient, and therefore requires a larger area than the silicon cells. Figure 6 shows a similar approach, using a liquid metal circulated by a thermoelectrically driven electromagnetic pump. The energy source can be either a nuclear or collected solar radiation with chemical storage. A somewhat different approach is shown in Figure 7. This system is slightly heavier than the previous one, but it has the advantage that chemical storage could be attached to each individual module, thereby increasing system reliability. For long missions, where reliability is the dominating criterion, a thermoelectric system has no serious competition in sight.

Larger power sources are still in an early stage of engineering. The 100-ekw unit shown in Figure 8 could be started immediately, with a high probability of achieving a long-lived, unattended power source for deep-submergence applications. Reactors with higher energy density and with liquid-metal heat transfer could reduce the size of this unit and increase power level to kilowatt range. Such units should be seriously considered for outboard engines on conventional submarines or for propelling small deep-sea craft. Ultimately it is hoped to have thermo-electric materials directly in-pile. Early results indicate that the

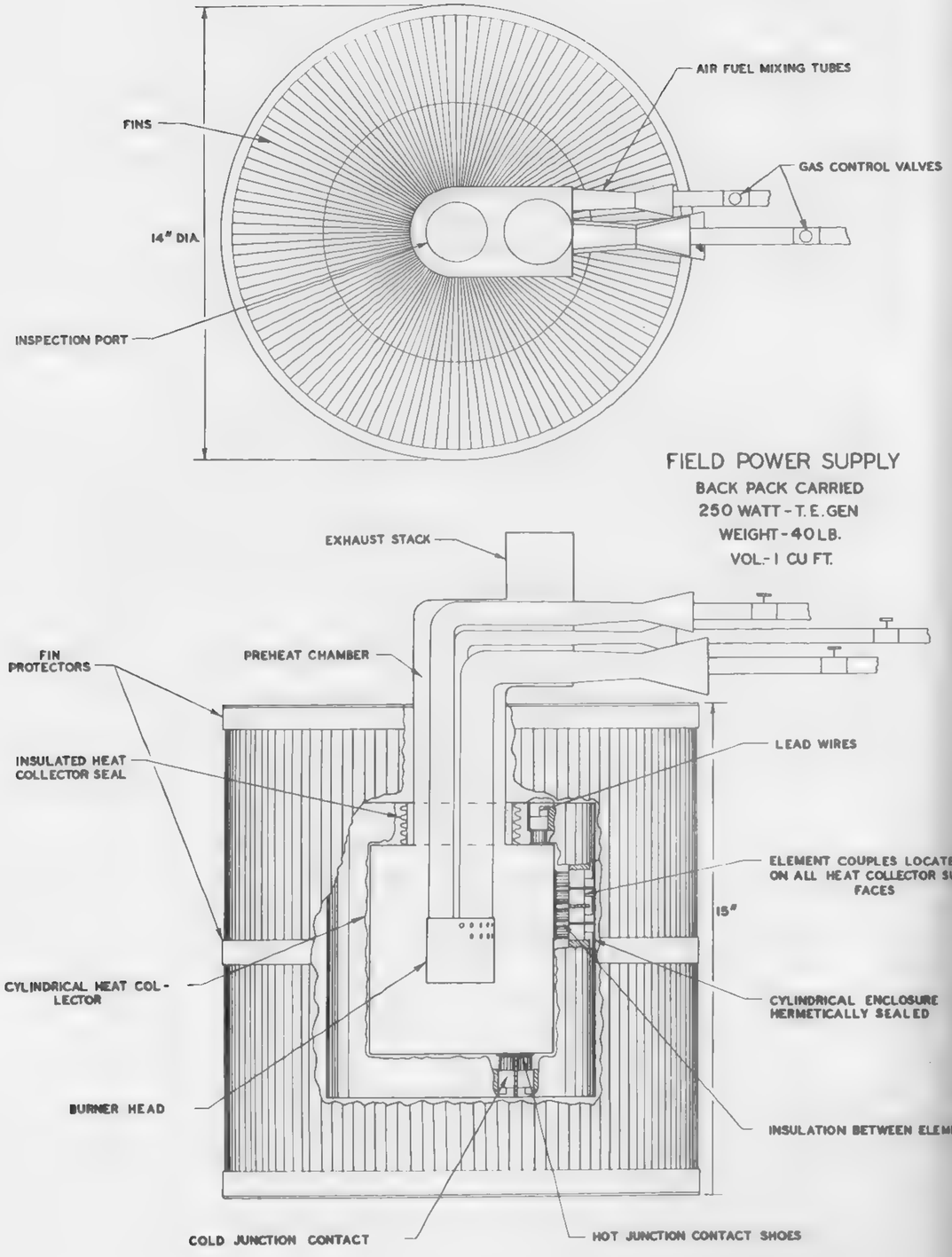


FIGURE 3

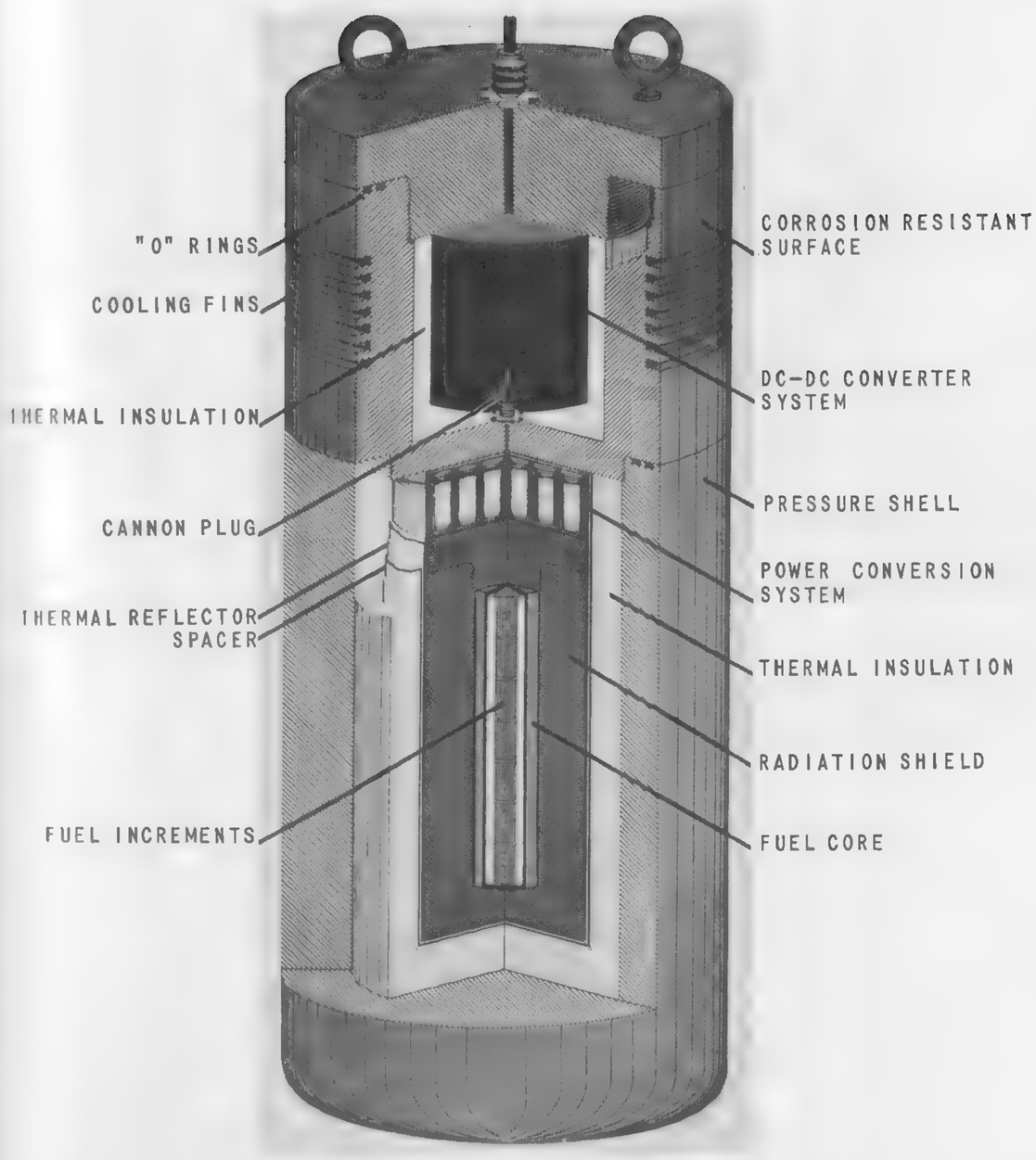


FIGURE 4

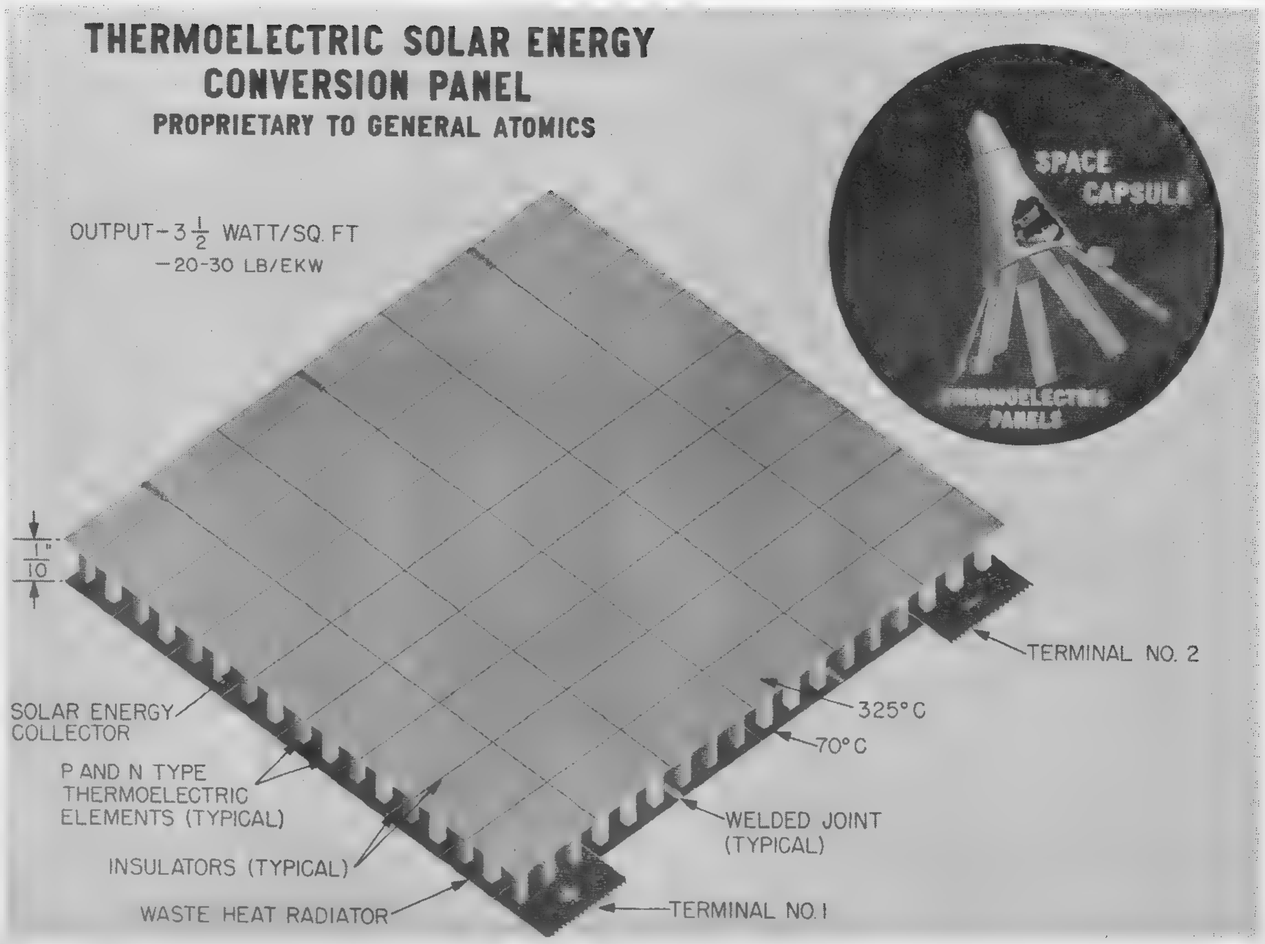


FIGURE 5

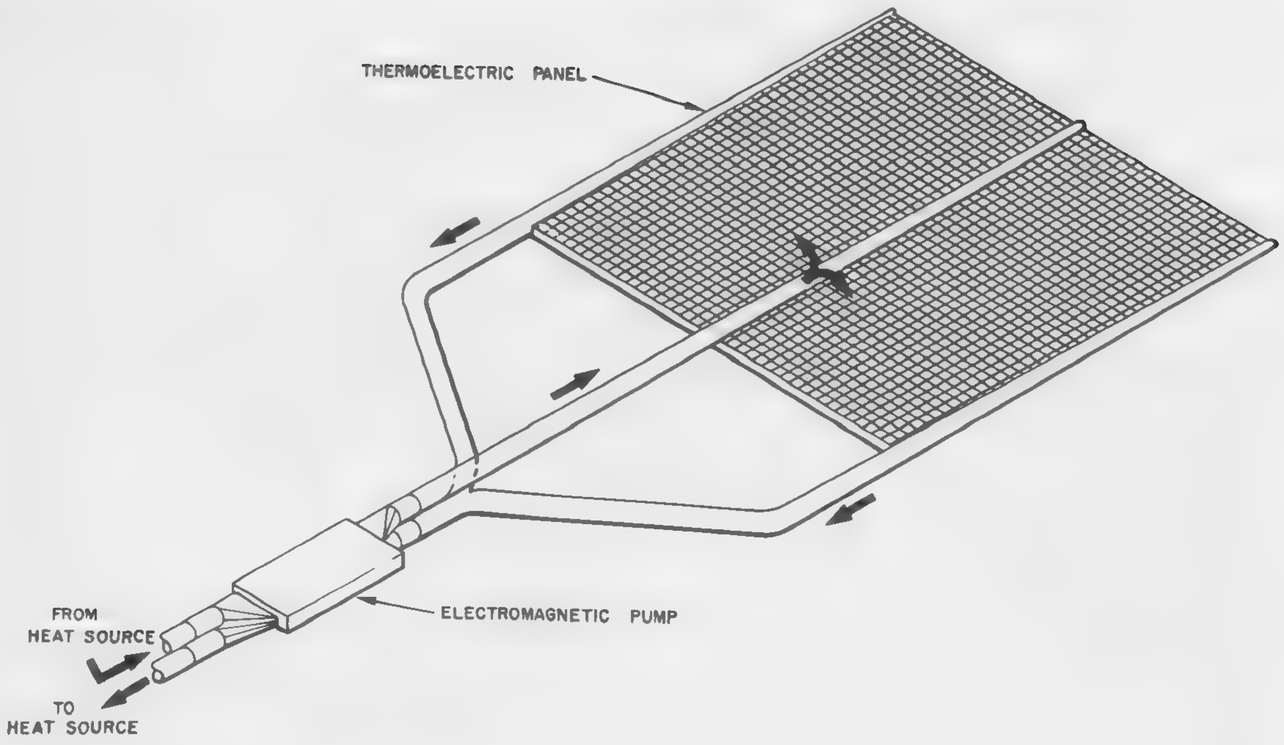


FIGURE 6

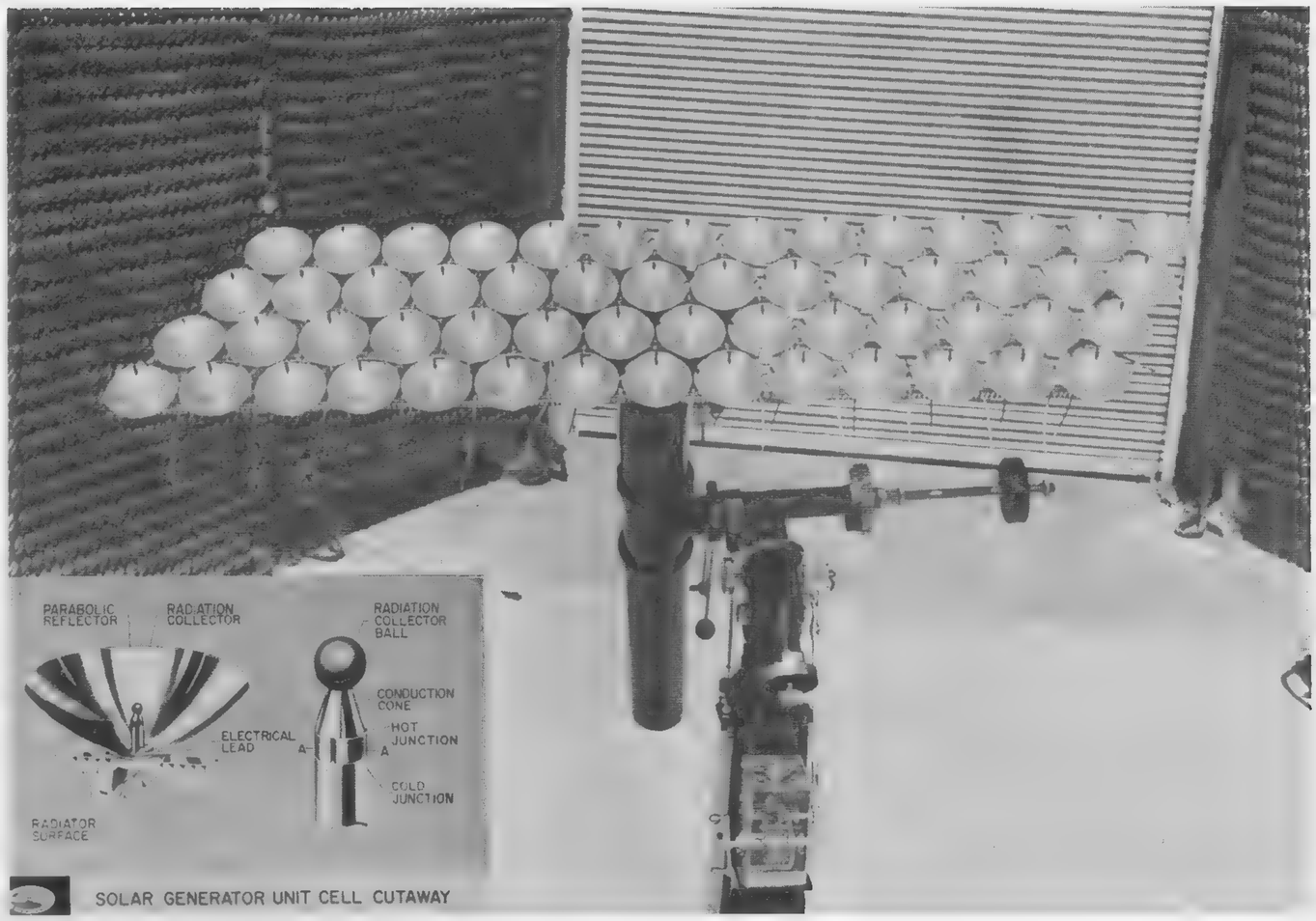


FIGURE 7

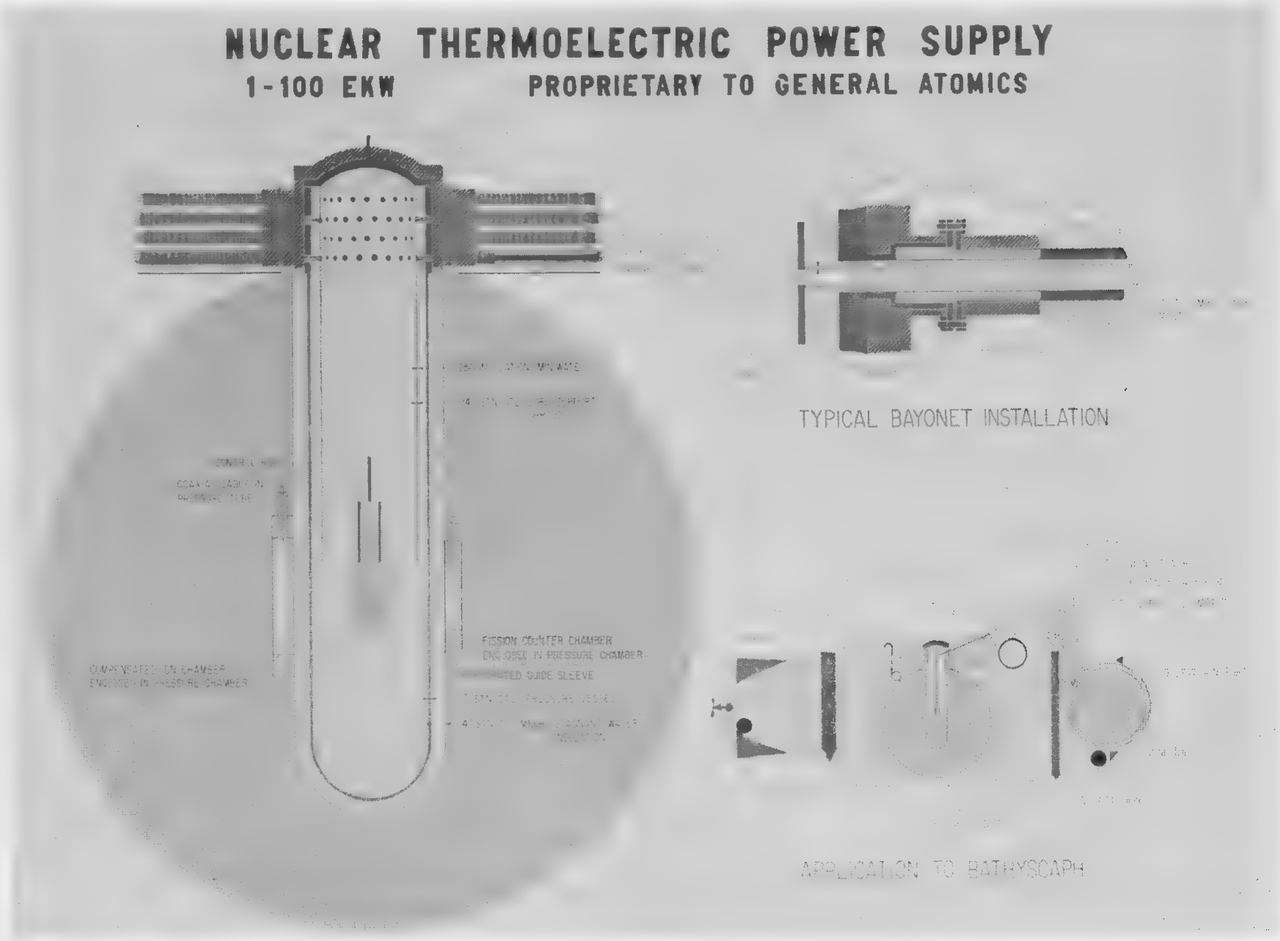


FIGURE 8

materials are not seriously damaged, but a successful system will require a solution to serious engineering problems.

THERMOELECTRIC COOLING

Air-conditioning and refrigeration devices are much further advanced toward shipboard applications than are power generators. For some submarine installations silence, small volume, ease of arrangement in the ship, and low maintenance requirements combine to make thermoelectric cooling technically attractive.

As in power-generating devices, however, small-capacity devices were the first to be successfully developed. A dew-point apparatus, various modules for cooling electronic components, cold traps for vacuum chambers, small cold chambers for laboratory devices, and small beverage coolers for hotel rooms are all commercially available.

Progress is excellent on larger installations. Unlike household refrigerators, which have a variable load and which must operate at times in a high-temperature environment, submarine requirements are reasonably steady, and they are of course in a water-cooled environment. Under these circumstances, thermoelectric units can be made competitive with the efficiency of mechanical systems, or they can compete in installed cost, though at present they cannot achieve both in the same design. Figure 9 shows a cooling module for a reefer box, and Figure 10 shows a section of an air-conditioning unit. Considerable further progress can be expected in reduced costs by perfecting fabrication techniques and by reducing the amount of thermoelectric material as shown in Figure 11. Because the work done depends on the ratio of electrical to thermal energy which moves through the material, the same work can be done by smaller pieces of material, so long as the length-to-cross-section ratio is kept the same. In practice this is limited by electrical contacts, which become an appreciable part of the total resistance, but progress on better contacts is encouraging. The amount of thermoelectric material required for a ton of cooling has been reduced from

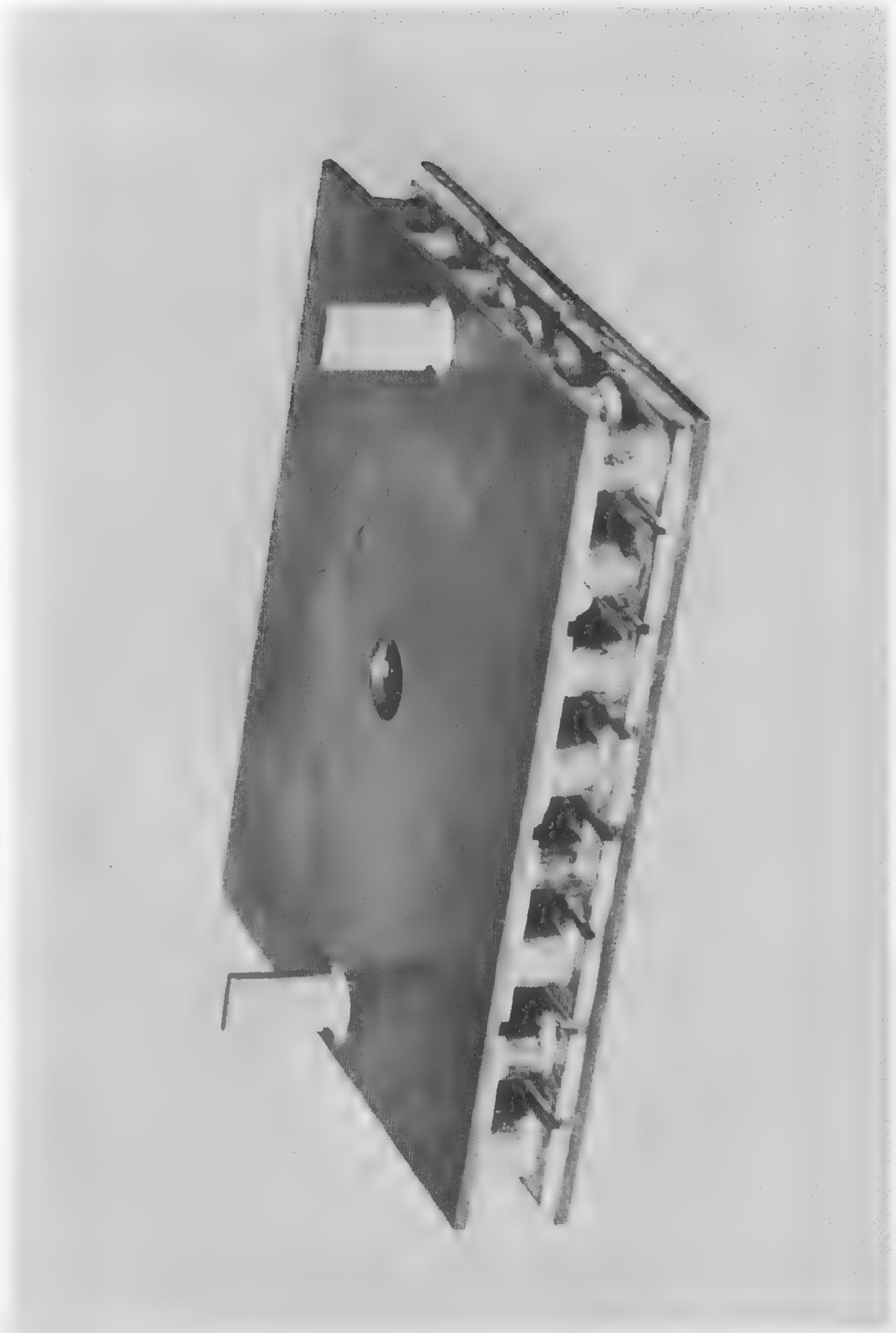


FIGURE 9

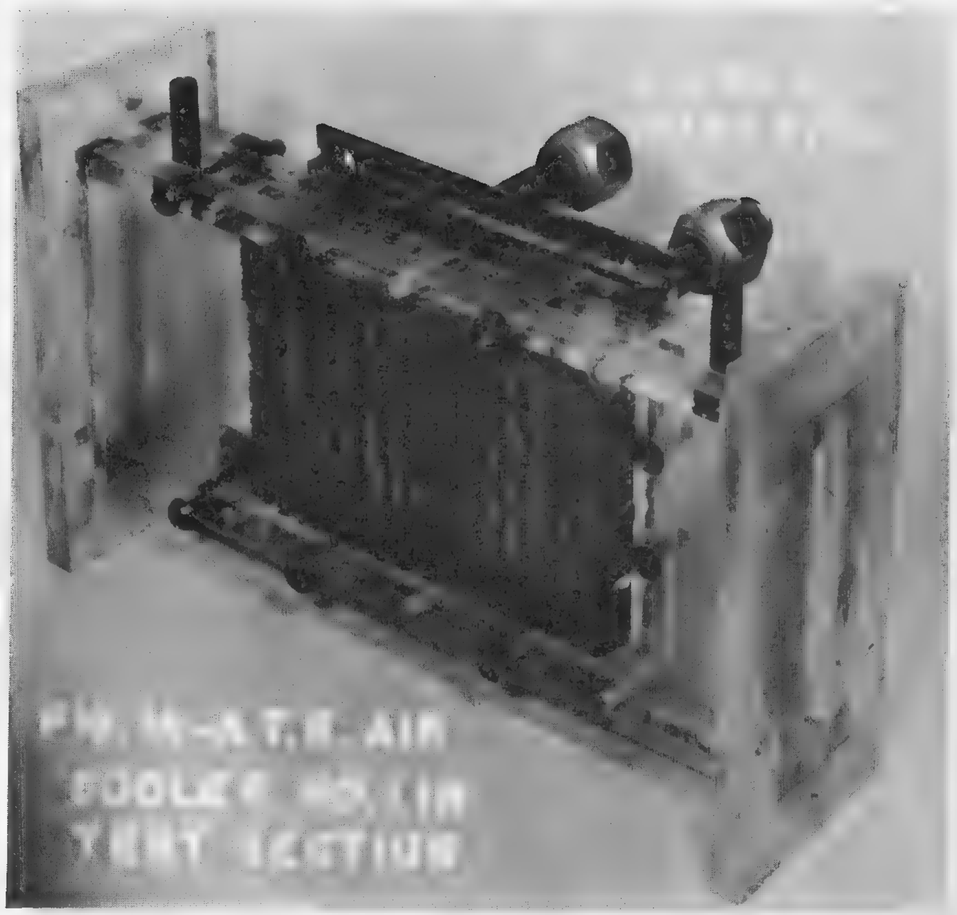


FIGURE 10

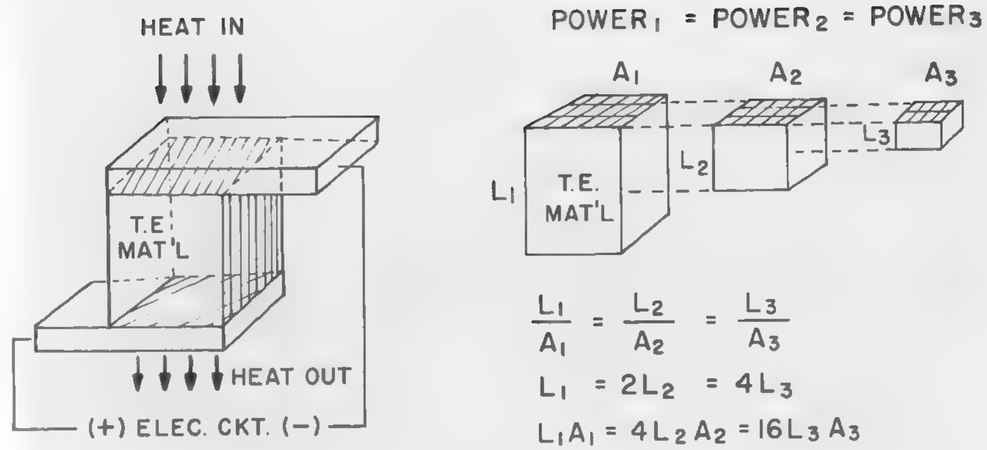


FIGURE 11

60 to 20 pounds, and amounts as low as four pounds per ton of cooling have been reported from laboratory experiments.

At this time it is clear that thermoelectric cooling devices can be highly reliable and maintenance free. Engineering studies indicate technical feasibility, with savings in space. The value of silence will probably result in the adoption of Peltier cooling on submarines within a few years.

HEAT PUMPING

There are a number of applications of thermoelectricity which depend on simultaneous use of cooling at one terminal and heating at the other or on the reversibility of heating and cooling depending on the direction of current flow. An example of the use of reversible heating and cooling is a chamber for controlling the temperature of frequency-control crystals (Figure 12). The availability of Peltier cooling at cryogenic temperatures will solve long-standing, important problems in regulating the temperature of radiation detectors. Food-handling problems for long air missions can be solved by refrigerating until time for use and then heating by simply reversing the current in the same thermocouples (Figure 13).

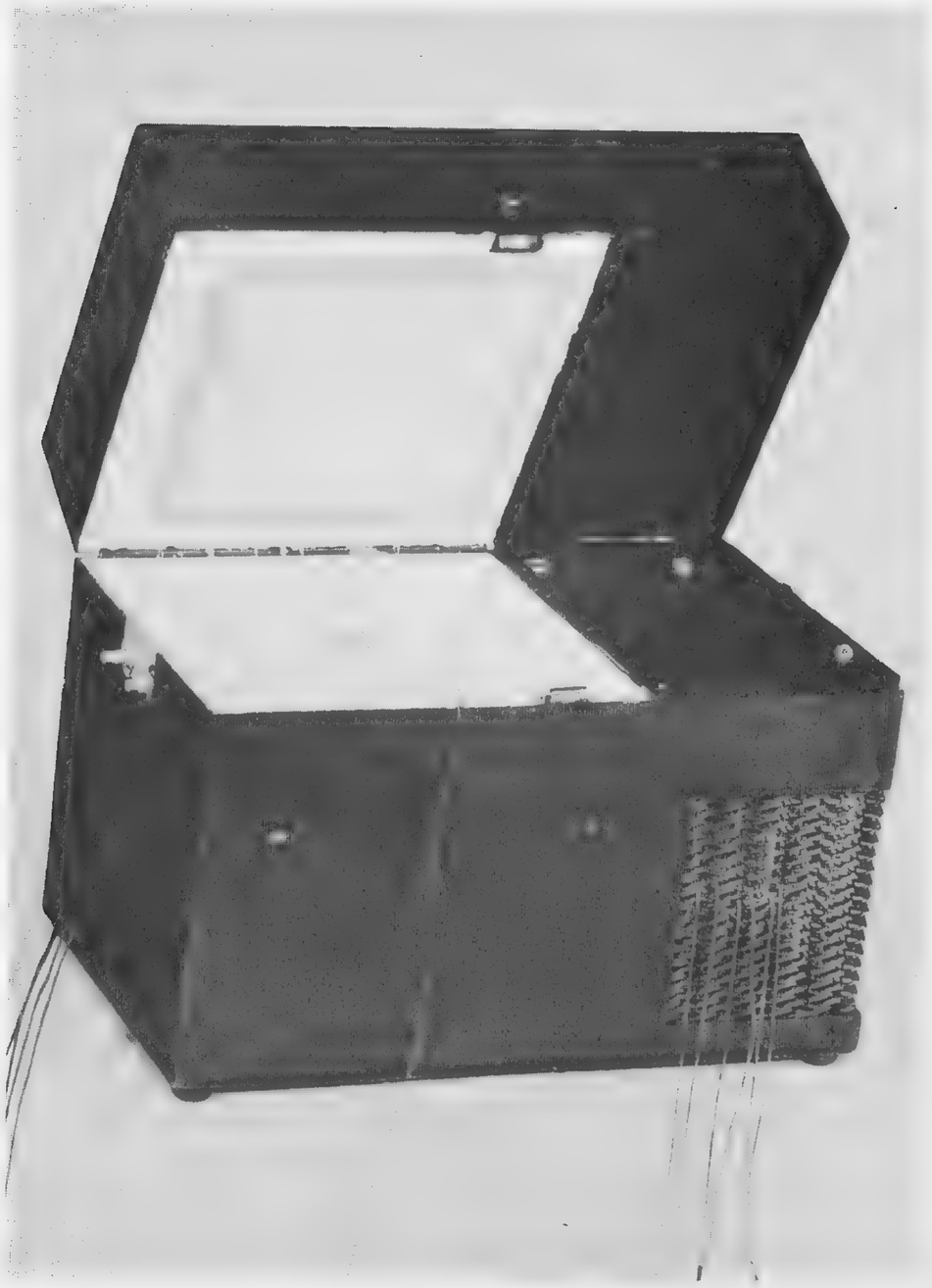


FIGURE 12

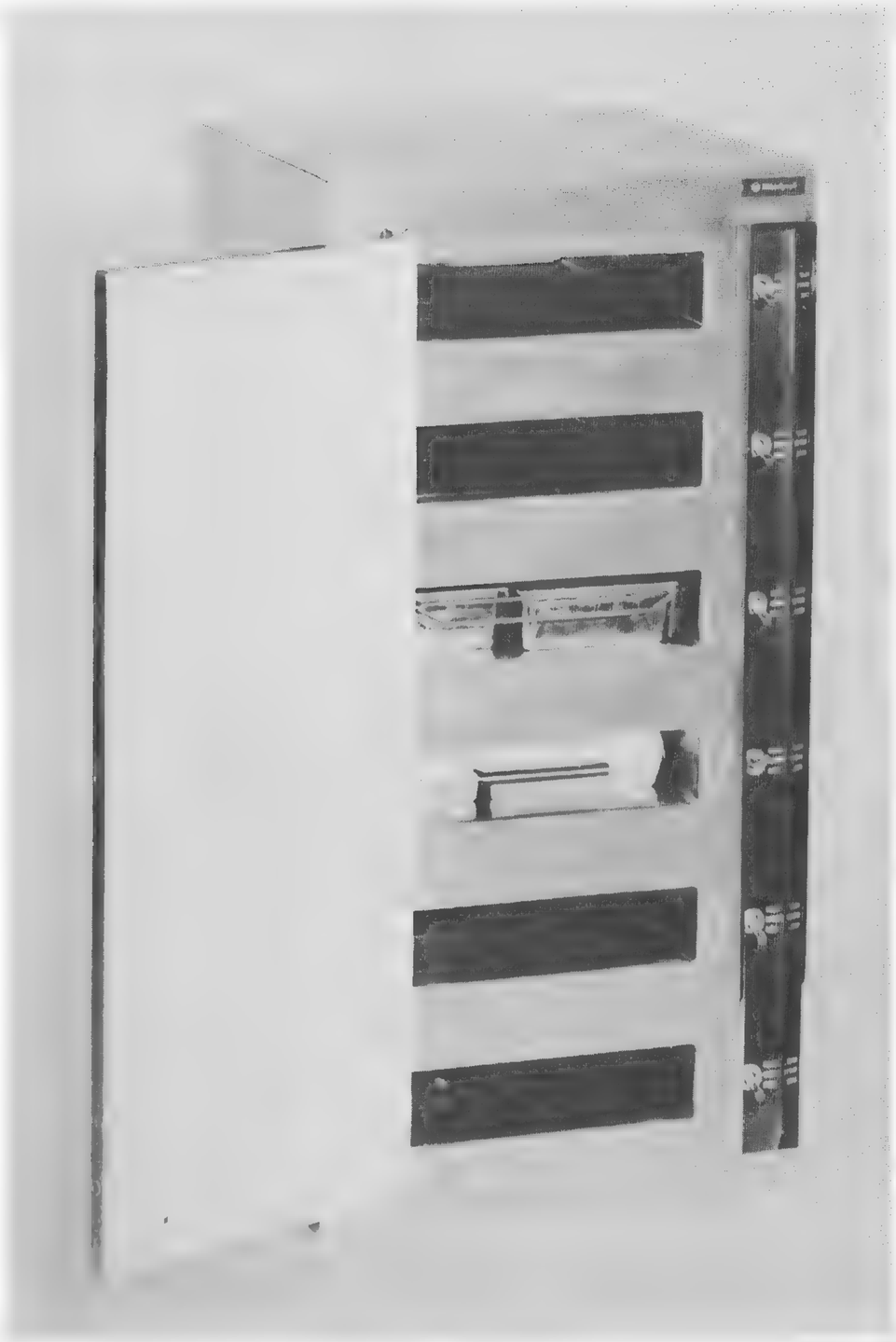


FIGURE 13

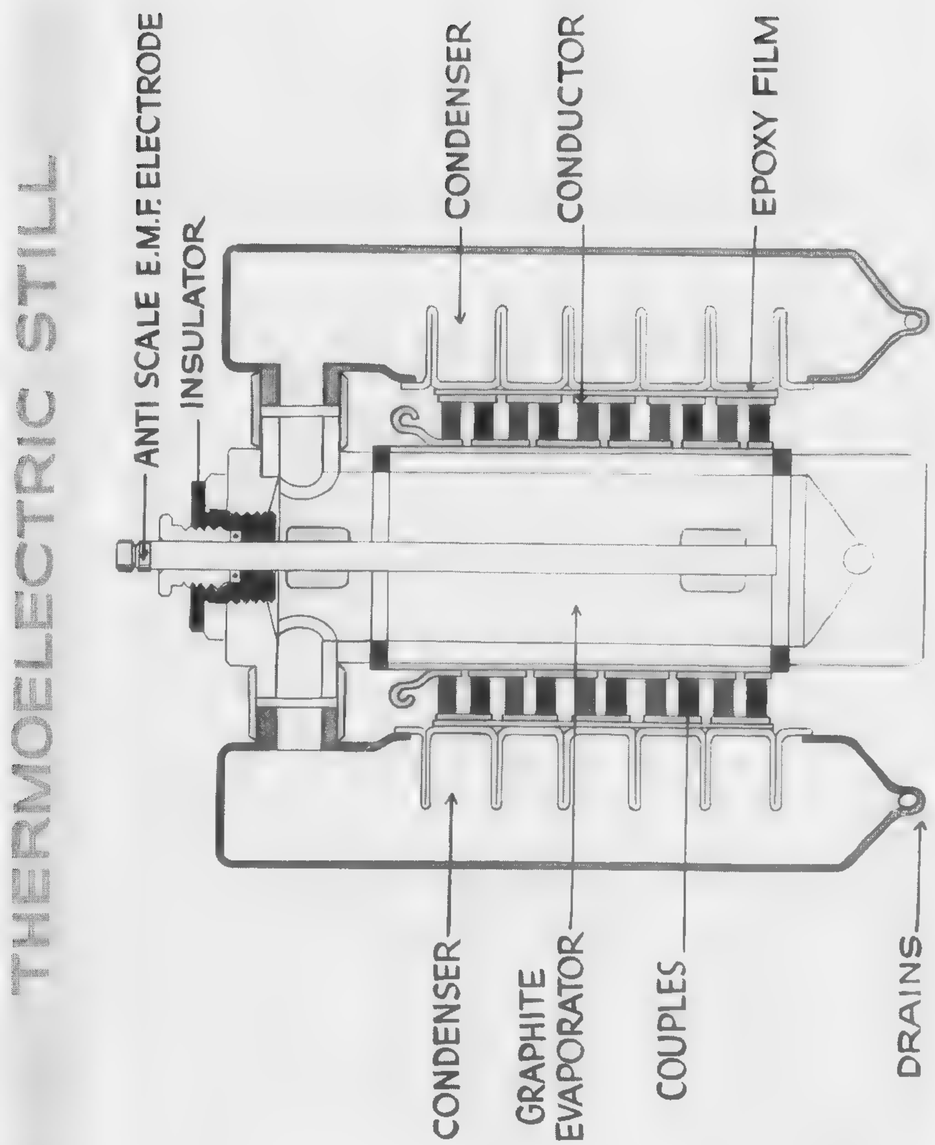


FIGURE 14

An important example of using both the hot and cold ends of a thermocouple simultaneously is in distillation (Figure 14). Liquid is evaporated by the hot side of the thermocouple, and the vapor condensed by the cold side. Again, small units appear practical immediately. A unit designed for water recovery from urine appears to offer the best solution to this problem for space flight. A sea-water-recovery unit with a capacity of a few hundred gallon per day appears feasible for use on small boats or for small remote military posts. Like large-scale air-conditioning, economical large-scale saline-water recovery by this process requires a reduction in the amount of thermoelectric material employed and improved fabrication techniques.

THERMIONIC EMISSION

The thermionic generator is receiving attention for advanced power systems because of the attributes of high power density (approximately 10 watts/cm^2), simplicity of operation (no moving parts) and high temperature heat rejection (up to 1000°C) which implies a small radiator.

The fundamentals of thermionic power generation are straightforward; a cathode is heated to incandescence and gives off electrons by thermionic emission, a colder anode is set opposing the cathode to collect the emitted current, and in most instances a plasma producing gas is introduced in the interspace which ionizes upon contact with the hot cathode and reduces the space charge effect. Several generators have now emerged from laboratory studies, differing in technical detail and operating range, but all operating on the same basic principle of thermionic emission. These may be listed as:

(1) Vacuum Cell. In this generator space charge neutralization is achieved by reducing the space below the point where space charge limited current exceeds saturated emission current. The required spacing depends on the design point of operation (power density, work function, temperature) but is considerably less than 0.001 in. for high performance. Both cathode and anode work functions are

predetermined by preparation of the electrode surfaces (e. g. oxide coating). Low surface work functions and spacing neutralization allow the generator to be operated at low cathode temperatures (approximately 1100°C). The principal life determinants are warpage tolerances for the electrodes, which must clearly be less than the spacing, and poisoning of the anode by material emission from the hotter cathode.

(2) Low Temperature Plasma Cell. In this generator space charge neutralization is achieved by the maintenance of the appropriate positive ion density usually cesium in the interelectrode region. The requirement of operating at low cathode temperatures (approximately 1200°C) means that ion generation does not automatically occur at the cathode surface. Hence auxiliary ion production methods are employed. One is to use a third electrode which is usually hotter and of higher work function than the cathode. Also, the third electrode must be biased so that its surface potential is nearly equal to the electrostatic potential of the plasma. Another proposed mode of operation is to operate at such a point that discharge (ion-multiplication) occurs in the plasma region. The cathode work function can be maintained by cesium wetting or by intrinsic preparation (such as by using a dispenser cathode). Spacing and gas pressure requirements are not fully determined.

(3) Refractory Metal Plasma Cell. The cathode is a refractory metal such as W, Ta, Mo or Re. The work function of both cathode and anode are determined by cesium coating, hence the term "wet cell." The operating temperature is sufficiently high (approximately 1600°C) that ion generation occurs at the cathode surface. Generally the work function corresponding to near-monolayer of cesium is 1.8V, while the completely uncoated refractory metal surface is about 4.0V. The cesium pressure and cathode temperature must be simultaneously adjusted to give appropriate ion generation (high work function requirement) and electron current density (low work function requirement). A work function intermediate between 1.8V and 4.0V is selected to give the correct balance; ion current density equals 1/500 electron current density. Such requirements dictate a high cesium

pressure, and as a consequence, close spacings are required to reduce electron scattering effects in plasma. Spacing requirements are typically 0.010 in. or less. If driven to the extreme case (high pressure, close spacing) spacing neutralization would occur, and the role of the cesium would be solely to coat both surfaces. Present limitations to performance is the ceiling placed on cathode operating temperature caused by cesium evaporation from the cathode.

(4) Carbide Cesium Cell. Space charge neutralization is caused by ion generation by the high temperature (approximately 1800°C) cathode. The anode work function is maintained by cesium wetting. The cathode work function (approximately 3.0V) is an intrinsic property of the cathode material. Hence the cesium pressure is dictated by the plasma ion density requirement rather than by the cathode work function requirement. Spacings are consequently greater than in the wet cathode cell. The cathode temperature limit is set by the cathode material emission, since the work function is intrinsic. Cathode sublimation is the determinant of cell performance and life, and excellent progress in stabilizing these materials promises several thousand hours of operation.

Small experimental thermionic generators have been operated in the laboratories at 10 to 15% over-all efficiency at current densities. It is expected that efficiencies of 25% or higher will be achieved in the laboratory in the next few years. Despite irresponsible claims, however, there are serious problems associated with the high temperature required for efficient operation before reliable, long lived hardware will be achieved.

Cathode stability is one obvious limitation. Figure 15 summarizes existing information on materials instability under various emission conditions. Relating this to the various modes of cell operation previously described, it becomes obvious that a high performance life over 1000 hrs. will be difficult to achieve by any of the approaches. Cesium corrosion of leads, seals and insulators is another area of concern, and this has stimulated work on other plasmas.

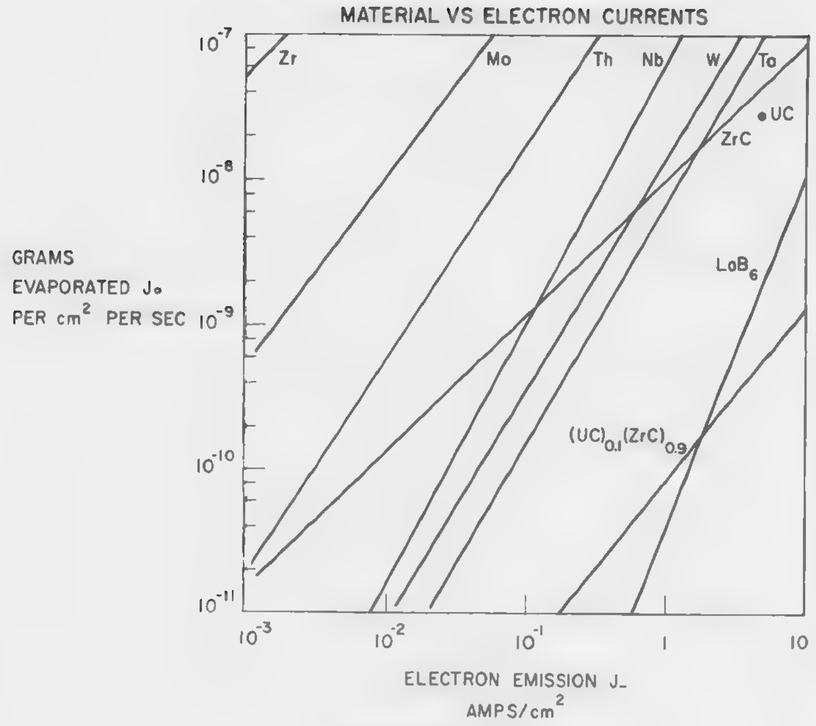


FIGURE 15

Aside from the converter, the heat source and storage systems necessary with solar energy present difficult problems. Solar collectors for temperatures above 1000°C require precision optics. Reactors which provide both high temperature and high energy density present another host of difficult problems. Even when the basic capability of constructing such reactors has been demonstrated, problems such as homogeneous temperature will remain difficult. All of these considerations make it appear that efficient long lived diodes are several years away. The weight and size advantage for large power supplies, however, makes it imperative that these problems be solved. A feasibility study of a solar heated diode system extrapolated from laboratory results indicated a system weight of 7.5 lb. per ekw. A similar study for thermionic cells in a reactor gave even more optimistic results. Figure 16 shows weights as low as 4.2 lb/ekw for the entire system, and the radiator area in the same study was 300 sq. ft. using two sides of the radiator. Even more impressive is the fact that weight remains below 8 lb/ekw for rather poor performance (5 watts/cm^2 at 6% efficiency). The situation improves still further for larger systems.

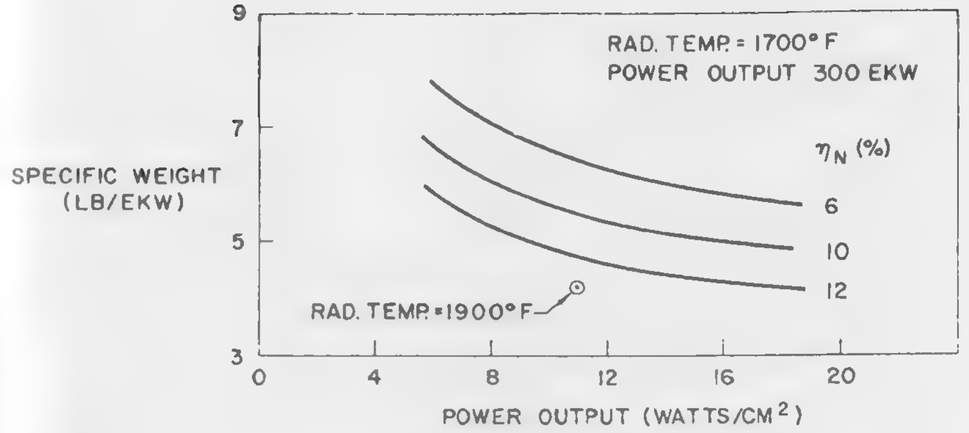


FIGURE 16

For short missions requiring large amounts of power (100 to 10,000 ekw) thermionic emission should receive immediate consideration. Moreover, recent encouraging results with new plasmas and new configurations which promise to ease the materials problem indicate a good possibility for long-lived applications within a few years. When this stage is reached, combined thermionic, thermoelectric systems will offer a wide range of design characteristics suitable for nearly all space auxiliary power requirements.

MAGNETOHYDRODYNAMICS

The final heat conversion process which is receiving any serious attention is magnetohydrodynamics, though in this instance there is more effort directed toward application as a propulsion device than as a source of electrical power. Conceptually an MHD generator is simply an electromagnetic generator in which the metal conductors of the armature are replaced by a stream of ionized gas. In its most simple form an MHD generator consists of a channel through which one passes a stream of electrically conducting gas with the top and bottom surfaces of the channel serving as magnet faces and the two sides as electrodes. Passage of the conducting gas through the transverse magnetic field

induces an electric field between the electrodes (electrons and ions move in opposite directions) and induces a current to flow in an external circuit (Figure 17). The current then reacts back on the gas flow to produce a force equal to the product of the current and the magnetic field.

The attractive feature is a high energy density and high efficiency since the turbine and generator are combined. The problem is to get a sufficiently conductive gas; the best efforts are likely to be a factor of a million short of copper wire.

To achieve any useful conductivity the temperature and pressure must be very high. A potassium seeded noble gas is generally used and must be at 2500 to 5000°K. This imposes horrendous material problems, and tricks like cooled electrodes introduce losses. Particularly difficult to imagine are the necessary high temperature magnetic materials.

The pressure-flow requirements of the hot gas stream are illustrated by the fact that the Atlas booster jet is just barely adequate to combine acceptable Mach numbers and static temperatures.

The system can only be large to support the losses and to avoid hydrodynamic problems. A ten-foot long tube, one foot in diameter is about minimum for one set of plasma conditions, but it might produce as much as 90 megawatts.

More elaborate configurations such as those shown at the bottom of Figure 17 offer some advantages but do not reduce the problems orders of magnitudes.

One of the major problems in terms of both cost and weight of an MHD device is the large field coil necessary to generate tens of thousands of gauss across a large channel. With the advent of superconducting coils, this problem can be vastly reduced.

To eliminate the difficulties inherent in high temperature requires a low temperature plasma. Some help in this direction, though with attendant costs in terms of expensive power supplies can be achieved with non-thermal ionizing processes such as with rf fields. What is hoped

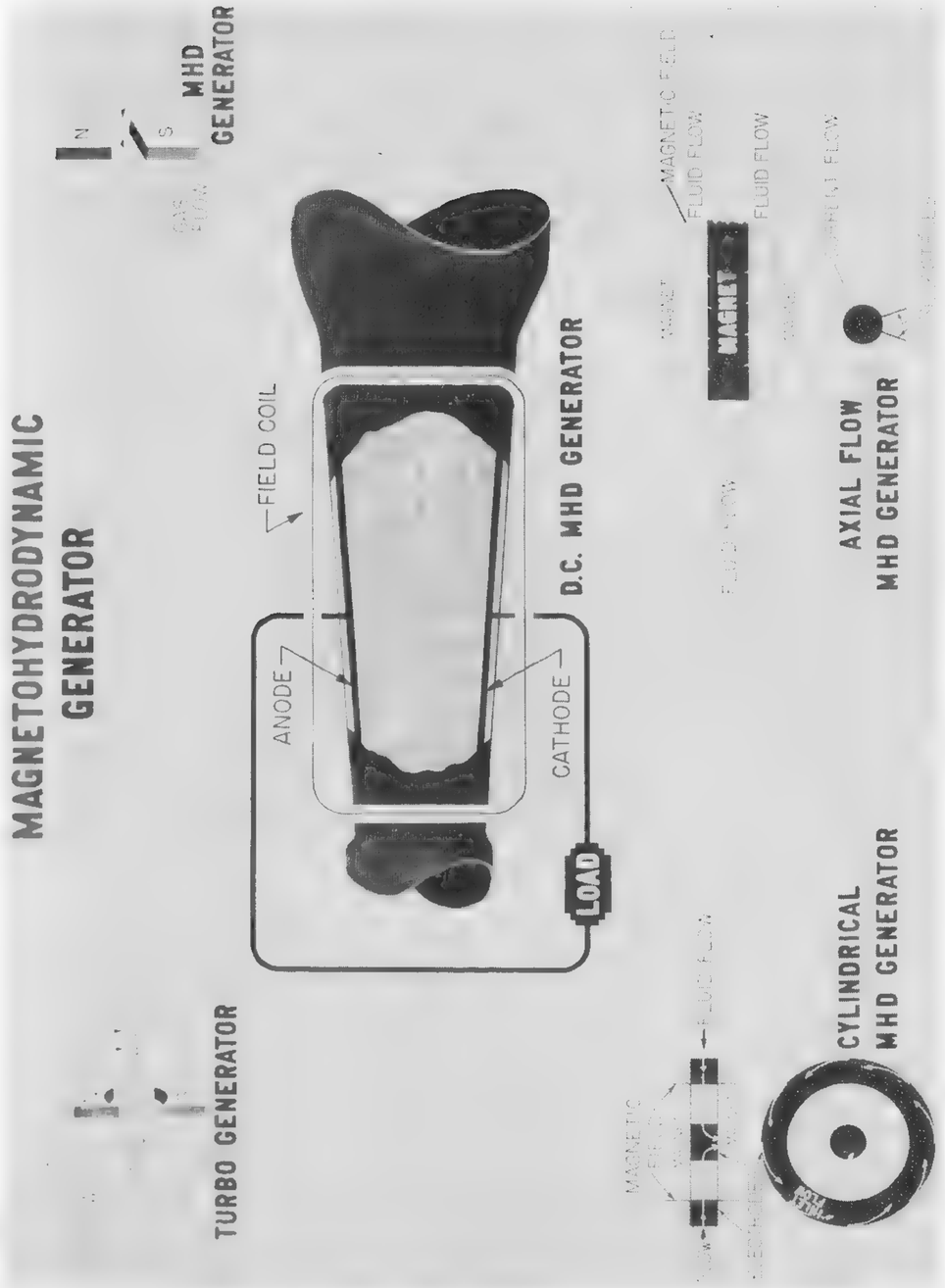


FIGURE 17

for is a stable, low temperature thermally ionized plasma and progress in this direction has been reported. Naiditch has achieved seven second stability with a complex sodium-ammonia plasma and believes that this can be improved by higher purity gases. Developments of this kind could make MHD attractive for many applications. Even the present short lived capability is likely to be important for military applications, and research should be vigorously pursued on this process as a possible power supply for advanced weapons systems requiring huge amounts of power from a small generator.

PHOTOELECTRIC PROCESSES

In this category are considered two energy conversion processes, one is that using the photovoltaic effect (solar cells) and the other is the photoelectric effect where electrons are emitted from a surface into the vacuum where they are collected by a transparent electrode. Both of these conversion techniques are quantum devices where individual photons from the sun (or other light source or radioactive material) cause quantum transitions in a metal or semiconductor to release charge carriers for electrical current flow in an external circuit. These are to be contrasted to the thermionic and thermoelectric devices which are heat engines. This report will be concerned chiefly with solar cells but a few remarks will also be made concerning true photoelectric devices at the end of the discussion.

Solar cells are the most highly developed of the direct energy conversion devices today. The most familiar form is a very perfect silicon crystal which is treated with traces of impurities that introduce extra positive and negative charges on the two sides of a thin wafer. These extra charges remain on their respective sides of the junction until light energy strikes the crystal. This radiant energy further disturbs the electrical balance of charges and starts them moving toward the surfaces and the junction. The current flow continues as long as light strikes the crystal.

The physics of this process is reasonably well understood. Theory tells us that as much as 25% of the incident radiation

can be converted to electricity, and under special conditions possibly as much as 40%. The best now reported from the laboratory is 14%, and substantial production quantities can be obtained that give a 10% conversion efficiency. The cells are reliable and operate with no loss in efficiency until damaged by meteorites or by high energy radiation.

Recent data on radiation damage has occasioned considerable alarm. An exposure of 10^{10} protons reduces the output of solar cells by 25%, and this may occur in as little as ten days in the peak fields of the Van Allen belt. Satellites in high orbits may therefore need to carry excessive shielding or turn to other power supplies. For most low orbits, this problem does not appear serious, and present solar cell designs are adequate. They are limited to small power supplies, however, because of their weight. Bare cells produce only 3 w per pound. In a satellite, they must be distributed over the surface of a free tumbling sphere, or a mechanism must be provided to keep them pointed toward the sun. Generally the cells are used as battery chargers and the batteries are inherently heavy so that the total system weight becomes excessive for large power supplies.

As large power supplies for ground stations, solar cells have the dual problem of size and cost. For example, a 10 kw generator suitable for a modern home power supply would occupy 100 sq. yd. and cost $2 million dollars.

Concerning the prospects of a solution to the problems posed by these various limitations, the situation is rather encouraging. For operating at higher temperatures such as required for light concentrating systems or for satellite missions near the sun, semiconductors with higher energy gaps are being developed. Where silicon at 100°C has a 50% reduced output from its 0°C value, gallium arsenide is reduced only 20% and gallium phosphide would suffer even less. Gallium arsenide cells of 8 or 9% efficiency are available, and good progress is reported on improved gallium phosphide.

One approach to the cost and weight problem has been various schemes for producing large area then layers of silicon in the form of films or embedded particles. In

general, the efficiency of these arrays was reduced to the point where other approaches such as the thermoelectric panels became competitive. More promising is the work on cadmium sulfide films. Efficiencies of about 8% have been achieved. Packaged in thin flexible plastic sheets, they appear to offer good performance at a moderate cost. At present terrestial applications are limited by rapid deterioration from water vapor, but vacuum stability appears good for space applications. Deterioration by high energy radiation has not been studied, but because they are majority carrier devices, it is reasonable to expect less damage than to silicon for some types of radiation.

On the basis of these developments together with improved battery reliability, solar cells are likely to remain the best source of power for satellites for many types of missions.

The photoelectric emissive converter has been intriging because it is inherently a large area, light weight, low cost device. Unfortunately, it also appears to be inherently a low efficiency device. In operation one has a photoemissive substance which is directly exposed to sunlight. Electrons are given off and collected by a grid or transparent electrode. It is assumed that the vacuum in outer space would be present so that no evacuated enclosure is required. A load is connected between the photoemitter and the collector and power is developed, thus completing the conversion of the solar radiation directly into electricity.

There are two basic modes of operation of this type of device, one where the emitted electrons are collected by virtue of their initial velocities; in which case, the lowest work function emitter and collector are used. The second mode of operation involves collection by a field produced by a difference in work function between the emitter and the collector. In this case, the lowest work function material is the collector, while the emitter is somewhat higher in work function. The voltage of the device is set by the difference in the work functions which can be 1/2 and 1 volt. In the first mode of operation, the voltage will be of the order of kT as is given by the initial velocity distribution.

The basic limitation of the photoemissive device is its long wavelength threshold. Well over 50% of the solar photons cannot cause the emission of an electron in the best photoemitter. Only 13% of the sun's spectrum in the outer atmosphere would yield a quantum efficiency greater than 10%. The longer wavelengths contribute negligibly. Neglecting other losses, it is obvious that a top conversion efficiency of about 1 to 2% is all that can be achieved. Using the method in mode 1, that of the initial velocities, the efficiency can be shown to be an order of magnitude less with the best emitters.

Much improvement in photoemitter characteristics is not to be expected. This is a field that has been worked over for at least 30 years and progress has been sporadic. The breakthroughs have been due to empirical experimentation rather than that of the basic understanding. The experts in the field do not anticipate the kind of improvement required to give a photoemissive device of even 10% over-all efficiency. Even with more efficient materials, it should be pointed out that many practical problems would exist such as large area--close space geometry, a collector with low light absorption properties, the reduction of series resistance in the surface and collector, etc.

For photoemissive devices to become attractive as power converters appears to require a whole new approach.

FUEL CELLS

Fuel cells offer excellent probabilities for a variety of important military applications and exciting possibilities for widespread commercial applications. Like other areas of the battery field, a bewildering array of chemical reaction systems is being explored. Among primary fuel cells (simple systems in which fuels are fed continuously and converted directly into an electric current) a fairly simple pattern is beginning to emerge. Most of the early work was concerned with hydrogen-oxygen cells and a variety of these cells are at an advanced stage of development. More recently a very large effort has been devoted to direct utilization of hydrocarbon fuels. There was hope that the right combination of catalysts and electrolytes would result in direct rapid

oxidation of hydrocarbons at a low temperature, but this condition has not materialized. The fuel most readily oxidized is hydrogen and consequently the fuel cell with the highest current density at room temperature is the hydrogen-oxygen systems. Next easiest are the soluble hydrocarbons such as alcohols and glycols and reaction rates are reasonable at moderate temperatures. The less reactive petroleum hydrocarbons require higher temperatures to achieve reasonable reaction rates and it is accordingly more difficult to engineer practical fuel cells. On this basis hydrogen-oxygen cells are likely to remain the most simple and efficient fuel cells; with their application limited only by the cost and difficulty of handling the hydrogen. Of the cells that operate near room temperature with a simple alkaline solution as the electrolyte, the most highly developed in this country is the Union Carbide cell, Figure 18. The electrodes are catalysed porous carbon. Typical operation is at 40°C with an output of 0.9 volts per cell and a current density of 50 amperes per square foot. Substantially higher current densities can be obtained with the cell developed by Professor Justi in Germany. The electrodes are a porous nickel structure with two layers of different pore size. Operation at 100 to 200 amperes per square foot for long periods appears to be well within the cells capability, and operation up to 500 amperes per square foot is reported. While these cells are reproducible in the laboratory, engineering problems such as water removal are at an early stage of development.

Efforts to take advantage of faster reaction rates at higher temperatures were initiated by Bacon in England and pursued by Patterson-Moos in this country. Difficulties with the porous nickel electrodes and the problems of maintaining a tight system at temperatures of several hundred degrees and pressures of several hundred pounds have not been solved and the effort has been early abandoned. Pratt and Whitney is exploring performance at less elevated temperatures and pressures with of course, less advantage in performance over room temperature cells.

Hydrogen-oxygen cells operating at high temperatures with molten alkali metal carbonate electrolytes have also been attempted, but the problems of the CO_2 balance and of materials failures have not been solved.

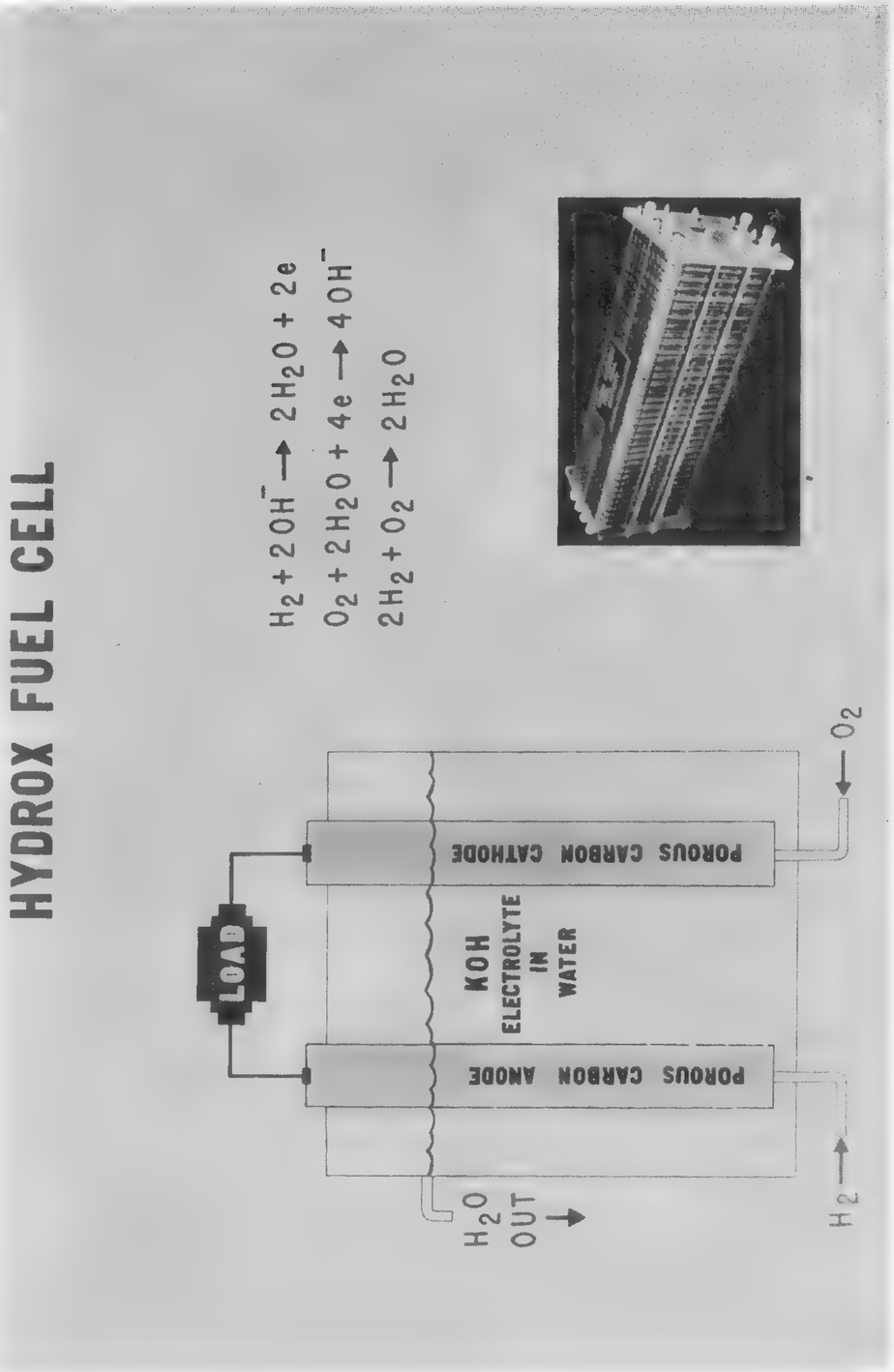


FIGURE 18

A novel approach by General Electric employs an ion exchange membrane instead of the alkaline solution electrolyte. Long-lived operation has been demonstrated at 50 amperes per square foot current density and membranes more resistant to damage at higher current levels have been developed. The absence of a electrolyte solution would appear to be a decisive advantage in a zero gravity space environment.

Substantial effort is now devoted to alcohol consuming cells. The simple approach is to use porous metal electrodes with concentrated alkali solution at slightly elevated temperatures as electrolytes. Methanol can be reduced to CO_2 but the problem of carbonate build-up in the electrolyte limits the operation. Acid electrolytes are under investigation, but so far have not produced good current densities for sustained periods.

Petroleum fuel consuming cells offer even more serious problems in CO_2 removal and corrosion difficulties with molten salt electrolytes. Practical cells by this approach seem many years away. An exciting new possibility for utilizing fossil fuels, possibly even powdered coal, is the use of solid electrolytes. This operates as a concentration cell with oxygen ions transported from the cathode through a porous dielectric which conducts ions but not electrons. The ionized oxygen recombines at the anode to form oxygen gas. A temperature near 1000°C is required for a useful current density but the absence of corrosive fluids minimizes the materials problem.

Another cell that deserves mention is the liquid sodium-oxygen cell developed by Yeager, Figure 19. Although sodium is an expensive fuel, this cell offers the advantage of a higher voltage and higher current density than any other and consumes substantially less oxygen and these are important considerations for applications where the entire fuel supply must be carried.

Closed cycle cells have been explored in a variety of systems. In these cells the reactants are generated by one of several means from the products of the cell reactions, Figure 20. Heat, ionizing radiation, chemical and photo-

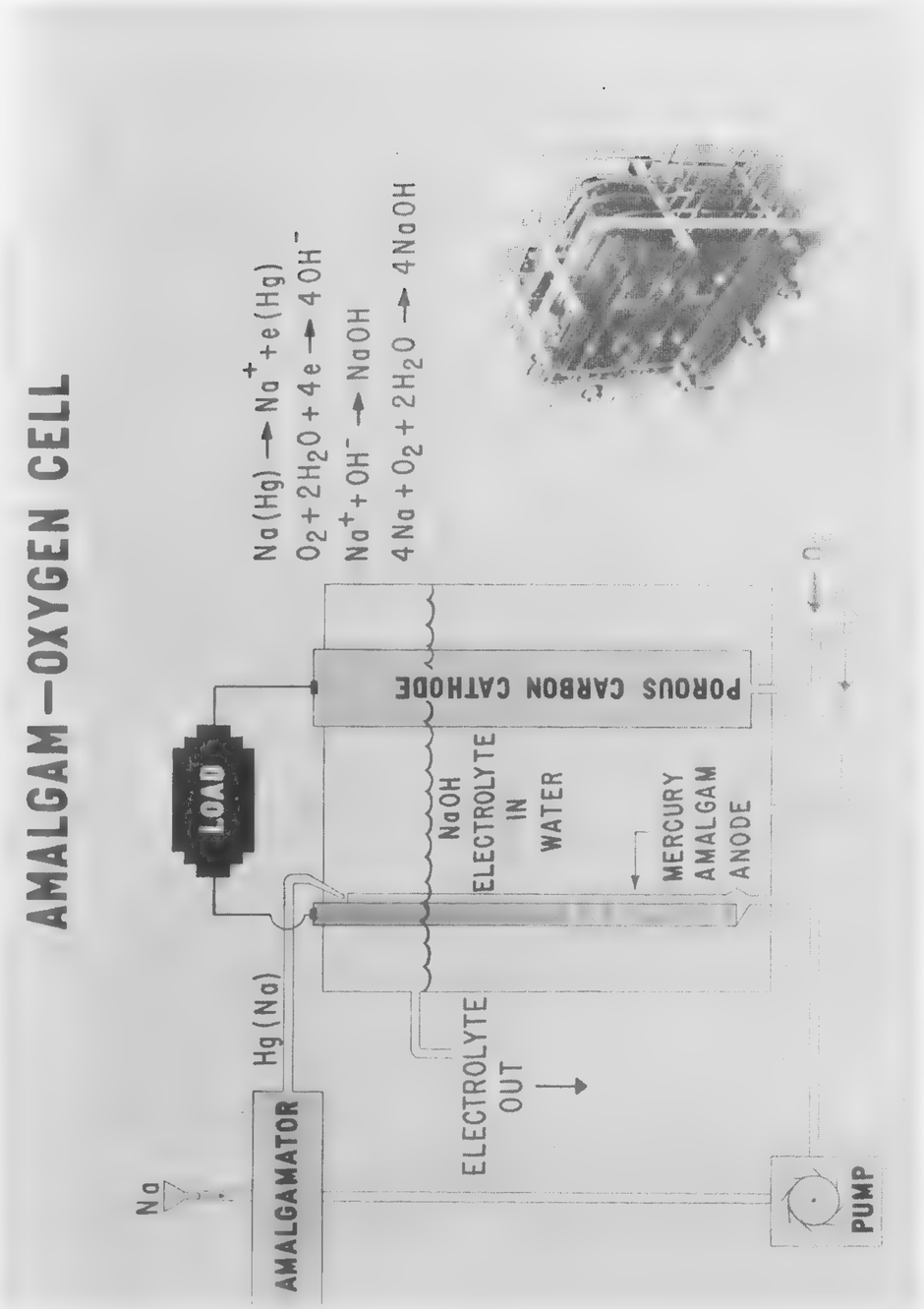


FIGURE 19

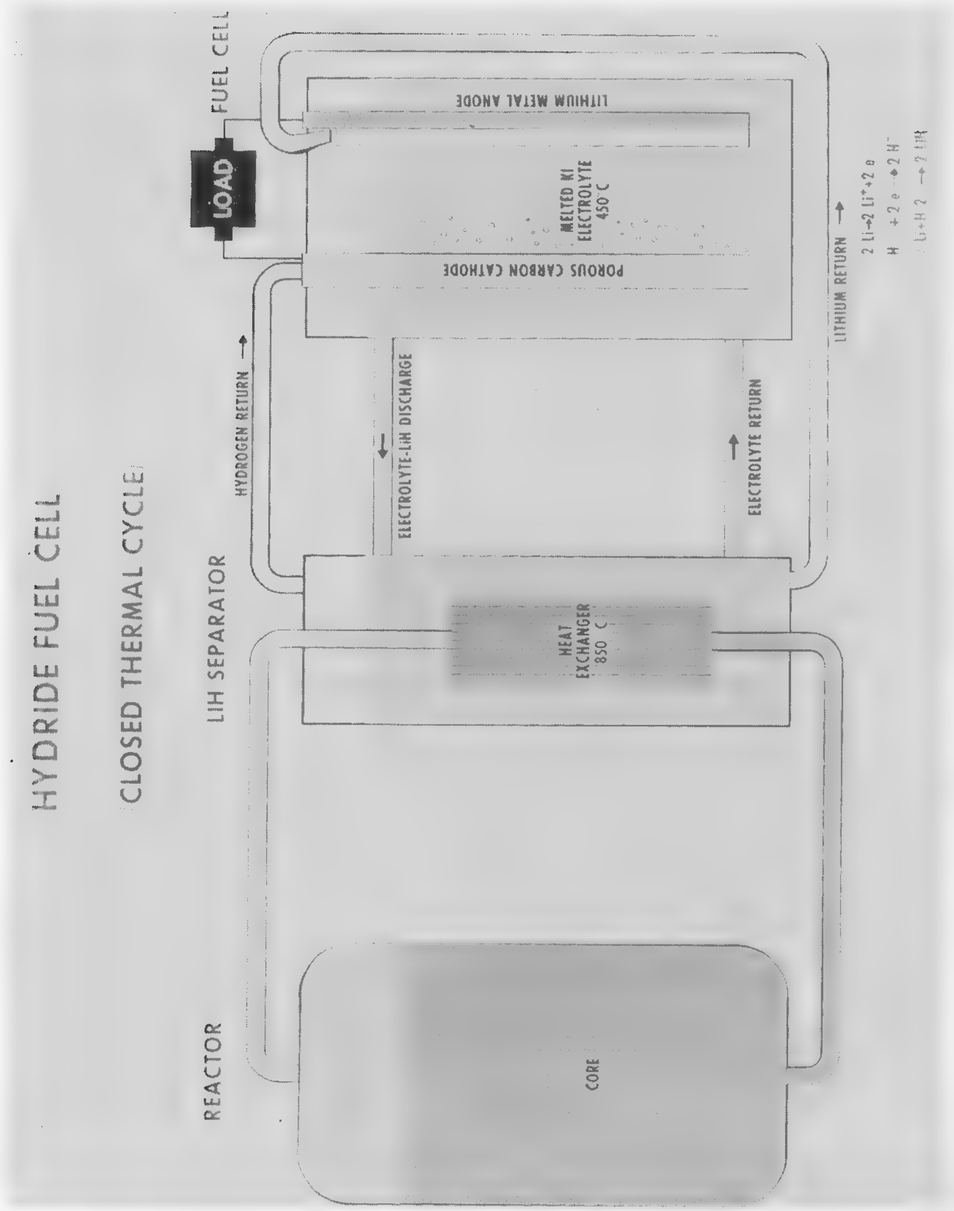


FIGURE 20

chemical reactions have all been considered, but most of the effort has been devoted to thermal regeneration. The problem to be faced is that most simple systems operate over a fairly narrow temperature difference between the cell operating temperature and the regeneration temperature. Thus, even though the cell operation is highly efficient, the total system efficiency is low because of Carnot limitations. The most thoroughly explored is a Li-H_2 system proposed by Mine Safety Research Corporation. Lithium and hydrogen are reacted in a LiF-LiCl eutectic at 450°C and the LiH_2 formed by the cell reaction is decomposed at 1000°C. The over-all efficiency thus cannot exceed 50% and in practice will be much less. More complex systems can exceed this limit, but at the cost of corrosion and chemical transfer problems.

ACKNOWLEDGEMENT

Material for several sections of this manuscript was taken from reports by acknowledged authorities in the several fields. Much of this material was in a report compiled for a NATO long range science study. The photoelectric processes portion of this NATO report were prepared by Paul Rapaport, the thermionic emission section by Lou Perry and the magnetohydrodynamics section by Arthur Kantrowitz. The information on fuel cells was drawn from papers by E. Yeager. In the section on thermoelectricity reference was made to unpublished work on materials by B. Abeles and by R. Wolfe.

SEMICONDUCTING MATERIALS FOR THERMOELECTRIC POWER GENERATION*

F. D. Rosi
RCA Laboratories
Princeton, New Jersey

INTRODUCTION

It has become apparent in recent years that the application of thermoelectricity to power generation is a problem which deserves the serious attention of the various scientific disciplines in solid-state research. With the advent of the transistor in 1948 and the subsequent rapid development of semiconductor technology, materials became available having a combination of thermoelectric properties which indicated the feasibility of power-generating thermocouples with much higher efficiencies than was possible with metals and metal alloys.

The present work is concerned specifically with research on semiconductor materials for thermoelectric power generation in the range 25-900°C. It is presently believed that semiconductors are the most promising materials for thermocouple operation in this temperature range, which coincides with potential heat sources such as chemical flame, focused solar and nuclear energy. The research described here is presented in three parts: (1) general considerations of efficiency factors leading to materials selection, (2) evaluation of compound semiconductors and their solid-solution alloys, and (3) fabrication of thermocouples to demonstrate power-generating efficiencies.

---

*Part of the work described in this paper was supported by the U. S. Navy, Bureau of Ships.

GENERAL CONSIDERATIONS

The application of thermoelectricity to power generation dates more than a century back to its discovery by Seebeck in 1822.[1] He showed that a current is obtained when the junctions of dissimilar materials forming a thermocouple loop are maintained at different temperatures. Such a circuit is shown schematically in Figure 1. In it, two dissimilar materials, an n- and a p-type semiconductor, are joined at

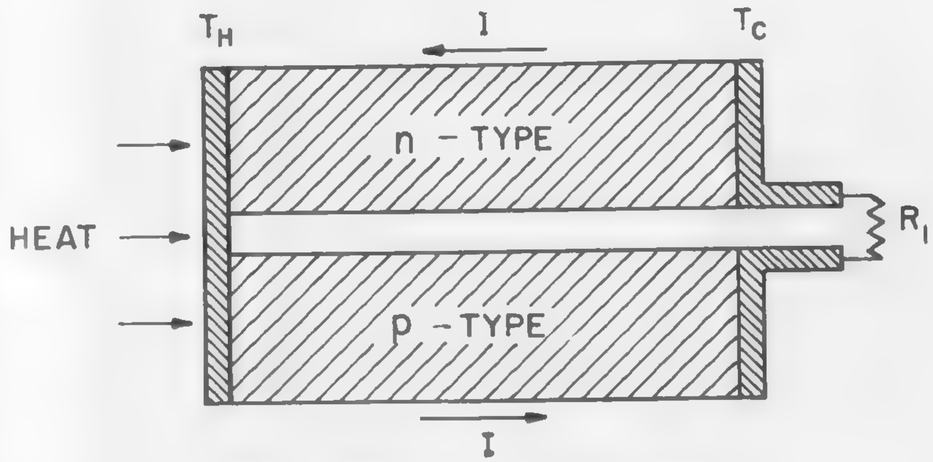


FIGURE 1 THERMOCOUPLE AS POWER GENERATOR

their ends by a metallic conductor. Heat is supplied to the hot junction, T_H, from an external source, and the other junction is maintained at a fixed lower temperature, T_C. As a result of the temperature difference, $T_H - T_C$, a current I flows through the branches of the thermocouple in the direction indicated by the arrows. By also allowing the current to flow through an external load resistance, R_L, inserted into the circuit between the cold junctions, the arrangement in Figure 1 represents a direct conversion of heat into electrical energy with a conversion efficiency, ϕ, given by

$$\phi = \frac{\text{power supplied to load}}{\text{heat absorbed at hot junction}} \qquad (1)$$

The useful power is simply I^2R_L; and, if the Thomson heat is neglected, the heat absorbed at T_H consists of the Peltier heat and the heat withdrawn from the hot junction by conduction

It can be shown by a consideration of the thermodynamics of this sample thermocouple circuit that under optimum load conditions and proper matching of the branch resistances, the expression for maximum efficiency is

$$\phi_{max} = \frac{T_H - T_C}{T_H} \frac{\sqrt{1 + z\overline{T}} - 1}{\sqrt{1 + z\overline{T}} + \frac{T_C}{T_H}} \qquad (2)$$

Here $$\overline{T} = \frac{T_H + T_C}{2}$$

and $$z = \frac{(\alpha_a - \alpha_b)^2}{\left(\sqrt{\rho_a K_a} \pm \sqrt{\rho_b K_b}\right)^2} \qquad (3)$$

where ρ_a, ρ_b and K_a, K_b and α_a, α_b are the resistivities, thermal conductivities and thermoelectric powers of the two branches in Figure 1, respectively. The quantity, z, defined by Equation (3), is commonly referred to as the figure of merit of the thermocouple.[2] If

$$\alpha_a = -\alpha_b \qquad \text{and} \qquad \rho_a K_a = \rho_b K_b ,$$

then

$$z = z_a = \frac{\alpha_a^2}{\rho_a K_a}$$

It is apparent from Equation (3) that the properties which are of primary importance in the evaluation of materials for thermoelectric power generation are the same as those for thermoelectric refrigeration. Moreover, it may be seen from Equation (2) that for optimum power-generating efficiency, it is desirable to maximize the factor, $z\overline{T}$, i. e., to obtain as high a value of z over as wide a temperature range as possible. This is demonstrated in Figure 2, which

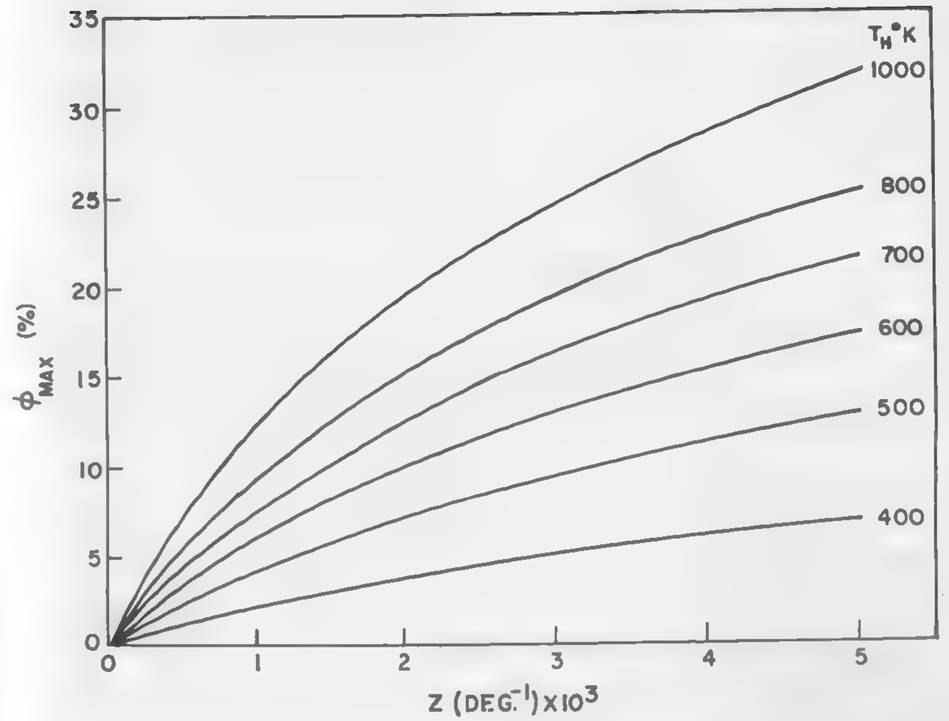


FIGURE 2 MAXIMUM COEFFICIENT OF PERFORMANCE ϕ_{max} AS FUNCTION OF FIGURE OF MERIT z FOR DIFFERENT HOT JUNCTION TEMPERATURES T_H. T_C = 300°K

shows the variation in ϕ_{max} with z for various hot junction temperatures and a fixed T_C of 300°K. It is assumed here that the resistivity, thermal conductivity, and thermoelectric power are constant within a branch over the temperature range considered and, consequently, that the Thomson coefficient can be regarded as zero.

Since this paper is concerned with research on semiconductor materials, it would be desirable to describe the figure of merit, as defined by Equation (3), in terms of semiconductor material constants. From semiconductor transport theory,[2] it can be shown that

$$z = C \left[\exp\left(\frac{|\Delta\epsilon_T|}{kT}\right) - 2\right]\left(\frac{m(N)}{m}\right)^{3/2}\left(\frac{T}{T_0}\right)^{3/2}\frac{\mu}{K}, \qquad (4)$$

where C is a numerical constant, T_0 is room temperature (300°K), μ is the carrier mobility, $m(N)$ is the density-of-states effective mass, m is the free-electron mass, $|\Delta\epsilon_T|$

is the kinetic energy term representing the average energy of the transported electrons relative to the band edge, k is Boltzmann's constant and K is the thermal conductivity. For extrinsic conduction, which is the case in the use of semiconductors for thermoelectric applications, the thermal conductivity is given by

$$K = K_{ph} + K_{el}. \tag{5}$$

Here, K_{ph} is the lattice thermal conductivity and may be regarded as independent of ρ, and K_{el} is the electronic contribution to K given by the Wiedemann-Franz relation,

$$K_{el} = \frac{S\left(\frac{k}{e}\right)^2 T}{\rho} \tag{6}$$

where S is a factor which depends on the type of scattering of the carriers and degree of degeneracy.

It follows from Equation (4) and (5) that the problem of finding new semiconductor materials with superior thermoelectric properties resolves itself into finding (1) materials with a maximum ratio, $(m^{(N)}/m)^{3/2}\,\mu/K_{ph}$, over the particular temperature range of application, and (2) the means for increasing the value of this ratio in a given material, such as by solid solution alloying.

It is also noteworthy from Equation (4) that some improvement in the figure of merit of a material can be expected at higher temperatures. Since the mobility μ can be expected to decrease with temperature as $T^{-3/2}$, then the factor $\mu T^{3/2}$ in Equation (4) would be constant. Thus, the variation in z with temperature would then depend on the value of K_{ph}, which usually has a T^{-1} dependence.

For optimum power-generating efficiency, it is desirable to obtain a high value of z over as wide a temperature range as possible (i. e., to maximize the factor $z\bar{T}$ in Equation (5)). Thus, the semiconductor material must have a large energy bandgap and a high melting point. A large bandgap is desirable, because it permits operation of the thermocouple

at high hot-junction temperatures without a prohibitive loss in thermoelectric properties. This follows from the knowledge that an increase in the bandgap of a semiconductor shifts the onset of intrinsic conduction due to thermal generation of electron-hole pairs to higher temperatures. Such electron-hole pair generation is to be avoided, because it results not only in a marked decrease in thermoelectric power, but also an increase in the thermal conductivity due to an ambipolar contribution, K_{amb}, resulting from the diffusion of electron-hole pairs from T_H to T_C.[3]

The need for a high melting point and corresponding chemical stability is obvious. Unfortunately, it is a general rule[4] that the higher the melting point, T_m, of a material, the larger is its Debye characteristic temperature, θ, and hence K_{ph} at a given temperature. This may be seen from the expression,

$$K_{ph} = \frac{\theta^2}{\gamma^2}\left[MV^{1/3}\left(\frac{\theta}{T}\right)\right]C, \tag{7}$$

recently derived by Leibfried and Schlomann.[5] Here, M and V are the atomic weight and volume of the material, respectively, $\gamma = \partial \ln \theta / \partial \ln V$, and C is a numerical constant. Equation (7) holds for the case where phonon-phonon interactions are the main source of thermal resistance, which is the usual situation at elevated temperatures. Since 0 is proportional to (T_m/M), it follows from Equation (7) that $K_{ph} \propto (T_m{}^3/M)^{1/2}$. This dependence could place an upper temperature limit to the usefulness of materials which exhibit semiconductor behavior at room temperature.

MATERIALS RESEARCH

In research on semiconductors for thermoelectric power generation, it became apparent that no one material could provide the figure of merit, or $z\bar{T}$ factor, necessary for high efficiencies over the temperature range of immediate interest, 25°-900°C. Consequently, attention was directed to a consideration of constructing thermocouple branches in

a sandwich-type arrangement, which makes use of a heterogenous distribution of materials from the hot to the cold junctions.[6] In the sandwich-type arrangement, materials are selected to provide a high average figure of merit over relatively narrow temperature ranges. With this principle of thermocouple construction in mind, data largely taken from the recent work of Rosi, Hockings, and Lindenblad[6] are presented on the evaluation of compound semiconductors and alloys for power generation over specific temperature ranges, and in addition of Ge-Si alloys.

Bi_2Te_3 Alloys

In the course of research on materials for thermoelectric cooling,[7] it became apparent that solid-solution alloys of Bi_2Te_3 with other V-VI compound semiconductors might also be useful in power-generating thermocouples operating with hot-junction temperatures up to 300°C. Consequently, the thermal and electrical properties of selected n- and p-type alloys were examined in the temperature range 25-500°C. For the n-type material, emphasis was placed on the 75% Bi_2Te_3 - 25% Bi_2Se_3 alloy doped with either CuBr or AgI, while alloys of Bi_2Te_3 - Sb_2Te_3 with excess Te or Se were examined for p-type material.

The results of the measurements of thermoelectric power, Q, and electrical resistivity, ρ, at various temperatures up to 550°C for n- and p-type alloys are summarized in Figures 3 and 4. In all cases, both Q and ρ initially increase with increasing temperature. The rise in Q is to be expected, and the occurrence of a maximum followed by a rapid decrease at the higher temperatures is associated with the onset of intrinsic conductivity. The appearance of a maximum in ρ is a direct result of the nature of the temperature dependence of the carrier mobility, μ, and carrier concentration, n. The initial sharp increase in ρ is due to the decrease in carrier mobility with increasing temperature, while the maximum and subsequent decrease in ρ reflect the exponential increase in n with temperature. It is further noteworthy that the maximum in Q always occurs at a temperature 100-200°C lower than that for ρ. This could be an indication that Q is a more sensitive parameter of the onset of intrinsic conductivity in these degenerate, or neardegenerate materials.

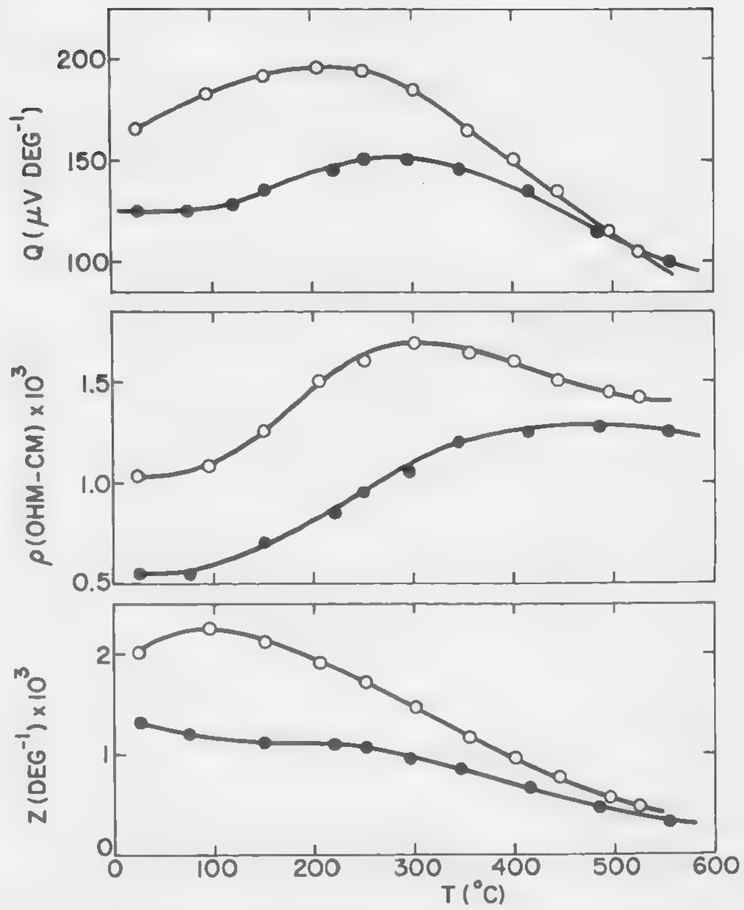


FIGURE 3 TEMPERATURE DEPENDENCE OF THERMOELECTRIC PROPERTIES IN N-TYPE 75% Bi_2Te_3 - 25% Bi_2Se_3 ALLOY

Figures 3 and 4 also show the temperature dependence of the figure of merit z, which was determined from the expression, $z = Q^2/(\rho K)$. Here the total thermal conductivity, K, at any given temperature was estimated from Equation (5) by calculating the electronic contribution, K_{el}, from the measured value of ρ, and assuming the room temperature value of the lattice contribution, K_{ph} (0.009 watt cm^{-1} deg^{-1}), to be invariant with temperature. The latter assumption represents a conservative approach toward estimating the temperature dependence of z, since in general K_{ph} varies as T^{-1} in crystalline solids. It may be seen from Figure 3 that an average z value as high as 1.9×10^{-3} deg^{-1} is obtained over the temperature range 25-300°C for the nondegenerate n-type alloy. For the p-type alloy in

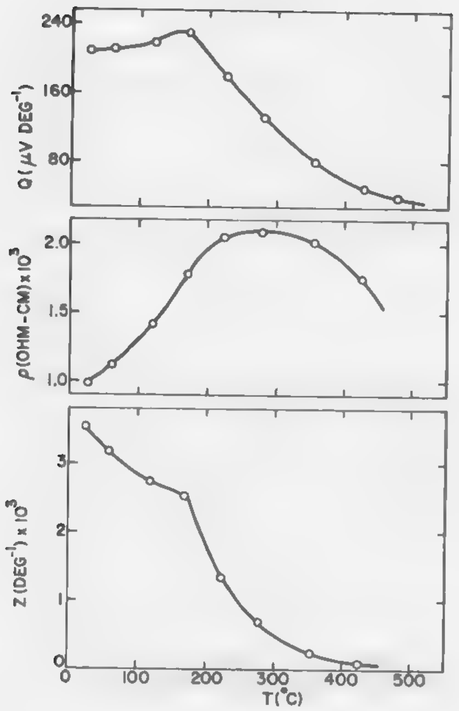


FIGURE 4 TEMPERATURE DEPENDENCE OF THERMOELECTRIC PROPERTIES IN P-TYPE 25% Bi_2Te_3 - 75% Sb_2Te_3 (1.75% Se) ALLOY

Figure 4 the average z value is approximately 2.5×10^{-3} deg^{-1} over the temperature range, 25-250°C. It is noteworthy that this alloy provided a z value of 3.6×10^{-3} deg^{-1} at 25°C.

Ternary Compounds

In the search for new and improved thermoelectric materials, attention was given to a class of compounds[8, 9] having the generalized formula, ABX_2. Here A is a Group I element such as Cu, B is a Group III or Group V element such as In or Sb, and X is a Group VI element such as Te. These ternary compounds represent one of the simpler compositional deviations from the more familiar III-V compound semiconductors, and in these compounds the ratio of bonding electrons to atoms is 4, as is the case for the Group IV elemental semiconductors.

The work on these ternary compounds was initially concerned with those having a cubic structure, in particular, the rock-salt and zinc-blende types. More than twenty compounds of these cubic types were prepared, and their thermoelectric properties determined. The data, summarized in a previous work,[10] showed that this new class of materials includes semiconductors that could be useful for power generation at intermediate temperatures. Of particular significance was the observation that the compounds which crystallize in the rock salt structure[9, 11] are all characterized by low lattice thermal conductivities (<0.0075 watt cm^{-1} deg^{-1}). Examples of these are $AgSbS_2$, $AgSbSe_2$, $AgSbTe_2$, $AgBiS_2$, and $AgBiSe_2$.

Of the large number of ternary compounds examined, $AgSbTe_2$ with the rock-salt structure[9] was found to be the most promising for power generation. This material has a lattice thermal conductivity[12] at room temperature of only 0.0063 watt cm^{-1} deg^{-1}, a hole mobility of ~140 cm^2 $volt^{-1}$ sec^{-1} for a carrier concentration of ~5×10^{18} cm^{-3}, and an energy bandgap of ~0.3 ev estimated from resistivity versus temperature data. From measurements of thermoelectric power and carrier concentration at 300°K, the density-of-states effective mass ratio, $m^{(N)}/m$, for holes was calculated to be 0.36 or 0.88, depending on whether a predominantly impurity or lattice-scattering is assumed, respectively, in assigning a value to the kinetic energy term, $|\Delta\epsilon_T| /(KT)$. Finally, data on the variation of thermoelectric power Q with resistivity ρ at 300°K show that Q values of 200-200 μV deg^{-1} can be expected in the resistivity range, 2-3 x 10^{-3} ohm-cm.

The principal drawback to the proper evaluation and utilization of $AgSbTe_2$ as a material for power generation is the present inability to adjust its electrical properties through controlled impurity additions. For example, it has not yet been possible to obtain either p-type material with resistivities below 2×10^{-3} ohm-cm, or n-type material. Attempts to obtain these electrical characteristics have failed in spite of a large number of experiments with elemental and compound doping. Perhaps this can be attributed in part to the presence of second phases in the as-prepared $AgSbTe_2$, which were recently reported by Armstrong et al[13]

and Wolfe et al.[14] It is possible that these second phases may have a higher solubility for impurities than the matrix material.

Measurements of thermoelectric power, Q, and electrical resistivity, ρ, were made on p-type $AgSbTe_2$ over the temperature range 25-525°C, and from these data the temperature dependence of z was determined. An average z value of approximately 1.6×10^{-3} deg^{-1} is obtained in p-type $AgSbTe_2$ over the temperature range 100-500°C.

Solid-Solution Alloys

It has been shown by a number of investigators[7, 10, 15-17] that the figure of merit of semiconductors can be improved by solid-solution alloying in the carrier-concentration range where the carrier mobility is limited by impurity scattering. Under these conditions, the lattice strains due to alloying are effective in scattering phonons, but are ineffective in scattering electrons which have longer wavelengths. Thus, at a constant resistivity corresponding to near-degeneracy, solid-solution alloying could improve the figure of merit by decreasing the lattice thermal conductivity, K_{ph}, without at the same time affecting the carrier concentration and, hence, thermoelectric power (i.e., K decreases while the ratio Q^2/ρ remains constant). This, of course, assumes no change in the density-of-states effective mass of carriers with alloying. In view of these considerations, the following alloy systems were examined: (1) $AgSbTe_2$ with the IV-VI compounds, PbTe, SnTe and GeTe, (2) PbTe-SnTe and (3) Ge-Si. Thermoelectric data on these systems are presented in the following sections.

1. $AgSbTe_2$ Alloys

The alloys of $AgSbTe_2$ with PbTe, SnTe and GeTe were selected for examination, because phase diagram determinations by differential thermal analysis indicated the existence of complete solid solubility.[6]

Data from electrical resistivity and thermoelectric power measurements made at room temperature for the three alloy systems are shown in Table I. On the basis of these results, as well as thermal conductivity measurements, the alloys with GeTe were considered the most promising materials for use in thermoelectric power generation. Consequently, detailed measurements were made on a selected number of p-type $AgSbTe_2$-GeTe alloys, and the temperature dependence of their figure of merit is shown in Figure 5. For comparison, the data for pure GeTe are also included. It may be seen from the curves in Figure 5 that the 10% $AgSbTe_2$-90% GeTe alloy appears to be the most promising for thermoelectric power generation in the temperature range 250-550°C where an average z value of $\sim 1.5 \times 10^{-3}$ deg^{-1} is obtained. Although this does not represent an improvement over the average z value for $AgSbTe_2$ in the same temperature range, it should be noted that the useful temperature range of the 10% $AgSbTe_2$-90% GeTe

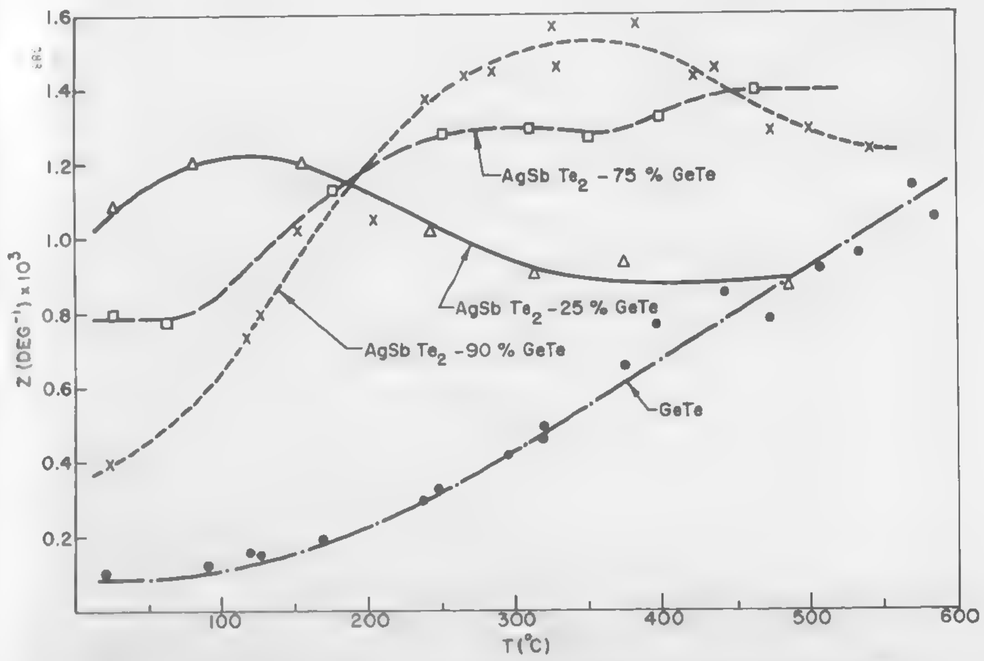


FIGURE 5 VARIATION OF FIGURE OF MERIT z WITH TEMPERATURE FOR P-TYPE $AgSbTe_2$-GeTe ALLOYS

TABLE I

ELECTRICAL RESISTIVITY AND THERMOELECTRIC POWER OF $AgSbTe_2$ ALLOYS AT 300°K

Alloy Composition	ρ (ohm-cm)	Q (μV deg^{-1})
75% $AgSbTe_2$ - 25% PbTe	3.1×10^{-2}	300
50% $AgSbTe_2$ - 50% PbTe	5.0×10^{-2}	350
40% $AgSbTe_2$ - 60% PbTe	3.0×10^{-2}	380
75% $AgSbTe_2$ - 25% SnTe	3.6×10^{-3}	110
50% $AgSbTe_2$ - 50% SnTe	4.8×10^{-4}	30
40% $AgSbTe_2$ - 60% SnTe	1.0×10^{-3}	71
20% $AgSbTe_2$ - 80% SnTe	6.4×10^{-4}	52
90% $AgSbTe_2$ - 10% GeTe	7.0×10^{-3}	235
75% $AgSbTe_2$ - 25% GeTe	5.5×10^{-3}	230
50% $AgSbTe_2$ - 50% GeTe	3.3×10^{-3}	212
25% $AgSbTe_2$ - 75% GeTe	1.1×10^{-3}	131
10% $AgSbTe_2$ - 90% GeTe	5.2×10^{-4}	70

alloy will be 50-100°C higher than that of pure $AgSbTe_2$. Moreover, the thermoelectric properties have not been optimized for the intended temperature range of application. One point of interest in connection with the data in Figure 5 is the marked improvement that is made in the figure of merit of GeTe over the temperature range 25-500°C by simply alloying with 10% $AgSbTe_2$.

2. PbTe-SnTe Alloys

Interest in an n-type thermoelectric material for use in the temperature range above that of the Bi_2Te_3 alloys led to an examination of the system, PbTe-SnTe, which had been shown to exhibit complete solid miscibility.[18] It was known from previous work[19] that PbTe is useful in this temperature range, and it was considered that solid-solution alloying with SnTe would provide a higher figure of merit by decreasing the lattice thermal conductivity.

A study of a number of n-type PbTe-SnTe alloys showed that one of the most promising compositions was 75% PbTe-25% SnTe, which has electrical properties comparable to PbTe. In addition, this alloy has a lattice thermal conductivity of 0.012 watt cm^{-1} deg^{-1} at 25°C, which is significantly lower than that of PbTe (0.017 watt cm^{-1} deg^{-1}).[19] Detailed measurements were made of the temperature dependence of Q and ρ for the 75% PbTe-25% SnTe alloy, and the data are summarized in Figure 6. It may be seen that the onset of intrinsic conduction occurs in these specimens at about 700°C, which probably represents the upper temperature limit for the use of this alloy in power generation. This is also indicated in Figure 6 by the dependence of z on temperature. The variation of z with temperature also shows a broad maximum which provides an average z value of $\sim 1.3 \times 10^{-3}$ deg^{-1} over the temperature range 300-700°C.

3. Ge-Si Alloys

To extend the useful temperature range of thermocouples above 500°C, the thermoelectric properties of Ge-Si alloys were examined up to 900°C. This work included measurements of electrical resistivity, thermoelectric power, and

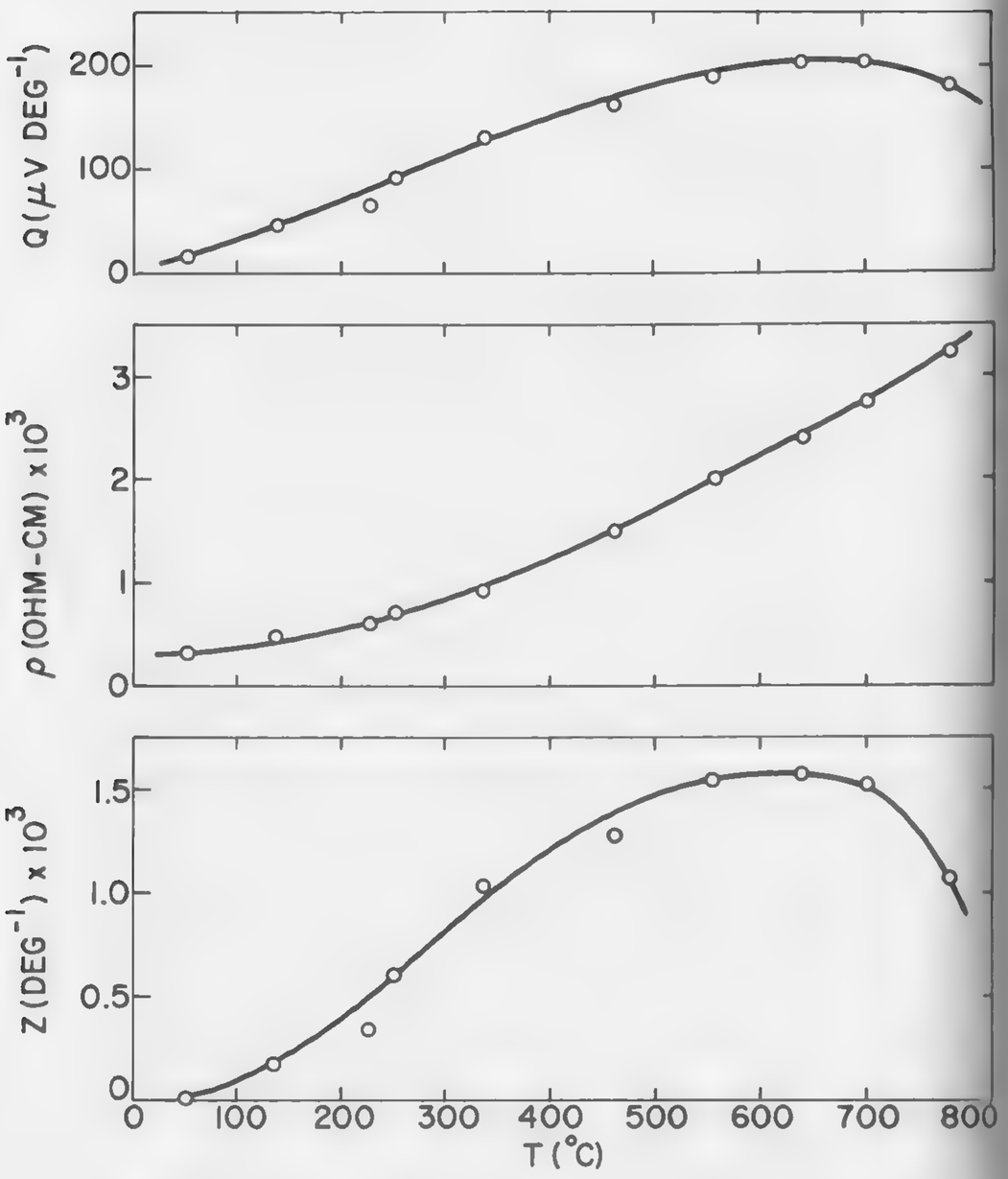


FIGURE 6 TEMPERATURE DEPENDENCE OF THERMOELECTRIC PROPERTIES FOR N-TYPE 75% PbTe - 25% SnTe ALLOY

thermal conductivity. The latter property was determined by the diffusivity method, as recently described by Abeles, Cody and Beers.[20] In this method one obtains a value of the ratio K/C_v, where C_v is the specific heat. The thermal conductivity is then obtained by calculating C_v from the DeLong-Petit Law.

The data on the lattice thermal resistivity, $W = 1/K_{ph}$, is shown in Figure 7, which was taken from the very recent work of Abeles, Beers, Cody and Dismukes.[21] It may be seen that the thermal resistance of the Ge-Si alloys increases with temperature at a more rapid rate than the pure Ge and Si. This unexpected behavior has been attributed by Abeles et al. to scattering in these alloys by umklapp and normal three-phonon processes due to anharmonicity, and to two-phonon momentum-nonconserving processes due to point defects. Equally important the data in Figure 7, in addition

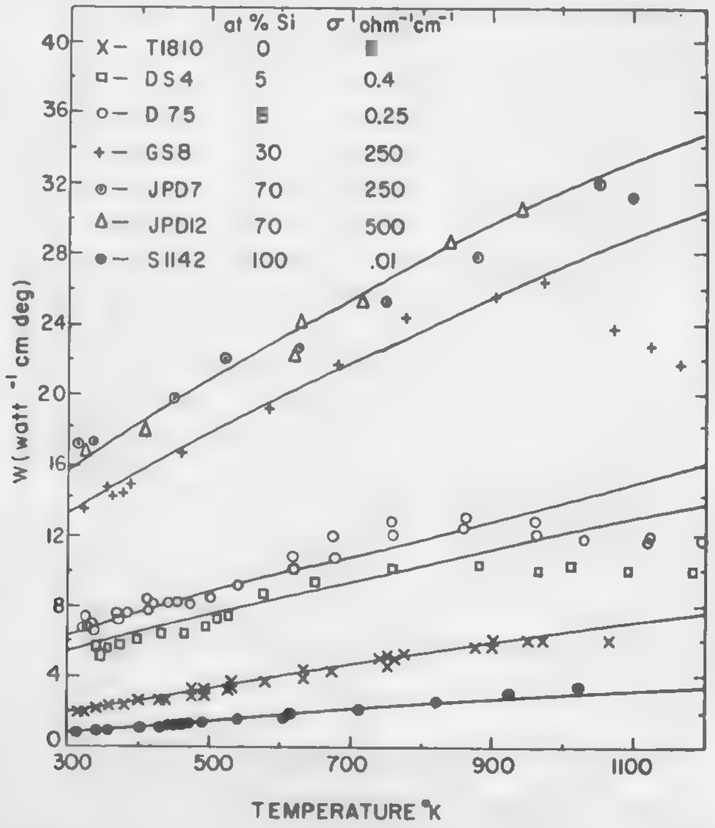


FIGURE 7 THE VARIATION OF THE PHONON THERMAL RESISTANCE W OF Ge-Si ALLOYS WITH TEMPERATURE AND ALLOYING (After Abeles et al[21])

to the Q and ρ measurements over the same temperature range, at once suggested the usefulness of these alloys for thermoelectric power generation up to 900°C.

n- and p-type Ge-Si alloys have been prepared with an average figure of merit for the n- and p-type branches in the thermocouple of approximately 0.7×10^{-3} deg^{-1} over the temperature range 300-900°C. In addition, the temperature dependence of z over this temperature range exhibits a broad maximum.

POWER-GENERATING THERMOCOUPLES

25-325°C Range

It was shown in the previous section that Bi_2Te_3 alloys could be useful for power generation at least up to 300°C. Consequently, a power-generating thermocouple, similar to the arrangement in Figure 1, was constructed from n-type 75% Bi_2Te_3-25% Bi_2Se_3 and p-type 50% Bi_2Te_3-40% Sb_2Te_3-10% Sb_2Se_3 alloys. In constructing the thermocouple, the metal-semiconductor junctions were made by soldering with an 80% Bi-20% Sb alloy, which provided a junction resistance at 25°C of at least one order of magnitude less than the sum of the branch resistances. Heat was supplied to the hot junction by a wire-wound resistance heater, and the cold junction was fixed at 25°C by circulating water.

Figure 8 shows the variation in power-generating efficiency, ϕ, (power output/heat input) with temperature difference of operation, as measured in a vacuum. It may be seen that a ϕ_{max} of approximately 6.5% is obtained for a $T_H - T_C = 300°C$ (i.e., $T_C = 25°C$ to $T_H = 325°C$). From the measured Q, ρ, and κ of the alloys in Table III over this temperature range, an efficiency of ~8% was expected.

20-550°C Range

Power-generating thermocouples for operation over the temperature range 20-550°C were constructed from semiconductor alloys in the sandwich arrangement shown

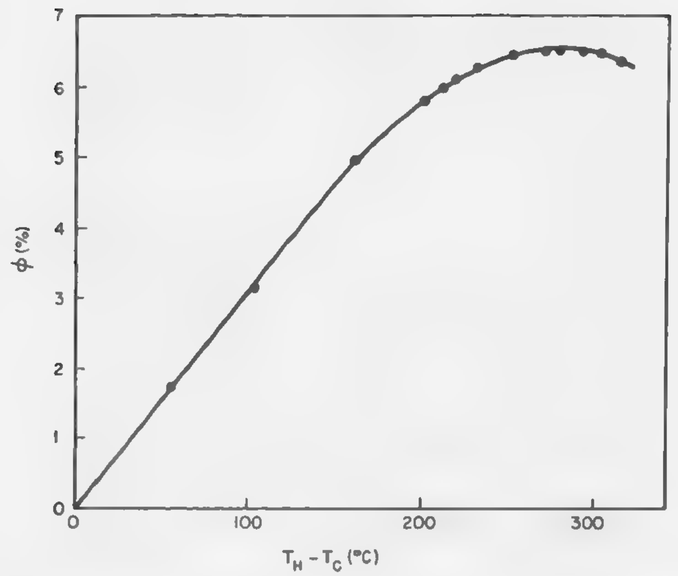


FIGURE 8 VARIATION OF POWER GENERATING EFFICIENCY ϕ WITH TEMPERATURE RANGE OF OPERATION. T_C = 25°C

schematically in Figure 9. It may be seen that the n-type branch consisted of alloys of 75% Bi_2Te_3-25% Bi_2Se_3 and 75% PbTe-25% SnTe, while the p-type branch was constructed from alloys of 25% Bi_2Te_3-75% Sb_2Te_3 (1.75 weight percent Se) and 10% $AgSbTe_2$-90% GeTe. The metal-semiconductor bonds at the cold and intermediate junctions for both the p- and n-type materials were made by soldering, while pressure contacts were used for the hot junctions. Heat was again supplied to the hot junction by a wire-wound resistance heater, and the cold junction temperature was maintained at 20°C by circulating water.

Measurements of Q, ρ, and κ as a function of temperature on the individual materials indicated that a power-generating efficiency of approximately 14% could be expected with the arrangement shown in Figure 9. The variation of ϕ with hot junction temperature T_H in Figure 10 shows that an efficiency of 10-12% was actually realized on operating in air up to a T_H of 550°C (i.e., a $T_H - T_C = 530°C$). The curves were obtained from two thermocouples, which were cycled over the temperature range of operation.

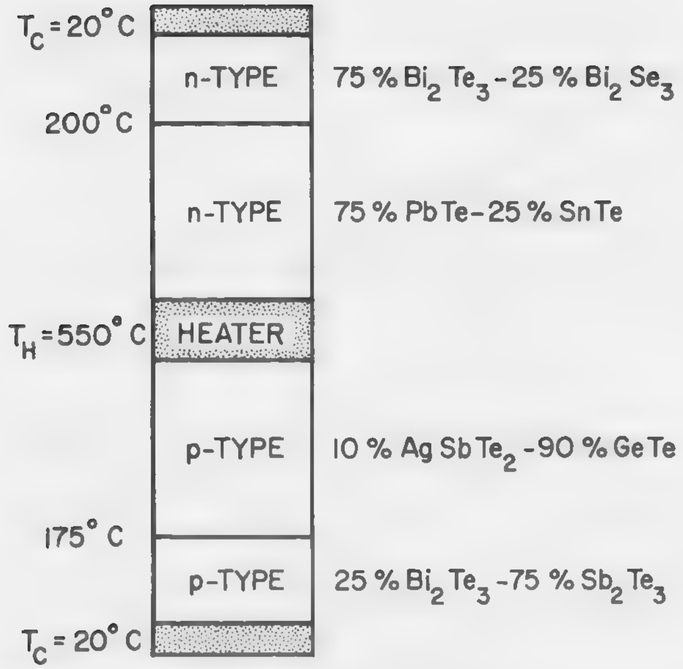


FIGURE 9 SCHEMATIC REPRESENTATION OF SANDWICH-TYPE POWER-GENERATING THERMOCOUPLE FOR OPERATION IN THE TEMPERATURE RANGE 20-550°C

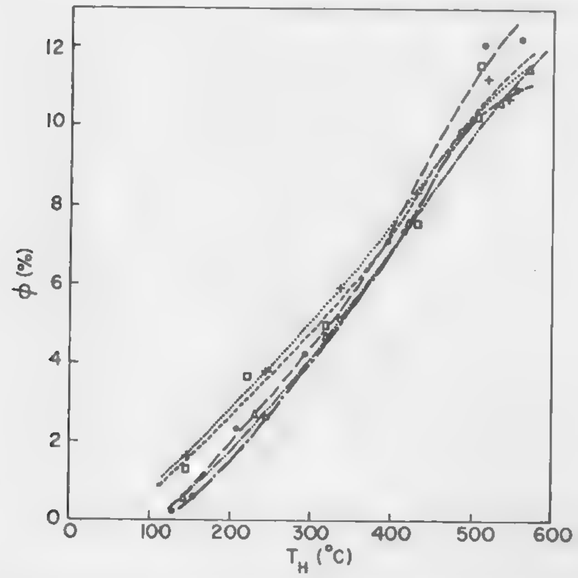


FIGURE 10 VARIATION OF POWER GENERATING EFFICIENCY ϕ WITH TEMPERATURE OF HOT JUNCTION T_H. T_C = 20°C

30-900°C Range

A power generating thermocouple was constructed from a degenerate, p- and n-type Ge-Si alloy in the form of bars, 1/4 in. x 1/4 in. x 1/2 in. The cold junction temperature was 33°C and the hot junction was 870°C. The heat to the hot junction was supplied by a wire-wound resistance heater. The power output into a matched load for this single thermocouple was 2.4 watts (12 amps and 0.2 v), and the measured power conversion efficiency was 7.3%. The efficiency predicted from the material properties was 10%; and the difference between the predicted and measured efficiencies could be entirely accounted for by electrical contact resistance and radiation losses. The high power density of the Ge-Si alloys at once suggests that a suitable arrangement of a ft^2 of thermocouples could provide a power output of 5-10 kilowatts.

To conclude this section, it is worth noting that the Ge-Si alloys are most suitable, from a figure of merit standpoint, in the temperature range 400-900°C. Therefore, it would be advantageous to include these alloys in a sandwich construction of thermocouple branches with the materials shown in Figure 9. Such a sandwich arrangement has not yet been constructed, but efficiencies in excess of 15% can be expected.

BIBLIOGRAPHY

1. Seebeck, T. J., Reports of the Prussian Acad. Sci. (1822-1823).

2. Ioffe, A. F., Poluprovodnikovye Termoelementy, Moscow-Leningrad (1956).

3. Price, P. J., "Ambipolar Thermodiffusion of Electrons and Holes in Semiconductors," Phil. Mag., Vol. 46, Ser. 7, p. 1252, November 1955.

4. Roberts, J. K. and A. R. Miller, Heat and Thermodynamics, New York, N. Y., p. 552 (1954).

5. Leibfried, G. and E. Schlomann, "Thermal Conductivity in Electrically Insulating Crystals," Gott. Nachr., Vol. IIa, p. 71 (1954).

6. Rosi, F. D., E. F. Hockings, and N. E. Lindenblad, "Semiconducting Materials for Thermoelectric Power Generation," RCA Review, March 1961, Vol. XXII, No. 1.

7. Rosi, F. D., B. Abeles and R. V. Jensen, "Materials for Thermoelectric Refrigeration," Jour. Phys. Chem. Solids, Vol. 10, Nos. 2 & 3, p. 191, July 1959.

8. Goodman, C. H. L. and R. W. Douglas, "New Semiconducting Compounds of Diamond Type Structure," Physica, Vol. 20, No. 11, p. 1107 (1954).

9. Wernick, J. H. and K. E. Benson, "New Semiconducting Ternary Compounds," Jour. Phys. Chem. Solids, Vol. 3, Nos. 1 & 2, p. 157 (1957).

10. Rosi, F. D., J. P. Dismukes and E. F. Hockings, "Semiconductor Materials for Thermoelectric Power Generation up to 700°C," Electrical Engineering, Vol. 79, No. 6, p. 450, June 1960.

11. Ramdohr, P., "Schapbuchite, Matildite, and the Silver and Bismuth Contents of Certain Galenites," Sitzungsber Preuss, Akad. Wiss. Phys. Math. K1, V1, p. 71 (1938).

12. Hockings, E. F., "The Thermal Conductivity of Silver Antimony Telluride," Jour. Phys. Chem. Solids, Vol. 10, No. 4, p. 341, August 1959.

13. Armstrong, R. W., J. W. Faust, Jr. and W. A. Tiller, "A Structural Study of the Compound $AgSbTe_2$," Jour. Appl. Phys., Vol. 31, No. 11, p. 1954, November 1960.

14. Wolfe, R., J. H. Wernick and S. E. Hasko, "Anomalous Hall Effect in $AgSbTe_2$," Jour. Appl. Phys., Vol. 31, No. 11, p. 1959, November 1960.

15. Ioffe, A. F., S. V. Airapetyants, A. V. Ioffe, N. V. Kolomoets, L. S. Stil'bans, "Increase in the Effectiveness of Semiconducting Thermocouples," Doklady Akademii Nauk. SSSR, V. 106, No. 6, p. 981 (1956); translation No. 3, Infosearch Russian Literature Survey, SEM-1-56; A. V. Ioffe and A. F. Ioffe, "Thermal Conductivity of Semiconductors," Izvestiya Akademii Nauk, SSR, Ser. Fiz. V. 20, No. 1, p. 65 (1956); Infosearch Translation IA-3-56.

16. Steele, M. C. and F. D. Rosi, "Thermal Conductivity and Thermoelectric Power of Germanium-Silicon Alloys," Jour. Appl. Phys., Vol. 29, No. 11, p. 1517, November 1958.

17. Gordyakova, G. N., G. V. Kokosh and S. S. Sinani, "Investigation of Thermoelectric Properties of Solid Solutions Bi_2Te_3-Bi_2Se_3," Zhurnal Tekhnicheskoi Fizuki, Akad. Nauk. SSSR, B. 28, No. 5, p. 977 (1958).

18. Abrikosov, N. K., K. A. Dyuldina and T. A. Danilyan, "On the System SnTe-PbTe," Zhur. Neorg. Khim., V. 3, p. 1632 (1958).

19. Fritts, R. W., in Thermoelectric Materials and Devices, Reinhold Pub. Corp., New York, N. Y., 1960, p. 143.

20. Abeles, B., G. D. Cody and D. S. Beers; Jour. Appl. Phys., Vol. 31, p. 1585 (1960).

21. Abeles, B., D. S. Beers, G. D. Cody and J. P. Dismukes, "Thermal Conductivity of Ge-Si Alloys at High Temperatures," in course of publication in Phys. Rev. (Jan. 1, 1962).

SOLAR ENERGY CONVERTERS

Dr. Bernd Ross
Manager, Space Projects Section
Hoffman Electronics Corporation
Semiconductor Division
El Monte, California

ABSTRACT

A short basic discussion of semiconductor P-N junctions will be given. This will be related to the operation of a photovoltaic device. A method of fabricating a silicon photovoltaic energy conversion device will be discussed. Considerations of spectral response and optimization to solar radiation resulting in the development of a solar simulator will be described. Special requirements of solar cells operating in earth space will be mentioned.

INTRODUCTION

Silicon solar cells are basically semiconductor P-N junctions optimized for photovoltaic response in the solar spectrum. In order to gain an understanding of the device parameters we shall examine the basic theory underlying P-N junctions.

In Figure 1 the boron, silicon and arsenic atoms are shown in schematic representation. It may be noted that the silicon atom contains 4 valence electrons whereas boron and arsenic have, respectively, 3 and 5 valence electrons.

A silicon crystal is built up of silicon atoms which are bound together by covalent bonding. Since all electrons are in bonding positions and are unavailable for conduction, such a crystal should be an insulator at low temperatures.

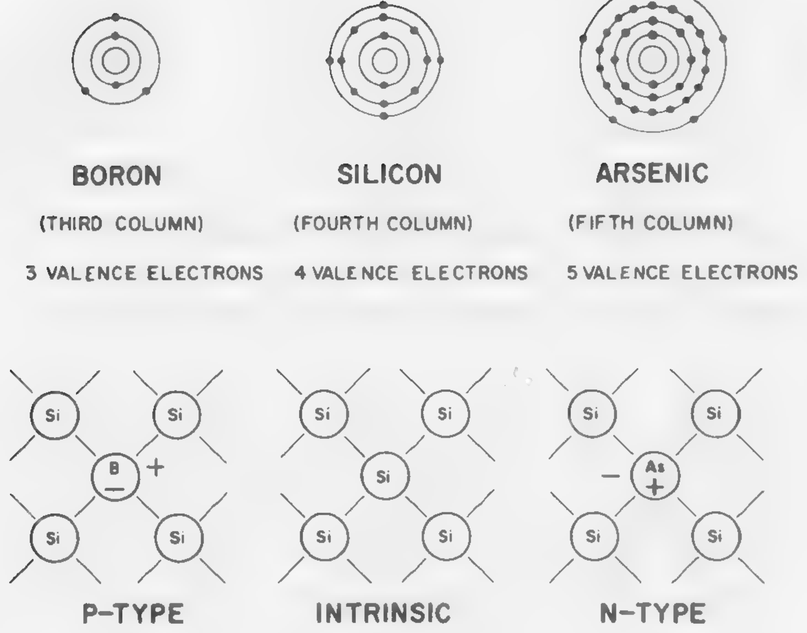
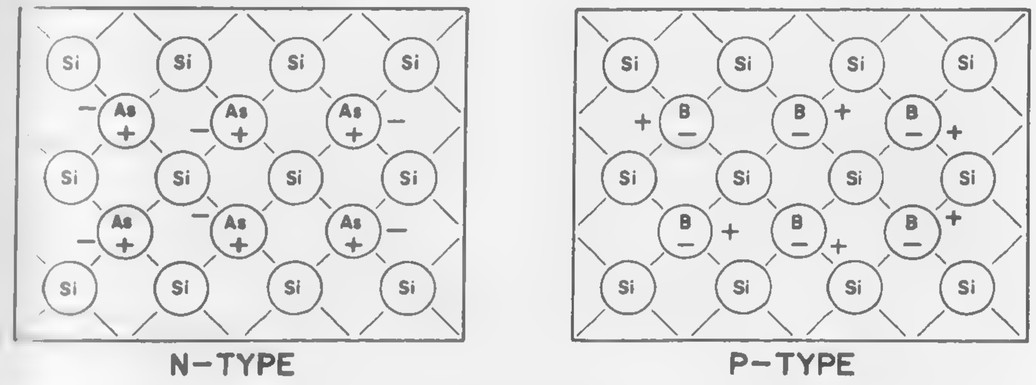


FIGURE 1 CRYSTALLINE STRUCTURES

When the crystal is heated, some electrons are boiled out of their bonding positions and may carry a charge through the crystal so that some electrical conductivity is obtained. A crystal of this type is called an intrinsic semiconductor.

One may produce a crystal which is inherently electrically conducting even at lower temperatures by including known impurities in controlled amounts in the crystal lattice. This can be done by introducing, for instance, arsenic (5 electrons in the outer shell). Since only 4 of the 5 valence electrons can be accommodated in the crystalline bond, the 5th electron assumes a wide orbit about the arsenic impurity center and will be ionized at relatively low temperatures (room temperature). When such an ionization occurs an arsenic atom gains 1 positive electronic charge, since charge neutrality for the arsenic atom requires 5 electrons in the outer shell. Therefore, for each arsenic impurity atom there will be 1 electron available for conduction in the crystal. Since conduction in this crystal takes place by electrons, this is called an N-type crystal (Figure 2).

A somewhat similar condition obtains when an impurity having 3 valence electrons is incorporated in the lattice, instead of the customary 4. In this case the covalent bonding of the boron atom to its neighboring silicon atoms is left unsatisfied since the boron atom only has available 3 valence electrons. Again, at room temperature there is a high probability that an electron from somewhere in the crystal will fill this unsatisfied bond. Such a crystal will exhibit electrical conductivity by reciprocal electron motion, that is, the electron nearest the open electronic bond may shift over and fill the empty bond. The second closest electron may move over into the position of the electron which has just jumped, and so on, until the open bond position has moved throughout the crystal. This is called hole conduction and the crystal in which it takes place is referred to as P-type (Figure 2). In this case the boron atom assumes a unit



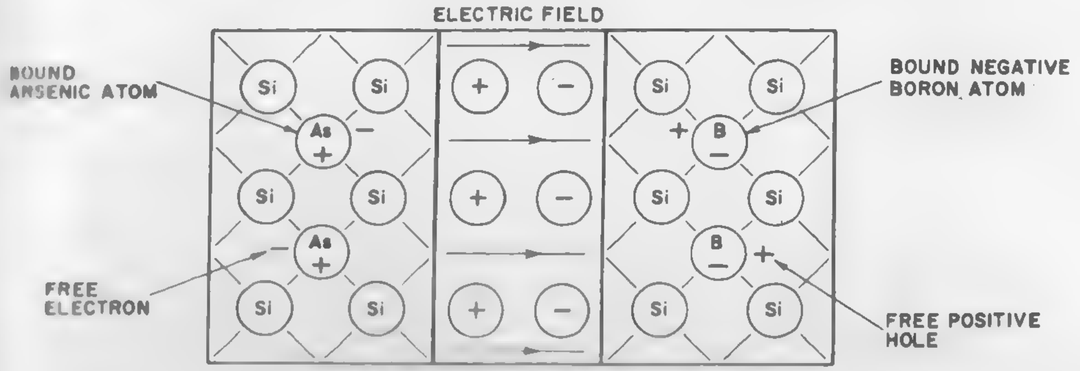


FIGURE 2 OPERATION OF A P-N JUNCTION

negative charge since there are only a sufficient number of positive charges in the nucleus to compensate for 3 valence electrons. The crystals having an electrical conductivity resulting from the inclusion of such impurity atoms are called extrinsic semiconductors.

When a crystal is fabricated such that a portion of it is N-type and the remainder P-type, a P-N junction results (Figure 2). Under equilibrium conditions, the electrons on the N side, and the holes on the P side will migrate by thermal diffusion across the surface dividing the 2 regions (the junction surface). The electrons which have thusly entered the P-type crystal are called minority carriers, as are the holes which exist inside the N-type crystal. These minority carriers are soon neutralized by recombining with the majority carriers (electrons on the N-type and holes in the P-type material). Since charge neutrality existed prior to the migration of carriers across the P-N junction, it follows that the above removal of electrons and holes by recombination has destroyed this charge neutrality. In this way, for each electron removed from the N-type portion of the crystal a positive charge was uncovered. The same applies to the holes in the P-type material. For this reason we have an inherent potential difference existing between the N and the P-type regions of the P-N junctions. This built-in field may be utilized for rectification or photovoltaic power conversion (Figure 3).

We will now digress in order to examine the interaction of light with an intrinsic semiconductor (Figure 4). If light of the proper energy strikes a semiconductor, the light particles (photons) will dislodge some of the valence bond electrons and give them a sufficient amount of energy to let them become conduction electrons free from their parent semiconductor atoms. The broken bonds (holes) may likewise contribute to conduction. When the source of photon excitation (light) is removed the electrons will drop back into the holes until equilibrium is re-established and the initial conductivity state re-obtains. The length of time necessary to re-establish the equilibrium after the light is shut off depends upon the crystal perfection, impurity content, type and number, and temperature. In the case of

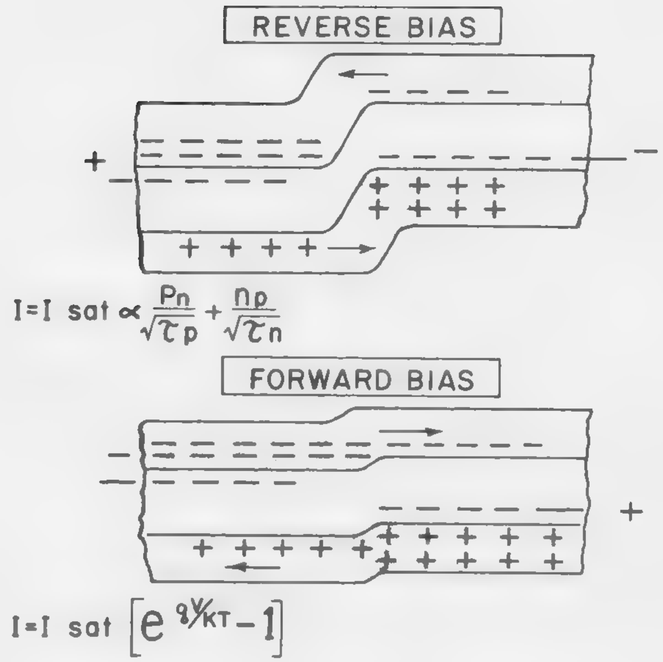


FIGURE 3 BIAS CONDITIONS ON A P-N JUNCTION

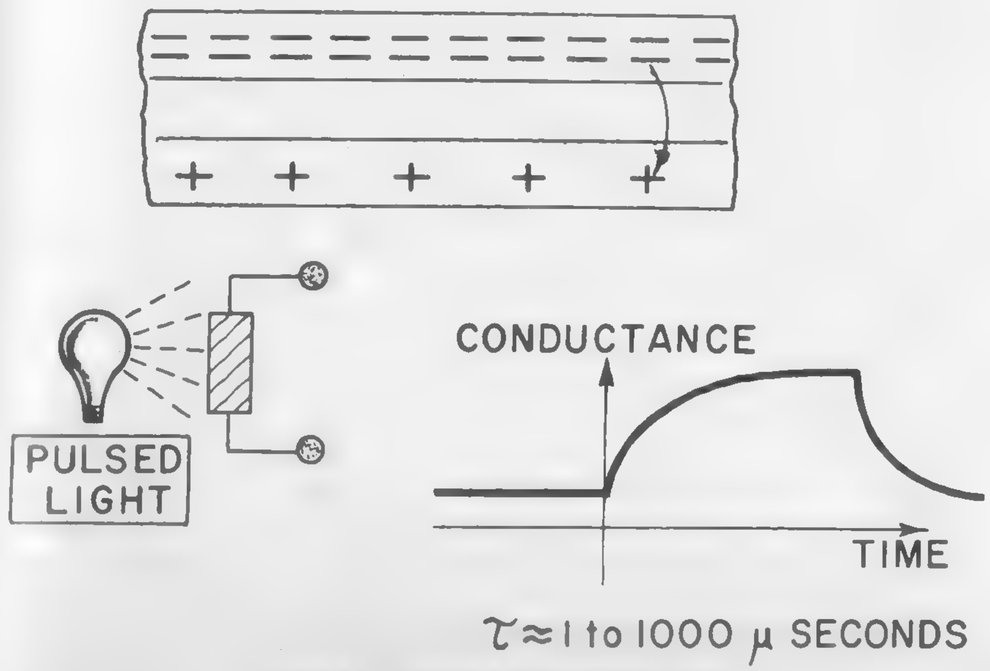


FIGURE 4 LIFETIME AND RECOMBINATION

an extrinsic semiconductor the re-establishment of equilibrium conditions is determined by the lifetime of the minority carrier. This is one of the most important parameters of photovoltaic converters, diodes, and transistors.

When light falls on a semiconductor, electron-hole pairs are created. Thermal motion will allow these pairs to wander throughout the crystal until they recombine in accordance with the minority carrier lifetime. If the crystal is dimensioned appropriately and the lifetime permits, the electron-hole pairs will have a good chance of reaching the P-N junction. At this point the pairs are separated by the built-in field and will cause an electrode potential to be set up which depends upon the temperature, the built-in field, the number of electron-hole pairs separated, and the leakage across the junction. Useful power may be obtained under these conditions by allowing the electrons (and holes) to return to their previous sites through an external path including an electrical load. It is obvious from the above discussion that one wishes to place the P-N junction in the crystal in such a position that the probability is high of photon produced electron-hole pairs to reach the junction within their lifetime. Furthermore, for a given configuration it is necessary to make the lifetime of the minority carriers sufficiently long that the electron-hole pairs may reach the junction. This can be done by exclusion of certain impurities, crystal annealing, etc.

The current generated by a photovoltaic junction depends chiefly upon the number of photons impinging, the efficiency of pair production, the probability of pair collection and the magnitude of current leakage through the junction. Since most electron-hole pairs are produced close to the surface of a crystal upon which a light is incident it follows that the junction will be placed close to this surface. However, the current flowing through the thin top region of the P-N junction will produce a voltage drop in accordance with the resistance of the top layer. This requires reduction of the resistance by utilizing high conductivity material and optimizing thickness between the electron-hole pair collection requirement and the resistivity limitations of the layer.

Figure 5 shows a simple representation of a rectangular solar cell with a metallic strip contact on the light incident side of the cell and a thin sheet of boron doped material comprising the P portion of the P-N junction. Below is shown the current-voltage behavior of such a device with and without illumination. The simplified relation giving the current-voltage behavior is

$$I = I_L - I_s(T) \exp \frac{q(V + IR_s)}{AkT}$$

where

- I = Output current
- I_L = The photon generated current (for practical purposes this is almost equal to the short circuit current of the solar cell)
- $I_s(T)$ = Saturation current which depends upon lifetimes, mobilities, impurity concentrations, and is a strong function of temperature
- q = Electronic charge
- V = Output voltage
- R_s = Series resistance (mostly the sheet resistance of the P-layer)
- A = A somewhat mysterious factor varying between 1 and 4
- k = Boltzmann constant
- T = Temperature on the absolute scale.

From this it can be seen that the output voltage varies logarithmically as the light input.

$$I = 0$$

$$V_{oc} = \frac{AkT}{q} \ln \frac{I_L}{I_s(T)}$$

The solar cell is produced by allowing an acceptor (P-type) impurity to diffuse into an N-type silicon crystal. The N-type crystal contains a doping impurity of approximately 10^{15} arsenic atoms/cubic cm. This amounts to an impurity

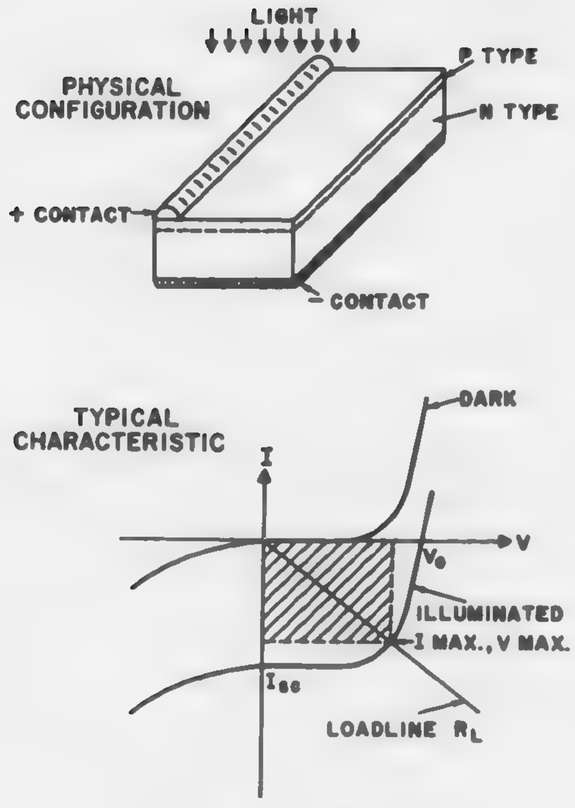


FIGURE 5 SOLAR CELL

fraction of about 1 millionth of a percent. Diffusion takes place by producing a glassy mixture of silicon and boron on the crystal surface and allowing the boron impurity to penetrate into the lattice at a temperature of approximately 1000°C plus. The boron impurity is allowed to diffuse a distance of approximately a micron (4/100,000 in.), that is, at this distance the diffused-in impurity has a concentration equal to that of the arsenic in the bulk crystal. This is where the P-N junction occurs. The concentration of the impurity, according to Fick's law goes in accordance with the error function complement, assuming an infinite supply of impurity atoms in the surface diffusion source C_o, and a diffusion constant which is independent of concentration.

$$C = C_o \operatorname{erfc} \frac{x}{2\sqrt{Dt}}$$

where

C = Concentration at a distance x into the crystal
C_o = Surface concentration of the impurity
D = Diffusion coefficient
t = Time.

The temperature behavior is inherent in the relation for the diffusion coefficient

$$D = D_o \exp \frac{-E}{kT}$$

where

D_o = Constant dependent upon the impurity and the crystal
E = Activation energy for the particular impurity in the particular crystal
k = Boltzmann constant
T = Temperature on the absolute scale.

The surface concentration is optimized to be as large as possible in order to obtain a high conductivity of the thin P-layer. In Figure 6 the error function behavior of the impurity gradient is shown. If one remembers from the earlier considerations that the impurity atoms represent charged atoms it is clear that this concentration gradient represents a charge gradient and this in turn implies an electric field. This electric field has the direction appropriate to expediting the minority carrier (electrons) towards the junction. This is a fortuitous but highly desirable consequence of the use of solid state impurity diffusion for photovoltaic junction fabrication. It allows an electron produced at the surface by photon impact ionization to reach the junction with a lifetime of 1/4 the value required if this field were not present. Shallower diffusions produce a sharper gradient with resultant higher fields. The energy bands of a diffused junction solar cell are depicted in Figure 7. Unfortunately, the theoretical considerations upon which Figures 6 and 7 are based, have been made somewhat doubtful by recent evidence uncovered at the Hoffman Semiconductor Division Laboratories. This was found as a result of painstaking etching experiments in which extremely thin layers of the

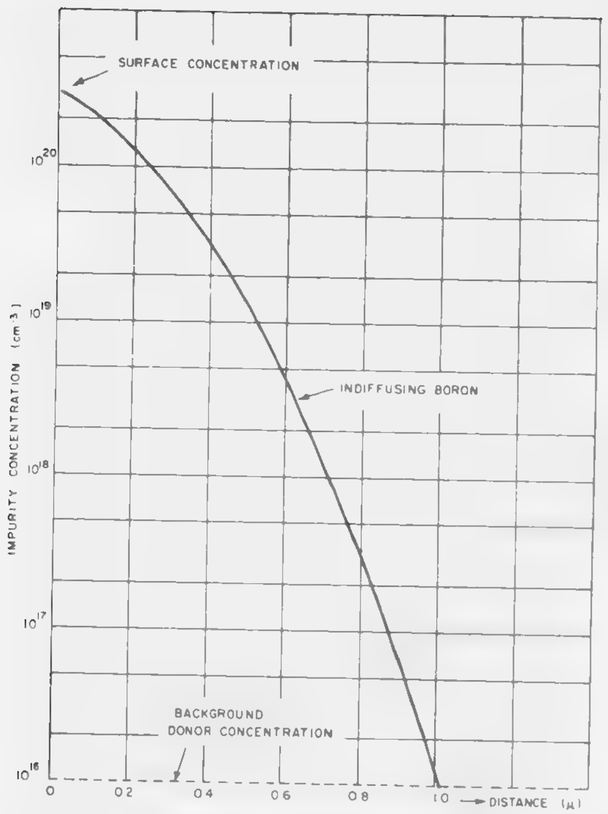


FIGURE 6 DIFFUSED IMPURITY GRADIENT IN SILICON

diffused material are removed successively. It appears that there is a serious departure from the predicted error function distribution near the surface. This may explain the insensitivity to ultraviolet radiation. Further work on the above is in progress and will be published upon verification. The spectral response of the solar cell depends upon the spectral absorption of photons, and the spectral collection of electron-hole pairs. The first is immutable once the semiconductor material has been selected. The latter is a function of lifetime, mobility and junction depth. The top of Figure 8 shows the effect of lifetime upon the spectral response whereas the bottom of Figure 8 shows the effect of junction depth upon the spectral response. An indication of electrode optimization on solar cells may be obtained by examining Figure 9, which shows the effect of applying collection grids upon the current-voltage behavior of a solar cell. Electrode optimization reduces the solar cell series resistance and therefore the internal voltage drop, and has a minimum effect upon shadowing the active area of the solar cell.

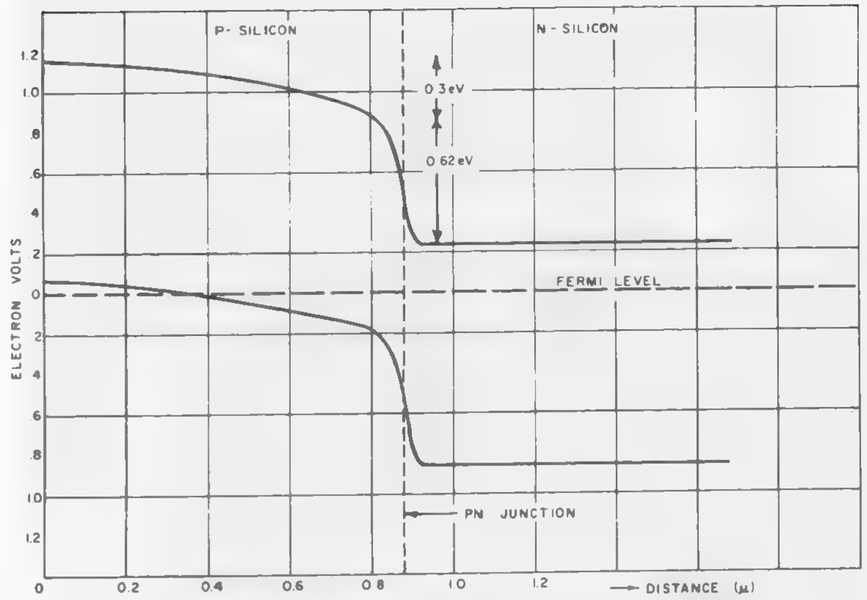


FIGURE 7 ENERGY BANDS OF A DIFFUSED SOLAR CELL

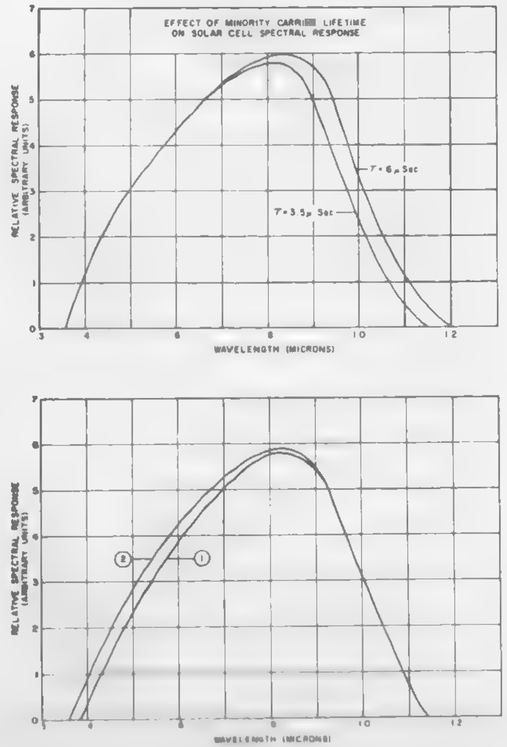


FIGURE 8 EFFECT OF JUNCTION DEPTH UPON SPECTRAL RESPONSE

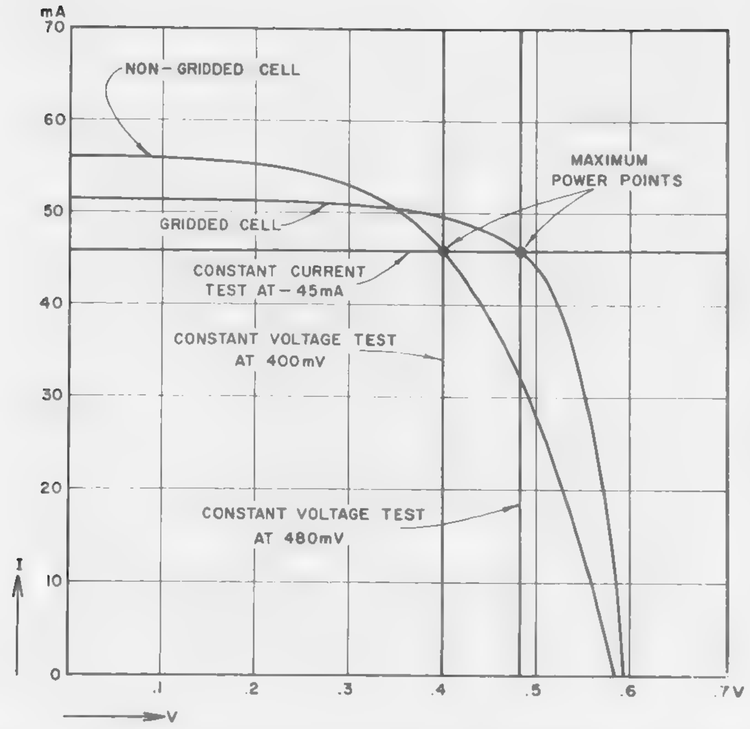


FIGURE 9 CONSTANT VOLTAGE AND CONSTANT CURRENT TEST OF SOLAR CELLS TYPE 120C, AT 25°C

Figure 10 shows an exponential plot of the current-voltage behavior of solar cells vs. illumination level. While the exponential plot gives an exaggerated idea of the rectangular behavior of the current-voltage characteristic, one may obtain a maximum power point which represents approximately 90% of the short circuit current and 80% of the open circuit voltage in good solar cells. These figures are based upon measurements on 100 cells of 11% space sunlight efficiency.

Since increased temperature boils electrons out of their valence bonding positions, increased temperatures increase back leakage (I_s) across the junction. This results in lower electrode potentials. Figure 11 shows the effect of temperature upon power output.

It was found that during the years of solar cell improvement under tungsten light a serious degradation of efficiencies resulted whenever cells were illuminated by other spectral

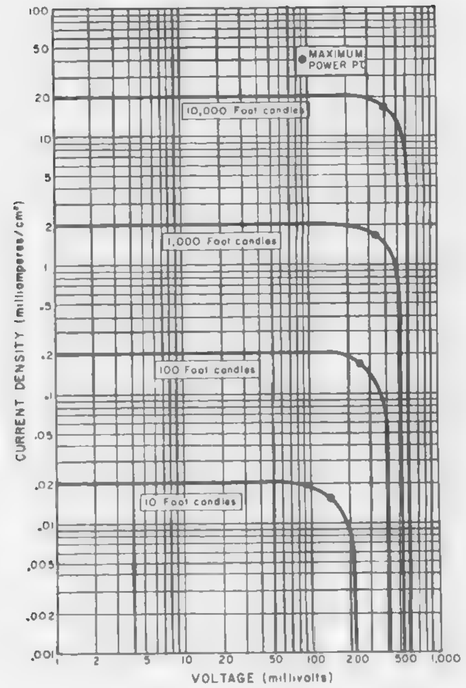


FIGURE 10 CURRENT VS VOLTAGE AT VARIOUS ILLUMINATION LEVELS FOR SILICON SOLAR CELL

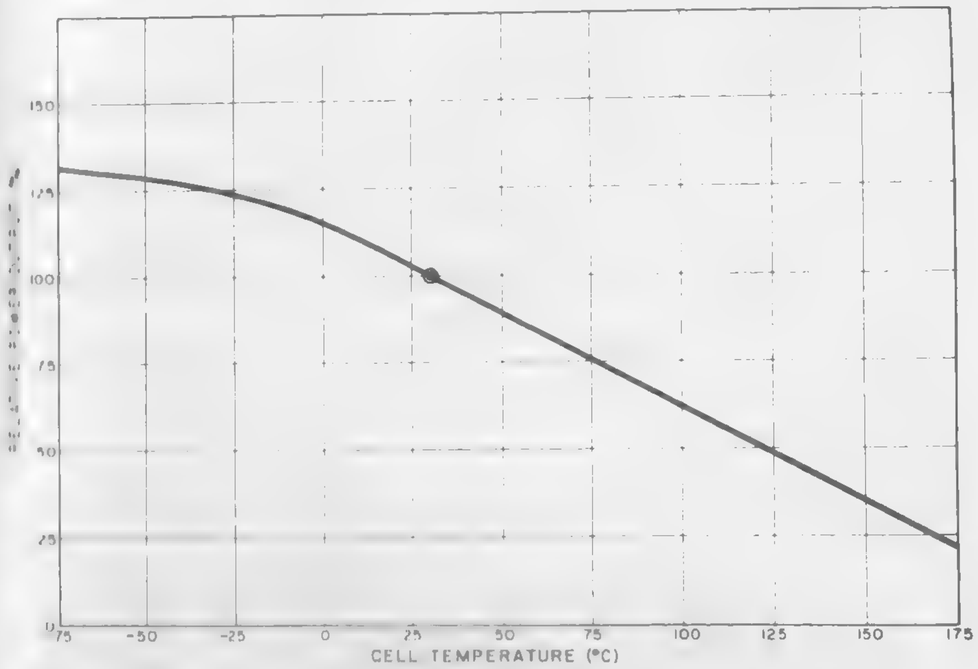


FIGURE 11 VARIATION OF OUTPUT POWER WITH TEMPERATURE CHANGE FOR SILICON SOLAR CELL

sources. Since recent requirements were based upon sunlight in space (Figure 12), it was necessary to attempt a laboratory duplication of the space sun. Such a sunlight simulator was built utilizing a zenon arc lamp in conjunction with a tungsten incandescent lamp, each appropriately filtered and blended such as to yield the best possible approximation to F. S. Johnson's curve of the space sun. This work was begun in late 1959 and completed in early 1961. Presently,

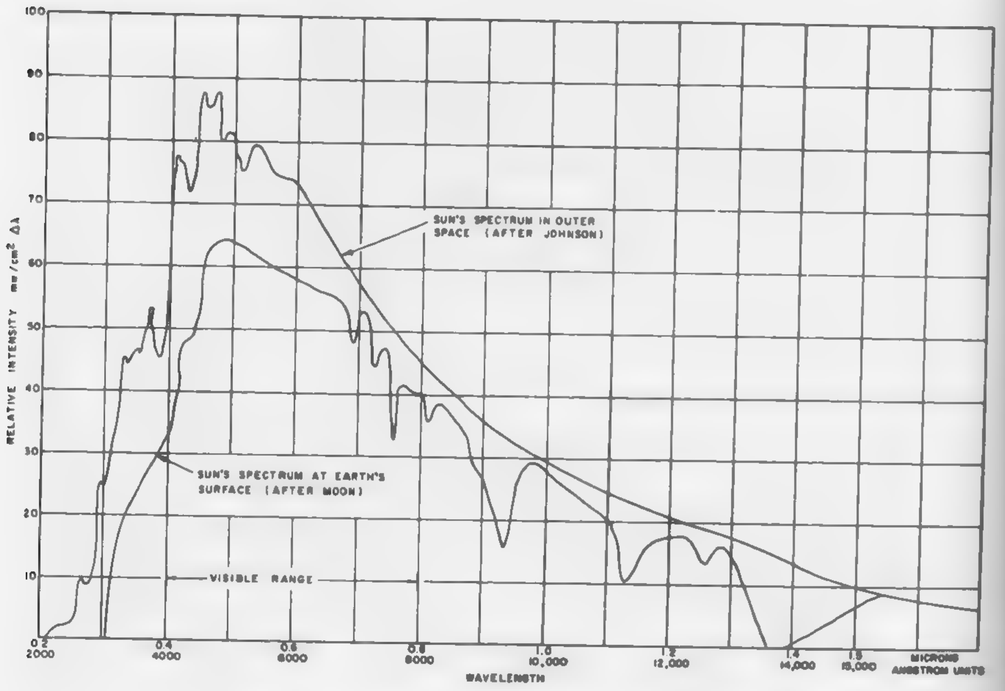


FIGURE 12 SPECTRAL DISTRIBUTION OF SUNLIGHT

Hoffman Semiconductor Division has two operating simulators on their premises, the early model being used for cell characterization, and the latest improved version operating as a module tester for 1" x 4" maximum modules. Figure 13 shows the spectral distribution of the earlier cell tester as compared to Johnson's curve. In the module simulator the spikes occurring between 0.8 and 1.0 microns

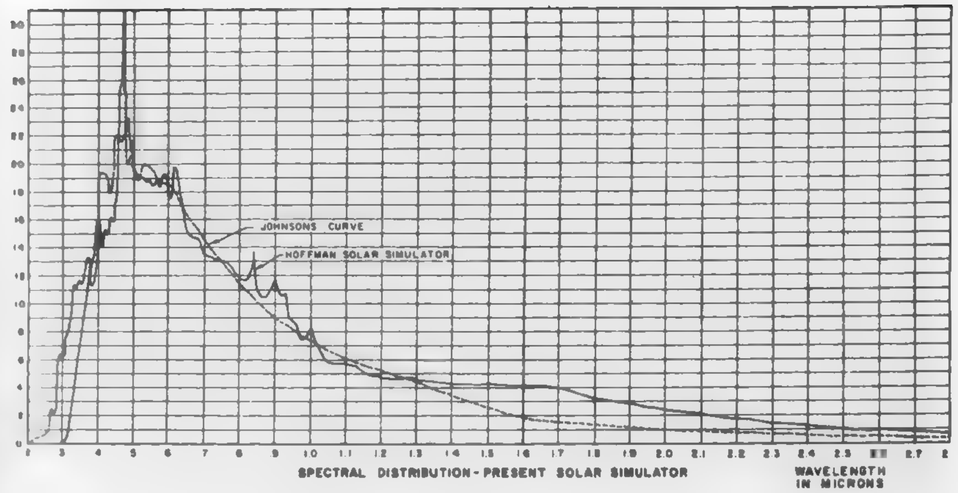


FIGURE 13

have been considerably attenuated. Figure 14 shows a photograph of the light sources of the cell simulator. Figure 15 shows a photograph of the module simulator in operation.

The use of the simulator allowed the optimization of diffusion and gridding processes to obtain a solar cell with maximum output in space sunlight. Figure 16 shows the spectral response of a solar cell prior to space sunlight optimization. Figure 17 shows the spectral response of a space optimized cell. The increase in blue response is largely due to a decreased diffusion depth. This increases the drift velocity of minority carriers in the p-layer due to an increased electric field. The increased sheet resistance of the thin p-layer is compensated by an increase in the number of lines of the collection grid.

An additional bonus obtained with the shallower diffusion is an increase in resistance to high energy particle radiation. According to measurements taken at Bell Telephone Laboratories which were communicated verbally (Dr. F. M. Smits),

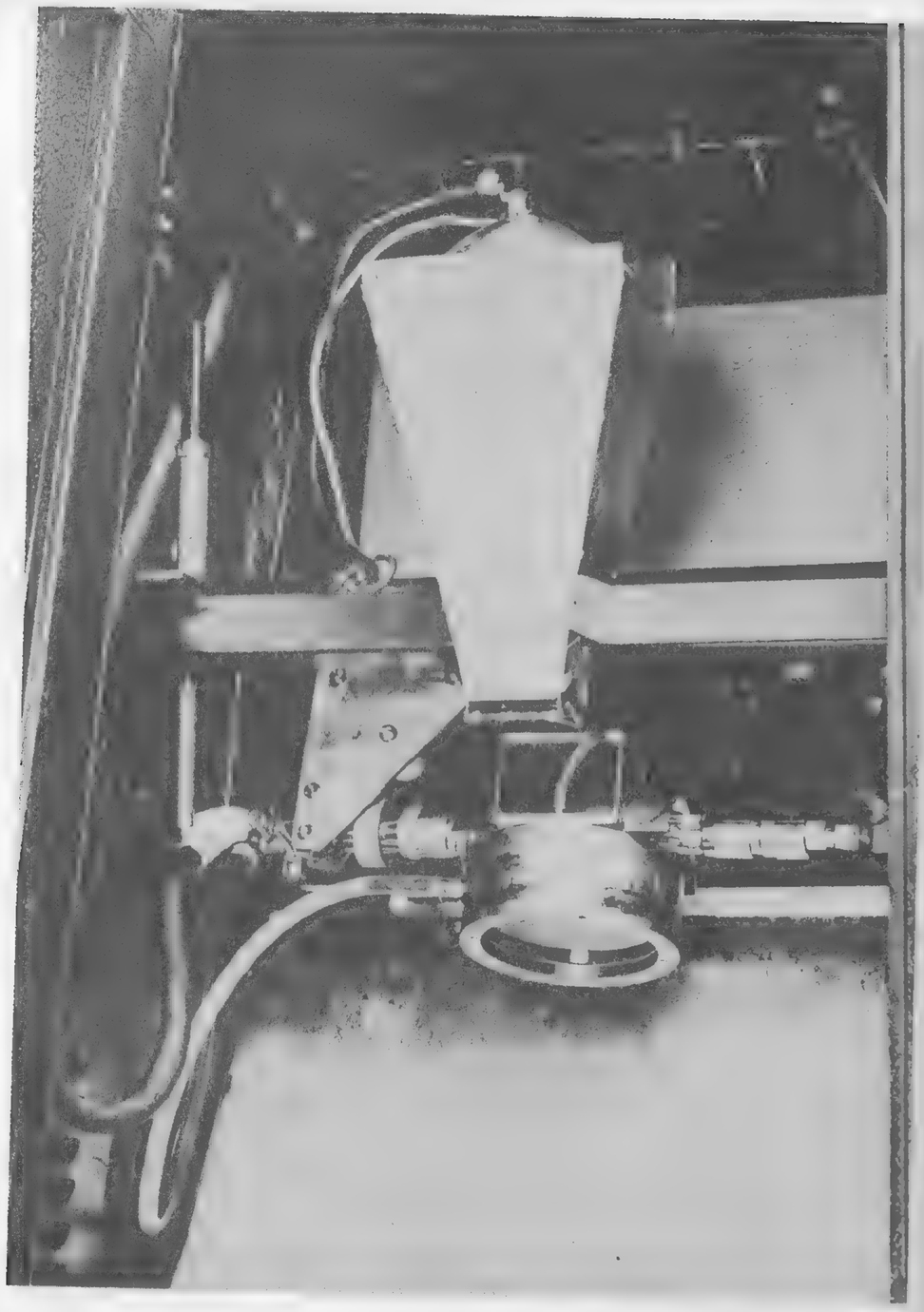


FIGURE 14 SOLAR SIMULATOR LIGHT SOURCES



FIGURE 15 SOLAR SIMULATOR FOR MODULE TESTING

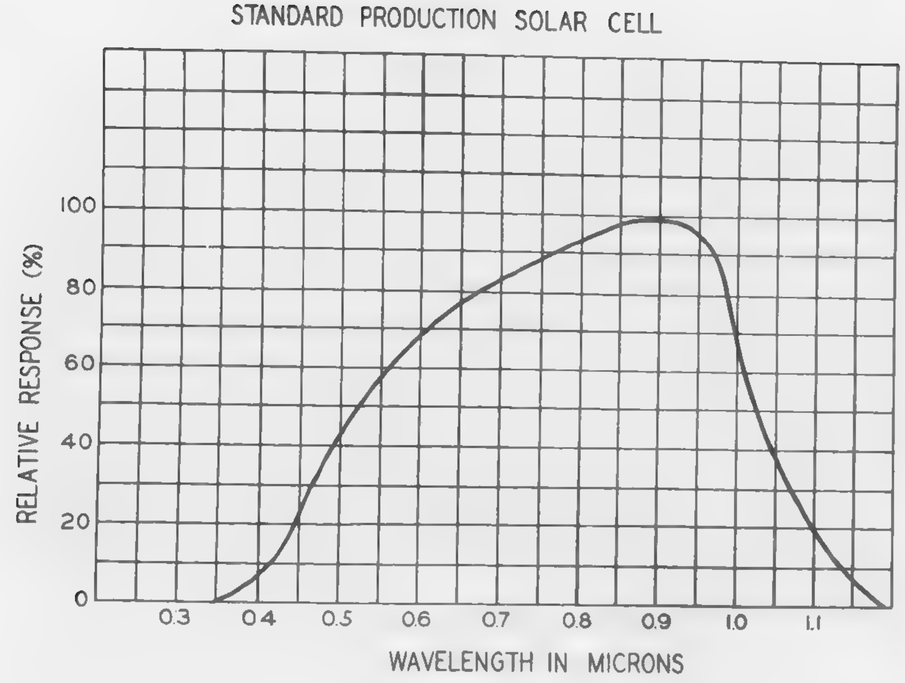


FIGURE 16

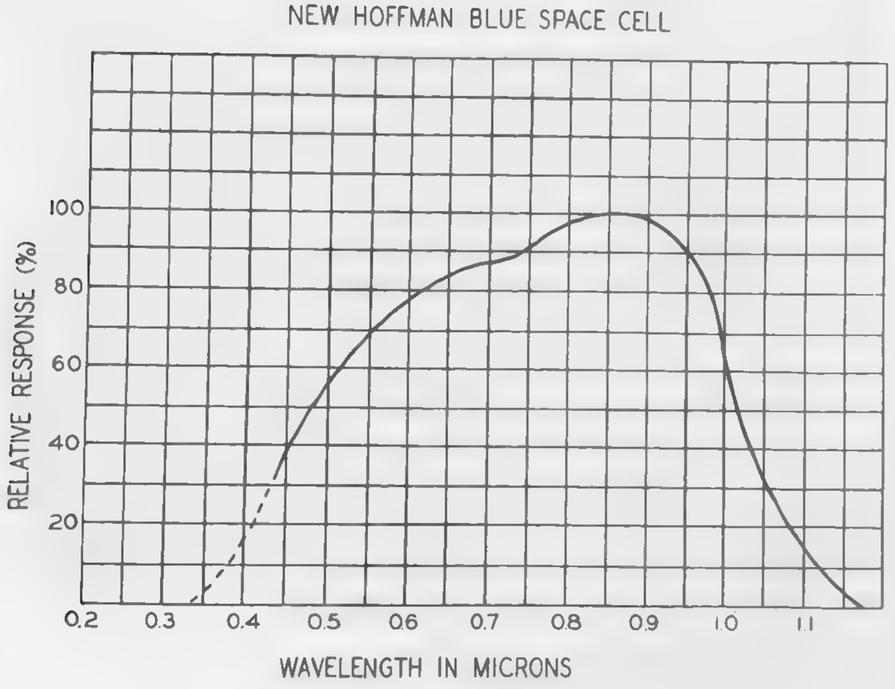


FIGURE 17

degradation from particle radiation is approximately cut in half. This means that a solar panel utilizing these cells will continue to deliver rated output in near earth space (Van Allen belt) for a period twice as long as the previously manufactured panels.

In addition to the above development, an N/P cell has been developed and proved out in pilot line production with space sunlight efficiencies up to 12% and having a spectral response very similar to the above cells. In Figure 18,

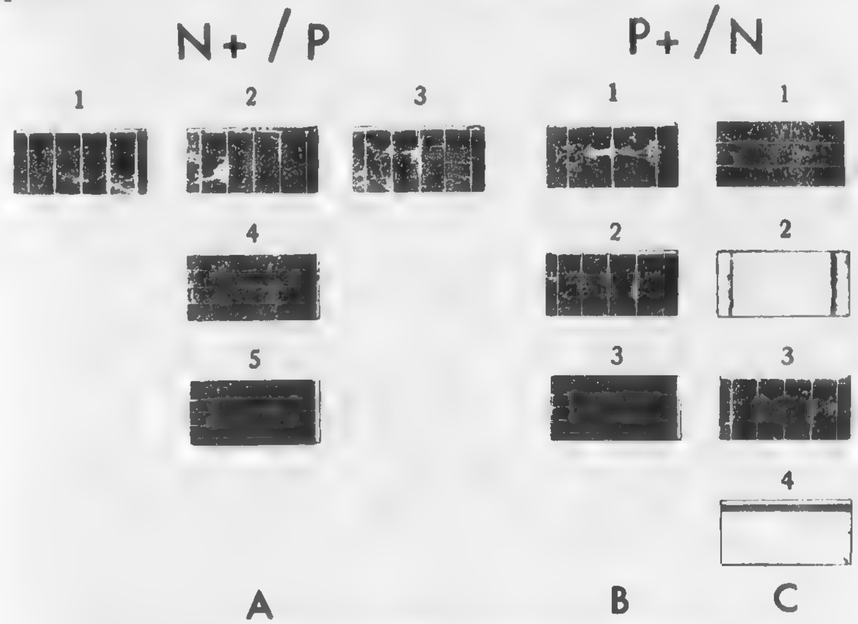


FIGURE 18 PHOTOGRAPH OF SEVERAL GRID CONFIGURATIONS OF CELLS

number of N/P and P/N cells are shown, including various grid configurations. In column B, cell No. 2 shows the collection grid for the "blue space" cell.

In order to achieve the best compromise between usable radiation received and degradation of output due to cell heating, optical filters with special properties are usually employed as coverglasses above the solar cell. These filters utilize antireflection coatings and interference films in order to reject light which cannot be properly used by present day solar cells. This light is normally below 450 millimicrons. Figure 19 shows a color slide of solar cells with filters applied. Due to the increased blue response of the "blue space"



FIGURE 19 SOLAR CELL MODULES WITH BLUE FILTERS APPLIED

cell, experimentation is presently carried out with filters with cutoffs at 435 millimicrons.

Filters are usually attached to the cell by means of an organic resin usually of the epoxy type. A considerable amount of development has been done in order to obtain a resin which meets the immediate requirements (optical transmission) and withstands the severe environmental conditions of space use (ultraviolet degradation, high temperature, vacuum soak, thermal shock, mechanical shock, low temperature (liquid nitrogen).

Figure 20 shows a picture of a solar panel fabricated for Jet Propulsion Laboratories, for use on the RANGER Spacecraft. These panels, utilizing the older cell (13% tungsten efficiency), are designed to deliver approximately 95 watts at 27 volts oriented to the space sun. A similar panel presently under construction with 12% tungsten efficiency is expected to have a space output of 102 watts.

Present investigations in the laboratories of the Hoffman Semiconductor Division include work on a radiation resistant solar cell concentration gradient on both sides of the junction which should result in a device which is considerably less dependent upon minority carrier lifetimes. Work is also being done on oxygen-free solar cells which have shown promise on a radiation resistance basis (Dr. J. Denney, Space Technology Labs.).

SUMMARY

A brief description of the semiconductor fundamentals for silicon solar energy converters has been given. Methods for optimizing solar cell efficiency for space power supply use have been mentioned. Such optimization has made it possible to realize power outputs of the order of 14 watts/square foot. The power/weight ratio varies from 6-10 watts per pound, depending upon panel construction. Environmental problems for space solar cells were outlined and some future trends in solar cell investigations were indicated.



FIGURE 20 SOLAR PANEL FOR JPL RANGER SPACECRAFT

MATERIALS FOR THERMIONIC CONVERTERS

Coleman Kaplan
Research Engineer, ASTRO
The Marquardt Corporation
Van Nuys, California

ABSTRACT

The basic theory of the thermionic converter is reviewed. Various methods of reducing the space charge limitation of current in a thermionic converter are discussed. In vacuum converters, the effect of space charge can be reduced by very close spacing or by the use of a crossed electric and magnetic field (the magnetic triode). Space charge can also be neutralized by introducing positive ions into the converter. In the cesium diode and triode, the plasmatron converter, and the pulsed diode, positive ions are supplied by ionization of a low pressure gas. Solid materials which emit positive ions when heated are also being investigated as a source of positive ions for space charge neutralization. The electrical and mechanical requirements for the emitter, collector and auxiliary electrode materials are discussed, as well as the problems related to insulators, seals, and electrical leads. The materials problems involved in using the thermionic converter with a nuclear reactor or a combustion chamber as the heat source are mentioned. The nuclear-heated application requires fissionable fuels and reactor structural materials that will withstand high temperatures and radiation damage. The combustion heated thermionic system requires materials with a reasonable lifetime when subject to corrosion and erosion by hot gases. Both applications require materials that are compatible with and can be joined to the electron emitters and insulators of the converter cells.

INTRODUCTION

Thermionic conversion is one of the techniques for the direct generation of electricity from heat. The underlying principle of the thermionic converter was probably first discovered by Thomas A. Edison, who described the operation of a thermionic generator in a patent almost 80 years ago. However, thermionic generation of electrical power at useful efficiencies was not attained until quite recently.

Figure 1 shows the operating principle of the thermionic converter. The basic converter consists of a hot electron emitter separated by a vacuum gap from a cooler electron collector. The emitter and collector are connected by an external circuit containing a load resistance. Electrons are evaporated from the emitter and cross the vacuum gap to the collector across a retarding potential. They are then returned to the emitter through the external load.

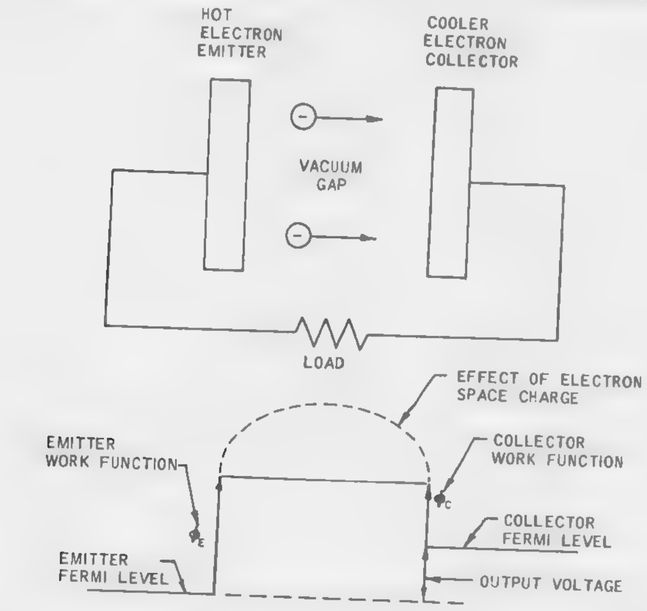


FIGURE 1 OPERATING PRINCIPLE OF THE THERMIONIC CONVERTER

The nature of the retarding potential for electrons is indicated in Figure 1, which shows the potential distribution of the converter. The average energy of electrons within the emitter is represented by the Fermi level. A potential barrier, known as the work function, is present to retard

the evaporation of electrons into the vacuum gap. Since there is a distribution of electron velocities, some of the electrons that arrive at the vacuum interface have enough energy to overcome the work function barrier and leave the surface. If the emitter temperature is high enough in relation to the magnitude of the work function, then very large electron emission currents can be obtained. The emitted electrons drift across the gap between emitter and collector, and fall through the collector work function to the collector Fermi level. If the work function of the collector is less than that of the emitter, then the difference in potential energy is available to the external circuit as useful electrical work.

It is necessary to consider the effect of space charge in the thermionic converter. Electrons emitted from the cathode form a cloud of negative charge in the interelectrode region, which reduces further emission across the gap. Since very little excess electron energy is available to overcome the space charge barrier, only minute currents will flow across the vacuum gap. The various techniques of overcoming this space charge limitation will be briefly reviewed.

Conceptually the simplest technique for the elimination of space charge is to use very close spacing between emitter and collector. The spacing required for reasonable power density and efficiency is several ten-thousands of an inch; the engineering problems of maintaining this spacing in a high temperature device are formidable. The lifetime of the close-spaced vacuum converter is limited, since small dimensional changes due to warping or evaporation of the emitter material cause short circuits, etc.

Another technique for reducing the space charge limitation in a vacuum converter is shown in Figure 2. A third electrode at a positive potential is used to accelerate electrons away from the emitter surface. A magnetic field is present at right angles to the emitter and collector, and turns the electrons around so that they reach the collector surface instead of intersecting the accelerating electrode. The efficiency of this converter is quite low, since the accelerating electrode collects electrons which are scattered

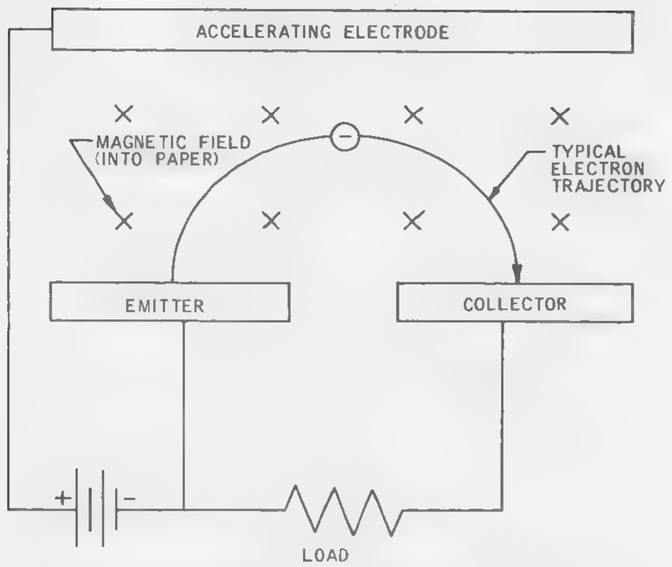


FIGURE 2 CROSS-SECTION OF THE MAGNETIC TRIODE

by electron-electron collisions. Due to the high positive voltage required at the accelerating electrode, the electrical power input is almost equal to the output power.

The methods of elimination of space charge which are receiving the greatest amount of attention in current research involve introducing positive ions into the emitter-collector gap. These positive ions serve as a grid in that they neutralize the electron space charge to yield a large electron current across the converter. Various techniques for producing positive ions in the thermionic converter are being studied.

In the cesium diode, cesium vapor is present in the interelectrode space and forms ions upon contact with the hot emitter surface. The cesium also serves to lower the collector work function to allow a greater output voltage. The emitter temperature required for this type of operation is generally very high, yielding problems due to evaporation; it therefore becomes very difficult to use conventional heat sources.

Under certain conditions the cesium thermionic converter appears to operate as a low voltage arc. Positive ions are then supplied by the collision of electrons with neutral cesium atoms in the emitter-collector gap.

The desirable temperature for operation of the thermionic converter is generally lower than the temperature needed to produce a sufficient supply of cesium ions. A possible solution to this problem involves the use of a third high-work-function electrode, at the emitter temperature, to ionize the cesium vapor.

The application of the "plasmatron" principle to the thermionic converter is currently under investigation at several laboratories. This consists of maintaining an auxiliary arc discharge within the converter, such that the power input to the auxiliary discharge is small compared to the power output of the converter. The auxiliary discharge is operated at a voltage high enough to yield copious ionization of the interelectrode gas. The resulting positive ions are used for space charge neutralization of the main current between emitter and collector.

Another method of ionizing the interelectrode gas, which is under investigation at Marquardt, is the application of a voltage pulse to the thermionic diode. In this type of converter, the anode is momentarily biased to a positive voltage with respect to the cathode. Electrons which are accelerated across the interelectrode gap collide with neutral gas atoms, ionizing them. The anode is then returned to a negative voltage so that the converter can produce electrical power. The positive ions resulting from the pulsed discharge are lost by recombination during the power output portion of the operating cycle, so that the converter must be pulsed on a repetitive basis to restore the ion density.

Another approach to the problem of space charge neutralization involves the use of ion dispenser materials, which emit positive ions when heated. The positive ion emitter which has been most extensively investigated for this purpose is beta eucryptite. This is a ceramic material which emits positive lithium ions when heated to about 1200°C. The most successful operation with an ion dispenser is achieved when the ion emitting material is used as a third electrode.

CONVERTER MATERIALS PROBLEMS

For the purposes of this paper, the materials problems related to the converter will be discussed separately from the materials problems related to the rest of the power generating system, although there is a great deal of relationship between these two areas.

Emitter Materials

The most important electrical characteristic of an emitter material to be used in a thermionic converter is the electron work function. The optimum value is determined by the desired operating temperature of the emitter. In the vacuum converters or the auxiliary ionization converters, where the emitter surface is not required to ionize cesium vapor, work function values of about 1.5 to 2.5 volts can be used. Materials with work functions in this range have been used for many years in the electron tube industry; these include rare earth oxides and other thin film emitters. For the intermediate temperature converters, emitter materials such as thoriated tungsten, lanthanum hexaboride, and dispenser materials such as the Phillips cathodes are being investigated. Finally in the high temperature converters where high emitter work function is allowable, the refractory metals and carbides are being investigated. In the arc-mode cesium converter, which uses high cesium pressure and intermediate values of cathode temperature, a molecular film of cesium is formed on a refractory metal emitter surface, lowering the work function to the desired value.

Another electrical characteristic of the emitter which must be considered is the bulk or interface resistance. This is important because the voltage drop across this resistance reduces the output voltage. If the converter is to be operated at high current densities, then this resistance is even more critical. Of course, the heat generated due to current flowing through this resistance must be considered if it has damaging effects upon the emitter surface. At the lower values of work function, the matrix emitters, using a mixture of oxides and metallic powder sintered onto a metal substrate, appear to be superior in this respect to the ordinary sprayed triple oxides.

The mechanical and thermal properties of the emitter surface must also be considered. The evaporation rate of the emitter will, of course, determine the converter lifetime. This is particularly true of close-spaced converters, where dimensional changes due to emitter evaporation must be reckoned with. Also, if the collector material is different from that of the emitter, the evaporation of emitter material and subsequent condensation upon the collector will alter the electrical characteristics of the converter.

If the emitter material is deposited upon a substrate of a different material then the problems of bonding the emitter to the substrate must be considered. There are many materials which would be useful in thermionic converters, except for the bonding and compatibility problem.

Collector Materials

The electron work function of the collector is another important parameter of the thermionic converter. In applications where the collector can be operated at low temperatures, the work function should be made as low as possible to maximize the output voltage, which is equal to the difference between the emitter and collector work function. The lowest work function surface currently known is a cesium oxide film on silver, which has a work function of about 1 volt. Serious difficulties are encountered in using this material in an operating thermionic converter. Further research is needed to develop very low work function collector materials.

If the collector is operated at higher temperatures, as might be required for space applications where the rejected heat of the conversion process must be radiated to space, or in conversion cycles where the heat rejected by the anode is accepted by another energy conversion cycle, then the collector work function must be higher to limit the emission of electrons from the collector surface. The problem then becomes one of achieving a collector work function close to the optimum, which yields the maximum power output for a given emitter temperature.

In converters using cesium vapor in the interelectrode space, the cesium is adsorbed on the collector surface, modifying the work function. In many applications, this is advantageous because it allows the use of metals such as copper or stainless steel for the collector.

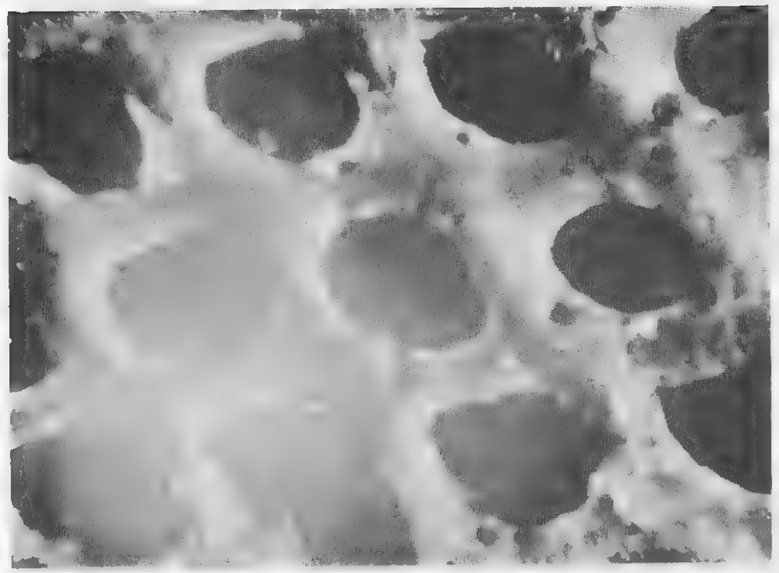
Ionizing Electrode Materials

In one type of converter described previously, the cesium vapor is ionized by coming in contact with a separate ionizing electrode. The chief property that this electrode must have is a high work function in the presence of cesium vapor. The adsorption process mentioned previously lowers the work function of metallic surfaces, thereby decreasing the ion yield to very low values. Also, in converters where the evaporation of emitter material is appreciable during the converter lifetime, the ionizing electrode should be capable of maintaining its high work function in spite of condensation of material from the low work function emitter.

Ion Emitter Materials

Materials which emit positive ions when heated have been studied by numerous workers for a period of several decades. One of the best positive ion emitters that has been observed in these studies is beta eucryptite. This is a ceramic material with the chemical formula Li_2O, Al_2O_3, $2SiO_2$. Positive lithium ions are emitted when this material is heated to temperatures in the range of 1000-1300°C. Beta eucryptite has the advantage of producing a relatively large current density of positive ions from a reasonably stable material.

Figure 3 shows a beta eucryptite coating fused onto a tantalum screen, used as an ion emitting grid in studies at Marquardt. A positive ion current sufficient to neutralize an electron current of several amps per cm^2 have been obtained from this grid.



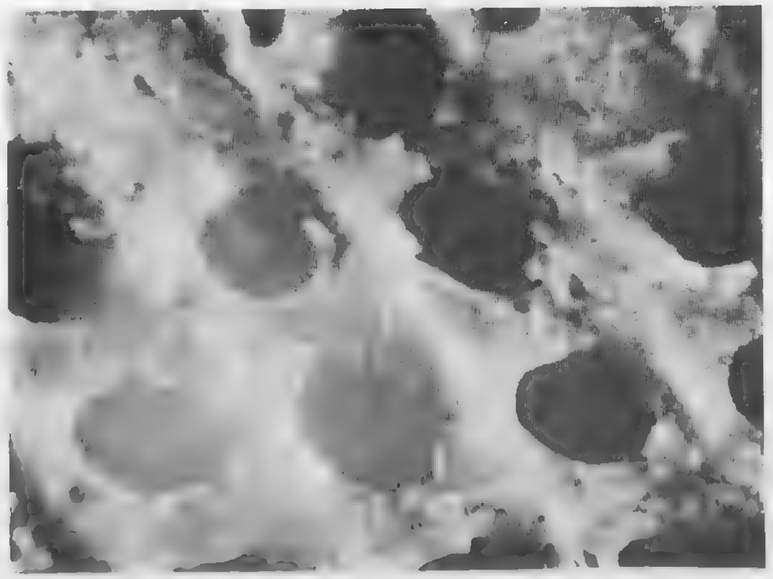


FIGURE 3 BETA EUCRYPTITE FUSED ON TANTALUM SCREEN (36 TIMES MAGNIFICATION)

Encouraging results have also been obtained at Marquardt with a material similar to beta eucryptite except that rubidium ions are emitted instead of lithium. The heavier rubidium ion has a lower velocity, so that a larger number of electrons can be space-charge neutralized per positive ion.

Further research will undoubtedly indicate other materials that can be used as ion emitters. The desirable characteristics are reasonable current density at intermediate temperatures, and long emission lifetime. For long term applications, it is desirable to have an emitter material such that the positive ions could be replenished in some manner, or to have a dispenser with a reserve supply of the material to be ionized.

Insulators

Problems are encountered in finding suitable insulating materials for the thermionic converter when high cathode and anode temperatures are to be used. These problems are even more acute when cesium vapor is present, since cesium attacks many of the common insulator and seal materials. Experience has shown that ceramic-to-metal seals using low expansion alloys brazed to metalized alumina are suitable for use in cesium thermionic converters at seal temperatures up to 600°C. Further research is needed to yield insulating seals that will be useful at higher temperatures.

Electrical Leads

The problem of suitable materials for electrical leads becomes evident when we consider that the thermionic converter is a high current, low voltage power generator. It is therefore desirable to have many converter cells in series. Each electrical lead in a series connection goes from a hot emitter to a cool collector; the heat conducted by the leads represents a decrease in the thermal efficiency of the converter. Even worse, this heat flow may cause a portion of the emitter to operate below its normal temperature, causing a decrease in electron emission. Of course, the electrical

leads cannot be made too small in cross section or the lead resistance will dissipate an appreciable portion of the electrical power generated. The optimum lead material is therefore, one which has a high electrical conductivity coupled with a low thermal conductivity. In addition, the lead materials may be required to serve as mechanical supports in some converter configurations, so that a high mechanical strength would be required.

HEAT SOURCE MATERIALS PROBLEMS

Many of the problems encountered in thermionic converter heat sources are common to all high-temperature systems. An attempt will be made to limit this discussion to those problems which are unique to the thermionic conversion power system.

Nuclear Reactor Heat Source

When used to convert heat from a nuclear reactor to electrical energy, the thermionic converter promises several distinct advantages as compared to other thermodynamic systems. The absence of rotating parts, high velocity gases, etc., allow the use of very high input temperatures to the conversion system. The upper limit to the operating temperature of the emitter in a thermionic converter is the temperature limitation of the fissionable material in the reactor, or the evaporation rate of the electron emitter.

Although the intrinsic temperature of the nuclear fission process is of the order of millions of degrees centigrade, the actual temperature that can be achieved in a reactor is limited by the materials problems of the fuel pins and reactor structural materials. In a thermionic converter located within a reactor core, there is also the problem of obtaining an emitter material which can be placed in thermal contact with the fissioning fuel. This problem is aggravated by the fact that at high temperatures many of the fission byproducts are released as gases, which must be removed from the core. There are also severe compatibility problems when conventional electron-emitting materials are used in contact with fissioning fuels.

A unique solution to the above problem, which is under study at the Los Alamos Scientific Laboratory and elsewhere, involves the use of uranium carbide fuel, which is also a good thermionic emitter. Zirconium carbide is added to improve the electron emission characteristics and the thermal and mechanical stability. However, this fuel pin is subject to swelling and warpage, which limits the converter spacing that can be used. Although encouraging results have been obtained from inpile tests of this material, much further work along these lines is needed before a practical nuclear thermionic power system can be obtained.

For some applications, it may be desirable to have the thermionic converter outside of the reactor core. The heat would be transferred from the reactor to a fluid or solid heat transfer medium and hence to the emitter of the thermionic converter. A major materials problem here is finding a suitable heat transfer medium which will be compatible with both the reactor and the thermionic converter materials.

Chemical Heat Source

The use of combustion gases to heat the emitter of a thermionic converter is being studied at Marquardt and elsewhere. The major problems in this area are caused by the corrosive nature of the moving combustion gases.

It is generally desirable to have separate converter cells which are arranged in a series connection, to raise the output voltage of the system. If these cells are in the same combustion chamber, then they must be electrically insulated from each other. This requires the use of ceramic to metal seals at the emitter temperature to prevent the flow of combustion products into the emitter-collector gap.

Various types of coatings such as sprayed alumina, etc., are available to protect the emitter from combustion gases. To date, the lifetime of these coatings has been very short due to thermal shock, differential expansion between the coating and the emitter, and due to erosion by the combustion gases. A definite need therefore exists for a coating that will protect the emitter for long periods of time.

ACKNOWLEDGEMENTS

The author wishes to thank his colleagues for helpful discussions; Figure 3 was supplied by K. R. Pinckney. The Marquardt program in Thermionic Conversion is supported in part by the U. S. Army Signal Research and Development Laboratory and by the Air Force.

THERMIONIC CONVERSION

BIBLIOGRAPHY

General References

Kaye, J. and J. A. Welsh. Direct Conversion of Heat to Electricity. Wiley, 1960.

Kohl, W. H.: Materials and Techniques for Electron Tubes. Reinhold Publishing Corp., 1960.

Proceedings of the 20th and 21st Annual Conferences on Physical Electronics, MIT, (1960 and 1961).

Electron Emitter Materials

Stout, V. L.: Thermionic Emission and Thermionic Power Generation. Published in "Thermoelectricity", Wiley, 1958 (P. H. Egli, Editor).

Plasmatron Principle

Johnson, E. O. and W. M. Webster: The Plasmatron, A Continuously Controllable Gas-Discharge Developmental Tube. Proc. I.R.E., Vol. 40, p. 645 (1952).

Ion Emitters

Couchet, G.: Contribution to the Study of Solid Ion Sources, (in French). Annales de Physique, Vol. 9, p. 731 (1954).

Surface Ionization of Cesium

Taylor, J. B. and I. Langmuir: The Evaporation of Atoms, Ions and Electrons from Cesium Films on Tungsten. Physical Review, Vol. 44, p. 423 (1933).

ADVANCED ELECTRON TUBES FOR HIGH FREQUENCY, HIGH POWER, AND LONG LIFE

Dr. Walter L. Knecht
Ass't. Chief, Thermionics Branch
Electronic Technology Laboratory
Aeronautical Systems Division
Wright-Patterson Air Force Base, Ohio

ABSTRACT

Great research efforts are spent on extending the state of the art of electron tubes for high frequency, high power, and long life. This research is required for anticipated aerospace systems. Electromagnetic radiation generated in the submillimeter range can be focused into narrow beams which will enable safe communication between two points. Submillimeter waves of high power are required to cover interplanetary distances. Space electronic systems will require electron tubes capable of operating reliably for a minimum of two years. In accordance with these requirements for high frequency, high power, and long life great emphasis is placed upon research designed to extend ultimately the state of the submillimeter art. This research, to some extent, covers the extension of present microwave tube technology as well as new ideas and concepts based on an attempt to analyze promising approaches aimed at extending the wavelength region from the submillimeter range to the optical wavelengths. Present designs, materials, and electron tube technology exhibit inherent limitations. New ideas will be required to achieve this goal.

INTRODUCTION

The challenge of space requires intensive research on electron tubes for high power, high frequency, and long life. The research on these electron tubes necessitates both phases of research work, namely, basic research and applied research. The basic research is directed toward an increase in fundamental knowledge in the microwave science. It covers theoretical analysis, exploration, and experimentation aimed at an increased understanding of the phenomena involved in generating electromagnetic radiation. The applied research, in turn, is concerned with the exploration of knowledge, material, and techniques from concept up to and including an experimental demonstration of feasibility of devices built. In establishing research programs in the area of submillimeter wave tubes, great emphasis is placed upon programs having a great potential pay-off even though they also have a high risk. Since the principal objective of this research work is aimed at submillimeter tubes the expression of submillimeter tubes is used collectively, that means, it will refer to both millimeter tubes and submillimeter tubes.

REQUIREMENT

Background

In general, microwave tubes are required for electronic equipment used for navigation, guidance, control surveillance, reconnaissance, tracking, fire control, communication, and electronic countermeasures. Superior microwave tube performance characteristics are required for the referenced applications. In illustration, microwave tubes used for radar systems must possess excellent performance characteristics in terms of stability, coherence, short pulse rise time, long pulse length, tunability, low noise figure, high power, high efficiency, and long life. These performance characteristics will control the performance of radar systems relative to high resolution significant for target recognition, increased range, and reduced vulnerability to electronic countermeasures. Microwave tubes used for communication systems

must satisfy high performance standards in regard to frequency stability, modulation characteristics, linearity, and multichannel operation. Finally, microwave tubes used for electronic countermeasure systems must exhibit optimum performance characteristics relative to wide bandwidth, high gain, and high power handling capability.

Submillimeter Waves

Submillimeter tubes are required because of their superior performance characteristics in regard to narrow beam width, high resolution, wide modulation bandwidth, high energy density, and distinctive atmospheric absorption phenomena. These superior properties suggest a variety of applications, including the following:

a. Transmission windows in the atmospheric absorption bands of submillimeter waves exist at the frequencies of 85 kmc/sec, 125 kmc/sec, 230 kmc/sec, and 850 kmc/sec as shown in Figure 1. For this reason, these frequencies may be used for space to earth communication.

b. The high resolution obtainable at submillimeter waves will make possible superior radar systems which will exhibit increased directivity at miniaturized antenna size. Submillimeter radars will have considerable range in space since the power density radiated is inversely proportional to the wavelength squared. The high resolution of submillimeter radars will make them useful for satellite inspection and homing as well as for lunar and planetary landing control.

c. The narrow beam width, the wide modulation bandwidth, and the high energy density obtainable at submillimeter waves will make possible superior communication systems covering large interplanetary distances.

d. Plasmas generated in front of hyper-velocity vehicles are transparent in the submillimeter wave region which, therefore, may be used for communication, guidance, and telemetry systems of re-entry vehicles.

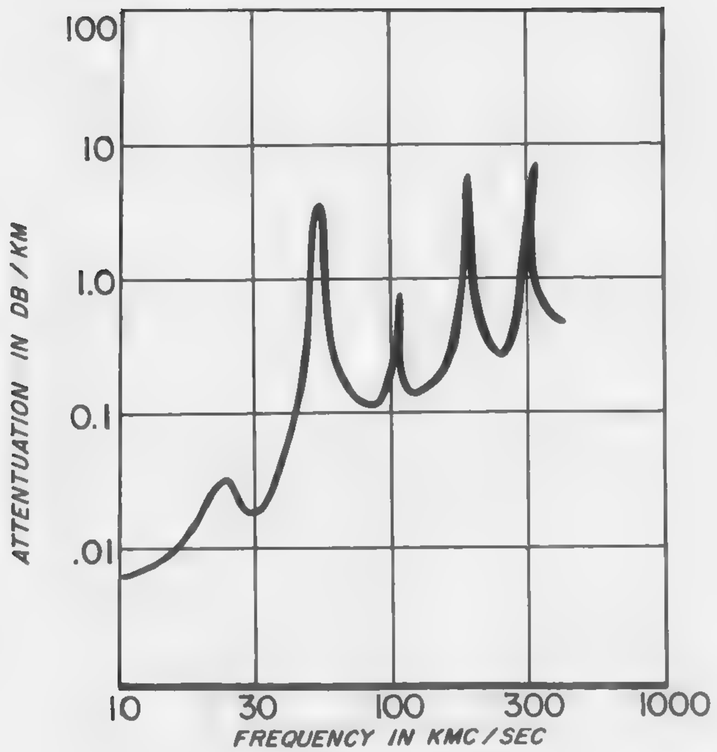


FIGURE 1 MILLIMETER WAVE ABSORPTION

e. Submillimeter waves will aid in electronic countermeasures by permitting the use of highly directional antenna beams. Furthermore, submillimeter waves will improve the performance of Doppler navigation systems, altimeter equipment, and high information rate data links.

f. Submillimeter waves will be used for spectroscopy giving access to a broader range of the spectrum than was previously available and so giving a clearer view of the structure of the matter. Submillimeter waves offer a tool for the investigation of fundamental properties of matter, including rotational spectra of molecules, fine and hyperfine intervals of atomic spectra, vibration spectra of solids or molecular crystals, electron paramagnetic resonance, cyclotron resonance of electrons in solids and gases, study of the superconducting state, and plasma investigations. Many

atoms, molecules, and crystals have sharp, strong spectral lines that can be measured with the high resolution and high precision methods of submillimeter wave spectroscopy.

g. Submillimeter wave astronomy is a potentially important field because a sharp probing of the universe, sun, moon, or planets can be made with an antenna which is small enough to be maneuvered. Submillimeter wave astronomy combines advantages of both optical and radio astronomy. Some free radicals, or molecular species, and excited atoms in the solar atmosphere, and perhaps some in outer space, have spectral transitions occurring in the submillimeter region.

High Power, Long Life Submillimeter Tubes

Electron tube power is a stringent requirement for space. Electronic equipment anticipated for use in space must be capable of covering interplanetary distances. Life is another stringent requirement imposed upon electron tubes used in space. Satellites, for instance, may last a minimum of two years. As a consequence, submillimeter tubes designed for space must have a minimum life of the order of 25,000 hours.

AVAILABLE HIGH POWER MILLIMETER TUBES

In general terms, existing microwave tubes may be broken down into five categories, namely, M-type backward wave oscillator, klystron, magnetron, traveling wave tube, and O-type backward wave tube. Each one of these categories represents a different approach to generating electromagnetic energy. Each one of these approaches may have its limit in regard to its capability of generating very short submillimeter waves. Figure 2 summarizes this information on the five approaches including significant performance characteristics, and the smallest wavelengths attainable at this time. In accordance with this information, the smallest wavelength may be generated by the O-type backward wave oscillator. In terms of high power generated by millimeter

tubes, Figure 3 shows representative and expected power levels of millimeter tubes covering a wide wavelength spectrum starting from approximately ten millimeters. Figure 3 lists the CW power of a representative series of O-type backward wave oscillators for the wavelength range from 6 mm to 1 mm. The boxes of Figure 3 list frequency ranges specified. In the frequency range extending up to 35 kmc/sec a growing number of millimeter tubes will become available. From 35 kmc/sec to 1000/sec, a small number of submillimeter tubes of limited power capability is available at present. A gap exists in the frequency spectrum, namely, from approximately 1000 kmc/sec to the optical frequencies. There exists no information on electromagnetic radiation devices capable of operating within the frequency region of this gap. The last box refers to the performance characteristics of the light amplification device accomplished by the stimulated emission of radiation, or in short, the laser devic

	GAIN	BANDWIDTH	EFFICIENCY	WAVE-LENGTH LIMIT MM
M TYPE BWO	—	HIGH	MEDIUM HIGH	5
KLYSTRON	HIGH	LOW	MEDIUM	3
MAGNETRON	—	LOW	HIGH	2
TWT	HIGH	VERY HIGH	MEDIUM HIGH	1.5
O TYPE BWO	—	VERY HIGH	LOW	.5

FIGURE 2 MICROWAVE TUBE LIMIT

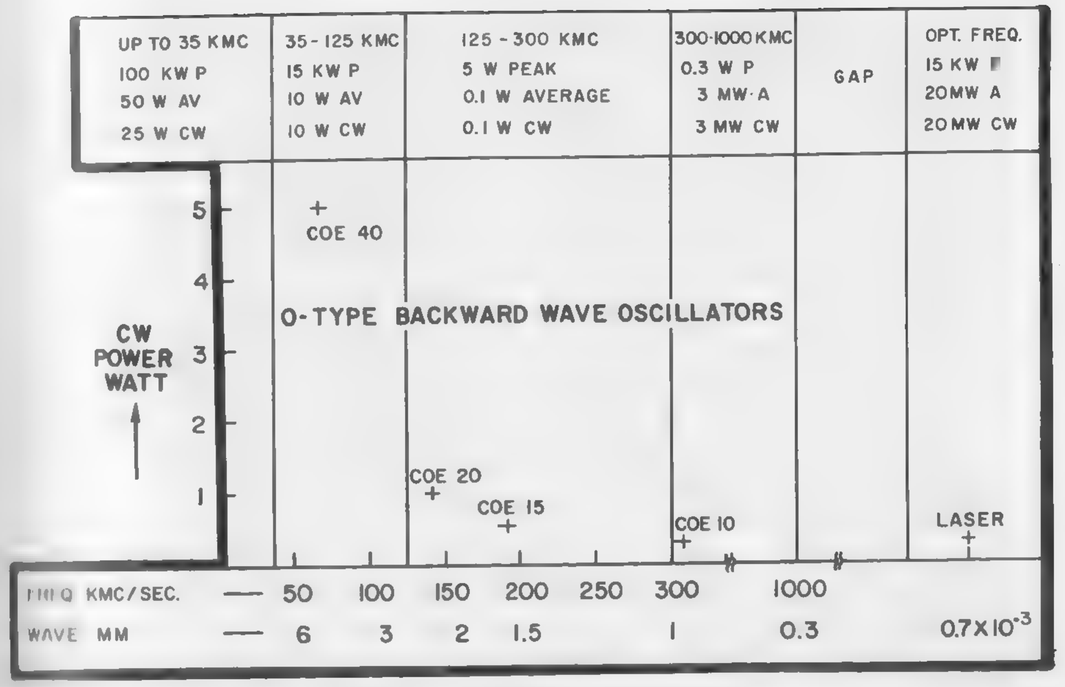


FIGURE 3 MILLIMETER TUBE POWER

APPROACHES TO SUBMILLIMETER TUBES

Many approaches are tried to close the existing gap in the electromagnetic frequency spectrum. This review is limited to the approaches which are aimed at the high power submillimeter tube rather than the low power device. A few approaches in this research area are discussed in the following.

Efforts Based on Established Device Concepts

A representative example of current efforts based on established device concepts is the approach designated Ubitron. It is a high power device which makes use of the cumulative interaction of an electron beam with a circuit

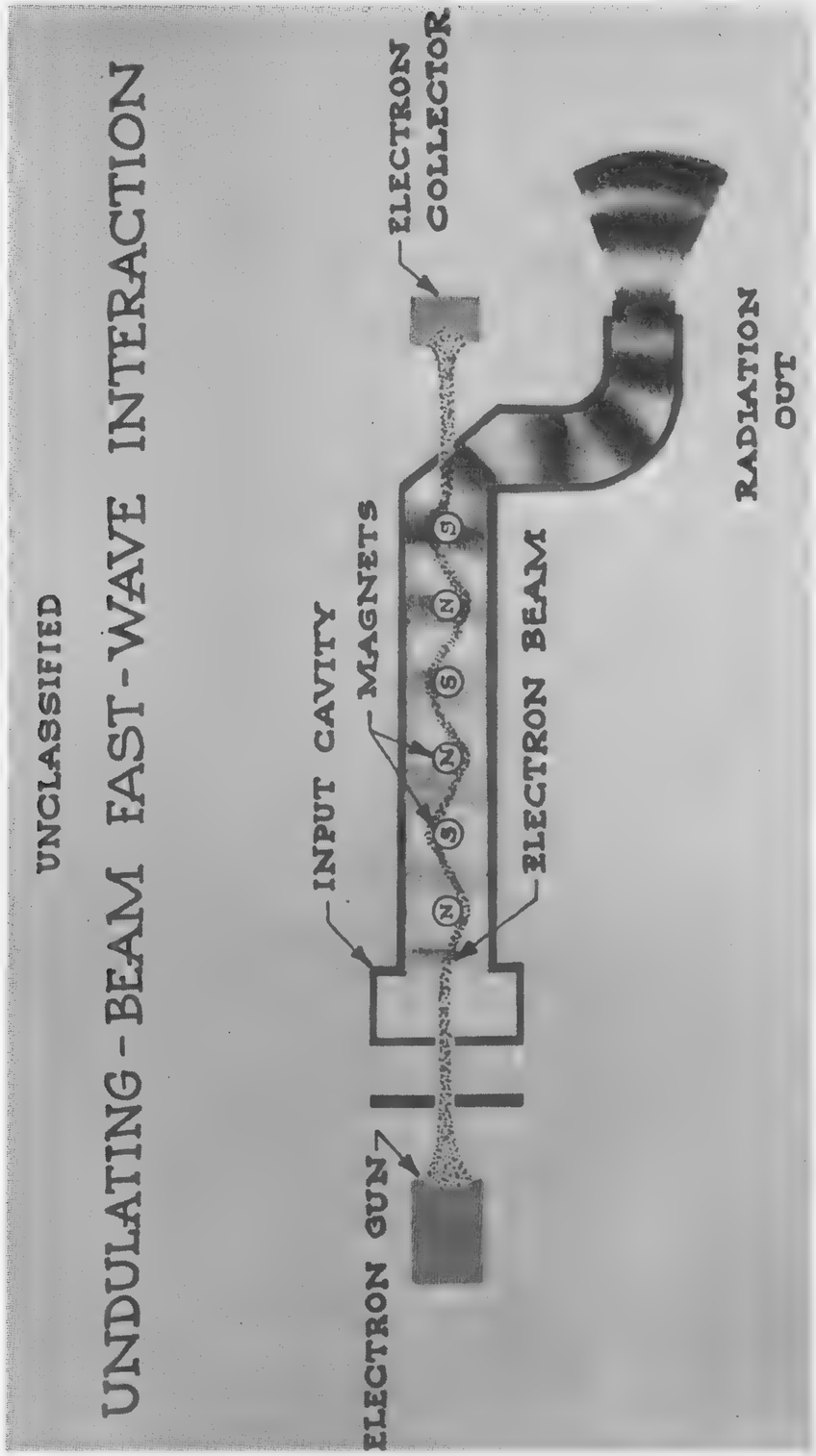


FIGURE 4 UNDULATING-BEAM FAST-WAVE INTERACTION UBITRON

wave that has a phase velocity greater than or equal to the free space velocity of light. Such waves are termed fast waves. This means that the circuit may be an unloaded cylindrical or rectangular waveguide as shown in Figure 4. An approach that appears promising for generating millimeter waves is to have the electrons transverse a periodic trajectory in an undulating magnetic field. The advantages of this approach are twofold. The circuit has a very simple geometry, and, in turn, the strongest RF field strength is in the beam region rather than at the conducting surface at the circuit. The limiting factors of this approach are the periodicity of the undulating magnet field becoming increasingly smaller with higher frequencies and, in addition, the electron beam flexibility which will decrease with increasing frequencies. The feasibility of this approach has been demonstrated at the approximate wavelength of 10 mm. As far as the potential power capability of this device is concerned, it is anticipated that such a device may be feasible up to a wavelength of the order of one millimeter with a potential peak power of some kilowatts. Major problem areas in this research relate to advanced magnet configurations to generate an efficiently undulating magnetic field, to electron gun structures capable of generating high density electron beams, and to efficient coupler devices.

A second example of current efforts based on established device concepts is the approach designated Rebatron, a short term for relativistic electron bunching accelerator. As shown in Figure 5, the Rebatron consists of an electron gun to generate an electron beam, and cavities to bunch and accelerate the electron beam. The feasibility of this device has been demonstrated at the approximate wavelength of 108 mm utilizing an electron beam of 0.1 ampere accelerated up to 1 megavolt, resulting in a beam power of 100 KW. The device generates beam harmonics up to the 34th harmonics which corresponds to a wavelength of 3 mm. This design concept can be utilized together with innovations to become a significant device at the fundamental wavelength of 10 mm. This device, if proven feasible, will be used for the generation of submillimeter wavelengths of smaller than 0.5 mm. The bunched electron beam of this device will be utilized for the generation of coherent electromagnetic radiation in

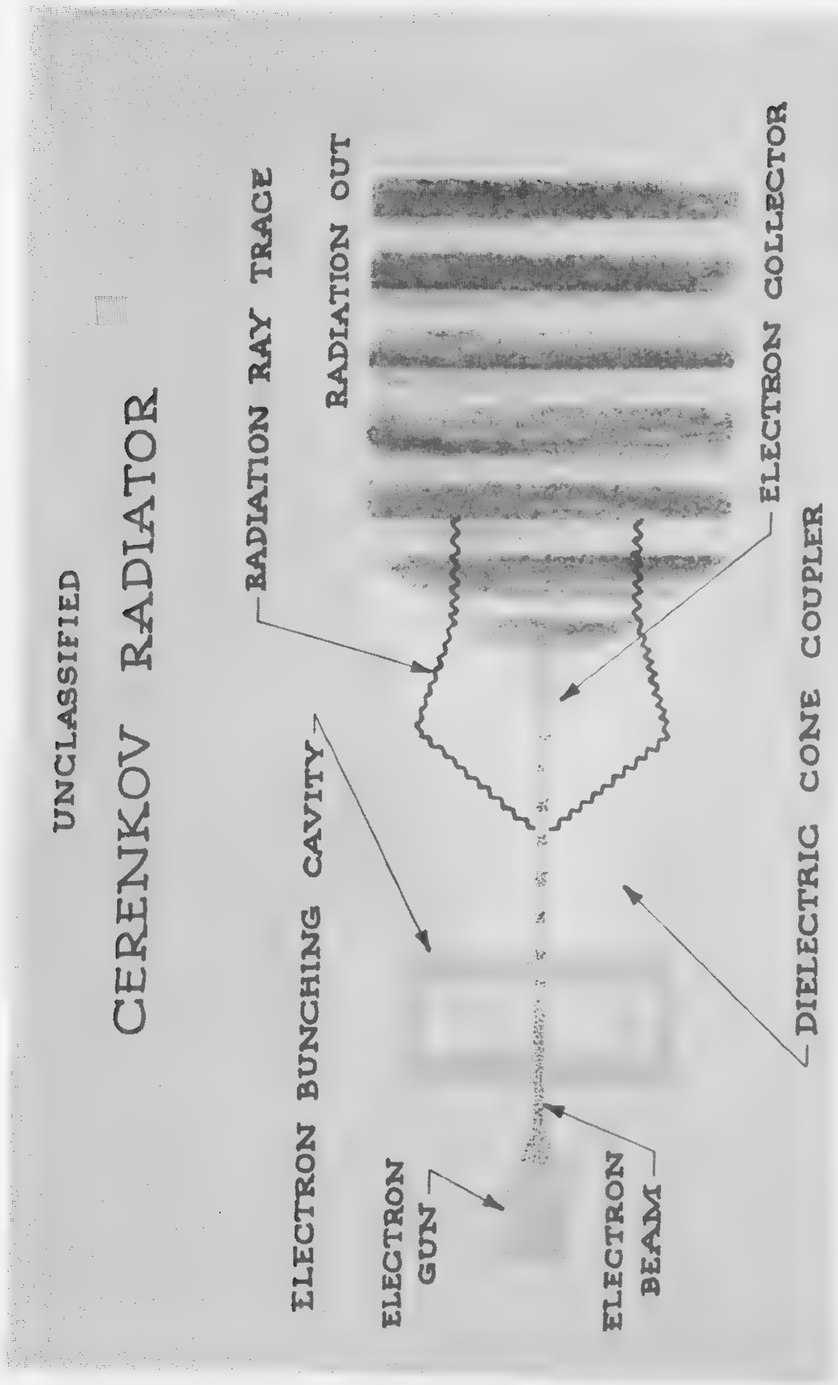


FIGURE 5 REBATRON

coupling schemes including the resonant scheme and the Cerenkov scheme. The difficulty of the resonant scheme is to inject the electron beam into the resonant structure. There are also problems of submillimeter waveguides as input and output structures. The interaction, is, however, strong. A Cerenkov device utilizing high voltage does not have the problems connected with mode separation and minute waveguide structures. A Cerenkov device will directly convert the kinetic energy of electrons into radiation within a dielectric device which may be built in the geometry of an optical lens transmitting the generated radiation as shown in Figure 5. Megavolt electronics underlying the Rebatron is a process of multiplication. It does not promise a self excited source of electromagnetic energy. In regard to the potential power level of this device, it is estimated that the application of this device may result in peak powers of tens of watts at the submillimeter wave region of 0.3 mm. This estimate is based upon an input of the magnitude of tens of kilowatts, resulting in an efficiency of better than 0.1%. Major problems existing in this research relate to generating tightly bunched, monoenergetic, high density electron groups at the wavelength region of a few millimeters, and, in addition, to dielectric couplers optimized in the selection of material and geometry.

Efforts Based on Known Technology

A representative example of current efforts based on known technology is the approach of scaling the propagating circuit structure down to the submillimeter region. The propagating circuit constitutes one of the foremost significant elements of microwave tubes. The electron beam penetrating the circuit will interact with the wave generated in the circuit. Cumulative interaction between an electron beam and an RF circuit field can be obtained by having the phase velocity of the circuit wave approximately equal to the beam velocity. Such a circuit wave is termed a slow-wave, since the phase velocity is less than the free space velocity of light. A slow-wave circuit may be obtained by periodic loading of circuits such as split-folded waveguide circuit, multiple ladder circuit, disk loaded coaxial line circuit,

coupled coaxial cavity circuit, waveguide circuit, interdigital line circuit, easitron circuit, vane line circuit, and ring and bar structure circuit. Characteristics of the slow-wave circuit system are the following. The RF field strength is greatest at the conducting surface and decays in magnitude approximately in an exponential form away from the surface. The periodicity of the loading is less than the free space wavelength. Both these characteristics make it difficult to achieve interaction with a slow wave circuit in the submillimeter wavelength region. The decay of the RF field strength away from the conducting surface means a decreased beam coupling impedance unless the beam is compressed into an area extremely close to the metallic walls. In this case, there are the problems of beam interception and heat dissipation.

New interest has been shown in the possibility of obtaining interaction between an electron beam and RF electromagnetic fields propagating at a phase velocity at, or greater than, the free space velocity of light. This has been termed "fast wave interaction." The advantages of this approach are: the tube can be simplified in that the propagating circuit structure can be an unloaded waveguide. The difficulty of fabricating a complicated structure whose periodicity is less than the free space wavelength is therefore eliminated. This is particularly advantageous at submillimeter waves. Since the interaction circuit is unloaded, coupling and matching problems are reduced, for there is no required transition from the interaction circuit and the normal transmission circuit. Interaction occurs in the region of the strongest RF field. Representative tube devices utilizing these advantages are the Ubitron and the cyclotron resonance backward wave oscillator.

The most common assembly procedure of circuits is straightforward stacking and brazing of laminated parts. When tolerances of a small fraction of a mil of an inch are approached, special brazing processes must be developed, and even these are often unsuccessful because of material warpage at brazing temperatures. The circuits of high heat dissipation capability are cut out of a solid piece of metal so that good heat conduction properties are obtained. Submillimeter wave circuits must be large in critical dimensions

in order to be constructed practically and accurately. The necessity for having periodic loading which is less than the free space wavelength introduces difficult fabrication problems at submillimeter wavelengths. Advanced fabrication methods are the method of spark machining, the photoengraving approach, and the hopping process resulting in precise dimensions and producing polished surfaces necessary to minimize circuit losses significant at submillimeter wavelengths. Figure 6 shows a representative propagating circuit structure designed for high peak power at the approximate wavelength region of 8 mm. The slot width in the shell is 5 mil of an inch. Present technology art may permit to construct propagating circuit structures for the submillimeter wavelength region of 0.5 mm. The fundamental limitations are the very small dimensions and construction irregularity as well as the attenuations of the circuits which will increase with the frequency. Furthermore, an arcing problem arises. The decreased dimensions lead to increased electric fields, to critical problems of confining and positioning the electron beam, and to construction irregularities which will weaken the optimum match between the electron beam and the propagating circuit wave. As a result, the efficiency will be decreased.

A second example of current efforts based on known technology is the approach of increasing the power density of electron beams used in submillimeter tubes. As the frequency is increased, the physical size of the interaction region is decreased, and maintaining a constant power level infers an increase in power density of the electron beam with the square of the frequency. The density of the electron beam can be achieved by either one of the following approaches. In the first approach, increased electron density of the thermionic emitter is obtained by increased operational temperature of the thermionic emitter as shown in Figure 7. However, life of the thermionic emitter will be shortened with its increased temperature. Figure 7 refers to a thermionic emitter device designated matrix cathode. It consists of the carbonates of barium, strontium, and calcium embedded in a tungsten matrix. Mixtures of these carbonates or aluminates constitute the most promising thermionic emitters with respect to high electron density and long life. Other



FIGURE 6 PROPAGATING CIRCUIT STRUCTURE

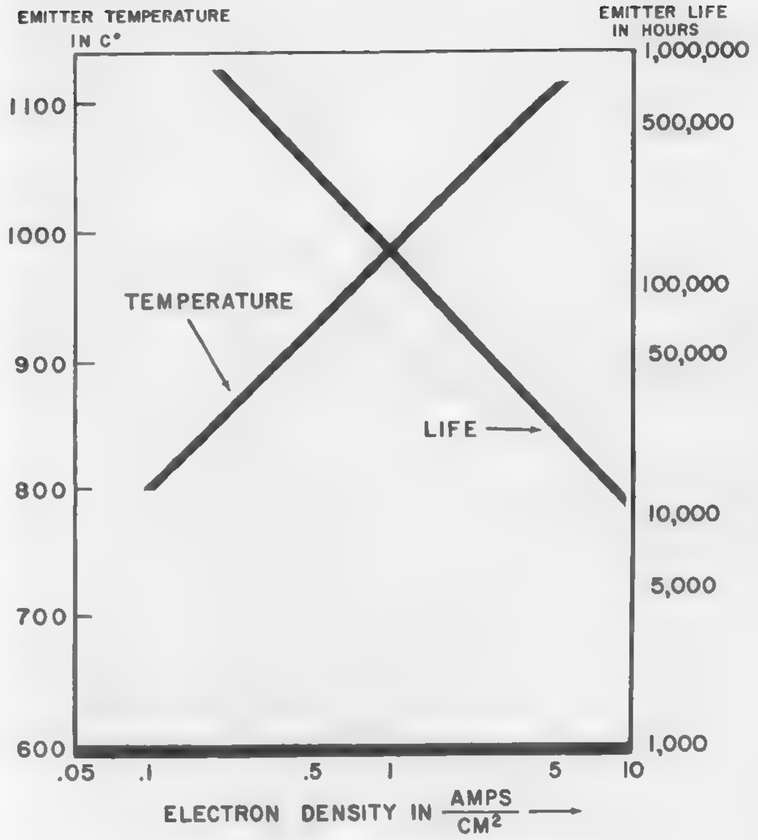


FIGURE 7 LIFE OF THERMIONIC EMITTER

cathode devices such as field emitters and tunnel cathodes do not yet fulfill the stringent requirements imposed by submillimeter tubes. In the second approach, increased power density of the electron beam is obtained by a high density electron gun shown in Figure 8. The large area of the thermionic emitter will be focused into a narrow electron beam. The use of converging guns has some drawbacks. The longitudinal and transverse thermal velocity spread of the electron beams issued from convergent guns can reach very high values, the mean quadratic spread of the initial velocities being multiplied by the gun convergence. Furthermore, the gun aberrations and the emission irregularities of the thermionic emitter can create a longitudinal velocity spread of the electrons. The resulting over-all spread of the electron velocities will constitute a serious limitation of submillimeter tubes. In illustration, it is

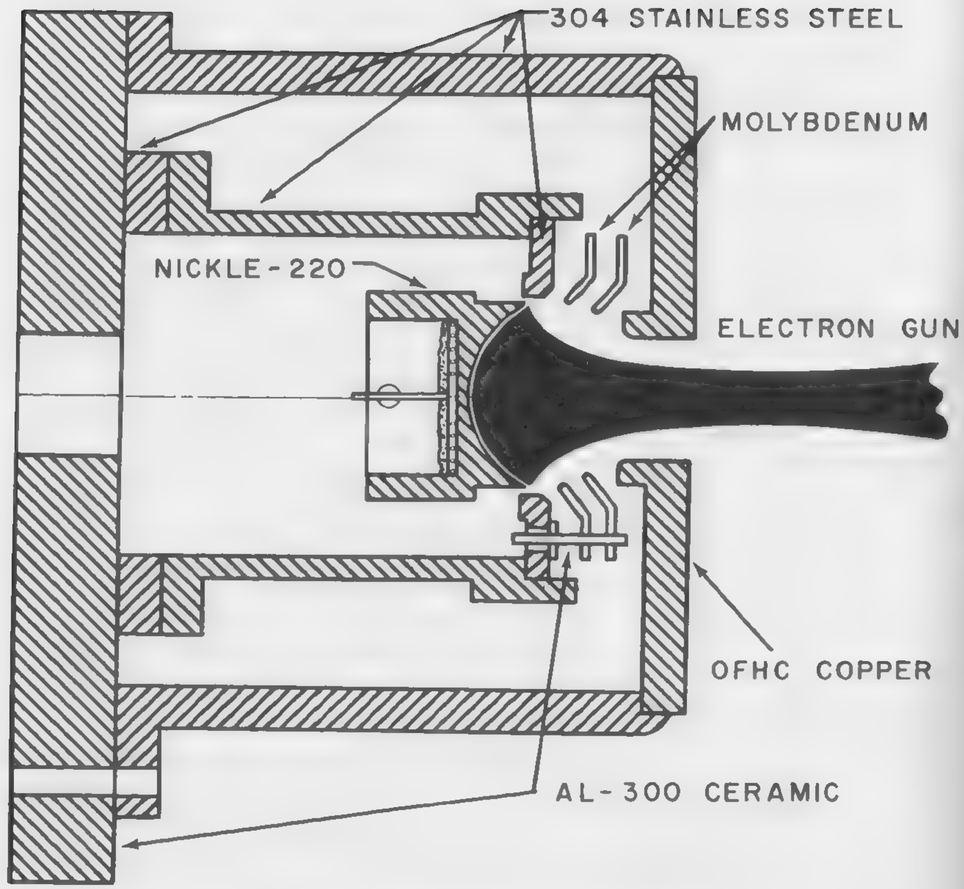


FIGURE 8 HIGH DENSITY ELECTRON GUN

feasible to build a high density electron gun with a convergent ratio of 100:1. It will form a narrow electron beam of 100 milliampere which will flow through a hole diameter of 0.008 inch, corresponding to the electron current density of 150 amperes per square centimeter while the emitted electron density at the thermionic emitter is 1.50 amperes per square centimeter only. In turn, it is considered feasible to compress this narrow electron beam by the application of an axial magnetic field of high strength. The resulting electron current density in the beam may be of the order of 300 amperes per sq cm. Electron current densities of this magnitude are required to generate submillimeter waves.

The need for high power capability of submillimeter tubes has stimulated research in hollow electron beams which offer distinct advantages over the solid beam. The hollow beam is preferable to a solid beam because of the high perveance obtainable. In the hollow beam, the useless center core is omitted resulting in improved efficiency. The electron beam coupling to the wave of the propagating circuit is only across a thin surface layer of the beam. Therefore, a large value of the impedance is possible in the case of the hollow beam. The use of a hollow beam promises another advantage. It avoids emitter surface damage caused by positive ion bombardment. The ions will concentrate near the axis and will strike the inner part of the gun rather than the emitter surface.

Efforts Based on New Concepts and Ideas

The approaches based on known technology do not seem to promise the closing of the gap between the submillimeter wave region and the optical wavelengths. New ideas for submillimeter power generation and amplification are studied. These ideas, if proven feasible, may considerably contribute to the submillimeter wave region. Four approaches to submillimeter tubes will be reviewed. They are considered representative of new concepts and ideas known at this time.

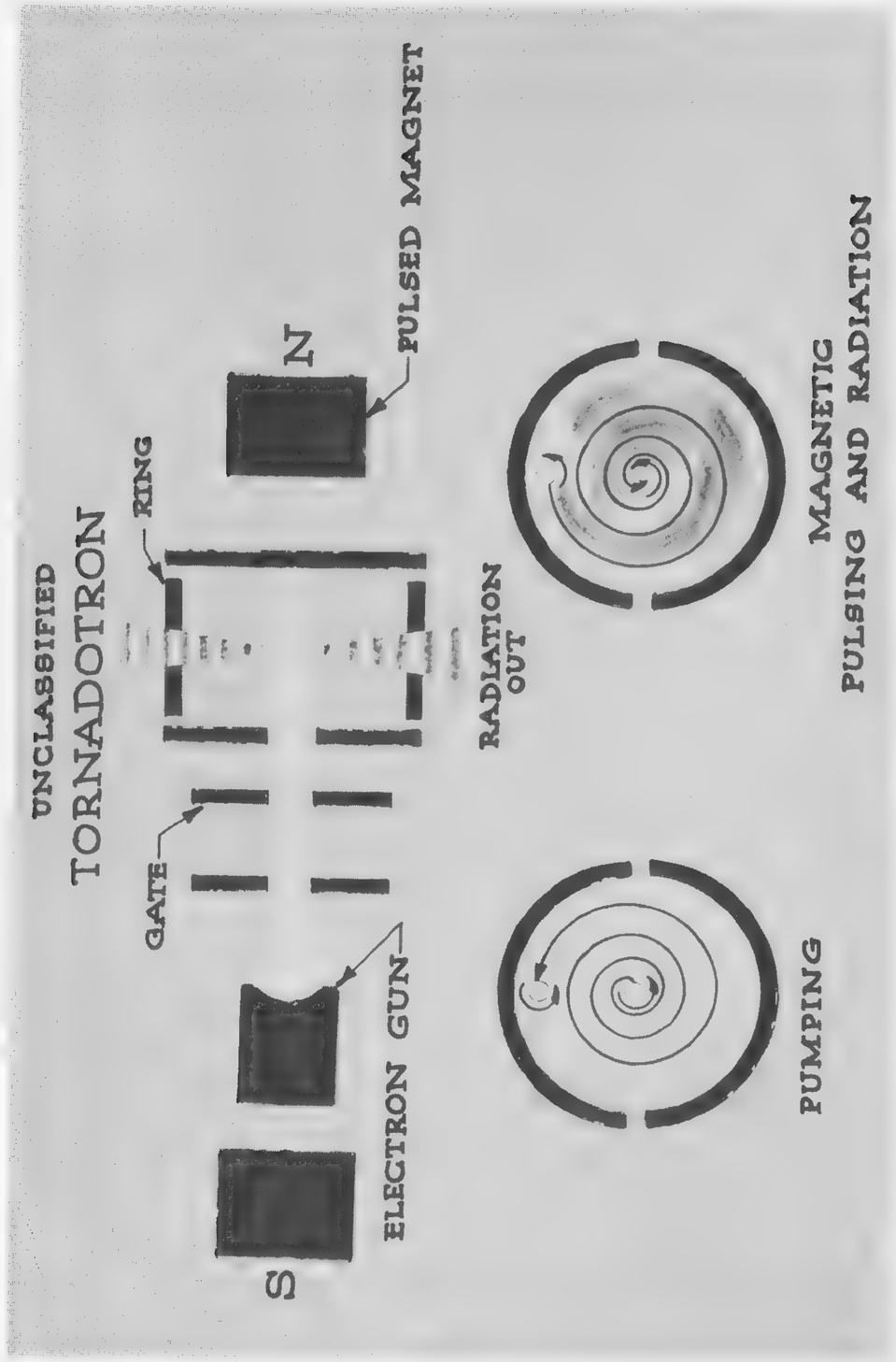


FIGURE 9 TORNADOTRON

a. The Tornadotron Device. The idea underlying the operation of this device is to inject and trap a cloud of electrons inside a resonance cavity, to produce cyclotron motion of the electron cloud by means of a transverse electric field, and to apply a fast rising magnetic field pulse to cause the electron beam to spiral back towards the axis. It is anticipated that while the electrons are spiraling back, submillimeter waves will be generated. A peak power of one kilowatt at the wavelength of 0.2 mm is predicted. The feasibility of this device is investigated at this time. A schematic picture of this device and its operational steps are shown in Figure 9. Problem areas are the following. The electron cloud contains a variety of unknown electron movements. The electron optical effects of the transverse electric field upon the configuration of the electron cloud are not yet known. It is difficult to minimize the Eddy currents in the resonance cavity which will be generated by the pulsed magnetic field. The pulse rise time of the magnetic field must be short. There exist great difficulties in regard to controlling the mode operation of the resonance cavity circuit and transmitting the generated submillimeter waves.

b. Electron Beam Plasma Interaction. The idea of this approach is to generate submillimeter waves by the interaction of an electron beam with a plasma defined as a gas in which the atoms have been separated into electrons and positively charged ions. This study showed that a longitudinal density modulation on an electron beam should grow as the electron beam is passed through the plasma. This density modulation may generate millimeter wave power. Promising features expected in the electron beam plasma amplifier relate to the gain theoretically attainable at submillimeter waves, to the gain per unit length and power conversion capability theoretically expected to be orders of magnitude greater than for linear beam interaction structures, to the size and weight of beam plasma devices potentially less than for devices having metallic resonant structures. A high density, highly ionized cesium plasma can be produced by contact ionization of the cesium atoms on a hot cylindrical tantalum wall if sufficient electrons can be provided for neutralization. Calculations show that power gain can be achieved at 300 kmc/sec if either one of the two conditions is fulfilled: electron densities of 10^{16} electrons per cubic cm

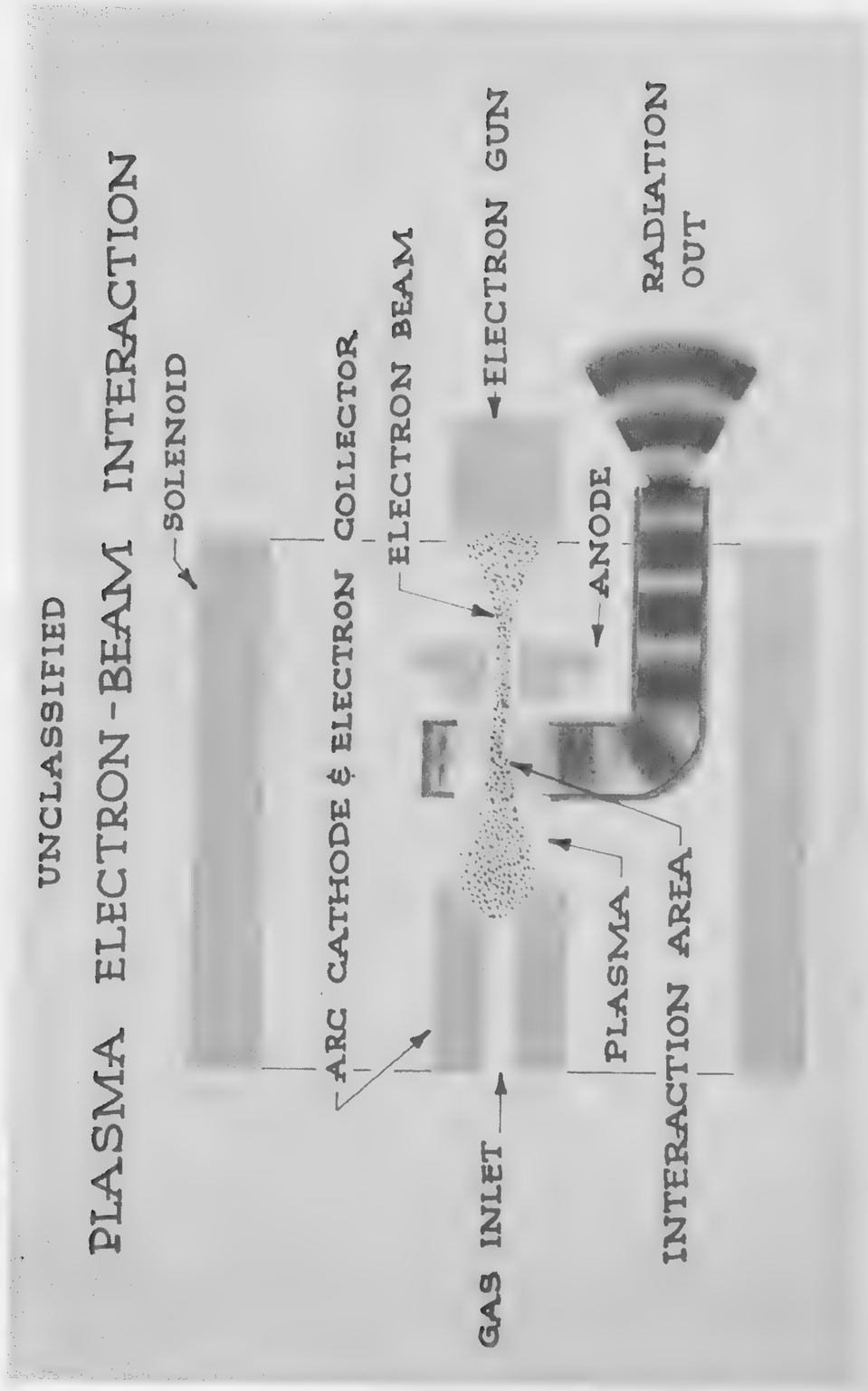


FIGURE 10 PLASMA ELECTRON BEAM INTERACTION

or a magnetic field strength of 100,000 Gauss. Feasibility of this device is investigated at this time. An illustration of a plasma electron beam interaction device is given in Figure 10. Problem areas are the production of a high density electron beam, highly ionized plasma, and coupling of the generated radiation.

c. Electron Beam Optical Grating Interaction. The idea of this approach has been tried in an experiment in 1953. In this experiment, an electron beam (current 5×10^{-16} amperes; voltage 300 KEV) passed close to the surface of a metal diffraction grating with 14,500 lines per inch moving at right angle as shown in Figure 11. The electron beam induced charges on the surface of the grating which traversed the hills and dales of the grating in a periodic motion. This periodic motion gave rise to incoherent electromagnetic radiation in the wavelength range from 0.38 to 0.65 micron. The color of the generated light changed with the angle of observation and beam voltage. The observed light was polarized with the electric vector perpendicular to the grating. The generated radiation per sq cm of grating surface, in milliwatts, was calculated to be four times the electron current density parallel to the surface in amperes per sq cm. Future research objectives in this area may consider the following items: to form thin, high density electron sheet which will flow parallel to the surface of the grating in a very close distance; to generate monoenergetic electron bunches; to establish a theory which will explain the operation and potential of this device.

d. Laser.

1. Background. The idea of the laser device is to amplify light by the stimulated emission of radiation. A representative example of presently available lasers is the ruby laser. It is a small cylinder rod with plane, parallel, partially reflecting mirrors at its end planes. The ruby material is crystalline aluminum oxide containing chromium in small quantity (0.05%). The ruby is surrounded by a light source which will pump light into the ruby. This light energy will move the excited chromium ions from their ground energy state, Level 1, into the broad absorption

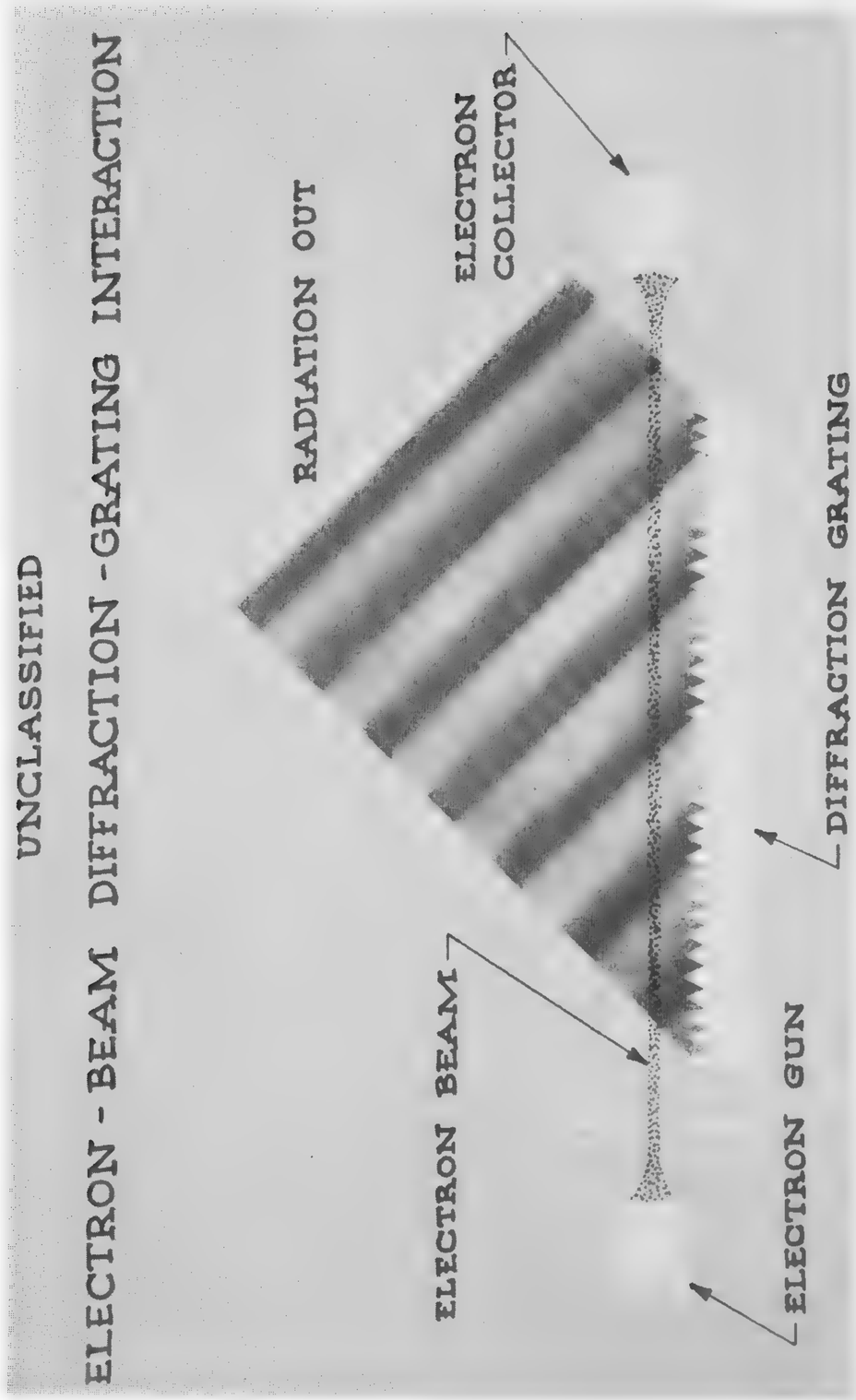


FIGURE 11 ELECTRON BEAM DIFFRACTION GRATING INTERACTION

band, Level 3, within 3×10^{-6} sec. In the next step, the ions will move to the metastable energy state, Level 2, by a non-radiative, thermal relaxation transition process within 5×10^{-8} sec. The ions have a tendency to relax and be trapped at Level 2. The time period of 300×10^{-6} sec is required to build up an excess of ion population at the Level 2. The ions trapped at Level 2 will return to Level 1 by a combination of spontaneous emission and thermal relaxation process within 5×10^{-3} sec. The spontaneous emission will result in fluorescent radiation which will stimulate the ions trapped at Level 2 to radiate. As a result, a net component of induced emission will be superimposed on the spontaneous emission. Induced emission will predominate over spontaneous emission and will lead to laser action. The induced emission will be reflected from the end planes back into the ruby rod. This feed-back mechanism will build up a powerful radiation output. For effective laser action to take place, the number of excited chromium ions must exceed the number of unexcited chromium atoms. In the case of 0.05% chromium atom content, the chromium ion density trapped at Level 2 must exceed 0.81×10^{19} ions per cubic cm. In order to fulfill this requirement, strong light pumping sources are employed. In general, the pulsed ruby laser will be illuminated by a bright burst of green light.

2. Performance. The laser is built into an optical frequency resonant cavity of extremely high selectivity. One currently favored is the Fabry-Perot interferometer etalon which is a pair of parallel plane mirrors of high optical quality, both as to flatness and reflectivity which are oriented accurately perpendicular to the line joining their centers and are separated by very many wavelengths at the desired resonant frequency. The resonant mode is then a pattern of plane standing waves between the mirrors. The resonant cavity must have a volume of very many cubic wavelengths for the short optical waves. This means that the cavity will have a very large number of possible resonant modes. The mirrors may be merely high reflectance layers deposited on the optically flat and parallel ends of the ruby rod.

The variety of laser devices existing includes the solid state laser, the liquid laser, and the gaseous laser. Pertinent laser performance characteristics are the following:

a. Pulsed Ruby Laser

Input to pumping source:	less than 500 joules
Peak power output:	more than 20 KW
Integrated output energy:	more than 2 joules
Pulse repetition rate:	3 pulses per min.
Pulse length:	500×10^{-3} sec
Over-all spectral width:	0.1 angstrom
Beam width:	15 min.
Radiated wavelength:	6943 angstrom

b. Super Pulse Ruby Laser. Pulsed reflector mode of operation of ruby lasers has the effect of rapidly switching the threshold so as to obtain a very large population inversion before the onset of oscillation. This method has produced giant output pulses with peak power multiplication factors of at least 100 to 1 when compared with the same laser operating in the normal mode. Peak powers of megawatts are now a feasible goal by varying the effective reflectivity of end walls in an appropriate manner as demonstrated in Figure 12.

c. Prospective CW Lasers. The following lasers may be suitable for continuous operation at very low temperatures. Firstly, a laser consisting of trivalent uranium in calcium fluoride generated a light output at 2.5 microns. This laser permits a very low pumping threshold for oscillation. The pumping power necessary to achieve stimulated emission is lower by a factor of 300 compared to pulsed ruby. The laser is cooled by liquid helium. The favorable energy level structure of this laser may result in a strong CW infrared light source. Secondly, a laser consisting of divalent samarium in calcium fluoride operated at 7082 angstrom. The quantum energy level structure of this laser approaches the ideal necessary to achieve continuous laser operation. Thirdly, a laser consisting of neodynium in calcium tungstate operated in the infrared

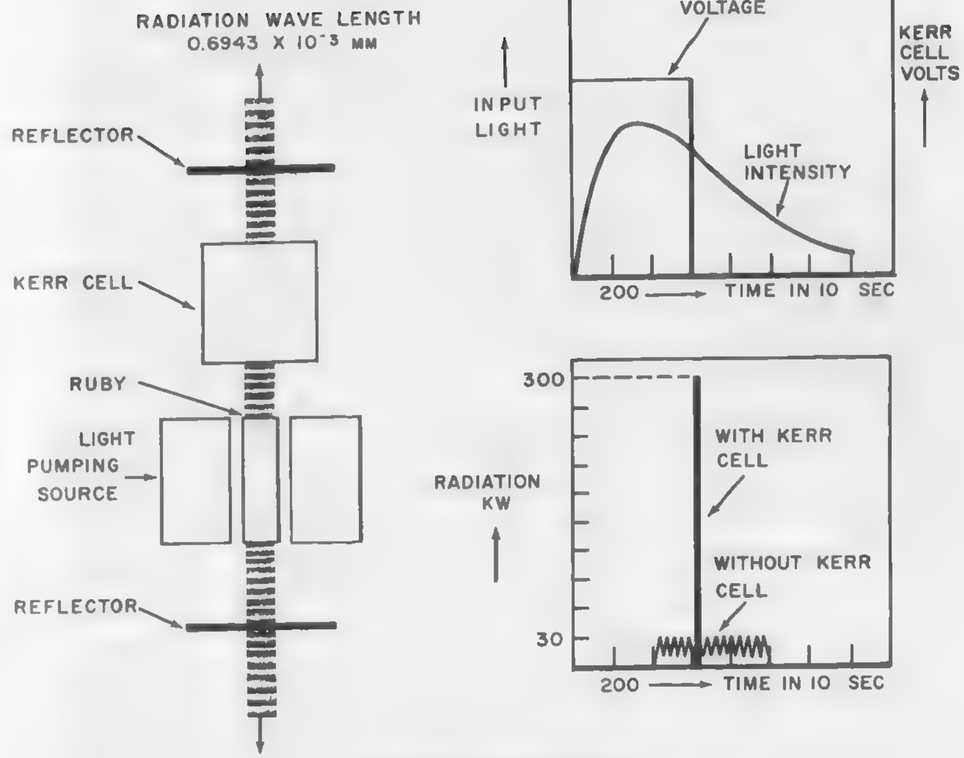


FIGURE 12 RUBY LASER

region at 10,600 angstroms with the small input power of 5 joules only.

d. Gaseous Lasers. A gas laser consisting of a helium neon mixture operated at 2.1 micron wavelength with a minimum of 50 milliwatt output power at continuous operation. The spectral line width is of the order of 10^{-5} angstrom.

3. Research Objectives. Continued research studies relate to continuous operation of the ruby laser, oscillation threshold as a function of pulse length, the effects of varying the chromium concentration in ruby, the effects of optical resonator alignment and spacing on light beam width and spectral composition, high levels of coherence, and the analysis of the pulsations observed in the pulsed laser output. Research will be continued in the material area including crystal growth technology, study of imperfection of crystal structure, and study of crystal uniformity. Materials studied will include solids, liquids, and gases. Optical pumping will be studied for optimum configuration and spectral output. Some critical problems are stated as optical perfection of the crystal, freedom from foreign atoms, and adequately reflecting and parallel and mirrors determining the mode of laser operation.

4. Applications. Many applications of the laser are foreseen because of its superior performance characteristics. The narrow width and the extreme directivity of the laser light suggests its application in a radar system. The laser light can be focused upon a small target area resulting in a high reflection percentage of the incident light. In a laser radar, a diverging lens may be used for wide search to determine the approximate location of the target. When the target has been located, the laser radar will utilize the narrow width of the laser light. The laser communication system will also utilize the high directivity of the laser light and, in turn, the enormous bandwidth available with the laser carrier frequency. The number of communication channels is almost unlimited. The laser carrier frequency is approximately 10^4 times greater than that of currently used microwave frequencies. Equivalent directivity of laser

systems could therefore be attained with antennas ten thousand times smaller than conventional microwave antennas. To illustrate, the beam for a 0.25 inch diameter ruby rod has an angular divergence of only 0.05 of a degree. Laser systems used in space may cover interplanetary distance. Problems related to laser communication systems as modulation, detection, and continuous operation remain to be solved. Other potential applications of the laser device are the following. At optical frequencies, electric field strengths greater than 10^5 volts per cm are possible. Such intensities might produce entirely new interactions between light and matter. Great acceleration of photochemical reaction rates initiated by laser light might result in new substances. The highly monochromatic nature of the laser beam might permit favoring production of one isotope rather than another. In spectroscopy, the heterodyning of light beams might be of significance. New technical applications such as high speed micro-photography may be within reach.

APPROACHES TO EFFICIENT, LONG LIFE SUBMILLIMETER TUBES

Space electronics requires considerable improvements in efficiency, reliability, and long life of submillimeter tubes.

Efficiency

Efficiency of submillimeter tubes can be increased by the following items. Depressed collectors designed to collect the spent electron beams in submillimeter tubes increase substantially the efficiency of submillimeter tubes by methods of sorting the electrons of the spent electron beam into electron velocity classes and collecting each velocity class at a potential appropriate to its electron velocity. Figure 13 shows efficiency as a function of multiple stage depressed collector. In order to minimize collector dissipation, the electrons of the spent electron beam are collected when their velocity is near zero so that they give up a negligible amount of energy to the collector and, in turn, produce a minimum number of secondary electrons. A minimum

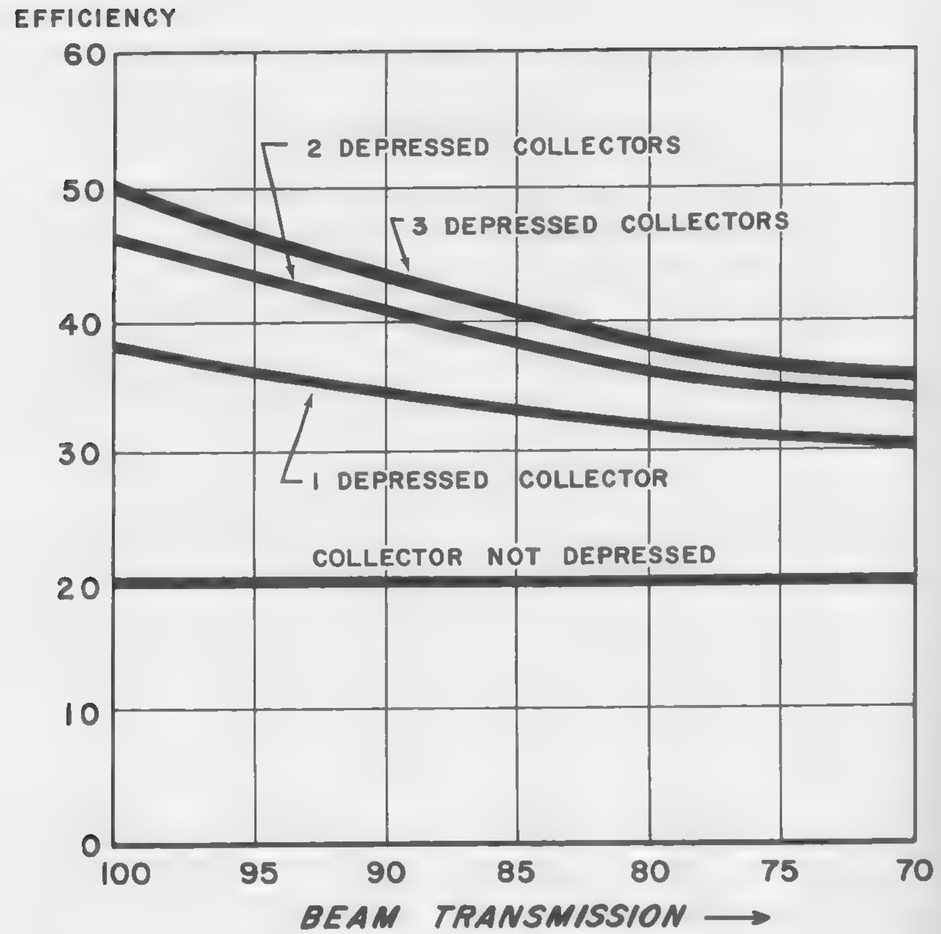


FIGURE 13 TUBE EFFICIENCY

number of secondary electrons is required in order to minimize the number of electrons returning to the RF ineraction region of the submillimeter tubes. In general, efficiency of submillimeter tubes is increased by high electron beam perveance, high interaction impedance, and low circuit losses. High perveance electron beams of small size and high current density with excellent laminar flow characteristics can be designed and built. They can be properly focused with a minimum interception with the propagating circuit structure.

Reliable Life

Reliable long life of submillimeter tubes can be obtained by optimized design features, materials, processing control, and operational conditions. A particularly significant parameter controlling long life is the operational temperature of the cathode as shown in Figure 7. The emitting surface of the cathode is quickly poisoned by traces of contaminants. Use of ion pumps will substantially enhance cathode life.

Materials

Materials used for submillimeter tube structures must exhibit superior properties in regard to high melting temperature, low vapor pressure, quick degassing capability, high thermal and electrical conductivity, erosion resistance, and good workability. Metallurgical research on new metals and alloys is performed. In illustration, columbium, hafnium, and binary alloys based on these metals were evaluated to determine their applicability for use in electron tubes. Alloying these metals resulted in improving their strengths at temperatures through 1000°C. Of the alloys investigated, a columbium - 0.65% zirconium alloy and hafnium alloys containing 2.5% and 5% columbium showed optimum combinations of workability, strength, and ductility. These alloys show considerable promise for use as structural electron tube materials suitable for high temperature use. In electron tube assembly, weld forms a significant step of production. Improved welds will increase electron tube reliability. In illustration, the characteristics of resistance

cross wire welds between various combinations of molybdenum and nickel were studied. The joint strength of molybdenum-molybdenum welds was shown to be a function of the recrystallized zone of molybdenum. The strongest welds were produced in joints having the smallest grain sizes and largest bond areas. Molybdenum to molybdenum cross wire welds were improved. However, even the best molybdenum welds had much lower joint efficiencies than nickel to nickel combinations. Joint strengths of molybdenum cross wire welds were increased 50 to 100% by using nickel-foil inserts.

Material problems arising in the area of submillimeter tubes include studies of magnetic materials to generate the magnetic lens systems required to focus electron beams along the axis of the propagating circuits of submillimeter tubes. Periodic magnetic focusing systems are developed. Present materials used for the periodic magnetic focusing systems do not permit satifsfactory operation of the electron tube over a widely varying ambient temperature range. Improved ceramic type magnets are used for this purpose because of their high coercive force. These magnets are of the barium ferrite variety. Their magnetic properties change greatly with the temperature. For this reason the barium ferrite magnets are used together with proper materials which will effect necessary temperature compensation. These materials are iron-nickel alloys. A new promising area of superconductive materials is investigated. This study is aimed at utilizing superconductive materials as a source of high magnetic field strengths required for generating submillimeter waves. Prospective material tried is niobium tin. The deposition of niobium tin on thin refractory metal wires has been successfully accomplished. Such wires have been grown reproducibly up to length of 300 meters. The wire is sufficiently ductile to be wound on 0.75 inch coil forms without loss of its superconducting properties. The wire supports current densities of 1×10^5 amps per sq cm in fields as high as 94,500 gauss.

SUMMARY

The electron beam techniques employed at millimeter tubes may be applicable to submillimeter tubes extending to the approximate wavelength region of 0.3 mm. The potential of electron beam-propagating wave interaction is far from exhausted provided creative imagination is exercised in the use of well-controlled multi-mode structures and new interaction principles. The final limitations of the conventional electron beam technology are given by the fine-grained slow-wave circuit structure beset by fabrication and thermal problems; the minute beam diameter with strong magnetic fields needed for thermal velocity confinement beset by the excessive power density of the electron beam; and the cathode loading problem. It is clear from physical principles that charge density requirements coupled with circuit attenuation will make electron beams unworkable as a practical source of electromagnetic power. Present new concepts and ideas on submillimeter tubes have not yet been proven feasible. The laser device designating light amplification by stimulated emission of radiation is in the process of opening up a major new area for application of electronic technology. This extension of microwave techniques and concepts, in modified form, for use with electromagnetic radiation in the infrared and visible frequency bands may prove to be one of the major breakthroughs in the history of electronics. New ideas will be required to extend the wavelength region from the submillimeter range to the optical wavelengths. An answer in this region appears to lie with plasmas, and since the density requirements are higher than can be maintained in gases, solid state plasmas appear most promising. The concepts here are still those of beam wave interaction, but the beam is now composed of free carriers in the crystal lattice. Because of the relatively low terminal carrier velocities available in a solid compared to electrons in vacuum, cyclotron resonance interaction or multiple streaming looks attractive. The answer is not known until sound experimental work is initiated, and, as is often the case in new areas, physical mechanisms not considered at all may prove to be the most powerful in real materials.

EPITAXIAL DEPOSITION

John E. Allegretti, Res. Associate
Peter I. Pollak, Director
Electronic Chemicals Research Department
Merck Sharp & Dohme Research Laboratories
Rahway, New Jersey

INTRODUCTION

The use of epitaxial deposition as a new semiconductor technology has been increasing since Theurer et al.[1] reported a successful transistor made from a silicon substrate prepared by epitaxial deposition. The transistor described by Theurer was similar to Early's[2] PNIP and NPIN transistors. This latter device maintained a low R_bC_c product chiefly by reducing the capacitance at the collector by introducing an intrinsic region between the base and collector of the conventional PNP and NPN transistor configurations.

Construction of the PNIP and NIPN transistor previously required a combination of alloying the diffusion processes. Although these technologies were both well understood and controlled, the epitaxial growth process laid the foundation for the large scale production of Early's transistor and for what is now called the epitaxial diffused transistor.

The general features of the epitaxial deposition process have been described previously.[3-7] It is the object of this paper to review principles of epitaxial depositions -- specifically as they apply to the epitaxial deposition of silicon. The epitaxial growth process is in principle analogous to the formation of electrically active regions in a silicon crystal by rate growing as reported by Hall.[8] The rate growing method is based on the fact that the effective distribution coefficient of an impurity between liquid and solid depends upon the rate of crystal growth. By properly choosing both an acceptor and donor impurity and by adjusting their melt concentration it is possible to incorporate

an excess of an acceptor in the crystal at one growth rate to give a p type semiconductor and an excess of donor at another growth rate giving N type.

To produce a rate-grown structure including both conductivity types, the concentrations of donor and of acceptor impurities in the melt must be such that exact compensation is obtained in the solid at some finite growth.[9]

In the epitaxial growth process, the original seed substrate can be part of the final structure as in an N^+N structure used in the epitaxial transistor, or it can simply be used as the seed crystal for initiating single crystal growth to form a structure made completely of vapor grown silicon. As in the rate growing method, a single crystal of silicon is continuously formed. However, in this instance this occurs by the vapor phase reduction of a silicon containing compound on a single crystal seed instead of crystallization from a silicon melt onto a single crystal seed. Instead of controlling the introduction of impurities by the rate of crystal growth, the epitaxial growth process operates at essentially a constant growth rate and impurities are introduced as part of the over-all reaction mechanism. The thermodynamics and kinetics of the silicon forming system and of the impurity system are designed such that a wide distribution in the ratio of silicon to donor or acceptor impurities can be attained.

Other methods used for the introduction of impurities for the formation of active P-N junctions are the alloying and diffusion processes. The diffusion process[10] has been of considerable importance in transistor technology. The diffusion process made it possible to control, with a high degree of precision, the concentration and gradients of either acceptor or donor impurities over very narrow regions. The exponential rate of change of impurity density in the base regions of a transistor due to diffusion laws produced a built-in field which improved the frequency response of transistors. Fick's laws of diffusion have been the subject of much theoretical and experimental investigations in solids and as a result many useful and basic ideas have been developed which made it possible to describe precisely the diffusion of impurities in silicon.

The alloying method for introducing impurities in silicon predates the diffusion process and has been widely used as a method for preparing junctions.[11] Two of the major considerations of any alloy technique are the selection of an alloying agent and of an alloy process. PN junctions are prepared by alloying donor and acceptor type elements into a single crystal silicon wafer of either N or P type. In most alloying processes advantage is taken of the natural tendency of the <111> plane in silicon to produce a flat recrystallized interface. The binary phase diagrams have been well established for silicon and the group III and V elements and the technology of alloying has been usefully and readily applied to the fabrication of semiconductor devices.

As each of the technologies became more widely applied and studied by a number of investigators, new and more effective devices were designed by device designers using the known technologies to advantage. Thus, many devices incorporated diffusion and alloying to improve the properties of the devices and the economics of their production. A similar pattern should also develop in the application of the epitaxial technology. As the fundamentals of epitaxial processes are more clearly defined, device designers will avail themselves more and more of this useful technique and bring forth new devices not now producible by alloying and diffusion processes alone.

Epitaxial growth has been the subject of a number of papers presented at technical meetings during 1960 and 1961. However, since the epitaxial growth process is relatively new to the semiconductor industry, the exact details incorporated to given vapor growth process often remain confidential information in particular with respect to process and equipment design. The properties of epitaxially grown silicon substrates are therefore only defined for the specific system that was used by a particular investigator.

The epitaxial growth of silicon involves a complex interdependency of many parameter variables which must all interact properly to allow an ordered growth of single crystal layers with predetermined characteristics.

Two of the major considerations of any epitaxial growth process are the selection of a chemical reaction system and the selection of a reactor configuration to carry out the growth process. In choosing a reaction system, one of the features of importance is that the reaction system shows favorable kinetics to permit the deposition of silicon by a surface reaction rather than by spontaneous gas phase separation of the solid. The reaction system should also be conducive to permit oriented growth to occur on a single crystal seed at a growth rate such that diffusion of impurities in the solid is not the controlling parameter in the resistivity control of structures.

The reaction system should also allow the simultaneous deposition of impurity atoms to permit formation of single crystal layers with active PN boundaries with controlled impurity concentrations and gradients. The advantage of epitaxial growth are, in principle, the combination of single crystal growth with impurity introduction to form a number of electrically active regions.

CHEMISTRY OF SILICON FORMING SYSTEMS

While it is, in general, true that the dividing line between chemistry and physics in the preparation of epitaxial layers is difficult to draw, there are three principal areas which in this field have become the primary problems of the chemist. These are: (1) the preparation of the epitaxial substrates prior to deposition, (2) the formation of a clean surface just before deposition, and (3) the deposition process itself.

The preparation of the substrate surface begins with the origin of the substrate single crystal. Epitaxial growth studies have been carried out which attempt to differentiate between float-zoned and crucible grown substrate origin, and some attempts have been made to interrelate point, line and area defects with epitaxial growth quality. In general, it appears as if dislocations can be originated at the epitaxial substrate interface, and that the growth of the highest quality will contain dislocations in 1:1 correspondence with the substrate.

A large number of mechanical, chemical and electrochemical procedures for the preparation of smooth substrate surfaces have been described. Here there are at least two schools of thought. One claims that a chemical etch must precede an epitaxial deposition before a good overgrowth can result. Others maintain that an optical mechanical polish is a better preparation of the surface than a chemical etch. The problem is made more ambiguous by the fact that some consider a very planar epitaxial growth as the ultimate criterion in epitaxial growth perfection, while others stress the over-all properties of the epitaxial layer as expressed in terms of electrical measurements and device performance. Obviously these two subjects are related, but it is clear that a perfect mechanical epitaxial surface does not necessarily imply a high quality epitaxial crystal layer.

In most processes the substrate surface used for epitaxial growth is not a clean silicon surface whatever the surface preparation. A further cleaning is essential in the epitaxial deposition ambient, and here a variety of chemical etches have been described. Most commonly, an exposure of the hot substrate to a stream of hydrogen is used. This system involves the reduction of silicon dioxide by silicon and hydrogen. The thermodynamics of these processes have been reviewed, and it is clear that the dominant reaction is the reduction of silicon dioxide by silicon to the monoxide which evaporates from the surface. Other systems which have been employed are the vapor phase etching of a hot silicon surface by silicon tetrachloride involving the equilibrium

$$Si + SiCl_4 \rightleftharpoons 2SiCl_2 \quad .$$

In addition, the etching of silicon substrates by hydrogen halide gases is also possible.

The thermodynamics of all these processes are fairly well understood. However, the kinetics have not been worked out. Considering the temperature region in which these reactions are carried out, it is probably a reasonable assumption to consider these processes as thermodynamically controlled.

The deposition of silicon itself is a special case of the Van Arkel[12] reaction where an unstable volatile metal derivative is converted to the metal below its melting point. From a practical point of view, three conditions must be present to adapt such a system to a worthwhile epitaxial process. These are: (1) the availability of an adequate growth vector under reasonable reaction conditions. The growth vector is defined as a linear growth rate in specific directions; (2) a system which allows the controlled introduction and variation of significant impurities; and (3) a system which permits epitaxial deposition with an optimum crystalline perfection. The difficulty of attaining these three process elements varies with the material to be deposited and the choice of volatile precursor. In general, the silicon chloride systems have been most widely employed as a silicon source for epitaxial deposition. The properties of silicon tetrachloride and the compounds obtained by successively replacing chlorine by hydrogen, shown in Table I, show that when the tetrachloride is converted to a chlorosilane, reduction to elementary silicon proceeds more easily. However, the thermal stability decreases with increasing hydrogen replacement so that trichlorosilane, for example, decomposes at about 900°C and silane (SiH_4) decomposes into silicon at about 400°C.

Table I

Compound	Molecular Weight	B. P. (°C)	ΔH (Kcal/mol)
$SiCl_4$	169.2	57.6	-145.7
$SiHCl_3$	135.4	31.5	-112
SiH_2Cl_2	101.0	12.0	- 80.3
SiH_3Cl	66.5	- 10.0	- 47.5
SiH_4	32.1	-112.0	- 14.8

In general, three types of reactions have been observed: (1) a homogeneous gas phase decomposition which is most pronounced in the case of silane; (2) a heterogeneous surface catalyzed decomposition; and (3) a reductive decomposition involving hydrogen which can occur in the solid-gas interface or can be surface catalyzed.

From a practical point of view, it is desirable to operate an epitaxial process at the lowest permissible temperature in order to permit precise geometrical control of impurity variations in the deposit. It is assumed here that these variations are governed by the usual diffusion processes. On the other hand, the temperature of the reaction system must be such that chemical reaction proceeds at a reasonable rate and that the crystal growth of the surface is not limited by growth on existing defects (such as edge or spiral dislocations) or by surface mobility. The chemistry of the decomposition of silane, for instance, can proceed by means of a first order process in the gas phase involving as reactive intermediate the species SiH_2. It can also proceed at a surface. Here the kinetics of the reaction are zeroth order with respect to silane and proportional to the available surface. The surface catalyzed reaction rate constant differs from the homogeneous gas phase reaction rate constant by a factor of $\sim$100. In the silane system the admixture of hydrogen leads to a decrease in the production rate of silicon. Analysis of the system indicates that the reason for this occurrence is a recombination of hydrogen with SiH_4 at a surface which reintroduces the silane thus formed into the steady state.

In the silicon halide cases the best understood systems are the silicon tetrachlorides and iodides. The so-called disproportionation system shown below has been examined, and it has been postulated that the rate is first order in silicon tetrachloride and first order in the surface.

$$Si + SiX_4 \rightleftharpoons {}_2SiX_2$$

where X = Cl, I

In the case of X = I, the system is complicated by a secondary reaction occurring at higher temperatures, i.e.,

$$SiI_2 \rightleftharpoons Si + I_2 \quad .$$

The reported energy of activation for these processes range from 25 to 40 Kcal/mol. They do not shed much light on their mechanisms; however, the effects of hydrogen on the kinetics of the reaction are marked but have not been analyzed.

Impurity atoms are introduced into epitaxial layers by essentially analogous reactions as those indicated above for silicon. Very few kinetic data are available, and thermodynamic calculations suffer from inadequate data on the heats of formation of a variety of precursor compounds. Recent evidence has been uncovered which indicates that the decompositions of halides of boron, hydrides of boron, halides of gallium, etc. are much more complicated than simple thermodynamic considerations indicate. Much work is required here before these systems will be understood to any reasonable degree.

Experience reported to date indicates that for good epitaxial growth it is probably preferable to operate in a chemical system which operates at a steady state with simultaneous deposition and erosion taking place, but with a small net difference in rates affording a net deposition. Under these conditions optimum integration of the depositing species into the existing host lattice is achieved. It is perhaps for this reason that epitaxial growths are better when carried out with halides than when carried out with hydrides or by vacuum deposition. The same considerations apply to the introduction of impurities, such as boron or arsenic. Here, however, because of the reversibility of the deposition reaction the concentration of these impurity atoms in the substrate has a controlling influence on the concentration of the same atoms in the deposited layers. Radioactive tracer experiments, coupled with measurements of electrical properties, have demonstrated conclusively that a

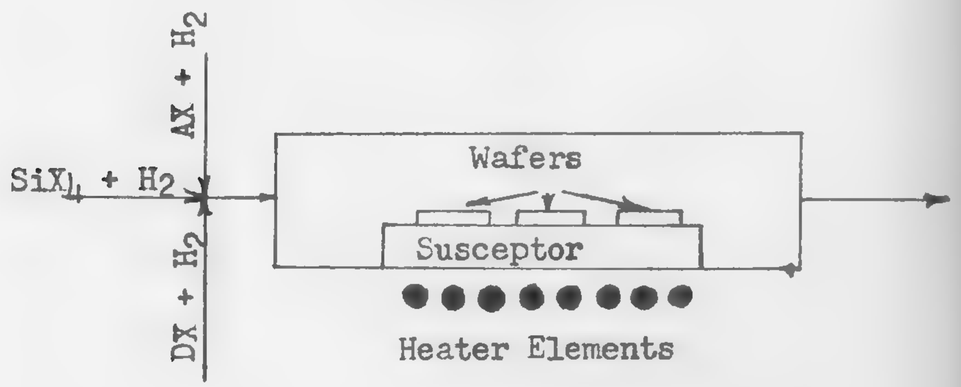
specific exchange occurs between the substrate and the growing film and that the extent of the exchange is a function of the chemical stability and equilibrium pressure of the volatile impurity in the process ambient.

It is further not surprising that rate and quality of the formation of epitaxial silicon layers is significantly dependent on the crystalline orientation of the substrate. Here the surface catalyzed reaction rate constant as well as the surface mobility of silicon atoms or precursor species varies with the surface energy of the substrate surface. However, further work is required to obtain quantitative correlations between growth rate and epitaxial surface orientation.

CONSIDERATION OF REACTOR DESIGN

With a knowledge of the chemistry for producing silicon and the impurity atoms, a reactor system is selected to carry out the growth process. Most reactor systems that have been reported on are based on a continuous flow concept. Figure 1 illustrates the principle requirements for an epitaxial reactor system.

FIGURE I



DX - Donor Element
AX - Acceptor Element

Since the compounds used in silicon chemistry are very reactive, and because of the high temperatures employed in the reaction, the choice of a material of construction for the reactor system is limited to fused silica or high purity graphite. The hydrogen employed is prepurified by either palladium diffusion units or by solid adsorbents. The impurity atoms are added either by premixing with the silicon containing compounds or as a separate gas stream.

Since the chemistry of the reaction systems that are generally used in epitaxial deposition are surface catalyzed, the reactants in the gas phase must reach the silicon surface before reaction can occur for incorporation into the lattice of the substrate surface. After reaction has occurred, the products of reaction must then be transported back into the bulk gas phase. These transport processes are used to determine the over-all reaction rate expressions involved in the chemical interaction and are required to form a basis for reactor design.

The over-all processes involved can be ascribed into five steps. (1) Transport of reactants from the bulk gas phase to the solid-gas interface; (2) Adsorption of reactants on the solid surface; (3) Reaction at the surface; (4) Deposition and crystallization of silicon with the desorption of products from the surface to the gas-solid interface; and finally, (5) Transport of the reaction products from the interface to the bulk-gas phase.

Under steady state conditions, the rates of the individual steps involved in transporting equilibrium reactants and products to and from the surface must be the same. The over-all reaction rates may be expressed by an over-all driving force involving concentrations in the bulk gas phase rather than interfacial concentrations which are difficult to estimate.

DIFFUSION

The transport of reactants and products to and from the semiconductor surface is by turbulent and molecular diffusion. If the gas velocities past the surface are large

by imparting sufficient thermal energy and kinetic energy into the gas stream, molecular diffusion can be neglected. The rate of mass transfer to the solid can then be described by an expression of the form:

$$N = Kg\ a\ (P_g - P_i)$$

where

N = rate of mass transfer g moles/hr/cm^2 surface area
P_g = partial pressure of reactant in bulk gas atm
P_i = partial pressure of reactant at solid surface atm
Kg = diffusion rate constant - g/moles/hr atm cm^2
a = area of surface.

In flow reactor systems the rate of reaction at steady state would be equal to the rate of diffusion if the reaction were diffusion controlled and can be expressed as:

$$r = Kg\ a\ (P_g - P_i)$$

where r is expressed in g moles Si formed/cm^2 area.

The diffusion rate constant (Kg) will be a function of the specie that is diffusing, and of the general fluid dynamics of the reactor system. If the diffusion constant is known, the partial pressure at the solid surface can be determined from a knowledge of a measured reaction rate and other known variables in the equation. If the difference $(P_g - P_i)$ is a small fraction of P_g then the diffusion resistances can generally be neglected. If $(P_g - P_i)$ is a large fraction of P_g, the reaction may be assumed to be diffusion controlled and that interfacial concentrations must be known to examine the reactions occurring at the surface.

The rate of adsorption of reactants at the surface after diffusion has occurred to the solid gas interface will be equal to the number of collisions the reactant molecules

will make with the surface multiplied by some efficiency factor representing this fraction of molecules that stick to the surface. Thus the net rate of adsorption will be as a function of the number of collisions which in turn is a function of temperature and also proportional to the partial pressure of the reactive specie at the solid-gas interface.

If we assume that the reduction of silicon tetrachloride to silicon proceeds by a mechanism which fits the experimentally determined reaction equation

$$\left[2SiCl_4 + 3H_2 \rightleftharpoons Si + SiHCl_3 + 5HCl\right]$$

as:

(1) $SiCl_4 + H_2 \rightleftharpoons SiCl_2 + 2HCl$

(2) $SiCl_2 + H_2 \rightleftharpoons Si + 2HCl$

(3) $SiCl_2 + HCl \rightleftharpoons SiHCl_3$

then we can analyze the rate expressions in terms of the gas composition found in the bulk phase. The molecular specie, $SiCl_2$, has not been isolated but is assumed to be formed in order to explain the presence of $SiHCl_3$ in the bulk gas phase.

In order to develop the kinetics of the adsorption process, it would be necessary to provide data relating the rate of adsorption with the partial pressure of the activated specie. As discussed previously, the rate of adsorption will be the function of kinetic energy of the molecular specie and collision rate with the surface. The adsorption rate would also have to be related to surface diffusion rates to prevent a pile-up of atoms which would result in disoriented crystal growth. Depending upon how the activated specie is adsorbed and how the reaction proceeds is of importance in obtaining useful kinetic data. If the reaction occurs between an adsorbed molecule of $SiCl_2$ and a gaseous molecule of hydrogen or between adsorbed molecules of both $SiCl_2$ and hydrogen, different rate expressions would evolve.

The desorption of the reaction product HCl would be treated similarly to the adsorption of $SiCl_2$ on the surface and the diffusion of HCl from the gas-solid interface treated similarly to the inward diffusion of reactants. It is obvious that the over-all rate expressions can become extremely difficult to evaluate and many simplifying assumptions must be made to interpret available kinetic data.

Once a satisfactory expression is known for the over-all rate of reaction, the problem of determining the optimun reactor configuration as a function of process variables becomes one of solving the rate equations. The number of variables that can be changed such as temperature, concentration of reactants, and mass velocity which are some of the more obvious variables must be optimized to obtain conditions conducive to good single crystal growth as well as optimum chemical reactions. The variables that play a role in epitaxial growth are numerous and much more investigation is required to further understand the process and to make the technology more applicable to the formation of useful devices.

BIBLIOGRAPHY

1. Theurer, H., H. Loar, J. Kleimack, and H. Christensen, Proc. IRE, 48, 1642 (1960).

2. Early, J. M., Bell System Tech. J., 33, 517-533 (1954).

3. Theurer, H. C., J. Electrochem. Soc., 108, 649-653 (July 1961).

4. Allegretti, J. E., D. C. Shombert, E. Schaarschmidt, and J. L. Waldman, Metallurgy of Elemental and Compound Semiconductors, Vol. 12. Ralph O. Grubel, Editor. Interscience Publishers, 1961.

5. Wajda, E. S., and R. Glang, Metallurgy of Elemental and Compound Semiconductors. Vol. 12. Ralph O. Grubel, Editor. Interscience Publishers, 1961.

6. Mark, A., J. Electrochem. Soc., 107, No. 6 (June 1960).

7. Mark, A., J. Electrochem. Soc., 108, No. 9, 880-885 (Sept. 1961).

8. Hall, R. N., Phys. Rev. 88, 139 (1952).

9. Bridgers, J. Appl. Phys. 27 (July 1956).

10. Fuller, C. S. F., Phys. Rev. 86, p. 136 (April 1952).

11. Pearson, G. L. and P. W. Foy, Phys. Rev. 87, p. 190 (July 1952).

12. Van Arkel, A. E., Physica 61, 316 (1925).

ELECTRON EMISSION FROM SINGLE CRYSTALS

Bruce Barnaby
Research Physicist
Eitel-McCullough, Inc.
San Bruno, California

ABSTRACT

Given the necessity of extending electron tube capabilities to higher power levels and operating frequencies, it is essential to isolate specific materials problems as early as possible and to concentrate suitable effort toward their solution. At present one of these problem areas is the cathode. It is important that no approach or point of view be overlooked and that all pertinent scientific disciplines be utilized. This paper describes the role of the cathode in electron tube design and some of the approaches to the development of improved cathodes. In particular experimental studies of electron emission from single crystals are discussed. Finally, some comments are made for employing the disciplines of crystallography in the search for cathode materials.

INTRODUCTION

Space communications systems will require electron tubes capable of extremely high power at ever higher frequencies. These power and frequency requirements are at present unattainable due primarily to certain materials limitations. One of these limitations is the cathode. Power level and operating frequency of electron tubes depend directly on current density in an electron beam. While the current density in this beam can be controlled by the use of

a suitable electron gun, the eventual limitation will be the emission current density of the cathode itself. An increase in cathode current density extends tube performance directly by increasing beam current and indirectly by permitting the use of a gun having less convergence, thus implementing lower noise level in the output and allowing simple construction of the electron gun.

The benefits to electron tube performance which could be brought about by a high current density cathode have been appreciated for a long time by industry and government agencies and each supports programs to improve cathodes. Some of these programs are conventional in that they attempt to improve existing types of thermionic cathodes by improved techniques and control of materials. Other programs use cathodes which operate on a mechanism other than conventional thermionic emission and adapt these to tube design. Still another type of program examines the fundamental processes involved in the mechanism of emission from a particular cathode so that significant generalizations can be made. All of these programs have achieved a certain amount of success, but none has been able to develop a cathode capable of satisfying the future needs of high power electron tubes. Thus, the cathode problem is still a pressing practical limitation on the power capabilities and operating frequency of electron tubes.

ELECTRON BEAMS, GUNS AND CATHODES

Rather than approaching the problem of cathodes from the point of view held by the physicist, it might be of some value initially to take the position of an electron tube engineer as he would be concerned with tube design, particularly an engineer who has no previous experience or prejudice in favor of a particular cathode. First, he looks at how his tube uses the cathode and then examines the handbooks for an acceptable cathode in terms of current density and temperature. Finally, he examines the literature to see what could be done about getting a more suitable cathode.

For beam-type tubes, the peak beam power of the electron tube imposes requirements on total beam current and beam voltage. The perveance of the electron gun places an additional restriction on these quantities. In some cases beam power is increased by further acceleration of the beam after it leaves the electron gun, but usually the gun perveance and beam power completely specify the beam current and voltage. The operating frequency, gain-bandwidth product and power dissipation due to beam interception place restrictions on the beam diameter. In this way, the over-all tube parameters have dictated the current density of the beam. Other types of tubes have similar considerations that determine the current density of the beam.

The function of the electron gun is to deliver the electrons emitted by the cathode to the electron beam with the proper current density, geometry and power. The gun parameters are the perveance and area convergence. The former is electrostatic in nature while the latter can be accomplished by electrostatic or electromagnetic means. The perveance determines beam current and voltage, while the area convergence relates beam area to cathode area, and thereby determines cathode emission current density. Since the emission current density of presently available cathodes is restricted, gun parameters, especially area convergency, have to be extended by design to give the required beam current density. This approach has been taken to give area convergences as high as 100:1, but at the expense of high noise level and other undesirable characteristics of the electron beam.

To insure stability, thermionic cathodes are normally operated in a space-charge limited condition. The emission is dependent on the applied voltage according to the equation:

$$I = GV^{3/2} \qquad (1)$$

where G is the perveance. This equation is valid only for a restricted range of voltage values and this range varies with the cathode temperature, becoming larger with higher temperatures. The upper limit of voltage and therefore the

upper limit of space-charge limited emission current is determined by the saturated emission current density given by the Richardson equation as corrected for the Schottky effect:

$$j_s = AT^2 \exp\left[\frac{-e\phi}{kT} + \sqrt{\frac{1}{4\pi\epsilon_o}}\,\frac{e^{3/2}(\nabla V)^{1/2}}{kT}\right]. \qquad (2)$$

Correction for the Schottky effect is negligible in practical cathodes, and for true space-charge limited operation is not even applicable. Therefore, the zero field form of the Richardson equation:

$$j_{so} = AT^2 \exp\left[\frac{-e\phi}{kT}\right]$$

is more significant in this discussion. In this equation, A is a universal constant equal to 120 amps/cm^2, while ϕ the work function is the energy required per electron to move a group of electrons from a point just inside a solid to a point just outside of the solid. The work function is of particular significance because it is the first parameter involved in the electron beam current density that is strictly a material parameter. Further, the exponential dependence of emission on work function is such a strong one, that for some temperature regions a change of a factor of two in the work function can cause a change of many orders of magnitude in emission current density.

The tube engineer has now reduced his electron beam current density requirement to the perveance of the electron gun, G, and the work function of the cathode, ϕ. The former is a geometrical factor over which he exercises design control while the latter is a materials parameter, which he can merely choose from those available. Concentrating on the work function, he finds that its value has been measured for a great many clean metals and composite surfaces either thin film or semiconductor. These measured values are tabulated in convenient references.[1,2,3] In addition to the work function, the tables give other measured emission constants; the temperature coefficient of the work function and A values which, in some cases differ

TABLE I

ELECTRON EMISSION CONSTANTS

Material	Work Function (ev)	A (amps/cm^2)	Operating Temperature (^{o}K)
Tungsten	4.5	70	2680
Tantalum	4.1	37	2680
Thoriated Tungsten	2.4-2.7	4	2000
Lanthanum Boride	2.6	29	1680
Barium Nickel	1.8	2.0	1300
Barium Dispenser	1.53	0.14	1100°CB
Oxide Cathode	1.2	0.1	1100 1200
Tungsten	(110) face 5.99		
	(100) face 4.56	15	
	(112) face 4.69	125	
	(111) face 4.39	35	
	(116) face 4.39	0.5	

considerably from the theoretical value of 120 amps/cm^2. The work functions of individual crystallography directions of a single crystal are listed in these references for some metals. Table I contains some typical emission constants that are found. This list is not sufficiently complete to allow the tube engineer to arbitrarily select a material with a certain work function and naturally the range is limited in the direction of the low work function that represents higher current densities. However, this is the situation as it now stands. Actually, there is considerable latitude of choice in cathode materials and some electron tubes operate at power up to megawatts and frequencies in the tens of kilomegacycles. But the tube engineer is not satisfied; his requirements are not met by available cathode materials; and he turns his attention to see what can be done about achieving higher current densities.

CATHODES AND WORK FUNCTIONS

The significance of the work function is specified by the definition but the factors which control it are much less apparent. In fact, no general method has been found for calculating the work function of an arbitrary material. An approximate method, due to Wigner and Bardeen[4] appears to hold for metals at the left-hand side of the periodic table. This method yields the following expression for the work function:

$$e\phi = (-e\bar{\Phi}_a - E_f) + \frac{0.611e^2}{r_e} + \frac{0.29e^2}{(r_e + 5.1a_H)} + \frac{0.10e^2 r_e}{(r_e + 5.1a_H)^2} \qquad (4)$$

The term $(-e\bar{\Phi}_a - E_f)$ represents the energy difference between the top of the Fermi distribution and the potential energy of an electron just outside of the surface, a_H is the Bohr radius = $\hbar^2/me^2 = 0.531$ Å; and r_e is the radius of a sphere whose volume equals the volume of the metal per free electron.

This expression is not expected to hold for practical cathode materials such as transition metals or composite layer emitters. It does point out the significant factors involved in such a calculation, and the difficulties of performing this calculation in a general way.

There is an alternative theoretical approach to thermionic emission. The composite emitters, which exhibit the lowest known work functions, can be considered from a semiconductor point of view.[5] In this case, the zero field saturated emission current density is given by the equation:

$$J_{os} = A^{*}T^{5/4} \exp - \left[\frac{X + E_f}{kT} \right] \qquad (5)$$

where X is the electron affinity and E_f is the position of the Fermi level with respect to the bottom of the conduction band. The electron affinity and the Fermi level occupy a position similar to that of the work function in the case of metals. Since the calculation of these quantities encounters the same kind of difficulties that are found in calculations of work functions, the model would not seem to be a great improvement. In fact, however, there are the following advantages: (1) Low work function emitters, such as oxide cathodes or thoriated tungsten can be described in terms of the semiconductor model; (2) The semiconductor model lends itself to an interpretation of the various chemical constituents of these composite cathodes via a donor hypothesis; (3) The vast amount of data available on semiconductor materials can be used in cathode development, thereby reducing the amount of experimental work necessary for cathode development. This last advantage is especially significant. What it implies is that other disciplines such as solid state physics in the case of the semiconductor approach can assist in cathode development. The rapid advance of semiconductor physics over the last decade should be quite beneficial to cathode development if exploited completely.

The tube engineer has now found that there is no material available to solve his immediate cathode problem. He has found little solace in his hope that there is an impending

break-through in the theoretical understanding of the work function by conventional methods. He has, however, found that other disciplines such as semiconductor physics do offer a new point of view that can be beneficial. This approach is being pursued in some cathode programs. If he looks closely, he will find similar assistance from other disciplines. One of these is implied in the table of electron emission constants referred to above. That is, the variation of work function with crystallographic direction in single crystals. This fact alone implies a relation between crystallography and electron emission. It remains to be seen if this relation can be exploited to any practical advantage. To some extent this depends on finding a relation between electron emission and parameters measurable by crystallographic techniques so that the experimental results of the crystallographer may be employed directly in cathode development without duplication. This relation is not available yet, but an indication is available in the experimental evidence of electron emission from single crystals.

EXPERIMENTS ON SINGLE CRYSTALS

The first quantitative experiments to correlate thermionic electron emission with crystallography were done by Nichols using a tungsten filament.[6] The measurements have been confirmed by others. The experiment is performed in a cylindrical diode using a single crystal filament. The anode of the diode has a narrow slit through which electrons emitted from a small segment of the cathode can pass to be collected separately. Since the accelerating voltage is applied at the anode proper, this structure amounts to a sensitive probe that detects the electrons emitted from the small segment of the cathode without disturbing the overall emission of the cathode. A balance must be made between sensitivity and resolution. It is desirable to have the probe look at a very narrow segment of the cathode but this limits the total emission current available. The total current can be increased by making the probe very long but it is difficult to grow the required long crystals.

The cathode can be rotated within the anode so as to expose the surface of the cathode to the measuring probe segment by segment. That is, the electron emission is measured as a function of polar angle. Figure 1 is a polar plot of the data taken in this kind of an experiment. The tungsten single crystal is usually grown by a simple, but specific heat treatment schedule sometimes employing a thermal gradient or

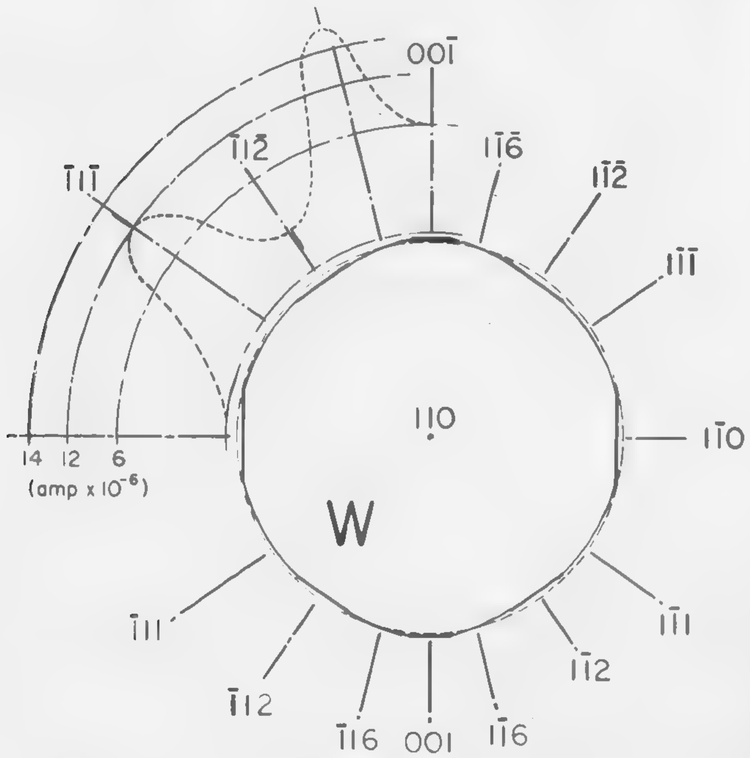


FIGURE 1 POLAR PLOT OF THERMIONIC EMISSION FROM A TUNGSTEN SINGLE CRYSTAL (6)

mechanical stress. The wire recrystallizes into crystals occupying the entire cross-section of the wire, and with proper conditions the crystals are several centimeters long. Due to the stress applied during the drawing process, the wire has a face diagonal very closely aligned with the axis of the wire. This orientation is maintained during recrystallization. Since the wire is round and smooth, this orientation causes all crystal directions which have the Miller indices of the form $\langle hhk \rangle$ to be normal to the surface of the wire. Figure 1, then, is a plot of emission as a

function of $\langle hhk \rangle$ directions. The emission is non-uniform within each quadrant, but is repeated in reverse order from one quadrant to the next as would be expected from a crystal with cubic symmetry. For convenience, the emission is plotted for one quadrant only. The principle directions, that is, the directions exhibiting a maximum or minimum in emission, are marked. Emission maxima are observed at the $[111]$ and $[116]$ directions, while emission minima are observed at the $[110]$, $[211]$ and $[100]$ directions. In general the minima are broad, while the maxima tend to be peaked. The emission variation observed in this plot represents a work function difference of about 0.5 ev between the maximum and minimum. Microscopic examination of a cross-section of a wire from which data of this type were taken revealed plateaus at the directions corresponding to the emission minima. The actual outline of the cross-section is shown in Figure 1 by the heavy line, while a circular outline is dashed for comparison. Careful measurement of diameters using an optical technique also showed the presence of plateaus at these directions.

Photographs taken of Field Electron Microscope images show the variation of electron emission with crystallography in a more dramatic, but no more convincing manner. The microscope operates on the principle of emission of electrons from a surface into a vacuum by the action of high (5×10^7 volts/cm) electrostatic fields. The high field is achieved by applying a moderate voltage (5000 volts) across a diode in which the cathode is in the form of a fine wire etched to a sharp tip (0.5 μ radius). The high curvature of the tip brings about a surface electrostatic field of the proper magnitude. The electrons emerging from the emitter tip have very little kinetic energy, and therefore follow the lines of force of the electrostatic field. The emitted electrons continue their flight through the vacuum along these radial trajectories. The anode is made a conducting fluorescent screen so that the impinging electrons produce an image which can be viewed directly or photographed for later study. The material under investigation is used as the emitter, and the image formed on the screen is a very much magnified (10^5X) electron emission map of the emitting tip.

Figure 2 is a photograph of the image of a Field Electron Microscope using a tungsten emitter. Since the emitter tip is usually smaller than the average grain size of the metal, the image is formed by the electrons emitted from a

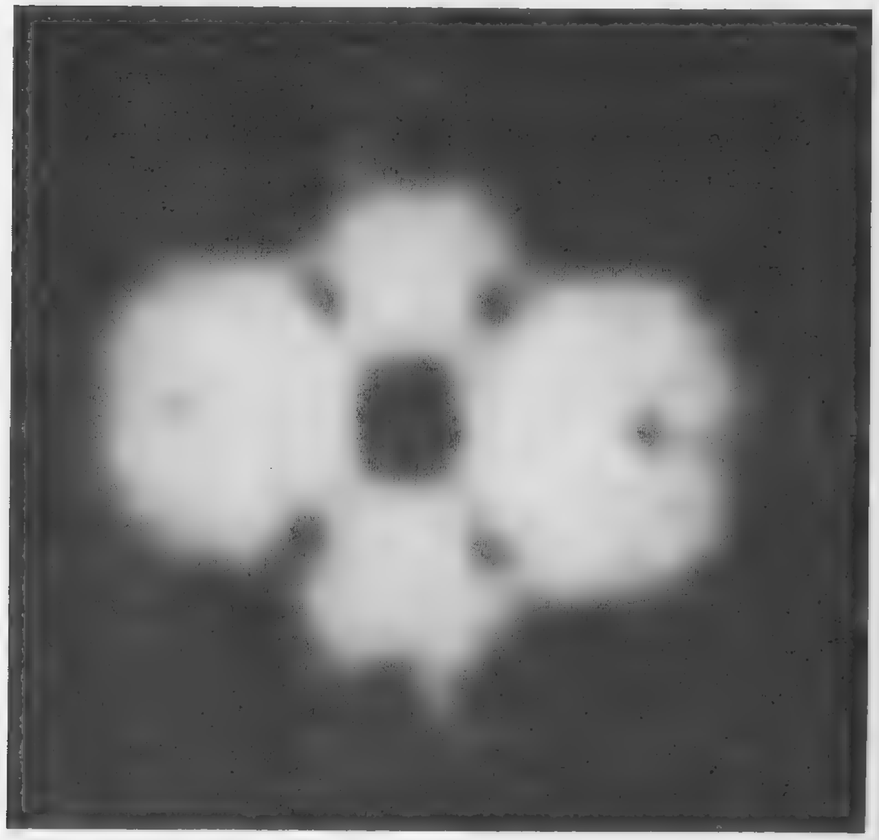


FIGURE 2 FIELD ELECTRON MICROSCOPE PATTERN OF TUNGSTEN

single crystal and can be considered as the characteristic pattern of electron emission from a single crystal of the metal. The light and dark areas correspond to regions of high and low emission respectively. The emitter pattern may be compared to a [110] oriented projection of a body-centered cubic crystal as shown in Figure 3. The symmetry for this type of structure is preserved in the emission

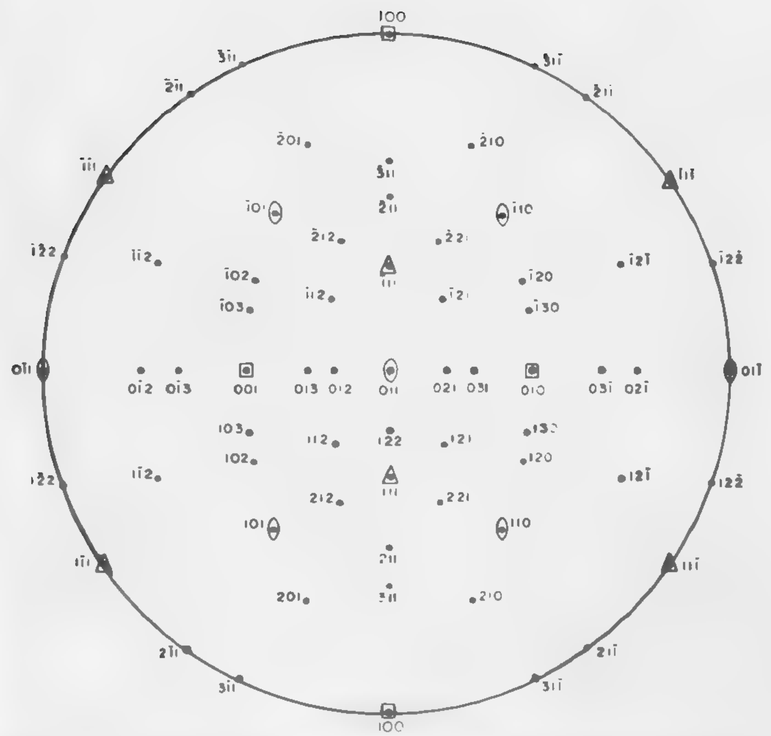


FIGURE 3 PROJECTION OF THE BODY-CENTERED CUBIC CRYSTAL DIRECTIONS

pattern. The main axes of the symmetry can be readily identified as the two-fold symmetry about the [110] direction and the four-fold symmetry about the <100> directions. The pattern appears dark at these directions indicating emission minima similar to the results of the thermionic measurements described above. The three-fold axis of symmetry about the <111> directions can be identified in the pattern as the region of high emission. Though it is difficult to identify emission in this region as a maximum by visual observations alone, careful measurements have shown that it is indeed a maxima, again conforming to thermionic measurements. From these axes of symmetry other details of the pattern can be determined. The dark spots about the <111> directions appear at the <211> directions and represent emission minima, while the bright regions about the <100> directions correspond to the maximum in emission observed at the <116> directions in the thermionic case. Thus, all the major features of the crystallographic distribution of emission as determined

from thermionic emission are also found at least qualitatively in the Field Electron Microscope pattern.

Dyke and his co-workers[7] have analyzed field emission patterns quantitatively by means of densitometric analyses of calibrated negatives. Some of their results are shown in Figure 4. The pattern on the left in Figure 4 is a hypothetical construction of a tungsten field emission pattern

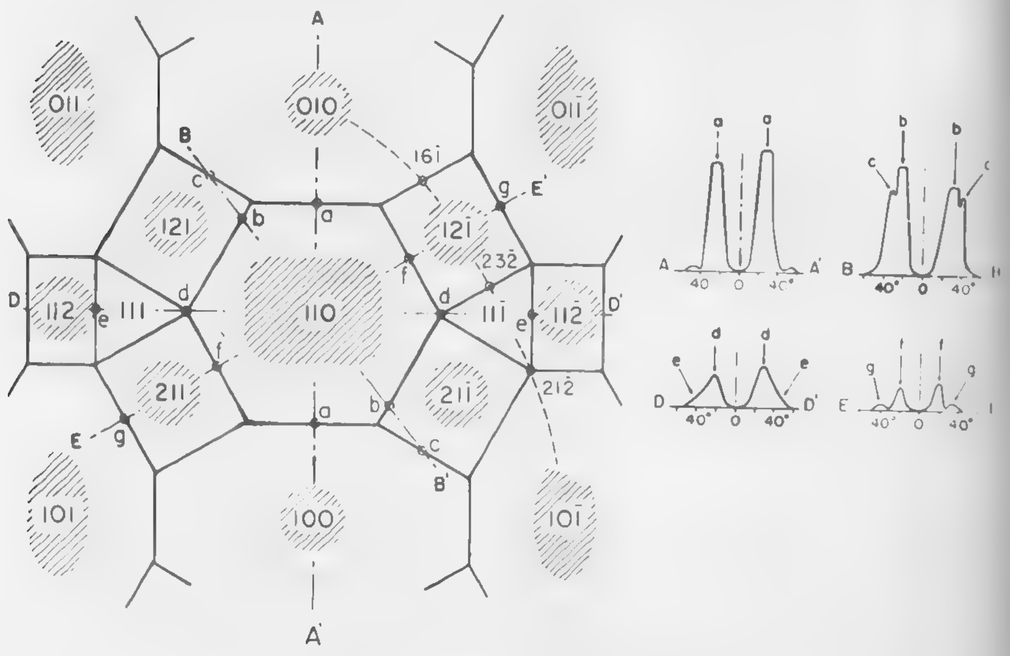


FIGURE 4 DISTRIBUTION OF FIELD EMISSION FROM TUNGSTEN (5)

showing the main crystallographic directions with their proper symmetry. The negatives of the Field Electron Microscope pattern are scanned with a photodensitometer along the azimuths indicated as AA, BB, DD, and EE. The densitometer readings are inverted to correspond to a positive image and plotted on the right of Figure 4 as a function of polar angle measured from the central [110] direction. These plots, therefore, represent relative emission on an arbitrary scale as a function of crystallographic direction along selected azimuths that pass through the center of the emission pattern. For ease of interpretation from the plots to the hypothetical pattern, certain prominent points on the plots are identified by the letters: a, b, c, etc., and the

corresponding points on the hypothetical pattern are similarly marked. The ⟨110⟩ directions have the lowest minima. The maxima indicated by "a" appear at directions of the form ⟨01k⟩. The maxima indicated by "d" appear at directions of the form ⟨hkk⟩. The crystallographic directions of the other maxima can be similarly identified with varying degrees of accuracy. Perhaps, the most significant point of these data is the sharpness of the maxima peaks and their occurrence at the high index directions like the ⟨016⟩, which occur at the intersections of low index planes. These intersections of low index planes do not occur as sharp edges as indicated in the hypothetical pattern, nor is there a smooth transition from one to another. Rather, the intersection occurs in a series of lattice steps of varying width between the two low index planes which are facets. These data confirm in a quantitative way the thermionic measurements and extend the measurements to crystallographic directions not observable in a cylindrical system.

The variation of electron emission with crystallographic direction has been observed for metals other than tungsten. The patterns observed with the Field Electron Microscope offer a convenient, though somewhat qualitative measure of the crystallographic distribution of emission. A qualitative study can be made after the manner of Dyke, but the general features of the emission can be determined merely by inspection of a pattern. This is demonstrated by Figure 5 which is the Field Electron Microscope pattern observed using a tantalum emitter. Tantalum like tungsten has a body-centered cubic structure and the pattern oriented with a ⟨110⟩ direction normal to the plane of the photograph displays that same symmetry. Tantalum can be etched to the necessary sharp tip almost as readily as tungsten. It is somewhat more difficult to get a truly clean surface by heating the tantalum but this can be done satisfactorily. An inspection of the tantalum pattern shows minima of emission at the ⟨110⟩ and ⟨100⟩ directions. Emission maxima are observed at the ⟨111⟩ directions and the region about the ⟨100⟩ directions. All these features are the same as observed for tungsten. The difference between the two is the absence of dark spots or regions of low emission at the ⟨211⟩ directions in the case of tantalum. The emission in

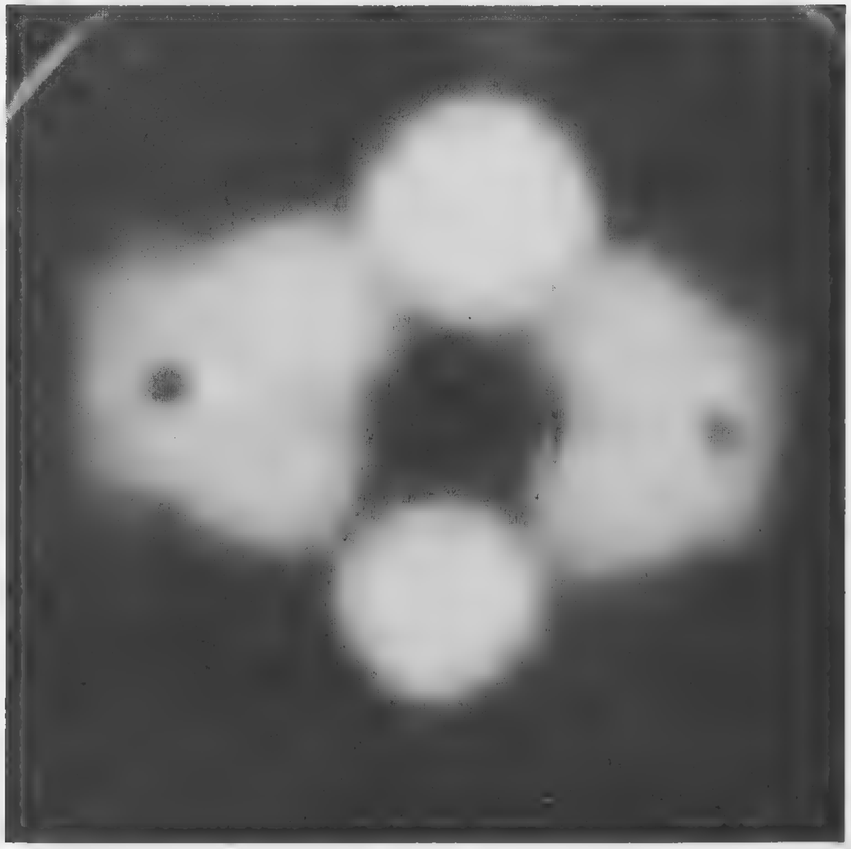


FIGURE 5 FIELD ELECTRON MICROSCOPE PATTERN OF TANTALUM

this region is high except for a narrow strip of low emission that appears to separate the ⟨111⟩ regions from the ⟨100⟩. Experiments on the thermionic emission from single crystal wires of tantalum confirm all these features, though the thermionic measurements have not been carried to the same state of refinement as those on tungsten. The thermionic emission exhibits peaks and minima at the same crystallographic directions at which they are observed in the field emission pattern. Careful examination of the surface of the single crystal wires of tantalum revealed the presence of plateaus at the ⟨110⟩ and ⟨100⟩ directions, but not at

the ⟨211⟩ directions again in contrast to tungsten. This fact establishes further the presence of a plateau on the surface at a direction which has a minimum in emission, even to the point that if the plateau is not present the emission minimum is not observed.

These experiments establish that the electron emission varies markedly with crystallographic direction, but that the variation is not a unique function of the bulk crystallography.

CATHODES AND CRYSTALLOGRAPHY

A first naive step toward a useful employment of the variation of work function with crystallographic direction might be to make cathodes of tungsten, tantalum, molybdenum in which the low work function or high emission regions dominate the surface. That is, make a cathode, say of tungsten, in the form of a ribbon; the surface of which is composed of a plane normal to the ⟨111⟩ directions. Figure 6 shows some of the principle planes of the tungsten body-centered cubic structure. In each sketch, the basic

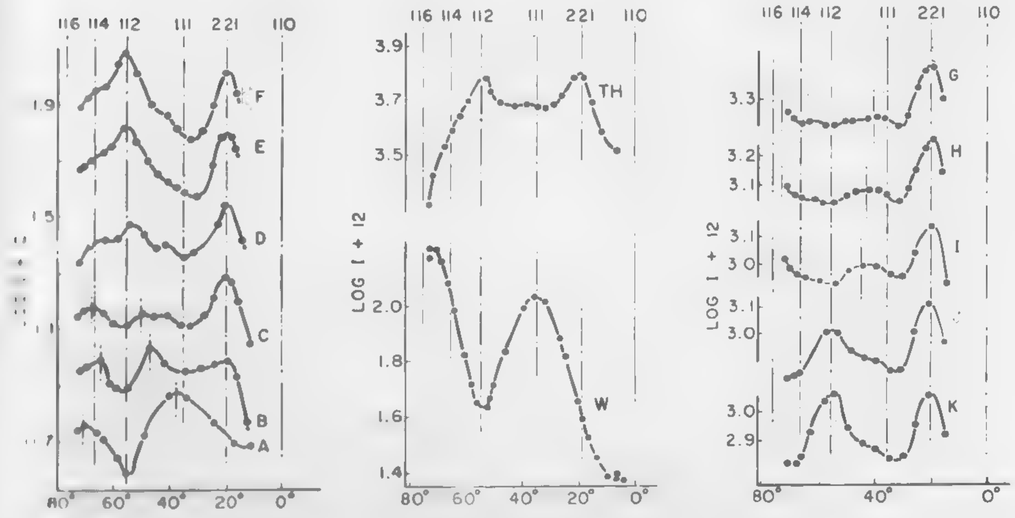


FIGURE 6 CRYSTALLOGRAPHIC PLANES OF THE TUNGSTEN BODY-CENTERED CUBIC STRUCTURE

unit cell or a group of unit cells is drawn in dotted lines while the indicated plane is set in bold lines. The interatomic spacings are indicated and σ is the surface packing factor for that particular plane. The poorly emitting planes are the (110) (100) and (211). Therefore, the cathode should be made in such a way that the surface has only a minimum of these while concentrating on the high emitting planes such as the (111). An attempt to make a cathode of a single crystal having such characteristics would be quite formidable if not physically impossible. Single crystals are difficult to grow, and it is even more difficult to grow crystals having preferred orientations. Secondly, the surface free energy of some of the desirable crystal planes may be such that it would be impossible to maintain the desired structure at the operating temperature for a significant time. But, most important in the case of the refractory metals, is that even the lowest work function directions have work functions in excess of 4.0 ev, which means it will give of the order of 40 milliamps/cm^2 of emission at 2000°K. This is not our high current density cathode. Thus, even if a desired crystal structure of a clean metal could be made, the results would hardly be worth the effort.

The low temperature cathodes in present use are far from single crystal metals, but rather are chemically complex, polycrystalline materials. They fall into two general classifications: the thin film dispenser-type cathode, such as thoriated tungsten, or the complex sintered layer, such as the alkaline earth oxide cathode. Are these cathodes also possessed of a crystallographic dependence of emission, which might be exploited? Fortunately, there are some data available on this point.

Experiments on the distribution of electron emission with crystal direction for a thoriated tungsten cathode have been performed.[8] The apparatus and method are similar to that used by Nichols for experiments with clean tungsten and are described above. The thoriated tungsten was approximated by depositing measured amounts of thorium onto a tungsten single crystal filament. The results of this experiment are shown in Figure 7. The measured emission current is plotted as a function of polar angle at the filament.

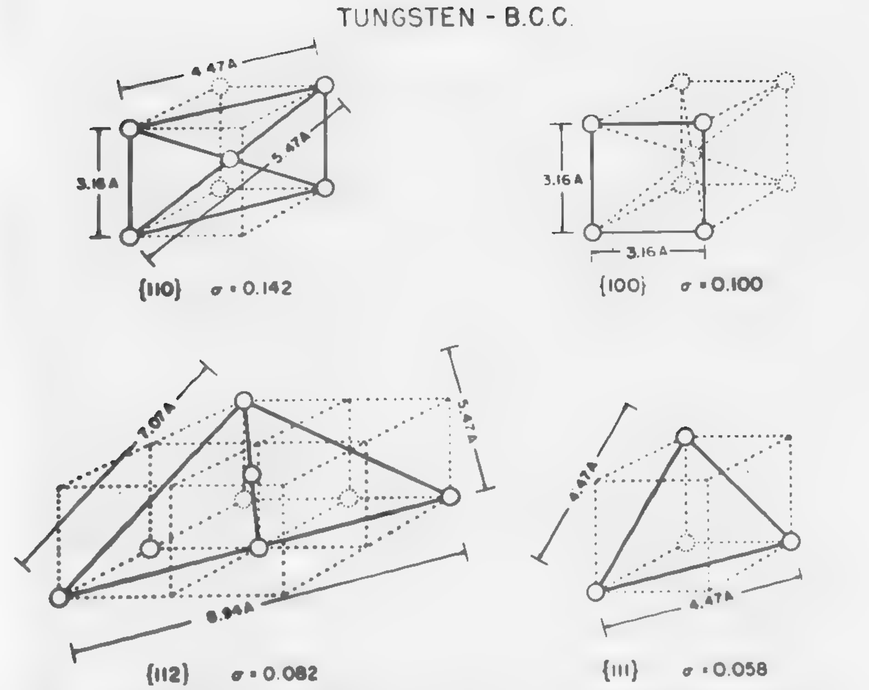


FIGURE 7 DISTRIBUTION OF THERMIONIC EMISSION FROM TUNGSTEN SINGLE CRYSTAL WITH ADSORBED THORIUM (6)

At the top of each plot, the positions of the principle crystallographic directions of the single crystal of tungsten are indicated. The curves labeled A, B, C, . . . K in the left- and right-hand plots are the emission distributions observed for various stages of adsorption of thorium. The center plot shows the distribution of emission for maximum total emission from thorium on tungsten and for comparison the distribution of emission from clean tungsten.

The total emission increased with the amount of thorium adsorbed to a maximum in accordance with other experiments for thorium on polycrystalline tungsten. As described before, the emission distribution "W" for a clean tungsten exhibits a maximum at the $\langle 116 \rangle$ and $\langle 111 \rangle$ directions. As the quantity of adsorbed thorium increases, these peaks become less pronounced, curves "A", "B", and "C", even as the total emission increases. Further accumulation of thorium is accompanied by the appearance of an emission peak at the $[221]$ direction, curves "C" to "F". An emission peak also appears at the $[112]$ direction, and seems

to develop by the [116] and [111] peaks moving together until they coincide at the [112] direction, curves "A" to "F". During this build-up of peaks at the [221] and [112] directions, the clean tungsten peaks at the [111] and [116] directions disappear and actually become minima. The sharp contrast between the distribution for clean tungsten and throium adsorbed on tungsten can best be seen in the center plot, curves "W" and "Th". The emission minima at the [110] persists throughout. The [116] approaches the [100] minima and the [111] becomes part of a broad shallow minima.

The cause of these shifts in the emission distribution is not understood but it should be pointed out that the crystal directions quoted are for the tungsten single crystal which acts as the substrate. Since the atomic details of the adsorbed layer are not known, there is no reason to assume the crystal structure of the adsorbed layer is the same as that of the substrate. More likely, the thorium is adsorbed in epitaxy on the tungsten surface. Consideration of the interatomic spacing of the tungsten crystal faces and the thorium face-centered cubic lattice suggest the accommodation of the (100) of thorium to the (110) of tungsten.

The principle significance of this work is that it demonstrates that electron emission depends on crystallographic direction for composite emitters just as it does for clean emitters. The details of the distribution differ considerably indicating an adsorption process which is highly dependent on crystallography. However, the main point is abundantly clear. Certain crystallographic directions give significantly greater electron emission than the average. Since the normally measured work function for polycrystalline thoriated tungsten is 2.4-2.7 ev, the correlation of electron emission with crystallography has been extended to work functions where high current densities at moderate temperatures have been realized. As a matter of practical interest, the increase in useful emission which could be gained by the preferred orientation of a thoriated tungsten filament is not sufficient to warrant much development interest. However, the areas of cathode development utilizing the disciplines of crystallography are more clearly understood and may be summarized as follows.

SUMMARY

Increases in useful emission from clean metal cathodes such as tungsten, may be realized by using single crystal cathodes of preferred orientation. However, it would be a difficult task to develop the necessary crystallographic techniques and most of the gain in emission could be realized by changing to a cathode of lower work function, such as thoriated tungsten. Different limitations of operating temperature and life are thereby imposed but they can be accepted. Again, the useful emission of the thoriated tungsten could be increased by preferred orientation of the crystal structure, but this is not a simple task. Instead, other cathods of the dispenser-type such as the barium-nickel matrix cathodes having lower work functions may be employed to give some increase in useful emission or a lower operating temperature. The use of this cathode involves a switch to some other set of inherent shortcomings, but these are usually preferable to a difficult development program. This procedure may be repeated over the entire list of available cathodes shown in Table I. That is, until the work function of the oxide cathode becomes the limiting factor. This is the lowest work function presently available. None of the effort of the last two decades devoted toward development of the oxide cathode has shown the way toward a lower work function cathode, that is, a cathode that can give higher emission at the same operating temperature or equivalent emission at lower temperatures. Still, from all that is known about the basic physical properties of the work function values lower than 1.2 ev are certainly feasible. This then is the region in which research effort could make a significant contribution. Present limitations are definite and of long standing. The research effort cannot be restricted to the point of view of crystallography, but since the problem is basically one of materials any effort would lean heavily on the disciplines of crystallography and metallurgy.

BIBLIOGRAPHY

1. Handbook of Chemistry and Physics (Chemical Rubber Publishing Company, Cleveland, Ohio, 1957).

2. Wright, D. A.: Proc. Inst. Elec. Engrs. 100, 125 (1953).

3. Müller, E. W.: J. Appl. Phys. 26, 732 (1955).

4. Wigner, E. and J. Bardeen: Phys. Rev. 48, 84 (1935).

5. Nergaard, L. S.: R.C.A. Rev. 18, 486 (1957).

6. Nichols, Myron H.: Phys. Rev. 57, 297 (1940).

7. Dyke, W. P., J. K. Trolan, W. W. Dolan, and F. J. Grundhauser: J. Appl. Phys. 25, 106 (1954).

8. Davey, J. E. and E. A. Coomes: Bull. Am. Phys. Soc. 30, 25 (1955).

SOME RECENT STUDIES OF THE HIGH-TEMPERATURE MECHANICAL PROPERTIES OF URANIUM CARBIDE AND BERYLLIUM OXIDE*

R. Chang, G. G. Bentle, and F. E. Ekstrom**
Atomics International
A Division of North American Aviation
Canoga Park, California

ABSTRACT

The high-temperature flow characteristics of polycrystalline uranium carbide and beryllium oxide are compared and discussed with regard to the possible importance of crystal structure, stoichiometry, and purity of the materials. The mechanism of flow for polycrystalline uranium carbide (and zirconium carbide) is that of the climb of dislocations. The flow behavior of polycrystalline beryllium oxide (and aluminum oxide) is at present not entirely understood but may possibly be controlled by the diffusional mechanism of Nabarro and Herring. The current status of the preparation of high purity uranium carbide and beryllium oxide is described and further work to produce higher purity materials than presently available for property measurements is recommended.

---

*Paper to be presented at the 1962 Golden Gate Metals Conference, February 15, 1962, Fairmont Hotel, San Francisco, California. The work was supported by the United States Atomic Energy Commission.

**The authors are respectively, Section Leader, Senior Research Engineer, and Laboratory Associate of the Mechanical Properties Section, Research Division, Atomics International.

INTRODUCTION

While uranium carbide is a potentially important fuel, beryllium oxide is an equally interesting moderator, both for high-temperature nuclear reactor applications. Beryllium oxide has the wurtzite structure (a = 2.698 ± 0.001A, c = 4.378 ± 0.001A, theoretical density 3.008 g/cc), while uranium carbide has the sodium chloride structure (a = 4.9600 ± 0.0005A, theoretical density 13.63 g/cc). Property wise the two materials are in some ways similar and in others different. Both have approximately the same melting point and are good conductors of heat. Electrically beryllium oxide is an insulator, uranium carbide is a metal. Currently available data on the thermal conductivity and electrical resistivity of the two materials are shown in Figures 1 and 2. While beryllium oxide is nearly stoichiometric at all temperatures, the nonstoichiometry range

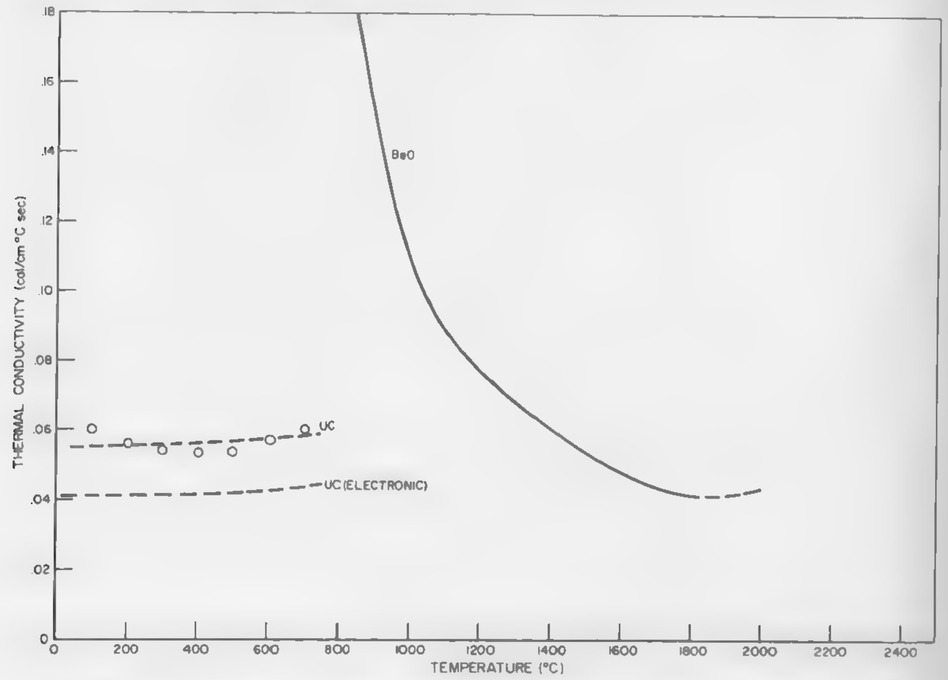


FIGURE 1 THERMAL CONDUCTIVITY OF UC AND BeO VERSUS TEMPERATURE

of uranium carbide is considerable at high temperatures. The lattice parameter of rapidly cooled (such as liquid nitrogen quench from 1,850°C) uranium carbide containing slight excess of uranium increases from 4.952A to 4.960A

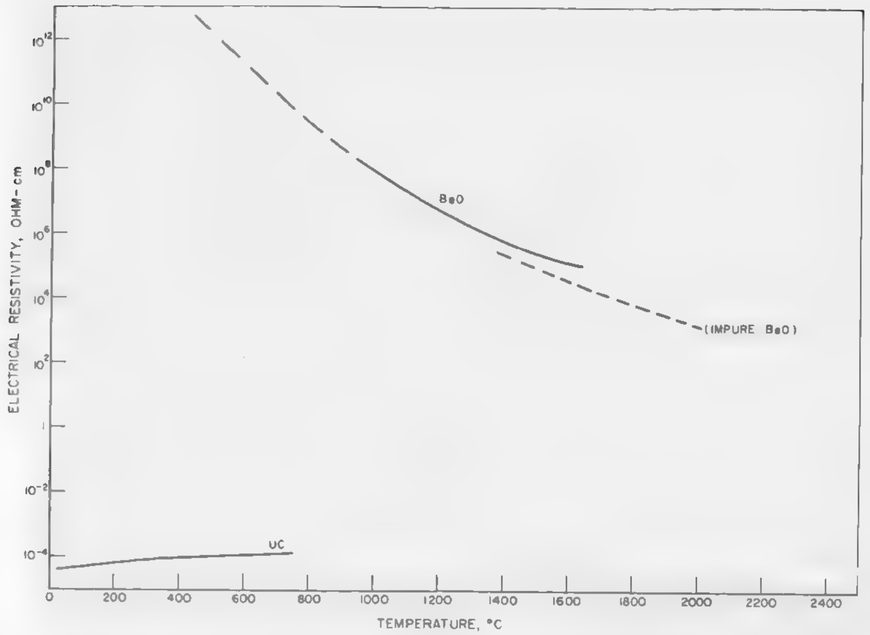


FIGURE 2 ELECTRICAL RESISTIVITY OF UC AND BeO VERSUS TEMPERATURE

in a systematic manner with increasing carbon content. These variations in lattice parameter are believed to be due to departure from stoichiometry on the uranium-excess side. In addition to the field of nuclear energy, the carbides and oxides in general are also potentially important as high-temperature load-bearing materials. It is the main objective of this paper to present some of our recent studies on the high-temperature mechanical properties of these materials. The differences in the high-temperature mechanical behavior of beryllium oxide and uranium carbide are rather striking. The experimental evidence indicates that crystal structure, stoichiometry, and purity, are important factors to be considered for an intelligent selection of materials for high temperature applications.

EXPERIMENTAL PROCEDURE

Compression testing was used exclusively in this study. Test specimens, approximately 1 cm long and 0.3 cm in diameter, were compressed between two tungsten rods located within a heated region of about 7 (or 10) cm long by

4 (or 7-1/2) cm in diameter inside a water-cooled stainless steel vacuum chamber mounted between the cross heads of a table model (or standard) Instron. Temperatures were determined with an optical pyrometer sighted through a quartz window at the interior of a small aluminum oxide tubing (one end closed) placed beside the specimen to simulate black body conditions and were maintained constant within the precision of the pyrometer during a given test. Pressure within the test chamber was approximately 10-5 mm of mercury at all times.

The uranium carbide specimens used in this study contained about 50 ppm Fe, 40 ppm Si, 15 ppm Ni, and a few ppm each of a number of other metallic impurities typical of reactor grade uranium. Microstructurally the material was composed of fully dense single phase UC having an average grain size of about 350 microns and containing a few specks of metallic uranium as isolated inclusions. Since only traces of metallic uranium were present as isolated inclusions, it is not believed that these inclusions per se would have any appreciable effect on mechanical properties but may possibly exert an indirect influence on the degree of nonstoichiometry of the material, as will be discussed later.

The beryllium oxide specimens, approximately 20-40 microns in grain diameter and 99.8+ per cent of theoretical density, were hot-pressed from (1) the highest purity BeO powder available or (2) BeO powder containing one weight per cent MgO as additives.

In addition to uranium carbide and beryllium oxide described above, zirconium carbide (supplied by the Carborundum Company) and aluminum oxide (supplied by the General Electric Company under the trade name Lucalox) specimens were also tested for comparison purposes.

RESULTS AND DISCUSSION

Uranium Carbide

Since uranium carbide has the same crystal structure as sodium chloride which slips predominantly on (110) type planes and in [101] type directions, multiple slip in uranium carbide is easy. Consequently the individual grains of a polycrystalline uranium carbide aggregate can deform readily under stress providing that the temperature of deformation is high enough. The flow characteristics of metal-excess uranium carbide in the temperature range 1,500-1,900°C is summarized in Figure 3,[1] suggesting that

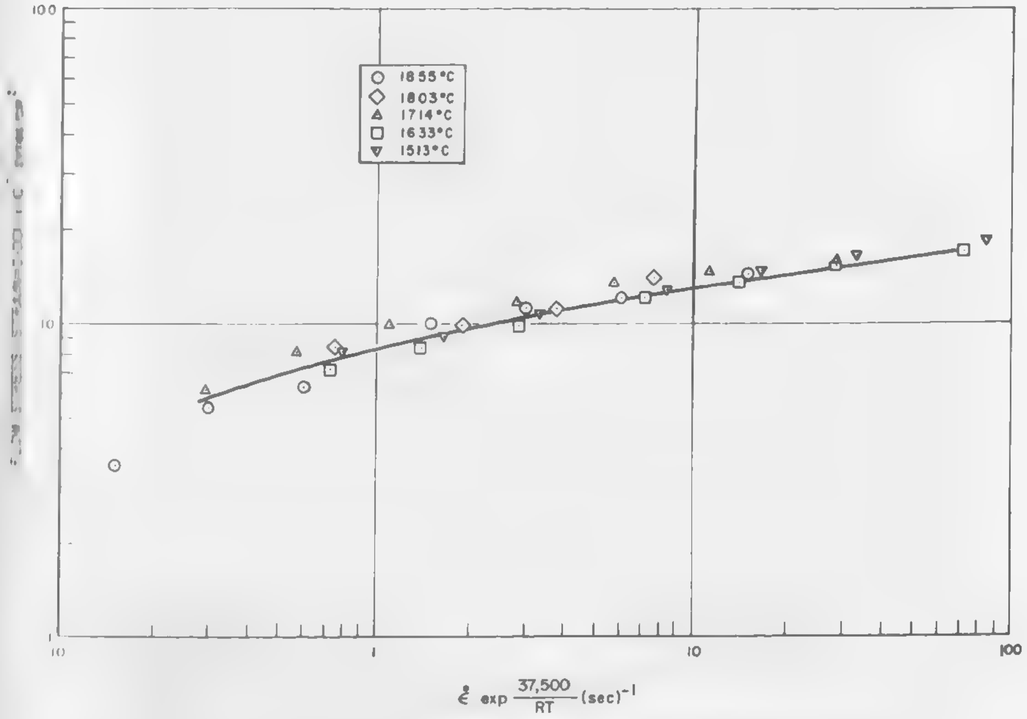


FIGURE 3 DEFORMATION BEHAVIOR OF UC (METAL-EXCESS) BETWEEN 1,500 AND 1,900°C

the controlling mechanism is dislocation climb. A typical microstructure of specimens after a compression strain of about 5% at 1,513°C is reproduced in Figure 4, showing

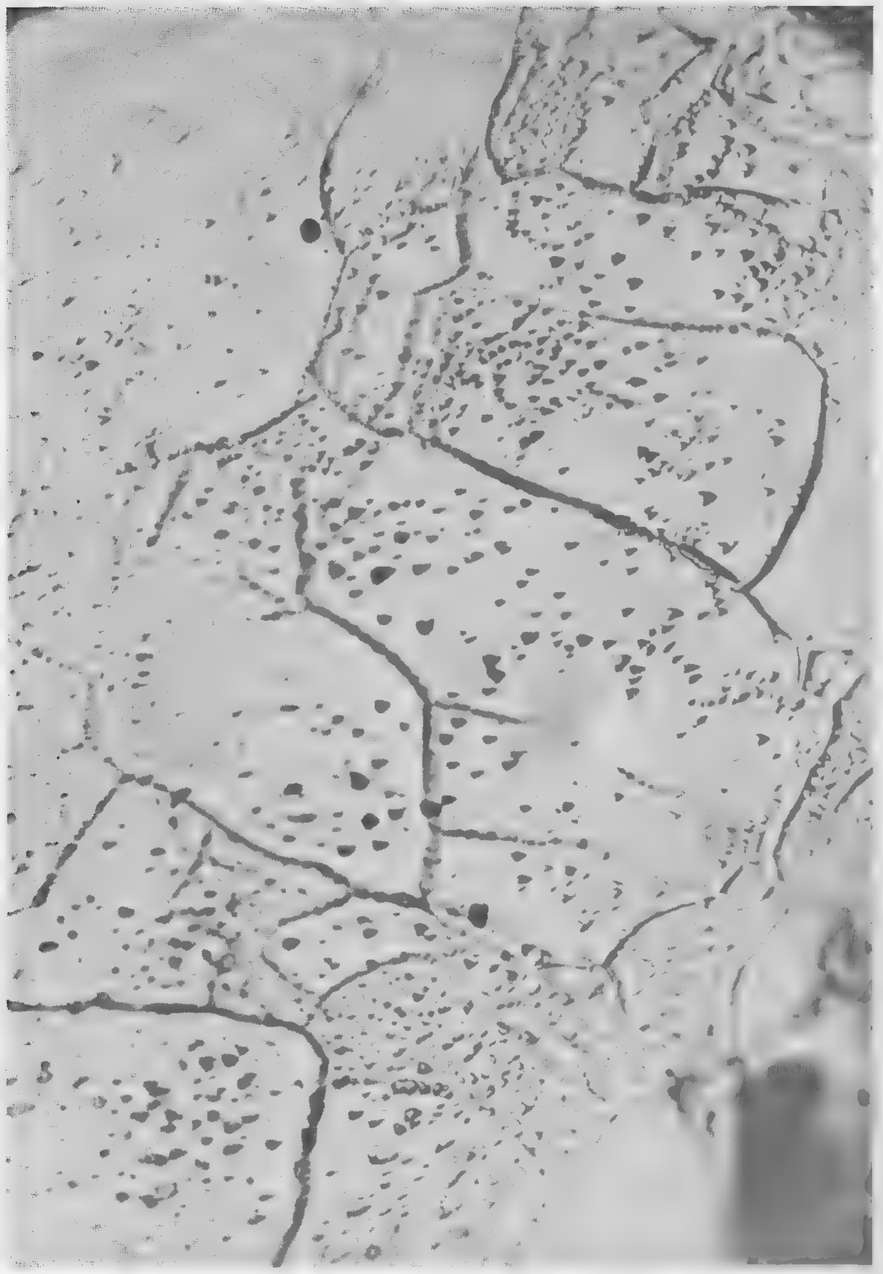


FIGURE 4 MICROSTRUCTURE (ETCHED TO SHOW SUBGRAIN BOUNDARIES) OF UC AFTER COMPRESSION-STRAINED SEVERAL PERCENT AT 1,513°C. 1000X

subgrain formation but no slip bands. The apparently low activation energy, 37,500 calories per mole (Fig. 3), suggests immediately that the activation energy for flow in uranium carbide is markedly dependent on the degree of stoichiometry of the material. The strong dependence on nonstoichiometry of the activation energy for flow in AB type intermetallic compounds of the cesium chloride structure has been reported by several investigators.[2] Further investigations of the effect of nonstoichiometry of uranium carbide on its high-temperature flow properties are still in progress in the laboratories at Atomics International.

Similar flow characteristics have been found for zirconium carbide (supplied by the Carborundum Company), which also has the sodium chloride structure. Typical flow data for this material are illustrated in Figures 5 and 6. Detailed results will be reported separately in the near future.

Beryllium Oxide

Since beryllium oxide is hexagonal and slips presumably on the basal plane, flow of the individual grains in a polycrystalline aggregate is restricted. In fact, the tensile and bend creep behavior of polycrystalline beryllium oxide (and aluminum oxide, which also is hexagonal in structure) has been shown to follow predominantly the diffusional mechanism of Nabarro-Herring:[3]

$$\eta = \frac{\partial}{\dot{\epsilon}} = \frac{kTR^2}{10\,D\,\Omega} \qquad (1)$$

where η is the viscosity; ∂, stress; $\dot{\epsilon}$, strain rate; k, Boltzmann constant; T, absolute temperature; R, average grain radius; D, diffusion coefficient; and Ω, atomic volume. However, inconsistencies have been discovered upon further investigation: First, the diffusion coefficients calculated from tensile and bend creep date[4, 5] according to Eq. 1 are about two orders of magnitude larger than the tracer diffusion coefficients for both beryllium oxide and aluminum oxide. They are compared in Figures 7 and 8. Second, the same experiments cannot be duplicated by

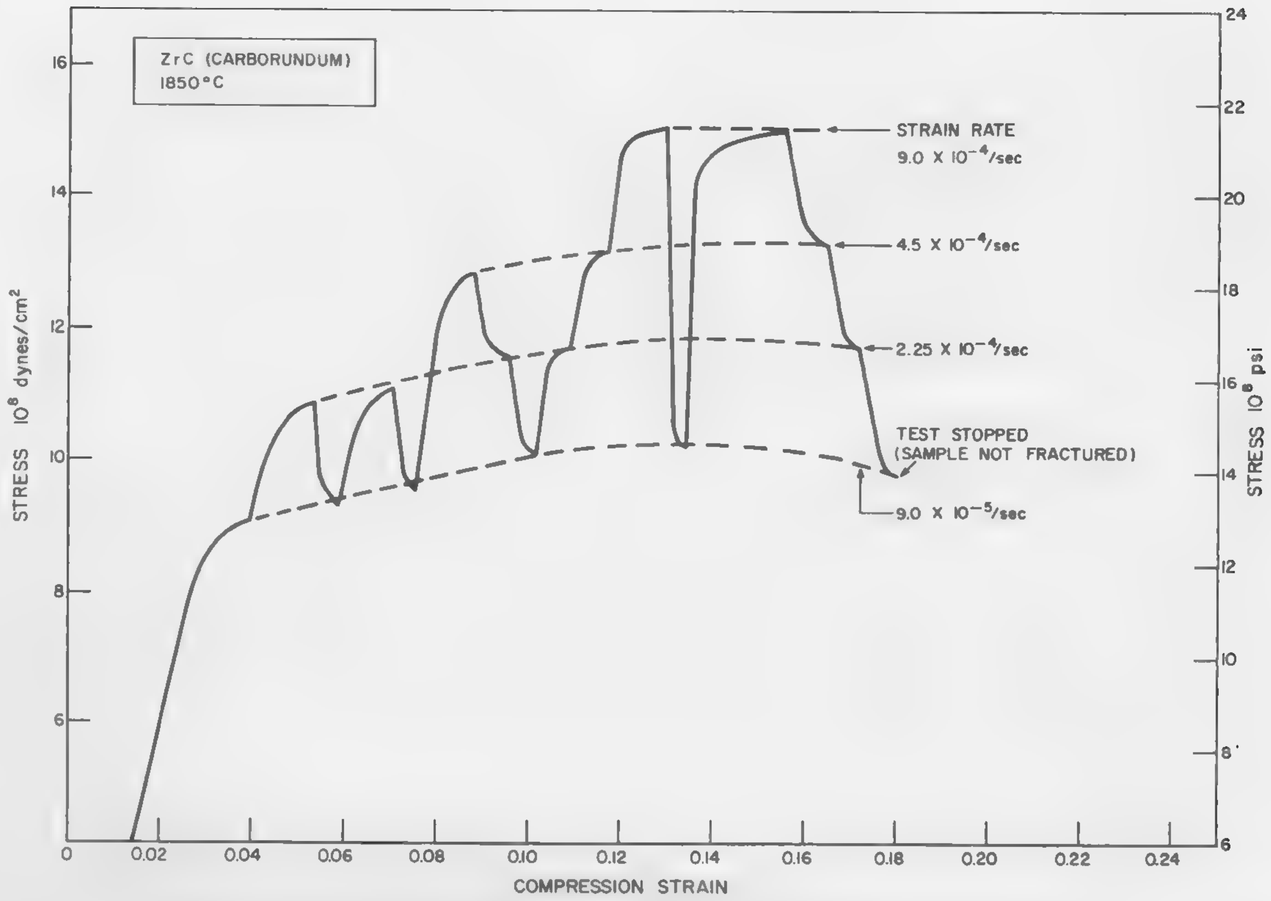


FIGURE 5 TYPICAL COMPRESSION STRESS-STRAIN CURVE FOR ZrC (INCLUDING SUDDEN STRAIN RATE CHANGES)

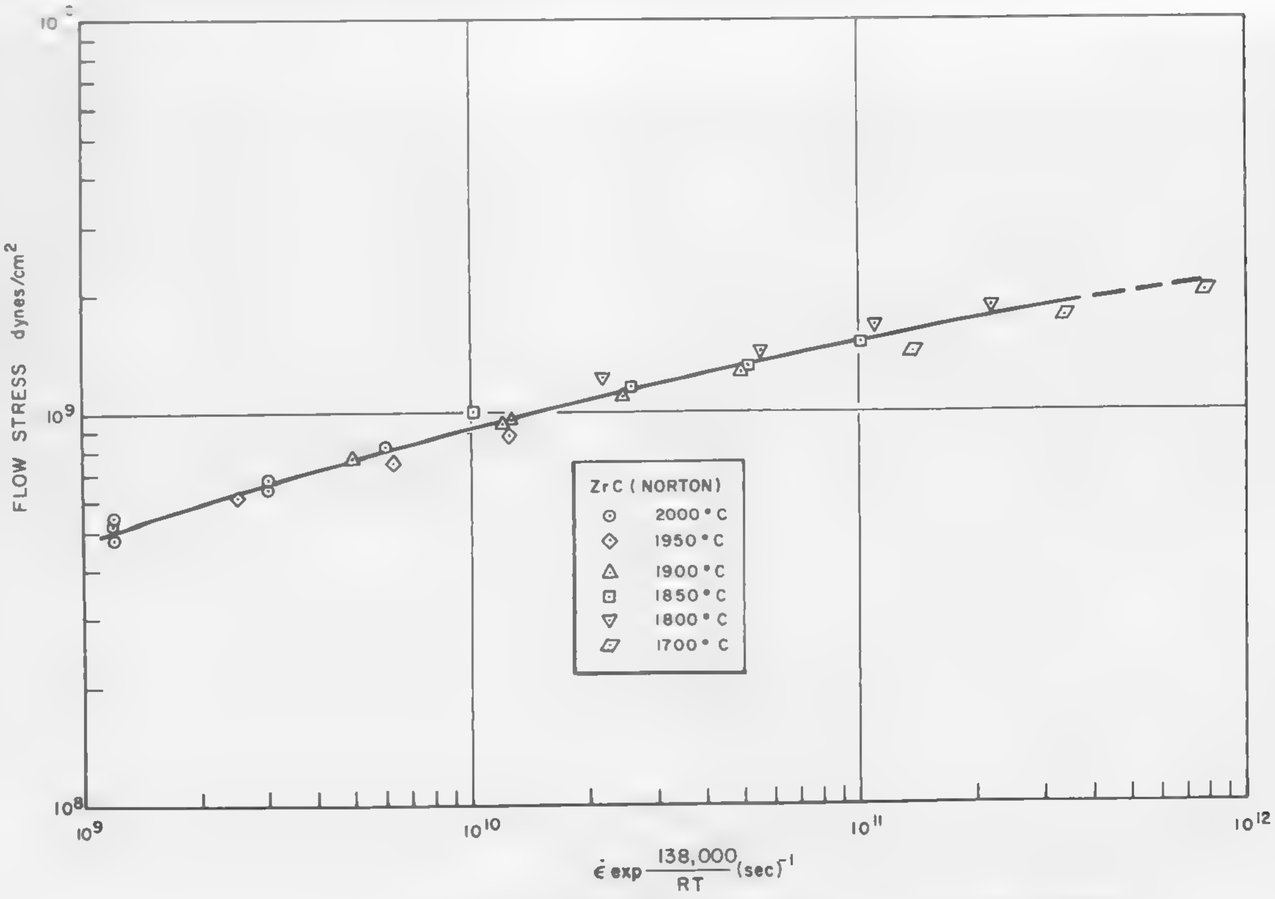


FIGURE 6 SUMMARY OF DEFORMATION BEHAVIOR OF ZrC (CARBORUNDUM) BETWEEN 1,700 AND 2,000°C

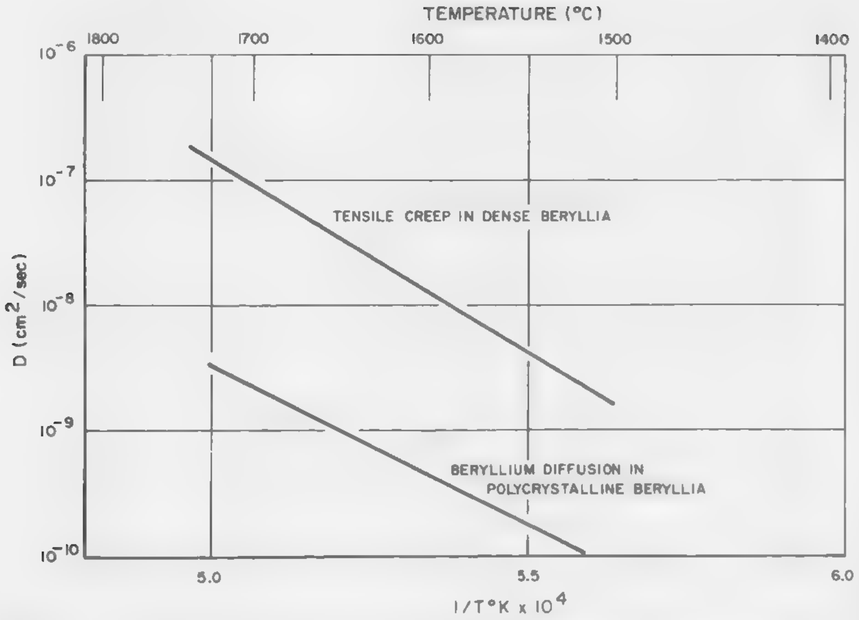


FIGURE 7 COMPARISON OF CREEP (TENSILE) AND TRACER DIFFUSION COEFFICIENTS FOR POLYCRYSTALLINE BeO (REFERENCE 4)

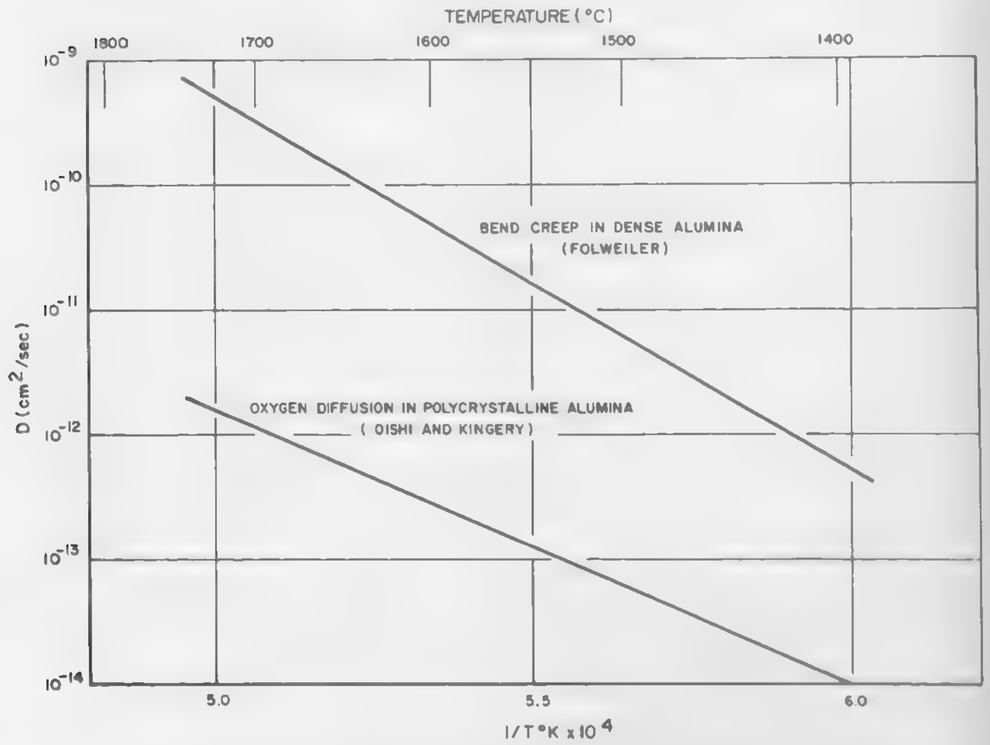


FIGURE 8 COMPARISON OF CREEP (BENDING) AND TRACER DIFFUSION COEFFICIENTS FOR POLYCRYSTALLINE Al_2O_3 (REFERENCE 5)

compression creep. Typical compression stress-strain curves (temperature and strain rate constant) are shown in Figure 9 for beryllium oxide and in Figure 10 for aluminum oxide. Horizontal arrowheads are placed at the

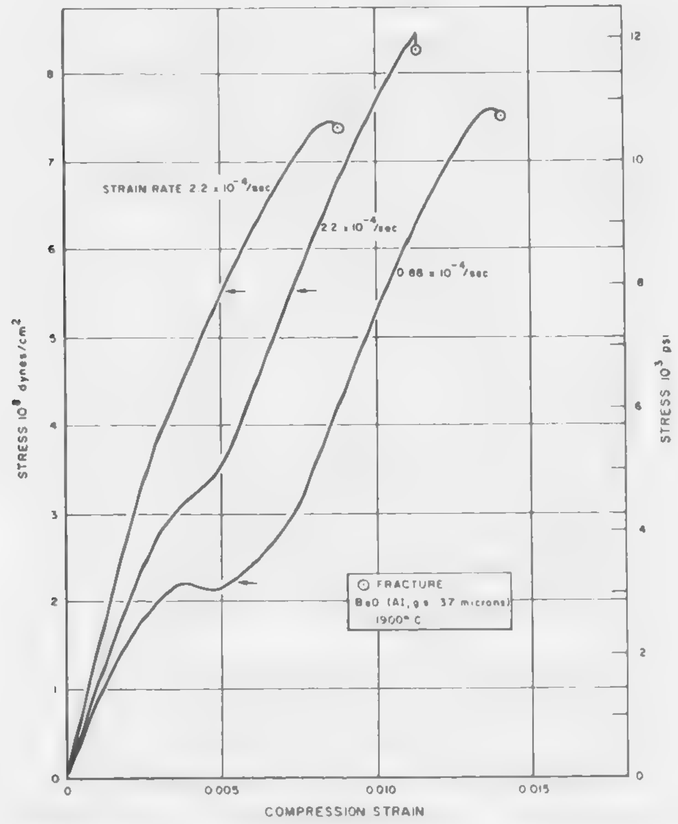


FIGURE 9 COMPRESSION STRESS-STRAIN CURVES OF POLYCRYSTALLINE BeO AT 1,900°C AND STRAIN RATES OF 0.88 TO 2.2 x 10^{-4}/SEC.

stress levels where Nabarro-Herring diffusional flow is expected if the creep diffusion coefficients given by the upper curves of Figures 7 and 8 are used. Extended flow was not observed in any of the six tests conducted at the indicated stress levels. The limited strain shown by the lowest curve in Figure 9 at the indicated stress level is probably due to "grain boundary flow" and cannot be pure diffusional creep nor dislocation-slip since the stress-strain curve continues upwards almost elastically until fracture. Further evidence of limited "grain boundary flow" is shown in Figure 11 for the compression testing of aluminum oxide, where the

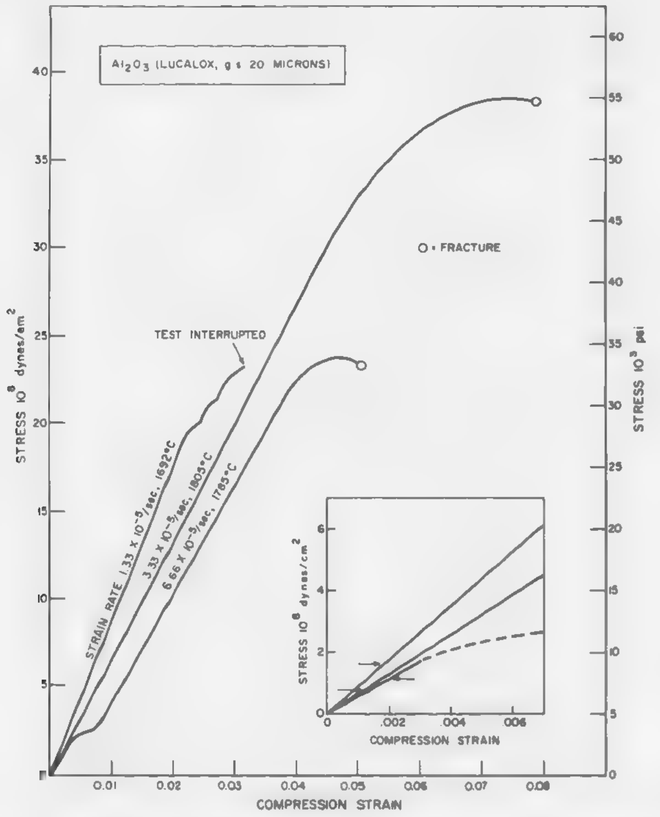


FIGURE 10 COMPRESSION STRESS-STRAIN CURVES OF POLYCRYSTALLINE Al_2O_3 AT ~ 1,800°C AND VARIOUS STRAIN RATES

stress at which flow occurs corresponds fairly well to the creep diffusion coefficients 1.1 to 1.3 x 10^{-9} cm^2/sec at 1,780-1,795°C given by the upper curve of Figure 8.

Very recently, compression creep and deformation work at Atomics International has been successfully carried to temperatures near 2,000°C at very low strain rates. Only then was extended deformation by compression observed. A typical compression stress-strain curve for beryllium oxide at 1,900°C and a strain rate of 9 x 10^{-5}/sec is presented in Figure 12. Here it is interesting to find that polycrystalline beryllium oxide can sustain plastic strains greater than 5% without strain hardening (in fact, the observed stress-strain curve suggests strain softening). Assuming that the extended deformation is due to Nabarro-Herring flow, the diffusion coefficient calculated from the

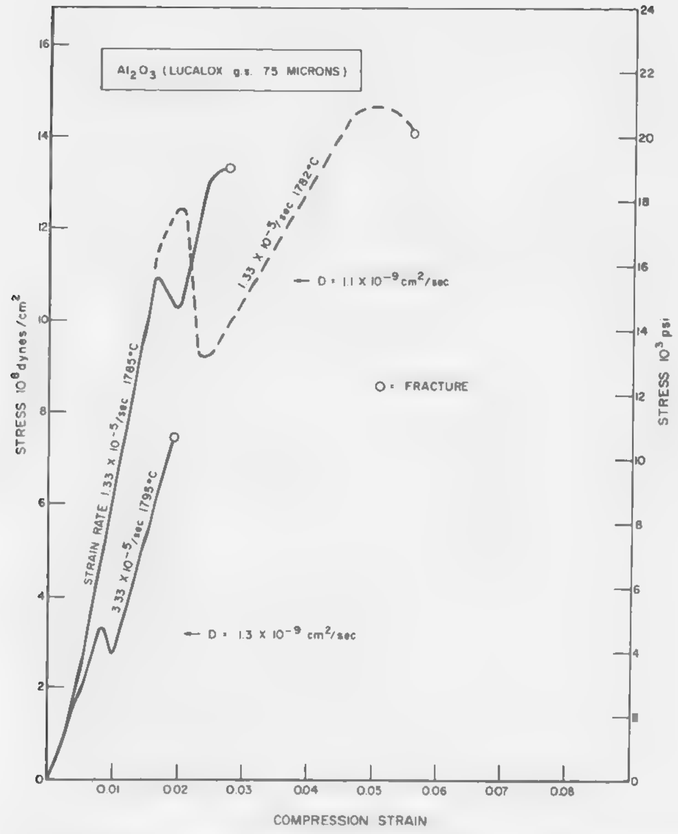


FIGURE 11 FURTHER COMPRESSION STRESS-STRAIN CURVES OF POLYCRYSTALLINE Al_2O_3 AT 1,700 TO 1,800°C AND VARIOUS STRAIN RATES

necessary parameters according to Eq. 1 agrees quite well with the tracer diffusion coefficient shown by the lower curve of Figure 7. Figure 13 reproduces the compression stress-strain curve of aluminum oxide at 1,950°C and a strain rate of 1.3 x 10^{-4}/sec. Extended flow without strain hardening was again observed. The diffusion coefficient calculated according to the new data also agrees reasonably well with the tracer diffusion coefficient shown by the lower curve of Figure 8 for aluminum oxide. These experiments suggest that (a) "Steady-state" creep formerly observed by Chang[4] and Folweiler[5] by means of tension and bending is most probably due to "grain boundary flow", the nature of which is presumably sensitive to variations in impurity content, density, etc., and (b) true Nabarro-Herring diffusional creep does seem to exist in polycrystalline beryllium oxide

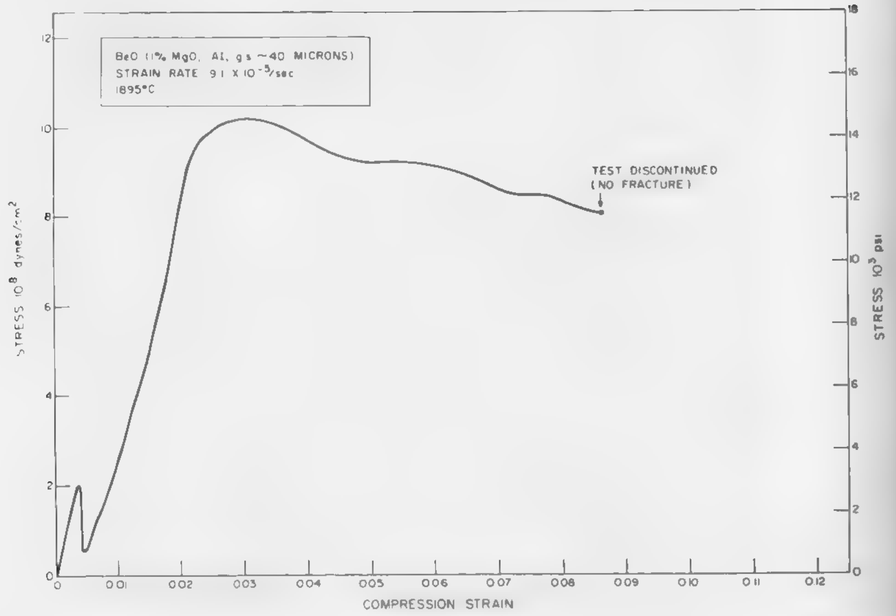


FIGURE 12 COMPRESSION STRESS-STRAIN CURVE OF POLYCRYSTALLINE BeO AT 1,900°C AND STRAIN RATE 9.1 x 10^{-5}/SEC SHOWING EXTENDED DEFORMATION

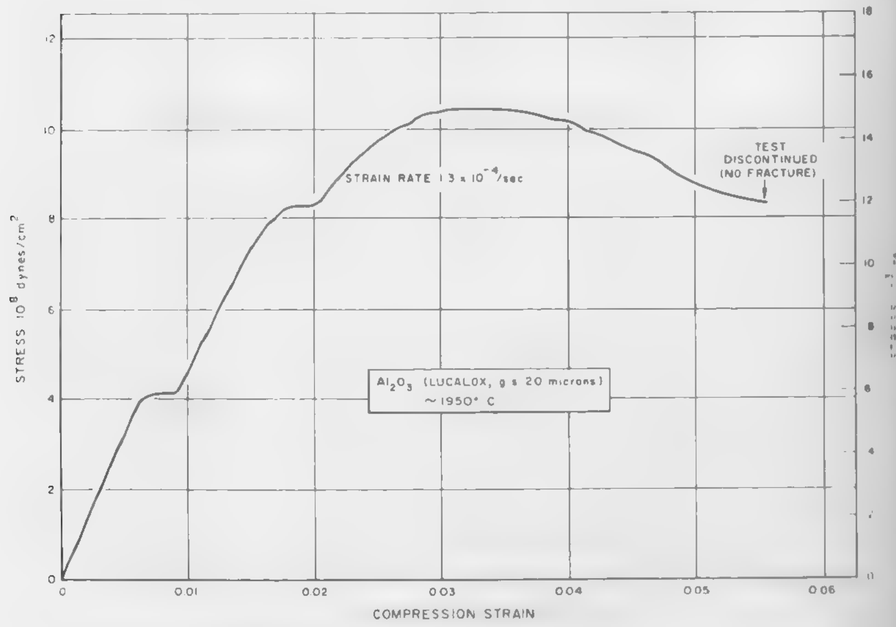


FIGURE 13 COMPRESSION STRESS-STRAIN CURVE OF POLYCRYSTALLINE Al_2O_3 AT ~ 1,950°C AND STRAIN RATE 1.3 x 10^{-4}/SEC SHOWING EXTENDED DEFORMATION

and aluminum oxide. More detailed studies, however, are necessary in order to establish unambiguously that the extended deformations shown in Figures 12 and 13 are true diffusional flow of the Nabarro-Herring type. Such work is still in progress in the laboratories of Atomics International. It is also possible that basal and prismatic slip take place concurrently near 2,000°C for both beryllium oxide and aluminum oxide so that deformation of the individual grains within a polycrystalline aggregate can occur. Current data presented here and by others,[6] suggests, however, that the dual slip hypothesis is unlikely.

CURRENT STATUS OF THE PREPARATION OF HIGH PURITY URANIUM CARBIDE AND BERYLLIUM OXIDE

Uranium Carbide

At Atomics International, purification of uranium carbide is accomplished by means of floating-zone electron-beam melting. A picture of the melting chamber is shown in Figure 14, and that of a zone melted rod is shown in Figure 15. Presently reactor grade uranium carbide rods made by arc casting or powder metallurgical techniques are used as the starting material. Comparison of the impurity contents of uranium carbide before and after zone-melting is shown in Table I. It is noted that a single zone pass results in marked reduction of the metallic impurities. Upon using higher purity starting material and making more zone passes, it is believed that uranium carbide of the highest purity can be obtained by this technique. Because of the relatively high uranium vapor pressure and wide composition range of uranium carbide at high temperatures, composition control of the material during zone-melting is difficult. The zone-melted product is usually slightly hyperstoichiometric in carbon, a typical microstructure of which is shown in Figure 16. The excess carbon is finally removed by treating the zone-melted rod in a hydrogen atmosphere. The heat treatment is also used to control the stoichiometry of uranium carbide. A combination of electron-beam floating-zone melting and heat-treating has successfully produced

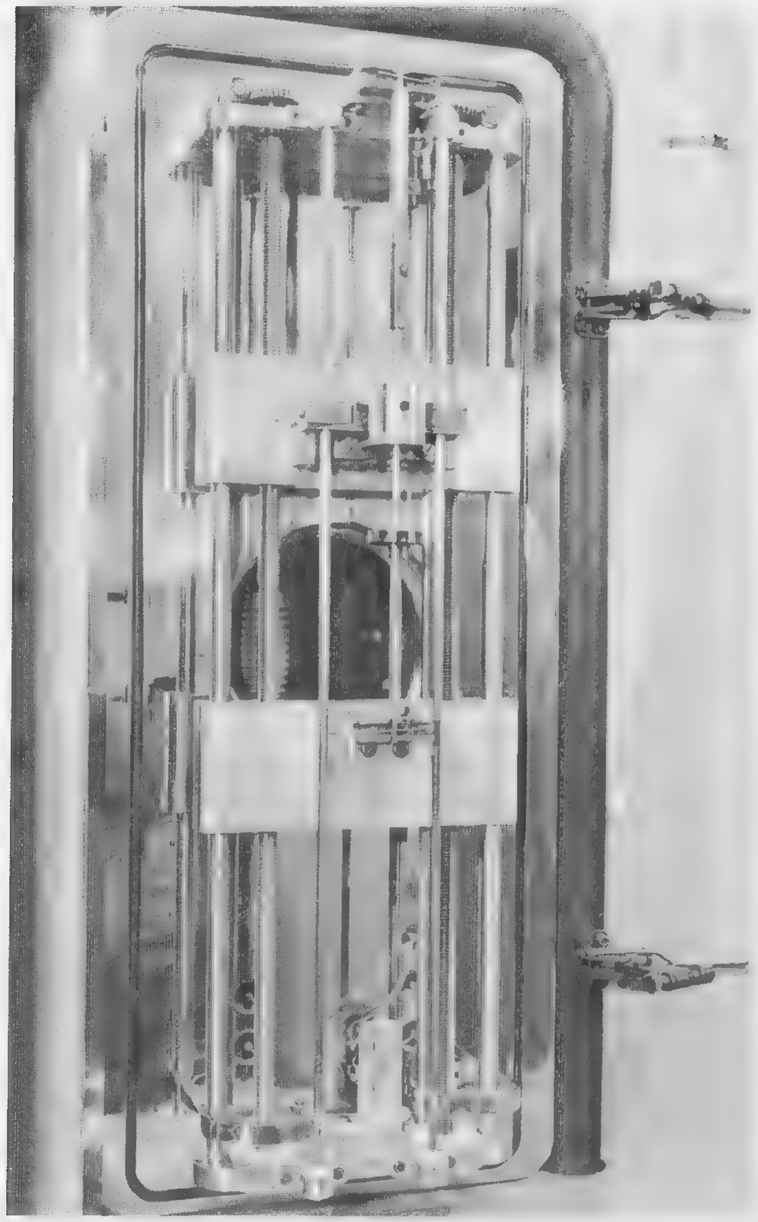


FIGURE 14 PHOTOGRAPH SHOWING SPECIMEN AND GEAR SYSTEM OF ELECTRON-BEAM FLOATING-ZONE REFINER



FIGURE 15 PHOTOGRAPH OF A ZONE-MELTED URANIUM CARBIDE ROD (ONE END CLEAVED)

TABLE I

REDUCTION OF IMPURITIES AND COMPOSITION CHANGES IN URANIUM CARBIDE BY FLOATING-ZONE REFINING (SINGLE PASS)

Element-ppm	Arc Cast	Zone Refined	Arc Cast	Zone Refined	Arc Cast	Zone Refined	Arc Cast	Zone Refined
Al	<10							
Be	1.5	1	0.2	0.2	< 0.2	< 0.2	< 0.5	< 0.5
B	0.5	0.5	0.75	0.75	0.75	0.75	< 0.5	< 0.5
Cd	< 0.5							
Ca	5	5	5	5	5	5	< 5	< 5
Co	< 2							
Cr	5	< 5	< 5	< 5	10	10	5	10
Cu	2	< 2	< 2	< 2	2	2	2	2
fe	65	30	65	20	125	<10	50	< 5
Mg	< 2							
Mn	< 5							
Mo	< 5	10	< 5	< 5	< 5	< 5	< 5	< 5
Ni	35	< 5	35	< 5	50	< 5	10	< 5
Pb	< 1							
Si	30	15	40	15	40	15	100	< 5
Sn	< 2							
Ti	< 2							
V	1	< 1	5	< 1	5	< 1	4	< 1
O_2							1835	835
N_2							675	140
H_2							35	15
Carbon w/o	4.24	4.86	5.17	5.5	4.46	5.16	4.96	5.23
Rate of zone travel-in/hr		4		1		1.5		1.5
Specimen		32		34		39		45

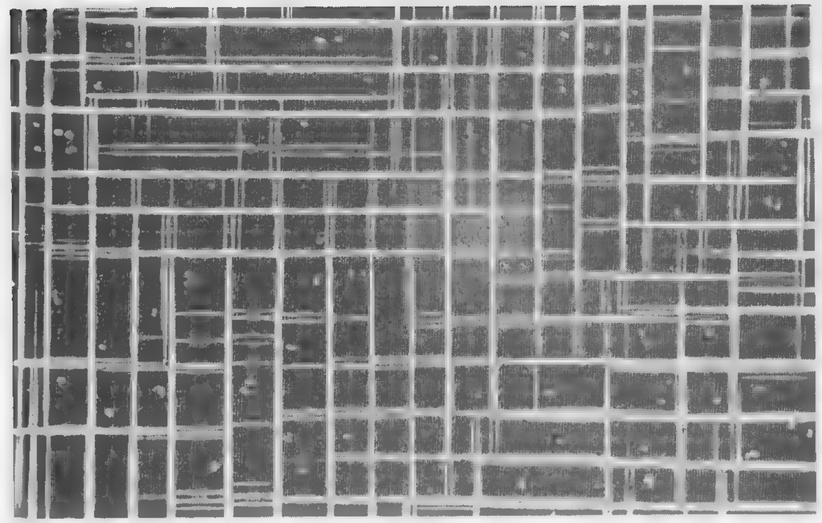


FIGURE 16 MICROSTRUCTURE OF ZONE-MELTED URANIUM CARBIDE ROD SHOWING THE PRESENCE OF UC_2 PLATES IN UC MATRIX, 500X

high quality uranium carbide rods, 5-6 mm in diameter and 2-10 cm long, in both polycrystalline and monocrystalline forms.

Beryllium Oxide

The purification of beryllium oxide powders by means of wet chemistry has been a widely studied subject which will not be discussed here, except to mention that the use of sulfuric acid or hydrofluoric acid results in powders containing considerable amount of sulfur or fluorine as anion impurities. At Atomics International two additional methods of producing high purity beryllium oxide crystals are studied:

a. The Alkali Molybdate Method

The precipitation of beryllium oxide crystals from alkali molybdates, principally Li_2MoO_4-MoO_3 saturated with BeO, resulted in the production of crystals up to 5 mm (imperfect) and 2 mm (clear, well-defined) in size.

Although several techniques have been tried, a slow cooling rate of 25-1.5°C per hour, starting at 1,400°C was found most suitable. The crystals commonly developed some modification of the pyramidal habit as a growth form, but under near equilibrium conditions prismatic crystals were developed. Typical photographs are shown in Figures 17 and 18. Most of the metallic impurities present in the crystal were below the limits of detection by spectrographic analysis. Persistent impurities present are B (0-1,000 ppm), Si (0-1,500 ppm), Li (5-50 ppm), and Mo (1,000 ppm and higher), depending on the purity of solvent and solute oxide and clearness of the grown crystals.

b. The Water Vapor Transport Method

Beryllium oxide crystals were also grown by a method employing a reversible reaction between the oxide and water vapor at high temperatures. The reaction product $Be(OH)_2$, formed at temperatures between 1,300 and 1,800°C, was allowed to decompose to the oxide and water vapor at a temperature several hundred degrees lower. Clear whiskers, platelets, rods, and massive crystals were formed depending on the temperature and pressure conditions. The principal interference with growth of large well-formed crystals was found to be impurities derived from the furnace, water, and the nutrient oxide placed in the furnace. Crystal growth mechanisms probably involve various types and orientations of dislocation structures, impurity poisoning of growth steps, spurious nucleation of new orientations by impurities, etc. By suitable control of the crystal growth system, crystals of 5 mm (diameter) by 1 mm (thickness) as platelets or 2 cm (length) by 1 mm (diameter) as rods were produced. Typical photographs are shown in Figures 19 and 20. The principal impurities found in the crystals are Al, Ca, Fe, and Si (up to several hundred ppm each).

Aside from wet chemistry methods, the purification of beryllium oxide by the above crystal growing techniques merits further study. Under favorable conditions, it may even be permissible to use these crystals as starting material for the production of high purity polycrystalline bodies.



FIGURE 17 PHOTOGRAPH OF BeO CRYSTALS MADE BY THE ALKALI MOLYBDATE METHOD



FIGURE 18 SAME AS FIGURE 17



FIGURE 19 PHOTOGRAPH OF B_2O PLATELETS MADE BY THE WATER VAPOR TRANSPORT METHOD

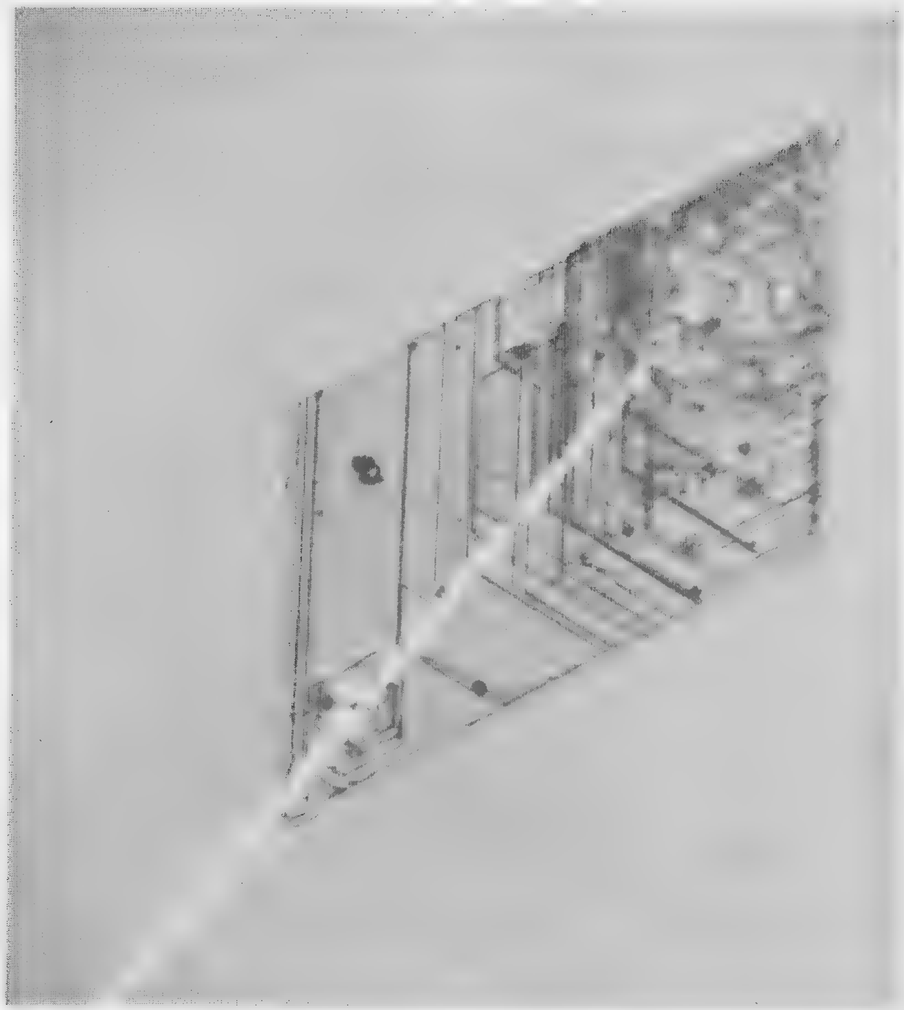


FIGURE 20 SAME AS FIGURE 19

SUMMARY AND CONCLUSION

Uranium carbide and beryllium oxide (as well as other carbides of the sodium chloride structure and oxides of hexagonal structure) are materials potentially important for high-temperature nuclear reactor and load-bearing applications. Their contrasting mechanical properties are presented and discussed with regard to the possible importance of crystal structure, stoichiometry, purity, etc. The present status of the preparation of high purity uranium carbide and beryllium oxide indicates that additional work is necessary in order to produce high purity bodies in suitable forms and sufficient quantities for property measurements as criterion for further evaluation of the potentialities of these materials. Although it could not be assured whether further work to obtain purer materials than presently available will lead to new information, our experiences so far have been both fruitful and stimulating.

ACKNOWLEDGMENTS

The authors wish to thank the following colleagues of Atomics International in providing them with certain information described in this paper: S. B. Austerman (BeO crystal growth), H. Nadler (UC zone refining), and R. E. Taylor (portions of the thermal and electrical property data).

BIBLIOGRAPHY

1. Chang, R., paper accepted for publication in the Journal of Applied Physics.

2. Hagel, W. C. and J. H. Westbrook, Trans. A. I. M. E. 221, No. 5, 951 (1961).

3. Herring, C., J. Appl. Phys. 21, 437 (1950).

4. Chang, R., J. Nuclear Materials 1, 174 (1959).

5. Folweiler, R. C., J. Appl. Phys. 32, 773 (1961).

6. Beauchamp, E. K., G. S. Baker and P. Gibbs, "Impurity Dependence of Creep of Aluminum Oxide," University of Utah, Scientific Report to WADC, September 1961.

FIBER-REINFORCED STRUCTURAL MATERIALS

David W. Levinson
Metallurgical Advisor
Armour Research Foundation
Chicago, Illinois

ABSTRACT

This paper will discuss fiber reinforced materials, both organic and inorganic, from the standpoint of the relationship between constitution and properties. Current applications will be discussed, and possibilities for future special purpose and general applications will be considered.

INTRODUCTION

The reinforcement of a material of construction with a fibrous or filamentary form of another is usually done to make capital of the tensile properties of the filaments. As will be seen in the following pages, this is not the only reason for making such composites, physical properties as well as mechanical properties being amenable to control.

The most common example of a fiber-reinforced structural material in everyday commerce is the autombile tire. The bulk of the ability of the tread portion of the tire to resist elongation derives from the presence of longitudinal nylon or rayon fiber cords bonded to the tire rubber; and similarly, the bulk of the burst resistance of the sidewall derives from an incorporated set of similar fibers wound bi-directionally so as to maximize the resistance of the composite to biaxial tension. To appreciate the remarkable degree of strengthening thereby obtained one need only compare with it the obvious lack of strength of the unreinforced inner tube whose wall thickness was typically between one-third and one-fifth of the tire sidewall thickness. The

inner tube could not, by itself, even begin to sustain the normal working pneumatic pressure, let alone the opera stresses encountered in service. There are many other pre-space age examples of fiber-reinforced materials ranging from glass fiber reinforced plastic fishing rods rubberized fabric barrage balloon bags. The concept is certainly not new, but the possibilities are exciting and numerous. Reinforcement of elastomers, plastics, met and ceramics with fibers of glass, plastics, metals, and ceramics has been under intensive study in many places recent years and always for the purpose of rectifying so basic structural or physical deficiency in the base mater

BASIC CONSIDERATIONS

To understand how this may obtain we can consider several specific examples. The most primitive possibili is that of reinforcement for simple tension. Consider a body of cross-sectional area A in physical parallel with n fibers each of area a. If the fibers are bonded to the b the strain will be homogeneous as a first approximation that conditions will exist as shown in Figure 1. If a load is applied, the strain ϵ will result when the sums of the back forces in the two components are equal to P. The computation of this strain is simple so long as the syster is Hookean--that is, so long as the components are deforming elastically.

Since the strain ϵ is the same in both components

$$\epsilon = \frac{\text{stress}_B}{E_B} = \frac{\text{stress}_f}{E_f}$$

where

E_B = Young's modulus of the body material
E_f = Young's modulus of fiber material

or

$$\frac{p_1}{AE_b} = \frac{p_2}{naE_f}$$

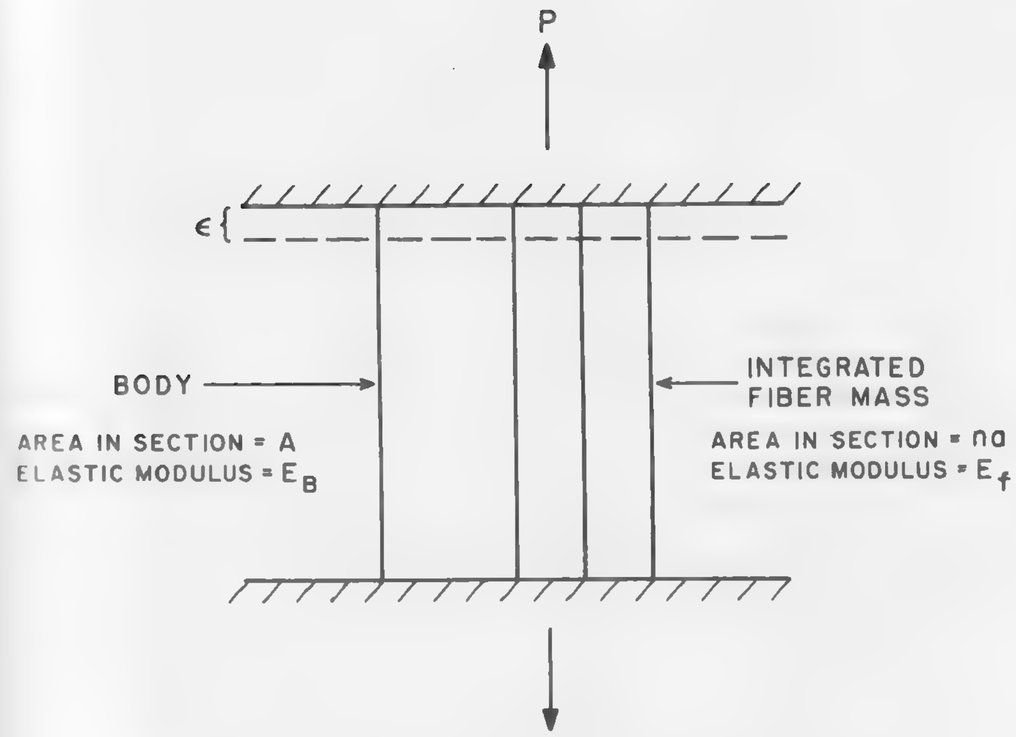


FIGURE 1 SCHEMATIC BEHAVIOR OF FIBER REINFORCED BODY

where

$$p_1 + p_2 = P.$$

Thus it may easily be seen that the effect of the fibers is to absorb part of the load in direct proportion to the integrated cross-sectional area and to the ratio of the elastic modulus of the fiber material to that of the body. Thus, the incorporation of glass fibers having a very (relatively) high modulus into a plastic of low modulus makes eminently good sense, the fibers in this case absorbing most of the tension per unit cross-sectional area of each. In a similar way flexural, torsional, and compressional behavior of such composites can be computed. The elastic moduli of several important glass fibers are shown in Table I, and in Figure 2 as a function of annealing temperature, so that the values and their variability can be appreciated. This very simple picture applies strictly only if the fibers are continuous and are oriented along the long axis of the body. The picture applied also only within the limitation imposed by the boundary conditions. When these conditions are fulfilled, the

TABLE I[6]

GLASS FIBER PROPERTIES

Glass Fiber	Specific Gravity	Modulus of Elasticity (10^6 psi)	Tensile Strength of Single Fibers (10^3 psi)*
E Glass	2.55	10.7	500
E Glass (heat treated)	2.57	12.3	--
Imperial N-672	2.92	17.3	520
YM31A (com'l BeO glass)	2.89	16.0	500
Fiberglas X-37B	2.6	13.2	580
Bjorksten Silica	2.2	10.7	200-500

* Tested at 50% relative humidity.

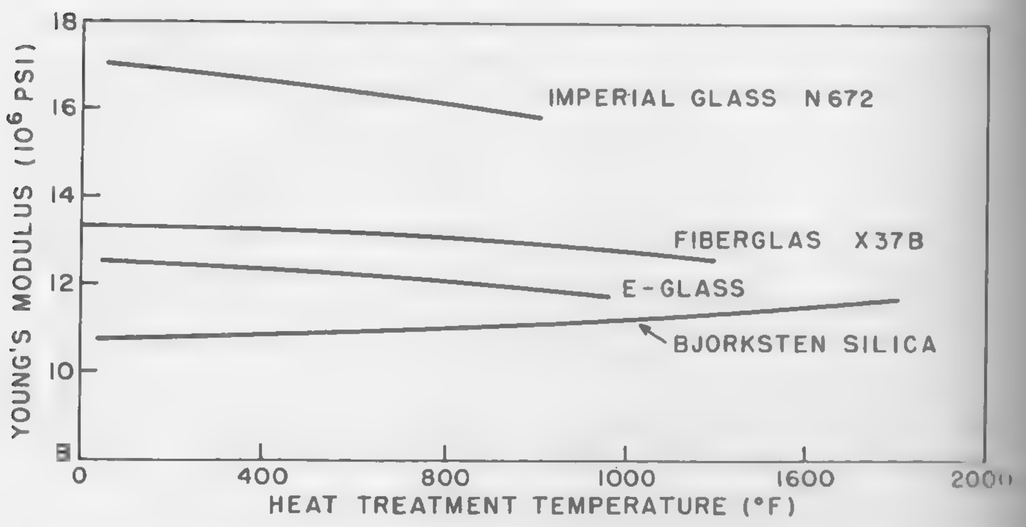


FIGURE 2 HEAT TREATED GLASS FIBER MODULI (DATA FROM OTTO, W.H., REFERENCE 1)

essentially elastic behavior of the composite is quite predictable.[2, 3] When, however, the composites are stressed to levels at which elastic behavior no longer results, the strength values become rather less predictable, and failure, which appears to be progressive, is complex. The manner in which the elements in the structure participate in the failure process is obscure. Attempts have been made to predict the properties of composites such as these under non-ideal loading conditions, and it has been found that, with the assumption of orthotropic behavior, this is fairly successful. A succinct discussion of the conditions under which the mechanical properties of glass-resin composites can be predicted is given by McGarry.[4] The strength properties of composites with short, randomly oriented fibers are also difficult to predict. New variables appear such as interfiber spacing. The effects, as shown in Figure 3, are best determined experimentally. The same rules apply to the degree allowed by the initial and boundary conditions to all fiber-composites, and sometimes rather spectacular advantage can be taken of the strength increases afforded, particularly at elevated temperatures. The so-called fiberglas composites are among the highest strength-weight

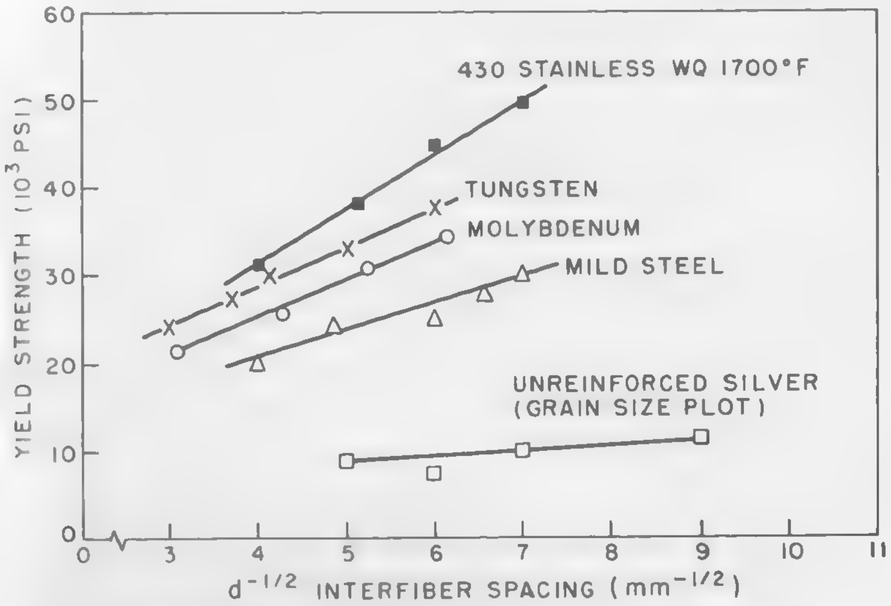


FIGURE 3 STRENGTH OF REINFORCED SILVER COMPOSITES

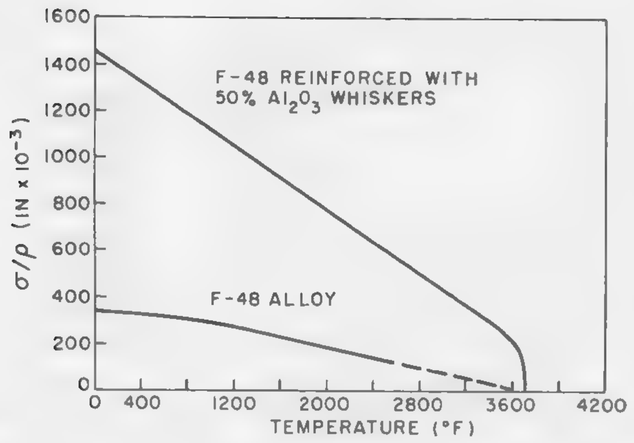


FIGURE 4 STRENGTH-TO-DENSITY RATIO FOR F-48 ALLOY UNREINFORCED AND REINFORCED WITH Al_2O_3 WHISKERS

ratio materials known. Shown in Figure 4 is the predicted effect of sapphire fibers (whiskers) on the properties of a columbium-based alloy known as F-48. The assumptions in the calculations involve only parallel whisker orientation and interfacial bonding between the matrix and whisker. This case represents, of course, two departures from the previous discussion. The fibers are now not assumed to run the entire length of the composite and the fibers are, in this case, true whiskers and have tensile (fracture) strengths as high as 1,400,000 psi--that is, strengths approaching the theoretical. While the spectacular predicted increases in strength of F-48 have not to my knowledge as yet been verified, the very same sapphire whiskers have been incorporated within aluminum, and one sample containing 12.5% whiskers exhibited a fivefold increase in tensile strength.[5] These examples reflect a common and predictable increase in the mechanical properties of a resin by glass reinforcement, and of a metal by ceramic reinforcement. Particularly the latter is an example of the sort of improvement that can be realized if cognizance is kept of the exact nature of the two microconstituents. Reinforcement of aluminum with true whiskers of Al_2O_3 is quite different from results obtained from experiments in which the aluminum was reinforced with polycrystalline alumina fibers, alumina flour, or by the natural oxide coating aluminum powder. The inability of alumina or

other polycrystalline ceramics to support tensile loading is well known and is quite unlike the behavior of virtually lattice defect-free whisker crystals.

This general deficiency of ceramics in tension can to some degree be rectified by a fiber composite which, if properly made, becomes the analog of prestressed concrete. Consider a metal M and a ceramic C for which the expansion coefficients are, respectively, α_m and α_c where $\alpha_m > \alpha_c$. Implicit in this discussion will be the same boundary conditions as for the case of simple reinforcement.

Assuming equal areas for simplicity, the ceramic and metal will be bonded at, say, 2000°C, a temperature at which the ceramic will densify and one at which the metal is still a good solid.

Initially, the situation is as represented in Figure 5a. If the two components were allowed to cool individually to room temperature (0°C), the situation would be as pictured in Figure 5b. We now apply tension to the metal component so that it is at room temperature equal in length to that of the untouched ceramic, l_c. This, of course, places the metal under tension σ'_m (Figure 5c). Imagine, now that the two are bonded together and the force applied to the metal is released. The residual tension in the metal will force the ceramic into compression until the stresses equilibrate as shown in Figure 5d. The dependence of the equilibrium

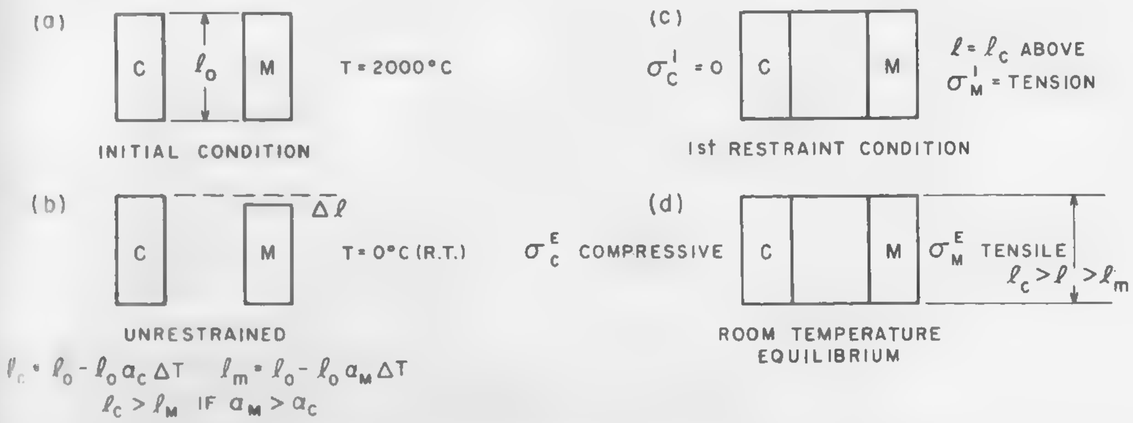


FIGURE 5 ANALYSIS OF PRE-STRESSING

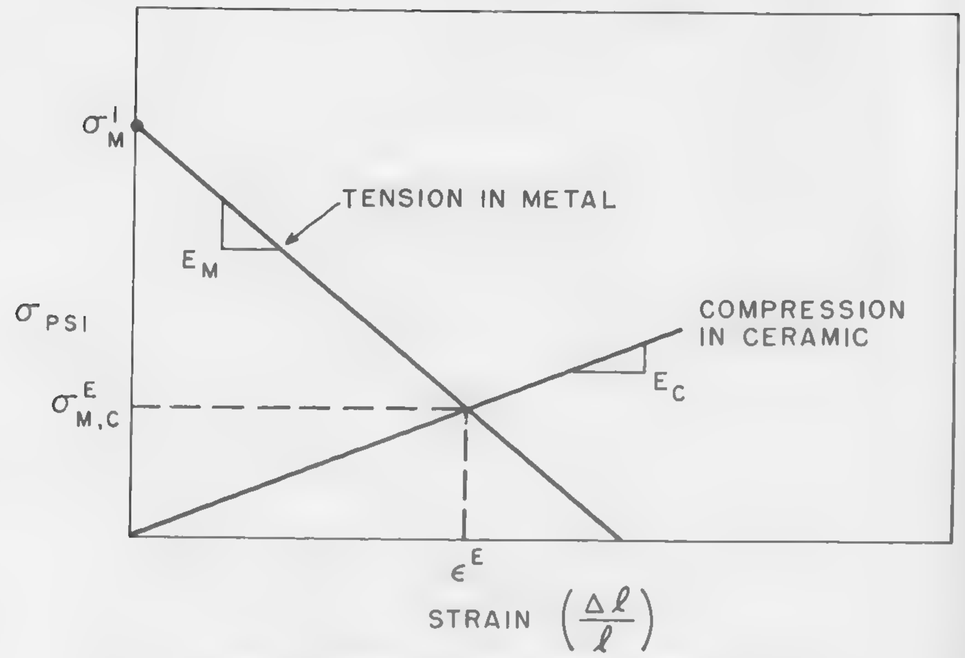


FIGURE 6 STRESS VARIATION IN PRE-STRESSED COMPOSITES

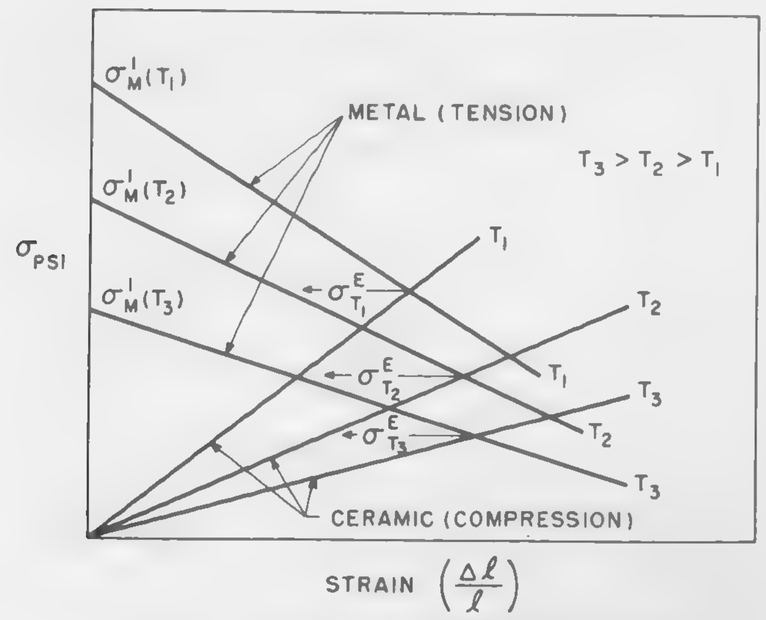


FIGURE 7 DEPENDENCE OF PRE-STRESS ON TEMPERATURE

stresses on the elastic moduli is shown in Figure 6, and the dependence of the prestress on temperature in Figure 7 in which the slopes are exaggerated for clarity. One needs only values of E_m, E_c, α_m and α_c (and their temperature dependencies) to determine the degree of prestress which will be active at any particular temperature. The possibility, of course, exists of placing the ceramic in hydrostatic pre-compression by dispersing randomly oriented fibers of the proper metal. Some experimental values of the elastic modulus of composites are shown in Table II. These values are for 10 v/o molybdenum fibers randomly dispersed. Note especially the case for Momullite, in which the expansion coefficients are evidently very nearly equal, and the effect of negative prestressing of ThO_2 and MgO, both of whose expansion coefficients are appreciably

TABLE II

ELASTIC MODULI OF PRESTRESSED CERAMICS

Metal	Oxide	Modulus (10^6 psi)
Mo	--	46
	$6ZrO_2.CeO_2$	8.2
Mo	prestressed composite	19.6
	ZrSiO	14.0
Mo	prestressed composite	20.6
	$3Al_2O_3.2SiO_2$	18.8
Mo	prestressed composite	18.8
	ThO_2	36.4
Mo	prestressed composite	26.9
	MgO	34.7
Mo	prestressed composite	16.3

greater than that of Mo. It was found that Mo-ThO_2 composites became rather fully cracked during cooling, as one would expect. However, the relatively ductile Mo fibers acted as very effective crack stoppers, and the bodies maintained apparent integrity even when subjected to repeated and severe thermal shock.

The general resistance of metal fiber-ceramic composites to thermal shock is far superior to that of the ceramic alone. This may be due, in part, to the prestressing but is also due, at least in part, to the improved thermal conductivity afforded by the incorporated paths of metallic conductivity. Here too, the properties are quite predictable based on the effective cross section of the fibers, the individual thermal conductivities of the phases, and well-known laws of conduction by networks. Ideal geometries can, of course, permit simple parallel conductivity behavior. Graded fiber densities can provide high conductivity surfaces which act both to reduce maximum surface temperatures and also reduce temperature gradients.

Thus, to a good first approximation, mechanical and thermal properties of fiber-filled composites can be estimated. The results have been sufficiently encouraging to warrant intensive study of actual composites for many critical applications.

SOME COMPOSITES OF CURRENT INTEREST

The uses of filamentary composites for improvement of strength are perhaps the most numerous. Of the structures that people are currently willing to openly discuss, the two most common are the glass fiber reinforced plastic pressure vessel and the metal wire reinforced thin-walled metal pressure vessel, both promising as high strength-weight ratio rocket motor cases.

The former of these involves the use of some of the newer high-strength glasses and many new laminating resins which remain stable, at least for short periods up to 800°F. For comparison, some strength properties are shown in Table III.

TABLE III

PROPERTIES OF SOME PRESENTLY AVAILABLE STRUCTURAL MATERIALS

Property	Filament-Wound Glass Fiber-Resin Composites	Steel	Titanium
Density	0.08	0.285	0.163
TYS (psi)	250,000	220,000	180,000
TYS/Density (in.)	3.12×10^6	0.77×10^6	1.10×10^6
Modulus of Elasticity (psi)	8.5×10^6	30×10^6	16×10^6

The figures in Table III are of a qualitative nature for comparative purposes only. To be sure, both the steels and the titanium alloys can be used at higher strength levels than those indicated, but not without attendant difficulties in fabrication of pressure vessels. Similarly, the "tensile yield strength" of a fiber glass composite is not, as was mentioned earlier, definitive to the same degree as in the case of the metallic materials.

In addition, when actual vessels (rather than sample test samples) are made, several disadvantages accru to what is otherwise the obviously superior material (glass fiber composites). The relatively poor ability to sustain high bearing loads poses many problems in design since loading ports, nozzle ports, and skirt fastenings must be kept small. This complicates the problems in winding the vessel, loading propellant, and making adequate closures. The relatively low elastic modulus also poses problems that are soluble only by thickening, which imposes weight penalties. The result is that the metals are still distinctly competitive in this application.

Some work, previously mentioned, is presently concerned with the distribution of inorganic fibers (in the case mentioned, Al_2O_3 whiskers) in metals. Here the fibers are variously carbides, metals themselves, and other oxides, the preponderance of real interest being devoted to whiskers or very small polycrystalline filaments. Currently attempts are being made to capitalize on what appears to be a true size effect, since it has long been known that ordinary structural alloys are stronger in wire form, in sizes below about 2 mils, than in bulk. The magnitude of such strengthening can be appreciated by consideration of Figure 8.

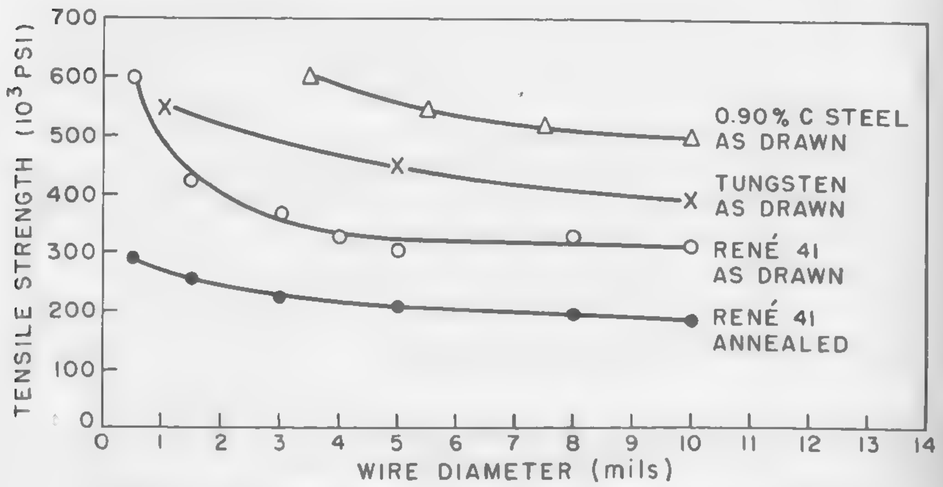


FIGURE 8 SIZE DEPENDENCE OF TENSILE STRENGTH OF FINE WIRES [9]

Two features of these data are of interest. First, the curves display a linear portion sloping gently towards higher strength values. They then become concave upwards, suggesting a real strength bonus in very fine diameters. Unfortunately, the random frictional influence of debris and die imperfections normally prevent wire from being drawn by conventional methods to sizes below 1 mil.

Much of the current work in which metals are internally reinforced with metals involves short fibers rather than continuous filaments, although very fine fibers are of particular interest where obtainable. One system of importance is the lead-steel system in which commercial grades of pure lead and dilute alloys have been reinforced with either tin bronze or mild steel. The obvious need here is for simple

strengthening (especially in creep). Rather successful composites have been made at volume fractions of fibers of the order of 20%. In this case, relatively coarse fiber aggregates, resembling fine steel wool, were used. The composites were made by infiltrating a presintered mat of the order of 20% dense with the molten alloy which then is allowed to freeze. This type of composite has been found[7] to be useful in other ways. It has been found, for example, that remelting the matrix phase does not necessarily produce runout of the liquid and that the composites were, therefore, rather interesting in their behavior as unlubricated bearings under conditions where unreinforced bearings of the same composition summarily failed on melting. Similarly, stainless steel-teflon composites have shown promise for high-temperature seals and some bearing applications.

In a quite different way the magnetic properties of essentially elongated single domain particles of iron (dendrites 150A in diameter) have been put to commercial use by fabricating a composite with either a plastic lacquer, lead, or copper. These so-called ESD magnets are described most recently by Luborsky et al.[8] While here one capitalizes upon the high intrinsic coercive force of elongated iron particles of this optimum diameter, the composite structure is required to take practical advantage of the excellent permanent magnet characteristic of the ESD particles. Here, then the composite is made, not strictly in the sense of improving the properties of the matrix by adding the fibrous second phase, but rather to permit one to utilize the properties of the fiber particles themselves. Analogous structures to utilize the nearly theoretically strong true whiskers of both metals and ceramics are also being made.

There are thus four kinds of fiber or filament-matrix composites of current interest: the continuous filament or woven composite, short fiber composites (either oriented or random), sintered or bonded fiber matrix composites in which all fibers are bonded to one-another at all points of contact as well as to the matrix, and whisker composites.

The most widely used of these today is the continuous filament type typified by many fiber glass and reinforced metal fabric composites. The unbonded fiber type is perhaps best typified by the ESD magnets.

The full co-continuity of metal and pore networks in sintered (or otherwise bonded) fiber metal leads to the obvious conclusion that by filling the pores with another material, composite materials may be almost ideally constituted. Some of the material combinations which have received extensive attention at the Foundation are listed in Table IV. Because an essentially unbroken network of both metal and matrix material can be achieved, the reinforcement of a weak or brittle matrix material is accomplished without excessive alteration of the desired matrix properties. For example, the creep strength of lead has been increased 800% by incorporating only 15 weight per cent of mild steel in the form of sintered fiber metal. Aluminum oxide bars of identical size, one reinforced with 20 volume per cent molybdenum fibers and the other unreinforced, have been partially quenched in water from 2000°F. The unreinforced bar shattered while not even surface cracks developed in the composite bar. A molybdenum-reinforced thoria bullet has been fired through concrete without damage.

The engineering possibilities offered by composites are becoming apparent at a time when almost impossible demands are being made of materials. Brittle materials must be ductile; nonconductors must conduct heat and electricity; intrinsically weak materials must support loads; molten metals must not flow. The only answer is, in many of these cases, a composite. Molten metals may easily be held in place by the blotter-like action of a sintered fiber skeleton. Materials with a precise modulus of elasticity can be designed: the tungsten fiber-copper system shows a continuous variation in E from 12 x 10^6 psi to 25 x 10^6 psi between 0 and 50% (by volume) of tungsten fiber. The same system shows a controllable variability in electrical resistivity (and correspondingly in thermal conductivity) from 2-8 microhm-cm over the same range. Gradations in these properties may be built into the same piece! In other words, the capability to achieve properties in a fully controlled fashion intermediate between metals or alloys, ceramics, or plastics is now becoming available.

As has been implied, the most exciting possibilities lie in the realm of true whisker composites. It is unlikely that true whiskers can be bonded to one another and still

TABLE IV

SOME COMPOSITE MATERIALS BASED ON SINTERED FIBER METAL

Fiber Network Material	Matrix
	A. Metal - Metal
Tungsten	Beryllium Copper Silver
Mild Steel	Lead Magnesium Silver
Stainless Steel (Type 430)	Silver Copper
Copper, Bronze, and Brass	Lead
	B. Metal - Ceramic
Molybdenum	Alumina
Tantalum	Alumina
Tungsten	Titanium Carbide Hafnium Carbide Tantalum Carbide Zirconium Carbide
	C. Metal - Plastic
Stainless Steel	Epoxy Phenolic Furfural Alcohol

retain their whisker character. However, it has been shown that they can be bonded with apparent success to other materials without suffering drastic losses in strength, and accordingly there is great interest in composites for the future utilizing their enormous strengths. An analysis by Hoffman[10] indicates that the worth in use of whisker material can be of the order of $4000 per pound. This allows reasonable latitude in the ultimate cost of mass producing the whisker, a problem which at the moment is a challenging one.

One may thus conclude that the fibered composites are, for good reason, rapidly joining the family of new structural and special purpose materials, and that much worthwhile research and technological development in this area remains before us.

BIBLIOGRAPHY

1. Otto, W. H.: Properties of Glass Fibers at Elevated Temperatures. Presented at 6th Sagamore OMRO Conference, Raquette Lake, N. Y., Aug. 18-21 (1959).

2. McGarry, F. J.: Plastics Technology 5: p. 44 (1959) Feb.

3. McGarry, F. J., and R. E. Chambers: ASTM Bull. No. 238, p. 38 (1959) May.

4. McGarry, F. J.: Properties of Glass Fiber Reinforced Plastics Presented at Sixth Sagamore OMR Conference, Aug. 20, 1959, Raquette Lake, N. Y.

5. Sutton, W. H.: Contribution to Refractory Composite Working. Group Meeting, Dallas, Tex., Aug. 8-10, 1961. This work is under Contract NOw 60-0465d by General Electric Co., Philadelphia, Pa.

6. Runck, R. J., and B. W. King: DMIC Memo No. 110 (1961) June 6.

7. Fisher, J. I., et al.,: An Investigation of Fiber-Reinforced Lead, unpublished.

8. Luborsky, F. E., T. O. Paine, and L. I. Mendelsohn: Powder Met. 4:57 (1959).

9. Data from DMIC Memo No. 80 January 20, 1961, Compiled by D. A. Roberts.

10. Hoffman, G. A.: Future Possibilities in Fibered Material. Rand Corp. Publ. P-1760, 13 July 1959.

RECENT DEVELOPMENTS IN COLUMBIUM PHYSICAL METALLURGY

Warren I. Pollock
Research Supervisor
Pigments Department - Metal Products
E. I. du Pont de Nemours and Company
Experimental Station
Wilmington 98, Delaware

ABSTRACT

This paper presents new information concerning the effect of second phase strengthening as obtained by the solution treatment and subsequent aging of columbium alloys. The susceptibility to age hardening, as well as dispersion strengthening, is imparted to columbium-base alloys by additions of both zirconium and hafnium. The interaction of zirconium with carbon and oxygen is detailed. Phase identification and metallographic studies are reviewed. Suggested avenues of future research are also presented.

INTRODUCTION

Of the refractory metals melting above 4000°F (2200°C), columbium (niobium) is most attractive because of its relatively low density, excellent ductility and natural abundance. Commercially pure, unalloyed columbium, when compared to tantalum, molybdenum, and tungsten, has lower strength and modulus values. However, marked increases in strength and moderate improvements in modulus are easily obtained by simple alloying. Further, columbium attractively possesses susceptibility to age hardening, as well as dispersion strengthening, by the addition of small amounts of zirconium and hafnium.

Columbium physical metallurgy is in an active state of development. Gemmell[1, 2] and Begley[3] have studied the effect of solute elements on the tensile strength of columbium and Anders[4] has reviewed the metallurgy of columbium and its alloys. The Defense Metals Information Center of Battelle Memorial Institute has undertaken to periodically issue brief memoranda concerning major developments in the technology of columbium (and tantalum). The subject of this paper is therefore to discuss second phase strengthening and identification in columbium alloys, particularly with respect to recent investigations detailing solution treating and aging phenomena.

Cb-1% Zr

The very important influence of dispersion hardening was observed early in physical metallurgical studies of columbium. R. T. Begley[5] undertook investigations to obtain basic creep rupture data on annealed and cold worked columbium. The columbium tested exhibited surprisingly high strength, the 100 hour rupture of the annealed columbium being more than twice that of pure molybdenum at 1800°F (982°C) and 2000°F (1093°C). The high strength was attributed to the presence of approximately 0.6% zirconium in the columbium used in the test program: apparently zirconium was an impurity resulting from the ore beneficiation. "Since it appeared that the high strength could not be entirely attributed to simple solution hardening, there was a possibility of interaction between the zirconium and interstitial impurities present in the starting material or picked up during test."[5] Soon after this discovery, there was a large demand for columbium mill products and to fill this request, columbium containing approximately 1% zirconium was selected based, among several factors, on its elevated temperature strength advantage over unalloyed columbium. Today Cb-nominal 1% Zr is of prime importance as a refractory metal structural material.

Extensive physical metallurgical studies on Cb-1% Zr have been undertaken by Stewart, Lieberman, and Rowe,[6] Gregory and Rowe,[7,8] Hobson[9, 10] and Chang.[11, 12] It is

beyond the scope of this paper to review in detail the excellent analysis of the recovery and recrystallization mechanisms of this alloy by Stewart et al nor to detail the comprehensive discussion of the mechanisms of creep as advanced by Gregory and Rowe. Only contributions to the subject of solution annealing and aging will be reviewed.

The phase diagram for Cb-Zr[13] is shown in Figure 1.

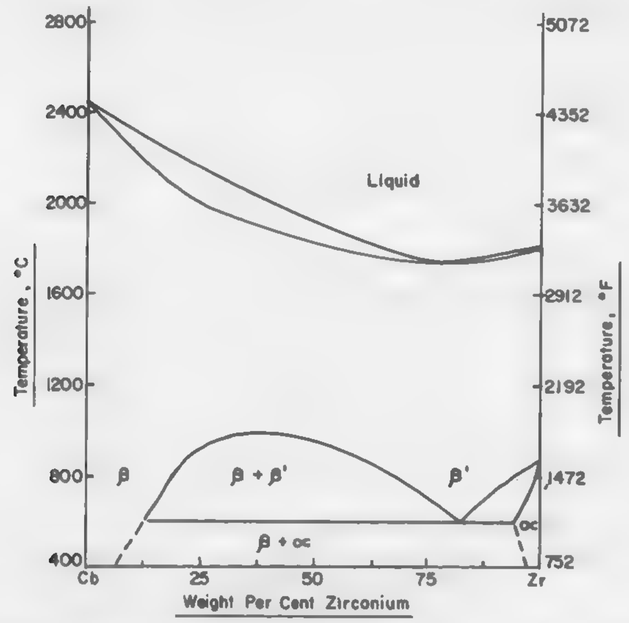


FIGURE 1 COLUMBIUM-ZIRCONIUM DIAGRAM (ROGERS AND ATKINS)

Above approximately 2000°F a continuous series of solid solutions exists. At the monotectoid temperature of 1130°F (610°C), there is equilibrium between the two immiscible solids of 82.8% (the monotectoid composition) and 13% zirconium, as well as the 93.6% zirconium composition. A β (b.c.c. Cb)/β + α (h.c.p. Zr) transus is postulated starting at 13% Zr and 1130°F and decreasing to lower zirconium contents at lower temperatures; there are no data points. However, the solid state reactions in the high columbium alloys are sluggish and no β' (b.c.c. Zr) nor α have been metallographically detected in alloys with zirconium contents up to 20% which have been slow cooled in vacuum annealing furnaces from temperatures above 2000°F.[14] However, microstructures of Cb-Zr binary alloys to at least

20% zirconium, Figures 2-4, made by several different techniques to insure the highest possible purity show copious quantities of "second" phases. These phases come from solidification as well as aging during processing anneals, and are broken-up and redistributed in fabrication.

Other investigations of the Cb-Zr binary system have indicated that several portions of Figure 1 might be in error. Temperatures both substantially higher and lower than 1130°F have been proposed as the monotectoid temperature and some experimental data[15] indicate a continuous series of solid solutions exists only above 2150°F. An intermediate phase between 20 and 40% zirconium has been suggested although experimental proof for this has not been advanced. With recent discoveries of superconductivity in high magnetic fields at high current densities in columbium-zirconium alloys with 25-50% zirconium[16, 17] and, as noted later, the large interaction of interstitials with columbium-rich Cb-Zr alloys, the need for a systematic metallographic investigation under proper experimental conditions seems warranted.

Stewart and co-workers[6] have shown that heating as-cast Cb-1% Zr to 3200°F (1760°C) followed by a rapid cool, resulted in virtual disappearance of the precipitate which was present in the as-cast structure as a relatively uniform precipitate, Figure 5. Electron microscopy, however, revealed an extremely fine phase which formed on cooling. Reheating to 1500°F (816°C) resulted in further precipitation, now readily visible with optical microscopy. Aging material up to 30 hours at 1700°C (927°C) after rapid cooling from 3200°F resulted in a marked increase in hardness; longer aging times resulted in a lowering of hardness indicative of overaging. Other studies indicated that one hour at 2200°F (1200°C) after an anneal at 3200°F resulted in a "maximum" amount of precipitate which was in an overaged condition. The ingot used for these investigations contained oxygen less than 100 ppm, nitrogen less than 125 ppm, carbon less than 175 ppm, and zirconium about 0.815% (8150 ppm).

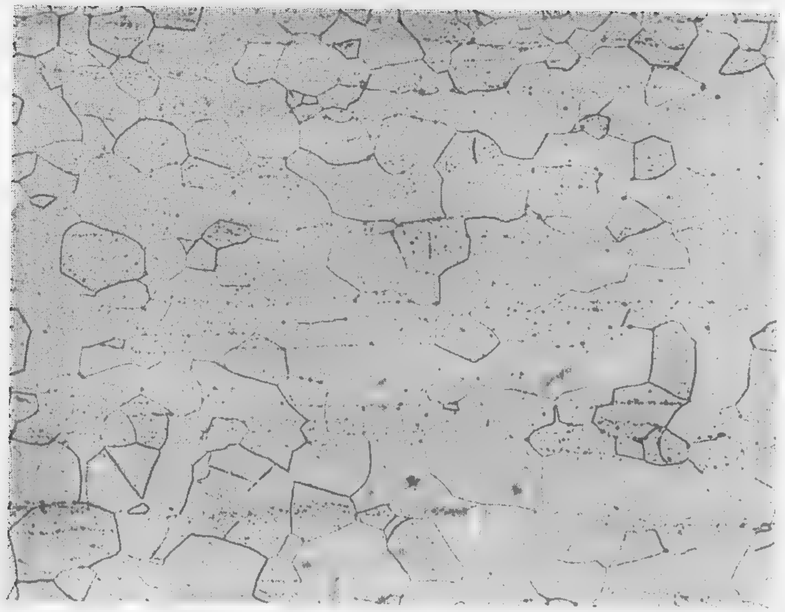


FIGURE 2 Cb-1 1/2% Zr ALLOY ANNEALED 14 HOURS AT 2550°F (1400°C) 250 X (GEMMELL)

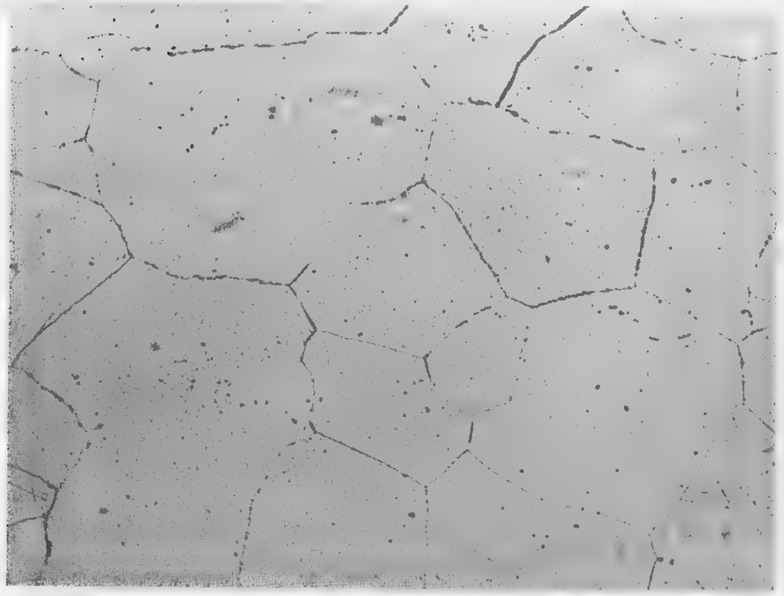


FIGURE 3 Cb-7% Zr ALLOY ANNEALED 14 HOURS AT 2550°F 250 X (GEMMELL)

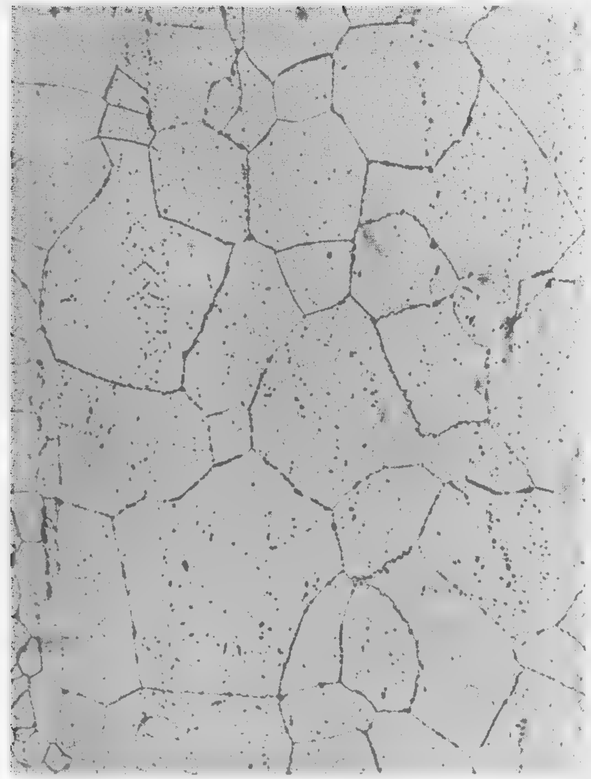


FIGURE 4 Cb-10% Zr ALLOY ANNEALED 14 HOURS AT 2550°F 250 X (GEMMELL)

Hobson[9, 10] has extended the studies of Stewart, Lieberman, and Rowe and has made a signficant contribution to the aging phenomena in columbium-base alloys. Columbium-nominal 1% zirconium alloys with a fairly wide range of interstitials (oxygen from 24 to 1200 ppm) were aged for times up to 500 hours at temperatures 1500°F and 1700°F after vacuum anneals at 2200°F (1200°C), 2550°F (1400°C), 2910°F (1600°C), 3270°F (1800°C), and 3630°F (2000°C). Figure 6 shows typical aging results as obtained with an ingot analyzing 1.07% zirconium, 145 ppm oxygen, 160 ppm nitrogen and 210 ppm carbon. For specimens which were aged following a 2910°F anneal, maximum strength occurred after 75 hours; further aging resulted in decreased strength indicating overaging, although in the overaged condition the tensile strength was still 28% above the as-annealed value. Aging resulted in a decrease in ductility: 9% elongation in a 2-in.-gauge length for as-annealed condition vs. 6% for maximum strength condition vs. 4.5% for the overaged condition.

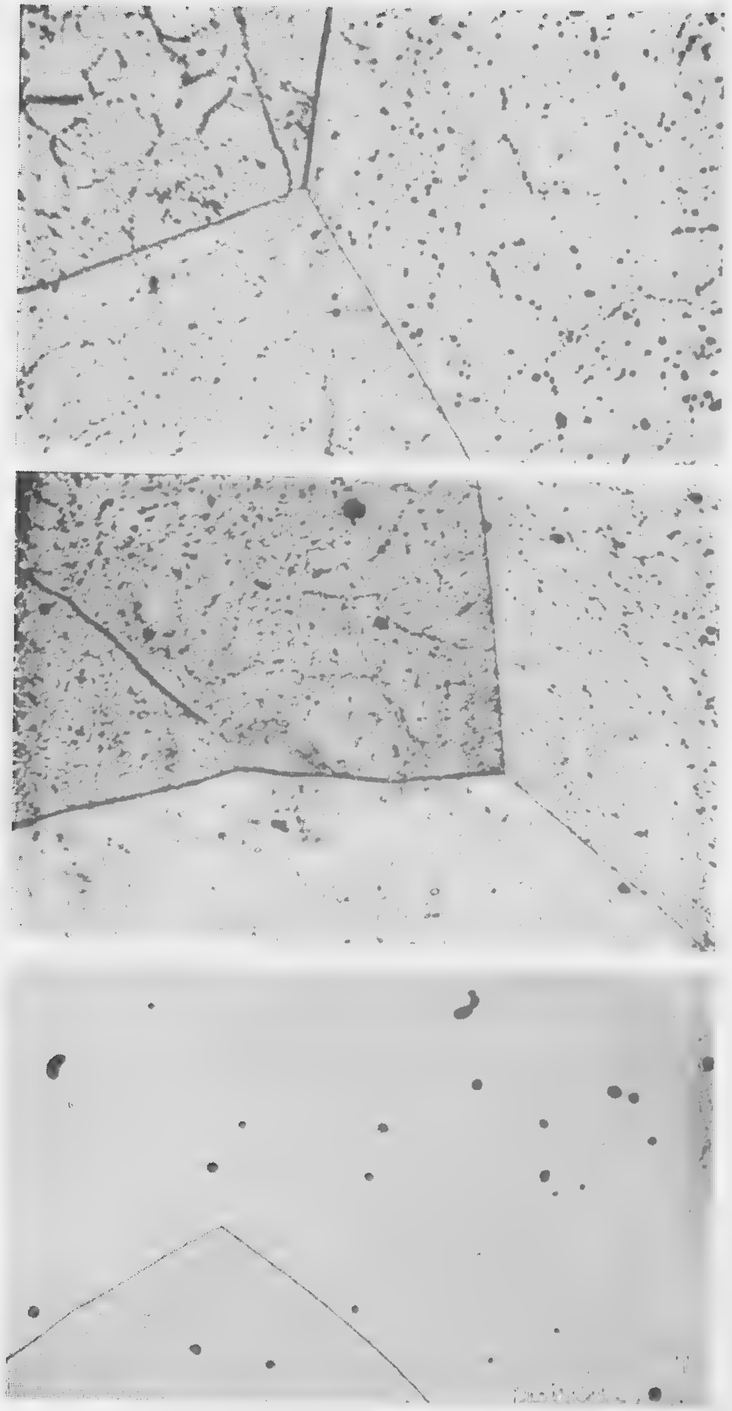


FIGURE 5 STRUCTURE OF Cb-1% Zr INGOT. TOP - AS-CAST. MIDDLE - ANNEALED 1 HOUR AT 2200°F (1200°C) BOTTOM - ANNEALED 1 HOUR AT 3200°F (1760°C) 12X (STEWART, LIEBERMAN AND ROWE)

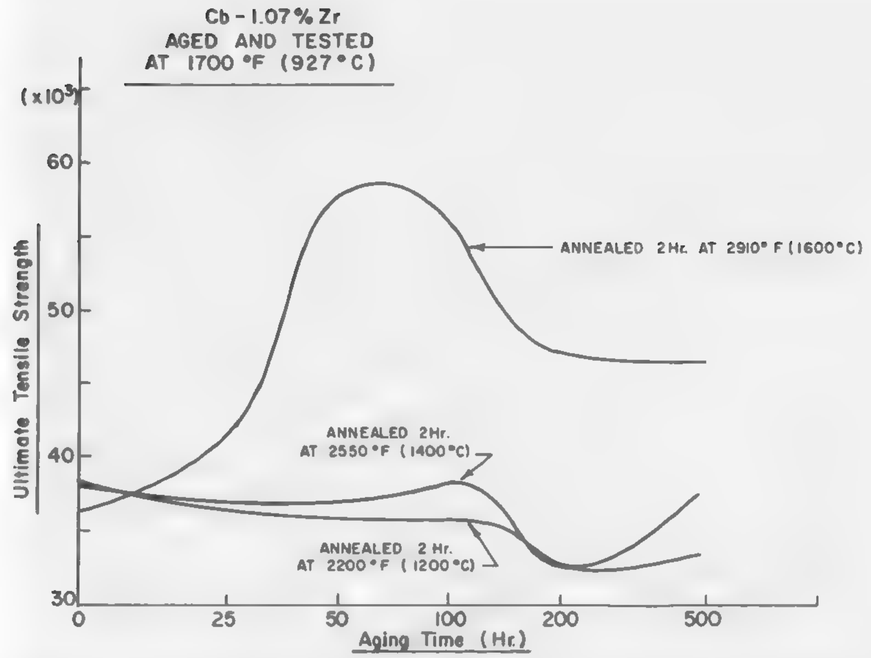


FIGURE 6 TENSILE RESULTS OF Cb-1.07% Zr (145 ppm OXYGEN, 160 ppm NITROGEN, AND 210 ppm CARBON) ALLOY ANNEALED 2 HOURS AT 2200, 2550 AND 2900°F; AGED THROUGH 500 HOURS AT 1700°F. (HOBSON)

Some grain-boundary phase was present after 50 hours of aging. After 100 hours, corresponding to the peak of the aging curve, some matrix precipitate was present. As the alloy overaged, as shown in 200- and 500- hour aged specimens, more of the phase was precipitated in the matrix. Some depletion of the phase occurred in areas adjacent to the grain boundaries which in turn showed an almost continuous phase.[9] It is possible that electron microscopic examination would show much finer precipitation particles after aging times less than 50 hours and also after the annealing heat treatment.

Hobson, examining whether the Cb-nominal 1% Zr alloys aged or did not age following a 2910°F anneal, noted that if the oxygen content was higher than approximately 300 ppm, there was no reaction as indicated by strength when the alloy subsequently "aged". Heats of Cb-.86% Zr specially alloyed with various oxygen contents ranging from 470-1200 ppm showed no aging reaction at 1700°F after anneals at 2910°F. However, those specimens with

oxygen contents of 700 ppm or less showed an aging response if annealed at 3270°F.

Summarizing his results, Hobson clearly pointed out, Figure 7, the role of oxygen in the aging of Cb-1% Zr alloys

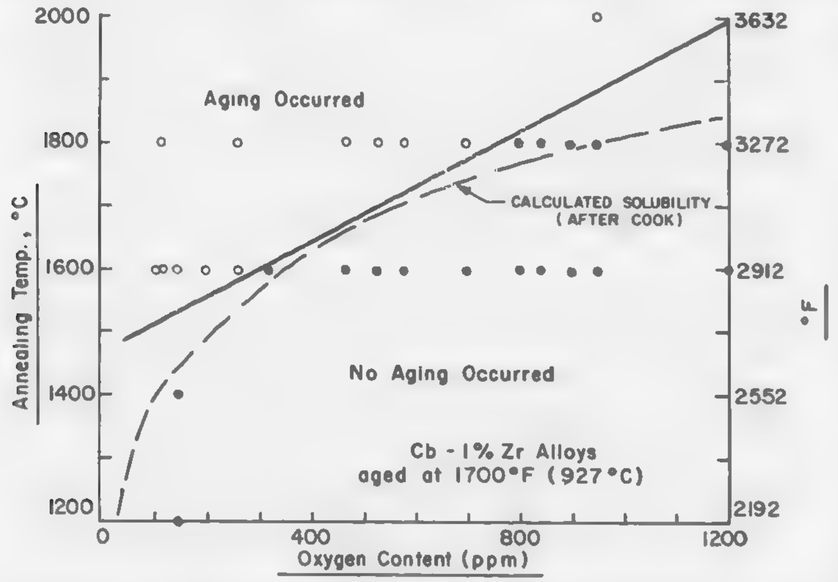


FIGURE 7 SUMMARY OF THE EFFECT OF ANNEALING TEMPERATURE VS. OXYGEN CONTENT OF Cb-NOMINAL 1% ZIRCONIUM ALLOYS. (HOBSON)

with respect to the effect of annealing temperature. Drawing a line between the regions of "ageability" and "nonageability", Hobson has indicated that this line is related to the solvus line between the single phase β (Cb-Zr-O)* and the two-phase region, β + precipitate.

Hobson[10] has proposed a 2900°F Cb-Zr-O ternary diagram, Figure 8, which illustrates the very marked decrease in oxygen solubility with very small zirconium additions. The solubility of oxygen at 2900°F for columbium is approximately 6500 ppm[18] while for Cb-1% Zr, Figure 9, the solubility is less than 200 ppm. A calculation of the

*To conform with Figure 1, β is used throughout this manuscript to signify the columbium-rich solid solution.

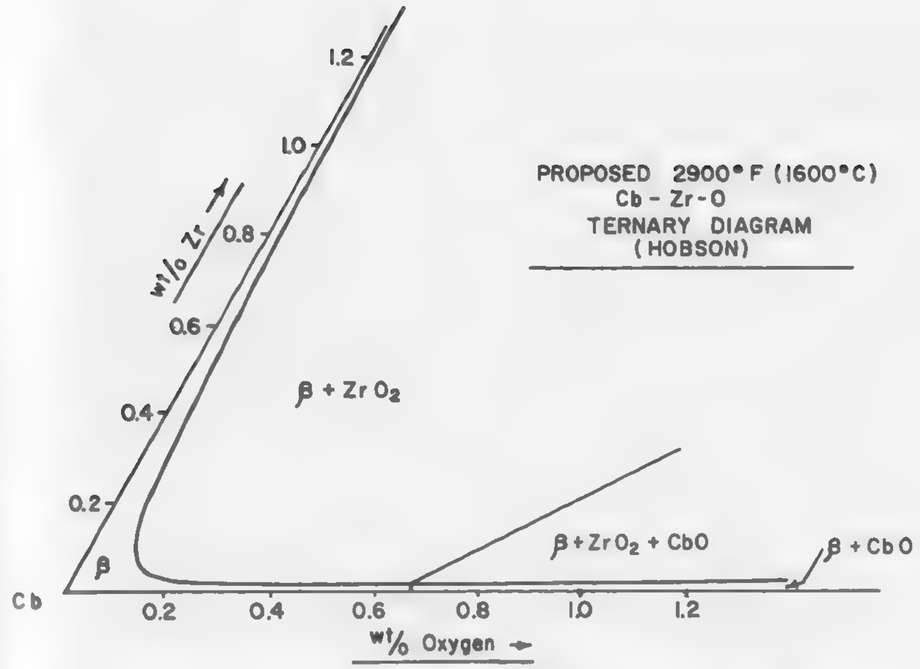


FIGURE 8 PROPOSED 2900°F Cb-Zr-O TERNARY SECTION. (HOBSON)

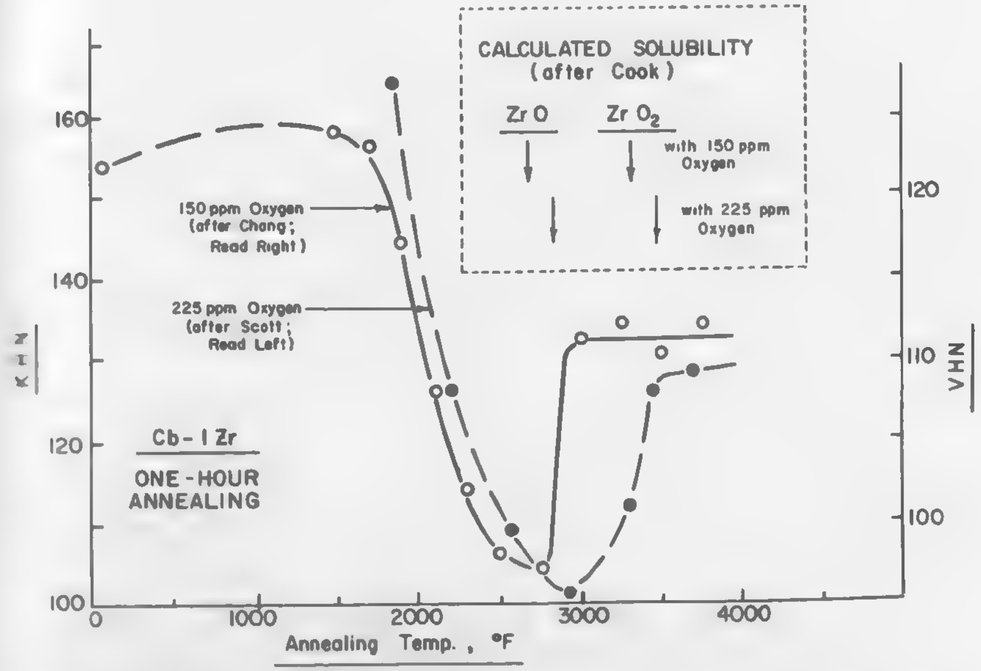


FIGURE 9 EFFECT OF ANNEALING ON ROOM TEMPERATURE HARDNESS OF Cb-1% Zr ALLOYS (CHANG AND SCOTT)

ZrO_2 solvus line at 2900°F by Cook[19] indicates 50 ppm and this lower solubility appears to be in line with recent experimental data.

Chang[11] has studied the influence of heat treatment on microstructure and properties of Cb-1% Zr alloy containing 150 ppm oxygen, 100 ppm nitrogen and 50 ppm carbon. Annealing this alloy for 1 hour at 1500-4000°F, Figure 9, resulted in a decrease in room temperature hardness up to 2750°F, increased strength from 2750-3000°F and constant hardness from 3000-4000°F. The hardening at temperatures greater than 3000°F is due to solution of "second" phases. Scott[20] has done a similar experiment with Cb-1Zr containing a greater amount of oxygen (225 ppm) and 50 ppm each nitrogen and carbon. Increasing the oxygen content increased the temperature at which there is a sudden rise in hardness, Figure 9.

Chang has aged Cb-1% Zr after solution anneals above 3000°F for temperatures up to 2600°F. Aging below 2000°F for one hour caused little change in hardness and little effect on microstructure, either in matrix or along grain boundaries. Long aging times, 12 hours, at 1750°F resulted in softening and enhanced grain boundary precipitation. Softening occurred on aging for one hour in the temperature range of 2000-2590°F: increasing aging temperature gave lower room temperature hardness. With higher oxygen (225 ppm), minimum hardness does not occur until 2800-3000°F.[20] Chang has pointed out that age softening is due to grain boundary precipitation which depletes the matrix of solution strengthening without benefit of dispersion hardening associated with general precipitation.

McNutt and Gemmell[21] have extensively studied the metallography of Cb-Zr binary alloys up to 20% zirconium and oxygen contents up to 600 ppm and have shown that alloys with this range of compositions have "second" phases in their as-cast structures which can be taken into solution and re-precipitated. The general phenomena exhibited by Cb-1% Zr alloy carries over to zirconium containing columbium alloys up to, at least, 20% zirconium.

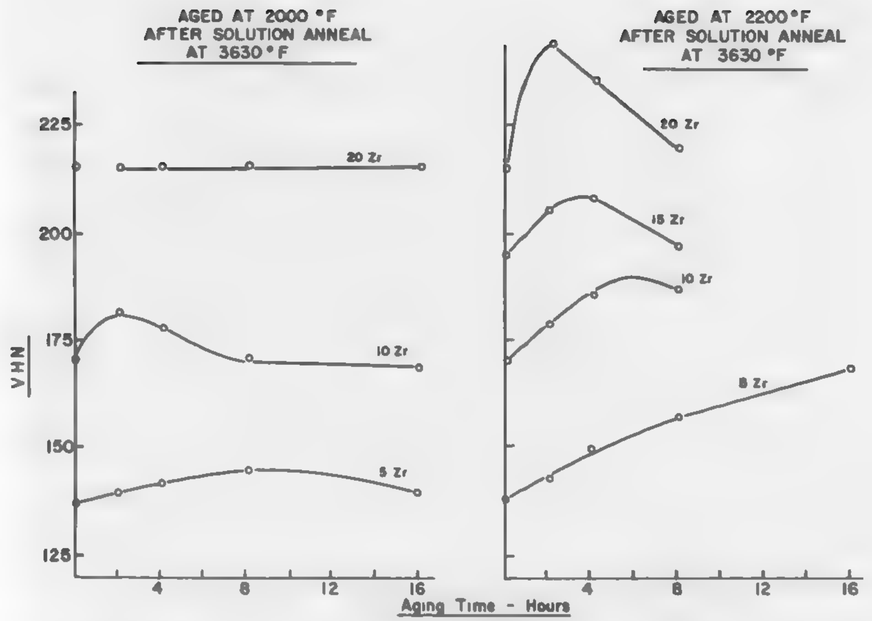


FIGURE 10 EFFECT OF AGING AT 2000 AND 2200°F, AFTER ANNEALING AT 3630°F, ON ROOM TEMPERATURE HARDNESS OF Cb-Zr ALLOYS. (McNUTT AND GEMMELL)

The room temperature hardness of columbium alloys with 5, 10, 15, and 20% zirconium after anneals at 3620°F and aging treatments at 2000 and 2200°F is shown in Figure 10. These data indicate that:

1. Increasing zirconium content in the columbium-zirconium binary system increased the overall hardness (strength).

2. Increasing the zirconium content decreases the time for maximum hardness resulting from aging at both 2000 and 2200°F.

3. Increasing the temperature of aging from 2000-2200°F after solution anneal at 3630°F, increases the time required to obtain maximum hardness.

McNutt and Gemmell have shown that in Cb-Zr alloys with zirconium contents greater than 1-1/2% overaging occurs by discontinuous or cellular precipitation. This means that during aging at low temperatures the coherency

stresses associated with small particles of the second phase are sufficient to cause recrystallization of the matrix leading to formation of new matrix grains. Cellular precipitation is an integral part of the generalized sequence of microstructures expected as a result of precipitation during aging and has been observed in many different age hardenable alloy systems. Geisler[22] has pointed out that in some alloy systems the grain boundary reaction does not begin until after the precipitation process is complete; in others, it starts before the general precipitate is optically resolvable and before the composition of the solid solution has changed much. In the Cb-Zr system cellular precipitation is seen after matrix precipitate has been observed. Increasing zirconium content increases the tendency for cellular precipitation. Figures 11 and 12 show Cb-10% Zr solution annealed at 3630°F and aged for

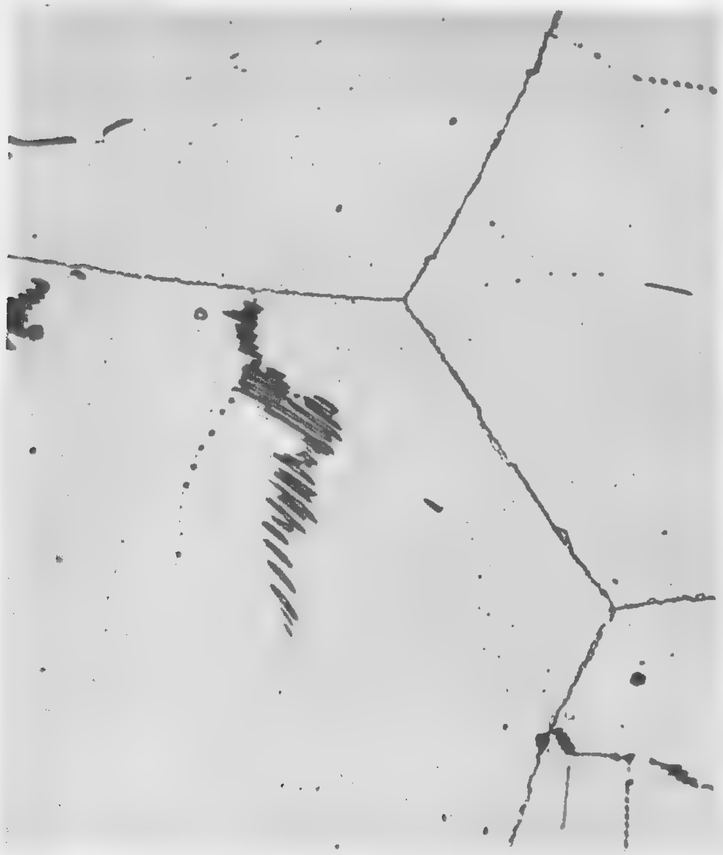


FIGURE 11 Cb-10% Zr ALLOY. SOLUTION TREATED 4 HOURS AT 3630°F AND AGED 4 HOURS AT 2000°F. 650 X. (McNUTT AND GEMMELL)

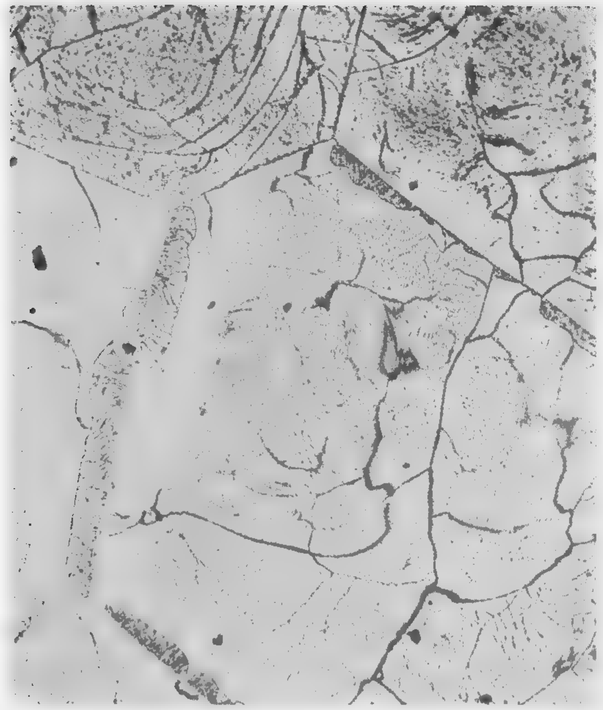


FIGURE 12 Cb-10% Zr ALLOY. SOLUTION TREATED 4 HOURS AT 3630°F AND AGED 16 HOURS AT 2000°F. 650 X (McNUTT AND GEMMELL)

4 and 16 hours at 2000°F. With 20% Zr, cellular precipitation occurs after 4 hours at 2000°F, Figure 13. Cellular precipitation can occur in Cb-5% Zr, Figure 14. From the studies of Hobson, it may be inferred that no cellular precipitation has been observed after aging times up to 500 hours in Cb-1% Zr although extensive grain boundary precipitation is observed. Probably an important factor contributing to dependence of overaging on zirconium content greater than 1% is that the recrystallization temperature for columbium-zirconium alloys,[1, 3, 20] reaches a maximum at about 3% zirconium and beyond this percentage the recrystallization temperature decreases with increasing zirconium.

Overaging begins first in regions where precipitation begins first; these regions are grain boundaries, subgrain boundaries, and regions of high zirconium content, residual from casting and not entirely removed by subsequent processing. As aging proceeds, a colony of recrystallized



FIGURE 13 Cb-20% Zr ALLOY. SOLUTION TREATED 2 HOURS AT 3630°F AND AGED 4 HOURS AT 2000°F. 1,125 X. (McNUTT AND GEMMELL)

alloy initiated at a grain boundary subsequently grows both along the boundary and into the grain. Turnbull[23] states that general precipitation of a coherent structure often precedes and sometimes precludes the cellular reaction; but that, once nucleated, the cells containing incoherent precipitation grow at the expense of the generally distributed coherent precipitate particles. The relative rates of cellular nucleation and subsequent growth of these regions vary with temperature so that at low aging temperatures (2000°F) grain boundaries may be covered by recrystallized cells while only a few volume per cent of the alloy as a whole has overaged; on the other hand, at higher aging temperatures (say 2200°F) the overaged colonies grow more rapidly into grain interiors while fewer new colonies are nucleated at grain boundaries.[21] Thus, a given volume per cent of recrystallized material can be formed for various times at a number of temperatures; at lower



FIGURE 14 Cb-5% Zr ALLOY. SOLUTION TREATED 2 HOURS AT 3630°F AND AGED 100 HOURS AT 2000°F. 1500 X. (McNUTT AND GEMMELL)

temperatures this volume per cent will be concentrated at grain boundaries, but at high temperatures grain interiors will be consumed by the overaging cells relatively fast.[21] The volume per cent of overaged structure increases regularly with time at a given aging temperature. The kinetics of the aging process are dependent on the zirconium content and the general features of this classical process are illustrated in Figures 11-14. Since the recrystallized, overaged lamellar zones contain incoherent precipitate, these cells are always appreciably softer than the volumes which have not yet overaged. Further, it should be pointed out that it is not necessary to give a special solution treatment in order for overaging to occur by cellular precipitation; samples cast, worked and aged without a special solution or annealing treatment show overaging by this mechanism after appropriate aging times.[21]

Increasing oxygen content increases the tendency for cellular precipitation in the 10 and 20 weight per cent

zirconium containing columbium binary alloys. High oxygen containing alloys have been prepared by careful additions of ZrO_2 and Cb_2O_5 to the melt. Also, contamination by oxygen from heat treating atmospheres shows a soft case whose microstructure is identical to the lamellar products of overaging.[21]

Extremely fine, well oriented, coherent precipitation can be obtained in Cb-Zr alloys. One example of this, Figure 15, is a Cb-10 Zr alloy containing approximately 370 ppm oxygen and less than 70 ppm each of carbon and nitrogen which was annealed at 3630°F and aged 4 hours at 2200°F. McNutt[14, 21] has identified this coherent precipitate using extraction replica techniques and electron diffraction as "ZrO" (cubic rock-salt type compound). Interestingly, ZrO does not exist in the simple zirconium-oxygen binary system, but has been reported in other alloy studies.[24] Columbium conceivably stabilizes a ZrO lattice with some Cb substituted for Zr in the structure. The coherent

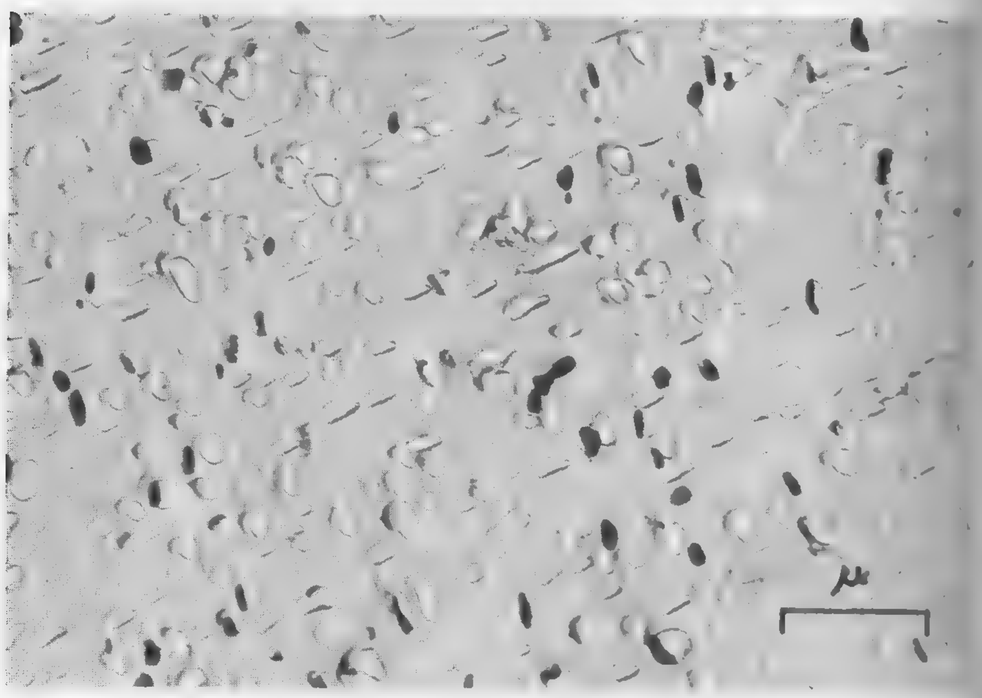


FIGURE 15 Cb-10% Zr ALLOY. SOLUTION TREATED 2 HOURS AT 3630°F AND AGED 4 HOURS AT 2200°F. 20,000 X. (McNUTT AND GEMMELL)

precipitate is no doubt quite complex with respect to its exact chemistry as some nitrogen and carbon are probably substituted for oxygen at interstitial sites. Reference to the phase as "ZrO" is therefore an over-simplification.

The incoherent precipitate in the cellular zones, as well as the coarse precipitate optically observed after aging and also incomplete solution annealing heat treatments, has been identified by McNutt and Gemmell as ZrO_2. The crystallographic phase most frequently observed for ZrO_2 is monoclinic although other modifications of ZrO_2 have tentatively also been identified. Stewart et al[6] and Begley et al[25] have also identified ZrO_2 in Cb-Zr alloys. McNutt has therefore concluded that "ZrO" is an intermediate phase and the precipitation process is:

$$(Cb\text{-}Zr\text{-}O) \longrightarrow \text{"ZrO"} \longrightarrow ZrO_2$$

"ZrO" is metastable and with increasing aging times at appropriate temperatures coarse, massive ZrO_2 will be found: in columbium alloys with greater than 5% zirconium, coherent ZrO_2 has not been observed.

C. M. Cook, Jr.[19] has recently carried out an interesting thermodynamic analysis of the phase relationships in the Cb-Zr-O system and has been able to predict the solubility of both ZrO and ZrO_2. Viewing the formation and dissolution of these phases as physico-chemical reactions, he has shown that the solubility of ZrO_2 would be lower than that of ZrO at all temperatures. Thus coherent "ZrO" phase, characteristic of precipitation hardened zirconium-containing alloys, is metastable at all temperatures. The calculated ZrO solubility has been drawn in Figure 7 which summarizes the data of Hobson concerning the regions of "age hardenability" and "nonage hardenability" for Cb-1% Zr alloys as a function of oxygen content and annealing temperature. The calculated ZrO solubility curve agrees very well with the line drawn to separate the two regions, and which was suggested by Hobson to be similar to a solvus line. Cook has pointed out that the line separating the two fields must slope downward as the oxygen content decreases to zero per cent, similar to the predicted solubility curve. The

"age/nonage" line of Hobson is therefore apparently related to the ZrO solvus. According to Cook, the predicted ZrO_2 solvus would be considerably above the ZrO solvus.

The calculated ZrO and ZrO_2 solubilities[19] for Cb-1% Zr alloys containing 150 and 225 ppm oxygen have been indicated in Figure 9 which shows annealed hardness data of Chang[12] and Scott.[29] The theoretical solubilities agree well with the experimental data confirming that the hardness plateau beyond 3000°F for the alloy containing 100 ppm oxygen is due to solution of the "second" phases: ZrO would be dissolved and beyond approximately 3270°F, any ZrO_2 present would also be dissolved. As would be expected, increasing zirconium content increases the temperature for the solubility of both ZrO and ZrO_2.

There is good agreement between Cook's analysis and the experimental observations of McNutt and Gemmell, e.g., Nb-12% Zr containing ca. 400 ppm oxygen retains considerable quantities of zirconium oxide when annealed for long times at 3270°F because this temperature is below the solvus. Good agreement also exists with the Cook analysis and the studies of Gregory and Rowe.[8] The calculated solution temperature of ZrO_2 for Cb-1% Zr with 125 ppm oxygen is above 3250°F which agrees with their experimental observations.

Cb-Zr-C System

Few details have been reported concerning the Cb-Zr-C system. Most studies have dealt with high strength alloys which also contain molybdenum and/or tungsten.[12, 26] Hiltz and Laverty[27] studied Cb-0.13 w/o C alloys with various zirconium contents ranging from zirconium-to-carbon atomic ratios of 1:1 to 5:1. Examination of the as-cast structures showed massive carbide precipitation, in most cases with Widmanstatten plate-like morphology, Figure 16. Heat treatment at 2950°F (1620°C) indicated that the solvus temperature was not crossed but annealing at 3200°F (1760°C) was high enough to be in the single phase region. On cooling from 3200°F, a significant amount of

carbide came out as Widmanstatten plates, Figure 17. For the particular cooling rate employed by Hiltz and Laverty, some aging also occurred on cooling and a fine precipitation was also noted. Aging the solution treated alloys for 7 to 10 hours at 2000°F resulted in a large amount of carbide precipitation. Extractive techniques on the Cb-1Zr-0.13C alloy were used by Hiltz and Laverty to identify the precipitate as ZrC or ZrC·CbC.

In the columbium-carbon system, β-Cb is in equilibrium with the hexagonal subcarbide Cb_2C. The addition of zirconium apparently stabilizes the rock-salt type ZrC lattice. The solubility of carbon in columbium is low (about 500 ppm at 2900°F[28]) and there is not sufficient data to indicate whether additions of zirconium appreciably lower the carbon solubility further. Although the ZrC solvus line in Cb-Zr-C alloys has not been determined, it appears to be similar to that for "ZrO". Here, however, the similarity with the Cb-Zr-O system ends. There are no microscopically metastable intermediate phases and ZrC transforms to no other zirconium carbide structure on aging. No cellular precipitation has been found in overaged structures of Cb-Zr alloys containing up to 5% Zr; overaging appears to be due to normal growth and agglomeration of ZrC particles. Cooling at rates normally obtained in cold-wall vacuum furnaces from temperatures above the carbide solvus, results in some large Widmanstatten ZrC plates; although this might be due to the relatively large percentage of carbon (500-1300 ppm) purposely added to, say, Cb-1% Zr, the same amount of oxygen added to Cb-1% Zr does not result in a Widmanstatten oxide precipitate on cooling from solution annealing temperatures.

The profile of room temperature hardness after one hour annealing at elevated temperatures of Cb-1% Zr with nominal 500 and 1000 ppm carbon, Figure 18,[29] is similar to that obtained with Cb-1% Zr containing low carbon (Figure 9) but accountable by the physical metallurgical behavior of ZrC (or ZrC·CbC). The hardening upon annealing above 3000°F is due to solution strengthening even though microstructures show massive precipitation, Figure 19.

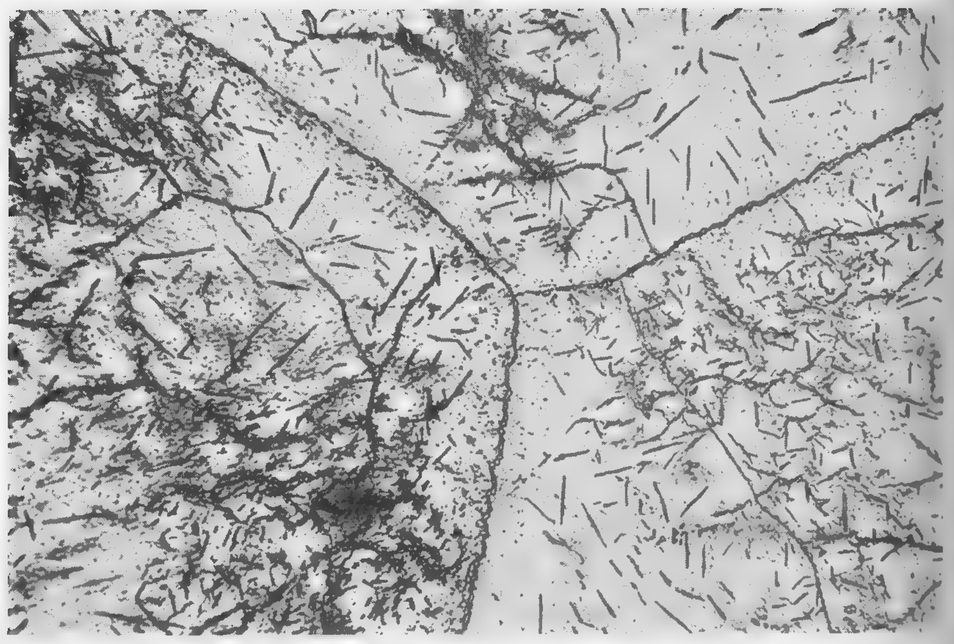


FIGURE 16 Cb-2 1/2% Zr-0.1% CARBON ALLOY. AS-CAST. 500X (HILTZ AND LAVERTY)

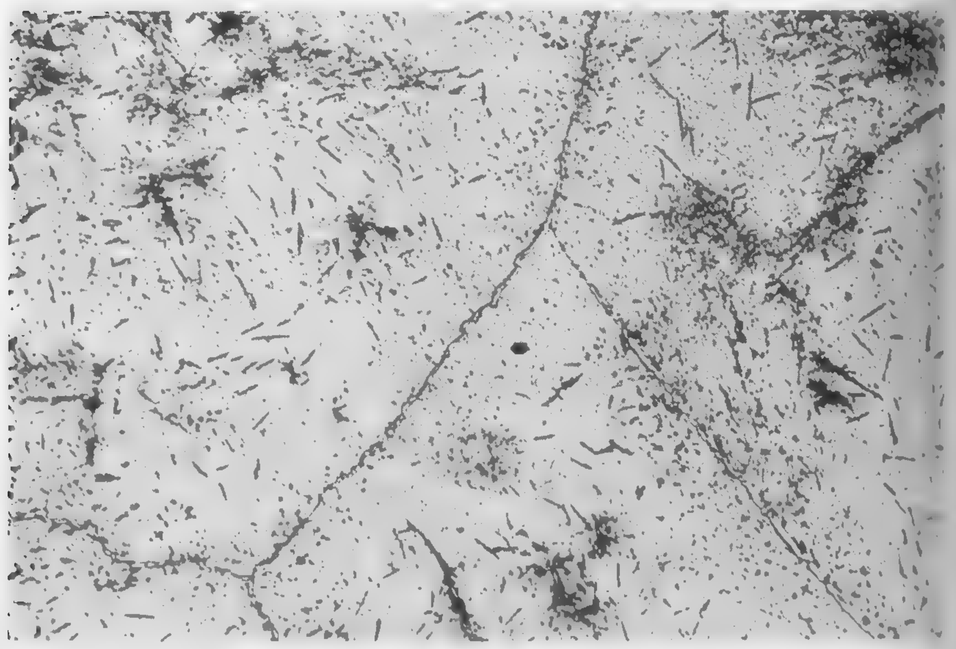


FIGURE 17 Cb-2 1/2% Zr-0.1% CARBON ALLOY. ANNEALED 1 HOUR AT 3200°F. 500X (HILTZ AND LAVERTY)

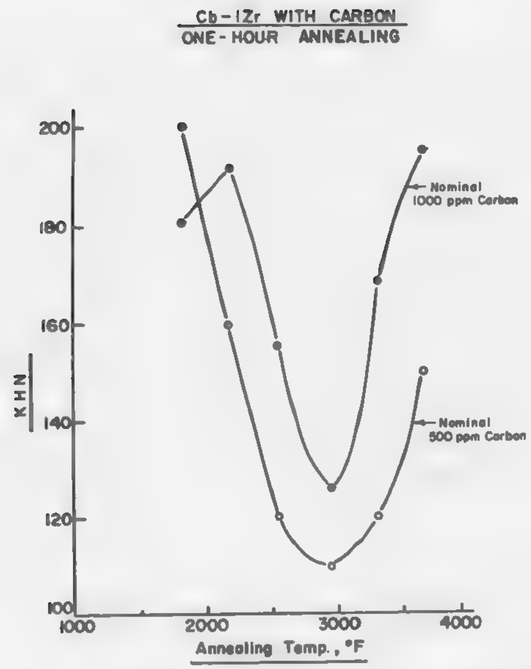


FIGURE 18 EFFECT OF ANNEALING ON ROOM TEMPERATURE HARDNESS OF Cb-1% Zr-0.1% CARBON ALLOY. (SCOTT)



FIGURE 19 Cb-1% Zr-0.05% CARBON ALLOY. ANNEALED 1 HOUR AT 3270°F. 500X. (SCOTT)

Clark[26] has studied the importance of the zirconium-to-carbon atomic ratio in columbium-tungsten alloys with up to 20 weight per cent tungsten. Using extraction techniques, he has examined the residue from Cb-20W-0.9 Zr alloys containing carbon contents up to 3000 ppm and has shown that the "relative abundance" of the phases ZrO_2, ZrC·CbC and also Cb_2C changes with the amount of carbon in the alloy. At 50 ppm carbon, ZrO_2 is the main phase found in the Cb-20W-0.9 Zr alloy containing 600 ppm oxygen. As carbon is added, deoxidation of the alloy system occurs and less ZrO_2 is found: at Zr/C=1 atomic ratio (1200 ppm carbon) ca. 300 ppm oxygen was present and at 2000 ppm carbon the alloy contained 200 ppm oxygen and no ZrO_2 was found. In addition to the oxide, a complex ZrC·CbC phase is formed and the amount of this phase increases with increasing carbon up to approximately the Zr/C atomic ratio of 1. Beyond this, the "relative abundance" of ZrC·CbC decreases. Clark also reports that the subcarbide, Cb_2C, is also present at carbon concentrations as low as 500 ppm and the amount of this phase increases with increasing carbon content. There is also a difference in the size of the precipitates as a function of carbon content, and a marked dependence of mechanical properties on the Zr/C atomic ratio.

Chang[12] has studied the influence of heat treatment on microstructure and properties of Cb-5Mo-15W-1Zr-carbon and Cb-5Ti-5Mo-15W-1Zr-carbon alloys. Both of these alloys respond to solution annealing and aging in a classical manner. Chang has identified the various phases formed at different annealing temperatures for these alloys, pointing out the complexity of these systems. The monocarbide phase in these alloys contains a significant amount of the metallic elements constituting the matrix, e.g., Cb, Mo and W as well as Zr.[30] The mono-oxide and the mono-nitride of zirconium have similar (rock salt type) crystal structures and high mutual solubility, and it also would be expected that the extractions from complex type alloy systems of commercial purity levels should also contain a significant amount of oxygen and nitrogen. Since the important elements in these alloys for dispersion strengthening are zirconium and carbon, reference to it as simply "ZrC" or "ZrC·CbC" seems therefore justified.

Cb-Hf SYSTEMS

Some investigations in the Cb-Hf-O system have been carried out by Begley et al[31] and in the Cb-Hf-C system by both Hiltz and Laverty[27] and Begley et al.[25] Although much less work has been performed, especially with respect to kinetic studies, these systems appear to be very similar to those with zirconium. HfO_2 has been identified in Cb-5% Hf, 670 ppm oxygen alloy[25] and HfC (or HfC·NbC) has been identified in Cb-Hf-carbon alloys with Hf/C atomic ratios from 1 to 5.[27] An important consideration in Cb-Hf studies is the atomic weight of hafnium as compared to zirconium: Cb-5 weight per cent Hf is ca. Cb-2-1/2 atomic per cent Hf.

CONCLUSIONS AND RECOMMENDATIONS

Most of the columbium base alloys commercially available today in mill product form, e.g.,

Cb-1Zr
Cb-33Ta-1Zr (Fansteel FS-82, DuPont D-32)
Cb-5Zr (DuPont D-14)
Cb-10Ti-5Zr (DuPont D-36)
Cb-10Hf-1Ti (Wah Chang C-103)
Cb-5Mo-15W-1Zr-Carbon (G.E. F-48, DuPont D-40, Wah Chang C-120)

make use of dispersion hardening obtained with zirconium (or hafnium) and oxygen or zirconium and carbon as an important part of their high temperature strengthening mechanisms. Almost all of the alloys currently in advanced stages of development, e.g.,

Cb-10W-1Zr-0.1C (DuPont)
Cb-4Zr-10W (DuPont D-35, Haynes Cb-752)
Cb-20W-1Zr-0.1C (G.E. AS-30)
Cb-27Ta-12W-0.5Zr (Fansteel 85)
Cb-5V-10W-1Zr (Westinghouse B77)

employ zirconium interstitial interactions to supplement the solution strengthening obtained with tungsten, for this latter form of strengthening is not sufficient to give desired mechanical properties. More studies need to be done before a firm understanding of the physical metallurgy of these systems is obtained. New studies along these lines will, however, not be easy. A criticism against all of the previous investigations is, because of equipment limitations, that the cooling rates were not fast enough from the solution annealing temperature to suppress precipitation. Precipitation is usually seen in alloy systems forming zirconium oxides, and Widmanstatten plates occur in alloy systems forming zirconium carbide.

Extraction techniques need improvement. The two techniques used, bromine-methanol and electrolytic, do not always give "clean" separations. To identify the various metallic elements in the complex phases, the electron probe seems necessary: this tool has been very helpful in carbide chemistry identification.[30] Transmission electron microscopy of thin films of Cb-1Zr is currently under investigation[8] and should be extended to higher zirconium containing columbium alloys as well as systems forming carbides.

Enrietto et al[32] have shown that annealing columbium rod, which originally contained 300 ppm oxygen, for 11 hours at 3800°F in a high vacuum reduced the oxygen content to 5-10 ppm. McNutt[14] has seen different solution treating and aging characteristics in the core and at the edge of Cb-Zr samples attributable to different oxygen concentrations resulting from vacuum high temperature deoxidation. In columbium alloys containing relatively large quantities of carbon, the amount of both the carbon and oxygen can be significantly reduced in very high temperature anneals. Obviously, care must be taken in interpreting physical and mechanical properties when using very high temperature annealing heat treatments.

The full potentialities of columbium-base alloys still remain to be revealed. A better understanding of the applications of the principles of second phase strengthening is needed. As pointed out by Anders,[4] there is no one colum-

bium alloy. But the columbium alloys of the future all will make use of second phase strengthening and the basic principles will be generally applicable.

ACKNOWLEDGMENT

The author wishes to thank D. O. Hobson, J. E. McNutt, C. M. Cook, Jr., A. G. Scott, R. H. Hiltz and D. P. Laverty for allowing review of material in advance of publication. A. S. Nemy and R. W. Heckel read and criticized the manuscript.

BIBLIOGRAPHY

1. Gemmell, G. D., "Some Effects of Alloying on the Strength Properties of Columbium at Elevated Temperatures," Trans. Met. Society AIME, Vol. 215, 1959, p. 898.

2. Gemmell, G. D., "Temperature Dependence of Tensile Properties of Binary Columbium Alloys," paper presented at the AIME Fall Meeting, Detroit, Michigan, October 1961.

3. Begley, R. T., and J. H. Bechtold, "Effect of Alloying on Mechanical Properties of Niobium," J. Less Common Metals, Vol. 3, 1961, p. 1.

4. Anders, F. J., Jr., "Metallurgy of Columbium and Its Alloys," Refractory Metals and Alloys, Interscience, N. Y. 1961, p. 219.

5. Begley, R. T., Development of Niobium-Base Alloys, WADC Technical Report 57-344, Part II, March 1959.

6. Stewart, J. R., W. Lieberman and G. H. Rowe, "Recovery and Recrystallization of Columbium-1% Zirconium Alloy," Columbium Metallurgy, Interscience, N. Y. 1961, p. 407.

7. Gregory, D. P. and G. H. Rowe, "Mechanism of Creep in Columbium and Columbium-1% Zirconium Alloy," Columbium Metallurgy, Interscience, N. Y. 1961, p. 407.

8. Gregory, D. P. and G. H. Rowe, "Solid-State Metallurgical Studies of Pure Columbium and Cb-1Zr Alloy," Report PWAC-359 under Contract AT(11-1)-229, June 30, 1961.

9. Hobson, D. O., "Aging Phenomena in Columbium-Base Alloys," paper presented at the AIME High-Temperature Materials Conference, Cleveland, Ohio, April 1961.

10. Hobson, D. O., Oak Ridge National Laboratory, private communication.

11. Chang, W. H., Study of the Influence of Heat Treatment on Micro-Structure and Properties of Refractory Alloys, Quarterly Report No. 3, 1960 under Contract AF 33(616)-7125, Report DM60-279.

12. Chang, W. H., Study of the Influence of Heat Treatment on Micro-Structure and Properties of Refractory Alloys, Quarterly Report No. 4, 1961 under Contract AF 33(616)-7125, Report DM61-87.

13. Rogers, B. A. and D. F. Atkins, "Zirconium-Columbium Phase Diagrams," Trans. AIME, Vol. 203, 1955, p. 1034.

14. McNutt, J. E., E. I. duPont deNemours & Co., private communication.

15. Domagala, R. F. and D. J. McPherson, "Discussion on 13," Trans. AIME, Vol. 206, 1956, p. 618.

16. Berlincourt, T. G., R. R. Hake and D. H. Leslie, "Superconductivity at High Magnetic Fields and Current Densities in Some Nb-Zr Alloys," Physical Review Letters, 6, 1961, p. 671.

17. Kunsler, J. E., "Superconductivity in Magnetic Fields at High Current Densities," Review of Modern Physics, Vol. 33, 1961, p. 501.

18. Elliott, R. P., "Columbium-Oxygen System," Trans. ASM, Vol. 52, 1960, p. 990.

19. Cook, C. M., Jr., E. I. duPont deNemours & Co., private communication.

20. Scott, A. G., E. I. duPont deNemours & Co., private communication.

21. McNutt, J. E. and G. D. Gemmell, "Precipitation-Hardening in Columbium Alloys," paper presented at AIME Fall Meeting, Detroit, Michigan, October 1961.

22. Geisler, A. H., "Precipitations from Solid Solutions of Metals," Phase Transformations in Solids, Wiley, N. Y., 1951, p. 387.

23. Turnbull, D., "Theory of Cellular Precipitation," Acta Metallurgica, Vol. 3, January 1955, p. 55.

24. Schonberg, N., "The Structure of the Metallic Quaternary Phase ZrTaNO," Acta Chem. Scand. 8, 1954, p. 627.

25. Begley, R. T., W. N. Platte, Development of Niobium-Base Alloys," WADC Technical Report 57-344, Part IV, May 1960.

26. Clark, J. W., "The Effect of Interstitials on the Properties of Cb-rich Alloys in the Cb-W-Zr System," paper presented at AIME Fall Meeting, Detroit, Michigan, October 1961.

27. Hiltz, R. H., Jr. and D. P. Laverty, Thompson-Ramo Wooldridge Co., private communications.

28. Elliott, R. P., "Columbium-Carbon System," Trans. ASM, Vol. 53, 1961, p. 13.

29. Scott, A. G. and W. I. Pollock, "Mechanical Properties of Cb-Zr-W and Cb-Zr-Mo Alloys," paper presented at AIME Fall Meeting, Detroit, Michigan, October 1961.

30. Bartlett, E. S. and F. F. Schmidt, Review of Recent Developments in the Technology of Columbium and Tantalum, DMIC Memorandum 115, Battelle Memorial Institute, July 7, 1961.

31. Begley, R. T., W. N. Platte, A. I. Lewis, R. L. Ammon, Development of Niobium-Base Alloys, WADC Technical Report 57-344, Part V, January 1961.

32. Enrietto, J. F., G. M. Sinclair, and C. A. Wert, "Mechanical Behavior of Columbium Containing Oxygen," Columbium Metallurgy, Interscience, N. Y. 1961, p. 503.

WELDING AND BRAZING OF SPACE AGE MATERIALS

H. C. Emerson
Manager, Manufacturing Engineering
Rohr Corporation
Chula Vista, California

ABSTRACT

A cursory review of the more commonplace joining processes for the space age metals from the viewpoint of the manufacturing engineer. Metallurgical peculiarities of the materials are correlated to equipment and tooling abilities and limitations. Recent facilities, developments and techniques for metal joining by high speed brazing, electron beam and ultrasonic welding are discussed.

INTRODUCTION

The basic materials that will be used in the fabrication of the space age vehicles of the foreseeable future are known to us today. The basic processes for joining these materials have been discussed in many papers and are being worked daily in many of the laboratories throughout the country. Why then do we make this the subject of another paper? Perhaps because we have gained sufficient knowledge about these processes and materials to appreciate the tremendous problems that exist in the transition of our techniques from the laboratory phase to the production line concepts of the metal working industry.

As a major subcontractor to the aero-space industry, we at Rohr are tremendously concerned with the problems of this transition period. This paper therefore is oriented toward the manufacturing engineer's approach to this subject and it is hoped that many of the questions posed will

prove to be sufficiently provocative to stimulate a considerable increase in manufacturing research effort in this area in order to reduce the gap that presently exists between the design engineer's requirements and our industry's manufacturing capabilities.

At this point, we should identify the so-called space age materials and processes with which we, in manufacturing, are presently concerned.

These materials can be roughly listed under three main categories:

1. The exotic or super alloys and reactive metals
2. The refractory metals and their alloys
3. The ceramics and cermets.

Materials such as Hastelloy, A286, Inconel, Rene' 41, titanium and its alloys, zirconium and beryllium, may be considered in the first grouping and are looked upon as the mainstay metals of the aero-space and some related atomic applications of today.

With the exception of beryllium, sufficient manufacturing technology exists today to permit joining these materials under production type environments.

Granted these techniques, as in the case of welding the alpha-beta type of titanium alloys, become somewhat tricky, but nevertheless are possible and are now practiced in many plants including Rohr's.

The second grouping of materials consists of columbium, molybdenum, tantalum, tungsten and their alloys. This group contains those metals which may permit our space vehicles to operate at temperatures above the 2000°F range, but also are the ones causing premature gray to appear on the heads of our manufacturing specialists today.

Inasmuch as the bulk of our operations at Rohr are primarily concerned with the materials covered by the first two groups, this discussion will be limited to these and will not endeavor to enter into the realm of ceramics and cermets.

Having identified the space age metals, perhaps a look at the joining processes is now in order.

Basically the joining processes with which we are presently concerned are as follows: Brazing, fusion, and ultrasonic welding.

Limiting our discussion to the above processes, we shall endeavor to analyze specific peculiarities of each technique and relate these to the idiosyncrasies of the materials being joined in order to determine the compatibility of the metals to the process. Following this, compatibility of the metal process combination to production philosophy will be reviewed in an effort to determine the areas which require further effort on behalf of our manufacturing research technology.

BRAZING

The brazing of precipitation hardening alloys is currently being accomplished on a production basis with little technical difficulty. Brazing temperatures range from 1750°F to 2050°F, depending upon the selection of braze alloy. Silver-lithium alloys are being used in the lower temperature ranges while nickel base alloys are employed for the higher temperature elevations.

Several techniques exist in the matter of heat application. In addition to furnaces, during the last few years radiant quartz lamp heaters, electric blankets and nichrome strip heaters used in conjunction with glasrock braze fixtures have come into use. See Figures 1 and 2.

Impetus for the development of these techniques was furnished first by the metallurgical requirements of the braze cycle and second as an expedient to production economics, the latter consideration being primarily concerned with a reduction of the total braze cycle time and lower cost tooling and facilities investment.



FIGURE 1 CONTROL PANEL FOR A BATTERY OF GLASROCK BRAZING FIXTURES



FIGURE 2 GLASROCK BRAZING FIXTURE IN OPERATION

In this respect, undoubtedly many manufacturers, just as Rohr, are even now developing means of achieving production advantages that would permit more competitive pricing of brazed products.

Refinements in cooling techniques as well as heat source media are being explored and/or incorporated into the production operations of the immediate future.

Facility investigations at Rohr during the past three years, have centered about the development of a cold wall brazing platen capable of reducing the braze cycle to about 50% of that formerly required by standard brazing furnaces.

This equipment (Figure 3) is designed for brazing honeycomb panels up to 2' x 4' and is being used in our Manufacturing Research Lab for experimental purposes. The heat source within the platen can be furnished by means of a graphite cloth blanket or nichrome strip heaters depending upon the braze temperature required. Provisions within the brazing facility permit introduction of any desired type of brazing atmosphere and cooling medium. A vacuum system capable of pump down to 28" Hg is also provided. All necessary electrical control and recording connections are contained within the brazing chamber. An additional innovation includes provisions for pneumatic pressure pad fixturing.

Although details of this system are considered of a proprietary nature by our company, I am at liberty to discuss briefly the sequence of events that take place during the normal braze cycle.

Lay-up of the panel is accomplished within the platen in a manner that provides sandwiching the panel between two graphite blankets or nichrome strip heaters. A pneumatic pressure pad maintains a predetermined positive pressure on the assembly.

The platen is sealed and evacuated to 28" Hg during purge cycle and backfilled with the desired atmosphere. Heat up cycle is started once the desired conditions,



FIGURE 3 LAY-UP OF PANEL IN ROHR DESIGNED BRAZING PLATEN

regarding atmosphere within the platen, have been established. Temperatures are recorded by a Minneapolis Honeywell Multipoint recorder. At the appropriate time, power input is controlled to maintain the desired braze temperature. At the termination of the required time at temperature, power to the heat source is cut-off and the cooling cycle started. Liquid nitrogen manifolded in proximity to the panel accelerates the normally rapid cooling experienced with the braze platen technique.

In this manner, the sub zero cooling cycle may also be performed within the braze platen along with the heat treat required after brazing. A novel gas purification system and purity monitoring device is used in conjunction with the braze platen. This system was first developed and used on a zirconium production welding job at Rohr and will be described later in this discussion. The concept of the braze platen technique is such that panels up to 4' x 6' may be brazed in this type of facility.

At the present time, a production facility is in the final stages of completion and existing backlog on certain Rohr contracts scheduled for this new equipment.

A cursory analysis of this Rohr developed technique is capable of demonstrating its economic advantages and metallurgical potential.

For example, significant response rate to heat application and removal due to the intimate contact of the heat source to the workpiece, portends use of this equipment for the brazing of titanium and other materials wherein short braze temperature cycles are mandatory for high strength joints.

Operating costs are reduced substantially due to restriction of heat input to the workpiece only and not dissipated in massive furnace structures and large areas within the working chamber.

Elimination of the brazing envelope or retort with its attendant costs also carries us another step toward the

production of economically brazed honeycomb products for which we all strive.

Obviously, however, the braze platen and the glasrock heated fixture concepts suitable to honeycomb panel structures will not fill the bill for other types of brazing applications; wherein, part configuration precludes lay-up of the braze structure over a reference tool or surface. Typical examples of such products are the many turbine engine components being brazed today. Nozzle boxes, compressor stator assemblies, exhaust collectors and many similar items are normally brazed in high temperature furnaces and in all probability will continue to be for a long time to come. The need for new thinking regarding braze furnace designs, in our opinion, will be directed by the necessity of joining reactive materials such as titanium and other metals wherein braze joint strength is directly related to minimum time at braze temperature. Although titanium can be brazed in a furnace, this is not an entirely satisfactory operation because of the long furnace temperature recovery and cooling rates which take place while the braze alloy is in the liquid state. Excessive time at temperature during the liquidus state results in excessive diffusion of braze alloy into the base metal with subsequent formation of undesirable compounds. If high strength joints are required, the brazing cycles must be shorter than those used for other metals. Time required for heat-up is not critical up to the liquid state of the braze alloy, but the time at braze temperature is.

In this connection, WADC tests have indicated considerably higher strength levels for induction brazed titanium joints than for furnace or torch brazed specimens. The tests, reported in TR 52-313, Part 2, dated December 1953, produced a marked difference in the amount of diffusion and compound formation between the heating cycle for furnace brazing and the heating cycle for the induction technique.

Shear strength levels on single-lap joints produced readings of 30,600 to 35,000 psi for the induction brazed specimens and only 13,300 to 17,100 for the furnace brazed parts. Pure silver was used as the brazing alloy in each

case. Cycle time was ten minutes for the furnace brazed specimens and 14.5 seconds for the induction brazed parts. Argon atmosphere was used in both methods.

In the face of evidence of this nature, reaffirmed during the years, it is normal to assume that application of heat energy by means of the induction technique will receive a high degree of consideration in the design of facilities for the brazing of titanium and other reactive metals.

Much has already been accomplished in the area of induction brazing and units are commercially available today that are phenomenal in performance. Induction equipment, such as the Induction Heating Corporation's new 25 kilowatt machine, capable of joining 1800 cams per minute, yet occupies an area little more than 4' x 6' may well point the way for the development of similar equipment for the aero-space industry.

Ability of focusing heat input primarily in the braze area without having to subject the attendant brazing tool or fixturing to elevated temperature, creates an ideal condition from the tool designer's viewpoint. Design problems associated with thermal stresses, dissimilar materials expansion and heat absorption are eliminated. Relatively simple fixturing can be resorted to a lower cost and with a higher degree of reliability, thus making induction brazing attractive from the tooling angle.

Much ingenuity, however, is required in the design of tooling for the more conventional furnace brazing processes. Typical examples of this can best be illustrated here by the fixturing employed at Rohr for the brazing of a honeycomb cylinder and gas turbine honeycomb seal assemblies. See Figure 4. The principle involved in this tooling is that of differential expansion. Material selected for the fixture must expand at a rate that will insure sufficient clamping pressure on the braze assembly throughout the thermal cycle. In the assemblies illustrated, the materials used are Inconel for the honeycomb products and 321 for the tooling.

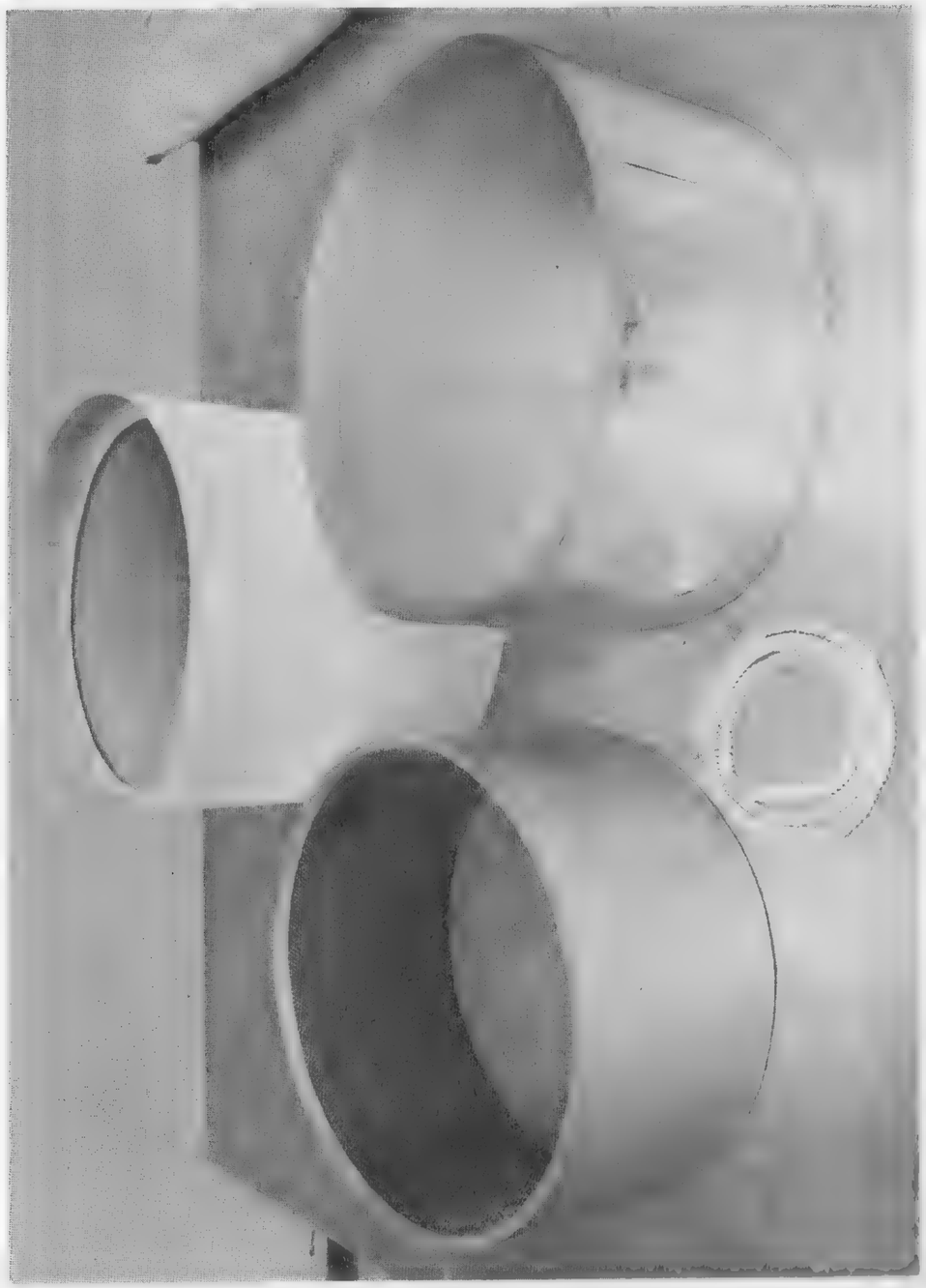


FIGURE 4 TYPICAL LAY-UP OF HONEYCOMB CYLINDER ASSEMBLY SHOWING OUTER SKIN AND CORE (LEFT) INNER SKIN WITH BRAZE FOIL (RIGHT) AND FIXTURING CYLINDER (REAR)

Fixturing problems imposed by the difference in thermal expansion of two dissimilar materials in the braze assembly can at times appear insurmountable as in the case of the gas turbine eductor assembly shown in Figures 5 and 6. The inner shell of this assembly is made of Incoloy 901, while the outer casing is of 321 material explosively formed. Tack welding of these components prior to brazing would be futile because of the difference in their thermal expansion coefficient. The obvious solution (after considerable cogitation) consisted of strapping the 321 casing to the 901 shell with two narrow 901 bands welded into hoops. In this manner, the 321 casing was contained between the 901 material and permitted movement only along the peripheral plane during the brazing cycle.

On the basis of the above, it would then appear that adequate information is available upon which facilities, tooling and manufacturing concepts for the brazing of the super alloys and titanium can be predicated. Considerable cost reductions have been accomplished during the past five years.

Validity of this statement can best be based upon our own experience at Rohr, wherein brazed honeycomb and other structures of the exotic materials are being produced daily for experimental purposes and as saleable products. Figure 7 illustrates, in chart form, our present status with respect to brazed honeycomb structures and their availability.

Emphasis in recent years, on the refractory alloys as prime structural members and thermal barriers, has created an important new challenge in manufacturing technology. This challenge, first accepted by materials producers, is now facing the manufacturing organizations of the aero-space industry and its facilities and equipment suppliers. Basically, the need for refractory metals structures now exists and the industry must prepare itself to furnish them. Furthermore, the techniques and equipment used must provide these products at a profitable level in a highly competitive market. In order to achieve this goal, it is important for us to understand the metallurgical obstacles confronting us, have intimate knowledge of the laboratory techniques used to

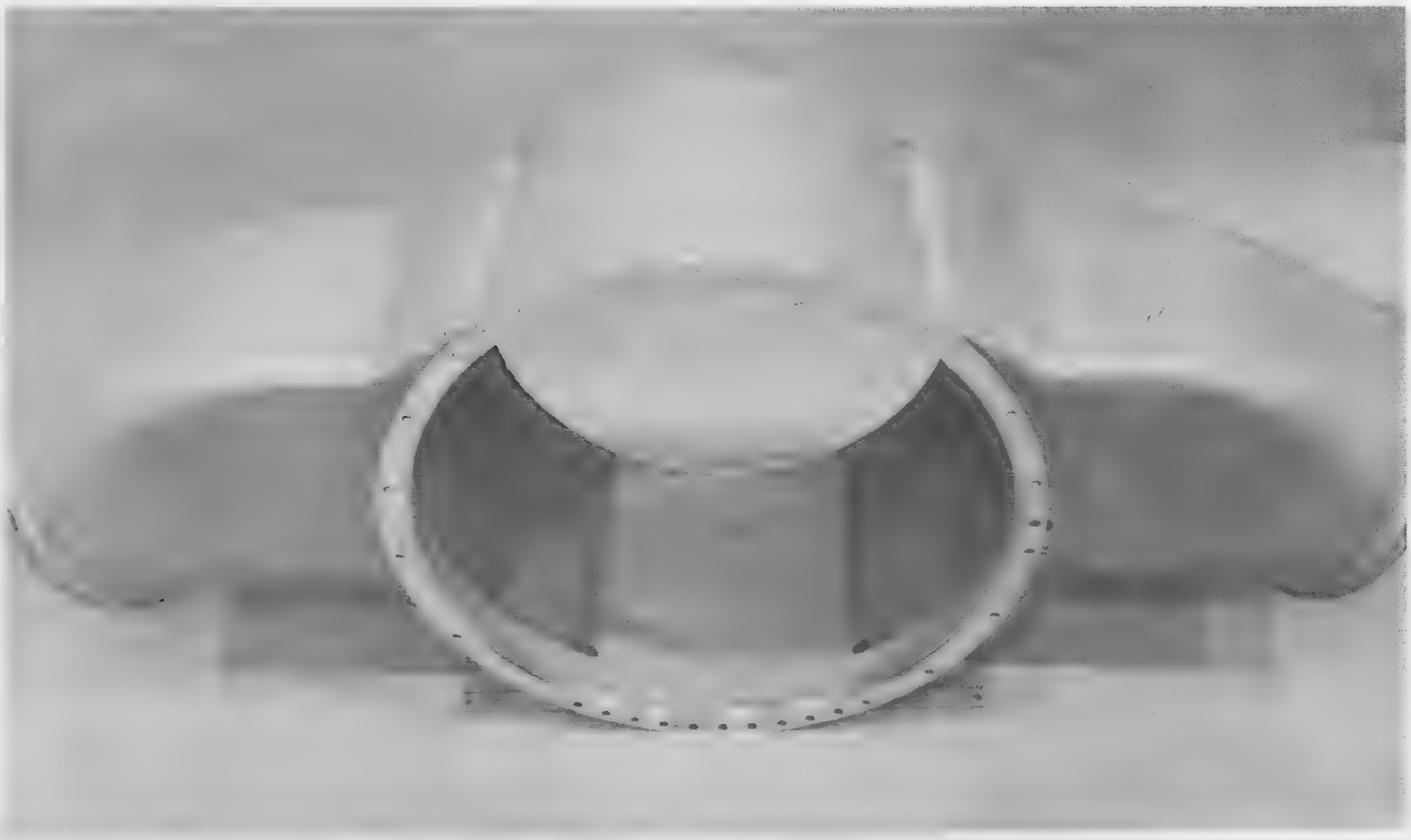


FIGURE 5 AND 6 VIEWS OF TURBINE ENGINE EDUCTOR ASSEMBLY CONSISTING OF INCOLOY 901 AND 321 BRAZED DETAILS

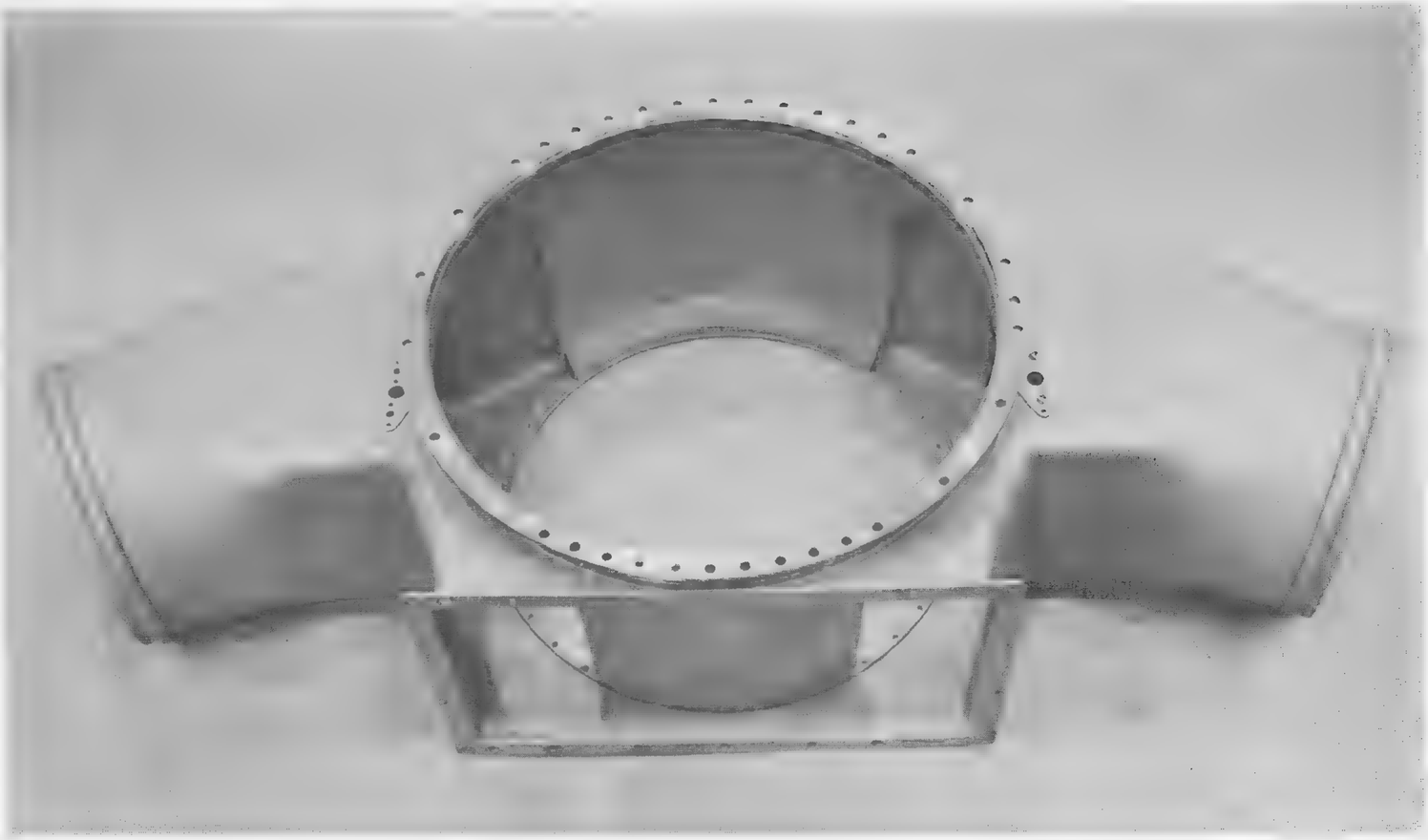


FIGURE 5 AND 6 VIEWS OF TURBINE ENGINE EDUCTOR ASSEMBLY CONSISTING OF INCOLOY 901 AND 321 BRAZED DETAILS

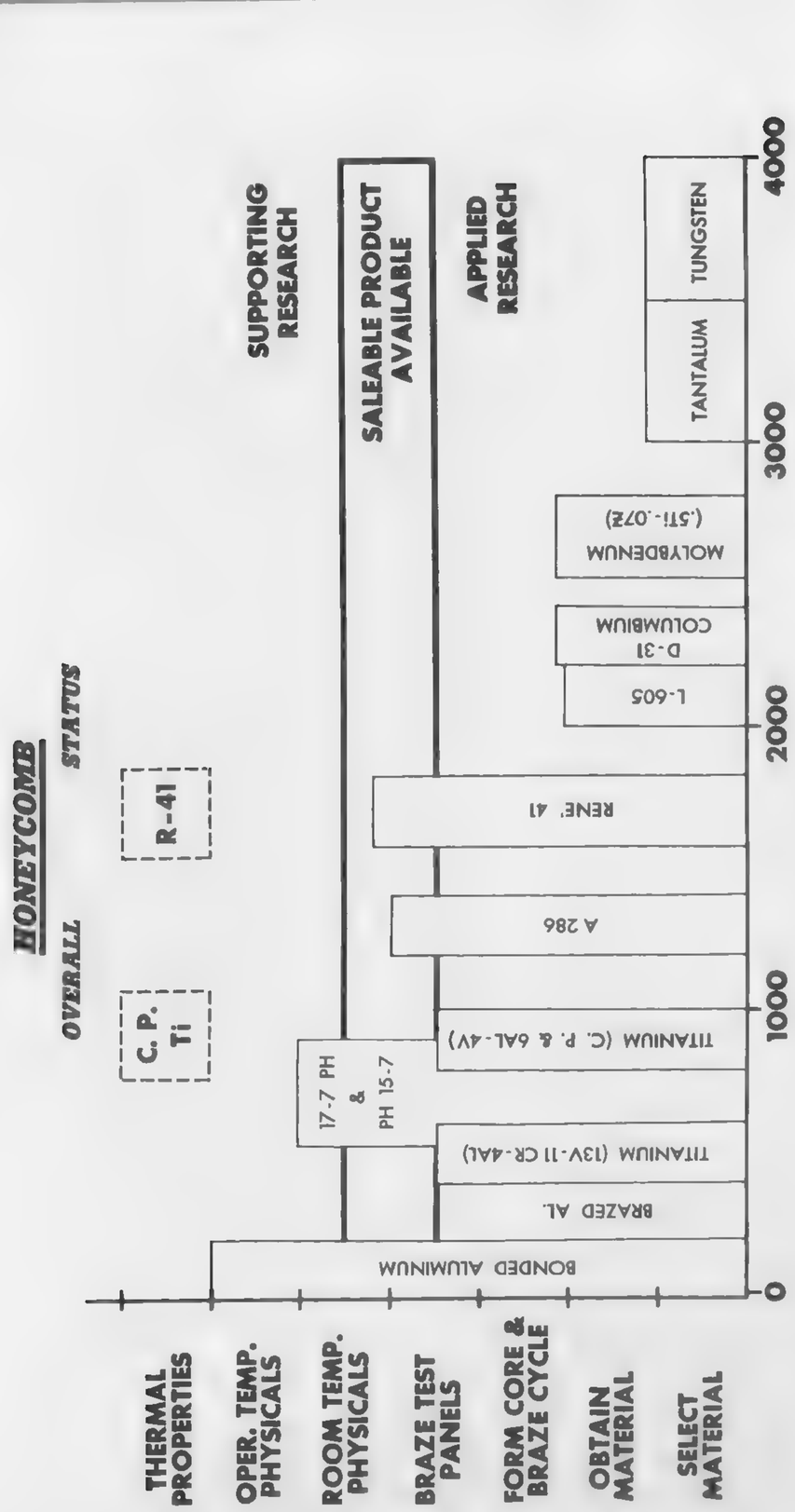


FIGURE 7 CHART OF STATUS AND AVAILABILITY OF HONEYCOMB SANDWICH

circumvent these problems and translate these techniques into production methods through the proper selection of tooling and equipment.

We all know that braze alloys suitable for use in the 3000° to 4000°F temperature range are limited. Recrystallization temperature and the brittle transition range are major problems that must be surmounted prior to achieving full utilization of the refractory metals as structural components at the temperature levels wherein their properties show advantage. Improved alloys are needed with higher recrystallization points. The high temperature resistance of the refractories to oxidation (particularly molybdenum) is notably poor, making it mandatory to provide a very high degree of purity in the braze atmosphere or else a vacuum in the order of approximately 1×10^{-5} mm of Hg.

Conventional brazing techniques require a filler metal with a liquidus temperature below the melting point of the base material and several hundred degrees above the expected service temperature of the brazed assembly. Service temperatures for the refractory alloys would require filler metals with a liquidus above the melting point of present steels and super alloys. Facilities capable of 3000° to 4500°F will be required. Currently, temperatures of this order have been limited to laboratory equipment, such as the small cold-wall internal-element vacuum furnace used by the Martin Company of Baltimore, Maryland, described in the April 1961 issue of the Welding Journal, and to induction-fired vacuum furnaces used in metals refinement operations.

Cold wall internal element vacuum furnaces have been in use for a number of years and a sufficient fund of knowledge exists as to their advantages and limitations. From this background data, the relatively ideal equipment designs of tomorrow will emerge. The Martin furnace may well be the link between the technology of yesterday and the furnace of tomorrow, for through its advanced concepts, many of the earlier cold wall limitations may be overcome.

Operation of this equipment, however, is presently serving a dual purpose, for in addition to its function as a prototype facility, it is being used for brazing sandwich structures of refractory alloys and much useful metallurgical data is being accumulated as a result of this work.

Preliminary tests and literature surveys indicate that the best available materials for use as tools and fixtures in the brazing of refractories are the refractories themselves. Certain borides and carbides still in the development stages have shown promise, but to our knowledge have yet to be proven in use. The Brush Beryllium Company's beryllide intermetallics may also have application here.

Because of the limited availability of the refractory metals in the past, and especially in the gages needed for brazed products, such as honeycomb sandwich structures, not too much background exist upon which to base tooling concepts.

The extremely high cost of high temperature facilities has also impeded broad experimentation in this area; however, with the demands placed upon industry today, considerable work should be forthcoming in the not-too-distant future.

While a considerable impetus is being given to production techniques for brazing the refractories, other methods for joining these materials are not being overlooked.

WELDING

Welding process developments, the advent of electron beam and ultrasonic welding, have furthered the technology for joining the refractory alloys.

The metallurgical problems associated with brazing these materials for the most part are present in the welding. However, through judicious control of process variables, and environment, these can be restricted to a tolerable level.

With the exception of electron beam and ultrasonics, wherein contaminant pickup from atmospheric environment is obviated, the necessity for the development of suitable atmosphere purification systems for production welding is of paramount importance.

Our own experience, at Rohr, has indicated the need for independent systems separate from plant-wide distribution of gasses normally used in production welding. In addition to an independent gas purification system, extensive use of the dry box has been found most helpful. A means by which the purity of the inert gas can be quickly monitored is also most desirable.

Systems capable of 200 cubic feet per hour of inert gas dried to below -100°F dew point, are in operation at our plant. These purification trains consisting of molecular sieve driers, and a series of specially constructed heated "getter" chambers packed with titanium, zirconium, and uranium chips produce an atmosphere in which bright welds in zirconium and other reactive metals are commonplace production operations. Coupled between the purification train and the dry box, is a monitoring device consisting of a glass bell jar-like container, housing a roll of thin foil material (titanium or other similar reactive metals). See Figure 8. A means is provided for resistance heating a portion of this foil to the desired degree of incandescence. Any discoloration of the foil is related to inert gas impurity and welding is not started within the dry box until sufficient purity of gas has been obtained and the foil remains bright upon cooling.

With a well constructed leak-tight dry box, this technique has proven extremely reliable and inexpensive. Figure 9 illustrates this set-up being used in welding a 26' long zirconium process tube. The welding chamber or dry box shown is approximately 30" x 24" x 24". Seals are provided at each end of the box in order to permit passage of the reactor tube through the chamber. A typical example of the finished weld is shown in Figure 10. Note the brightness of the completed weld. This is typical of the type of results that are possible due to a well-functioning gas



FIGURE 8 ROHR DEVELOPED GAS PURITY TESTER

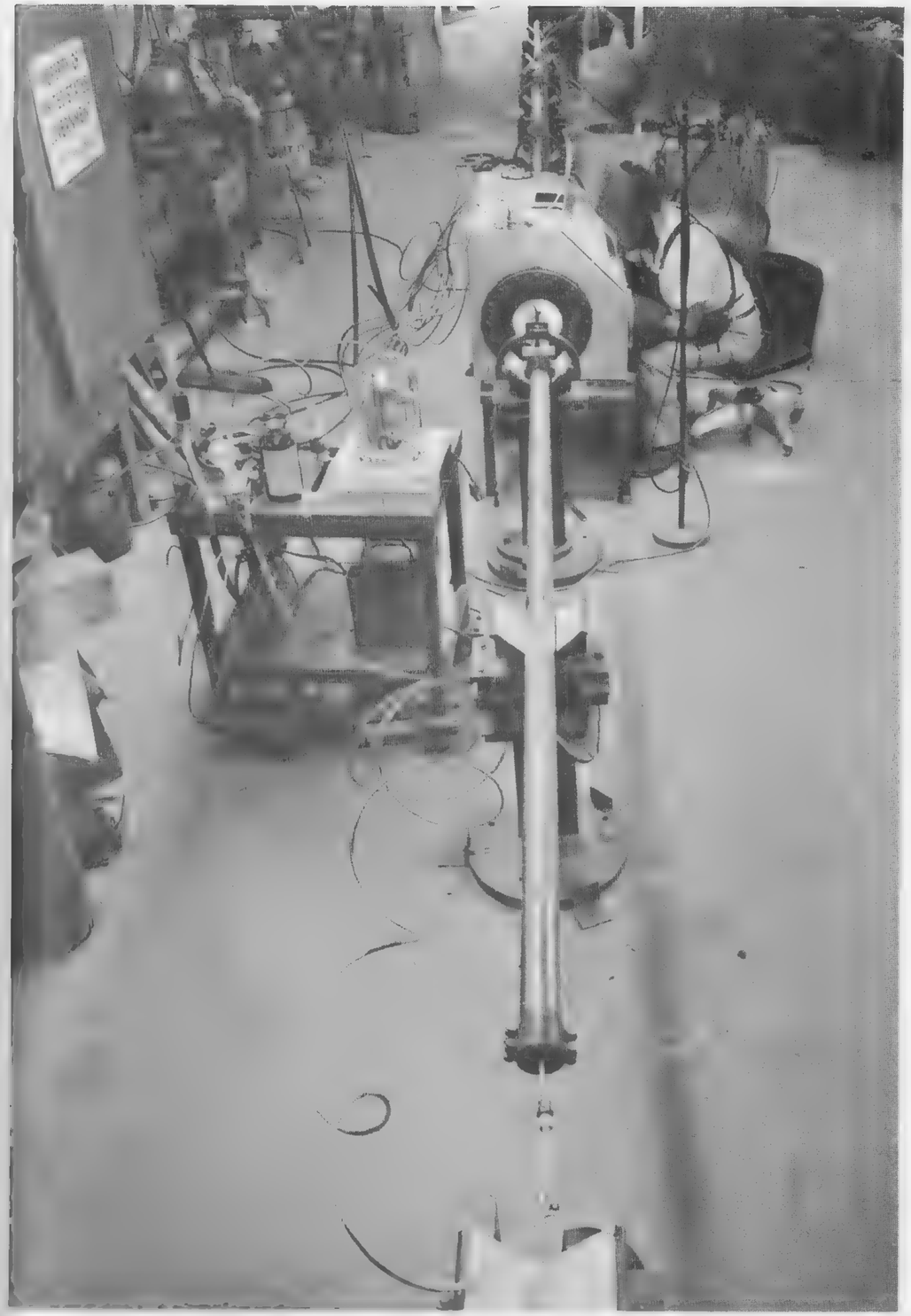


FIGURE 9 DRY BOX WELDING SET-UP USED FOR WELDING ZIRCONIUM REACTOR ROD



FIGURE 10 TYPICAL WELD PERFORMED ON ZIRCONIUM IN ROHR DEVELOPED DRY BOX

purification system. Figure 11 illustrates the completed tube, jacketed in an aluminum casing and ready for shipment.

The tungsten inert gas process is the most versatile process applicable to the welding of refractories on an economical production basis. Electron beam undoubtedly is, and ultrasonic welding will eventually become far more desirable from a metallurgical aspect; however, both these techniques present manufacturing limitations today that restrict their general use as good production operations at this time.

Both automatic and manual welding of the refractories, molybdenum, columbium and tantalum, are possible by the tungsten inert gas process; however, extreme care must be exercised in providing the needed inert gas shielding on both the top and back side of the weld joint throughout the welding cycle. In addition, this atmosphere should not only protect the molten portion of the weld, but also the solidified portions that are cooling. Because of the extreme "tramp-like" characteristics of these refractories for "pick-up" of trace impurities, it has been our experience that welding chambers are a "must." In this respect it is also necessary to state that tools or fixtures destined for use within the chamber should be of such configurations as will will not permit entrapment of shop soils or gaseous pockets that could be a potential source of contamination.

Filler wire may be used with the tungsten inert gas process if this is necessary. Manual welding of tantalum is difficult due to the need for maintaining the required arc length and should not be attempted without some provision for maintaining the position of the welding head at a constant distance from the work.

Joining of tungsten for aero-space applications by other than electron beam has not proven feasible to date, because of the extremely embrittled joint that is produced. Some work has been accomplished in an attempt to control the chilling rate of the molten weld, but this has by no means been the solution to the total problem.



FIGURE 11 COMPLETED REACTOR TUBE READY FOR SHIPMENT

The electron beam, therefore, appears to be the brightest hope to date for achieving any degree of success with the welding of the cantankerous refractories. Many laboratory tests have substantiated its metallurgical advantages and these are undoubtedly better known to you than they are to us.

Of prime concern to us, however, are the techniques to be developed in order to effectively utilize the beam as a profitable and routine production process. Evaluations currently in progress at our plant, on a two-shift basis, are concerned with the development of feasible techniques for production application of the electron beam equipment. The latest Hamilton-Standard electron beam equipment (Figure 12) is being used for this investigation.

The objective of these studies is primarily to develop tooling capable of increasing the versatility of movement within the chamber and establishing tooling concepts to be used in planning new production assignments for facilities of this nature. In addition, a considerable amount of work is being done toward establishing the capability limits of this process as related to existing production tasks. In this area, a wealth of information is presently being compiled on joint design, fit-up requirements and assembly techniques.

With the advent of ultrasonic welding, there has been a great deal of interest in the feasibility of joining both dissimilar and refractory metals of the aero-space trade. However as the principle of ultrasonic welding is relatively new, and the properties of the refractory alloys are not too well defined, acceptance of this process is being attempted on an extremely cautious basis. Since there is no correlation between the development of heat, as in resistance welding, and the development of vibratory energy, as in ultrasonic welding, we should avoid making simulations between the two processes and treat each independently of the other. Unlike resistance welding, the ultrasonic process, although limited to joining thin gages in the refractory metals, is more suited to producing welds of greater structural integrity. Ultrasonic welding has the distinct advantage of not having to generate heat to produce a bond as compared to

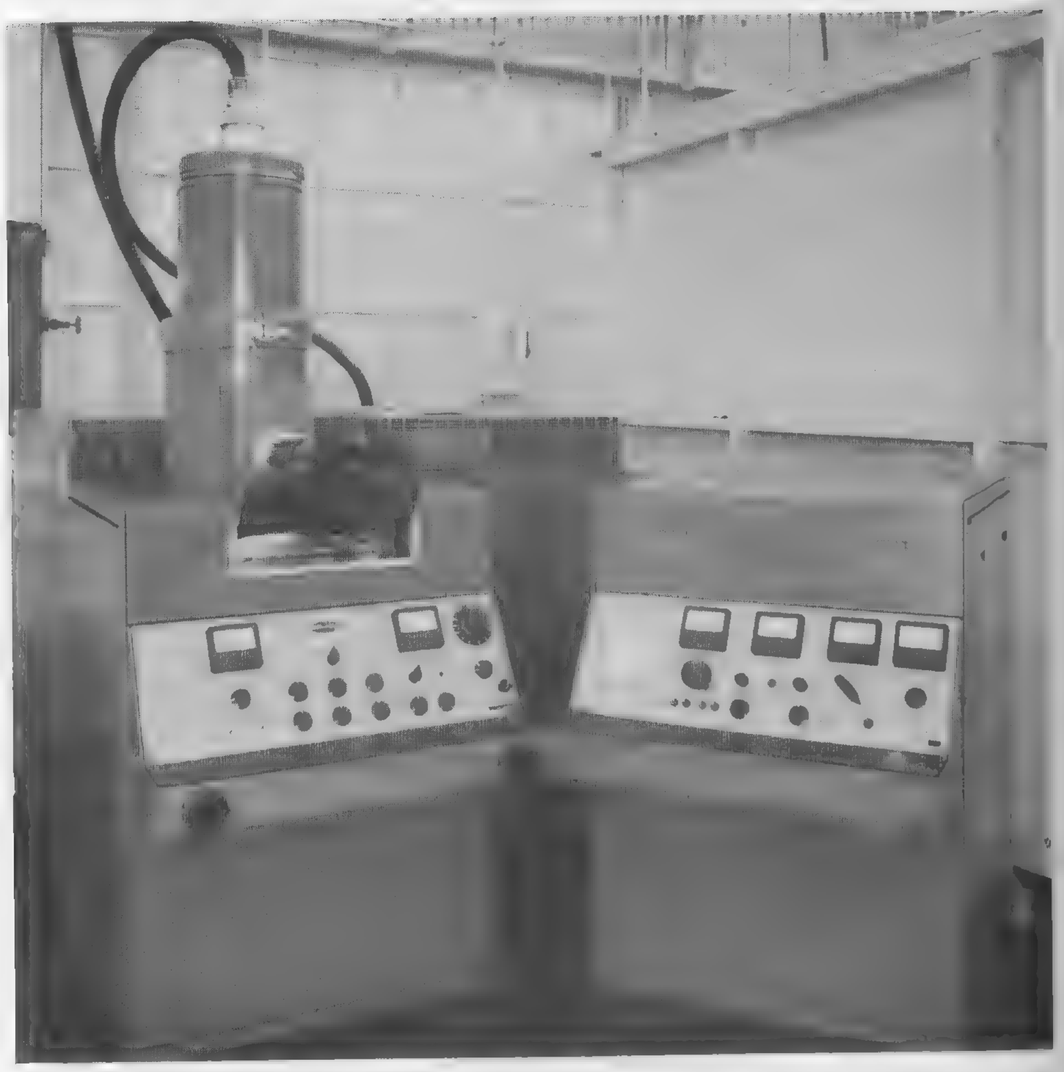


FIGURE 12 HAMILTON-STANDARD ELECTRON BEAM WELDER BEING USED IN THE ROHR PRODUCTION TECHNIQUES EVALUATIONS

fusion or resistance welding. The heat generated in the ultrasonic weld is a by-product of the process and can generally be controlled at levels well below the recrystallization temperature of the refractory alloy. Since the formation of an ultrasonic weld is not dependent upon melting, grain growth, recrystallization, and diffusion of the bond, are of little consequence. Metallurgically, this advantage is of tremendous value.

At the present time, ultrasonic equipment is limited in vibratory power output due primarily to the low efficiencies of the transducer and transducer coupling system.

A serious drawback to ultrasonic welding is the effects of vibration set-up within the weldments resulting in high shear stresses of the weld. In some cases, this vibration will cause the complete fracture of the weld and it has on occasion caused crack failures in the parent metal. Vibrations set-up within the weldment are unwanted and considered lost energy. If this superfluous energy was not of a dangerous potential, it could be disregarded. However, because of its hazardous potential, it must be contained by dampening to an acceptable level or preferably absorbed completely. The natural resonant frequency of the weldment must be altered by fixturing devices, clamps or application of absorbent materials, thereby complicating the job of tooling and reducing the extent of process application. Careful preparation of all edges of detail parts is of prime importance in order to reduce parent metal cracking. Tip sticking is still a problem. The method of attaching tips to the sonotrode by silver brazing, represents a delicate and costly operation when considering the life span of the tips. The pressure system requirements for ultrasonic are not as demanding as with resistance welding. Power supply can be placed reasonably remote from the welding head as to provide excellent accessibility around the weldment area.

If we can rely on the time-tested validity of the old adage "necessity is the mother of invention" we of the aero-space industry may well expect to see a tremendous surge of improvement in the techniques of joining the metals of our trade for never before has there been a greater necessity for "invention" nor the stakes as high.

HIGH ENERGY RATE FORMING OF SPACE AGE MATERIALS

Warren G. Mang
General Sales Manager
Advanced Products Department
General Dynamics Corporation
San Diego, California

Mr. Chairman, members of the American Society for Metals, and guests. It is an honor and privilege to take part in this informative and vital conference and in such distinguished company. The advanced technological information being exchanged in these sessions will certainly improve our combined positions in aerospace industry. On behalf of the Advanced Products Department of General Dynamics Corporation, I would like to extend our appreciation to the ASM for the opportunity to participate in this Golden Gate Metals Conference and with it offer our congratulations and sincere wishes for continued success in the highly technical fields represented here today.

High Energy Rate Forming of Space Age Materials requires, first of all, a basic understanding of the problem--the problem that is consistently reduced by the constant assault made on the hard-to-work super alloy and refractory materials by advanced techniques in metalworking and, in particular, forging techniques.

The development of high energy rate forging equipment has reached a practical application stage at a time when new techniques are urgently needed to meet the rapidly increasing demands for working super alloy and refractory materials so vitally needed in the aerospace industry. Stronger, more complex parts made from these advanced metals are in urgent demand; and the current, critical status is serious in space age manufacturing. Current demands for stronger, more reliable parts made from these materials and this is

very important--have exceeded the capabilities of obsoleted, conventional, more costly mechanical forging methods.

In recent years, the concept of introducing energy at high rates to a metal workpiece has received a great deal of attention. The purpose of applying high energy rates has been to reduce size and cost of equipment needed to forge larger parts. This, it has been proven, provides the capability to form parts from the materials that are not easily worked by conventional methods. It also provides the capabilities to produce improved dimensional tolerances and reduce over-all production costs with increased material savings. Significantly, it greatly reduces waste metal. To achieve this purpose, we have seen the rapid development of high energy rate forming methods based on three types--Chemical, Electrical, and Pneumatic Mechanical.

This general classification of high energy rate forming can be divided further into existing processes to encompass forming by:

Detonation of explosives
Combustion of propellants or gases
Release of stored electrical energy to produce spark discharge
Release of stored electrical energy to produce high intensity electromagnetic fields
Rapid expansion of compressed gases to activate the piston or ram of a press.

To be specific and concern ourselves with High Energy Rate Forming of Space Age Materials, let us consider primarily the problem of forging the hard-to-work super alloy and refractory metals into useable parts. This involves the pneumatic mechanical, high energy rate forming by rapid expansion of compressed gases to propel a ram into high velocity, transferring kinetic energy to impact. To illustrate, this is the basic concept of the DYNAPAK high-energy rate machines which we shall compare to conventional forming processes which use forming velocities up to about 5 feet per second. The high energy rate forming machine shown here is capable of velocities up to 60 feet per second.

The machine structure, its principle, and its operation are not complicated. To better understand the high energy rate technique, perhaps an explanation of concept and operation is in order here.

To prepare the machine for operation, a gas pressure of approximately 100 psi is introduced into the lower cylinder which forces the ram, or driving-piston, up against the orifice plate. Gas pressure is introduced into the set pressure system moving the set pressure piston down and against the orifice. The driving pressure, which may vary from 200 psi to 2000 psi, is contained in the upper cylinder. The set pressure piston prevents the driving pressure from acting on the ram piston. The set pressure is adjusted to one-third the driving pressure.

To actuate the machine, a small quantity of gas is introduced into the orifice cavity through the trigger pressure line. This gas pressure is sufficient to lift the set pressure piston off the orifice but not sufficient to move the ram piston downward. Lifting the set pressure piston allows the driving pressure to act upon the ram piston moving it toward the bolster. Since the driving pressure is three times the set pressure, the set pressure piston is driven rapidly upward. The upward motion of the set pressure piston is retarded by metering the gas trapped in the set pressure cylinder.

The machine is supported in its structural frame by shock absorbers on each guide rod. Each shock absorber cylinder is divided into two compartments around the guide rod by the guide rod piston. The lower and upper compartments are pressurized with nitrogen gas. The entire actuator is free floating as the gas pressure is the only means of support between the structural framework and the foundation.

The force of the driving pressure gas on the ram piston rapidly accelerates the ram assembly. As the ram moves toward the bolster plate, the bolster plate moves toward the ram. Consider the machine at this point as composed of only two basic elements--the ram assembly and the actuator

assembly. The ram assembly is composed of the piston, column, and the ram itself. The actuator assembly consists of the cylinders, guide rods, bolster, etc. At the instant the punch contacts the billet we have a light mass (the ram assembly) at a high velocity impacting a heavy mass (the actuator assembly) at a low velocity in the opposite direction. The kinetic energy of both assemblies is equal and opposite. Surplus energy not utilized in deforming the billet is thus dampened out and heavy foundations or cushion plates are not required. The machine can be mounted on a conventional concrete shop floor.

After the working cycle is completed, the machine is re-energized by turning it into a compressor. Hydraulic oil is pumped into the lower cylinder compressing the ram back-pressure gas against the ram piston, overcoming the residual driving pressure and the weight of the ram assembly, to force the ram piston against the orifice plate. The hydraulic oil and the ram back-pressure gas are separated by a floating piston to prevent aerating the hydraulic oil. This action results in the driving-pressure gas reassuming its original volume and pressure. The orifice cylinder and the set pressure piston are driven downward by forcing hydraulic oil into the volume over the orifice cylinder. As the set pressure piston seals against the orifice plate, the gas trapped in the orifice is vented to atmosphere. The hydraulic oil in the lower cylinder is bled off by the force of the ram back-pressure gas which was highly compressed. The back-pressure drops to approximately 100 psi when all the oil has been forced from the system. As this operation is completed, the hydraulic pressure is released from the orifice cylinder in the set pressure assembly; thus, the orifice cylinder is driven upward by the compressed set-pressure gas driving out all of the oil and allowing the set-pressure to return to normal. The machine is now ready to recycle.

Velocity has two distinct functions, which can not be divorced in this process. Since the kinetic energy of the ram is equal to one-half the mass times the velocity squared, the faster the ram is propelled, the greater the energy level imparted to the billet on impact. Thus, through velocity,

high unit pressures are generated. These pressures are of sufficient magnitude to cause the material being formed to behave plastically and flow into the die. The rate of strain is also a function of velocity.

In the high energy rate forming of exotic materials, this all means that no-draft forgings are economically feasible. It means that complex sections employing narrow, stronger webs can now be forged. It means that tolerances measured in thousandths of an inch are possible rather than in fractions of an inch. It means that the refractory and exotic materials now in demand in aerospace requirements can be forged as well as can the conventional metals. It means, in addition, that many parts can now be forged in one blow that would normally be considered impossible, regardless of the number of blows or size of equipment.

In order to fully realize the potential of pneumatic source, high-energy rate forging, current forging requirements will require review and correlation with these advanced capabilities.

High energy rate forgings consistently exhibit reduced grain size. Grain sizes of 8 to 10 are normal. By the nature of the process, grain flow can be directed and controlled to allow the maximum utilization of material strength in the forged parts.

With a machine of this concept set up to forge a given part, it is now possible to forge any number of subsequent parts with exactly the same amount of energy at the same deformation rate. The energy available to strike the billet is always known by the exact control of the driving pressure. To illustrate this significant point, permit me to introduce a summary prepared from a report made by Douglas Aircraft Company of Santa Monica, California, on energy variance and, more specifically, of the DYNAPAK high energy equipment which we are comparing with conventional equipment and methods here this afternoon.

The test which formed the basis for this report was practical. It involved a conventional air-hammer and an

experienced operator, who had 20 years of applied operating background on this particular hammer. "In each test the operator endeavored to hit the form block as hard as possible. The speed before impact varied between hits from 120 to 156 inches per second indicating that precise speed control is difficult to obtain, "--on conventional equipment. The velocity variation represents a percentage difference of 30%. Consider now, that because energy varies as the square of velocity, the true variation area is 69%. A conventional hammer blow at energy levels other than peak output is even more dependent on the "feel" of the operator. The forging of super alloy and refractory materials requires a more sophisticated, scientific, and advanced approach than the mere "feel" of an operator. The element here of human error factors does not have a place in space age production.

In contrast, the energy per blow of the high energy rate concept equipment has been clearly demonstrated to not vary more than 5% over the entire practical operating range--which in the case of DYNAPAK is 100% to less than 10% of machine capacity. In other words, at any level the energy may be accurately pre-set and accurately recorded. This capacity and capability is basic in pointing out the utility of high energy rate methods in the closed die, precision forging field. The ability to produce a single-blow closed die forging depends entirely on accurate adjustability with precise repeatability and reliable performance--blow after blow. Such capability in high energy rate forging is not shared by more conventional equipment. High energy rate forging methods are unique and, at this stage of aerospace requirements, invaluable. Forging is, indeed, in a more scientific area today. With high energy rate methods, it is conclusive that once data is tabulated regarding the level of energy required to deform a given material a given amount, the operator is able to calculate the exact energy requirement and machine settings.

Tool design presents somewhat of a challenge at this point. However, our experience to date would suggest that accepted tool design fundamentals can be applied wherever possible if consideration is given to the probable flow of material, the developed stresses, and the velocity of the

material as it passes and/or fills each surface of the punch and die. The selection of punch and die materials and their proper heat treatment are understandably important and critical. To date, H-13 and H-11 die steels, heat treated to Rc 50-52, have proved to be most satisfactory die materials. S-1 shock resistant tool steel, heat treated to Rc 48-50, is compatible punch material.

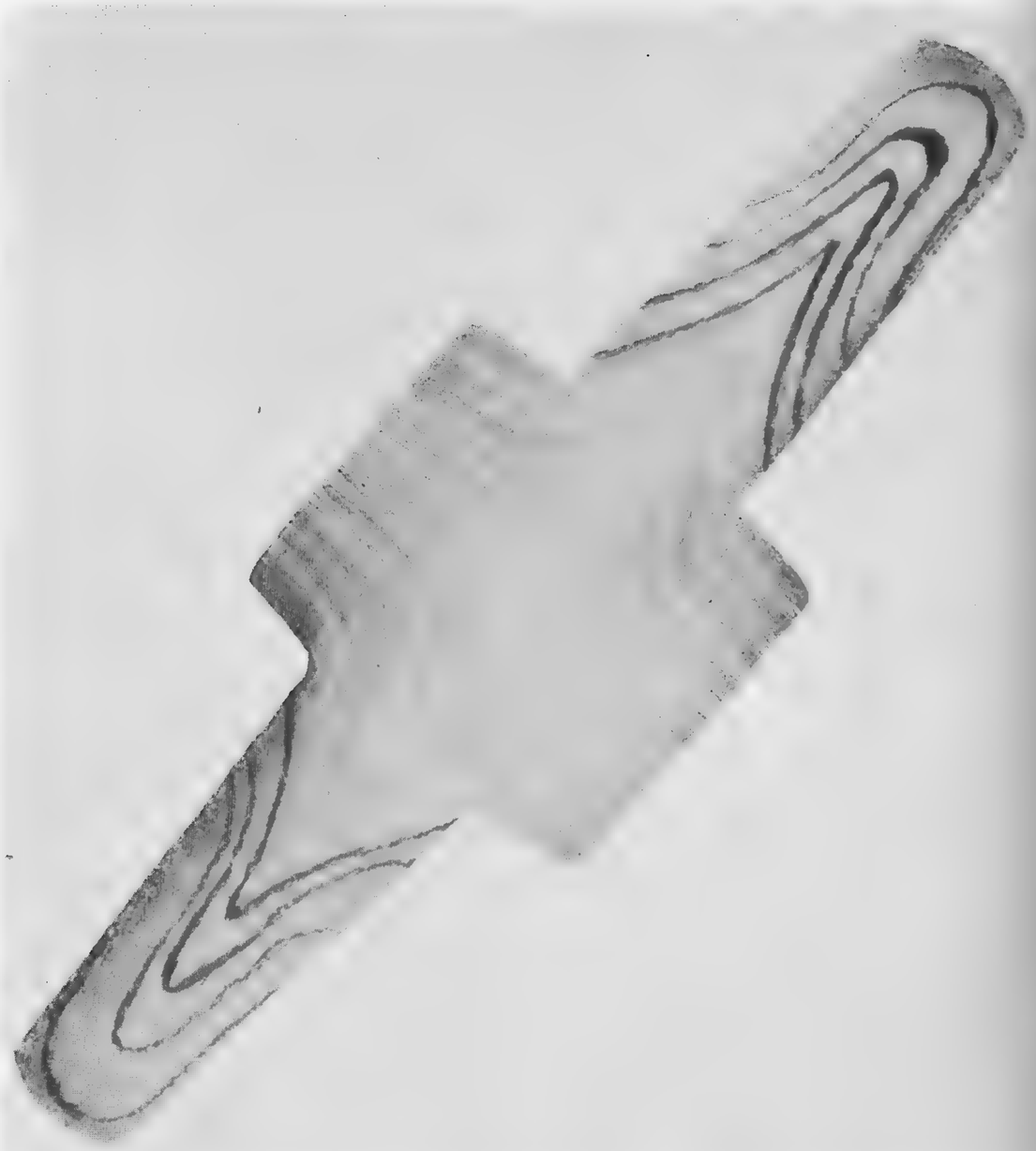
Tool life will vary with the process involved; also, the complexity of the part, the abrasiveness of the material to be formed, and the lubricant used are factors in tool life. With so many variables, die life can not be generalized. However, twenty-four hundred H-11 tool steel diaphragms shown here for reference were forged with one die set without re-dress.

It is interesting to remember that many of the parts forged need not be forgings from a design standpoint. They can be forged by this high energy rate concept to effect savings in material and labor; and at present, this is exactly what is being done in many plants.

What future High Energy Rate Forging of Space Age Materials holds for all industrial and military progress is dependent upon the acceptance of this new manufacturing technique. This metal forming equipment with combined technological and mechanical efforts opens an entire new era which offers a new dimension in capabilities to work super alloy and refractory materials into useable parts. It offers a means to strike back and make further advances in other manufacturing areas once available only to costly, demanding, chip-making conventional methods. Again that time worn slogan, "It is better to move the metal than remove it," is realistic. This potential will be fully realized if industry is willing to change many of its present concepts regarding the design and the method of manufacture of many parts. It is critical to adopt this positive approach to progress.

Our continued greatness as a Nation depends on individual men like those of you in this audience this afternoon, lots of individual men. It depends on the recognition and use the spirit of individual excellence which lies within each of us

Gentlemen, exchange, discuss, examine, and evaluate technical findings. Re-examine the conventional materials as well as considering the super alloy and refractory metals. Approach aerospace material parts manufacturing problems with the capability and compatibility of advanced techniques developed in high energy rate forming. It's expedient most of all. Finally it is change, risk, improvement, and growth, these, the ingredients of success.



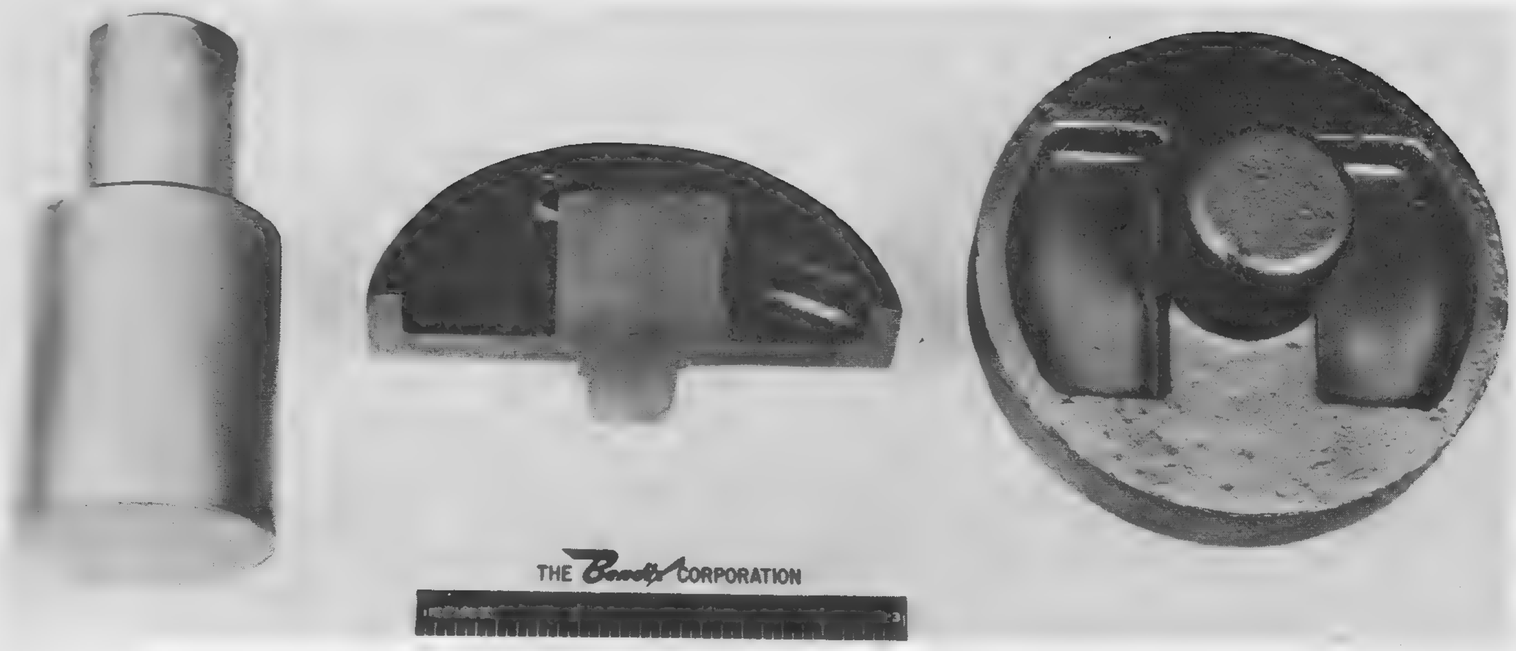

10
9
8
7
6
5
4
3
2

642

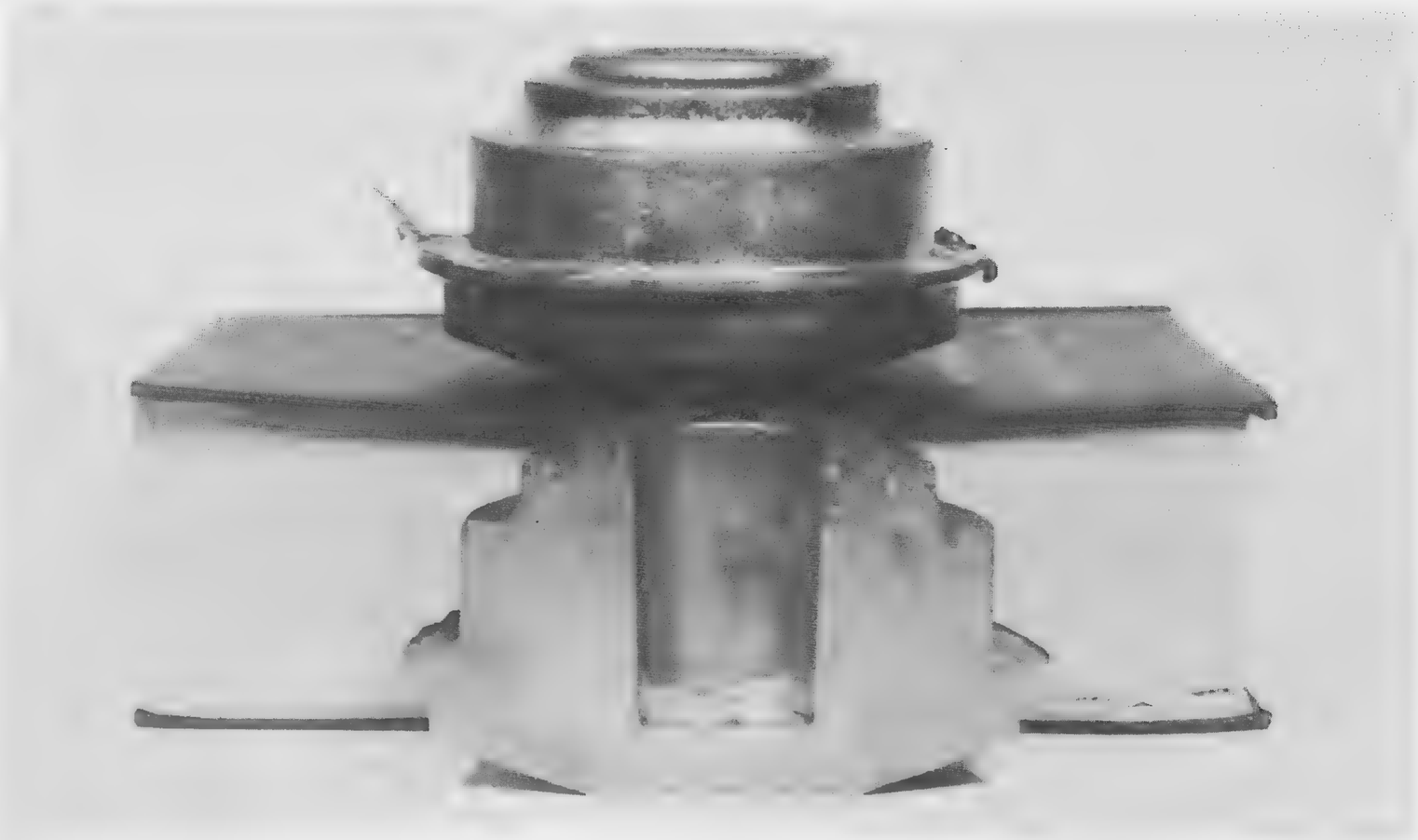


Port Plate
Material: Hastelloy "C"
Temperature: 2225°F
Fire Pressure:
Billet Size: 1/2" x 1" x 2-1/2"

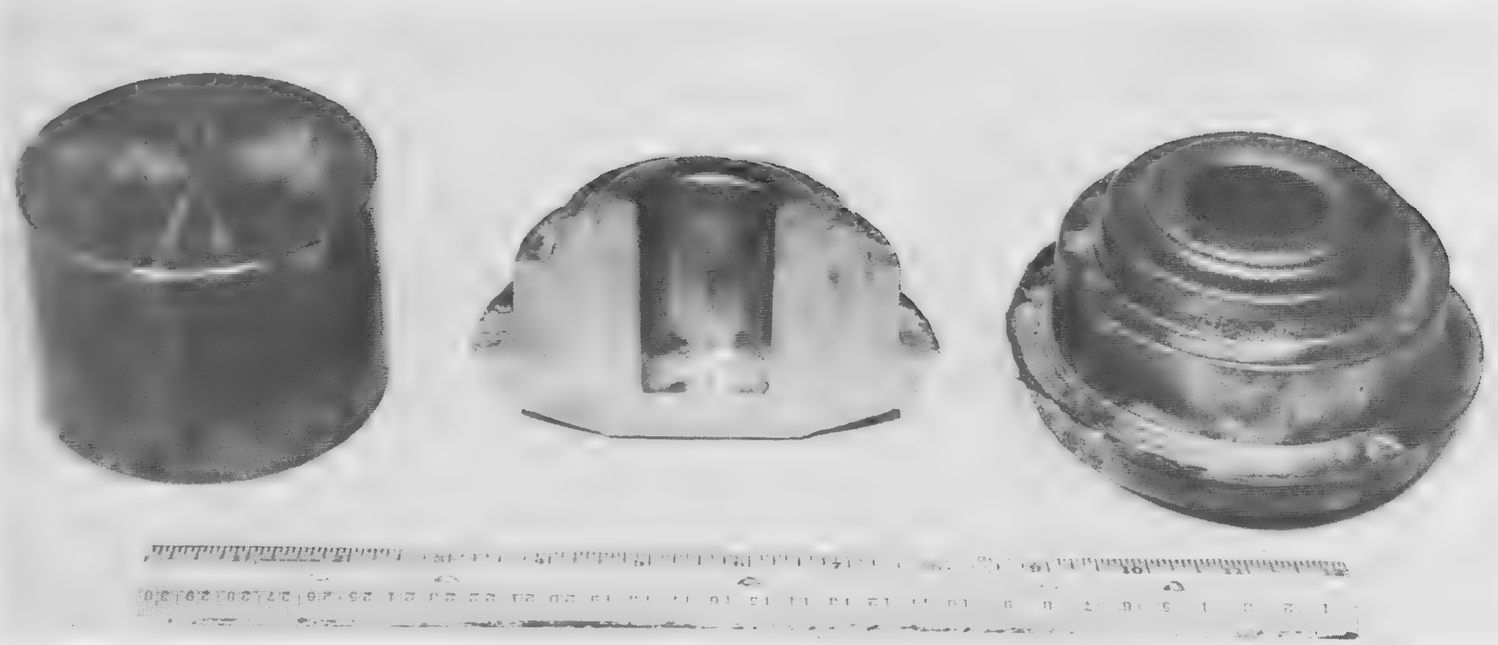
643



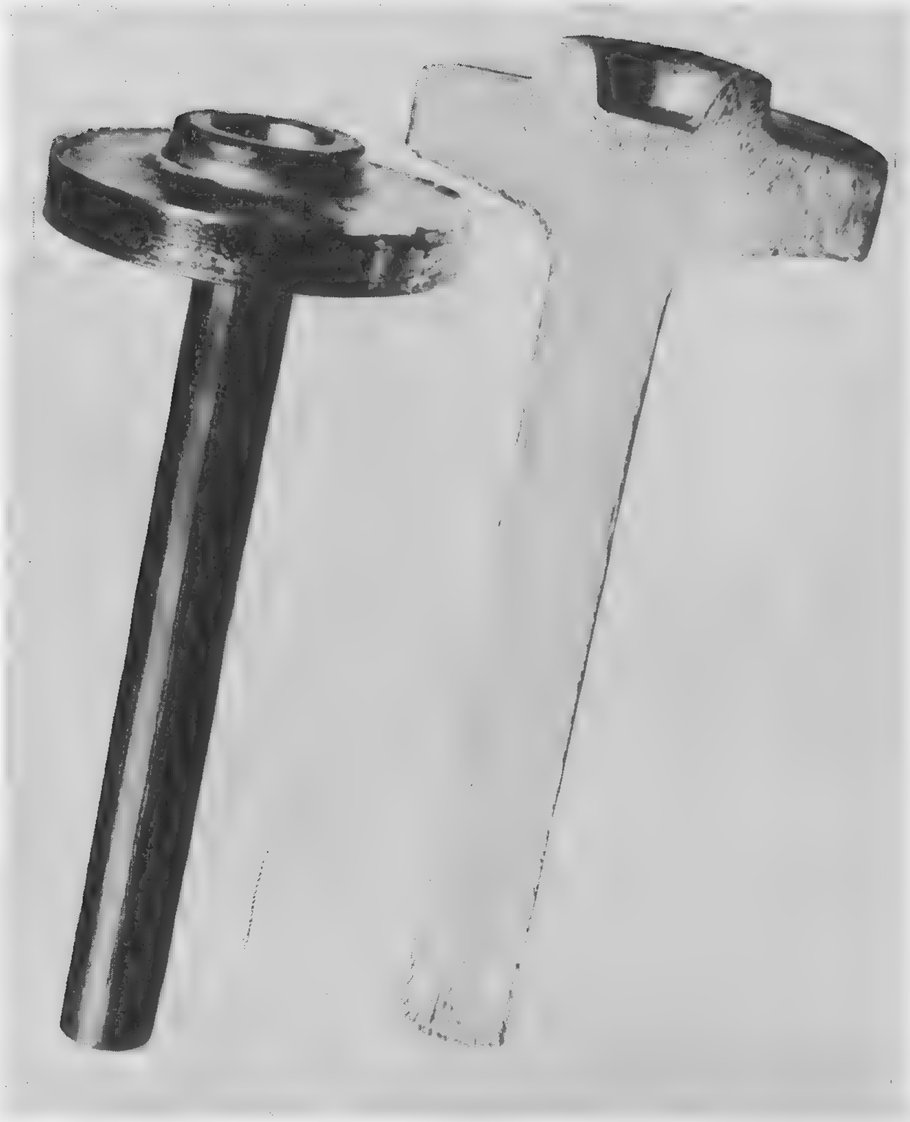
Spline Plate
Fire Pressure: 525 psi
Temperature: 2150°F
Billet: 1-1/2"D x 3-1/4" long
Stroke: 6"
Material: 8740



This tough pitch copper oxygen nozzle can be produced with improved qualities by utilizing a powdered metallurgy technique on DYNAPAK.



This is a copper nose cone for an oxygen nozzle used in a steel mill blast furnace. This product was successfully forged on DYNAPAK. The original copper billet weighs 9.10 lbs. The finished nozzle 8.90 lbs. It has a 1-1/4 inch diameter hole pierced to a depth of 2-1/2 inches.



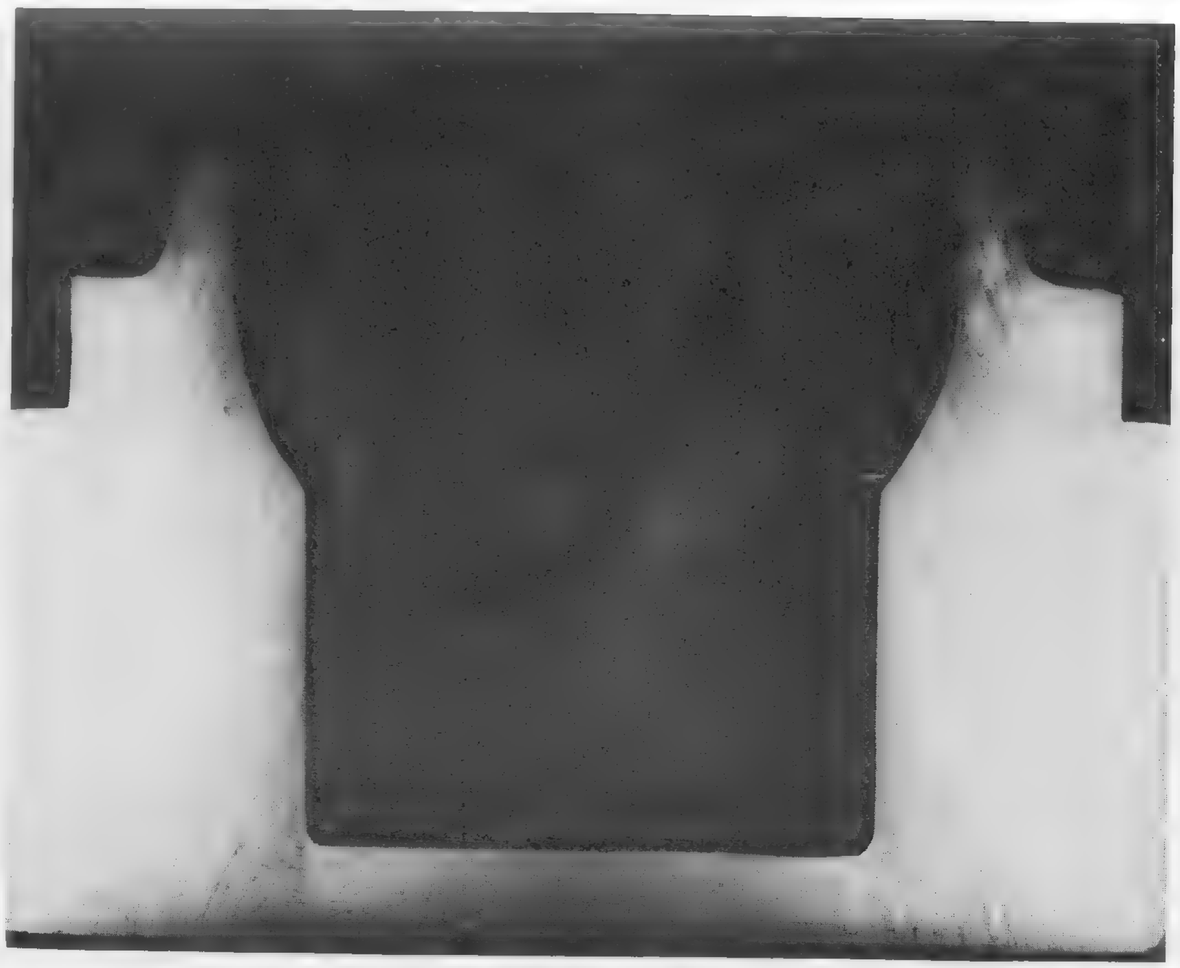
Part No. 642384 Shaft
Material; 4350 Steel
Billet;
3.600 dia. X 1.250 Lg.
Extruded Length 10 in.



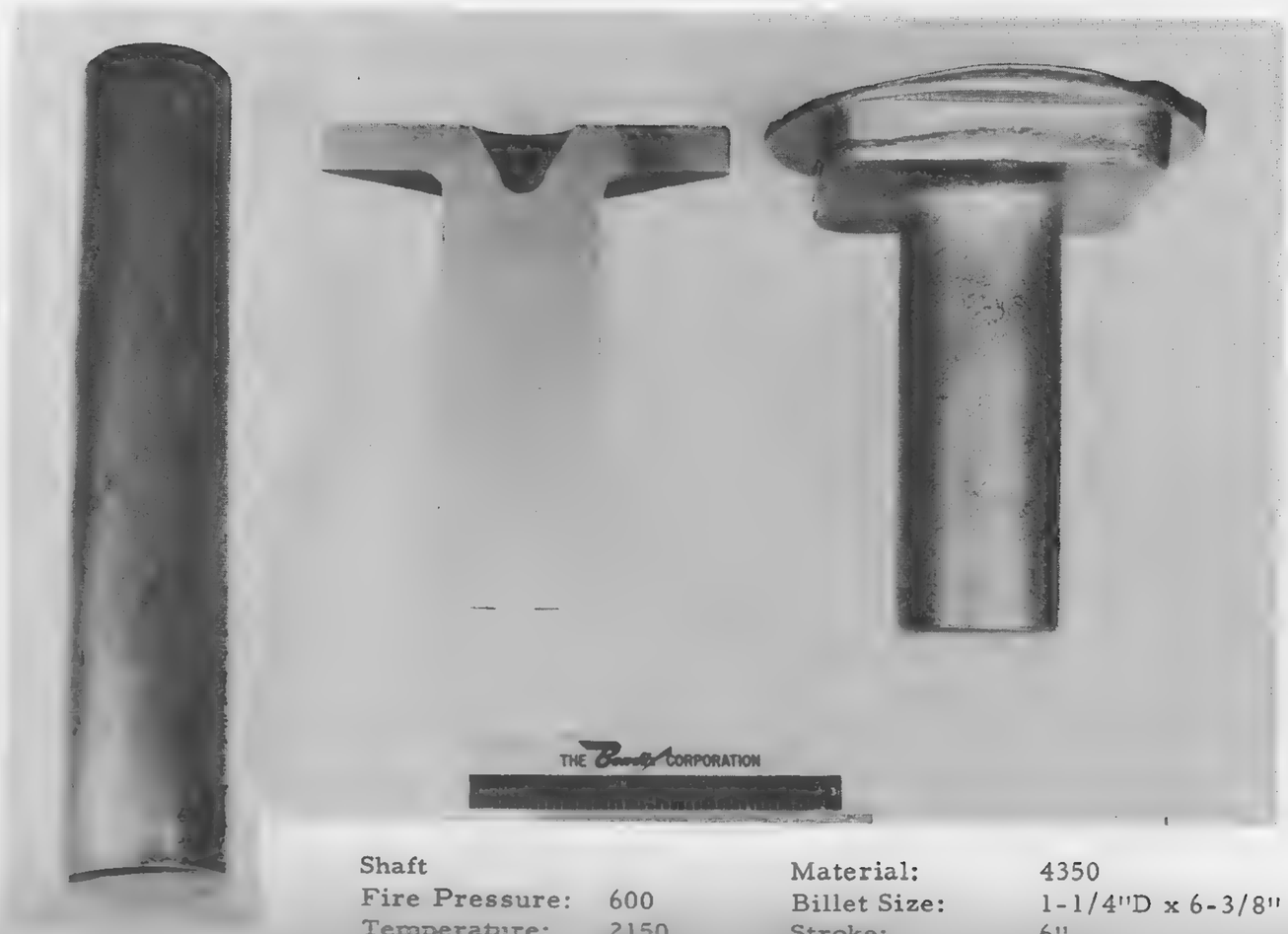
Part No. 642256 Gear - Material: 9310 Steel
Billet: 1.400 dia. X 4.750 Lg.



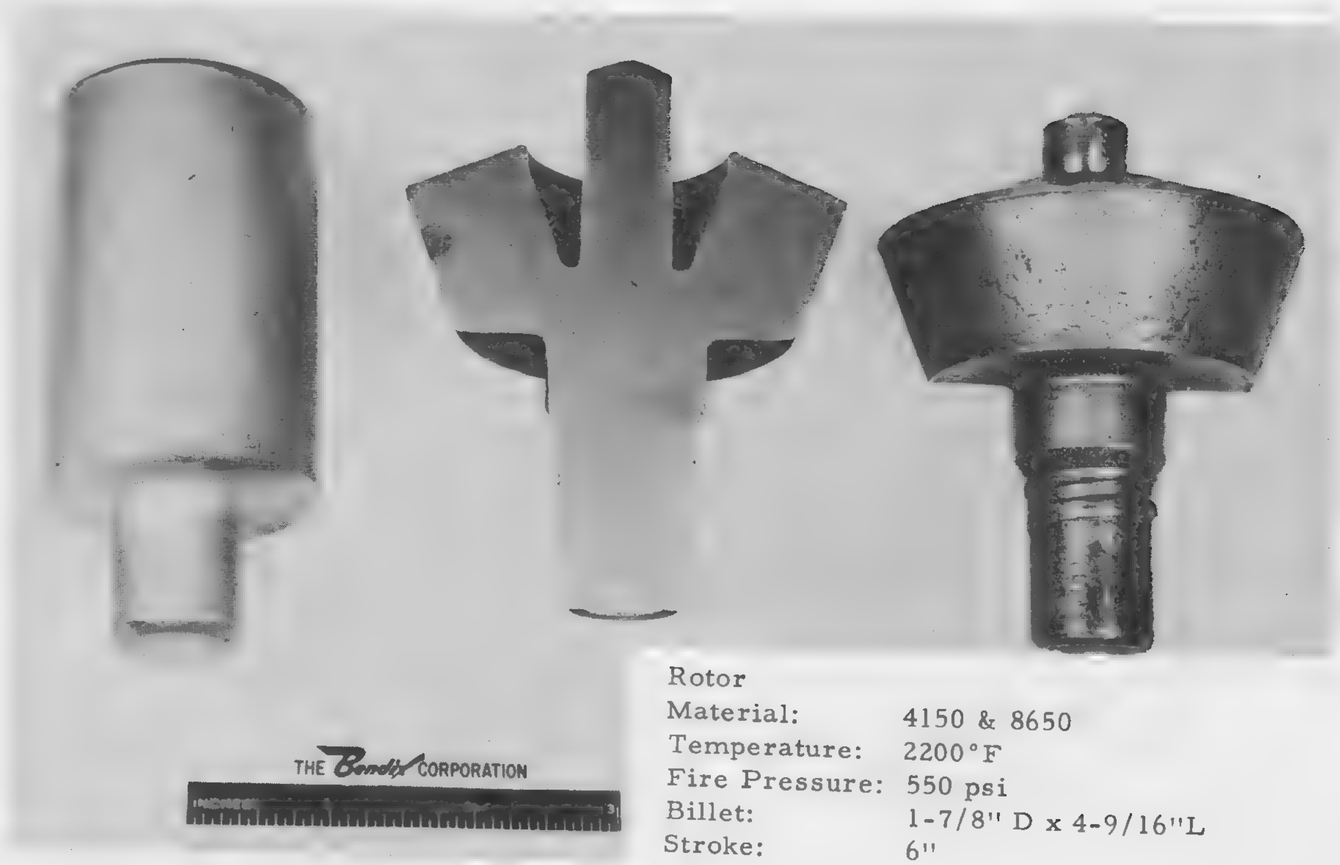
Part No. 646499 - COMMERCIAL DIAPHRAGM
Material - Halcomb 218
Billet Size - 1.343 Dia. x 1.282 Lg.
Billet Coating - Copper Plate - Flash
Die Material - Halcomb 218 - 44 Rc
Punch Material - Halcomb 218 - 44 Rc
Die Coating - Colloidal Graphite in H2O
Forging Temp. - Soak at 1650° for 30 Min. Heat to 2000°F Hold 15 Min.
DYNAPAK Forged: 1 Blow at 900 PSI Fire Pressure
7" Total Stroke
Time From Furnace to Impact -- 9 Sec.



650

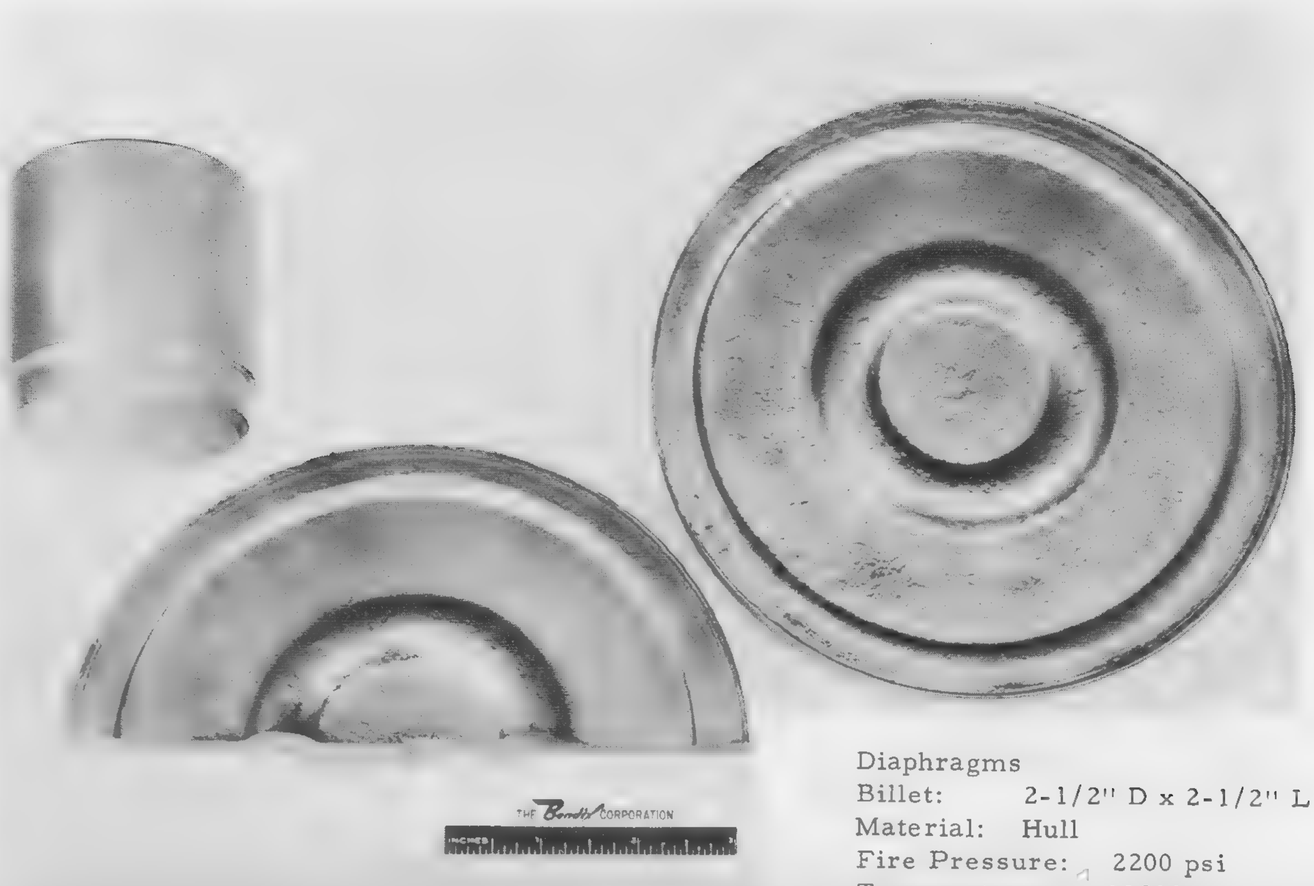


Shaft			
Fire Pressure:	600	Material:	4350
Temperature:	2150	Billet Size:	1-1/4"D x 6-3/8"
		Stroke:	6"



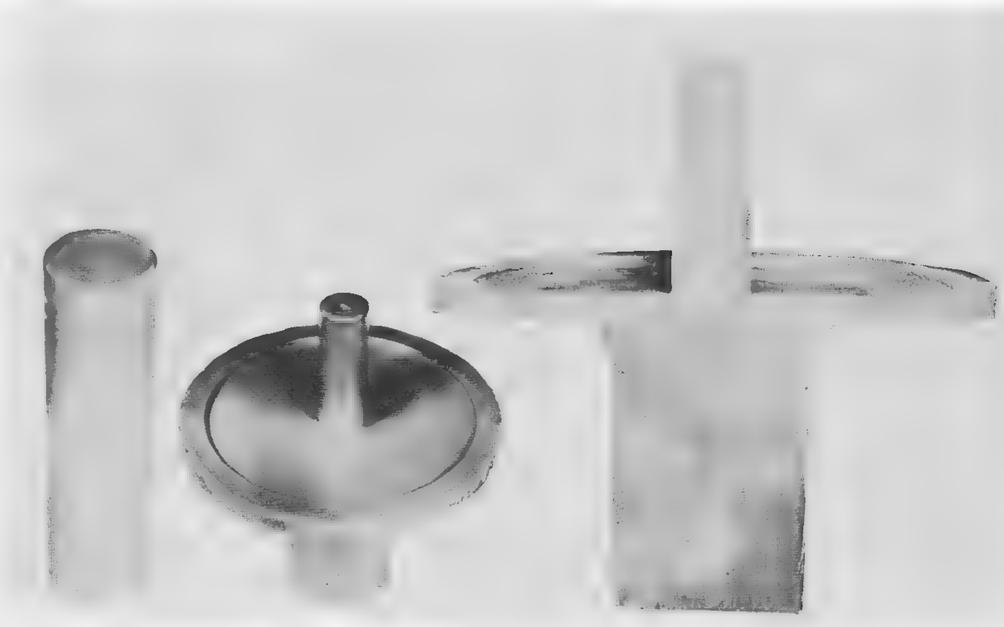
Rotor	
Material:	4150 & 8650
Temperature:	2200°F
Fire Pressure:	550 psi
Billet:	1-7/8" D x 4-9/16"L
Stroke:	6"

652



Diaphragms
Billet: 2-1/2" D x 2-1/2" L
Material: Hull
Fire Pressure: 2200 psi
Temperature: 1980°F

653



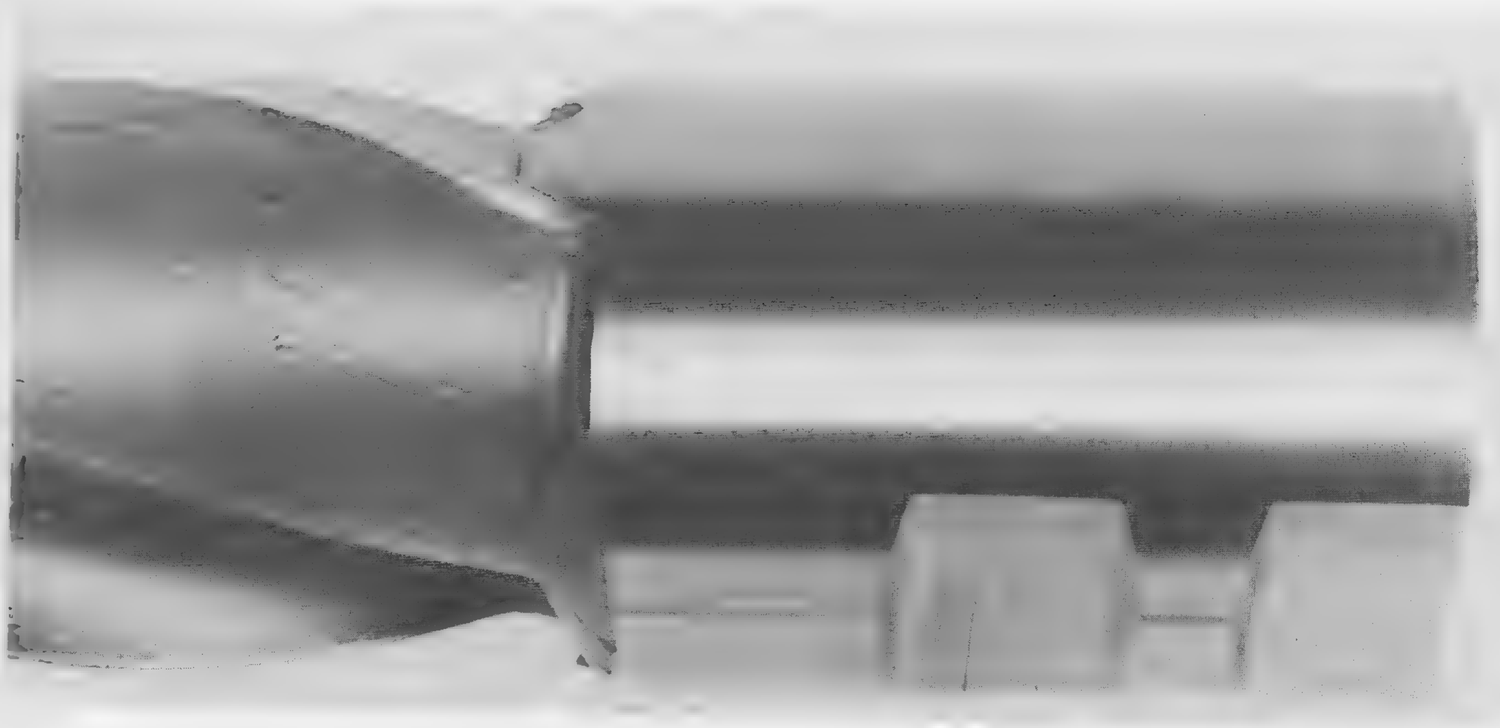
PART NO. 642044 & 5 - FLANGE
Material - 9310 Steel
Billet Size - 1.225 Dia. x 4.000 Lg.
Billet Coating - Copper Plate - Flash
Die Material - Latrobe VDC 40-43 Rc
Punch Material - Halcomb 218 (Tool Steel) 44 Rc
Die Coating - Colloidal Graphite in H_2O
Forging Temp. - 2000°F.
DynaPak Forged: 1 Blow at 900 PSI Fire Pressure
7" Total Stroke
Time From Furnace to Impact -- 9 Sec.
NOTE: Surface imperfections due to poor atmosphere control - To be corrected

654



1 1/2 diameter end mill in as extruded condition.

655



1 1/2 diameter end mill.
Material: Type-1 Tool Steel

PLASMA-ARC SPRAYING OF SPACE-AGE MATERIALS

Donald R. Mash
President and Technical Director
Advanced Materials and Processes, Inc.
Los Altos, California

ABSTRACT

Plasma-arc spraying is a versatile process which is only beginning to realize the potential predicted for it. Although current applications still largely involve refractory materials such as zirconia and tungsten used in liquid and solid fuel rocket motors, the technology is expanding rapidly to include other materials and other technical areas. Many problems inherent in the fabrication of refractory metals and compounds are being solved by means of plasma-spray techniques. This approach is expected to serve to an increasing extent in the fabrication of the refractory hard materials (carbides and borides) which are growing in importance for aerospace and other advanced applications.

Technology developed in connection with aerospace applications is already finding use in other areas. Techniques such as gradated coatings and plasma-forming are widely applicable.

Continued efforts to produce better equipment, to improve spray materials and techniques, to understand the effects of process variables, and to develop useful product specifications in certain areas of application will all contribute to the growth of this important fabrication process.

INTRODUCTION

Although serious application of the plasma-arc in materials technology is only a few years old, this technique may not generally be considered new any more. This is probably because plasma-spraying attracted attention and immediate recognition as an important metallurgical tool in connection with advanced missile and space projects. Early applications included zirconia coatings as thermal barriers as well as tungsten coatings and free-standing shapes for thermal shock and erosion-resistant rocket-nozzle liners. These still represent major production applications for plasma-spraying, indicating the very early stage of development of the plasma-arc as a general fabrication technique.

The plasma-arc is extremely versatile. Typical applications within the scope of materials technology are listed in Table I. There are, of course, numerous other real or suggested uses for this equipment in the general fields of science and engineering.

TABLE I

TYPICAL PLASMA-ARC APPLICATIONS IN MATERIALS TECHNOLOGY

Spraying	Spherodizing
Melting	Surface hardening
Welding	Deoxidation
Cutting	Crystal growing
Machining	Materials testing and evaluation

In many past discussions, unfortunately, real accomplishments of the process have not been distinguished from potential applications, leading to considerable confusion and, in some cases, disappointment. Happily, this type of presentation is disappearing, and the plasma-spray field in general has settled down to steady growth. To emphasize the broad potential for applying plasma-arc spraying techniques, Table II presents a compilation of materials and substrates which have been employed either in research or in production. Although not complete, this table indicates the possibilities available through use of plasma-arc techniques. By comparison, only a limited number of applications currently involve plasma-arc spraying on more than a trial basis. Some typical established applications for plasma-spraying are shown in Table III, a rather modest list when compared to the previous table. The conclusion is reached easily that plasma-arc technology, from a materials standpoint, is still young. Progress must be made in materials and equipment, in processing and evaluation methods, and in the development of suitable product specifications. A large portion of this work will be done by organizations conducting plasma-arc operations on a regular basis. However, close cooperation with equipment manufacturers and ultimate consumers is necessary to achieve the desired result.

THE PLASMA-ARC PROCESS

Advantages

Advantages of this process over previously available methods of spray deposition relate to the extremely high flame temperature of the plasma-arc as well as the ability to operate in inert atmospheres. From Table IV, comparing various heat sources,[1] it is clear that the plasma-arc is 2-4 times hotter than the nearest flame condition (oxy-acetylene). Advantages of the plasma-arc are summarized in Table V.

Process Description

The plasma-arc process has been described many times in the past and, therefore, will not be covered in detail in

POTENTIAL PLASMA-SPRAY APPLICATIONS SPRAY MATERIALS AND SUBSTRATES

Oxides	Nitrides Silicides & Sulfides	Carbides	Borides	Metals, Alloys	Cermets & Composites	Substrates
Al_2O_3	Si_3N_4	TiC	TiB	Cr, Fe	TiC Cr	Metals & alloys
CaO.				Co, Cu	TiB_2 + Ni	Ceramics
ZrO_2· MgO.	ZrN	B_4C	TiB_2	Ti	ZrB	Plastics
Y_2O_3				Th	Haynes LT	Steels
ZrO_2· SiO_2	TiN	WC	ZrB	W, Ta, Cb	Fe	Stainless steel
SiO_2				Mo, Nb, Re	Cr	Inconel
BeO	$MoSi_2$	TiC+B_4C	MoB	Ni, Monel	WC + Ni	Kovar
50% TiO_2+Al_2O_3				Cd	Al	Molybdenum
Al_2O_3+SiO_2	MoS_2	HfC	ZrB_2	Cr+Ni+B	Si	Aluminum
Mixed Oxides				Coast Metals,	Mo	Silicon
Cd_2O_3	$CrSi_2$	TaC	B + metal	Nos. 63,	40Co+ZrO	Magnesium
Oxide + metal			mixtures	54, 55, 56	WC+12%Co	Beryllium
mixtures	$TiSi_2$	ZrC		"Si"	40Ni+Al_2O_3	Copper
ThO_2, Y_2O_3				"B"	ZrO_2+40%Co	Zirconium
UO_2		Cr_3C_2	CrB	Sn	Al_2O_3+40%Ni	Graphite
HfO_2				Stainless	60CrC-Co	Oxides
MgO		CbC	CrB_2	Steels	Moly+Mn mix-	Hi-temp plastics
TiO_2				Stellite #1	tures	Fused silica

TABLE II (continued)

Oxides	Nitrides Silicides & Sulfides	Carbides	Borides	Metals, Alloys	Cermets & Composites	Substrates
R. E. oxides				Stellite #6	Kenface + 40%	
CeO_2				Misc. alloys	Colmonoy #6	
Porcelain powder				Colmonoy #6		
Glass (fixed m. p.)				Au, Ag		
$BaTiO_3$				Pt, Pd, Zn		
$MgO \cdot Al_2O_3$				Inconel		
				Al		
				Be		
				Zr		
				80Ni-20Cr		
				Brass, Bronze		
				Haynes alloys		
				Nicrobraze		
				Hastelloy C		

TABLE III

TYPICAL CURRENT APPLICATIONS
FOR PLASMA-SPRAYING

$MgO \cdot ZrO_2$ coatings on graphite melting crucibles
ZrO_2 coatings as thermal barriers for liquid rocket engines
Tungsten coatings on graphite for solid rocket nozzles, exit cones, etc.
Refractory metal coatings on refractory metal billets for mill processing
Tungsten free-standing shapes for melting crucibles
Spheroidizing materials such as UO_2, ZrO_2, WC, B_4C
X-ray targets
Experimental nuclear fuel elements and control rods (UO_2, B_4C)
Electrical contacts
Experimental rocket and missile parts, including plasma-formed tungsten, tungsten-coated graphite, and TaC-coated graphite
Miscellaneous industrial applications for protective coatings to resist wear, abrasion, and erosion (Al_2O_3, WC, Cermets)
Miscellaneous applications for thermal and for electrical insulation (ZrO_2, Al_2O_3, ThO_2, BeO)

TABLE IV

COMPARISON OF HIGH TEMPERATURE HEAT SOURCES[1]

Heat Source	Approximate Temperature °F	Gas Velocity F. P. S.	Atmosphere Control	Operating Pressure ATM	Maximum Gas Enthalpy Btu/lb	Maximum Heat Transfer Rate Btu/ft^{2}sec
Open flames, air and oxygen	3000-7500	1-600	O_2, C, H_2, present	1	4700 O_2 1300 Air	10 Air 700 oxygen
Enclosed flames, air and oxygen	3000-7500	1-9000	O_2, C, H_2	Vacuum-600	4700 O_2 1300 Air	100 Air 1400 Oxygen
Open arc, low intensity	6000-8500	1-30	Almost any gas depending on electrode choice	Vacuum-200	25,000 N_2 1,000 A	14,400
Open arc, high intensity	6000-10,000	1-100	"	Vacuum-200	30,000 N_2 8,000 A	14,400
Plasma Jet, arc contained within device	500-30,000	1-30,000	H_2, N_2, A, He, Air, etc.	Vacuum-200	130,000 H_2 15,000 N_2 8,000 A	6000
Plasma Jet, arc transferred to object receiving heat	6000-60,000	1-40,000	H_2, N_2, A, He, Air, etc.	Vacuum-200	200,000 H_2 30,000 N_2	29,000
Solar and arc image furnace	6500	0	Any gas	Vacuum-up	---	1000-1070
Adiabatic compressor	7000	Vacuum-100	---	Vacuum-up	2000 N_2	---
Pebble bed heaters	5000	---	Any gas	Vacuum-up	1500 N_2	140
Shock Tubes	15,000	0-30,000	Any gas	Vacuum-up	See Plasma Jet	5000

TABLE V

ADVANTAGES OF PLASMA-SPRAY PROCESS

Minimum heating of substrate (2-400°F usual range)

High deposition rates and efficiencies

Inert or reducing atmospheres can be used

Process is widely applicable due to high flame temperature and control of environment

Minimum porosity of deposits, especially if coupled with subsequent densification steps

High level of adherence, especially if care taken to control deposition conditions and to employ techniques such as gradation

Minimum contamination and, often, purification of some materials as-deposited in reducing or inert atmospheres

Broad range of deposit materials and substrates can be employed

this presentation. Equipment generally employed for spray applications is of the nontransferred arc type, using either argon or nitrogen as the primary gas. Hydrogen (up to 15% by volume) often is added to raise the arc voltage, improve heat transfer to particles, and provide reducing conditions for atmospheric protection. A number of 40 KW commercial units are available, each with individual design features. None are sufficiently versatile to meet the broad range of applications found in the laboratory although each can be optimized to perform well on a particular job. Both vortex and gas-sheath stabilized arc designs are suitable for individual applications and can produce deposits of excellent quality if conditions are properly adjusted. Limited electrode life continues to be the principal difficulty with current equipment, and this has a definite influence on the economics of the process. Also, miniaturization in current standard torch designs has been achieved at the expense of the rugged construction needed for constant usage on a broad range of applications. Better equipment at lower cost is definitely needed for both routine and research usage. Manufacturers and operators must work together to accomplish this end.

Proper selection of operating conditions for each application requires that the effect of process variables be understood. In this connection, the relationship between plasma enthalpy and temperature shown in Figure 1 must be appreciated. For efficient heat transfer from plasma to particle, it is clearly desirable to employ a diatomic gas. However, the importance of this relationship depends on design of a particular plasma-arc torch and upon the materials to be deposited. It is important that a plasma-arc torch be able to reach high enthalpy levels; therefore, the equipment must operate at sufficiently high power levels for a given arc gas flow range. Besides choice of plasma gas, other process variables exercise more or less of an effect on the deposition characteristics of materials. This subject has been covered to some extent in previous articles[2, 3] and will be discussed here only in connection with specific materials and applications.

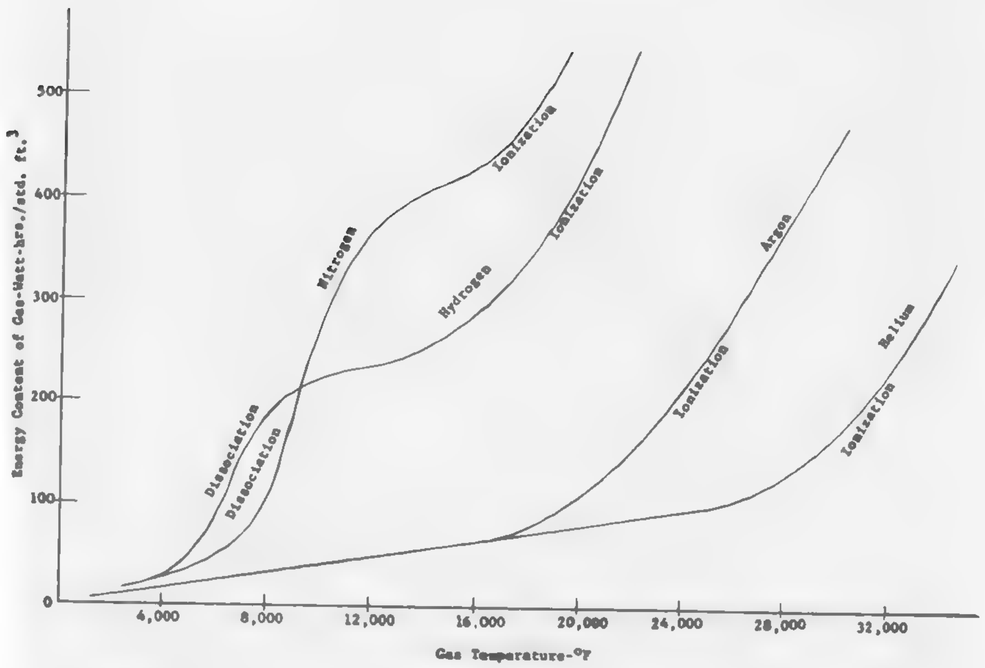


FIGURE 1 PLASMA TEMPERATURE AS A FUNCTION OF GAS ENERGY CONTENT AT ATMOSPHERIC PRESSURE

PLASMA-SPRAY APPLICATIONS AND MATERIALS

Space age materials include those with very high temperature capability such as refractory metals, oxides, carbides, borides, nitrides, and silicides. These offer attractive physical properties for missile and space component uses and, in general, can only be deposited satisfactorily by the plasma-arc technique. As indicated previously, major emphasis to date has been placed on the fabrication of such highly refractory materials for aerospace applications.

The balance of this paper will be devoted to an examination of current applications and of recent developments in technology from which future applications would be expected to arise.

The Effect of Environment

Since a very wide range of materials can be sprayed, the effect of environment must be understood to insure that the resulting deposit composition truly represents what was sprayed. Considerable data is available to show that the atmosphere must be carefully controlled in many cases. Some of this data is summarized in Table VI. Furthermore, Table VII shows that purification of tungsten is possible by employing a high purity argon atmosphere and a partial pressure of hydrogen in the plasma-gas.

Refractory Metals--Tungsten

The plasma-arc process represents a promising fabrication tool for forming intermediate and finished shapes from refractory metals and compounds. This is well supported and exemplified by the current status of tungsten plasma-spraying technology.

Tungsten is sprayed on graphite rocket nozzles as a coating for erosion resistance and is plasma-formed on a removable mandrel to produce free-standing melting crucibles, rocket nozzle liners, and tubes. As-sprayed densities of 95% theoretical are achieved with values as high as 99% reported after a subsequent heat treatment.

Graphite rocket nozzles are coated on the inside diameter with tungsten, with or without an undercoat of tantalum or rhenium to minimize a graphite-tungsten reaction at very high temperatures. Tungsten provides excellent protection from exhaust gases at high temperatures and pressures and maintains throat erosion within permissable limits.

Development of the plasma-arc spray process for the fabrication of free-standing tungsten shapes from laboratory scale to full-scale production has been described.[4] Tungsten cylinders and cones have been produced weighing over 100 pounds and over 1-inch thick. Decreased contamination and increased density was observed for tungsten deposits

TABLE VI

EFFECT OF ATMOSPHERE ON COMPOSITION OF VARIOUS PLASMA-SPRAYED DEPOSITS[3, 8]

Material	Post-spray Diffraction Pattern	As-received	Sprayed in Air	Impure Argon	High Purity Argon
TiC	TiC + Ti	20.7% C	14.1% C	17.8	20.5
WC	W + α W_2C				
TaC	TaC + Ta + Ta_2O_5	6.4% C	4.3		5.4
	TaC + Ta_2C				
CbC	CbC + Cb + CbO_2	11.2	4.9		9.5
ZrC	ZrC + ZrO_2 + Zr	13.0	6.6		10.2
Al_2O_3	γAl_2O_3 + αAl_2O_3				
TiO_2	TiO_2				
ZrO_2	ZrO_2				
UO_2		O/U = 1.95	2.34-2.41	2.05-2.08	1.93-1.98
HfC	Hf(CN) + HfO_2 + ZrO_2	6.0	4.5		5.6
4TaC:1HfC		6.3	4.1		5.3

Note: Plasma gas was Argon in each case.

TABLE VII

OXYGEN ANALYSIS OF SPRAYED TUNGSTEN[3]

As-Received powder	. 019% O_2
Sprayed with Argon plasma-gas	. 044%
Sprayed with 95% A + 5% H_2 plasma-gas	. 0078%

Notes: 1. Vacuum fusion analyses
2. Sprayed in Argon atmosphere chamber produced in an inert atmosphere chamber as compared to spraying in air. This is true for both free-standing shapes and for coatings.

The plasma-spray and sinter technique has been developed as a new, convenient method of fabricating tungsten shapes. The product is generally equivalent to commercial recrystallized material produced by cold pressing and sintering. The flexibility and low tooling cost associated with the plasma-spray approach looks attractive. The development of tungsten forgings using sprayed preforms, appears promising and offers potential advantages of increased strength and toughness. Table VIII presents some typical properties of plasma-sprayed tungsten.

The plasma-spray and sinter technique offers several advantages, including (1) no size limitation, (2) simple tooling, (3) consistency of properties in each piece from mid-radius to edge, and (4) flexibility of contour design.

Such techniques are applicable to a number of space age materials and must be considered because conventional forming techniques often cannot handle these hard, strong, heat-resistant metals and compounds. Often advanced compositions require entirely different ideas in fabrication. Where a new approach is needed, plasma-spraying may be a solution.

TABLE VIII

SOME TYPICAL PROPERTIES OF PLASMA-SPRAYED TUNGSTEN

	Cold Pressed and Sintered*	As-Sprayed	As-Sprayed and Sintered	As-Sprayed, Sintered and Forged
Density	93%	85-95%	92-98%**	97%
Ultimate tensile strength, psi	60,000	22,000	72,000	115,000
Modulus of rupture, psi	300	250	320	400
Hardness, DPH		44,000	57,000	
Young's modulus, psi		22×10^6	34×10^6	
Structure	Equiaxed fine grain	Lamellar	Equiaxed very fine grain	Elongated very fine grain

* Shown for comparison purposes.
** 2 hours at 1400°C.

Process Variables--Tungsten

High deposition efficiency and density can be achieved only with complete particle melting. For a given material and particle size range, therefore, it is worthwhile to examine these deposition characteristics as a function of plasma enthalpy, since this factor determines complete particle melting. Power input and arc-gas flow rate, in turn, determine enthalpy. In addition, arc-gas flow rate influences deposition efficiency by fixing particle residence time in the plasma jet and contributes to density as a result of the impact velocity imparted to the injected particles. Such effects can be separated to some extent by comparing deposition characteristics as a function of arc-gas flow rate at constant enthalpy. Optimum process parameters are established when both density and deposition efficiency are maximized.

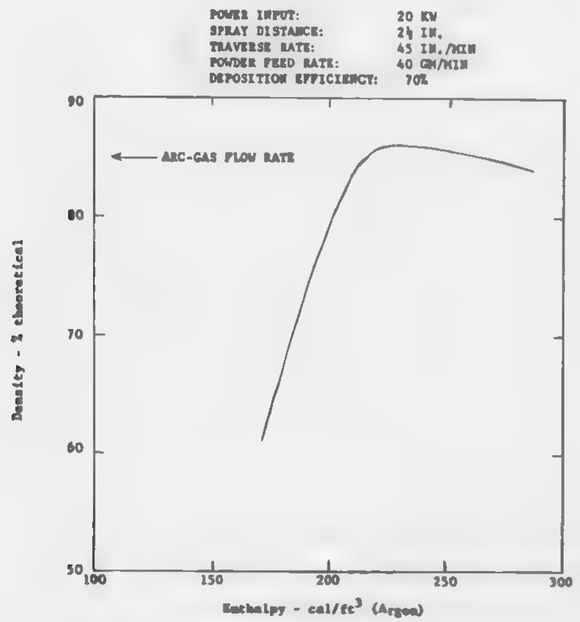


FIGURE 2 EFFECT OF PLASMA ENTHALPY AT CONSTANT POWER INPUT ON THE DENSITY OF PLASMA-SPRAYED TUNGSTEN (3)

Figure 2 presents density-versus-enthalpy data for plasma-sprayed tungsten in which the effect of adequate particle melting and the supplementary influence of particle velocity are combined. This latter effect can be separated,

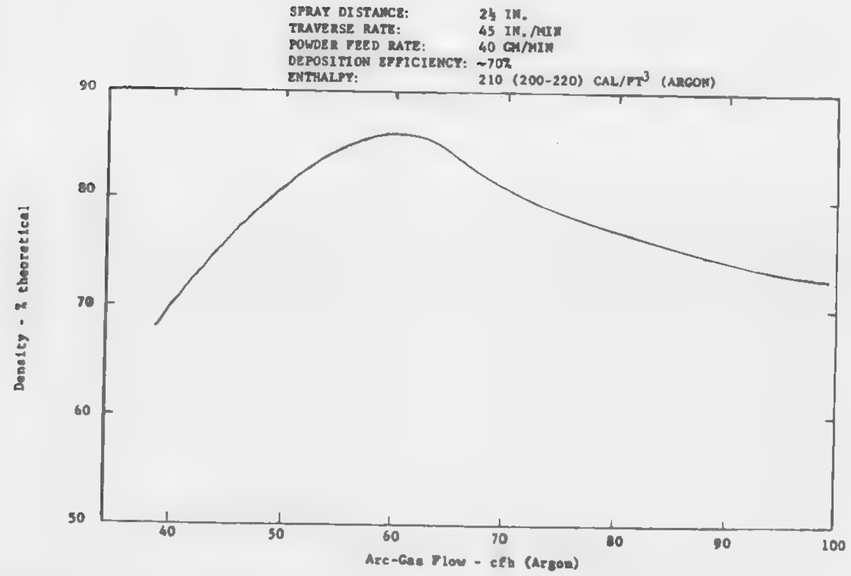
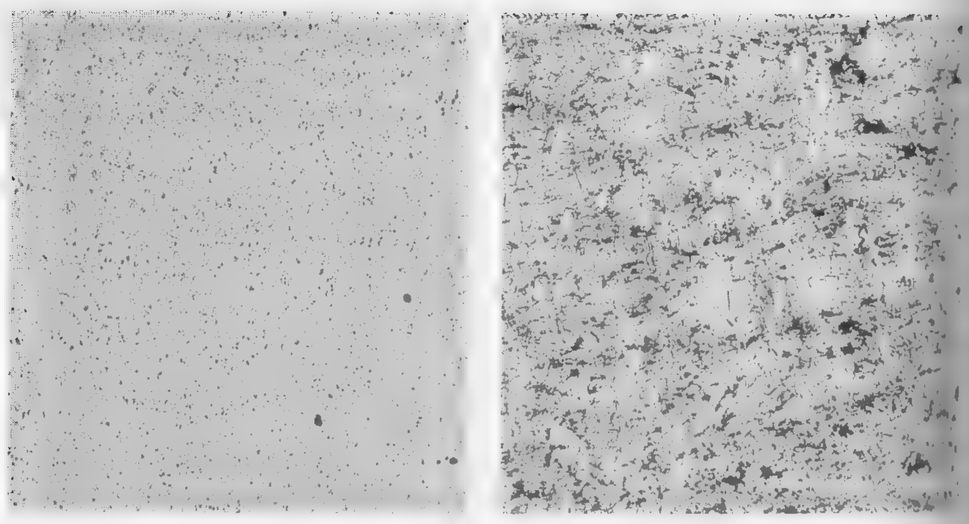


FIGURE 3 EFFECT OF ARGON ARC-GAS FLOW AT CONSTANT PLASMA ENTHALPY ON THE DENSITY OF PLASMA-SPRAYED TUNGSTEN (3)

as shown in Figure 3 where density is plotted against arc-gas flow at constant enthalpy. Maximum density of about 85% of theoretical was achieved using argon arc-gas. Addition of about 5% hydrogen to the arc-gas resulted in densities of greater than 90% of theoretical density, chiefly as a result of improved heat-transfer properties of the mixed plasma. Density increased somewhat with decreasing particle size. Interlayer porosity is almost eliminated and density increased to over 90% by using hydrogen additions to the argon arc-gas or by subsequent hot rolling.

Single-layer tungsten bars 8" x .700" x .080" have been sprayed with densities of greater than 90% of theoretical.[5] Densities as high as 97% were obtained; however, the density was normally about 92-93%. This was accomplished by spraying -325 mesh tungsten powder using 95Argon-5H_2 arc gas. A slow traverse rate was used, and the graphite mold was oscillated beneath the torch. Power input of 30-35 KW was used at a spray distance of 2-1/2 inches without cover gas. Typical photomicrographs of as-sprayed tungsten are shown in Figure 4. The pores are on a very fine scale and are not interconnected providing a vacuum tight material even in the as-sprayed condition.



(A) As-polished (B) Etched in NH_4OH-H_2O_2 Reagent

FIGURE 4 MICROSTRUCTURE OF PLASMA-SPRAYED TUNGSTEN

Oxides

Zirconia and alumina are, by far, the most widely used oxide protective coatings for thermal and electrical insulation and, in the latter case, for wear resistance. Current plasma-spray applications follow directly from conventional use of these materials as the main workhorse ceramics of the oxygen-fuel gas flame-spray field. Applications requiring higher density and adherence than previously available require the plasma process to replace earlier methods.

Extensive use has been made of ZrO_2 as the thermal barrier coating in rocket engines. Densities of 85-90% are easily obtained under spray conditions which are not too critical.

Although still in the experimental stage, plasma-sprayed UO_2 fuel elements are attractive and have been investigated rather extensively. Arc-fused uranium dioxide powder has been used throughout most of the investigation. Coatings have been made on 304 stainless steel and on Zircaloy-2 substrates. Substrate thicknesses as low as 0.020 inch have been sprayed with coatings up to 0.100 thick.

Uranium dioxide is sprayed in a vacuum-purged inert-atmosphere chamber under argon. This procedure is necessary to prevent oxidation to U_3O_8 or an intermediate oxide (see Table VI).

Densities as high as 90-91% theoretical (10.98 gm/cc) have been obtained. Variables studied include power input, spray distance, the use of cover gas, arc-gas flow, powder type, and powder size. Increasing power input and decreasing spray distance resulted in improved coating densities but increased the tendency for cracking and spalling of the coatings. Cracking and spalling were reduced or eliminated by use of helium cover gas to provide surface cooling.

The influence of arc-gas flow rate on coating density at constant enthalpy is shown to be very significant. Maximum densities of 88 to over 90% theoretical, depending on spray distance, were observed at values of about 75 cfh argon. Deposition efficiencies were maximized at about 60 cfh argon, and somewhat lower enthalpy values achieved (Figure 5) indicated the need for close particle-size control to establish optimum parameters.

Fused UO_2 powder produced coatings of higher density than did sintered powders. This is due primarily to the fact that the fused particles are nearly 100% of theoretical density, while the sintered particles contain a considerable amount of porosity. Similar effects were noted previously when spraying fused and sintered zirconia powders.

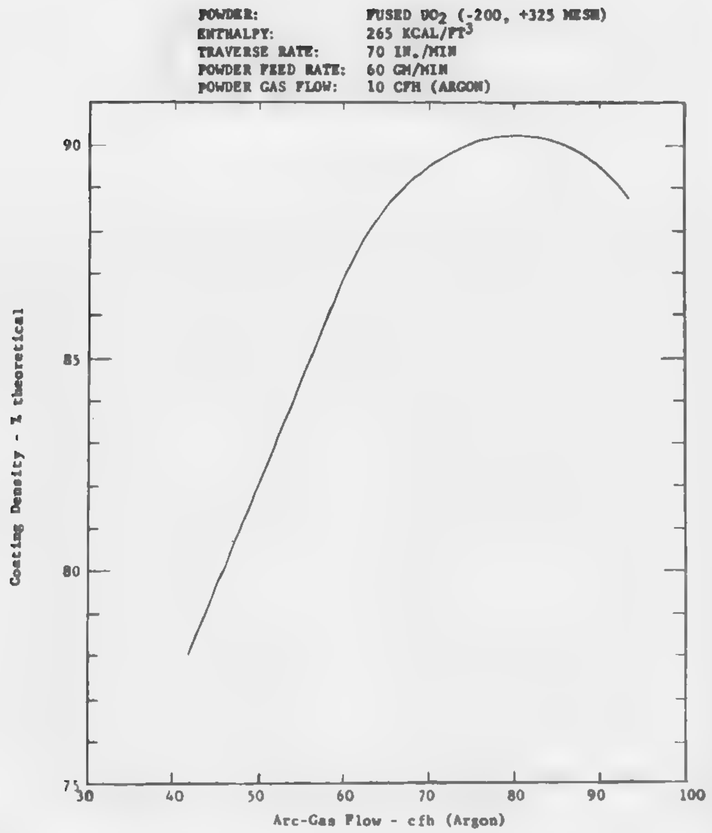


FIGURE 5 EFFECT OF ARC-GAS FLOW ON THE COATING DENSITY OF URANIUM DIOXIDE AT CONSTANT PLASMA ENTHALPY [3]

Powder particle size is more critical when spraying uranium dioxide than zirconia. The best results have been obtained using -200, +250 mesh powder.

A major advantage of a sprayed fuel element is an integral bond between the fuel and the cladding. Adherence of sprayed UO_2 fuel is, therefore, of prime importance. Coating adherence has been found to be a function of substrate type, surface preparation, thermal history during spraying, geometry of the spray pattern, and coating thickness.

More adherent coatings are produced on Zircaloy-2 substrates than on stainless steel because slightly rougher surfaces are produced on Zircaloy under identical grit-

blasting conditions and because Zircaloy possesses a thermal expansion coefficient about 40% of that for stainless steel.

To date, substrate surfaces have been prepared by grit blasting to provide a strong mechanical bond. On thin substrates, this is followed by straightening and annealing. Silicon carbide, sand, garnet, and iron-blasting media have been tried. Of these, sand is the least desirable. Although the remaining three media provide an adequate surface, silicon carbide is preferred since it provides the cleanest surface for spraying. Bend tests have been made of coatings sprayed on 0.030-inch thick substrates. Figure 6 shows four



(A) (B) (C) (D)

FIGURE 6 BEND-TESTED COUPONS OF URANIUM DIOXIDE ON STAINLESS STEEL SUBSTRATES PRESSURE-BLASTED WITH: (A) IRON, (B) GARNET (C) SiC, (D) SAND (THICKNESS OF COATING IS 0.050 IN. ON 0.030 IN. THICK SUBSTRATE)

specimens bent around a 1-inch radius. Even though cracks occurred during bending, the coatings remained adherent in all cases, except for surfaces blasted with sand.

The effect of thermal history on the distortion resulting from spraying and on coating adherence has been studied. Conclusions of this study were:

1. Substrate temperatures must be kept below 500°C, while the coating must be maintained at a temperature below 870°C. Helium cover gas can be used to provide the required degree of temperature control.

2. The substrate must be in the fully annealed condition prior to spraying.

3. At spray distances below 4 inches, without the use of cover gas, traverse rates of 71 in./min or higher must be used at power levels of 22-25 KW and arc-gas flow rates of 55-75 cfh argon.

Coating thickness also influences adherence, since increasing coating thickness results in increased residual stresses at the interface. Coating thicknesses up to 0.050-0.060 inch are very adherent. However, coatings about 0.100-inch thick are less adherent and will not accept a severe bend such as that shown in Figure 6.

Plasma-sprayed coatings for high temperature extrusion dies have been given attention,[6] and this application appears to be firm enough to merit mention. Dies coated with aluminum oxide are reported to extend the practical extrusion temperature range to 3200°F and use of ZrO_2 facings extends it to at least 4150°F. In addition to improved die life and a marked increase in the practical extrusion temperature range, use of ceramic-faced dies results in a general reduction of extrusion pressures. Plasma-sprayed ZrO_2 shows superior bond strength and density for this application although somewhat more costly than flame-sprayed methods. However, because of the greater range of

materials which can be handled, plasma-spray methods are definitely promising for improved coatings for extrusion dies and other high temperature wear and oxidation problems.

Gradated Coatings

A useful technique which has been employed to some extent in connection with several programs involves a gradation from substrate to surface coating to produce greater compatibility between materials of different thermal expansion characteristics. In this manner, thermal shock resistance and adherence of coatings are improved. Gradation may be affected in step-wise or continuous manner depending on materials, equipment available, and the ultimate application. Feed rates and/or mixtures must be selected on the basis of experimental data since it has been determined that composition of the "as-sprayed" composite material differs greatly from that of the pre-mixed powder feed due to differences in density and thermal properties. Table IX shows the results of typical runs of pre-mixed cermets. Gradated coatings have been under investigation for the X-15 liquid rocket thrust chamber[7] since zirconia applied as an erosion and heat barrier developed failures after several firings.

Refractory Hard Materials--Borides and Carbides

The great potential for applying borides and carbides in military and industrial equipment can not be realized unless unique methods of production and fabrication are developed. For many applications, the plasma-jet offers attractive possibilities. Although not established as a production process as yet, this approach is now being explored, and it is safe to say that use of the plasma-spray technique will grow with the growing application of these relatively new materials. Table X lists some of the properties and suggested applications for typical borides and carbides. As a group, both borides and carbides possess high hardness, oxidation and corrosion resistance, high melting points, wear, abrasion, and thermal shock resistance. In addition, several borides are not wet by non-ferrous liquid metals. Aerospace

TABLE IX

ANALYSIS OF "AS-MIXED" AND "AS-SPRAYED" GRADATED COATINGS[7]

Powder Mixture Analysis		Sprayed Deposit Analysis	
Nichrome V	Zirconia	Nichrome V	Zirconia
73.7	26.3	90	10
60	40	75	25
48	52	70	30
Nickel	**Alumina**	**Nickel**	**Alumina**
61	39	77.5	22.5
47	53	51	49
17.5	82.5	48.5	51.5

Table X

TYPICAL PROPERTIES AND APPLICATIONS FOR CARBIDES AND BORIDES

Materials	Density (g/cc)	Thermal Conductivity (cal/cm sec °C)	Knoop (100g) Hardness (Kg/mm^2)	Melting Point °C (°F)	Some Suggested Uses
TiB_2	4.40	0.0624	3400	2900 (5232)	Cathodes in Al reduction cells Catalyst for hydrocarbon synthesis
CrB_2	5.60	--	1800	1850 (3262)	
ZrB_2	6.10	0.0550	1750	3040 (5500)	Molten metal containers Jet and rocket engine liners
MoB_2	7.80		1280	2100 (3810)	Brazing alloy for refractory metals
CbB_2	7.20	0.0400	2595	2900 (5250)	
TaB_2	12.60	0.0260	2537	3000 (5430)	
TiC	4.25	0.0410	3200	2700 (4892)	Cutting tools Arc welding electrodes Gas turbine blades Liquid metal pump components High temperature bearings
Cr_3C_2	6.68		1300	1895 (3440)	Turbine blade coatings Die-casting machines Hot extrusion dies
TaC	14.48	0.0530	1800	3875 (7007)	Rocket nozzle liner coatings Filaments Cutting tools
HfC	12.20			3887 (7030)	Nuclear reactor control rods
CbC	7.82	0.0340	2400	3500 (6332)	
ZrC	6.70	0.0490		3530 (6386)	Refractory coatings for rocket and missile parts

and many other advanced applications will require such interesting materials.

Other Plasma Processes

In addition to spraying, several other metallurgical uses are being developed for the plasma-arc using the transferred arc design. Plasma-arc welding has several useful features, including ability to make butt joints in thick materials without edge preparation, high depth-to-width ratio in weld zones, and uniformity of penetration. Weld surfacing with powder additions is also feasible, and any alloy powder compatible with the base metal can be applied. A low velocity, ultra-high enthalpy plasma with very low gas flows and a 10-20 inch flame is used for particle spheroidizing.

Machining and cutting also have been developed to some extent. Most of these transferred arc-techniques are currently under development and should find uses for special applications.

BIBLIOGRAPHY

1. Thorpe, M. L., "The Plasma-Jet and Its Uses," Research/Development, January 1960.

2. Mash, D. R., N. E. Weare, and D. L. Walker, "Process Variables in Plasma-Jet Spraying," Journal of Metals, V. 13, No. 7, July 1961.

3. Mash, D. R., "Refractory Coatings Research," Fifth Meeting of the Refractory Composites Working Group, August 8-10, 1961, Dallas, Texas.

4. Singleton, R. H., E. L. Bolin, and F. W. Carl, "Tungsten Fabrication by Arc Spraying," Journal of Metals, V. 13, No. 7, July 1961.

5. Weare, N. E., private communication, December 1961.

6. Harvey Engineering Laboratories, "Activities in the High Temperature Inorganic Refractory Coatings Field," HA-1755, presented at Refractory Composites Working Group Meeting, Dallas, Texas, August 8-10, 1961.

7. Unger, R., "Arc Sprayed Gradated Coatings," presented at the National Meeting S. A. M. P. E., November 14-15, 1961, Dayton, Ohio.

8. Bennett, P. L., "Plasma-Spray Program," presented at Fourth Refractory Coating Meeting, November 15-17, 1960, Cincinnati, Ohio.

HEAT TREATMENT OF SPACE AGE MATERIALS

Cecil C. Lacy and Leopold Albertin
Manufacturing Development Section
Aero-Space Division
The Boeing Company
Seattle, Washington

ABSTRACT

Boeing uses new heat treat techniques to fabricate super alloys and refractory alloys for application. Cleaning processes prior to heat treatment, heat treat cycles used and their effect on welding, age cracking, recrystallization, contamination and final mechanical properties are discussed. Special furnaces as well as other auxiliary heat treat facilities are described.

INTRODUCTION

In designing winged re-entry vehicles, engineers are faced with the difficult task of selecting materials suitable for the environments of space and re-entry, and of overcoming fabrication problems associated with these materials. The principle characteristics of metals, which ensure their extensive use as structural materials in space application, are: (1) a favorable strength-to-weight ratio (particularly at elevated temperatures), (2) an ability to sustain high temperature stresses with a high degree of reliability, and (3) a relative ease of fabrication of most shapes and sizes desired.

The strength-to-weight-versus-temperature properties of metals and alloys are constantly being improved to meet engineering requirements. These properties become particularly significant in space structural considerations when

one realizes that approximately 100 pounds of propellant are required to get each pound of payload into orbit.

On the basis of strength-to-weight-versus-temperature data, super alloys are the best choice in the temperature range of 1000-1800°F. Super alloys have adequate oxidation resistance up to 1800°F. Refractory alloys operating in their effective temperature range of 1800-3000°F require an oxidation resistant coating system to prevent catastrophic oxidation.

At present, molybdenum and columbium alloys such as Mo-0.5% Ti and Fansteel 82 are being considered for application where temperatures exceeding 1800°F are expected. Structures subjected to more moderate temperatures are fabricated from such nickel and cobalt base alloys as Rene' 41 and H.S. 25. However, with the advancement of metal technology, particularly in the field of refractory alloys, this material selection is by no means final.

The advent of a whole new family of space age materials, coupled with the need for thin gages and close tolerances, has markedly affected heat treat techniques and their applications. Some of these techniques, as practiced at Boeing, are discussed below. They include solution annealing and aging Rene' 41 structures as well as stress relieving and coating of Mo-0.5% Ti and columbium alloy F.S. 82.

CLEANING PARTS PRIOR TO HEAT TREATING

Clean surfaces are an important requirement when heat treating space materials. There are two important steps in the preparation of a metal surface for heat treating. One is the removal of organic substances such as oil and grease; the other is the removal of metal particles embedded by the tooling dies.

With the wider use of heat resistant materials, special cleaning and surface conversion methods have been used. Figure 1 summarizes the cleaning schedules used at Boeing

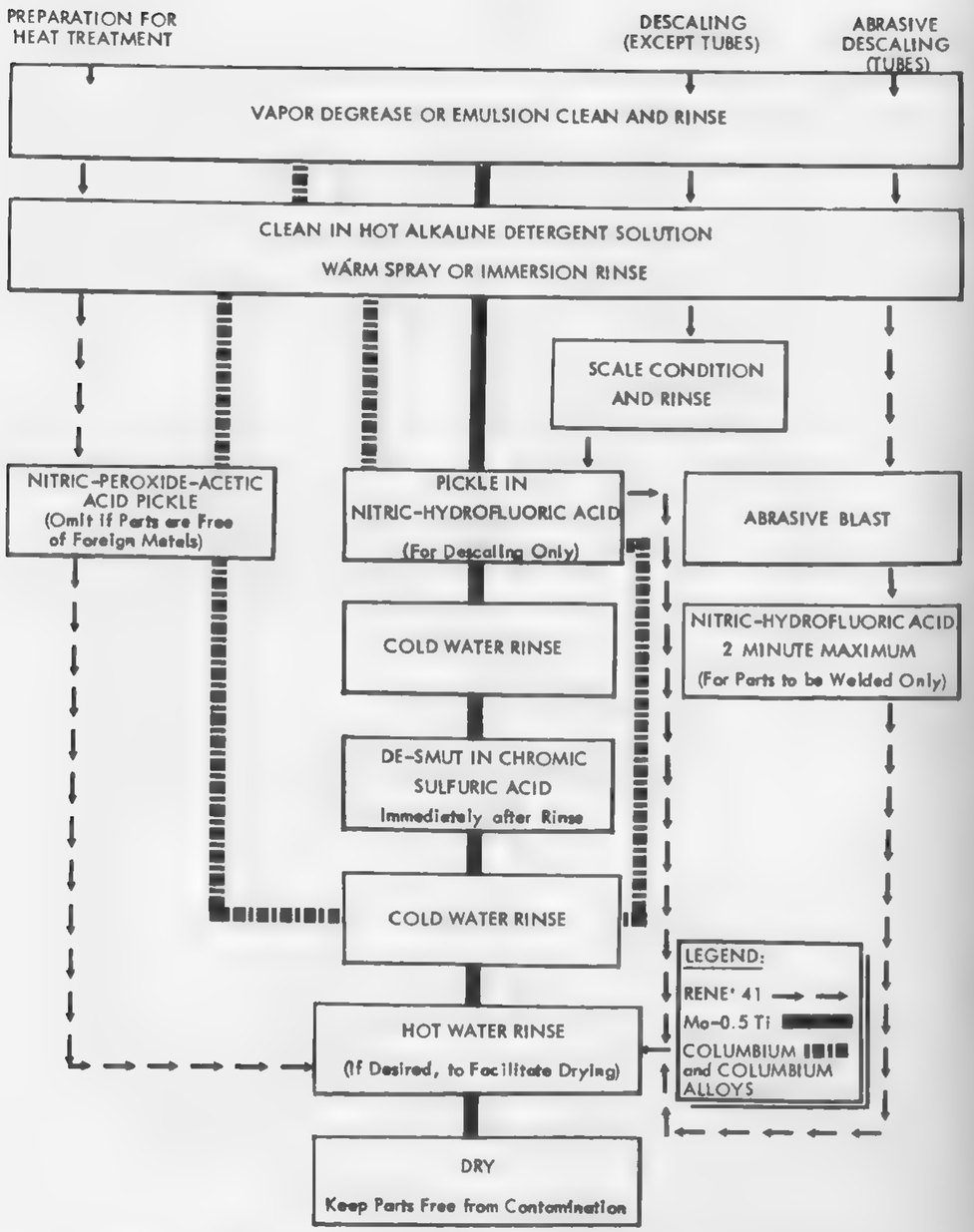


FIGURE 1 SUMMARY OF CLEANING SCHEDULES FOR RENE' 41, Mo-0.5% Ti AND COLUMBIUM ALLOYS

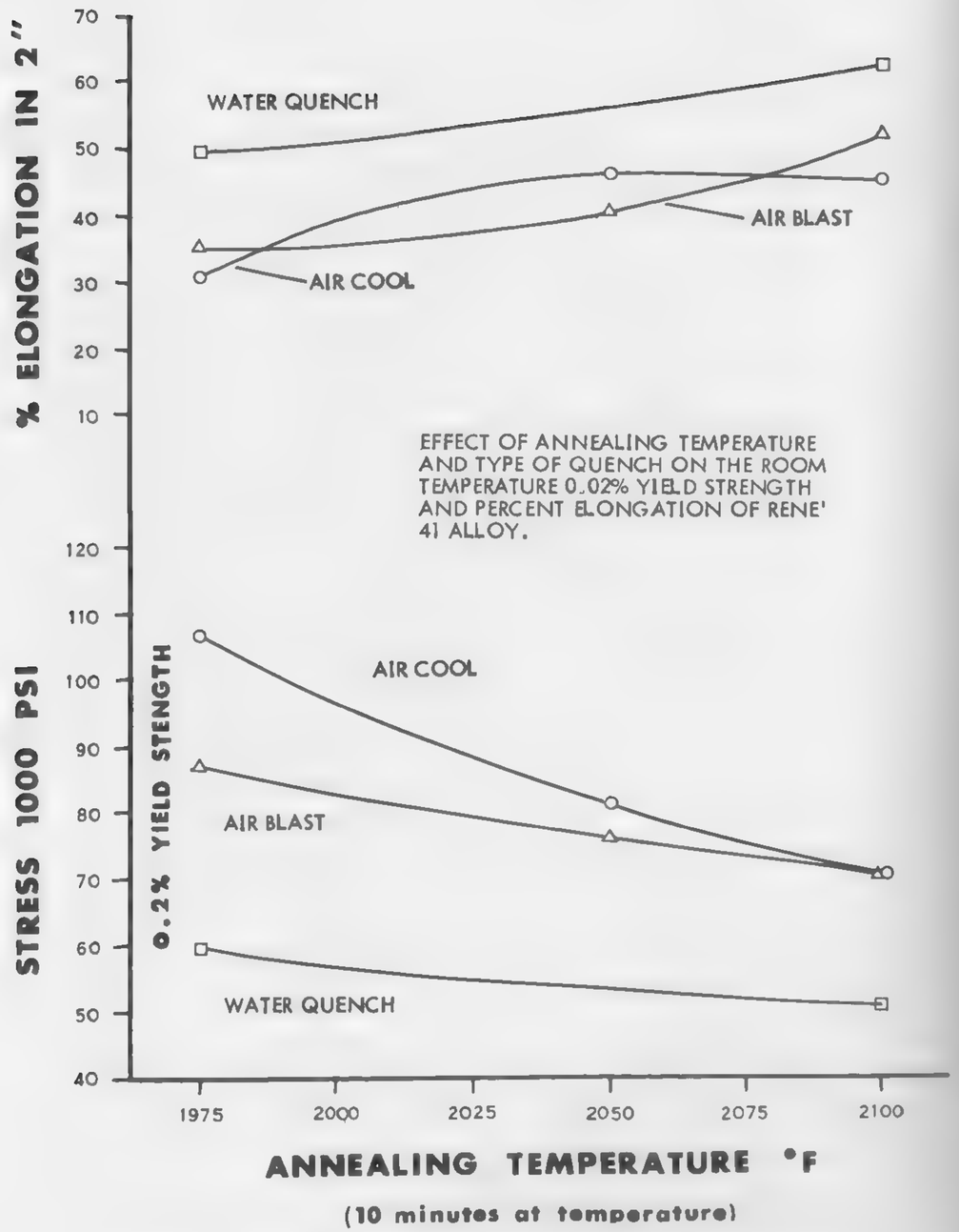
in preparing Rene' 41, molybdenum, and columbium for thermal treatments. A major problem in the cleaning technology of these new materials is to determine the minimum degree of cleanliness necessary, and then to devise quality control methods which will effectively ensure that this standard is met.

SELECTION OF HEAT TREAT PROCESSES TO MEET RENE' 41 FABRICATION REQUIREMENTS

It is generally accepted that the high strength of nickel-base alloys is related to a precipitation reaction which occurs during aging at temperatures above 1200°F, and which produces a fine dispersion of precipitate particles throughout the alloys. One of the newer production alloys of this type is Rene' 41. Rene' 41 derives its high temperature properties mainly from the precipitation of the intermetallic gamma-prime phase which is structurally similar to the Ni_3Al phase of the nickel-aluminum system. Gamma-prime precipitates very rapidly; a water quench is necessary to retain it in solution, thus preserving ductility for forming operations. Quenching is generally carried out from temperatures above 1950°F where gamma-prime is completely in solution.

Two other phase reactions are of great importance in the heat treatment of Rene' 41. These involve the carbides, $M_{23}C_6$ and M_6C. Investigations conducted by W. H. Chang[1] and H. J. Beattie[2] have shown that the M_6C carbide normally found in Rene' 41 will go into solution at 2150°F and will precipitate as a continuous grain boundary film of $M_{23}C_6$ at temperatures between 1300° and 1800°F.

Effects of the annealing temperature and quench rate on ductility and yield strength are shown in Figure 2. This figure illustrates that higher solution temperatures and faster quench yield more favorable properties for forming. However, exposure to temperatures at which the carbides dissolve promotes formation of brittle grain boundary films, with a resulting loss of weldability and ductility.



EFFECT OF ANNEALING TEMPERATURE AND TYPE OF QUENCH ON THE ROOM TEMPERATURE 0.02% YIELD STRENGTH AND PERCENT ELONGATION OF RENE' 41 ALLOY.

FIGURE 2 EFFECT OF ANNEALING TEMPERATURE AND QUENCH RATE ON DUCTILITY AND YIELD STRENGTH

The solution-treated structure of Rene' 41 is very important from the welding standpoint. Experience in welding tubular components, solution annealed at 2100°F, has shown that cracking is often a serious problem, even though the high temperature annealing is followed by a solution heat treatment at 1975°F prior to welding. Solution treating at 1975°F after a 2100°F anneal precipitates M_6C instead of $M_{23}C_6$. However, this carbide appears along grain boundaries, resulting in cracking when the alloy is welded and subsequently aged.

Beattie's work[2] has shown that the M_6C carbides begin to dissolve between 2025° and 2100°F. Consequently, the solution annealing temperature at Boeing has been established at 2025 ±25°F instead of 2100°F. In addition, a modified aging cycle has been developed to overcome the dilemma of cracking in welding components without adversely affecting mechanical properties. Various aging tests were conducted on tensile and plug-weld restraint specimens in the temperature range of 1400-1650°F to determine the aging temperature which eliminated cracking, yet retained mechanical properties. Welding and aging were performed on material solution-treated at 1975°F. The results are shown in Table I and Figure 3. Several microcracks were observed in welded and aged specimens which were aged at temperatures ranging from 1400-1550°F. Cracking was not observed in the specimens that were single-aged at 1600° and 1650°F, or aged at 1650°F for one or two hours followed by a ten hour aging cycle at 1400°F. The mechanical properties obtained by the latter treatment are slightly less than those obtained by the standard 1400°F, aging cycle. However, cracking is eliminated by such treatment.

From these welding and aging experiments a modified heat treatment for welded components has evolved in which such components are first aged for one hour at 1650°F, then for ten hours at 1400°F. Parts subjected to mild forming, and which are not welded, are aged for 16 hours at 1400°F.

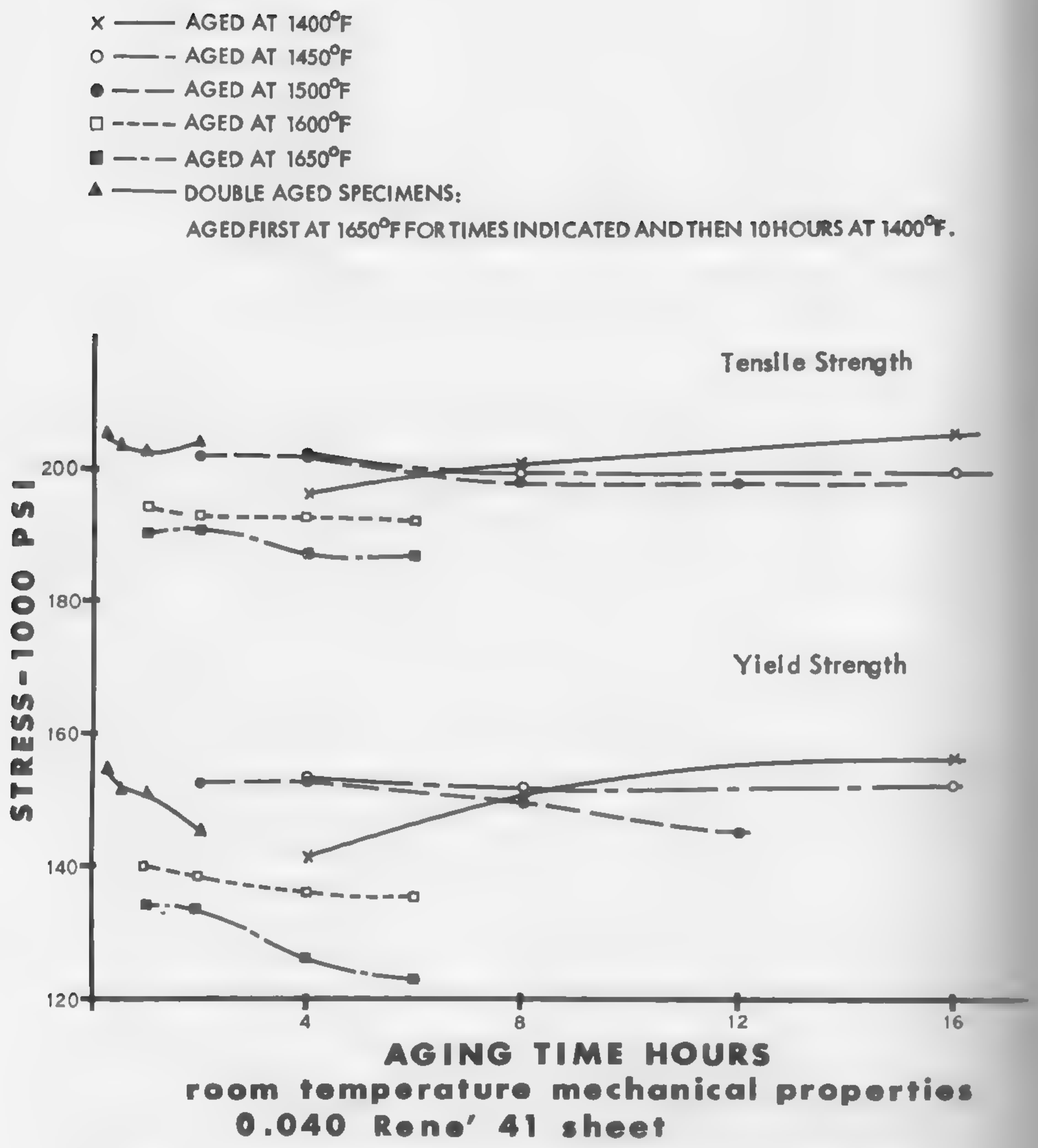


FIGURE 3 TENSILE AND YIELD STRENGTH VS AGING TIME AND TEMPERATURES

TABLE I

INFLUENCE OF AGING VARIABLES UPON STRAIN AGE CRACKING TENDENCIES IN MANUAL TIG FUSION WELDED RENE' 41 FORGED BAR

Aging Time (hours)	Aging Temperature (°F)	Results of Metallographic Inspection
4, 8, 16	1400	Microcracks, weld cracks
4, 8, 16	1450	Microcracks, weld cracks
4, 8, 16	1500	Microcracks, weld cracks
4, 8, 16	1550	Microcracks, weld cracks
4, 8, 16	1600	No cracks
4, 8, 16	1650	No cracks
1, 2	1650 (plus 10 hours at 1400)	No cracks

SHRINKAGE OF RENE' 41 DURING AGING

For design purposes a moderate contraction of components must be taken into consideration. Aging studies at Boeing have shown that an average contraction of 0.0013 inches per inch can be expected after an aging cycle of 1400°F for 16 hours or for an aging treatment of one hour at 1650°F, followed by ten hours at 1400°F. This average contraction value reflects measurements on both longitudinal and transverse specimens, three heats of Rene' 41, and the following conditioning treatments prior to aging:

1. Solution treated at 1975°F
2. Solution treated at 1975°F, annealed at 2025°F, re-solutioned at 1975°F.

Dilatometric measurements indicate that contraction is essentially complete within six hours after the aging temperature is reached.

INCOMING MATERIAL AND QUALITY CONTROL

The quality control of purchased Rene' 41 material is of great importance in ensuring final mechanical properties after all fabrication steps are completed. Sheet, strip, or bar material, generally purchased from the mill in Condition IB or IIB, is mill annealed at 1975°F and water quenched or is mill annealed and aged at 1400°F for 16 hours respectively. The mechanical properties of both conditions are specified in Table II. Bar stock is purchased in the IB condition without specifying the mechanical properties. However, the vendor must certify that mechanical properties after aging are met as shown in Table II for Condition IIB material.

Tubing is generally purchased in one of the following types: (1) type A, welded and solution treated; (2) type B, welded, cold drawn, and solution treated; (3) type C, seamless, and solution treated. The tensile properties of tubing as supplied must conform to the following properties as shown in Table III. The specified tubes must meet the same tensile properties after aging at 1400°F for 16 hours as those shown in Table II for Condition IIB material.

DIFFERENT HEAT TREAT METHODS EMPLOYED FOR SPECIFIC RENE' 41 COMPONENTS

The Rene' 41 components consist of sheet structures such as panels, tubular components, and fittings.

Sheet structures experiencing moderate cold working are generally spot welded and double aged in air furnaces without a prior re-solution treatment. Although desirable, re-solutioning introduces damaging distortion effects which are more detrimental to the structure than any benefits obtained by it. Air atmosphere is used during aging to provide a tight, adherent, dark scale which is useful for emissivity purposes in actual flight conditions. Sheet structures are freely suspended from heat treat fixtures to ensure uniform heating and cooling. Very little warpage occurs

TABLE II

SPECIFIED MECHANICAL PROPERTIES FOR RENE' 41 SHEET AND BAR STOCK

Condition	Test Temp. (°F)	Ultimate Strength (KSI) 0.020" gage & above	Ultimate Strength (KSI) below 0.020" gage	Ultimate Strength (KSI) bar	Yield Strength 0.2% Offset (KSI) 0.020" gage & above	Yield Strength 0.2% Offset (KSI) below 0.020" gage	Yield Strength 0.2% Offset (KSI) bar	% Elongation (In 2 Inches) 0.020" gage & above	% Elongation (In 2 Inches) below 0.020" gage	% Elongation (In 2 Inches) bar
IB	R. T.				100 max	100 max		30	30	
IIB	R. T.	180	180	180	135	135	140	12	10	10
IIB	1400	140	140	135	110	110	110	3	3	3

TABLE III

TENSILE PROPERTIES OF TUBING

Ultimate Strength (KSI)	Yield Strength 0.2% Offset (KSI)	% Elongation (In 2 Inches)
Not specified	100 max	30 min

during aging. A typical sheet structure suspended from a heat treat fixture is shown in Figure 4.

In fabricating tubular components which are reduced at the ends by swaging, multiple annealing is frequently required to remove cold work. Annealing is carried out in a specially designed swing tube furnace (Figure 5). The swing furnace has a three zone control, low voltage element system capable of continuous operation up to 2200°F. Six Inconel elements form a 15-inch diameter, 11-foot long vertical heating chamber. The chamber, insulated with Fiberfrax, is enclosed in an air-tight, water-cooled jacket. An inert atmosphere within the furnace is provided by a variable flow, argon gas system. The design also includes a mechanical system for remote controlled loading and quenching. Tubes are annealed in an argon atmosphere having an oxygen content of not more than 400 parts per million, and a dew point of not higher than -5°F. The annealing temperature is held just below the carbide solubility temperature (2025 ± 25°F) for 5 minutes. The tubes are then quenched in water in less than 3 seconds. The total intergranular attack on the material after three interstage anneals is generally less than 0.3 mil.

Aging of tubular components is carried out in an air-atmosphere furnace.

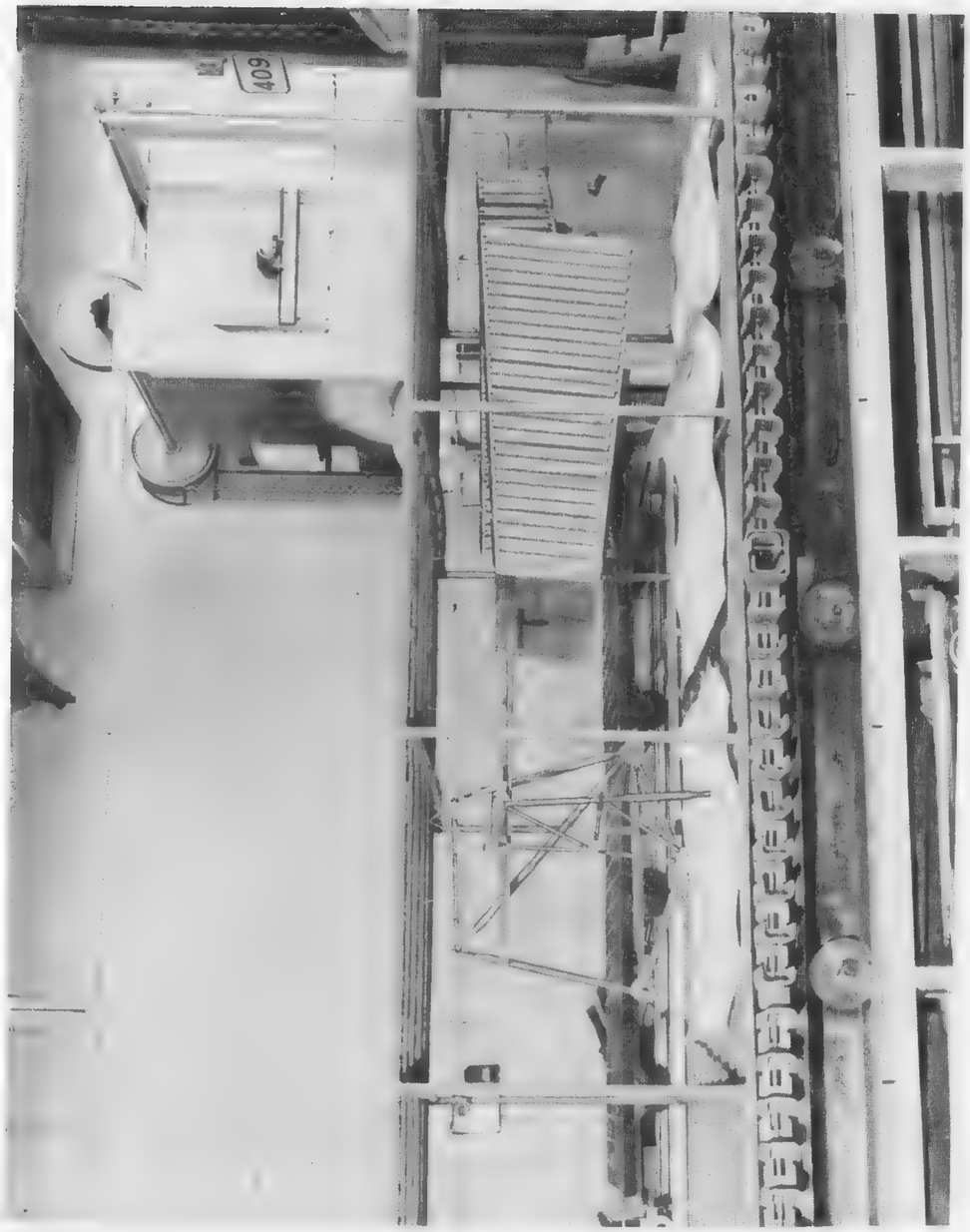
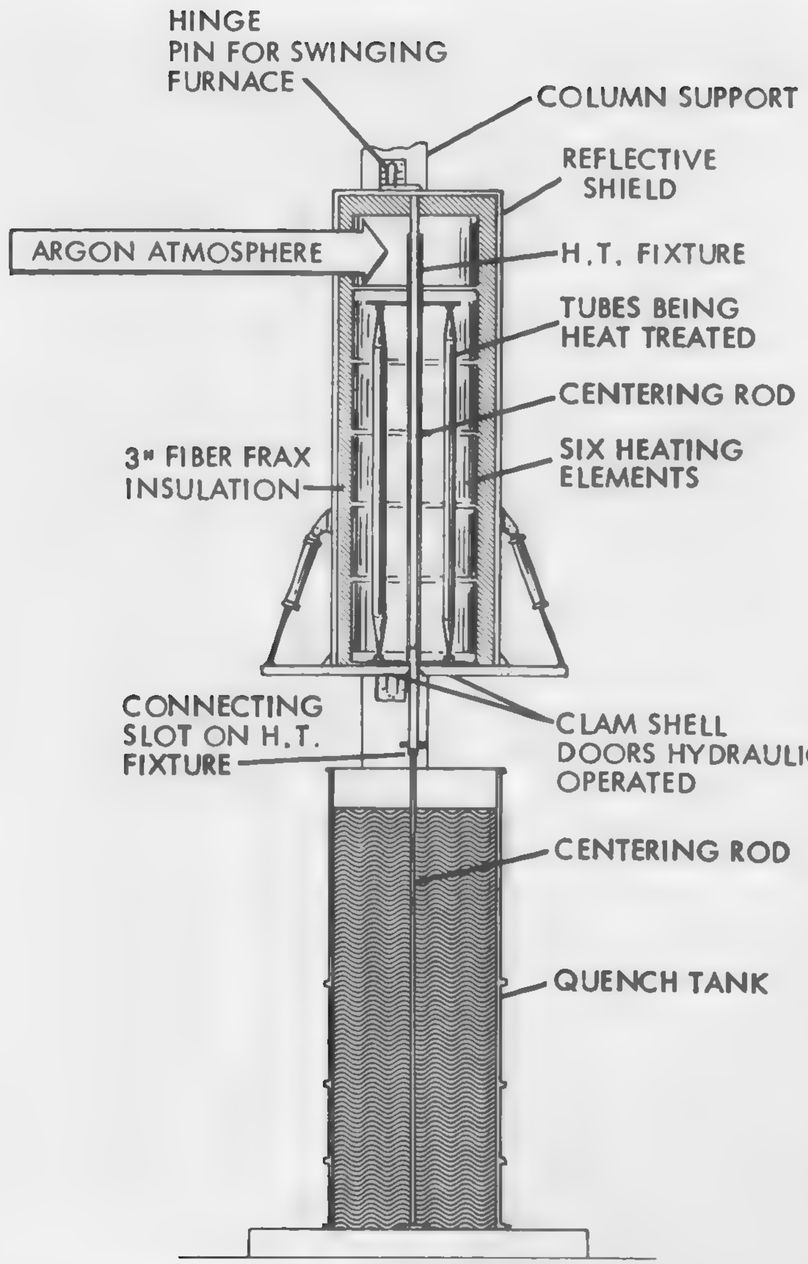


FIGURE 4 SHEET PANEL SUSPENDED FROM A HEAT TREAT FIXTURE



CAPACITY: 15 inches X 110 inches

FIGURE 5 SWING FURNACE FOR ANNEALING RENE' 41 TUBES

Joint fittings constitute the last group of major structural components. Until recently, joint fittings were predominantly machined from forged Rene' 41 bar stock. Problems in machining were encountered primarily from the high strength of the material and its tendency to work-harden. The optimum heat treat condition for machinability has not been established. However, it is generally felt that machining is more easily done with material in the solution heat treated condition. If cold work is too severe for further machining, an interstage anneal is frequently employed prior to the final machining operation. Such annealing is usually carried out in a high temperature, neutral salt bath. While the use of a salt bath both as a heat transfer and a protective agent does prevent scaling, it does not completely eliminate intergranular attack. Preparation of the salt bath, its control and rectification procedures are all of great importance in maintaining the neutrality of the bath. The total alkalinity of the bath should not exceed 1.5% BaO during the annealing treatment. With such process controls, intergranular attack can be kept below 0.5 mil per annealing cycle. A typical joint fitting is shown in Figure 6.

Because joint fittings are subsequently welded, cracking is the main problem with these parts. Special welding fixtures are used to facilitate rapid cooling from the welding temperature, thus reducing precipitation of a carbide film along grain boundaries. Figure 7 illustrates the extensive use of copper as a cooling medium.

Recent advancements in Rene' 41 fabrication have led to the production of forged parts which are now being evaluated for machinability. Intermediate annealing may then become unnecessary because forgings will require finish machining only.

THE INFLUENCE OF PREVIOUS MILL PRACTICES ON HEAT TREATMENT OF REFRACTORY ALLOYS

The heat treatment of refractory alloys such as Mo-0.5% Ti and columbium alloy F.S. 82 is to some extent dependent on the mill practices used. Both alloys are highly susceptible to interstitial contamination by such elements as

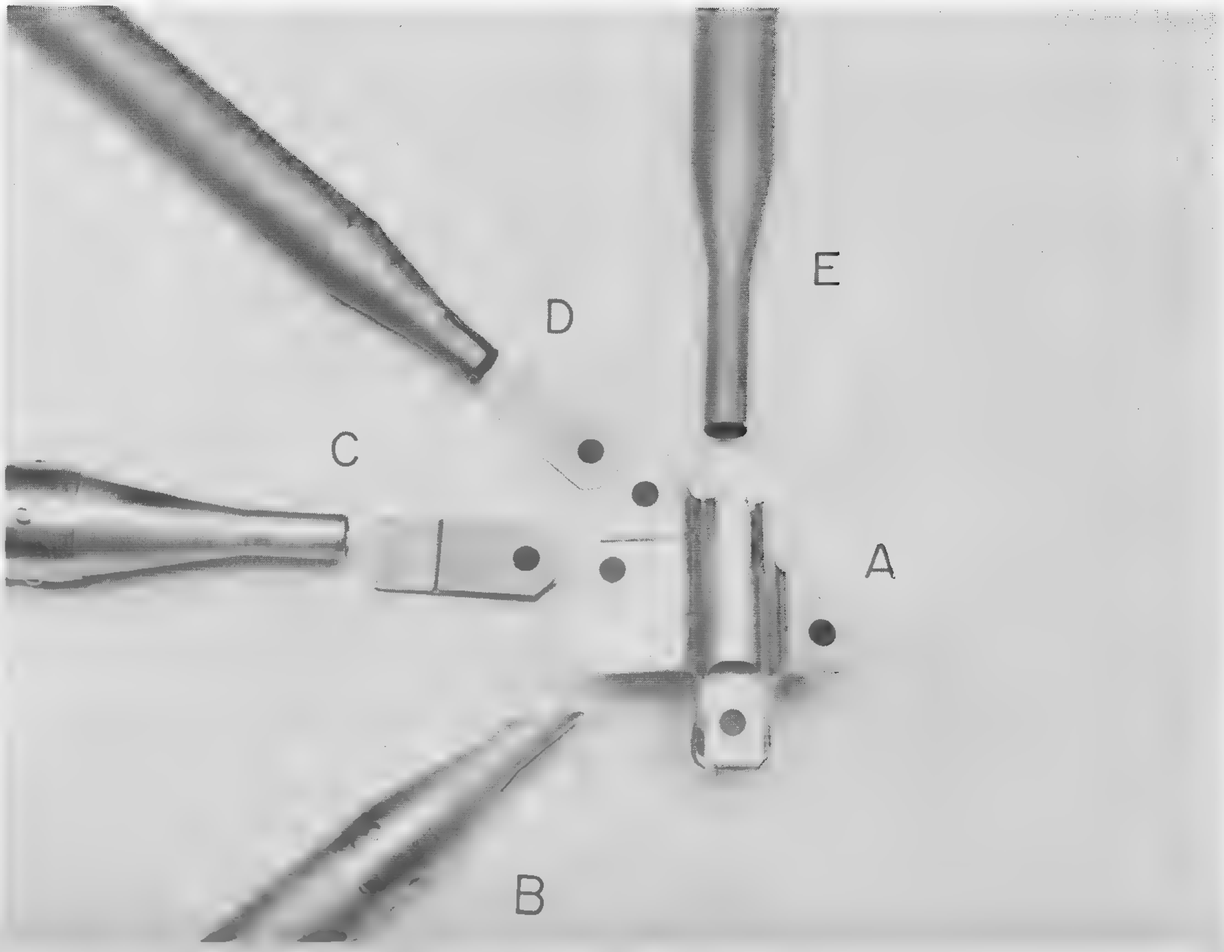


FIGURE 6 - JOINT FITTING

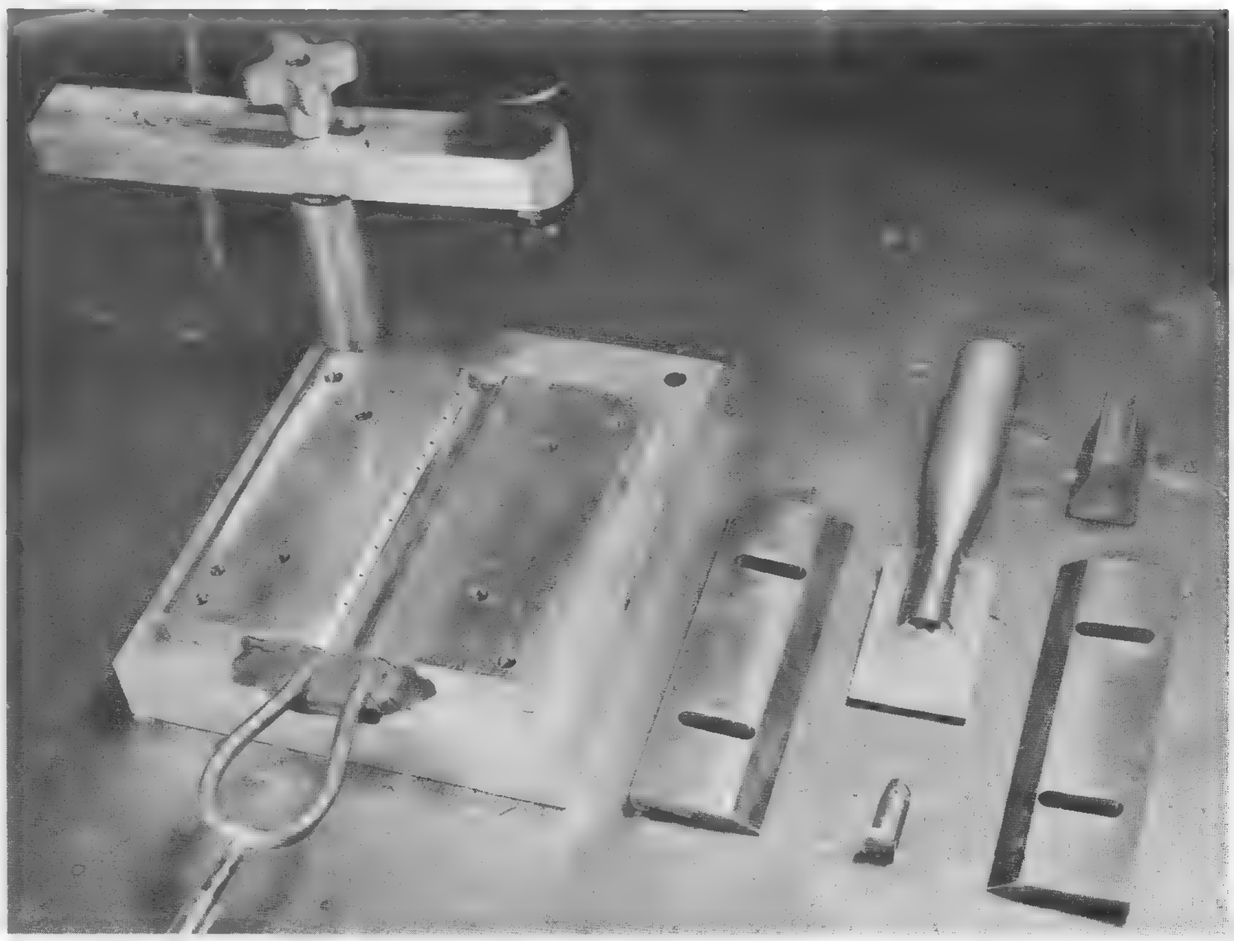


FIGURE 7 VARIOUS COPPER COOLING BARS USED IN WELDING RENE' 41

oxygen, nitrogen, hydrogen, and carbon. Melting and primary fabrication techniques recently developed can control the interstitial content to a level compatible with satisfactory secondary fabrication. However, oxygen, nitrogen and carbon are also effective strengthening elements, and some refractory alloys use these elements to improve strength characteristics. This makes secondary fabrication techniques and control of oxygen and nitrogen contamination more critical because interstitial diffusion increases hardening and embrittling.

Even when present in minute quantities, these impurities, strongly influence the room-temperature ductility of molybdenum. The ductile-brittle bend transition temperature depends greatly on the quality and fabrication history of the material. Figure 8 illustrates this point. The figure

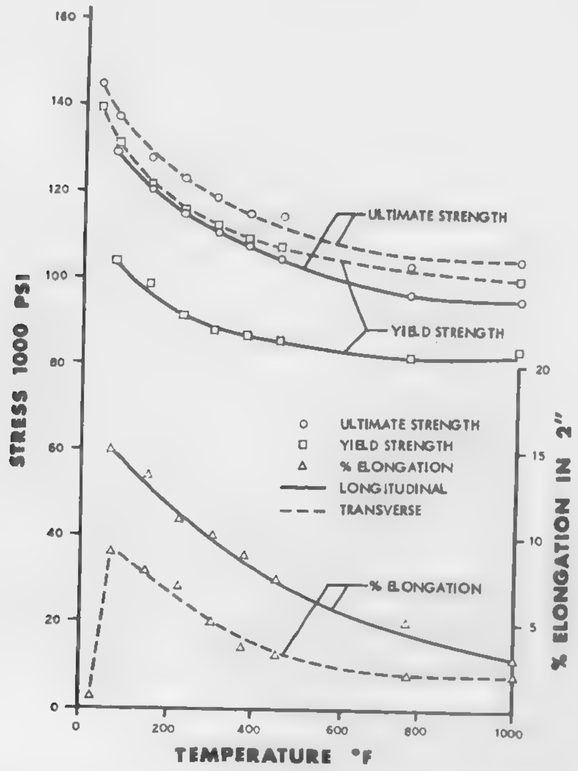


FIGURE 8 MECHANICAL PROPERTIES VS TEMPERATURE OF A 0.020" GAGE, Mo-0.5% Ti SHEET

shows longitudinal and transverse mechanical properties for a 0.020-inch gage, Mo-0.5% Ti sheet. The ductile-brittle bend transition temperature is close to room temperature, and it is significant that ductility decreases as the temperature increases.

The properties of cold-rolled Mo-0.5% Ti and F.S. 82 depend on the amount of cold work previously given the material. While strength properties can be increased by mechanical work, the working also reduces the recrystallization temperature, thus setting an upper limit to the operating temperatures and any thermal treatments at which the beneficial effects of mechanical work can be retained.

CONTROL OF STRESS RELIEF ATMOSPHERE AND TEMPERATURE

The stress relief of such refractory alloys as Mo-0.5% Ti Ti and F.S. 82 becomes necessary after secondary fabrication such as severe forming or welding. Usually, stress relief operations are carried out in vacuum furnaces because these alloys are highly susceptible to interstitial contamination. However, vacuum furnaces are expensive and often not warranted for low-production operation. In such cases, stress relief operations can be carried out in welded retorts, or in sand seal muffles purged with argon. The stress relief treatments can then be accomplished under protective atmospheres using conventional air furnaces. Purging rates are governed by the size of the retorts and the desired purity of the atmosphere during stress relieving. Table IV below shows purging conditions under which approximately 99% of the atmosphere can be replaced before starting the stress relief operation.

The flow rate during the stress relief operation is reduced so that a small positive pressure is maintained.

TABLE IV

DESIRED PURGING RATES OF RETORTS

Retort Volume(cu. ft.)	0-1	1-2	2-3	3-4	4-5
Flow Rate (cu. ft. /hr.)	18-20	18-20	27-30	36-40	56-50
Time of Purging (minutes)	15	30	30	30	30

Proper stress relief time and temperature parameters are determined by two independent techniques of relaxation measurement and recrystallization. The relaxation technique for determining stress relief parameters involves measuring the angle of springback of an elastically deformed specimen before and after being subjected to a one hour thermal treatment at a given temperature. This is generally related to the original springback angle and is expressed as percent of relaxation. Metallographic examinations of specimens heat treated for one hour at selected temperatures determine recrystallization and establish stress relief parameters. The degree of recrystallization of the microstructure is estimated from visual observation.

For all practical purposes, the temperature chosen for stress relief is defined as the minimum temperature at which the start of recrystallization can be observed after a one-hour thermal treatment. Figure 9 illustrates the percentage of relaxation which occurred at one-hour temperature exposure from 1400-2000°F in a Mo-0.5% Ti alloy. A comparison of this figure with the recrystallization curve in Figure 10 shows that roughly 85 to 90 per cent of the residual stress can be removed at an exposure temperature of 1850°F, and that this same exposure should not result in more than 20 per cent recrystallization. Similar recrystallization and relaxation studies with F.S. 82 alloy showed that a thermal treatment of one hour at 1800°F was adequate for stress relief.[4]

The effect on contamination produced in two refractory alloys using argon and hydrogen atmospheres during typical stress relief treatments under production conditions in

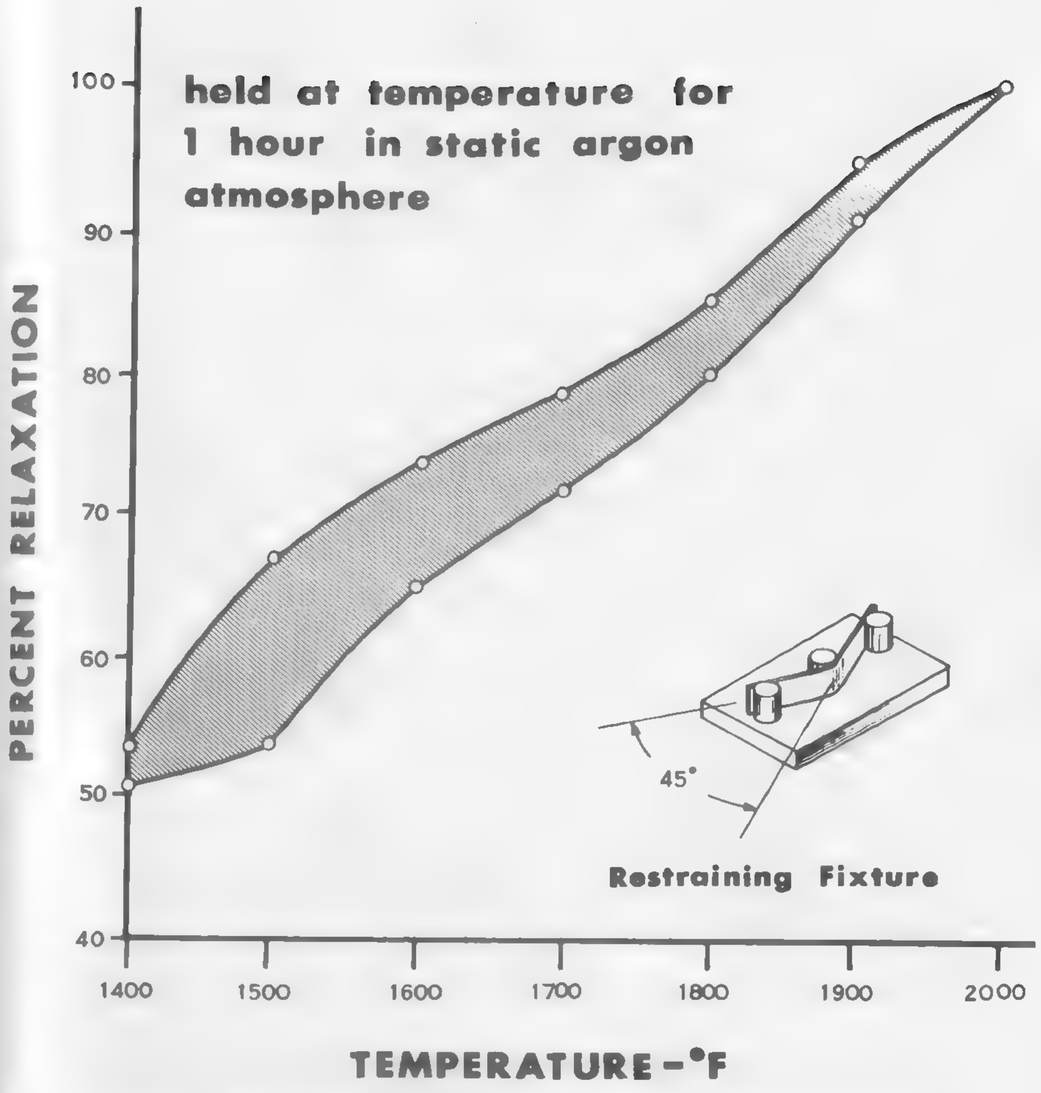


FIGURE 9 PERCENTAGE OF RELAXATION VS TEMPERATURE FOR 0.012" GAGE, Mo-0.5% Ti SHEET

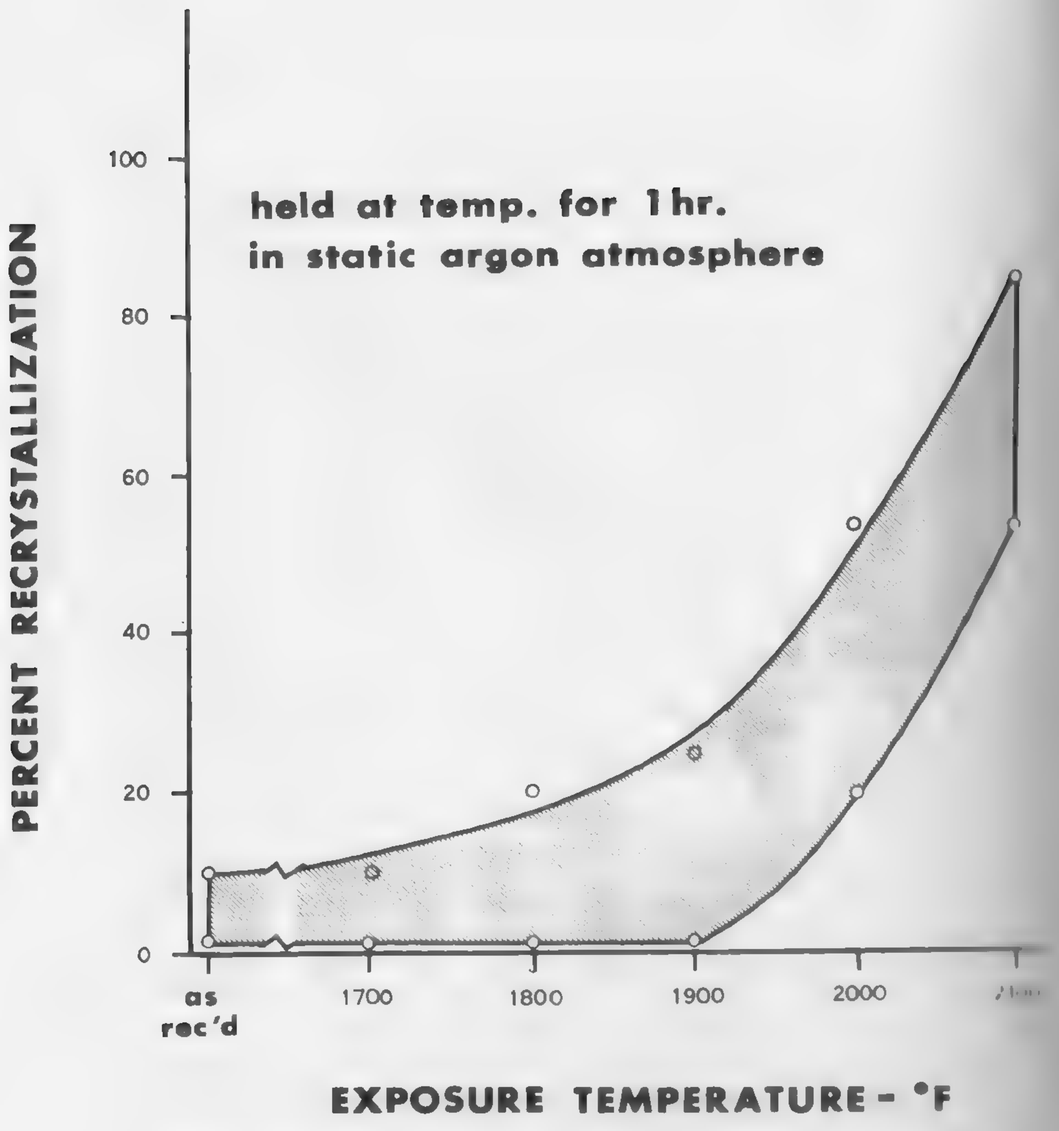


FIGURE 10 PERCENTAGE OF RECRYSTALLIZATION VS TEMPERATURE FOR 0.012" GAGE, Mo-0.5% Ti SHEET

shown in Figure 11. Best results were obtained on test parts which were stress relieved in a weld-sealed stainless steel retort under positive argon pressure. Cb-10 Ti-10 Mo alloy specimens were used in this test because of their high susceptibility to any atmosphere contamination. Parts stress relieved in retorts usually do not warp.

Mildly formed refractory parts such as the leading edge shown in Figure 12 are normally stress relieved during the coating process and require no separate stress relief treatment. Leading edges and panels are coated either with molybdenum disilicide or columbium disilicide depending on the alloy used. The coating operation is carried out in a fluidized bed shown in Figure 13. The bed consists of a long, vertical cylinder with provisions for heating and circulating an atmosphere of argon and iodine gas through a bed of fine silicon particles. The process is a closed system, completely contained within an exhaust hood except for the argon supply and system controls. The coating and stress relieving is accomplished at 1800-1850°F for 1 to 4 hours depending on the coating thickness desired. To reduce warpage, parts are supported by a 0.030-inch minimum diameter wire made of H.S. 25 alloy or by a H.S. 25 alloy rack especially designed for the fluidized bed. The use of these fixtures in no way interferes with the coating process.

CONCLUSIONS

The structural design of a re-entry glider requires formable refractory alloy sheet materials, which can withstand temperatures exceeding 1800°F. Mo-0.5% Ti alloy and columbium alloy F.S. 82 are two of the most promising materials for this application. Of the newly developed nickel-base alloys, Rene' 41 has outstanding strength characteristics at moderate elevated temperatures.

The advent of space age materials creates a need for new heat treat methods and their application. A better understanding of the structural changes occurring during

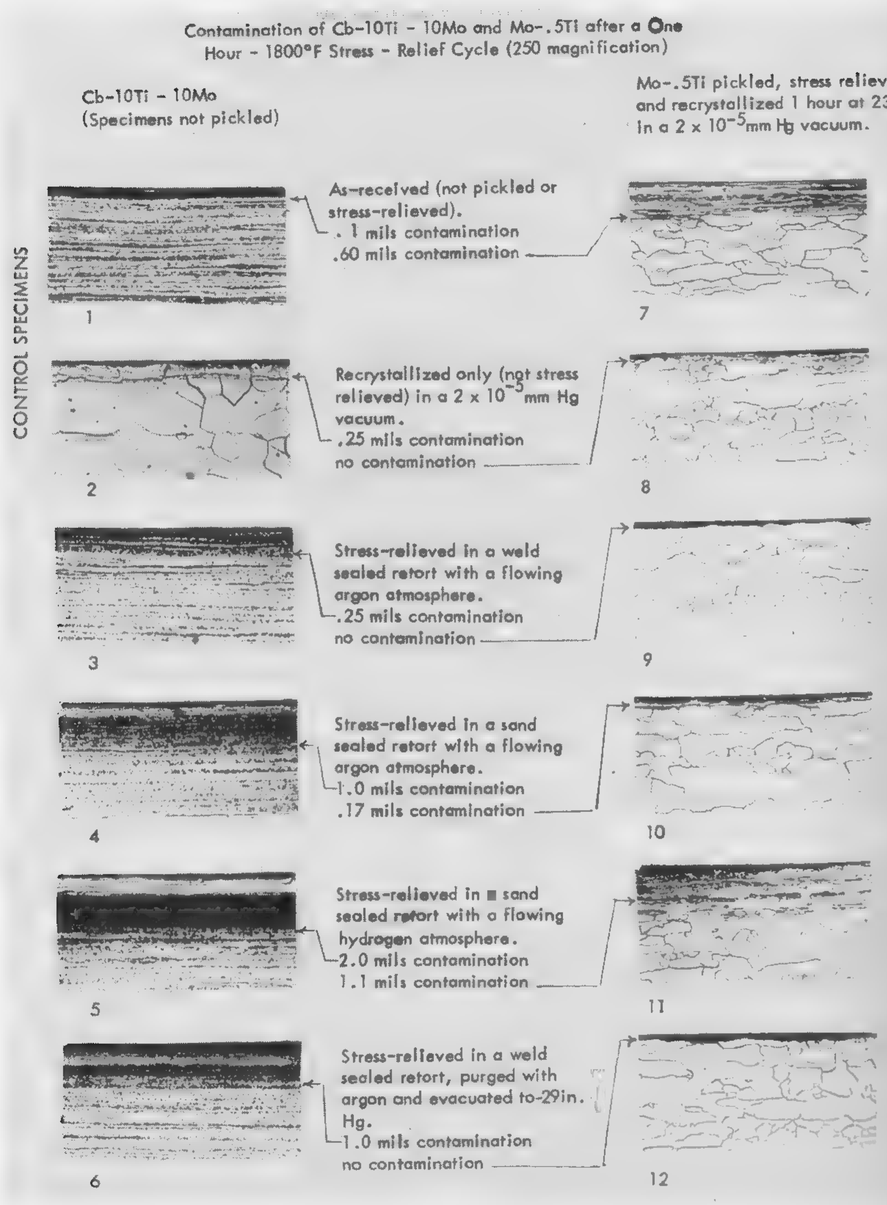


FIGURE 11 CONTAMINATION DUE TO ATMOSPHERE IN HEAT TREATING Mo-0.5% Ti AND COLUMBIUM ALLOY D31



FIGURE 12 LEADING EDGE OF COLUMBIUM

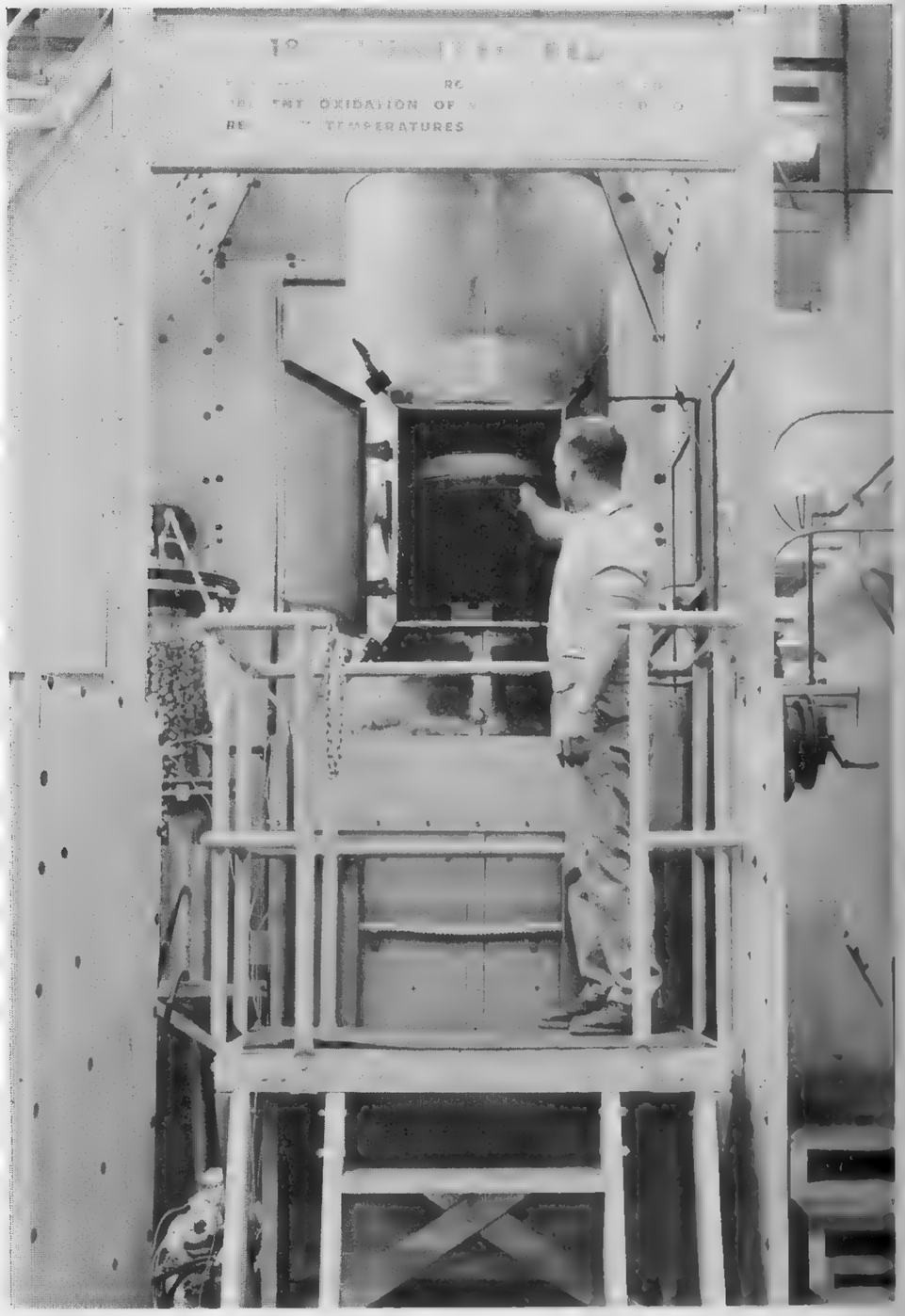


FIGURE 13 FLUIDIZED BED USED FOR COATING REFRACTORY ALLOYS

thermal treatments of Rene' 41 enables Boeing to maintain weldability and formability of the material by controlling annealing temperatures and thus preventing excessive solution of carbides. By using double aging cycles on welded Rene' 41 components, coupled with special welding fixtures to facilitate fast cooling, Boeing has virtually eliminated the cracking problem associated with welding this alloy.

Reliable methods for stress relieving Mo-0.5% Ti and F.S. 82 have been developed; welded retorts and controlled argon atmospheres are used to control oxidation and interstitial contamination. Expensive vacuum furnaces are not required.

In short, progress in heat treating of space age materials is one of many steps forward towards reliability, which means that heat treated structural components must work without fail under the extreme conditions of space flight.

BIBLIOGRAPHY

1. Chang, W. H.: Basic Cause of Cracking in Rene' 41 Sheet Alloy. General Electric Report DM-58302 (58AD-16) October 30, 1958.

2. Beattie, H. J., Jr.: Aging Reactions in Rene' 41. General Electric Report DF 59SL315. May 15, 1959.

3. Honebrink, D. A.: Fabrication Structural Parts from Mo-0.5% Titanium Sheet. The Boeing Company, paper presented at the 1961 Pacific Northwest Metals and Minerals Conference. Spokane, Washington, April 13-15, 1961.

4. Torgerson, R. T.: Evaluation of Forming Characteristics of Columbium Alloys. The Boeing Company, paper presented at the Columbium Metallurgy Symposium, Lake George, New York, June 7-10, 1960.

CORROSION AND MASS TRANSFER IN ALKALI LIQUID METAL SYSTEMS

John R. Weeks
Brookhaven National Laboratory
Upton, L. I., New York

ABSTRACT

Liquid alkali metals offer attractive properties as coolants for space-vehicle power sources. They are usually contained in the high-melting body-centered cubic transition metals and their alloys: steels at temperatures below 550°C and refractory metals at higher temperatures. Corrosion can occur by two mechanisms: dissolution of the solid metal into the liquid alkali metal, and a chemical -- as opposed to intermetallic -- reaction resulting from the presence of nonmetallic impurities in either the liquid or solid metals. Dissolution-corrosion is a function of solubility and hydrodynamic factors. It is rare in practical alkali metal systems except where high-Ni container alloys are used. "Chemical" corrosion is a function of the C, O, and N activity in both the liquid and solid metals; it is minimized by "gettering" both the solid alloy and the liquid metal for these impurities, and/or by cold-trapping the coolant to reduce the concentration of soluble oxides. Design of liquid-vapor systems requires knowledge of the relative aggressiveness of the bulk liquid and the fresh condensate.

INTRODUCTION

Compact power sources for space vehicle propulsion demand the high heat transfer and heat transport properties of liquid metal coolants. For long-term, sustained oper-

ation, nuclear fuels and liquid metal coolants are the most attractive and, indeed, the only possible compact, high-output power source. Liquid metals may be boiled to drive turbines or circulated without boiling to insure continuous contact with the high-temperature (nuclear) fuel in the absence of gravity. An attractive system, therefore, might be an all-liquid metal primary coolant with low vapor pressure exchanging its heat in a boiler to a second liquid metal with higher vapor pressure, which, in turn, would drive a turbine. The containment problems associated with both all-liquid and boiling-liquid metal heat exchangers must therefore be studied and understood.

The alkali liquid metals are particularly suited as coolants for space applications because of their low specific gravity. They offer a wide range of available turbine temperatures, as their boiling points range from 1330°C for Li down to 688°C for Rb. A two-stage coolant cycle might therefore involve an all-liquid enriched Li or Na primary coolant and a boiling K or Rb secondary coolant. It is thus necessary to consider the corrosion properties and containment problem of all of the alkali metals both in all-liquid and in boiling liquid systems. Table I reviews the temperature ranges of interest for each of the alkali metals in boiling and all-liquid systems, and the types of materials that can be considered for use in each. Materials for containing boiling Li and Na must be developed; Li, especially, is useful only in all-liquid systems at present. Heat exchange and turbine materials for boiling Cs, Rb, K, and perhaps Na are conceivable with present technology.

THE CORROSION PROBLEM

The chemical similarities among the alkali metals also carry over to their corrosive behavior and their tendency to alloy with container materials. Any generalized statements, however, must be carefully evaluated for subtle differences between these metals, since differences in their corrosion behavior do exist and are not always known or recognized.

TABLE I

TEMPERATURE RANGES AND MATERIALS OF INTEREST FOR HANDLING ALKALI LIQUID METALS

	Boiling Point at 1 atm. (°C)	Temperature Range of Interest (°C)		Available Materials	
		Boiling System	All-Liquid System	Boiling	All-Liquid
Li	1330	above 1400	below 1400	None*	Refractory metals
Na	892	1100-1400	below 900	Refractory metals	Refractory metals, ferritic steels, high-temperature alloys
K	760	900-1100	below 800	Refractory metals, high-temperature B.C.C. alloys	Refractory metals, steels, high-temperature alloys
Rb, Cs	688	750-950	below 700	Refractory metals, steels, high-temperature B.C.C. alloys	Refractory metals, steels, high-temperature alloys

* Fabricable refractory alloys of sufficient strength to be useful with boiling Li systems need to be developed.

The materials most resistant to corrosion by the alkali metals generally are high melting-point, body-centered cubic transition metals and their alloys. These metals, when pure, often are not detectably soluble in pure alkali metals by ordinary analytical techniques. However, solubilities of fractions of one part per million can produce severe dissolution and precipitation of the container material. Alloys best suited for containing alkali metals are steels and Co-base alloys for low temperature applications, and Cb, Ta, W, or Mo-base alloys for higher temperature (>600°C) application. Ni is generally somewhat soluble; and high-Ni alloys, particularly those which are face-centered cubic, are generally less resistant to attack at high temperatures.

Leaching of Ni appears to be less severe with the heavier alkali metals. Austenitic stainless steels and Ni-base alloys are severely attacked by Li;[1] however they have been used successfully to contain Na at temperatures below 550°C.[2] At higher temperatures (of the order of 800°C), De Van[5] has described corrosion rates of austenitic alloys by Na as generally increasing with the Ni content of the alloy; however, Hoffman[3] did not observe selective leaching of Ni from type 316 stainless steel in a loop containing K boiling at 816°C.

Ti, Zr, and their alloys appear resistant to pure Na[2] and Li;[1] however, they are scavengers for O and N in Na systems, and prone to severe embrittlement by O pickup. The solubility of Ti in Li (and presumedly the corrosion of Ti by Li) increases with the N content of the Li.[4] Ti and Zr were found[1] to be N, but not O scavengers from Li.

The mechanisms of corrosion of metallic container materials by any liquid metal fall into two classes: a solution-erosion (shall we coin a word - solosion?) process resulting from dissolution, transport, and precipitation of the container by the liquid metal; and a chemical (as opposed to intermetallic) reaction resulting from an interaction of nonmetallic impurities with both the liquid and the contained metals. Both processes are temperature-dependent. Each will be discussed separately.

The Solution-Erosion Process

Dissolution of a solid metal into a liquid metal is usually described as occurring in two steps, which are sketched in Figure 1. The first, or "dissolution" step can be pictured as the breaking of the metallic bonds that held the surface atom to its neighbors in the solid metal and the simultaneous formation of metallic bonds between the solute and solvent atoms. We know very little about the mechanism of this exchange;* we do anticipate it, however, to be highly sensitive to surface imperfections in the solid metal, as the

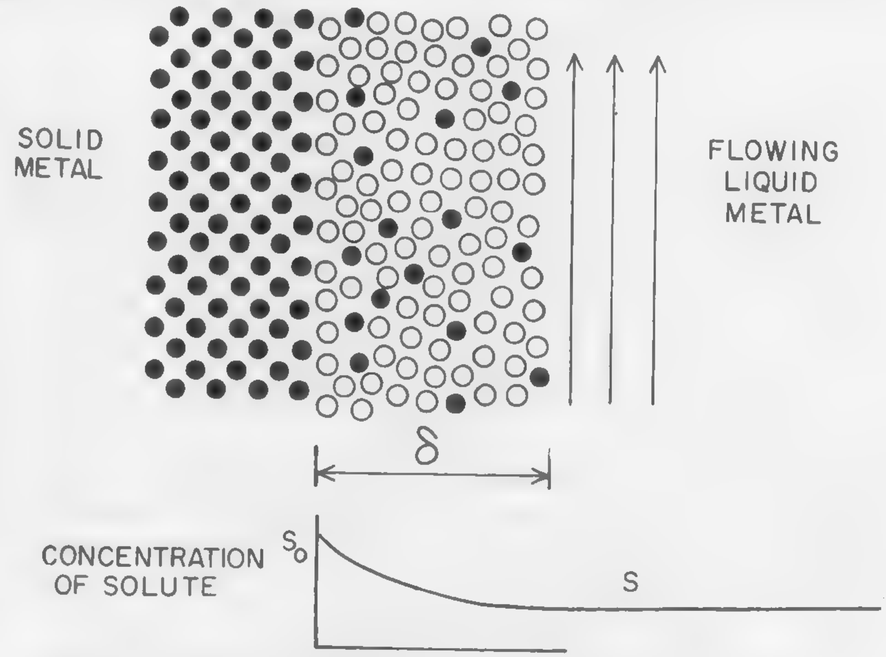


FIGURE 1 SCHEMATIC: DISSOLUTION OF A SOLID METAL INTO A LIQUID METAL

surface bond energies are related to crystal imperfections. Selective grain boundary attack and dislocation etching are, therefore, indicative of dissolution rate control by step I, especially when they are found in the absence of impurities in the grain boundaries.

---

*Obviously, for this reaction to occur, there must be intimate, atomic contact between the solid and liquid metals; the effects of intermediate layers and impurities will be described later.

Step II, diffusion of the solute species through the layer of solvent immediately adjacent to the container wall, is generally found, in pure systems, to be the rate-controlling process. This is indicated by sensitivity of the dissolution rate to flow of the liquid metal. The driving force for diffusion through the solvent layer is therefore the diffusion gradient, or the difference between the equilibrium solubility at the dissolution temperature, S_o, and the solute concentration in the bulk solvent, S, divided by the thickness of the solvent layer, δ:

$$J = \frac{D(S_o - S)}{\delta} \qquad (1)$$

from Fick's law, where D is the diffusion coefficient of the solute species in the liquid metal solvent. D is generally of similar magnitude for most liquid alloys. S (in a circulating system) is controlled by the precipitation of solute atoms, and therefore by the Δ T and the temperature coefficient of solubility in the system in question. δ is flow and viscosity dependent.

DeVan[5] has shown the mass transfer by Na at high temperatures of Ni-base alloys (Inconel) to be linearly dependent upon the flow rate at constant temperature, as seen in Figure 2, and upon the Δ T at constant flow rate, as seen

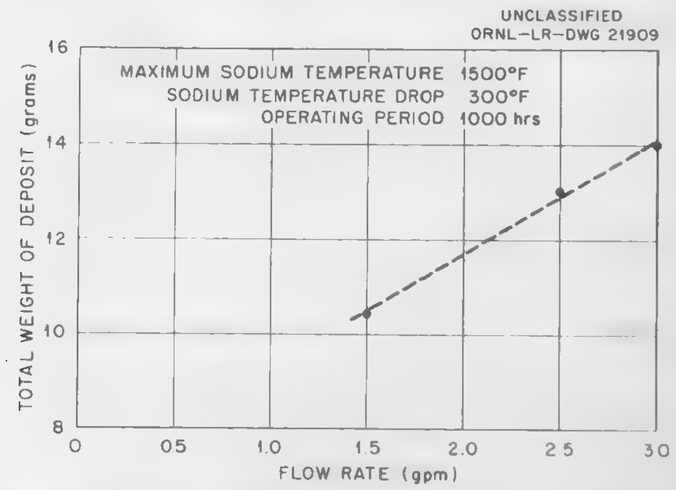


FIGURE 2 EFFECT OF FLOW RATE ON MASS TRANSFER IN Na-INCONEL PUMP LOOPS. FROM DeVAN. (5)

in Figure 3. These observations are in agreement with equation (1), and indicate liquid diffusion (of Ni) is the rate-controlling step in this mass-transfer system.

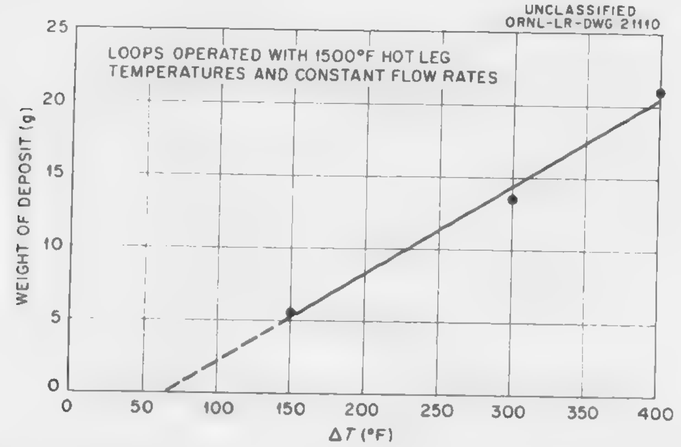


FIGURE 3 EFFECT OF ΔT ON MASS TRANSFER IN Na-INCONEL PUMP LOOPS. FROM DeVAN. (5)

Actual examples of dissolution control by step I are very rare in the absence of impurities. Lommel and Chalmers[6] increased the speed of a rotating cylinder of Pb during dissolution-rate experiments into liquid Pb-Sn eutectic alloy until the appearance of the Pb showed a structure-selective attack was occurring, indicating a shift from diffusion to dissolution control. Their data suggest the activation energy for step I (in their system) is lower than that for liquid diffusion. If this is generally the case, and data do not exist that either confirm or deny it, the energy required to break the bonds holding a surface atom to its nearest neighbors and replace them with bonds to the nearest liquid metal atoms must be small, < 5000 cal/gram-atom; this is of the same order of magnitude as the latent heat of fusion of most metals at their melting point.

In estimating the corrosion resistance of any material for a liquid metal application, it is necessary to know the equilibrium solubility of the container material as a function of temperature. This information is very difficult to obtain experimentally, both because of the exceedingly low solubilities that must be measured in any system of practical value, and the extreme complexity of the multi-component

practical systems. Further, there are no reliable means of predicting from the present status of alloy theory what the solubility of any pure solid metal in any pure liquid metal will be, or even if it will dissolve at all. In trying, two factors must be considered: the relative atomic diameters of the solute and solvent atoms in their liquid alloy and the electron-sharing between solute and solvent species (band structure of the liquid alloy). An empirical relation has been proposed by Strauss, White, and Brown,[7] suggesting minima in the heat of solution of solute species when the relative atomic radii of the solid and liquid metals are nearly equal, so that a liquid alloy can form with a minimum of distortion of the liquid structure, and when the solute atoms are sufficiently small to enter interstitially into the liquid structure. Maxima in heats of solution are suggested for those systems in which dissolution of the solute atom produces a maximum of distortion of the liquid structure, i.e., $r_{solvent}/r_{solute} = <0.85$, or $1.2 \rightarrow 1.4$. This interesting suggestion has substantiation in a number of selected alloy systems; however, there appear to be as many or more systems that are exceptions as are confirmations to the Strauss-White-Brown relationship. The results of Leavenworth and Cleary[8] on the solubility of container materials in liquid Li suggest that the relationship may be used, with caution, to estimate an equilibrium solubility curve when the solubility data scatter too badly to use other means of drawing the curve.*

The failure of the Strauss-White-Brown relation to predict generally the temperature-coefficient is probably due in part to its failure to take into account the electronic interaction forces - and therefore the related "ionic" radii of the dissolved solute atoms. These interactions are hard to evaluate. However, electrolysis of liquid alloys,[9] magnetic susceptibility measurements,[10] and correlations of diffusivities with atomic radii by the Stokes-Einstein relationship[9] all suggest that the dissolved species are ions in alloys with high concentration of solute atoms. In the very dilute systems of interest to liquid metal corrosion theory, however, these data are not generally available.

* However, their measured solubilities were dependent upon the N content of the Li,[7] and are therefore questionable as a test of this hypothesis.

Recently, Sherby and Simnad[11] have suggested that the valence of the metal is an important factor in liquid metal (and presumably liquid alloy) diffusion. Further knowledge of the structure of very dilute liquid alloys is therefore necessary to carry the discussion of the dissolution model further.

Effects of Dissimilar Metals in Contact with the Liquid Metal

Contacting two or more solid metals with the liquid introduces an additional complication resulting from their tendency to interact. For example, Ni was observed by Hoffman[12] to migrate through Na at 1000°C to form a reaction layer on a Mo surface; the deposit formed in 100 hours is shown in Figure 4. Also, at the point of contact of two

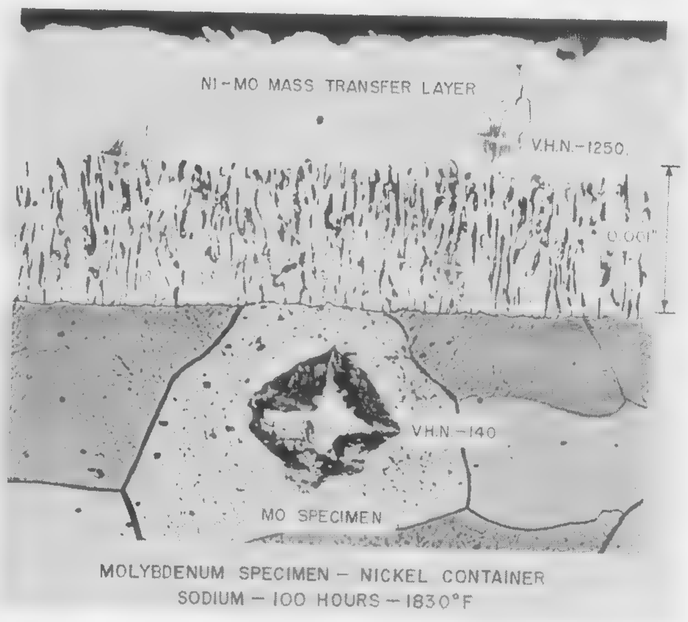


FIGURE 4 Mo SPECIMEN - Ni CONTAINER - CONTACTED WITH Na FOR 100 HOURS AT 1000°C. FROM HOFFMAN. (12)

dissimilar solid metals with the liquid, a local "dissolution cell" is conceivably set up, which, in view of possible electron-flow effects on dissolution, might result in selective dissolution of one constituent. Phenomena suggesting such

local acceleration have been observed in heavy liquid metal systems, [13] and perhaps exist in alkali metal systems also. Very complex mutual solubility effects have been observed during liquid metal attack on alloys; [13, 14] thus solubility information obtained from binary liquidus measurements is usually not applicable to the ternary and higher systems of most practical interest. Likewise, concentrations of dissolved atoms obtained after contacting a liquid metal for a given time and temperature with useful container alloys may not represent "solubilities" at all, and only represent the concentrations at a particular stage in the complex dissolution process. Steady-state concentrations for a given flow rate and temperature differential can be obtained by sampling the liquids in a circulating system as a function of time.

One, therefore, must conclude that the study of the solution-erosion process leads into a maze of interdependent complex phenomena. Precise multicomponent liquidus curves are necessary to predict corrosion resistance, and these are difficult to obtain. Precise binary liquidus measurements, however, are of great practical value in selecting base materials for container alloys, and of theoretical value in furthering the study of corrosion mechanisms.

The Chemical Dissolution Process

When contacting alkali liquid metals with ferritic steels or refractory metals, the equilibrium solubilities in most instances, when known, have been found to be negligibly small; dissolution mass-transfer accounts for only a small fraction of the containment problem. However, impurities, notably O and N, appreciably accelerate the dissolution rate presumably by increasing the solubility of the container metal. [13]

As a simple illustration, let us consider the possible effect of O on the dissolution and mass transfer of Fe by liquid Na. Throughout the system, the chemical reaction

$$Na_2O + Fe = 2Na + FeO \qquad (2)$$

is occurring. The equilibrium constant,

$$K = (Na)^2(FeO)/(Na_2O)(Fe)$$

is temperature-dependent, and thus varies throughout the system. Dissolved O has been shown to increase the "solubility" of Fe in Na, probably by formation of a soluble sodium ferrite, $(Na_2O)_x(FeO)_y$. * By far the major portion of the dissolved Fe can be considered to be in this form. Thus, at the steady-state, at an Fe surface, we have the reaction

$$yFe + (x + y)Na_2O = (Na_2O)_x(FeO)_y + 2yNa. \qquad (3)$$

This is endothermic as written and, therefore, tends to proceed to the right in the hot leg and to reverse in the cold leg. The O is then seen to "catalyze" the mass-transfer of y atoms of Fe from the hotter to the cooler part of the system. Examining the kinetic effect of O on Fe dissolution by this mechanism, we can assume the slow step in dissolution to be represented by equation 2, so that

$$d(FeO)/dt = k(Fe_s)(Na_2O); \qquad (4)$$

the dissolution of Fe is thus found to be first order dependent upon the O concentration of the Na. This has been reported by Haag [16] and Epstein. [17] It does not matter which oxide of Fe is selected; at the steady-state, the first order kinetics remain. Epstein also analyzed hydrodynamically the data on mass transfer of Fe by Na; he found it to be chemical-reaction controlled, in agreement with the above mechanism. Haag [16] also reported that mass-transfer of Co, Fe, Ta, and Mn is similarly a function of the O content of the Na, as determined by mass-transfer of radio tracers of these elements through Na from irradiated stainless steel (at 550°C).

*Horsley [15] has identified $(Na_2O)_2FeO$ in residues obtained from O-contaminated Na that had been held in Fe capsules. From its appearance he estimated it had precipitated from solution during cooling.

Holman[17] has suggested that, at higher temperatures (550° to 875°C) mass-transport rates are controlled simultaneously by processes occurring in both hot and cold regions; he observed a null-point (neither corrosion nor deposition) at an intermediate temperature in a circulating stainless steel loop system. This observation suggests that, at the steady-state, reaction 3 is at "equilibrium" for the intermediate temperature of the null point, and that both the forward and reverse reaction are slow compared to the Na flow rate in his experiments. The 50 ppm O in the Na of his experiments, if 100% efficient in catalyzing mass-transfer of Fe by reaction 3 (assuming x = 2 and y = 1), would have resulted in several orders of magnitude more mass transfer than he observed.

Impurities in the container metal, notably C, O, and N in refractory metals, may dramatically affect the corrosion behavior of these materials in alkali liquid metals at high temperatures. These interstitials tend to concentrate in the grain boundaries, and lead to severe intergranular attack by selective attack of grain boundary carbides, nitrides, and oxides by the liquid metal. They also tend to be introduced during welding.

Leavenworth and Cleary[8] also showed that the solubility of Fe, Ti, Cr, Cb, Ni, and Mo in Li was also highly dependent upon the concentration of N in the Li; all the concentration of dissolved metals, except Ni, in their data could be accounted for by this mechanism.

Hoffman[19] has shown that the principle species mass-transferred by boiling K in a type 316 stainless steel loop was $Cr_{23}C_6$. Decarburization was observed in a specimen from the boiler (870°C) and $Cr_{23}C_6$ deposits were found on a cold-leg specimen (710°C). These are shown in Figure 5. It is not clear whether the carbide was transferred as such, or formed in the cold leg as a result of simultaneous transfer of C and Cr. Hoffman also reported severe intergranular penetration of type 446 steel by Li, as seen in Figure 6.[1] This was accompanied by decarburization of the hot zone wall and deposition of $Cr_{23}C_6$ on the cold zone wall.



FIGURE 5 SURFACES OF TYPE 316 STAINLESS STEEL SPECIMENS FROM (A) BOILER (LIQUID - 870°C) AND (B) COLD LEG (LIQUID - 710°C) FOLLOWING 3000-HOUR EXPOSURE IN BOILING K - 316 STAINLESS STEEL LOOP TEST NO. 2. FROM HOFFMAN. (19)

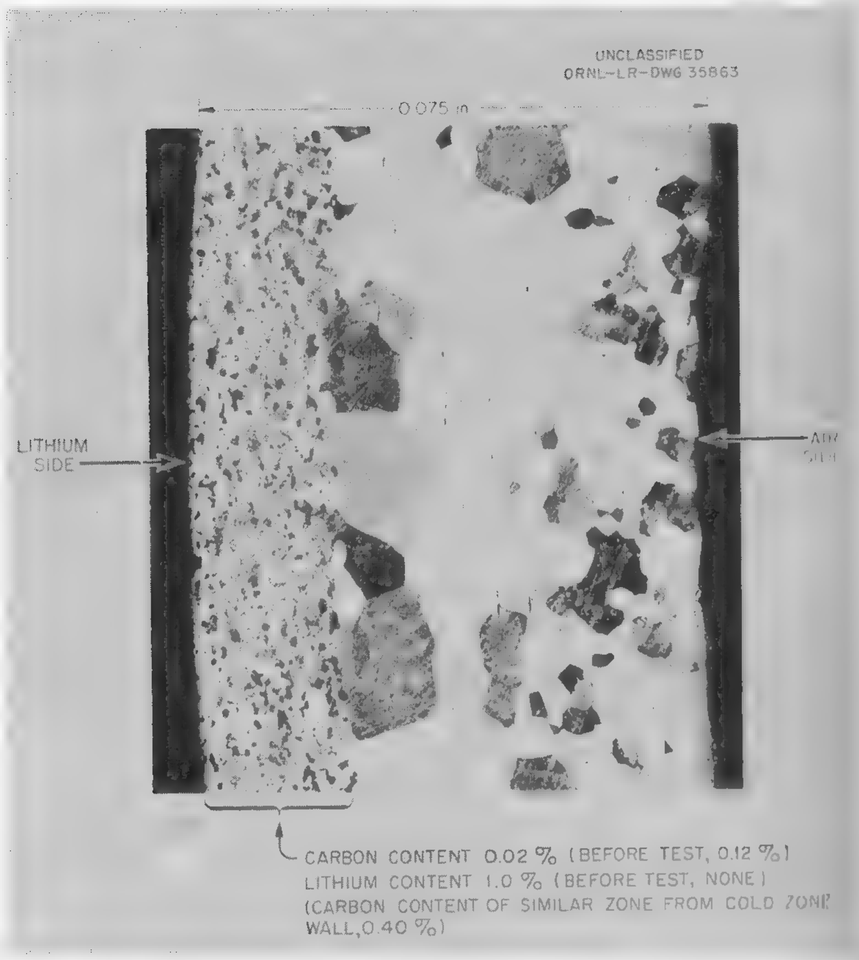


FIGURE 6 HOT ZONE WALL OF TYPE 446 STAINLESS STEEL SEESAW TEST CAPSULE AFTER CONTACT WITH Li FOR 100 HOURS AT 982°-704°C. FROM HOFFMAN. [11]

Severe decarburization of carbon steel by Na with concurrent carburization of stainless steel also in contact with the Na has been observed at lower temperatures.[2] The relatively low C activity in the stainless steel, as a result of its high Cr content, causes this material to act as a C sink, since thermodynamics require all steel surfaces in contact with the Na to have a uniform C activity.

The panacea for corrosion of steels and/or refractory metals by liquid alkali metals is thus: keep the system clean. O and N should be "gettered" in both the container material and the liquid metal, the former by alloying with Zr or Ti, and the latter by hot-gettering with Zr or Ti, and cold-trapping to precipitate out dissolved oxides. Surface oxides should be removed by flushing with liquid Na prior to starting the corrosion experiment. During an alkali metal loop experiment, the liquid must be monitored continuously for O and N in order to evaluate properly the results. This control is one of the most important - and most difficult to evaluate - factors in high-temperature alkali metal containment. In outer-space environments, a system, initially properly "gettered," should run safely for a long time.

Liquid-Vapor Systems

Boiling a liquid metal introduces three new factors in corrosion that need to be considered. The freshly-condensed vapor is probably solute-free, and therefore considerably more aggressive than the liquid in an all-liquid system, since the chemical potential for dissolution is greatly higher. It also may have a lower concentration of dissolved impurities, and be less aggressive. Thirdly, the dissolved corrosion product does not circulate through the circuit in a steady-state concentration, but instead tends to concentrate at the boiler interface, where it must either reach saturation and precipitate, back-diffuse against the liquid metal flow, or be entrained in droplets entering the vapor phase. In a working fluid in a practical system, calculations suggest back diffusion is too slow to prevent precipitation. Precipitation has been seen by Owens[20] at the boiler interface in boiling Hg circuits, and presumedly might also occur in alkali metal systems which were not properly "gettered,"

or in which materials of finite solubility were used. The probability of vapor-phase entrainment of small droplets is high in a small, high-output boiler.

SELECTION OF MATERIALS FOR CONTAINING HIGH TEMPERATURE ALKALI METALS

In selecting materials for service with high-temperature alkali metals, therefore, one must consider the following factors:

1. The purity of the liquid metal must be high; especially its O and N content must be a minimum.

2. The container materials must be of uniform composition to minimize dissimilar metal mass transfer.

3. The container materials must be weldable in such a manner as to prevent introduction of impurities, especially O and N.

4. The container alloy should be of such composition that

   a) the major constituents are essentially insoluble ($<$ 1 ppm at the maximum temperature in the system), and
   b) the impurity constituents (O, C, N) are stabilized and randomly distributed.

5. All surfaces that contact the liquid metal must be clean, and as oxide-free as possible.

6. Mechanical properties of the container alloys must be adequate at the maximum temperature of the system.

ACKNOWLEDGEMENTS

The assistance of Messrs. E. E. Hoffman, J. H. DeVan, R. E. Cleary, and J. Owens in making their previously unpublished data available to the author is gratefully acknowledged. The critical review of this paper by Dr. D. H. Gurinsky has been much appreciated. This work was carried out under the auspices of the U. S. A. E. C.

BIBLIOGRAPHY

1. Hoffman, E. E.: Corrosion of Materials by Lithium at Elevated Temperatures. ORNL-2924, 1960; Thesis, University of Tennessee, 1960.

2. Brush, E. G. and R. F. Koenig: Behavior of Materials in Nonagressive Liquid Metals. Nuclear Metallurgy, IMD Special Report Series #2, Am. Inst. Min. Met. Engrs., New York, 1956, p. 21.

3. Hoffman, E. E.: Private communication.

4. Cleary, R. E.: Private communication.

5. DeVan, J. H., Oak Ridge National Laboratory. Private communication. Also, Reactor Core Materials, May 1958, p. 28.

6. Lommel, J. M. and B. Chalmers: Trans. of Metallurgical Society of AIME, 212, 499 (1959).

7. Strauss, S. W., J. L. White, B. F. Brown: Acta Metallurgica, 6, 604 (1958).

8. Leavenworth, H. W. and R. E. Cleary: Acta Metallurgica, 9, 519 (1961).

9. Manglesdorf, Jr., P. C.: Electrolysis and Diffusion in Liquid Alloys. Physical Chemistry of Process Metallurgy, Pt. 1, p. 429, Am. Inst. Min. Met. Engrs., N. Y., 1961.

10. Bates, L. F. and E. M. Somekh, Proc. Phys. Soc. 56, 182 (1944).

11. Sherby, O. D. and M. T. Simnad: Am. Soc. for Metals Transaction Quarterly 53, 227 (1961).

12. Hoffman, E. E.: Liquid Metal Corrosion. Corrosion Fundamentals, University of Tennessee Press. 1956, p. 78.

13. Weeks, J. R. and D. H. Gurinsky: Liquid Metals and Solidification, Am. Soc. for Metals Symposium, pp. 106-161 (1958).

14. Elgert, O. J. and C. J. Egan: MTA-12, 1953.

15. Horsley, G. W.: J. Iron Steel Inst. 182, 43 (Jan. 1956).

16. Haag, F. C.: Liquid Metal Technology, Chem. Eng. Progress Symposium Series, 53, #20, p. 43 (1957).

17. Epstein, L. F.: ibid., p. 67.

18. Holman, W. R.: Mass Transfer by High-Temperature Sodium. AECU-4072, 1958.

19. Hoffman, E. E.: Boiling Alkali Metal and Related Studies. NASA-AEC Liquid-Metals Corrosion Meeting, Dec. 7-8, 1960. NASA-TN-D-769, February, 1961.

20. Owens, J.: Private communication.

JOINING OF REFRACTORY METALS FOR SPACE POWER APPLICATIONS

G. M. Slaughter*
C. W. Fox
E. A. Franco-Ferreira
R. G. Gilliland
Metallurgy Division
Oak Ridge National Laboratory**
Oak Ridge, Tennessee

INTRODUCTION

The ever-increasing role of space technology in the dynamic growth of our nation is apparent. As a result of the tremendous emphasis placed on space flight in the past few years, it is not surprising that the state of development in a number of fields has sometimes been hard pressed to fulfill the dictated requirements. One of the areas that has been pushed to the very limits of existing technology is materials and, in particular, the use of refractory metals as structural materials.

Since many proposed space power systems utilize refractory metals extensively, it is evident that a wide variety of components manufactured from these materials will be required. The joining problems[1-4] associated with the construction of reliable pumps, heat exchangers and nuclear fuel elements have received considerable attention, but it is generally realized that an even greater effort must be expended before the full potential of these metals can be exploited.

---

* Speaker

** Operated for the U. S. Atomic Energy Commission by the Union Carbide Corporation.

The developments reviewed in this paper cover some of the activities conducted along this line by the Metallurgy Division of the Oak Ridge National Laboratory (ORNL). Although this work was performed in support of long-range nuclear reactor technology, it is apparent that the results and findings of the research are also of interest in the space power field. Only a cursory look at a variety of subjects will be attempted in view of the scoping nature of this paper; however, more details have been given in the individual topical reports which have been prepared.

WELDING OF Cb-1 Wt % Zr ALLOY

Of the refractory metals, columbium and some of its alloys are of particular interest because of their good fabricability, their low nuclear cross sections and their good resistance to corrosion by liquid metals.[5] The Cb-1 wt % Zr alloy possesses higher strength than that of pure columbium, but an aging reaction has been observed in both wrought material and in welds. A program was undertaken to study the aging behavior of welds in this alloy since certain thermal treatments result in a severe loss in ductility along with an abrupt increase in strength.[6]

In order to conserve material, the room-temperature, longitudinal bend test was selected for a major part of the testing program. In all cases, bend testing was performed on single-pass, full-penetration, square-butt fusion welds in 0.060-in.-thick sheet with the bend radius being 2T (T = sheet thickness). The welding was performed in the inert-atmosphere chamber shown in Figure 1. Three criteria of ductility were established and are illustrated in Figure 2. These are (a) ductile, i.e., a full 180-degree bend with no cracking; (b) ductile with cracks, i.e., a full 180-degree bend with surface cracking; and (c) brittle, i.e., considerably less than a 180-degree bend where cracking was initially observed. A specimen which is susceptible to an aging reaction will show either the brittle or ductile-with-cracks behavior while an acceptable weld will always be ductile.

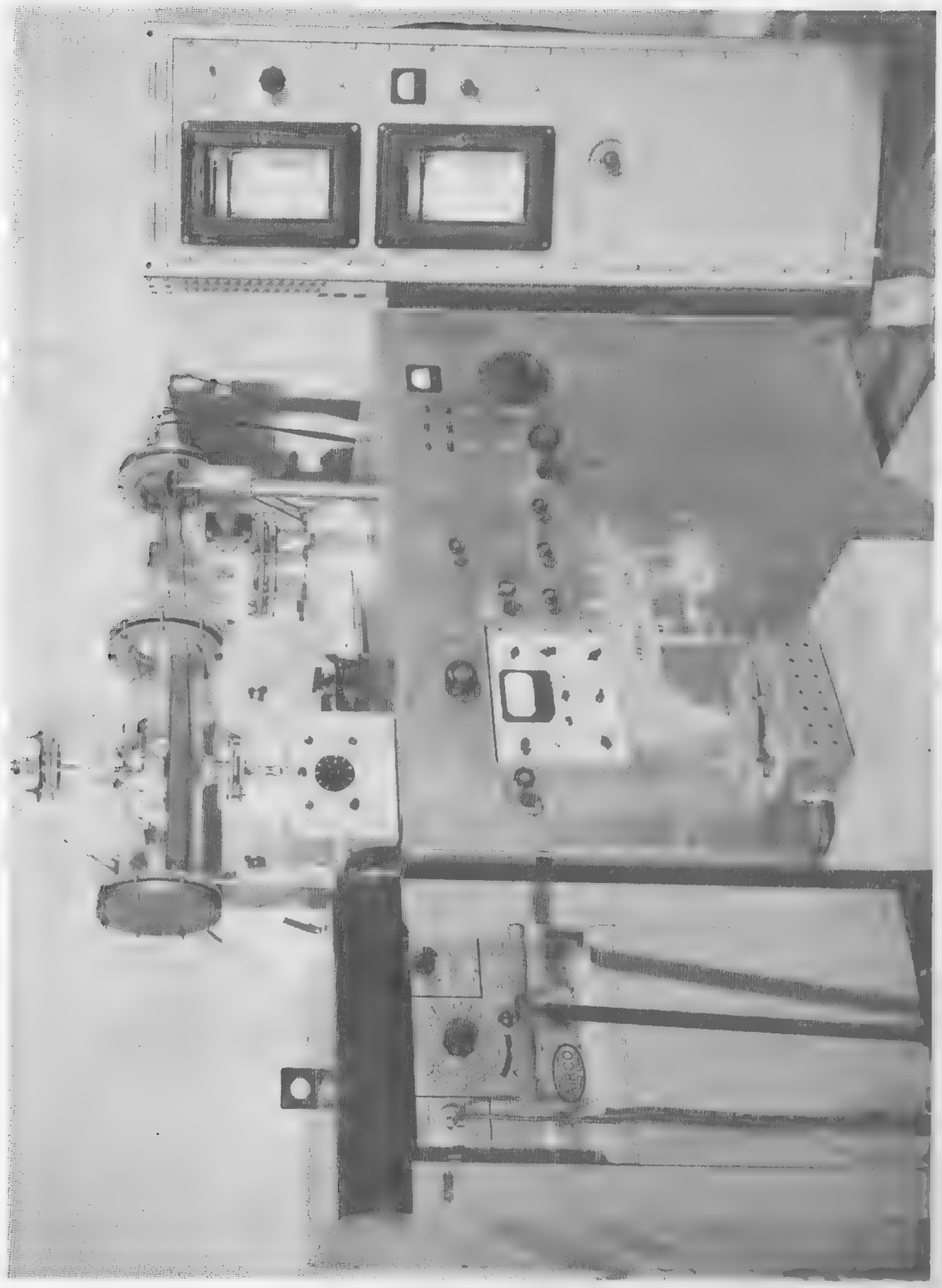


FIGURE 1 (ORNL PHOTO 50278) INERT-ATMOSPHERE WELDING CHAMBER USED IN Cb-1 WT % Zr WELD-AGING STUDY

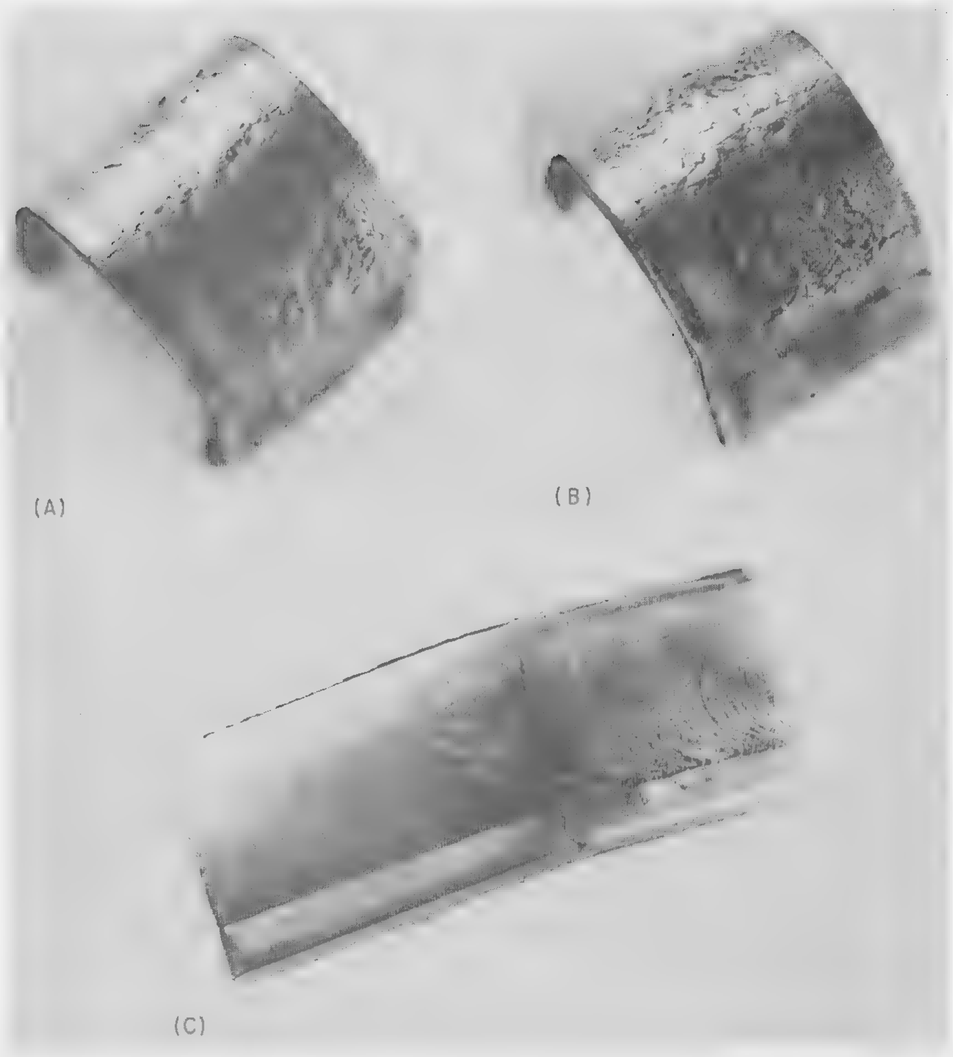
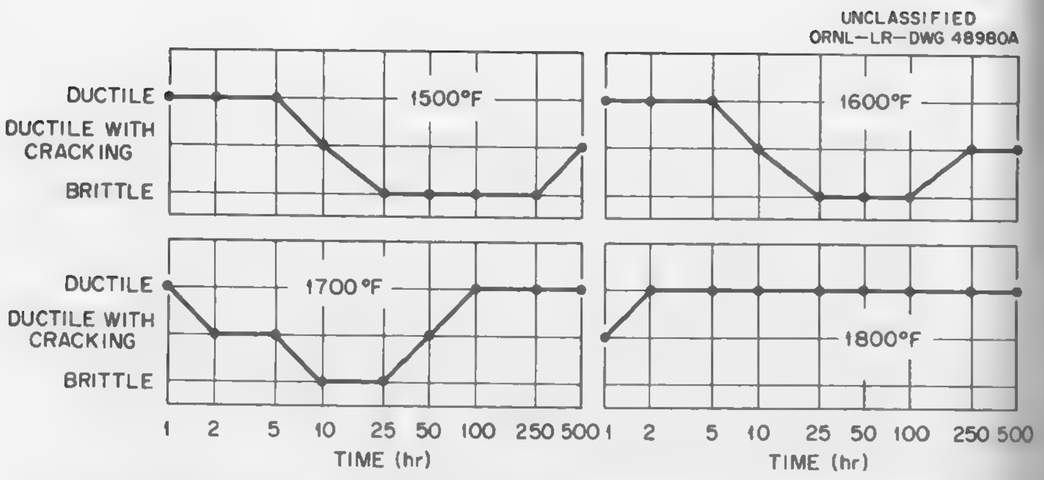


FIGURE 2 (Y-36223) ILLUSTRATION OF THE THREE BEND-TEST DUCTILITY CRITERIA FOR Cb-1 WT % Zr ALLOY WELDS. (A) DUCTILE: (B) DUCTILE WITH CRACKS: AND (C) BRITTLE. 2X



Influence of Aging Time at Various Temperatures on the Bend-Test Behavior of Cb-1% Zr Alloy (Heat XM-339).

FIGURE 3 (ORNL-LR-DWG 48980A) INFLUENCE OF AGING TIME AT VARIOUS TEMPERATURES ON THE BEND-TEST BEHAVIOR OF Cb-1 WT % Zr ALLOY

The result of a series of bend tests run on aged welds made in one heat of Cb-1 wt % Zr alloy are shown in Figure 3. The welds were aged at 1500, 1600, 1700 and 1800°F for times ranging from 1 to 500 hr. It appears that the aging reaction is a typical example of precipitation hardening and recovery through overaging. This contention is supported by Figure 4, a composite of microstructures representing as-welded, aged and overaged conditions. While no precipitate is visible in the as-welded microstructure, the as-aged structure reveals the presence of thin grain-boundary phases and the overaged structure shows a definite increase in the amount of precipitate in the subgrain network.

A postweld annealing treatment was found to be highly useful in preventing aging and its subsequent embrittlement. The improvement afforded by a 1-hr anneal at 2200°F before aging is shown strikingly in Table I. Welds 1 and 2 show the expected behavior when aging is encountered but Weld 3, after annealing, shows no embrittlement.

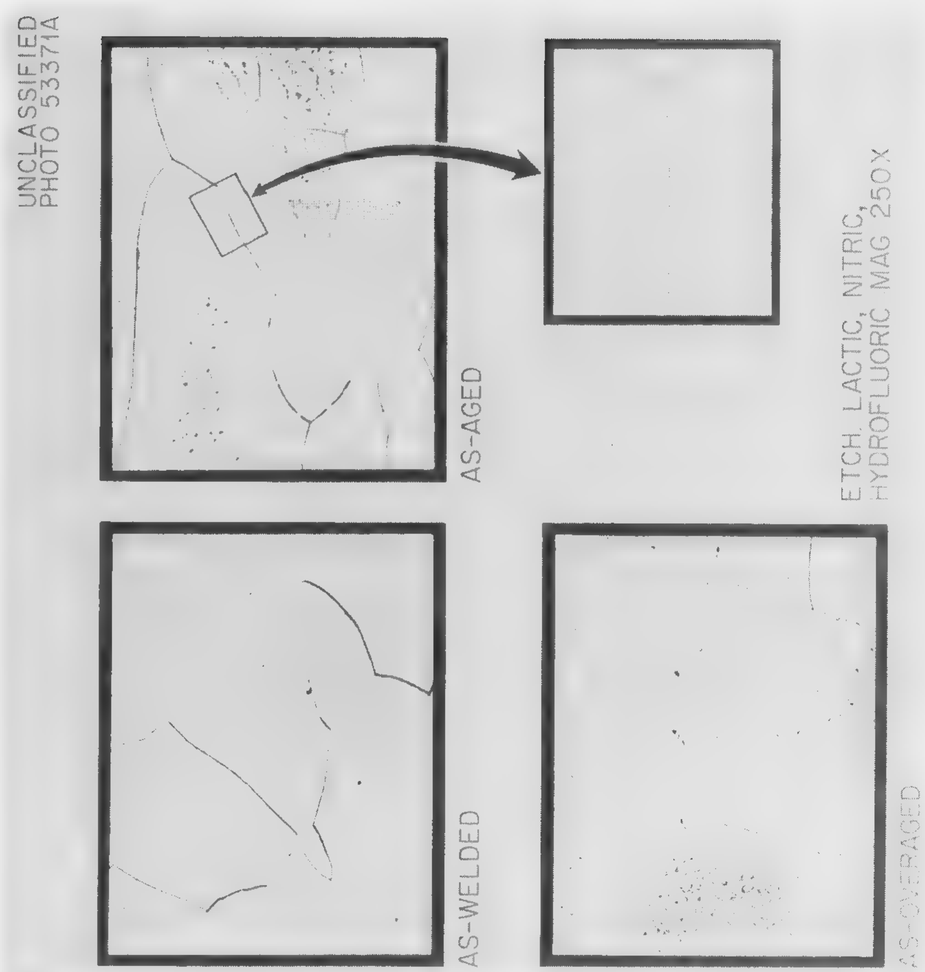


FIGURE 4 (ORNL PHOTO 53371A) AS-WELDED, AS-AGED AND AS-OVERAGED MICROSTRUCTURES IN Cb-1 WT % Zr WELDS. ETCH: MIXED ACIDS WITH HF (INSERT IS 1000 X). 250 X

TABLE I

RESULTS OF ANNEALING STUDIES ON WELDS

Weld No.	Annealing Treatment	Aging Treatment	Bend Test Results
1	As-welded		Ductile
2	--	100 hr at 1500°F	Brittle
3	1 hr at 2200°F	100 hr at 1500°F	Ductile

A metallographic survey was made of the specimens used in the heat-treating study. A portion of this survey, presented in the composite in Figure 5, compares the microstructures of the specimens annealed for 2 hr at the various temperatures. Microstructures of the specimens aged at 1500°F after annealing are also shown, as are the as-welded and as-aged microstructures. After annealing at 1700 and 1800°F, the microstructures show little difference from that of the as-aged weld. Upon annealing from 1900 through 2200°F, a precipitate forms which is heavier at the higher temperatures and the mechanical properties of the weld are improved. Subsequent aging for 100 hr at 1500°F did not cause embrittlement because the massive precipitate found with the high-temperature post-weld heat treatment was not altered.

The phase or phases causing the observed aging reaction have not been identified thus far but are believed to be associated with interstitial impurities in the parent material.

BRAZING OF COLUMBIUM

The potential advantages of high-temperature brazing in the fabrication of relatively complex components of columbium can be readily seen. However, the use of brazing for constructing these items (finned-tube heat exchangers,

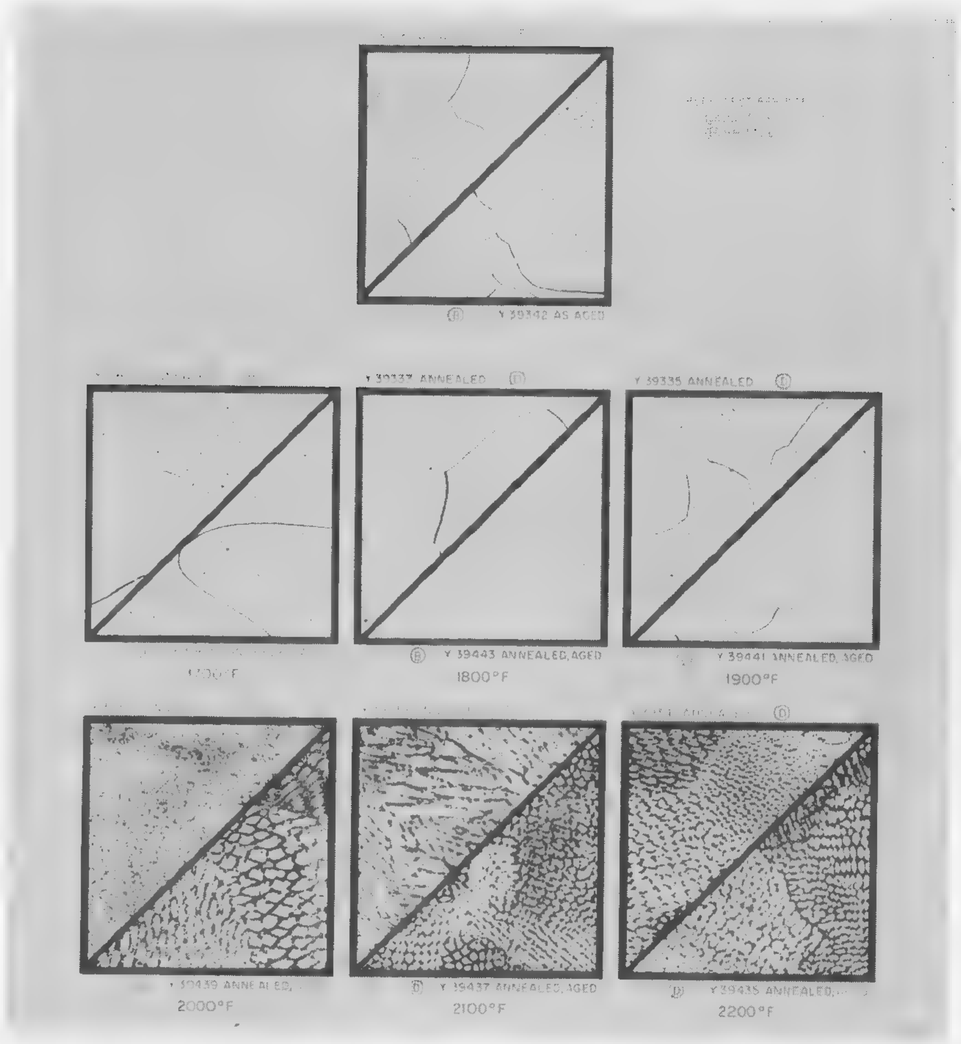


FIGURE 5 (ORNL PHOTO 53268R) PANORAMA OF MICROSTRUCTURES OF ANNEALED-AND-AGED WELDS (AGING TEMPERATURE - 1500°F). ETCH: MIXED ACIDS WITH HF

fuel elements, etc.) has been hindered by the lack of brazing alloys specifically developed for joining columbium.[7]

A study is under way at ORNL to develop suitable binary, ternary and quaternary alloys for brazing columbium.[8,9] Vacuum brazing is being used throughout this study since columbium is readily contaminated in other conventional furnace atmospheres, such as dry-hydrogen and low-purity inert atmospheres.

The survey of a large number of binary-phase diagrams revealed that some of the most promising alloys for liquid metal service lay in the titanium-base and zirconium-base systems. Since the vacuum brazing of large assemblies may be difficult to accomplish at high temperatures, a primary aim in the study was that the brazing alloys developed should melt below 2400°F. A minimum melting point of 1830°F was also set in view of the many potential service applications in the 1500-1800°F temperature range.

Several highly promising brazing alloys have been developed which readily wet and flow on columbium. Table II lists some of these alloys and their flow points.

TABLE II

PROMISING BRAZING ALLOYS FOR COLUMBIUM

Alloy (wt %)	Flow Point (°F)
67 Zr-29 V-4 Fe	2370
60 Zr-25 V-15 Cb	2340
48 Zr-48 Ti-4 Be	1920
45 Ti-40 Zr-15 Fe	1920
62 Ti-26 Fe-8 Mo-4 Zr	2280

An example of a columbium T-joint brazed with the 48 Ti-48 Zr-4 Be (wt %) alloy at 1920°F is shown in Figure 6. Excellent flowability is indicated. A photomicrograph of a joint brazed with the 45 Ti-40Zr-15 Fe (wt %) alloy is shown in Fig. 7. It can be seen that excellent base-metal wetting was obtained with little or no base-metal erosion or brazing-alloy cracking.

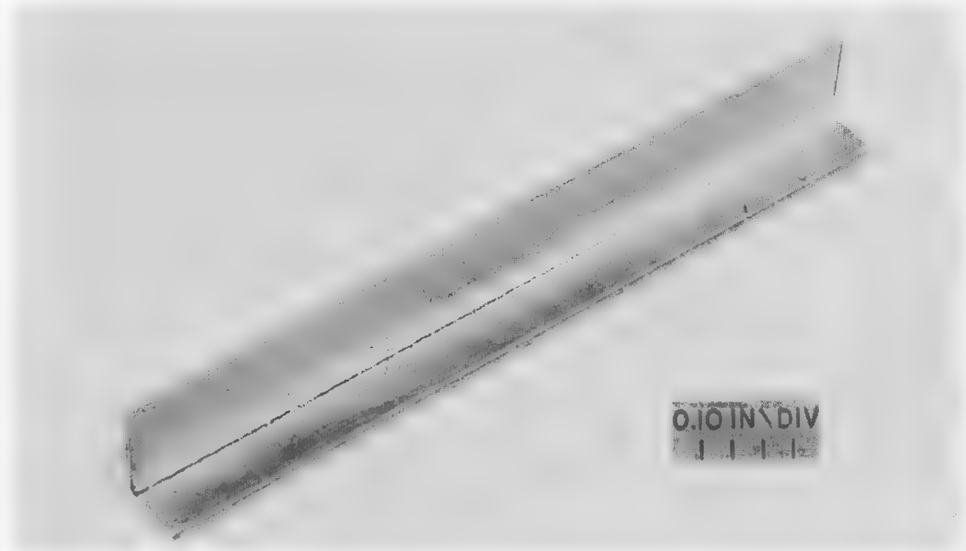


FIGURE 6 (Y-40367) COLUMBIUM T-JOINT BRAZED WITH 48 Ti-48 Zr-4 Be (WT %)

Room-temperature shear tests of the Miller-Peaslee[10] type have shown that joint shear strengths of at least 30,000 psi can consistently be made with these alloys. The determination of elevated-temperature mechanical properties and the behavior of joints after elevated-temperature aging and after thermal cycling are currently under study.



FIGURE 7 (Y-40899) PHOTOMICROGRAPH OF COLUMBIUM T-JOINT BRAZED WITH 45 Ti-40 Zr-15 Fe (WT %) ILLUSTRATING A SOUND JOINT. AS POLISHED

FABRICATION OF COLUMBIUM IRRADIATION TEST SPECIMENS

The fabrication of several miniature columbium in-pile irradiation tube-burst test assemblies was successfully undertaken and an exploded view of a typical assembly is shown in Figure 8. The end caps were welded into the columbium capsule by the tungsten-arc process. The electron-beam welding process was then used as a concentrated and rapid heat source to braze the thin-walled

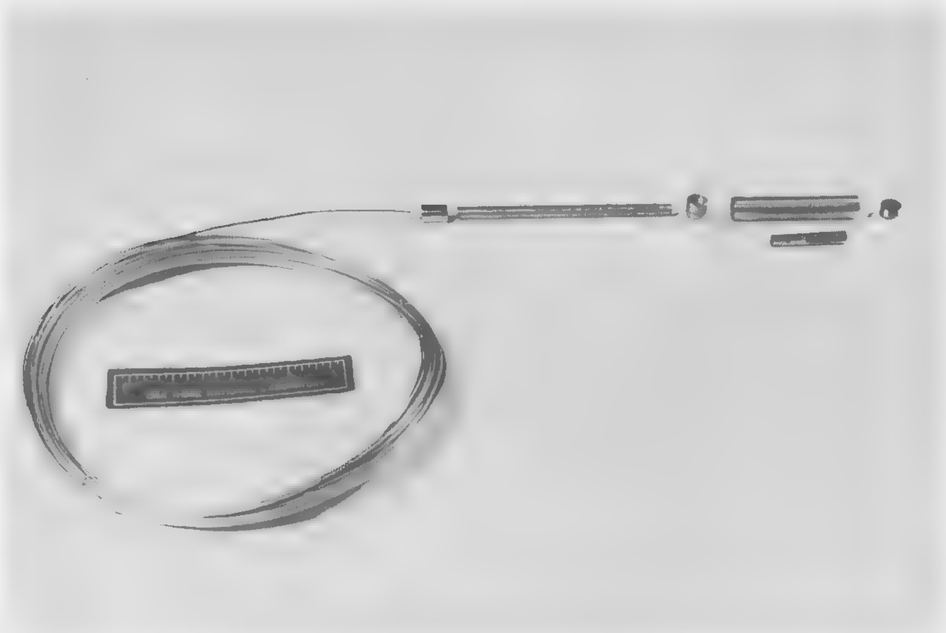


FIGURE 8 (ORNL PHOTO 51497) EXPLODED VIEW OF A TYPICAL COLUMBIUM IN-PILE IRRADIATION TUBE-BURST TEST ASSEMBLY

stainless steel capillary pressurizing tube to the columbium. A molybdenum transition sleeve was required between the stainless steel and columbium to permit the formation of a high-integrity brazed joint. The completed assembly is shown in Figure 9.



FIGURE 9 (ORNL PHOTO 51496) COMPLETED COLUMBIUM IRRADIATION ASSEMBLY

WELDING AND BRAZING OF BERYLLIUM

The unique properties of beryllium, such as its low-neutron absorption cross section, make it extremely attractive as a cladding material for advanced fuel elements. The obvious lack of suitable joining procedures, however, has been a major obstacle in the consideration of this metal for high-temperature nuclear applications. Serious weld-metal

and heat-affected zone cracking difficulties have been encountered by several investigators, and gross weld-metal porosity and brittle joints are other common salient defects.[11, 12] The development of brazing alloys for joining beryllium has been hindered by the generally poor wettability of this material and the rapid formation of brittle intermetallics along the base metal-braze metal interface. The development of suitable joining techniques for beryllium is therefore in progress in an effort to improve the over-all technology of fabricating advanced fuel elements.

The welding studies have been concerned with the production of sound, high-integrity, tube-to-end cap welds and optimum values of the important welding variables, such as welding current, welding speed, inert-gas flow rate and preheat, have been determined.[13] As a result of these studies, two beryllium-clad capsules containing UO_2 for irradiation investigations and over 200 beryllium tube-burst specimens for use in high-temperature in- and out-of-pile testing were successfully completed. Figure 10 illustrates a typical completed tube-burst specimen while a photomicrograph of a sound, high-integrity weld is shown in Figure 11. The stainless steel pressurizing tube was brazed into one end of each capsule with a 49 Ti-49 Cu-2 Be (wt %) brazing alloy developed at ORNL. A cross section of a joint revealing the excellent flow and integrity of the braze metal is shown in Figure 12.

SUMMARY

It is apparent that the fabricators of structural components of the refractory metals and beryllium are faced with a variety of problems since these materials are considerably more difficult to join than are the more common materials of construction. This paper has described some of the developments conducted at ORNL to assist in the utilization of these materials for useful components of construction. The aging of welds in the Cb-1 Zr (wt %) alloy was studied extensively and methods for minimizing the undesirable effects have been developed. Alloys and procedures for brazing columbium have been developed, as have satisfactory procedures for welding end closures in beryllium tubes.



FIGURE 10 (Y-37703) BERYLLIUM TUBE-BURST TEST ASSEMBLY

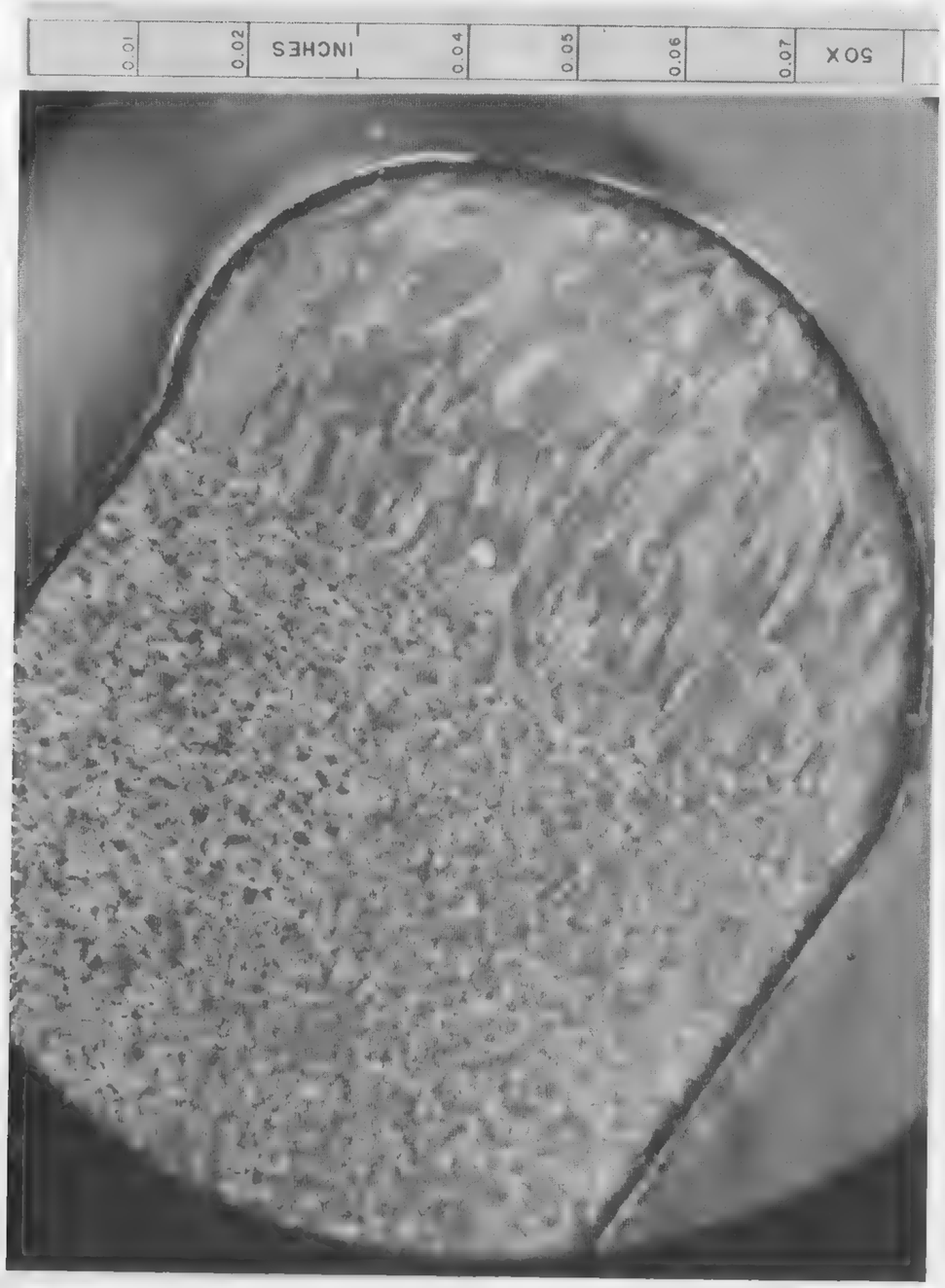


FIGURE 11 (Y-36565) SOUND BERYLLIUM TUBE CLOSURE WELD. AS POLISHED.

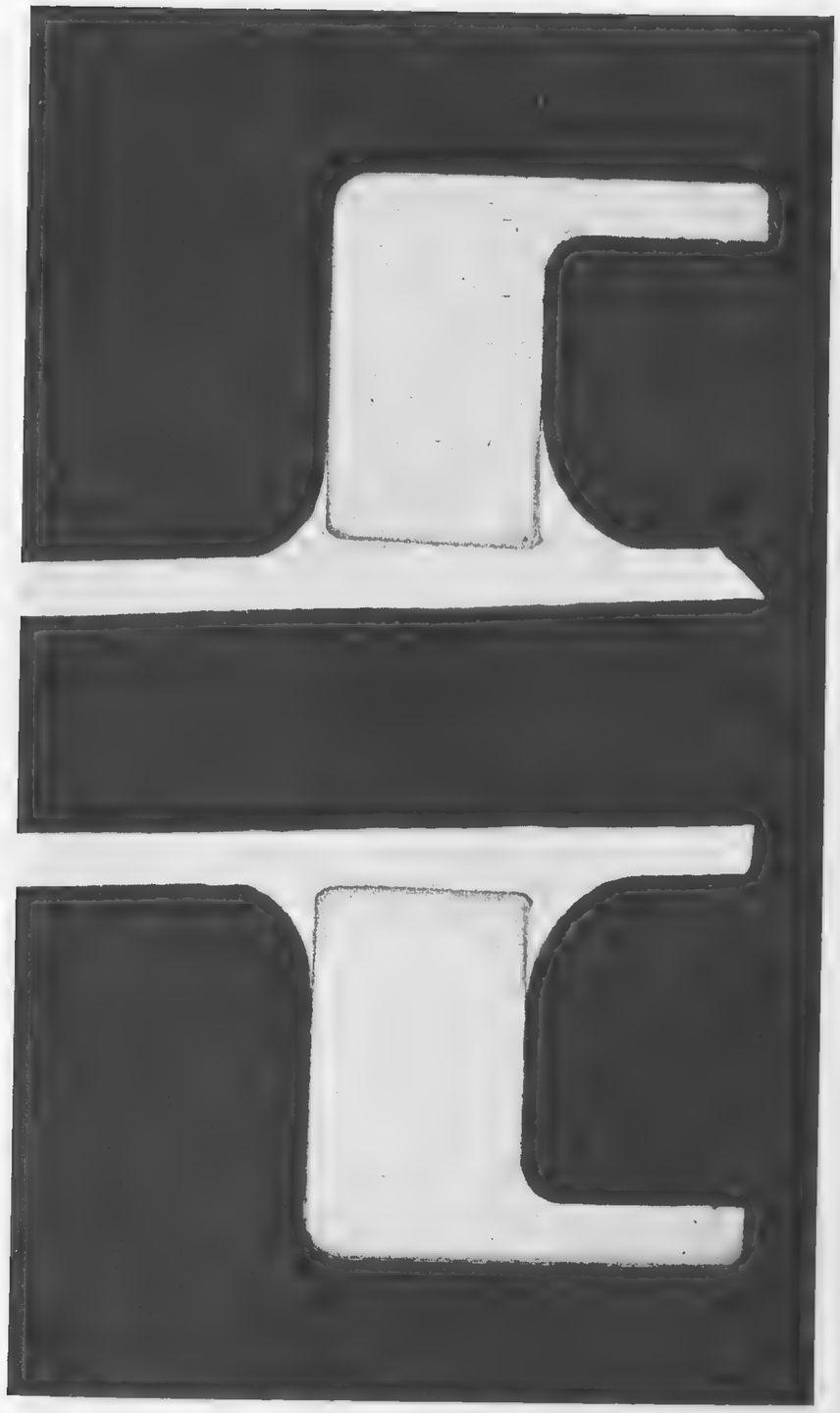


FIGURE 12 (Y-32357) BRAZED JOINT BETWEEN STAINLESS STEEL AND BERYLLIUM. THE BRAZING ALLOY IS A 49 Ti-49 Cu-2Be (WT %) COMPOSITION DEVELOPED AT ORNL

BIBLIOGRAPHY

1. "Materials Advisory Board Report of the Committee on Refractory Metals," Panel Reports, Chap. II, MAB-154-M(1) Vol. II (October 15, 1959).

2. Platte, W. N., "Welding of Molybdenum," The Metal Molybdenum, American Society for Metals (1958).

3. Schwartzburg, F. R., H. R. Ogden and R. I. Jaffee, Ductile-Brittle Transition in the Refractory Metals, DMIC Report 114 (June 25, 1959).

4. Slaughter, G. M., "Welding and Brazing of Refractory Metals," J. Soc. Automotive Eng. 69, 52-55 (1961).

5. "Columbium," Reactor Handbook, 2nd ed., Vol. I, Chap. 26, pp. 621-35, Materials, Interscience Publishers, Inc., New York, 1960.

6. Franco-Ferreira, E. A., and G. M. Slaughter, "Welding of Columbium-1% Zirconium," Welding J. (to be published).

7. Jahnke, L. P., R. G. Frank and T. K. Redden, "Columbium Alloys Today - Considerations in Design and Fabrication of Structures," Metal Progress 78 (1), 76-80 (1960).

8. Fox, C. W. and R. G. Gilliland, Progress Report on Brazing of Columbium, ORNL-CF-61-7-24 (July 5, 1961).

9. Fox, C. W., R. G. Gilliland and G. M. Slaughter, "Brazing of Columbium," paper to be presented at American Welding Society 43rd Annual Meeting, Cleveland, Ohio, April 9-13, 1962.

10. Peaslee, R. L. and F. M. Miller, Proposed Industry Wide Standard Procedure for Testing the Shear Strength of Brazed Joints, Wall-Colmonoy Corp., Detroit 3, Michigan.

11. Weare, N. E. and R. E. Monroe, Joining of Beryllium, DMIC Memorandum 13 (March 30, 1959).

12. GCR Quart. Prog. Rept. June 30, 1960, ORNL-2964, pp. 138-45.

13. Gilliland, R. G. and G. M. Slaughter, "Welding of Beryllium," paper presented at Fall Meeting of American Welding Society, Dallas, Texas, September 25-29, 1961.

A NUCLEAR FUEL ELEMENT FOR SPACE APPLICATION

Charles C. Woolsey
Assistant to Director
Fuels and Materials Department
Atomics International
Canoga Park, California

ABSTRACT

A nuclear fuel element has been developed for the SNAP-2 reactor. This reactor system is designed to provide 3 KW of electrical power to operate the instruments aboard a satellite vehicle. The reactor will develop 50 KW of heat which will be transferred at 1200°F by NaK to the boiler of a mercury turbo-generating plant.

The fuel element utilizes a solid-homogeneous fuel-moderator material, enriched uranium fuel in a matrix of zirconium hydride. The latter has the moderating capability of cold water but maintains this capability up to temperatures as high as 1400 or 1500°F. This temperature limitation results only from the increase in hydrogen dissociation pressure and the attendant hydrogen and pressure containment problems.

Properties of the fuel-moderator material have been studied extensively. The material is quite brittle, with mechanical properties somewhat like those of a ceramic. On the other hand, its thermal and electrical properties are more like those of a metal. Resistance to radiation damage is excellent for the limited exposures studied.

Cladding material development for the fuel element has been dictated primarily by the hydrogen and pressure containment requirements.

INTRODUCTION

There are several types of energy sources available to provide the power necessary to operate the instruments in the satellites presently in space. Batteries were used in the early vehicles, but these not only have a limited life but are rather heavy for the power they provide. Solar cells are limited in potential power level by the very large collecting and radiating surfaces required. As larger satellites are developed, greater power capabilities are required and longer operating lives are desired. The answer appears to lie in the use of nuclear reactor power plants. The SNAP programs are aimed at this target; in fact the term SNAP is created from its full name, System for Nuclear Auxiliary Power. The major objectives for such a system include:

1. Compactness and weight; costs of placing material in orbit have been estimated to run from $1,000 to $15,000 per pound; also space and weight not required for the power system can be replaced by payload (instruments, etc.).

2. Life; at least one year of operation.

3. Environment; the system must withstand the shock and vibration conditions encountered during vehicle launch and must be able to operate in the zero gravity and other conditions of outer space.

4. Remote startup capability; for safety reasons the reactor cannot be placed in operation until the vehicle is in its established orbit.

5. Reliability; the system must operate without maintenance throughout its lifetime.



FIGURE 1 SNAP-2 FLIGHT CONFIGURATION

The SNAP-2 program has been under active development at Atomics International for about five years. The SNAP-2 system will provide 3 kilowatts of electrical power continuously for a period of a year or longer. The system is composed of two major components, the nuclear reactor and the power conversion loop. The nuclear reactor generates 50 kw of heat which is transferred by a liquid metal coolant, NaK (sodium-potassium eutectic), to the boiler of the power conversion loop. The latter operates with a Rankine thermodynamic cycle with mercury as the working fluid. This was selected as the cycle with the highest probability of providing an optimum weight consistent with reliability and lifetime requirements. A view of a full-scale model is shown in Figure 1. The reactor is shown at the upper end of the vehicle, with a conical shield just below it providing the radiation attenuation necessary to protect the instruments which would be located in a section of the vehicle below the one shown.

Other SNAP systems under development at Atomics International include the SNAP-8 and SNAP-10A systems. The latter utilizes a nuclear reactor quite similar to that for the SNAP-2 system. However, it utilizes a direct conversion, thermoelectric unit for power generation. The heat generated in the reactor is transferred by a liquid metal coolant to the high temperature side of the thermoelectric elements; the low temperature side is thermally connected to a radiator. Efficiencies are somewhat lower but this is offset by the lack of any rotating machinery. The SNAP-10A reactor will provide 500 watts of electrical power, with the reactor generating 30 kw of heat.

The SNAP-8 system is a higher temperature, higher power version of the SNAP-2 system. It will provide 30 to 60 kw of electrical power, with a reactor only slightly larger than for SNAP-2.

THE NUCLEAR REACTOR

As was seen in Figure 1, the SNAP-2 reactor is quite small, perhaps about the size of a five gallon paint can. The reactor is shown in more detail in Figure 2. The heart of

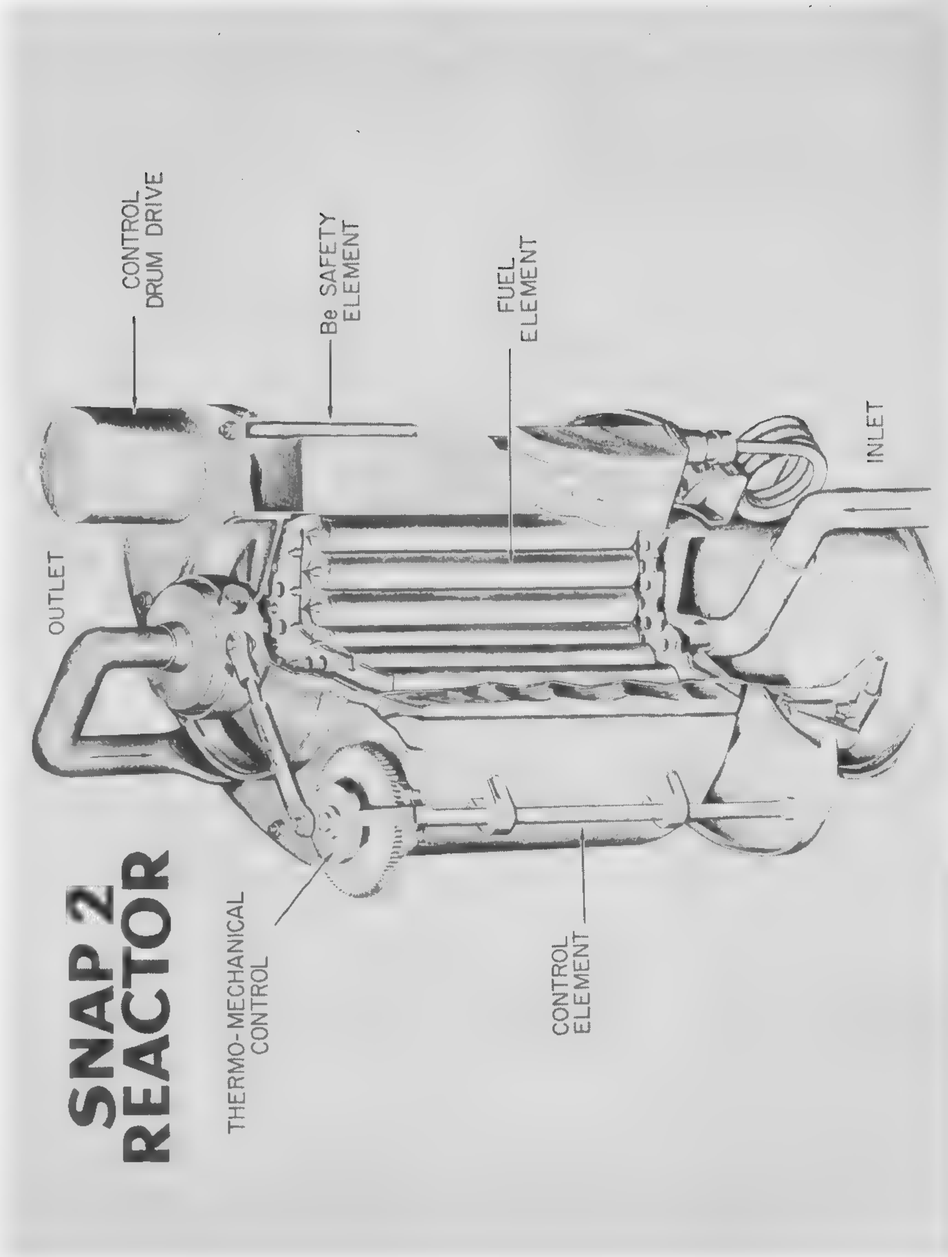


FIGURE 2 SNAP-2 REACTOR

the reactor is the nuclear fuel element, which contains a dispersion of uranium-235 in zirconium hydride. It is the fissioning of this uranium-235 that produces the heat that makes possible the production of power from nuclear energy. The zirconium hydride acts as a neutron moderator; other materials commonly used for this purpose include water and heavy water, graphite, beryllium, and organic materials. Zirconium hydride has about the same moderating ability as cold water. However, it can be used effectively well above the critical point of water, at temperatures up to 1400 and 1500°F, with essentially no loss in moderating capability.

The SNAP-2 reactor contains 37 rod type fuel elements in a cylindrical container. NaK is introduced at the lower end at 1000°F and is raised in temperature by the fuel elements to 1200°F. Maximum temperature in the fuel is 1300°F. Outside of the core vessel, a layer of beryllium metal acts as a neutron reflector. Both the moderation provided within the core by the zirconium hydride and the reflection provided externally by the beryllium are necessary to maintain the fissioning process in the fuel. Removal of some of the reflector can cause the reactor to become subcritical. This provides a method to control the reactor at the desired power level; a drum of beryllium turns out of the reflector, the amount of reflection determining the operating level of the reactor. This same principle is used for a safety element. A sector of the reflector can be made to fall away rapidly and thus make the reactor subcritical.

The SNAP-2 compact reactor concept has been aptly demonstrated by the operation of the first in a series of developmental reactors leading ultimately to the operation of one on a satellite in orbit. The SNAP Experimental Reactor (SER) started operation in the fall of 1959 and operated for the equivalent of half a full-power year before completion of the experimental studies planned for it. The second in the series of SNAP-2 reactors, the SNAP-2 Developmental Reactor (S-2-DR), began power operations last summer. Where the SER demonstrated the reactor system only, the S-2-DR will demonstrate the complete system, including the power conversion unit.

THE NUCLEAR FUEL ELEMENT

The fuel element for the SER is shown in Figure 3. The element is 1.0 inch in diameter by 13.5 inches in length. The components that make up the element are shown in the same figure; the fuel-moderator body, two beryllium metal reflector pieces, and the type 347 stainless steel cladding tube and end-closure caps. The SER core consisted of 61 such elements.

Advancements in processing techniques and in the state of knowledge of materials properties allowed a major design improvement for the fuel elements for the S-2-DR. The hydrogen content was increased, the uranium fuel content was increased, the fuel rod size was increased, and the number of elements decreased. The increased fuel loading density and increased moderation resulted in a higher power density and a decrease in reactor size and weight. Table I gives a comparison of elements for the two reactors.

TABLE I

FUEL ELEMENTS FOR SNAP-2 REACTORS

	SER	S-2-DR
Number of Elements	61	37
Diameter, inches	1	1.25
Length, inches	13.5	13.5
U in ZrH_x, wt %	6.88 (x = 1.7)	9.85 (x = 1.85)
Total U_{235}, kg	3.0	4.3
H in ZrH_x, wt %	1.68	1.81
N_H, H atoms/cm^3	6×10^{22}	6.5×10^{22}
Cladding	347 Stainless steel	Hastelloy N
Wall Thickness, mils	10	14
Heat Flux, average BTU/hr/ft^2	12,400	17,000
End Reflector	Be	BeO

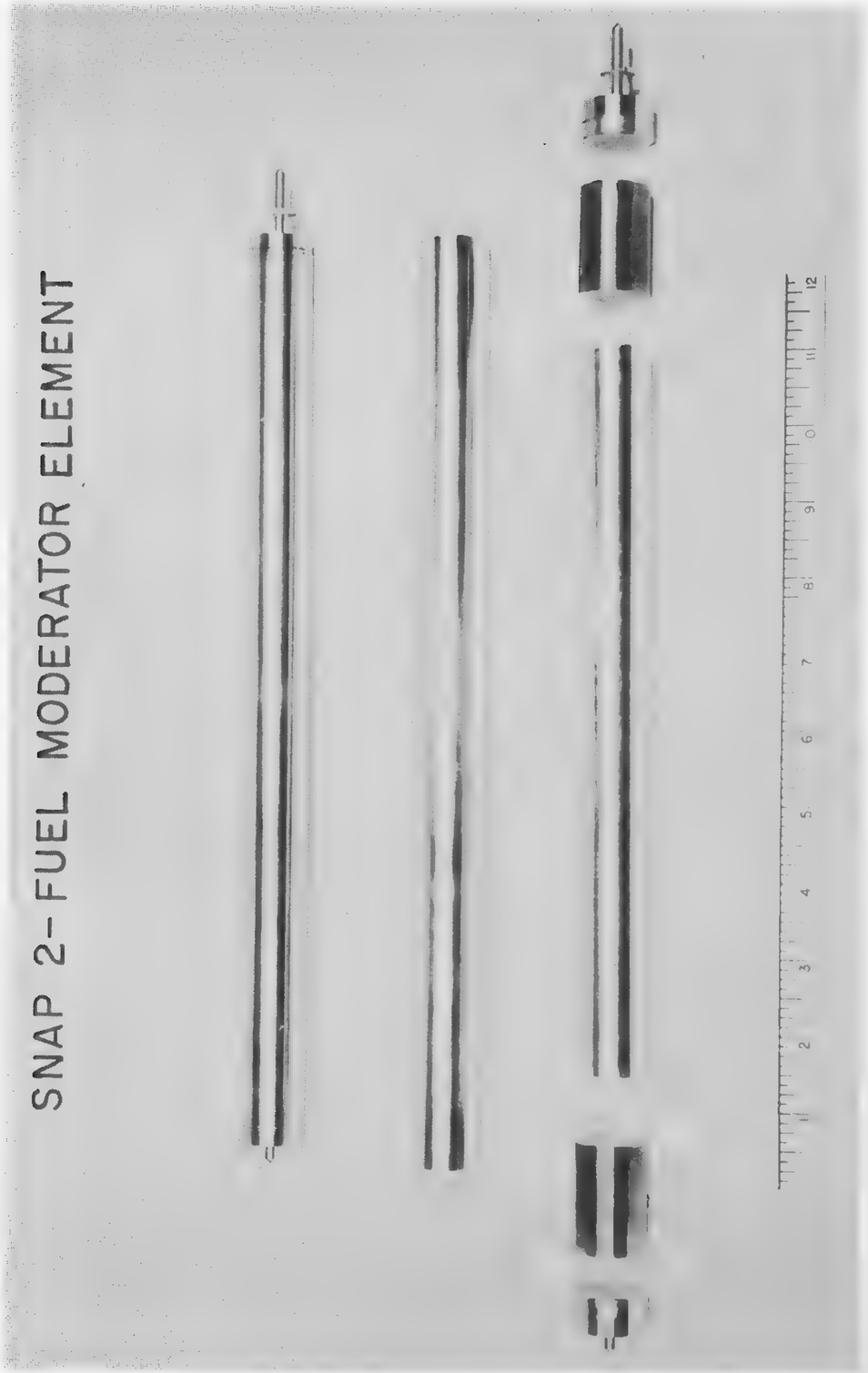


FIGURE 3 SER FUEL ELEMENT

The fuel-moderator rod is prepared by alloying uranium-235 with zirconium and hydriding the resultant alloy rod to the desired hydrogen content. The finished rod contains 9.85% uranium (93% of which is U-235), 1.8% hydrogen and the balance zirconium. It has a hydrogen atomic density (N_H) of 6.5×10^{22} H atoms per cubic centimeter.

The fuel-moderator rod and the two reflector pieces are slip fitted into the cladding tube. The end-closure caps are welded in place to complete the fuel element.

FUEL-MODERATOR MATERIALS

The properties of the fuel-moderator material have been studied quite extensively, to provide a basis for its selection initially, to extend this knowledge to provide an improved fuel material and to predict its behavior under the conditions of operation.

An important phase of this study concerned itself with the zirconium-hydrogen and zirconium-uranium-hydrogen systems. The phase diagram for such a system, in which one of the components is a gas, may be determined by measurement of the dissociation pressure, as a function of temperature and composition. A partial phase diagram for the zirconium-hydrogen system is given in Figure 4. This diagram has been determined at AI largely through studies of P-C-T relationships. X-ray diffraction data, metallography, and electrical properties were used to support the P-C-T studies for the establishment of the diagram. X-ray diffraction data also identified the crystallographic structure of the solid hydride phases.

The portion of the phase diagram shown in Figure 4 indicates two single phase (solid) regions, one a beta-zirconium containing dissolved hydrogen and the other the delta zirconium hydride phase. The former has a body-centered cubic structure. The delta phase appears to have two structural forms, dependent upon hydrogen composition and temperature. In the zirconium-rich regions the structure is face-centered cubic, and with higher hydrogen contents a face-centered tetragonal structure (delta prime) appears. There is evidence

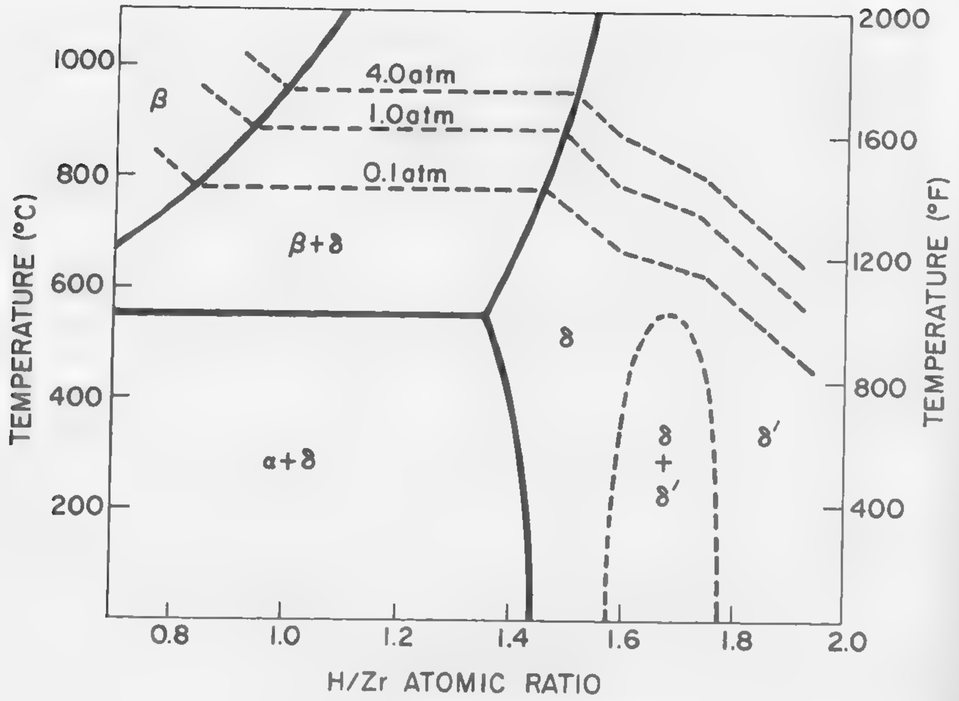


FIGURE 4 THE ZR-H PHASE DIAGRAM

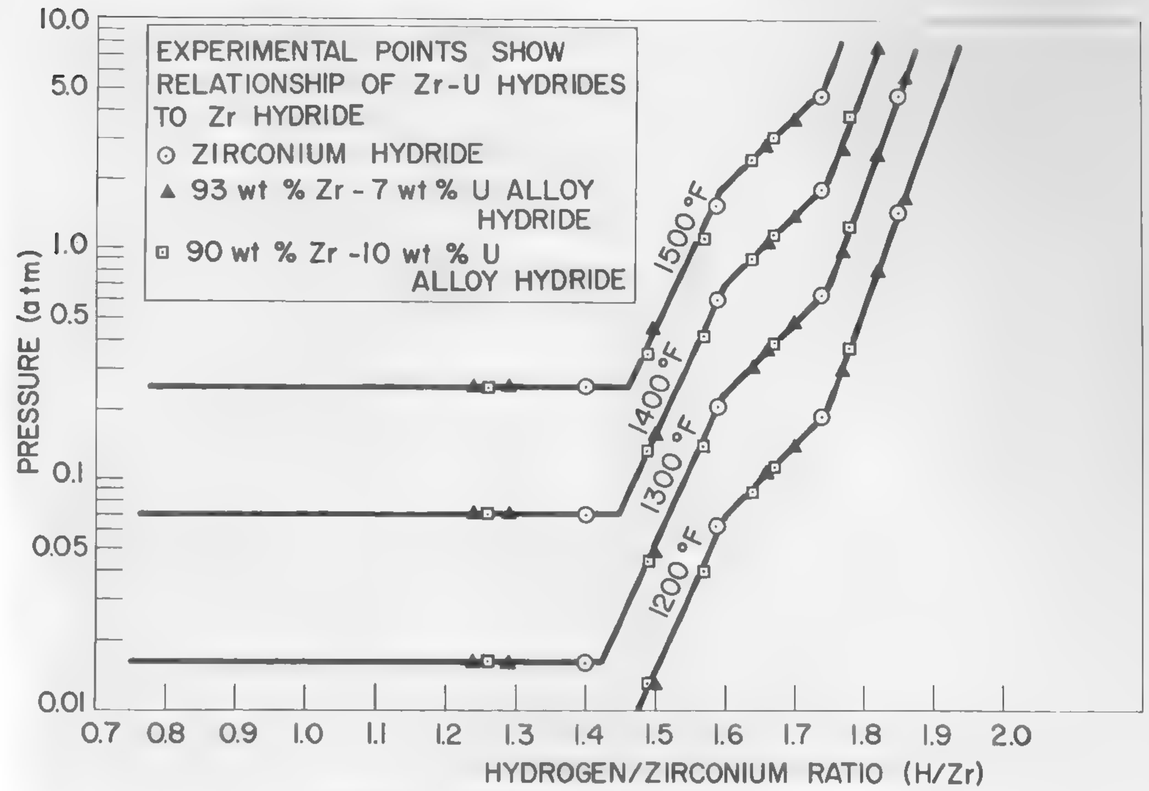


FIGURE 5 ISOTHERMALS OF ZR-H SYSTEM

that at temperatures below about 1000°F, a two-phase region exists. The effects of hydrogen pressure on this system are noted in the diagram by the three constant pressure lines. In a true two-phase region (beta plus delta) pressure is dependent upon temperature only, and is independent of composition. A change in the slope of these lines will be noted above the delta-delta prime region. It is believed that this is indicative of the delta-delta prime change being a second order effect, perhaps a distortion of the face-centered cubic lattice. High-temperature X-ray diffraction work is being carried out to help clarify this picture.

Pressure-composition-temperature studies on hydrided zirconium-uranium alloys have indicated that the uranium is precipitated from the solid solution alloy during the hydriding process. Four isotherms are plotted on the dissociation pressure-composition chart of Figure 5, the data being from hydrides of zirconium and two zirconium-uranium alloys. The composition is given in terms of the hydrogen to

zirconium atomic ratio. Since all points for a given temperature fall on the same line, it may be inferred that the uranium is behaving as an inert diluent.

The microstructure of the delta phase of fuel-moderator material with a H/Zr ratio of 1.7 is shown in Figure 6. It shows a banded or lamellar structure (in some of the darker grains) which is typical of zirconium hydrides of composition greater than 1.60 H/Zr ratio. The banding is associated with the face-centered tetragonal modification of the delta zirconium hydride phase.

The uranium is evenly dispersed throughout the zirconium hydride matrix and appears as the black specks of the photomicrograph. It precipitates from solid solution as hydrogen is added during the hydriding process. It is probable that this precipitate contains a small amount of dissolved zirconium. Because of the small particle size and small volume per cent of uranium in the material, the composition of the precipitate has not been determined.

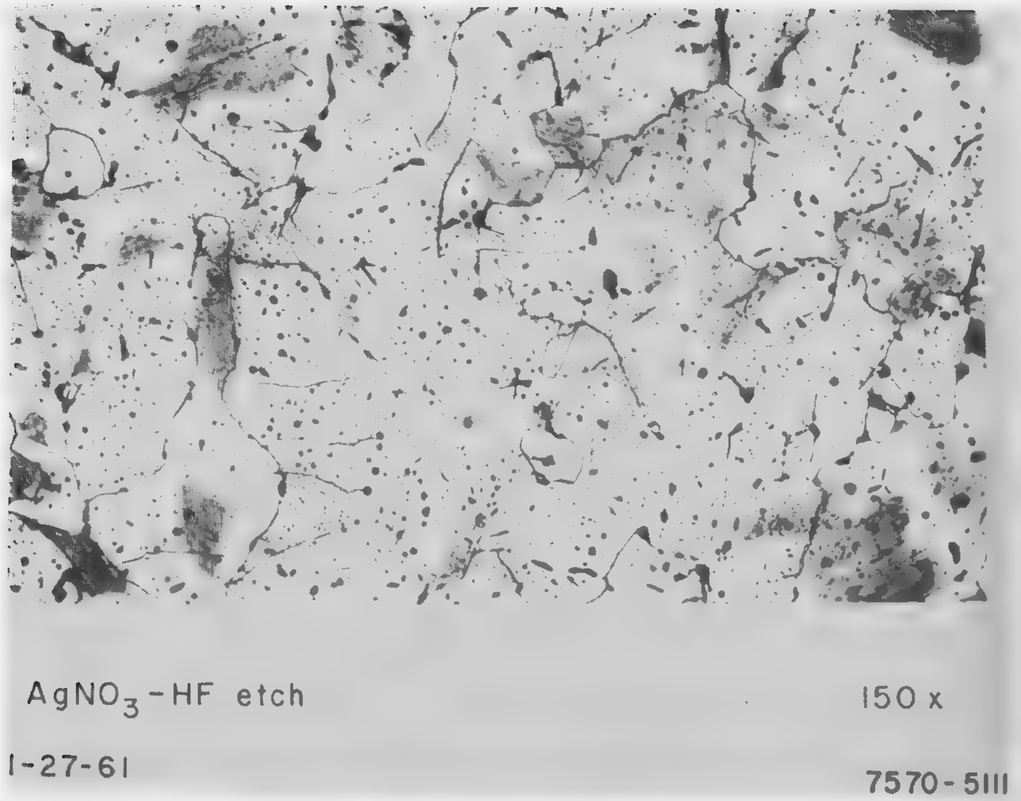


FIGURE 6 MICROSTRUCTURE OF HYDRIDED ZR-U ALLOY

The pressure-composition-temperature relationships discussed above and the relatively high degree of mobility of hydrogen atoms within a metal require a consideration of the effect of possible redistribution of hydrogen within the fuel rod under the influence of the reactor temperature gradient. Figure 7 shows the concentration profile in a specimen of $ZrH_{1.71}$ after being held in a 1000-1300°F gradient for 1344 hours. It is estimated that redistribution is approaching completion by this time and that only slight additional changes will take place. The hydrogen has increased at the cold end at the expense of that at the hot end.

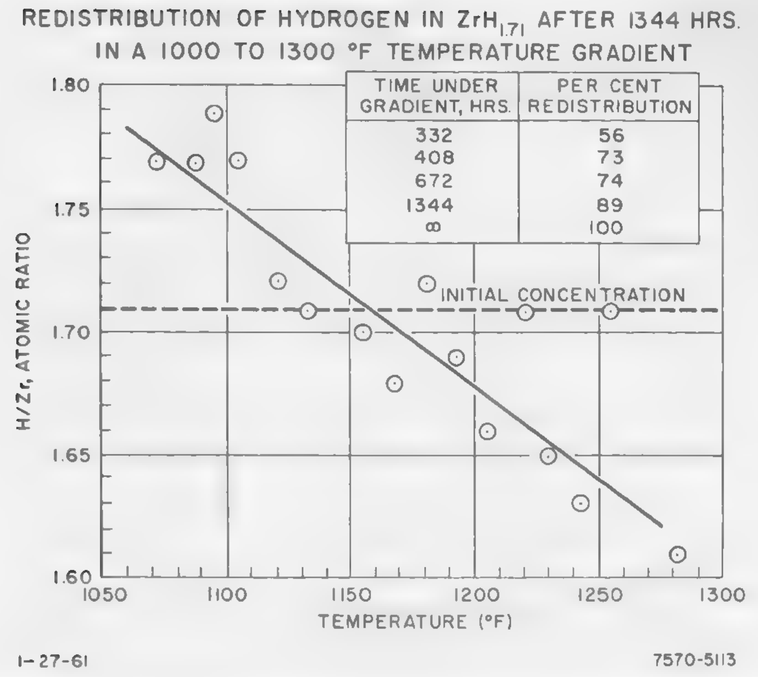


FIGURE 7 REDISTRIBUTION OF HYDROGEN UNDER TEMPERATURE GRADIENT

The over-all hydrogen content has remained the same, however, as a comparison of the area under the redistribution line (solid) with the original composition line (dashed) will show. The perturbation on the nuclear characteristics of the SNAP reactors as a result of this much migration of the moderator is not significant.

The delta hydride fuel-moderator material exhibits behavior characteristics of a brittle material. In fact, it is so notch-sensitive that meaningful values could not be obtained by standard tensile testing techniques. The use of the transverse bend test gave values for ultimate tensile strength considerably higher and more consistent from test to test than achieved with the standard tensile test. Ultimate tensile strength is about 24,000 psi and is little effected by temperature up to 1200°F.

Machining of this brittle material is readily accomplished by conventional centered or centerless grinding operations.

Its thermal and electrical properties are comparable to those of the austenitic stainless steels. The thermal conductivity is about 13 Btu /hr-ft-^{o}F. This favorable conductivity allows one to minimize the number of fuel elements required for a given loading, while still not being heat-transfer limited.

The average thermal coefficient of expansion of the fuel-moderator material is 6.56 microinches per inch per ^{o}F from room temperature to 1300°F, which is slightly less than that for the austenitic stainless steels, but comparable to the Hastelloys. The excellent expansion match of the latter alloys, together with their greater strength at elevated temperatures, was responsible for their selection as the cladding material for these fuel elements.

A list of the physical and mechanical properties of the S-2-DR fuel-moderator material (9.85 weight per cent uranium, 1.8% hydrogen) is given in Table II.

TABLE II

PROPERTIES OF FUEL-MODERATOR MATERIAL

(9.85 weight per cent U, 1.8 per cent H)

Density (unhydrided alloy)	7.0 gm/cc
(hydrided to 1.8% H)	6.0 gm/cc
Thermal Expansion (RT-1300°F)	6.56 x 10^{-6} in./in.-^{o}F
Thermal Conductivity (200-1200°F)	13. Btu/hr-ft-^{o}F
Electrical Resistivity (RT)	60 micro-ohm cm
Elastic Modulus (unhydrided alloy)	14 x 10^{6} psi
(hydrided to 1.8% H)	9 x 10^{6} psi
Transverse Rupture Strength (1200°F)	27 x 10^{3} psi

The irradiation stability for fueled zirconium hydride has been found to be satisfactory for SNAP-2 conditions of temperature and burnup. Samples 5/8 inch in diameter by 1 inch in length were irradiated in capsules in the Materials Testing Reactor to burnups of 0.026 metal atom per cent. Measured central temperatures ranged from 1165-1345°F. Dimensional stability and mechanical integrity were found to be excellent, as may be seen in the post-irradiation photographs of Figure 8.

A second source of irradiation data is in the operation of the SNAP Experimental Reactor. The fuel elements were subjected to about half the burnup to be achieved in the design reactor. No anomalous behavior has been noted in those elements which have been examined.

CLADDING MATERIALS

It will be noted in Figures 4 and 5 that in the regions of particular interest to the SNAP-2 reactor operations, the dissociation pressure between the gas and the solid increases markedly with either increased temperature or increased hydrogen content. In Figure 9 are plotted dissociation pressures as functions of temperature for various constant N_H values. Also plotted on this same graph are rupture pressures (for SER size, 1-inch diameter, 10-mil wall tubes) of Hastelloy B, Hastelloy N, and type 347 stainless steel as functions of temperature. These rupture pressures are calculated from the published high temperature ultimate tensile strength values for these materials. The intersection of a rupture pressure curve with a dissociation pressure curve fixes the maximum temperature at which that particular combination can be used. For example, with an N_H 6.3 fuel-moderator, one could operate for a short term excursion up to about 1575°F with type 347 stainless steel before rupturing the cladding, and up to about 1685°F with the stronger Hastelloys. For long-term operations, considerably lower temperatures must be used to avoid creep in the cladding.

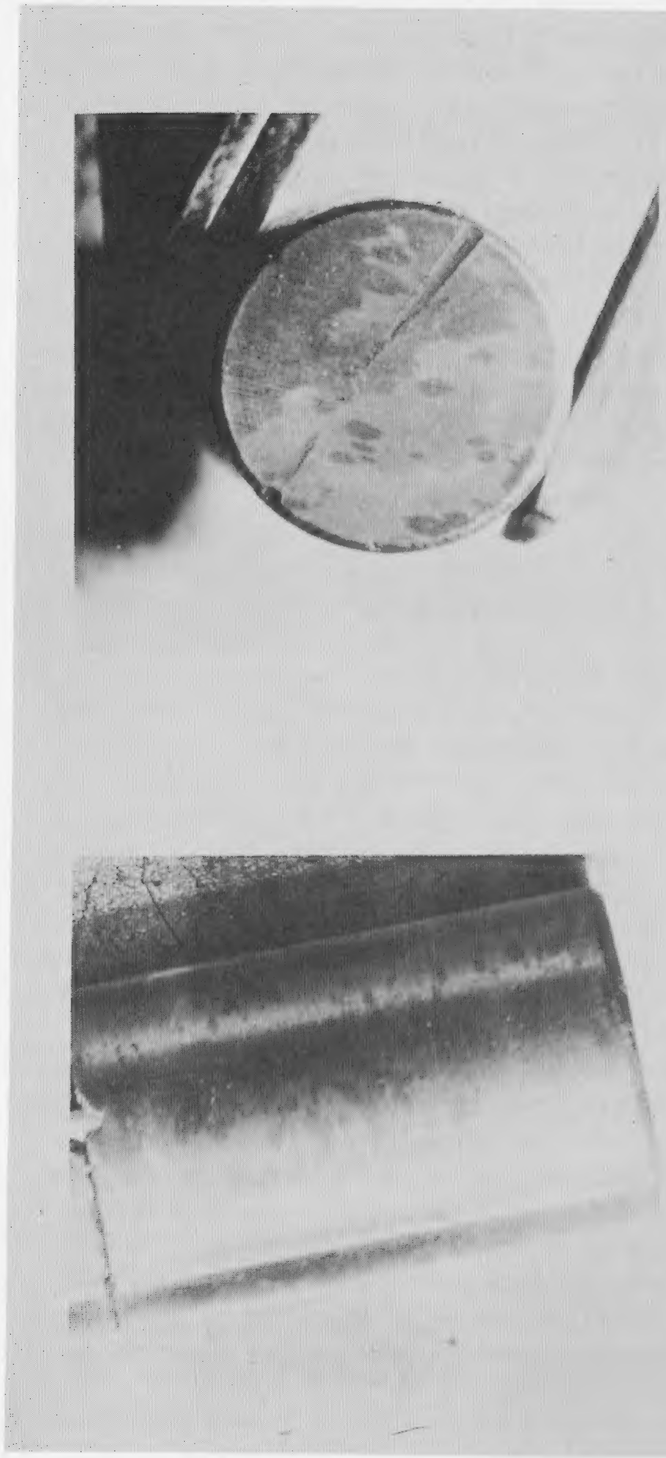


FIGURE 8 SNAP-2 FUEL-MODERATOR PELLET AFTER IRRADIATION

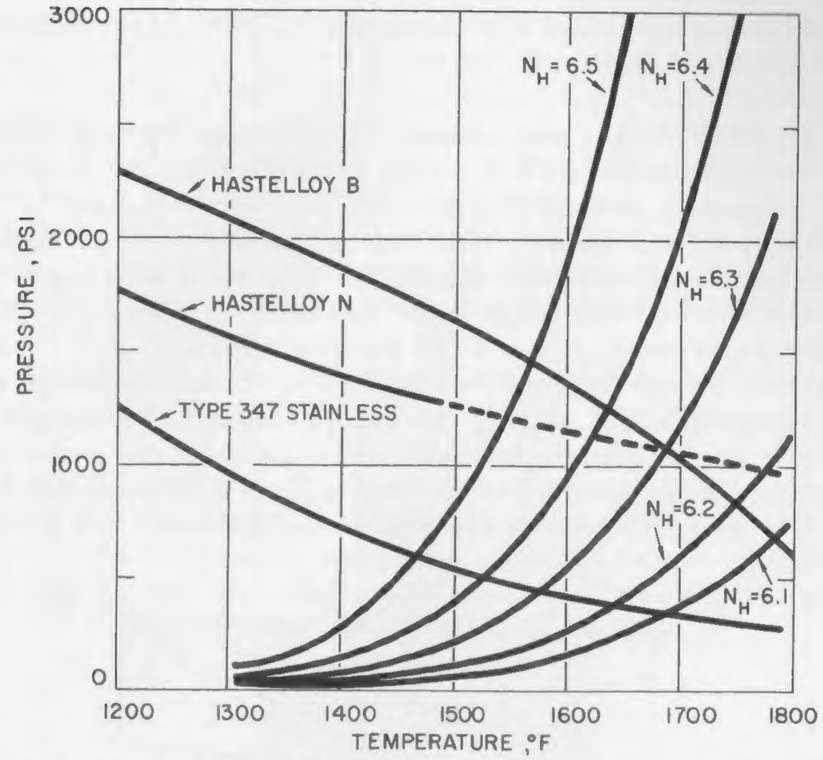


FIGURE 9 BURST TEMPERATURES OF VARIOUS COMBINATIONS OF FUEL AND CLADDING

Under normal operating conditions for the SNAP-2 reactor (about 1300°F peak fuel temperature) the dissociation pressure for the fuel-moderator is about 1.5 atmospheres. As mentioned earlier, the neutron moderation provided by the zirconium hydride is necessary to maintain the fissioning process. It is the hydrogen that is responsible for this, and any loss in hydrogen from the fuel element would result in a loss in reactivity. Hence, one must find a means for preventing appreciable loss of hydrogen.

The reactor control system compensates for some loss in reactivity but this is rather limited and some of it is required to compensate for other reactivity changes that occur. The limit for loss of hydrogen that can be tolerated has been set as 1% of the hydrogen initially in the fuel-moderator rod. This corresponds to a loss rate of about 0.3 cc (STP)

of hydrogen per hour from a rod. This in turn is equivalent to a loss rate through the surface area of the fuel cladding of about 10^{-3} cc/hr-cm^2.

At 1200°F, the permeation of hydrogen through molybdenum is the order of 100 times the rate that can be tolerated, as can be seen in Figure 10. For other metals, the rates are even higher. This led to a study of other types of materials for hydrogen retention. The most obvious answer was the use of a hydrogen-tight ceramic or glass cladding. Relative permeation rates for several types of glasses and ceramics are also given in Figure 10. It will be noted that fused quartz would satisfy the one per cent per year permeation requirement, but that other glasses are several orders of magnitude better. This allows a reasonable flexibility in selection to satisfy other requirements for a cladding material.

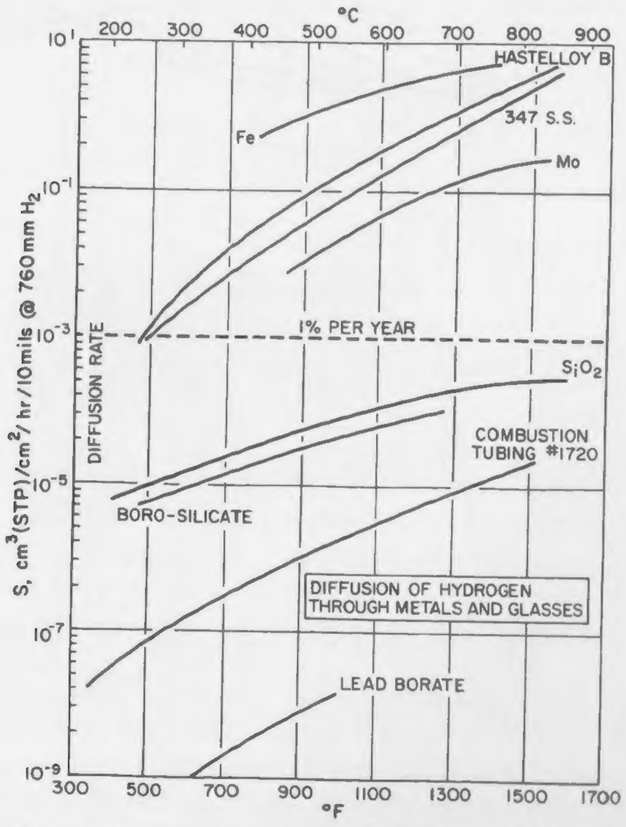


FIGURE 10 DIFFUSION OF HYDROGEN THROUGH METALS AND GLASSES

The use of a ceramic or glass as a cladding per se presents problems in handling, in possible fracture under operating conditions, in heat transfer from fuel to coolant, and in possible reaction with the coolant. These have been solved by using a metal backup for a thin ceramic coating--in other words, an enamel. The ceramic coating is placed on the inside of the Hastelloy N cladding tube and end-closure caps; thus, it is protected from any reaction with the NaK coolant. The coating does provide some thermal resistance in the heat transfer path; however, the coating is thin and the heat flux in the fuel elements is quite low, the average being about 17,000 Btu/hr-ft^2. Thus, the effect on peak fuel rod temperature is slight.

Laboratory tests of fuel elements using such a ceramic coating have shown that hydrogen losses can be held within the desired 1% per year under the operating conditions for the SNAP-2 reactor. The performance of fuel elements with such a hydrogen barrier coating in the SER have confirmed the success of this application.

CONCLUSION

The studies described have led to the successful development of a fuel element for a compact, light weight nuclear reactor for the generation of auxiliary power for space vehicles. Such studies are continuing, to provide improved reliability for the present systems and to provide the materials which may be required for the higher power, higher temperature demands for reactors of the future.

The work reported here is that of a sizable group of people at Atomics International. Some of this work is acknowledged by reference to already published work. The author wishes to express his appreciation to all contributors for their part in the successful development of the fuel element for the SNAP-2 reactor.

BIBLIOGRAPHY

1. Anderson, G. M., J. R. Wetch, H. M. Dieckamp: The Practical Application of Space Nuclear Power in the 1960's, (paper presented to the XI Astronautical Congress, Stockholm, Sweden, August 15, 1960).

2. Anderson, G. M.: SNAP-2--A Reactor-Powered Turboelectric Generator for Space Vehicles, paper 154B (SAE National Aeronautical Meeting, New York, 1960).

3. Anderson, G. M.: The SNAP Program--Present Status and Future Prospects, (paper presented at Atomic Industrial Forum, December, 1960).

4. Atkins, D. F.: Dissociation Pressures of Hydrided Zirconium-Uranium Alloys, NAA-SR-4245, Atomics International, February 15, 1960.

5. Barrer, R. M.: Diffusion in and through Solids, Cambridge University Press (1951).

6. Dieckamp, H. M., R. Balent, J. R. Wetch: Compact Reactors for Space Power, Nucleonics 19, No. 4, pp 73-76 (1961).

7. Flint, P. S.: The Diffusion of Hydrogen through Materials of Construction, KAPL-659, Knolls Atomic Power Laboratory, December 14, 1951.

8. Sommer, A. W. and W. F. Dennison: Thermal Diffusion of Hydrogen in Nonstoichiometric Zirconium Dihydride, NAA-SR-5066, Atomics International, October 1, 1960.

9. Vetrano, J. B. and D. F. Atkins: The Zirconium-Hydrogen System, Nuclear Metallurgy, Vol. III, IMD Special Report Series No. 10, AIME, pp 57-61 (1960).

10. Vetrano, J. B.: A Uranium Dispersion, Zirconium Hydride Matrix Fuel for Compact Space Power Systems, (paper presented at the American Nuclear Society Winter Meeting, San Francisco, December, 1960).

11. Woolsey, C. C.: Use of a Ceramic Coating for a Nuclear Fuel Element (paper presented at the American Ceramic Society, Fall Meeting of the Enamel Division, French Lick, Indiana, September, 1961).